Doctoral Theses at NTNU 2004:131

Kjetil Nordahl

A petrophysical evaluation of tidal heterolithic deposits

Application of a near wellbore model for reconciliation of scale dependent well data

Kjetil Nordahl

NTNU
Norwegian University of
Science and Technology
Doctoral thesis
for the degree of Doktor ingeniør
Faculty of Engineering Science and Technology
Department of Geology and Mineral Resources
Engineering

Doctoral thesis 2004:131 NTNU

ISBN 82-471-6487-6 (printed ver.)
ISBN 82-471-6486-8 (electronic ver.)
ISSN 1503-8181

A petrophysical evaluation of tidal heterolithic deposits

Application of a near wellbore model for reconciliation of scale dependent well data

by
Kjetil Nordahl

A Thesis Submitted in Partial Fulfilment of the requirements for the Degree of
Doktor Ingeniør

Department of Geology and Mineral Resources Engineering

Norwegian University of Science and Technology

Trondheim April 2004

To my late mother and father

Abstract

The main goal of this thesis, *A petrophysical evaluation of tidal heterolithic deposits: application of a near wellbore model for reconciliation of scale dependent well data*, is to give a better and less uncertain estimate of porosity and permeability in a challenging reservoir type. This is accomplished through an integrated study that takes into account both sedimentological and petrophysical well data, that are reconciled in a near wellbore model on which critical factors as sedimentological heterogeneity, biased sampling and scale transitions are evaluated.

A 25 m interval of the lower part of the Tilje Formation in Heidrun Field, Halten Terrace offshore mid Norway is parameterized with focus on factors affecting the petrophysical properties in the near wellbore volume. In tidal deposits, the amount and spatial distribution of low-permeable mud is a critical factor. A geostatistical near wellbore model is then created of this interval. The modelling approach is process-oriented and mimics the depositional process by displacement of mathematical surfaces to simulate deposition and erosion. The volumes between the surfaces are populated with petrophysical properties using a correlated Gaussian field approach. This process-oriented modelling tool is critically reviewed and transformations are proposed that are used to obtain input parameters from core observations such, as the sand and mud laminaset thickness distribution. The porosity and permeability values, that have to be specified at the lamina scale, are obtained from core plugs, which represent an average of several lamina types, through an iterative procedure. The result is a realistic representation of the sedimentological components and the petrophysical distributions in the near wellbore volume on which petrophysical parameters can be calculated on various scales.

In one of the lithofacies the vertical variation in sand laminaset thickness was analysed with time series analysis methods to quantify the degree of tidal influence. Although the data set is noisy, a few periodic components are significant: namely 11-16 and 50-60 sand laminasets per cycle. Furthermore, the internal stratification of the sand laminasets, the transition to the over- and underlying mud laminasets and the mean thickness of the mud laminasets, suggest that the shortest period recorded reflects a semi-annual tidal component. Incorporating vertical, periodic variation in mud fraction is important since it influences the bulk petrophysical properties.

Published flume tank studies are used to create a wide range of ripple-laminated, realistic bedding types with different mud fractions and correlation lengths but with constant petrophysical properties. These models are evaluated as a function of sam-

ple volume. A large variation in porosity and permeability between realizations, expressed as the Coefficient of Variation (C_V), is observed when the sample volume is small. This indicates that the volume of investigation is not representative. A representative elementary volume (REV) is here defined to correspond to the sample volume that gives a C_V below 0.5. For permeability there is observed a relation between the size of the REV and the bedding type (i.e. the correlation lengths of the sedimentological components). This relation is different for vertical and horizontal permeability. Porosity, being an additive property only dependent on the amount and not the spatial distribution of the components, shows no such dependency. From these experimental results, flow regimes and critical thresholds are identified that highlight the uncertainty in scale transition issues in these deposits. The results show that core plugs in general are inadequate to describe the effective permeability at the bedding scale and that this will affect the integration of core and log data.

The model set used to study the dependency with sample volume is expanded and evaluated with different porosity and permeability contrasts between the lithological components at a representative scale. The critical threshold for onset of vertical and horizontal flow is enhanced. The relation between the mud fraction and the effective vertical and horizontal permeability is expressed with different function types that are used to estimate a representative permeability value from a mud fraction estimate. Incorporating physical parameters that can be evaluated independently makes the relationship more generally applicable. The results can be used to guide the focus in data collection in these deposits by quantifying the influence of contrast between sand laminae or between the sand and the mud component in the different flow regimes.

The results form a basis for giving a better estimate of porosity and permeability in the selected interval. One method uses the near wellbore model, based on the detailed study of the interval, and forward models the porosity and permeability anisotropy at various scales. With this method individual lithofacies are studied and biased sampling is evaluated. A continuous estimate along the model is compared with existing estimates of horizontal permeability and porosity. A second method, being more general, uses the equations describing the relation between mud fraction and permeability. Using a wireline-based estimator of mud fraction, a continuous estimate of permeability anisotropy is obtained that differs from the traditional core-log method since the effective properties are calculated at a representative scale.

In summary, this study gives, as well as a contribution to scale transition issues in a difficult tidal heterolithic reservoir type, a formalised basis for analysis of petrophysical properties in a multi-scaled heterogeneous geological system.

Preface

This research project started in August 1999 and has been a part of the Formation Evaluation project at the Norwegian University of Science and Technology (NTNU). The project was financially supported by Statoil ASA, Norsk Hydro and Saga Petroleum. During this period I was employed at the Institute of Geology and Resources Engineering, NTNU, who also funded one year of this study. During the last part of the work, Statoil Research Centre offered me office and equipment to carry out the research part of the work.

A number of persons have contributed in different ways throughout the period and deserve credit for helping me completing this project.

- My supervisor at the Department of Geology and Resources Engineering, Førsteamanuensis Sverre Ola Johnsen is thanked for valuable support and comments during the whole period.
- Dr. Philip S. Ringrose is gratefully acknowledged for all the discussions, comments and suggestions for work through the whole period and for proofreading a large part of the manuscript. Without his contribution, this thesis could not have been completed.
- Project leader in the Reservoir and Uncertainty Modelling group (RUM) Dr. Allard W. Martinius is thanked for valuable comments, especially on the sedimentological part, and for letting me finalize this project after I started to work in the RUM project at Statoil Research Centre.
- Senior Geologist Carsten Elfenbein for interesting discussions on many issues and especially for making sure that I regularly got out of the office for a table-tennis match.
- Dr. Arve Næss for general support and introduction to the problem in an early phase of the project.
- Inge Bransæter and Dr. Alfhild Lien Eide for advice on statistical questions.
- Dr. Steven Morriss and Dr. Frank Antonsen for support on petrophysical issues.
- Dr. Renjun Wen and Geomodeling Technology Corp. for fruitful discussions and technical advices on the SBED tool.
- Fellow PhD.-students and staff at both the Department of Geology and Mineral Resources Engineering and Department of Petroleum Engineering and Applied Geophysics for offering a great environment to work in. Especially fellow student in the Formation Evaluation project and part time office mate, Bengt K.

Pedersen, is thanked for all the professional and not at least non-professional conversations during this period.

- Finally, my wife Siri is thanked for showing an enormous patient and understanding during this long period. All the long workdays have been a challenge also for her and I could not have carried out this work without her caring support. I am looking forward to spend more time with her and our little son Brage who arrived last autumn.

CHAPTER 1 *Introduction*

1.1 Background

Estimation of petrophysical properties, as porosity and permeability, has been and is an important activity in the petroleum industry. Even after decades of research, it is still little consensus of how to properly reconcile the available subsurface data in order to estimate these parameters. In heterolithic deposits, the estimation of permeability is particularly difficult because there is no reliable direct measurement of permeability in the subsurface, permeability is a non-additive, scale dependent property of the rock and the resolution of the measurements used is generally inadequate to describe the small-scale variability that influence on the flow properties.

Sedimentary architecture causes heterogeneity at many scales, which can affect reservoir performance (e.g. Haldorsen, 1986), and primary sedimentary structures at the sub-meter scale have been shown to significantly influence on the flow properties (Weber, 1982; Hurst, 1993; Hartkamp-Bakker and Donselaar, 1993a). However, because of computational limitations, these heterogeneities cannot be included explicitly in the reservoir simulator but have to be represented by a single representative value. To give a best estimate of that value, all the available and relevant data should be used. There are, however, some principal problems of integrating data representing different sample volumes (Haldorsen, 1986; Enderlin et al., 1991; Worthington, 1994; 2003a; Corbett et al., 1998). This is especially the case in tide-influenced deposits, which commonly show many scales of heterogeneities.

Brandsæter et al. (2001) showed that the ratio between vertical and horizontal permeability (k_v/k_h ratio) was one of the most important parameters influencing oil recovery in such deposits. At the lithofacies scale, thin mud layers intercalated with sand have a strong influence on the flow properties. These millimetre to centimetre scale heterogeneities are not well characterized by the core plugs or the wireline log measurements. Core plugs measure at a volume scale at or below the characteristic length scale of the heterogeneity and the wireline logs, measuring in general a larger volume of rock, tend to average out the response from the different components present. Integration between these two data sets is thus problematic. Heterolithic tidal reservoirs form a significant part of many of the hydrocarbon fields on the Halten Terrace, offshore mid Norway and are a reservoir type of growing economic importance.

Many methods have been proposed to calculate the effective permeability (for a review see Renard and Marsily, 1997). However, regardless of the upscaling technique, the question remains as to what scale the measurements should be rescaled to. Bear (1972) introduced the concept of Representative Elementary Volume (REV). At this volume, the parameter of interest is both homogeneous and stationary meaning that the value is insensitive to small changes in sample volume and location. Even though this concept is simple and intuitive, only a limited number of papers have been published on this issue, which can be related to the difficulty in experimental verifying the existence of such a volume (Baveye and Sposito, 1984).

Koltermann and Gorelick (1996) reviewed different methods for generating numerical models of sedimentary architecture. The majority of these focus on larger scale heterogeneities while some considered the scale of primary sedimentary structures. In this thesis, a process oriented stochastic modelling tool (SBED^{TM}, Wen et al., 1998) is used to generate realistic near wellbore models of the reservoir. The near wellbore model is defined here as a numerical representation of the sedimentological components and petrophysical properties in a rectangular shaped volume along the wellbore with a lateral dimension on the scale of the conventional wireline tools. This geostatistical, near-wellbore, 3D model can be regarded as an *earth model* common to the sedimentologist, the petrophysicist and the reservoir engineer since it can contain information relevant to all these disciplines. Having this model that spans geological length scales from the lamina scale to the bed set scale gives a possibility to reconcile conflicting well data and form a basis for better integration of static and dynamic data. This thesis will focus on a few of the possibilities this shared earth model can provide to reconcile conflicting welldata.

1.2 Problem definition and aim of work

Despite the acknowledgment of the principal problems with traditional integration methods of core and wireline data for estimation of porosity and permeability, it has been difficult to establish a consistent approach to this problem. For tide-influenced deposits, it is commonly observed that even after an interval is divided into lithofacies, the petrophysical variability, estimated from available well data, is large in each lithofacies and that the contrast between lithofacies is low. This indicates that the heterogeneity affecting these parameters is not well characterized with these well data types. The main goal of this thesis is thus to give a better and less uncertain estimate of porosity and permeability in such challenging reservoirs. This is a wide and cross-disciplinary topic and the following sub-tasks have been chosen to restrict this thesis:

- Focus on single-phase permeability anisotropy and porosity

- Evaluate the advantages and limitations of a shared earth model and develop consistent workflows that create realistic near wellbore models of these deposits giving an opportunity to rescale available data to the scale of interest.

- Evaluate, for some common tidal deposits, how porosity and permeability varies with sample volume, the size of a representative volume (if it exists) and its relation to the correlation lengths of the sedimentological components. Furthermore, evaluate the influence of varying the contrast between the lithological components on the parameters of interest.

- Apply the results and workflows to a specific reservoir interval in the lower part of the Tilje Formation, Heidrun Field on the Halten Terrace to give a better and less uncertain estimate of porosity and permeability at various scales.

These subjects address issues that can be regarded as more of academic interest and results that are directly applicable for the petroleum industry.

1.3 Organization of the thesis

This thesis consists of nine chapters in addition to appendices that contain necessary modelling parameters to recreate the results presented (Appendix A), two extended abstracts, one presented (Appendix B) and one accepted for presentation (Appendix C), and a paper that is submitted for publication (Appendix D). The nine chapters can be divided into five sections:

1. Theoretical background (chapter 2 and 3). Chapter 2 gives a general introduction to some petrophysical conceptual models, sedimentary processes and the implications on petrophysical properties, and different published methods for estimation of porosity and permeability from well data. Chapter 3 gives a review of tidal theory and the implications on the sedimentary record, which then forms as a background for chapter 5. Because of the cross-disciplinary aspect of this thesis, it is considered important to review these issues comprehensively. The result is that the reader may find some of the aspects reviewed unnecessary detailed. However, many of the concepts, terminologies and assumptions in the models in the different disciplines are often not well understood by a person not from that particular discipline. For example, a petrophysicist with a background in physics may find section 2.2 valuable both for introduction of common terms but also to appreciate better the geological part of the earth model. A sedimentologist, may however find that particular section trivial, but are perhaps more unfamiliar with the issues treated in for example section 2.3. Furthermore, these sections are then easy to use as reference in the subsequent chapters.
2. Geomodeling tool. Chapter 4 gives a description of the modeling tool used in this thesis and the results from a preliminary sensitivity study of the input and output parameters. A workflow and transformations to be used for detailed modelling of specific lithofacies, is given in the end of this chapter.
3. Detailed near wellbore model of a well interval. Chapter 5 gives a sedimentological description of a selected interval of the Tilje Formation with focus on aspects that influence the petrophysical properties in the near wellbore volume. The results from chapter 4 are used to build a realistic sedimentological model of this interval. Chapter 6 outlines a workflow that is used to populate the near wellbore model with petrophysical properties from core plugs. The combined result from these two chapters is a detailed near wellbore model that honours the available well data and that are applicable for near wellbore modelling in deposits where similar aspects affect the petrophysical properties.
4. Evaluation of conceptual tidal bedding models. Chapter 7 gives a set of conceptual tidal bedding models which input parameters are based on published flume tank studies. These models, representing a range of tidal bedding types with different mud fractions and correlation lengths, are then evaluated as a function of sample volume. An extended model set is used in chapter 8 to evaluate the influence of petrophysical contrast between the lithological components at a representative scale.
5. Application of results to example well. Chapter 9 uses the results from previous chapters to give a better estimate of porosity and permeability anisotropy in the selected well interval. One method uses the detailed near wellbore model from

chapter 5 and chapter 6, while another method uses the results from chapter 7 and chapter 8.

CHAPTER 2

Petrophysics and sedimentary processes

For a petroleum reservoir to be economical it is necessary that the reservoir rock under consideration has the ability to store hydrocarbons and that the hydrocarbons are allowed to flow through the rock. The first property is called porosity and the second permeability. An important task in petrophysics is to estimate these two parameters. This chapter will give the basic concepts regarding petrophysics and the intimate relation to sedimentary processes. In the final section, published methods to estimate porosity and permeability from common well data in the near wellbore region will be reviewed.

This thesis will focus on scale transition issues in tidal heterolithic reservoirs and the implications for core-log integration for estimation of porosity and permeability anisotropy. It will thus be essential to have a basic knowledge of the topics reviewed here to appreciate the challenges that are involved. As mentioned in the Introduction, some of the topics are reviewed on a rather detailed and basic level. This is however done with intention since the issue itself is cross-disciplinary and it is important that readers with different backgrounds are familiar with the terminology and model assumptions of the other disciplines.

2.1 Properties of porous media

In the following, a review of the basic theory for flow of fluid in porous media is given with emphasis on the assumptions of the petrophysical models. Most of the

material presented can be found in textbooks covering dynamics in porous media (Scheidegger, 1974; Bear, 1988; Bear & Bachmat, 1990; Dullien, 1992; Sahimi, 1995) and general fluid mechanics (Munson et al., 1994).

2.1.1 Description of porous media and the continuum approach

Simply stated, porosity is the capacity of a medium to store fluid and permeability is the ease of which fluid can flow through the porous material. Even though we may have an intuitive understanding of porosity, permeability and porous media, it turns out that they are difficult to define exactly. Bear (1988) outlines some essential characteristics of such a medium. A porous medium should be a multiphase matter, where at least one of the phases is not a solid. The solid phase is called the solid matrix and the void space between is called the pore space. Scheidegger (1974) used the term pore for void space of intermediate size between molecular interstices and caverns, which imply an indefinite limit. In order to be characterized as a porous medium, these 'intermediate sized' pores should be frequently distributed in the solid and at least some of the pores should be interconnected, even though the passages between them, the pore throats, often are narrow. Ideally, one would like to define a geometrical quantity that would characterize the pore system. However, the pore system of a natural porous body forms a very complex network, which is extremely difficult to describe geometrically. As a first approach, one would like to describe the pore with a diameter, and label this the pore-size. But attaching a (single) diameter to an irregularly shaped object is not a trivial task. The same problem is encountered when describing the grains. If the grains do not have a simple shape, a geometrical description of the volume or surface will be difficult. Scheidegger (1974) gives a good discussion of the difficulty of quantifying geometrical quantities of the porous media.

The complexity of the pore geometry makes it intractable to describe with exact mathematical formulations. Another approach, the continuum approach, ignore the details of the media and uses the hypothesis that the porous matter is a hypothetical substance that is continuous throughout the spatial domain it occupies. The matter can then be described in that domain by a set of variables, which are continuous and differentiable functions of the spatial coordinates and of time (Bear and Bachmat, 1990). The method of replacing a complex medium with a hypothetical homogeneous one has a long history and is often referred to as effective medium approximation (Bruggemann, 1935). Such an approach is appealing since measurements of extensive properties (see section 2.1.4) also represent an average over a certain volume of the porous media. Essential to the treatment of the porous media as a continuum is the concept of a particle that is associated with a certain volume. The size of the particle should be so large that the effect of the micro-geometry is averaged out,

but still so small that it is representative for the centroid of the particle. This suitable large volume is often labelled the Representative Elementary Volume (REV) (Bear, 1972). The introduction of this volume is associated with a length scale. It is thus important to evaluate the effect of various length scales at which the system may be considered homogeneous, especially since the continuum approach breaks down if the correlations in the system approach the linear size of the system (Sahimi, 1995). This issue will be discussed in more detail in chapter 7.

Before proceeding, some aspects of the porous media need to be considered. In a porous medium a property of interest may change as a function of the *position* in the medium and a medium is said to be *homogeneous* with respect to a certain property if that property is *independent of position* within the medium. Otherwise the medium is said to be *heterogeneous* (Bear and Bachmat, 1990). The property may also vary with the *direction* it is measured, and a medium is said to be *isotropic* with respect to a certain property if that property is *independent of direction* within the medium. If, at a point within the medium, a property of the medium varies with direction, the medium is said to be *anisotropic*. Depending on the measurement volume, most reservoirs are heterogeneous and anisotropic rather than homogeneous and isotropic.

Having described some of the characteristics of the porous media, the next step is to evaluate how macroscopic properties, as porosity and permeability, are influenced by the pore structure. A general useful approach when studying complex natural phenomena that is too difficult, or impossible, to handle analytically, is to construct a conceptual model that is amenable to mathematical treatment. Various parameters of the conceptual model can then be related to parameters from the real phenomena. In the following, published conceptual models that have been used to investigate the relationship between pore structure and macroscopic properties will be briefly reviewed.

2.1.2 Porosity

A simple conceptual model for a porous medium will be a packing of equally sized spheres (figure 2.1). Grafton and Fraser (1935) made an extensive analysis of packing of spheres and its relation to porosity and permeability.

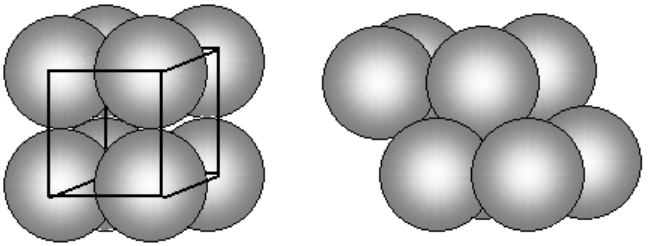

FIGURE 2.1 *Examples of different packing of equally sized spheres. Left: Cubic packing, Right: Rhombohedral packing.*

If we consider a unit cell of this model (inside the square to the left in figure 2.1), the pore or void *volume* can be calculated as the difference between the total volume of the cube and the volume of the solid spheres. The *total porosity* ϕ, a dimensionless property, is defined as the ratio between the pore volume and the total volume or the fraction of the total volume that is not solid:

$$\varphi = \frac{V_p}{V_b} = \frac{V_b - V_s}{V_b} \qquad \textbf{[2-1]}$$

Where V_p, V_b and V_s is the volume of the pore space, bulk or total, and solid, respectively. In the case of cubic packing, the total porosity is 0.476 while the rhombohedral packing has a porosity of 0.26. It should be obvious from the discussion above that porosity needs to be calculated on a volume of a certain size since the porosity at an infinitesimal volume can take the value 0 or 1 depending on the location.

Another geometrical quantity of the porous media is the specific surface area S. This is defined as the ratio between the total internal surface area of the pores (A_s) and the total volume:

$$S = \frac{A_s}{V_b} \qquad [S] = [m^{-1}] \qquad \textbf{[2-2]}$$

A variant of this quantity is the ratio between the specific surface area and the volume of the solid (S_S)

$$S_s = \frac{A_s}{V_s} = \frac{A_s}{V_b(1-\varphi)} \Rightarrow S = S_s(1-\varphi)\,. \qquad \textbf{[2-3]}$$

From such conceptual models it is observed that porosity is independent of the sphere size but dependent of the grain configuration (packing), while the specific surface area is dependent of the sphere size and that the latter will increase with decreasing radius (through the ratio between A_S and V_S). In natural sandstones where the solid matrix forms a complex surface, the same equations can be used, but the volume of the solid or the void space has to be found experimentally. In addition, not all the pores in a sandstone have to be in connection with each other and with respect to flow through a porous medium, only the interconnected pores are of interest. A quantity, termed the *effective porosity* ϕ_e can be defined as the ratio between the interconnected pore volume ($V_{p,e}$) and the total volume.

$$\varphi_e = \frac{V_{p,e}}{V_b}, \quad V_{p,e} + V_{p,ne} = V_p \qquad \textbf{[2-4]}$$

where $V_{p,ne}$ is the non-interconnected pore volume.

2.1.3 Permeability

In order to incorporate fluid flowing through the porous media, with the end goal of determining its permeability, details of the fluid dynamics are needed. In principal, the Navier-Stokes equation can be written and solved at the microscopic level. However, because of the complex surface bounding the fluid, the description and solution at the pore level is impractical and probably impossible. As a result, the continuum approach has been used where the phenomena is studied at a scale much larger than the pores. However, in some simple cases, it is possible to solve the equation exactly. For steady, laminar flow in a cylindrical tube the resulting solution is the Hagen-Poiseuille equation. In this case the flow rate through the tube, which is equal to the velocity distribution from the Navier-Stokes equation multiplied with the area of the tube, can be expressed as

$$Q = \frac{\pi R^4 \Delta p}{8\mu L} \qquad \textbf{[2-5]}$$

where R and L is the radius and length of the tube, respectively, and Δp is the pressure drop that occurs over the tube.

The macroscopic description of a fluid flowing through a porous medium was early experimentally investigated by a Henry Darcy in 1853 (Bear, 1972). Darcy used the experimental setup in fig 2.2. An incompressible fluid was percolated through the one dimensional sand filter and in open manometer tubes at the base and top of the filter, the liquid rose to the heights h_1 and h_2, respectively, above a defined datum (Z=0). From this experiment, Darcy concluded that the rate of flow (volume per unit time) Q is a) proportional to the constant cross-sectional area A b) proportional to (h_2-h_1) and c) inversely proportional to the length L. Combined, this gave the Darcy law or formula:

$$Q = \frac{KA(h_2 - h_1)}{L} \qquad [Q] = [m^3/s] \qquad \textbf{[2-6]}$$

Darcy law is valid in the case of incompressible fluid flowing through a homogeneous medium at a low speed (i.e. at laminar flow were the viscous forces are predominant). With other conditions, this relationship is not valid. This one-dimensional equation has later been extended and generalized to three-dimensional differential equations (see e.g. Scheidegger, 1974; Sahimi, 1995).

The ratio between the flow rate Q and the cross-sectional area A is called the specific discharge q. The coefficient of proportionality K, appearing in the Darcy formula is called the hydraulic conductivity. It expresses with which ease the fluid is transported through the porous matrix and has the dimension m/s. This coefficient depends on both the matrix and the fluid properties. Nutting (1930), proposed a relationship that separates the effect of the grain configuration (the matrix) and the fluid:

$$K = k\frac{\gamma}{\mu} = k\frac{\rho g}{\mu} = k\frac{g}{\upsilon} \qquad \textbf{[2-7]}$$

where g is the gravitation constant, ν is the kinematic viscosity and γ is the specific weight of the fluid. The parameter “k” is called the specific permeability or intrinsic permeability and has the dimension m^2. The specific permeability, denoted permeability in this thesis, is then only dependent on the matrix properties, while the ratio between the specific weight and dynamic viscosity is the effect of fluid on the hydraulic conductivity.

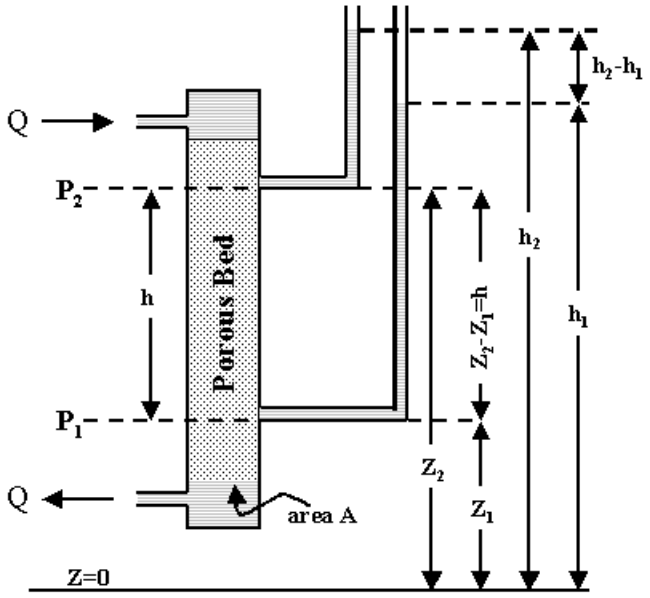

FIGURE 2.2 *The setup for Darcy's filtration experiment. Modified from Scheidegger (1974). The various terms are explained in the text.*

Over the years several models have been proposed to estimate permeability, often with porosity or grains size as independent parameters. Although they might give satisfactory results in some instances, a universal relationship between porosity and permeability is obviously not valid. A simple consideration of theoretical possibilities of the structure of porous media makes one realize that a general correlation between porosity and permeability cannot exist. The important question then is what geometrical quantities of the porous media influence the specific permeability. Since permeability has the dimension of a length squared, great effort has therefore been made to reveal what geometrical length factors of the porous media that affect this property. Intuitively, the pore size and more important the pore throats will affect the ability of a fluid to flow through the media. As a consequence, it would be desirable to be able to express these geometrical quantities with the equation of the surface that bounds the pore space. However, as we have seen previously, this surface is complex and irregular, which makes it intractable to express mathematically. In addition, the question whether the pore can be described adequately with a diameter is doubtful. As for porosity, conceptual models have been made so that the

effect of a simplified solid matrix on permeability can be investigated. The conceptual models should ideally capture the main features of the porous medium, but still be so simple that the Navier-Stokes equation can be solved.

One conceptual model is the capillaric model (figure 2.3). In this case the viscous, incompressible fluid is assumed to be restricted to flow in narrow tubes that resemble the pores. The flow of fluid is covered by the general differential equation of motion but can in this case be simplified to the Hagen-Poiseuille equation (eq. 2-5).

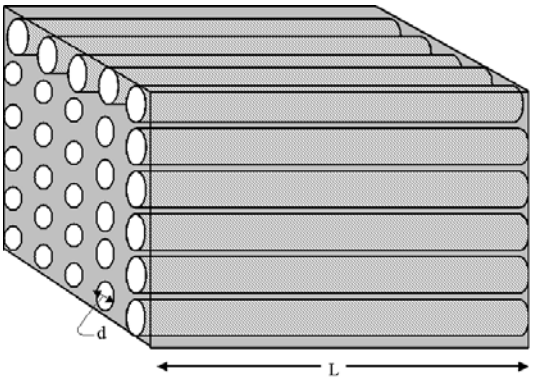

FIGURE 2.3 *A conceptual model of a porous medium as a bundle of straight, circular tubes (modified from Scheidegger, 1974).*

If there are n equal tubes per unit cross area with diameter d and length L, the specific discharge q (flow per unit area) becomes

$$q = \frac{n\pi d^4}{128\mu} \cdot \frac{\Delta p}{L} \qquad \textbf{[2-8]}$$

The porosity of this model is $\varphi = n\pi d^2/4$ and by comparing with eq. 2-6 and 2-7 it follows that the permeability of a bundle with capillary tubes is

$$k = \phi \cdot \frac{d^2}{32} \qquad \textbf{[2-9]}$$

It is clear that the capillaric model do not resemble a natural porous medium like a sandstone where the flow channels are more complex than straight tubes. There has

been proposed several modifications of the straight capillaric model by introducing flexibility to the length and radius of the tubes and by replacing the numerical factor by a arbitrary factor τ called the tortuosity, without increasing the actual knowledge of the influence of the matrix on permeability (see Clennel (1997) for a good discussion of tortuosity).

Instead of using the radius of the tubes, another possibility is to use the *hydraulic diameter,* which is defined as the ratio between the area of cross-section and the wetted perimeter. In a circular tube this would be equal to $(\pi r^2)/(2\pi r) = r/2$. Another definition of the hydraulic diameter is the ratio between the volume of the pore space and the wetted surface area of the same pore space.

One commonly used models for calculation of permeability, which is based on the hydraulic radius theory, is the Kozeny-Carman equation (Carman, 1937). In this case the porous media is modelled as a set of channels with equal length but variable cross-section. In this respect it resembles the capillaric models described previously, but it uses the hydraulic diameter instead of the tube diameter. By solving the Navier-Stokes equation simultaneously for all the channels the equation for permeability becomes (for a full derivation, see Scheidegger, 1974)

$$k = c\frac{\frac{\varphi^3}{(1-\varphi)^2}}{S_s^2} \qquad \textbf{[2-10]}$$

where S_s is the specific surface area of the solid as defined in eq. 2-3, and c a constant called the Kozeny constant. The constant c is also expressed as $1/\tau^2 c_0$, where τ is the tortuosity. With spherical grains of equal diameter d, eq. 2-10 can be written as

$$k = c\frac{d^2}{36} \cdot \frac{\varphi^3}{(1-\varphi)^2}. \qquad \textbf{[2-11]}$$

It has been shown experimentally that the Kozeny-Carman equation works well in well sorted sandstones. In the high or low porosity range, the relationship breaks down, and is no longer valid. This is mainly due to the porosity term, and based on this observation, Mavko & Nur (1997) incorporate a threshold porosity ϕ_c in the equation by replacing the ϕ-term with ϕ-ϕ_c, and obtain some improvements in the low porosity range. Sheidegger (1974) points out additional criticism, especially

that the theory neglects the influence of conical flow in the constrictions and expansions of flow channels (between pores and pore throats). The constant c, which usually is associated with the tortuosity of the porous media, is difficult to both interpret physically and measure experimentally. In the original equation, this constant is a scalar and has consequently no direction dependency, although permeability often exhibits this property.

Bear and Bachmat (1990) developed a porous medium model that is statistical in nature. That is, they treat the porous media with fluid as a continuum and calculate the average of the property over the entire model. Essential to this model is that the volume over which this average is taken has to be representative for that property (i.e. at the REV). In the model by Bear and Bachmat (1990), the Navier-Stoke equation is averaged in each channel in much the same way as the Kozeny-Carman model. This average flow value is assigned to the channel-axis. In the next step they average the flow properties in all the channel axis and obtain a general expression of the flow of an inhomogeneous incompressible fluid, through an anisotropic porous medium. For a homogeneous, incompressible fluid, this expression is reduced to an expression similar to the Darcy Law

$$q_i = -\left(\frac{k_{ij}\gamma}{\mu} \cdot \frac{\partial p}{\partial l_j}\right). \qquad \textbf{[2-12]}$$

The permeability, k_{ij} is here expressed as a second rank tensor, and is in this model calculated as

$$k_{ij} = \varphi B T_{ij} \qquad \textbf{[2-13]}$$

where, ϕ is porosity as before, B with dimension m^2 is called the conductance of channel related to the cross-section of that channel, and T_{ij} is the second rank tortuosity tensor. The factor B was introduces via a constitutive assumption that the force resisting the motion of a particle at a point inside the channel is proportional to the particles mass-averaged velocity V at that point and acting in the opposite direction to that local velocity vector:

$$\boldsymbol{R} = -\frac{\mu}{\boldsymbol{B}}\boldsymbol{V} \qquad \textbf{[2-14]}$$

All the above-mentioned theoretical models relate permeability or porosity to some geometrical factors in the model. The challenge is to relate these factors to some measurable parameters in the real porous media. The simple capillaric model obtains an exact expression of permeability, but it does not represent the true

porous media in a satisfactory manner. The Kozeny-Carman relation have been widely used and more complex version are also published (e.g. Panda and Lake, 1994; 1995). However, such complex methods require input parameters that are difficult to measure. In the same manner, the Bear and Bachmat model is quite sophisticated, since it allows flexibility to channel morphology, and allows permeability to be direction dependent. It was, however, necessary to include the tortuosity term in order to obtain an expression for absolute permeability of the media. The permeability constant in Darcy equation (k) is in this respect a parameter of ignorance since it incorporates *all* the geometrical effects of the porous medium, that is not expressed explicitly in the equation, into a single value. When a continuum approach is used to calculate permeability, coefficients are introduced that enable the passage from the microscopic to the macroscopic level. They are, however, only undetermined factors used in order to make the data fit the desired equations, as pointed out by Scheidegger (1974, p. 124). Some knowledge about the factors controlling these important petrophysical properties has however been obtained: porosity is mainly a function of packing but not as much of the grains size, but permeability is dependent on the pore throat size, geometry and the tortuosity of the pore channels.

All the equations derived so far have the assumption that only *one* fluid is flowing through the porous medium. In the case of several fluids, it becomes more complicated since one have to take into account the effect of the various fluid components in relation to each other. Relative permeability is a term used to describe the permeability of one of the flowing phases with respect to the absolute permeability. In this thesis, only flow of one fluid will be discussed and this will be called single-phase, absolute permeability, here just denoted permeability.

2.1.4 Extensive and intensive properties

In general, when considering a porous medium, two types of properties are evaluated. The first type, dependent on the quantity of the porous material, is called extensive properties. Mass and energy are examples of this type of property. Different from extensive properties are those properties, which denote concentrations or intensities of mass or energy. These are independent of the quantity or shape of the porous media and are called intensive properties. Temperature, density, pressure, porosity and permeability are examples of this property group.

The reason for introducing these terms is that most of the parameters that are measured on the porous material are intensive properties. Due to limitations of the measuring device, only a finite domain of this material can be measured. These

instruments act thus as an integrating device and provide data in a statistical sense. The result is an average of the measured properties over this sub domain. As a result, our understanding of the porous media is very much related to averaging.

Basic to the procedure of mathematical integration is the process of addition. A physical meaningful averaging procedure (i.e. integration that conserves mass or energy over part, or the whole of the porous media) must therefore have integrands that are additive. The additive relationship can be expressed as (Olea, 1991):

$$f(A \cup B) = f(A) + f(B) \quad \textbf{[2-15]}$$

This means that if f is a measure and A and B are two disjoint sets then the measured property of the A and B sub domains are equal to the summation of the measures from the two sub domains. Narasimhan (1983) showed that only extensive properties are additive and than intensive properties in general are not. However, methods have been proposed to take into account the non-additivity of intensive properties. Narasimhan (1983) argued that intensive properties could be transformed into extensive properties through a capacity function. For example the specific heat capacity can be used to link temperature (intensive property) and heat (extensive property). Hassanizadeh and Gray (1983) proposed to use the concept of REV to allow physical meaningful averaging of intensive properties.

In summary, this means that both porosity and permeability are intensive, non-additive properties. However, porosity is a volume-normalized parameter where the capacity function is unity. Hence, porosity can be regarded as an additive property. Because of this, it will be shown later that it is easier to define an average porosity value than an average permeability value.

2.2 Sedimentological factors controlling porosity and permeability

Previous section gave a review of theoretical equations for porosity and permeability based on conceptual porous media models. It was clear that these petrophysical properties were dependent on some aspects of the pore geometry, which again was influenced by both the shape, size and arrangement of the grains constituting the solid matrix. This section will give a review of the relation between the depositional process and the porosity and permeability anisotropy in the final sedimentary deposit. It is important to understand the fundamental pore-scale control on porosity and permeability in order to comprehend the effect of lamina and bedding structures (i.e. at a larger scale) on these petrophysical properties (Brayshaw et al., 1996). An important theme of this thesis will be to evaluate how these petrophysi-

cal properties vary as a function of the measurement volume using a process oriented modelling approach to model some tide influenced sedimentary rocks.

There is an additional motivation for including this section because the modelling tool used here (see chapter 4) requires an understanding of sedimentary terminology and depositional processes. Although the depositional process is not directly simulated with this code, its effect on porosity and permeability can be incorporated in the synthetic bedding models through bedform dependent trends. It is thus important that the processes that create these trends are reviewed for better understanding of the modelling method. Furthermore, the code is in part based upon some earlier results in describing and modelling the geometry of sedimentary bedforms (see section 2.2.2.3).

2.2.1 Texture and fabric

Water and air are the primary fluids to consider in erosion and transportation of sedimentary particles. Depending of the velocity and kinematic viscosity of the fluid in motion, two modes of flow can be defined. Laminar flow can be visualized with a fluid particle that follows smooth parallel streamlines, and occurs at low velocity or in high viscosity fluids. Turbulent flow is on the other hand characterized by a relatively irregular, eddying motion of the path that each fluid particle follows through the flow. This eddying results in an apparent increased viscosity and affects both the fluids ability to transport and erode the sediment bed.

The entrainment of a grain from a sediment surface is a function of several parameters: size, shape and orientation of the grain and the forces exerted on the grain by the fluid, neighboring grains and gravity. On a cohesionless near horizontal surface, the gravity will pull the grain downwards and the fluid exerts a lift force both due to the buoyancy force and the Bernoulli effect (see Allen, 1970b, p. 45-52). There is also a shear force or drag force from the fluid on the grain related to the boundary shear stress. On a cohesive surface the force needed to entrain the grain will in general be larger since the there is an additional attractive force between the grains. This is often the case with clay minerals since they have electrochemical bonds between them. The erosive power of a fluid on a cohesive surface is also dependent on the degree of consolidation (Terwindt et al., 1968; Terwindt and Breusers, 1972). Increasing consolidation will increase the force needed to erode the surface.

Once the grain is lifted from the surface, it is transported down-current by the fluid, and the rate of grains entrained increases with increased strength of the current (Allen, 1968, p. 24-28). Depending then on the energy and the physical properties

of the fluid combined with the shape, size and density of the entrained grain, two main modes of transportation can be described: suspension and bedload (e.g. Middleton and Southard, 1977; Allen, 1982a). The latter is conventionally defined as movement in substantially continuous contact with the bed. With increasing turbulence, the upward directed force from the fluid increases and the grain is kept in the fluid for a longer time than that could be predicted from the falling velocity in non-turbulent water.

The sedimentary particles will eventually settle on the bed surface and come to rest. The characteristics of the individual grains and the spatial arrangement of an aggregate of grains is called the texture of a sediment and is dependent on the prevailing depositional conditions. The individual grains have been described by various parameters as grain size and grain shape. Grain size and sorting has been used to interpret the depositional environment of the sedimentary rock (e.g. Visher, 1969; Middleton, 1976; McLaren and Bowels, 1985; Sun, 2002). However, as discussed in section 2.1.1 the grain size of natural grains is difficult to express exactly because of the complex and irregular surfaces and the grain size distribution of a sediment reflects more the depositional process and is not unique for a particular sedimentary environment. The shape of a sedimentary grain can be expressed with three independent properties; form, roundness and surface texture and Barret (1980) gives a review of the different methods proposed to measure these quantities. The orientation and packing of grain aggregates, called the fabric, have been studied extensively in order to evaluate the influence on porosity and permeability (Fraser, 1935; Pryor, 1973). Atkins and McBride (1992) devised a quantitative index to assess the packing of sediment, which measured the number of contact points between grains, known as the contact index. Non-spherical and angular grains will tend to have looser packing since there are more contact points between the grains.

Although the texture will influence on bulk physical properties as porosity and permeability anisotropy, the exact relation is a complex. Essentially, the factors that control the pore size and -geometry also control porosity and permeability at this scale. Beard and Weyl (1973) found, in an empirical study, that grain size and sorting are the most influential parameters followed by the fabric of the sediment and to a lesser degree shape and roundness. Porosity was found to be independent of grain size but decreased with decreasing sorting. The permeability however, depends on both grain size and sorting. Larger grains gave larger pore throats and hence higher permeability. In poorly sorted sediments, the finer grained material tends to block the pore throats giving a decrease in permeability. Figure 2.4 shows the effect of grain size and sorting on porosity and permeability.

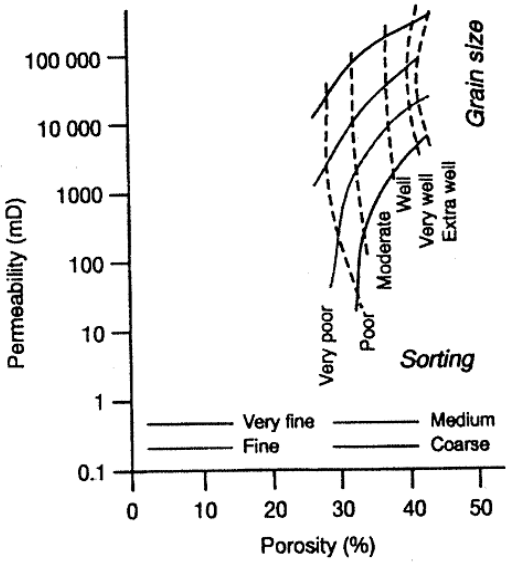

FIGURE 2.4 *The effect of grain size and sorting on porosity and permeability (from Brayshaw et al. 1996).*

The findings from the theoretical models of packing of spheres in section 2.1.2 agree with the empirical studies. In addition, the studies on natural sand-sized sediments indicate that sorting, shape and fabric of the sediment influences on the pore scale petrophysical properties.

2.2.2 Inorganic sedimentary structures and relation to petrophysical variability

The texture and the fabric controls porosity and permeability, and the direction dependency of the latter, at the pore scale. This information can be used to estimate porosity and permeability at the scale of the individual layers of grains as done by e.g. Bryant (1993). While the fabric is the microscopic (~mm) structural feature of a sediment, the macroscopic structural features (cm-m's) of a sediment are called sedimentary structures. The latter is often further divided into primary or secondary, and organic or inorganic structures (Reineck and Singh, 1980). Primary struc-

tures are those generated during or shortly after deposition, while secondary is formed some time after sedimentation. Organic structures are those generated by living organisms in or on the bed of deposition (both animals and plants). Inorganic sedimentary structures are, on the other hand, a result of "*...interactions between gravity, the physical characteristics of the sediment and fluid as well as the hydraulic environment*" (Brush, 1965).

2.2.2.1 Bedforms and relation to flow strength

A grain is entrained from a cohesionless granular surface once the threshold of motion is exceeded and transported down-current a distance related to the strength of the current and to the characteristics of the grain. The bed surface will remain plane under some flow conditions while during other it will shape into wave like features, dominantly transversely oriented with respect to flow direction. The size, shape and evolution of these bedforms, in addition to their internal structure, have been found to depend on the physical properties of the sedimentary grains and the transporting fluid, and the depositional process (e.g. Brush, 1965; McKee, 1965; Allan, 1968; Southard and Boguchwal, 1973; Reineck and Singh, 1980; Allan, 1982a,b).

The initiation of these wavy bedforms is dependent on the smoothness of the bed surface and characteristics of the flow. The granular bed is almost never perfectly plane, but has either some pre-existing irregularities or irregularities induced by the turbulent current (Middleton and Southard, 1977; Best, 1992). Southard and Dingler (1971) observed, in a unidirectional flow experiment, that no sand transport occurred until a mound was placed on the plane sand bed. Over these irregularities, a flow separation occurs and heightening of the turbulence on the lee side of the irregularity is created (Allen, 1982b, p. 102). The distributed flow scours into the plane bed and produce a new bedform downstream. Once the defect becomes higher than the viscous sub-layer, a more pronounced separation starts and scour or erosion will be enhanced where the flow reattaches the surface (Etheridge and Kemp, 1978). Downstream of the reattachment point turbulence decreases (Allan, 1982b, p. 121-127) and grains entrained will be deposited or re-distributed over the next bedform.

The further evolution of the bedforms, as a result of changing the hydrodynamic conditions and sediment characteristics, have for over four decades been studied in laboratory flume tanks and natural environments. An important question has been on which types of flow variables that characterize the bed configuration best. It is well established that it depends on the flow strength, but how to accurately describe flow strength has been the subject of some debate. Simons et al. (1965) presented a

diagram relating the bedform type to the stream power (the product of bed shear stress and mean velocity) and the grain size, while a plot based on flow velocity and grain size (figure 2.5) was given by Harms (1969) and Southard and Boguchwal (1973). The non-uniqueness of the bedshear stress and flow velocity and the depth dependency are among the difficulties encountered in these studies. Southard and Boguchwal (1990) and Allen (1982a, p. 336-343) reviewed and discussed comprehensively the different diagrams proposed.

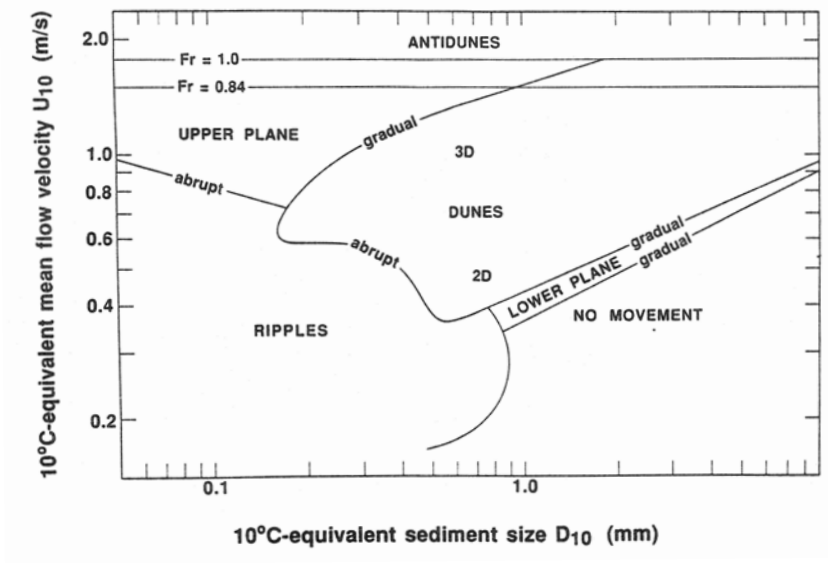

FIGURE 2.5 *The stability fields of bedforms in steady, unidirectional water flows for a specific grain size and water temperature (From Southard and Boguchwal, 1990).*

Based on the bedform configuration, mode of sediment transport, processes of energy dissipation and phase relation between the bed and water surface, Simons et al. (1965) classify two types of flow regimes: lower flow regime and upper flow regime. In the lower flow regime resistance to flow is large, sediment transport is low and the water surface is out of phase with the bedform. From a plane bed without movement, after a certain flow strength, small triangular shaped bedforms, called ripples develop when the grain size is below ~0.6 mm. By increasing the flow strength, these small bedforms develop into approximately equally shaped, but larger in size bedforms called dunes. In slightly coarser grained material, ripples do not form before dune development. At higher flow strengths (upper flow regime), ripples and dunes develop into plane bed and then anti dunes. The water surface is

in this case in-phase with the bedforms, the resistance to flow is small and the grains move continuously downstream in sheets.

The lower flow regime bedforms described above can vary in size, and there has been some inconsistency in the names used and the boundaries between the different groups. Based on hydraulic considerations, Simons et al. (1965) divided the bedforms into ripples and dunes. Also Allen (1968) noted a hydraulic difference between the two bedform types. Both large-scale ripples (Allan, 1968), megaripples (Klein, 1963; Reineck and Singh, 1980) and sandwaves (Middleton and Southard, 1977) have been used in addition to the more commonly encountered term dune (e.g. Harms and Fahnestock, 1965; Rubin and Hunter, 1982; Allan, 1982a, See also Middleton, 1965a for an early review) for the largest bedform population. Based on this inconsistency Ashley (1990) defined a dune to be all transverse bedforms from the lower flow regime with wavelengths larger than 0.6 m and heights higher than 7.5 cm. Hence, ripples are transverse, lower regime bedforms with a size below these values.

2.2.2.2 Geometrical description of lower regime bedforms

The transverse bedform created is normally described in a cross-section parallel to the flow (figure 2.6) and in plan view (figure 2.7). Although different in size, ripple and dunes are similar in shape in both plan view and profile (e.g. Allen, 1970b, p. 71; Rubin, 1987). Allen (1968) gives a thorough description of these bedforms, focusing primarily on the small-scale ripples. In cross-section, the lower regime bedforms can be divided into a crest and a trough. The bedform wavelength is the horizontal distance, at right angle to the crest, between the troughs or the crests of two adjoining bedforms. The bedform height is the vertical distance between the trough-point and the summit point, where the summit- and trough-point is the highest and lowest point on a bedform, respectively. Based on these point definitions, the stoss side is the gentle up-current slop of the bedform, extending from the trough-point to the summit-point, while the lee-side is the steeply dipping surface down-current of this point. The trough can then be defined as that part of the bedform, which in elevation is less than half the bedform height while the crest is the remaining upper part. The form of the bedform can be further described with the ripple- or vertical form index which is the ratio between the wavelength and the height of the bedform, and the symmetry index which is the ratio between the horizontal projection of the stoss side and the horizontal projection of the lee side (e.g. McKee, 1965; Reineck and Singh; 1980). Based on the pattern of the crestline, which is the line connecting the summit-points, Allen (1968) defined five different classes of bedforms: straight, sinuous, catenary, linguoid and lunate. When these

bedform appears in trains additional variation is possible and ten classes can be recognized (figure 2.7)

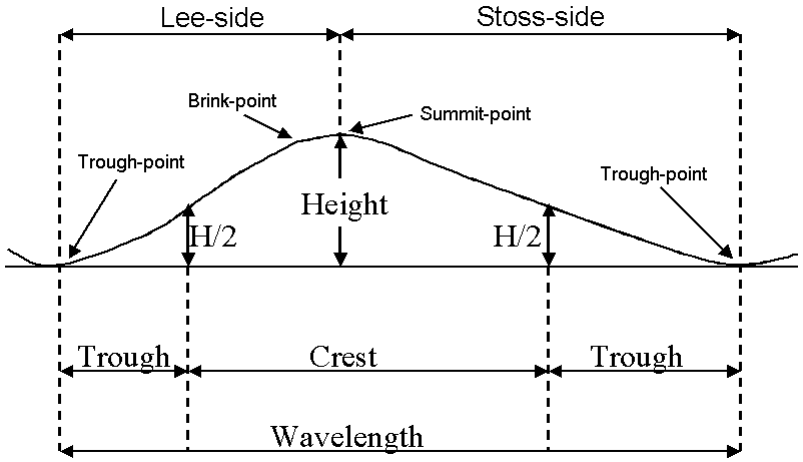

FIGURE 2.6 *Cross-section terminology of bedforms. Modified after Allen (1968).*

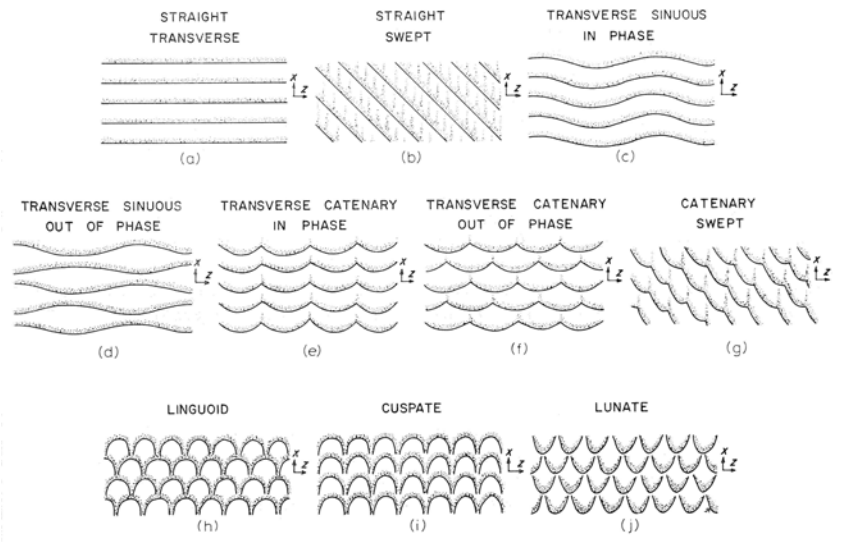

FIGURE 2.7 *Schematic form of ripple trains in planview. After Allen (1968)*

Several authors argue that the planform morphology, described by the crest line of the bedforms, becomes more complex and curved with increasing flow velocity (e.g. Simons et al. 1965; Allen, 1968, 1977; Harms, 1969; Ashley, 1990) and Allen (1969) relate the increased complexity of the bedforms to the streamwise corkscrew of vortices in the current. Although all the factors that control the shape are not well understood, the evolution of the bedform with increasing flow velocity is in general observed to be from straight crested to sinuous crested to linguoid and finally lunate. Middleton and Southard (1977), however, dispute these findings and conclude that no unique trend can be found, in particular for the small-scale bedforms. Furthermore, Allen (1968) reported that bedforms with in-phase crestlines formed in weaker flows than bedforms with out-of-phase crestlines. Baas (1994) suggest, based on flume tank experiments, that all bedforms will evolve into equilibrium shape, which is a linguoid shape, regardless of the flow strength, but dependent on the time. Given long enough time, all flow velocities will shape the bedform into this equilibrium state. However, the stronger the current, less time is need for development of an equilibrium shape. This independency of increasing shear stress was also suggested by Briggs and Middleton (1965).

2.2.2.3 Migration of bedforms and cross-stratification

The bedforms in the lower flow regime described above develop in time and space as a result of *bedform migration*. The process of grain movement and migration is different in the lower and upper flow regime (Simons et al., 1965), and in the following, the former process will be outlined. The migration of bedforms starts with that the entrained grains from the stoss-side moves upwards as bedload traction and accumulates near the top of the bedform. At the back of the bedform, a thin (a few grain-diameters thick) layer of bedload and suspension, often called a heavy fluid layer (Simons et al., 1965, Jopling, 1965b) develop, although this layer is more clearly definable in the upper flow regime. At the ripple crest, the boundary layer separates from the bed (Allen, 1965). Figure 2.8 shows the separation of flow with the associated distribution of grains over a wavy bedform. The heavier grains settle on the bedform crest or on the upper part of the leeside, while the lighter grains are projected out from the separation point.

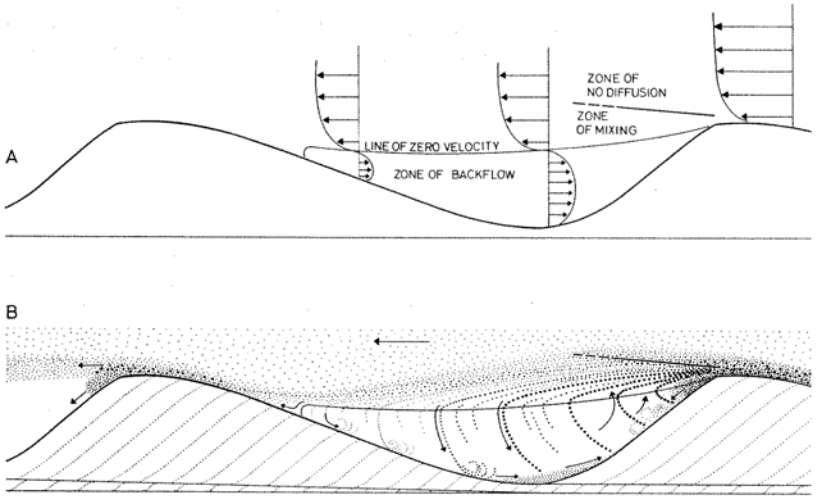

FIGURE 2.8 *A: Flow pattern and velocity distribution over a lee side of a wavy bedform (ripple). Three flow zones are illustrated. B: Flow pattern and sedimentation process over the same bedform as in A. Heavier grains avalanche directly down the lee-side. Some sediments are moved upcurrent in the backflow zone and deposited at the toe of the bedform. After Reineck and Singh, 1980.*

The factors influencing the shape of the lee-side has been investigated by several authors both in flume tank studies (McKee, 1957, 1965; Allen, 1965; Jolping, 1965a,b; 1966; 1967; Simons et al., 1965; Harms, 1969) and in the natural environment (Brush, 1965; Harms and Fahnestock, 1965; Imbrie and Buchanan, 1965; Doucette, 2002). In general, increasing velocity, increasing amount of sediment in suspension and increasing depth-ratio, favours more tangential lee-sides. At low velocities, the grains pile up at the crest and avalanche down the lee-side at the angle of repose (~30°). On the other hand, with a higher velocity or a higher concentration of sediment in suspension, more grains are carried off the crest and settle in the trough. In addition, Imbrie and Buchannan (1965), assumed that at higher velocities, a velocity component from the fluid acts along the lee-side and decreases the angle of repose by several degrees. The avalanching process down the lee-side results in a sorting of the sediment (Brush, 1965). However, for that process to be effective, it requires that the length of the lee-side to be relatively long (Reineck and Singh, 1980). Regarding packing of the individual lamina, Imbire and Buchanan (1965), noted that the steep avalanched deposits were looser packed than the more tangential accretion lamina. Consequently, the depositional process controls the lamina fabric and grain sorting of the foreset lamina and, as outlined in section 2.2.1, this also has an effect on porosity and permeability.

The migration of bedforms through formation of lamina on the lee-face has been suggested to be a result of several processes: variability in the composition of the sediment mix discharged over the forset slope, selective transport due to differential settling velocity and stream flow velocity pulsations (Jopling, 1966). The avalanche process is often intermittent, especially at small transport rates, (Jopling, 1966; Allen, 1965, 1970b), and the selective transport process of avalanching bedload and fall out of finer grained material (i.e. silt and clay) from suspension can result in a distinct layering of the foresets. In addition, changes in the sediment composition and periodic short-term fluctuations in the stream, relates to bedform migration (Jopling, 1966). However, the latter process was thought to be of minor importance.

The migration process described above for the lower regime bedforms produces an internal pattern of inclined, lithologically homogeneous or gradational layers. In the literature there exists many classifications schemes and names for the different parts of the sedimentation units and the most commonly used are those by McKee and Weir (1953), Campbell (1967) and Reineck and Singh (1980). This thesis will primarily use the terminology of Campbell (1967) who focus on the depositional process and not the scale of the sedimentation unit (as McKee and Weir, 1953). In Campbell's (1967) terminology (and in accordance with McKee and Weir (1953) and Reineck and Singh (1980)), a lamina is the smallest unit in a sedimentary sequence and it is relatively uniform in composition and texture and not internally

layered. A lamina is formed under essential constant depositional conditions during a relatively short time period. It is not distinguished between lamina deposited by traction or suspension. When the lamina has an angle relative to the depositional surface, the term cross-lamination is used. Planar lamination can thus be found in both suspension deposited mud and traction deposited sand in the upper flow regime. Although equal terminology, it will be clear from the text which of the two kinds that are meant. Furthermore, a laminaset consists of a group or set of conformable laminae that compose a distinctive structure within a bed (Campbell, 1967). This is in the opposite sense to Reineck and Singh (1980) that term this a bed. Similar laminaset bounded below and above by a bedding surface (sensu McKee and Weir, 1953), are termed by Campbell (1967) a bed. A bed constitutes thus a complex of laminasets. Allen (1963) termed this a coset of strata. In tidal deposits (see chapter 3), the terminology proposed by Reineck and Wuderlich (1968) is well accepted and much used. They give, however, no names for the different elements. Following the terminology by Campbell (1967), the sand layers bounded above and below by a contrasting lithology (mud), should be named laminasets, while a bed should be a unit bounded above and below by a bedding surface. Figure 2.9 shows the terminology that will be used in this thesis.

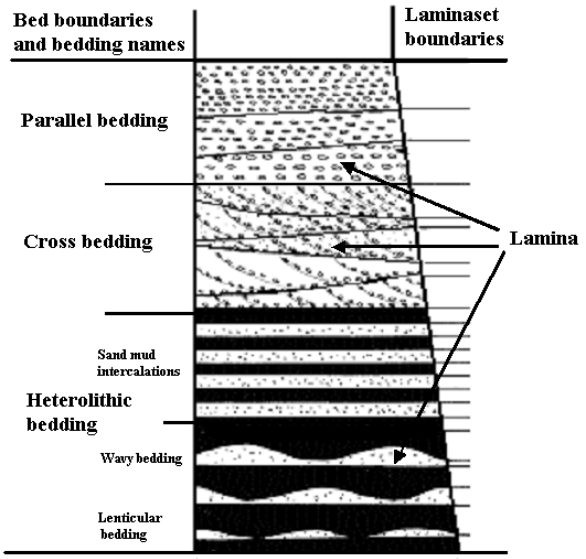

FIGURE 2.9 *Nomenclature for sedimentary units used in this thesis. Modified from Reineck and Singh (1980).*

In order for these cross-strata to be preserved in the rock record some conditions must be fulfilled. While determining the flow conditions from bedform morphology and behavior mainly is a problem of fluid dynamics, the reconstruction of bedforms from cross-stratified deposits is primarily a geometrical problem (Rubin, 1988). Allen (1968) presented a geometrical model for which a pattern of an idealized triangular ripple migrates through space under defined conditions of sediment flow. The shape and arrangement of the erosional and depositional elements were then evaluated (figure 2.10). In this figure, ξ' is the angle of the stoss-side, ξ'' is the angle of the leeside and ζ is the angle of the bedform migration with velocity U.

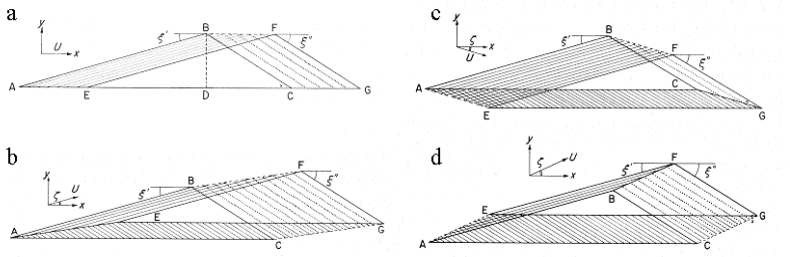

FIGURE 2.10 *Migration of a single triangular shaped bedform with varying bedform migration angle ζ with respect to the stoss side angle ξ', and baseline AC. a: the bedform advances parallel to the base. b: bedform advances at an angle less then the stoss side ($\zeta < \xi'$). c: bedform advances downward relative to the baseline. d: bedform advances at an angle greater than the stoss side ($\zeta > \xi'$). Modified after Allen (1968).*

Consider first the case in figure 2.10a where the bedform of constant height travel parallel to its base (AC). The quantity of sediment removed from the stoss side equals the quantity of sediment deposited on the lee-side and it is clear that;

$$\underset{\text{(eroded from stoss-side)}}{\text{area ABEF}} = \underset{\text{(deposited on leeside)}}{\text{area BCFG}} \quad . \qquad \textbf{[2-16]}$$

The mass rate of transport i_b of sediment involved in the bedform movement is (Allen, 1970a)

$$i_b = \frac{1}{2} H U_b \gamma_s \qquad \textbf{[2-17]}$$

where, H is the height of the bedform, U_b is the bedform migration speed (along AC) and γ_s is the sediment bulk density. In this case, beneath the bedform there occurs neither erosion or deposition on a scale larger than the bedform and the transport rate remains constant along the line of flow. In order for a cross-stratified deposit to be preserved the migration must stop and the bedform buried, usually by a contrasting sediment like mud. A preserved cross-stratified layer like this is called

a formset (Imbrie and Buchanan, 1965). In figure 2.10c the bedform migration path is inclined below the baseline and there occur an overall erosion. The net rate of erosion can be expressed as

$$\underset{\text{(net erosion)}}{\text{area ACEG}} = \underset{\text{(eroded from stoss-side)}}{\text{area ABEF}} - \underset{\text{(deposited on lee-side)}}{\text{area BCFG}} \quad \text{[2-18]}$$

and only a part of the cross-stratified set can be preserved if the migration stops and becomes abruptly buried. When the angle of bedform migration is above the baseline, there is a net deposition. In the case where the bedform angle of climb is below the angle of the stoss-side, only sediments on the lee-side is deposited (figure 2.10b). Preserved leeside deposit can be expressed as

$$\underset{\text{(net erosion)}}{\text{area ACEG}} = \underset{\text{(eroded from stoss-side)}}{\text{area ABEF}} - \underset{\text{(deposited on lee-side)}}{\text{area BCFG}} \quad \text{[2-19]}$$

If the angle of bedform migration is larger than the stoss-angle (figure 2.10d), the stoss-side sediment is also preserved and the minus sign in equation 2-19 is replaced with a plus sign. Allen (1968, 1970a) extended these results from one ripple to a ripple train and he expressed the conditions of sediment flow in terms of the general quantity $\partial i_b / \partial x$, where i_b is the sediment transport rate and x is the distance measured downstream in the direction of flow. As the bedform migrates, its trough moves through space and defines a bounding surface (McKee and Weir, 1953) with respect to the underlying strata. If no net deposition occurs, these bounding surfaces coincide and this is the situation in figure 2.11b (equation 2-16). In figure 2.11a, the bedform migration path declines with respect to the baseline and only incomplete formsets can be preserved. Figure 2.11 c-e have overall net deposition, but different boundaries between the cross-stratified sets. When $\zeta < \xi'$ there is an erosional contact and a subcritical (or stoss erosional; Hunter, 1977) set is formed. In the case where $\zeta = \xi'$ the boundary is non-erosional and the set is termed critical and when $\zeta > \xi'$ a gradual contact is present and the deposit is called supercritical or stoss depositional climb. Alternative models for development of cross-stratified deposits are reviewed in Rubin and Hunter (1982). The thickness of the cross-stratified set can, under constant conditions, be calculated from (Rubin and Hunter, 1982):

$$T \cong -\left(\frac{HL}{2i_b} \cdot \frac{di_b}{dx}\right) \quad \textbf{[2-20]}$$

where L is the bedform wavelength.

This geometrical model, valid for two-dimensional (straight crested) bedform, was extended to three-dimensional bedforms. In that case, the boundary surfaces became trough-shaped in the direction normal to flow.

In addition to Allen's theoretical model, several authors have evaluated the development of cross-stratification, the shape and the characteristics of the stoss- and lee-side laminae in flume tank studies (e.g. McKee, 1957, 1965; Allen, 1965; Jopling, 1965 a,b, 1966, 1967; Harms, 1969; Arnott and Southard, 1990; Storms et al., 1999) and in natural conditions (e.g. Harms and Fahnestock, 1965; Imbrie and Buchanan, 1965; Douchette, 2002). One important aspect has been to relate bedform morphology to the cross-stratified deposit, and thereby having a means to interpret the paleoflow conditions (for a review see Allen, 1968, p. 96-100; Allen, 1982a, p. 346-349). Various parameters have been considered like the shape of the cross-strata, the bounding surface, scale and lithological variability. However, regardless of scale, both McKee and Weir (1953) and Allen (1968, 1982a) emphasis that the three-dimensionality of the bedform is reflected in a three-dimensionality in the cross-stratified deposit. Rubin (1988) also point out that three-dimensionality of cross-stratification not only is dependent on three-dimensionality of the bedform, but also influenced by bedform variability, behaviour and angle of climb. Based on this, Rubin (1988) presented a classification with four groups of bedforms forming distinct stratification structures: two and three dimensional bedforms that could be either variable or invariable with time. The degree of variability causes dispersion in inclination of bounding surfaces, in contrast to the dispersion in dip-direction of the cross-strata caused by three-dimensionality of the bedform. Variability in bedforms can arise from both changes in flow conditions and from bedform interactions like superpositioning of one set of bedforms on another. Along with this new classification, Rubin (1988) presented a computer program that simulates the migration of various synthetic bedforms with displacement of sine curves. The modelling tool used in this thesis is based on this classifications scheme, and in part the equations used (see chapter 4).

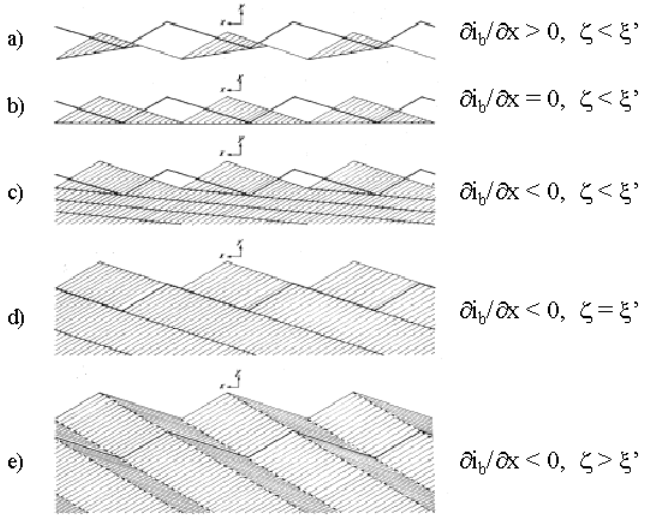

FIGURE 2.11 *Equilibrium of a train of ripples of constant height and wavelength for different conditions of* ζ *relative to* ξ' *and* $\partial i_b/\partial x$. *After Allen (1968).*

The term facies can be defined as a body of rock that formed under certain conditions of sedimentation, reflecting a particular process, set of conditions or environment (Reading, 1996, p.19). Anderton (1985) distinguished between descriptive facies, based on features such as grain size, geometry and structure, and interpretative facies, which use the interpreted depositional process or environment of a certain rock volume. The term lithofacies is used if lithological attributes are emphasized (Anderton, 1985; Reading, 1996). A facies can further be divided into subfacies or grouped into facies associations, forming a useful hierarchy of scale for describing rocks. In this thesis, units of rocks will be identified from core (chapter 5) that are assumed to have different influence on petrophysical properties and more specific on the ratio between vertical and horizontal permeability. This will often coincide with a division into units based on lithological characteristics (e.g. ratio between sand and mud). In addition, focus will also be on the interpreted depositional process since a process oriented modelling tool will be used.

2.2.2.4 Petrophysical variability in stratified deposits

It should be clear from above that porosity and permeability is controled by the texture and fabric of the sediment. Permeability is most influenced by grain size and sorting while porosity mainly by the latter. The degree of anisotropy in permeability is influenced by the packing and orientation of the grains but is mostly evident at the scale of the laminaset or at the bed scale. Numerous studies have verified that sedimentary structures have an effect on petrophysical properties and in particular on permeability (e.g. Weber, 1982; Stalkup, 1986; Gibbons et al., 1993; Brayshaw et al., 1996). As a consequence, it is of fundamental importance to understand the depositional process in order to best model the spatial variability of porosity and permeability.

The minipermeameter (see section 2.3.1) is able to measure permeability at the mm-scale, i.e. at the lamina scale (Halvorsen and Hurst, 1990). Dreyer et al. (1990), Robertson and McPhee (1990), Harkamp-Bakker et al, (1993, a, b) and Tidwell and Wilson (2000) have used this device and were able to correlate the permeability variations to the sedimentary structures. In particular, it is observed that there are variations in the foreset lamina where the basal part on average has lower permeabilities than the upper and middle part and this is related to the sorting process previously described. If sample spacing is close enough, it has been shown that there is a close relation between the permeability distribution and the sedimentary structure (Corbett and Jensen, 1993). Laminascale anisotropy is, however, more difficult to measure directly although overall trends can be inferred (Brensdal and Halvorsen, 1993). Even in reservoirs where larger scale connectivity is the dominant factor, petrophysical variability in the sedimentary structures affect factors as water breakthrough time (Hurst, 1993; Jones et al., 1995). Ultimately this will affect the recovery efficiency of such reservoirs (Weber, 1986; Lasseter et al., 1986).

2.3 Estimation of petrophysical properties in the near-wellbore volume

In the two sections above, porosity and permeability have been connected to several geometrical factors of the porous medium (2.1) and have further been related to grain characteristics and depositional processes (2.2). In this section, the main types of data sampled from the well are described, with emphasis on their sample volume and how porosity and permeability are estimated from them. In the end of this section, a review of some published methods of calculating the effective permeability of a porous medium will be given. Combined, this will give a reference frame and a means of comparison with the results in chapter 6 to 9.

2.3.1 Core Data

From selected sections of the reservoir cores are retrieved while drilling. These cores vary in diameter from 10-20 cm. The cores are further analysed in a laboratory and the results represent a direct measure of the reservoir rock. This section will give a brief overview of the most common measurements made on core material. There is no intention here to give an elaborate overview. For such an overview see among others Monicard (1980), Blackbourn (1990) or Torsæter and Abrahi (2000).

From the retrieved core, standard industry practice is to take small, cylindrical samples (core plugs), 1-1.5 inch (1 inch = 2.54 cm) in diameter and length, about every 30 cm of the interval. Core plugs are taken both parallel and perpendicular to the bedding plane. The vertical core plugs are often less densely sampled then the horizontal core plugs. After cleaning of the core plugs and removal of fluids, porosity is determined from the grain volume and the bulk volume of the sample. Depending on the technique used, different types of porosity are estimated. With a gas expansion method, the connected porosity is measured, while with destruction of the sample to estimate grain volume, a measure of total porosity is obtained. To determine the permeability of the core plugs, a Hassler cell device is often used. Here, the core plugs are placed in a compliant sleeve within a steel cylinder. A pressure on the sleeve ensures that the injected gas or liquid flows parallel the core plug axis. Fluid ,usually gas, is injected with an inflow pressure and flows quasi-linearly through the plug to atmospheric pressure. The permeability is then determined from Darcy's Law. Due to difference in flow physics between gas and liquid, especially in low permeable media, a correction is done on the gas or air permeability (Klinkeberg correction).

Ejipe and Weber (1971) were among the first to measure permeability distributions in consolidated and unconsolidated samples using a probepermeameter (or minipermeameter). This equipment consists of a probe that is pushed to the investigation surface and letting a gas flow into the sample. The flow rate can then be converted to air permeability through a modified version of the Darcy law (Goggin et al., 1988). Further details on this measurement device can be found in Halvoresen and Hurst (1990). This measurement device has successfully been used to describe the permeability variation in cores and outcrops representing a range of depositional environments (e.g. Dreyer et al. 1990; Hurst, 1991; Corbett and Jensen, 1993; Halvorsen, 1993; Hartkamp et al., 1993a, b). The volume of investigation depends on the probe-tip area, conditions of the surface and the operating conditions, but are generally found to be of two order of times the internal probe diameter ($2\text{-}8*10^{-7}$

m^3) (Corbett, 1993). In this respect, the probe permeameter is able to measure the permeability of the individual lamina.

In summary, the core data represent a direct measure of the petrophysical properties of the reservoir. However, the laboratory conditions are different from the subsurface conditions and the correction factors used are often based on empirical relations. Furthermore, the retrieved core plugs represent only a fraction of the near wellbore volume. To illustrate this, consider a core with a diameter of 15 cm and that the core plug dimension is 1 in. in diameter and 1.5 in. in length. The total number of possible core plugs, per feet, in the cored interval is then 277. Hence, a randomly drawn core plug from this population of 277 samples is assumed to represent the petrophysical properties of the cored interval. The discussion of how representative this core plug is for the one feet interval will be a matter of this thesis.

2.3.2 Wireline log data

Geophysical wireline logs (or well-logs) can be described as “a recording against depth of any of the characteristics of the rock formations traversed by a measuring apparatus in the well-bore” (Serra, 1984a). The measuring apparatus, called a wireline tool is lowered to the base of the drilled well on a cable and pulled up at a constant speed while recording the characteristics of the formation which that tool is designed to respond to. It is common to divide wireline tool measurements to those arising from natural (or spontaneous) phenomena and those arising from induced phenomena. The first group of wireline tools only consists of a detector while the latter consists of an emitter that induces a response from the formation and a detector. A range of different wireline tools are available and specific details about the physics of the conventional logging tools can be found in Serra (1984a), Tittman (1986) and Ellis (1987) while petrophysical and geological interpretation of the measurements can be found in Serra (1984b) and Rider (1996).

Associated with a measurement is the terms (vertical) resolution, volume of investigation and quality (Lovell et al., 1998). The quality is defined by the precision, accuracy and bias of the measurements. Precision refers to the closeness of the results if the same experiment is performed several times under the same conditions, while accuracy refers to the closeness of the result to the true value. Precision can be quantified by running the same wireline log several times in same section. Accuracy is more difficult to assess since the true value is not known (as discussed below). The vertical resolution of a wireline measurement device can theoretically be defined as (Theys, 1999): *The full width at half the maximum of the response of the measurement to an infinitesimally short event.* This means that if the logging

tool is to measure a parameter and yield a true value for even a limited portion of the bed, then the bed thickness must be at least as large as the vertical resolution. Consequently, the vertical resolution will be a function of the tool design (e.g. the distance between the emitter and detector) in addition to bore hole and formation characteristics and logging speed. A feature thinner than the emitter-receiver distance may still be identified, but the value indicated on the log will, however, only be a percentage of the true reading. In reality, where lithologies vary rapidly and individual layers are thin with respect to the tools vertical resolution, it is only an average value that appears on the log. At the boundary between two relatively thick contrasting beds (contrasting with respect to the parameter measured), the "averaging" effect is also evident as the tool responds to both beds and resulting in a "shoulder effect". The volume of investigation is determined by the vertical resolution, the depth of investigation and the geometrical shape of the response volume. The depth of investigation is again a function of the tool characteristics, the conditions of the borehole and the formation. Common practice is to define the depth of investigation to that distance into the formation where some specified fraction of the response originates from (e.g. 90% of the signal). Also, the geometry of this volume is different for different tools, some measuring a spherical volume around the wellbore while others are focused to one of the wellbore sides and measures and hemi-ellipsoid. The geometrical factor is also an idealized concept, and the shape of the investigated volume may change due to the configuration of the physical contrasting beds (Rider, 1996)

Examples of conventional wireline tools are: 1) The single detector *gamma ray tool* that measure the natural radioactivity of the formation. The response of the tool is a function of the concentration by weight of the radioactive mineral in the rock and the density of the rock. 2) The *density tool* senses formation density by measuring the attenuation of gamma-rays between source and detector. The gamma rays emitted from the source, travel into the formation where they collide with electrons that cause them to loose energy and scatter in all directions in a process called Compton scattering. This process is only dependent on the electron density of the formation, which is closely related to bulk density with minor corrections in the presence of water (hydrogen) (Rider, 1996). 3) The *neutron tool* emits energy into the formation and measures the formation response in a detector system. In this case, high energy neutrons are emitted into the formation, the neutrons collide with the atoms present and loose energy. The most efficient atoms to slow the neutrons (through elastic scattering) is hydrogen since they are of approximately equal mass.

In addition, a range of other tools have been developed that measure other physical characteristics of the traversed formation; the electrical resistivity or conductivity, the spontaneous potential between an electrode in the bore hole and a reference

electrode on the surface, the ability to transform acoustic waves, detection of different elements and investigation of the free precession of proton nuclear magnetic moments in a magnetic field, just to mention a few. These conventional wireline tools are further described in Dewan (1983), Jordan and Campell (1984), Serra (1984a), Ellis (1987) and Rider (1996).

The vertical resolution and the depth of investigation is closely related since usually a higher vertical resolution gives a shallower depth of investigation. The corresponding volume the measurement averages over will then be affected. Also knowing that the volume of investigation depends on the conditions in the borehole and the surrounding formation makes it difficult to establish exact how much formation each tool measures at each point in the well. Figure 2.12 in section 2.3.3, gives however a general idea of the volume characteristics for some selected tools.

From this brief description it is clear that the wireline tools measure a physiochemical signature of the rock that has to be converted to the petrophysical parameter of interest such as porosity and permeability. This is in general not a trivial task as will be discussed further below. This thesis has no intention to evaluate the physical basis of the different tools or the corrections that are made to the measurements due to e.g. hole conditions. The wireline data and the interpreted curves used here are taken from the Statoil database. However, it is important to bear in mind the assumptions associated with the processing and interpretation of these wireline log data.

A final group of well data to mention is the measurements of formation pressure vs. time at specific depths. The Repeat Formation Tester (RFT) is a wireline tool that is positioned in the wellbore and allowing fluid to flow into its chambers. Through drawdown and build-up of the pressure, the permeability can be estimated from the pressure derivative and other specialized plots (see Bourdet et al., 1989; Ahmed et al., 1991). This group of well data is then characterized as dynamic (measure flow directly) as opposed to the static data of core and conventional wireline data. In the same manner, but measuring a larger volume, well tests provide permeability estimates from larger sections of the near wellbore volume. Although permeability from such pressure build-up analysis is representative of the in-situ conditions, they are still subject to uncertainties. In particular, some assumptions have to be made about the thickness of the production interval and about the nature of the flow. None of these dynamic data types were available in this study.

2.3.3 Scales of heterogeneity and well data support

The term scale has hitherto been used without further explanation. Some geological parameters are associated with a specific point, while others, as porosity and permeability, are spatial averages and indeed have a volume associated with each measurement. There is however a conceptual difference between the volume of a sample and the scale of characteristic length scales in the porous media (Koltermann & Gorelick, 1996). Support is a common term in geostatistics and refers to the volume of a sample. The volume is completely specified when it includes its geometrical shape, size and spatial orientation. A change in any of these characteristics of a support defines a new regionalized variable (Olea, 1994). Support may then be related to the measurement method while scale is related to the size of features that often influence on the spatial distribution of petrophysical properties. Heterogeneity of some property is then a result of spatial variability of that property. The terms scale and support have often been used indistinguishable in the literature, but this thesis will distinguish between these two terms.

In addition to the above mentioned use of scale, the labeling of different length scales vary considerable, often with terms like micro-, meso- or mega- as prefix. Regardless of the prefix, the major divisions of the scales are rather similar for different authors that have focused on the size of geological structures (e.g. Weber, 1986). As discussed above (section 2.2.2.4) the petrophysical distribution shows a close relation to the sedimentological structure, which again is related to the depositional process. A useful classification of scale should therefore include geological features that affect heterogeneity. Following Koltermann and Gorelick (1996), the smallest relevant scale is on the multiple pores where it is possible to defined porosity and permeability and the latter may show anisotropy due to texture and lamina contrast. The next scale, called depositional flow regime features, is the structural organization of the laminae into different (cross-)stratified deposits and anisotropy can be evident in the bounding surfaces (Pickup et al., 1999; Schatzinger and Tomutsa, 1999). The division of the depositional flow regime features into beds is the next scale defined by Koltermann and Gorelick (1996). Channels, depositional environments and sedimentary basins are recognized as larger scale elements without those being described further here. It will be clear later that the scales that are relevant in this thesis are the three smallest mentioned above, and with most focus on the scale from the lamina to bedding scale since the heterogeneity at the bedding scale is affecting flow properties in tidal deposits significantly.

Figure 2.12 shows the how the different geological length scales relate to the vertical resolution and sample support of the well data described above. The upper and lower values of the wireline tools are based upon published limits (e.g. Serra,

1984a), but there are significant uncertainties associated with them and especially regarding the volume of investigation. The values will also change with borehole conditions, logging speed and service company specific tool designs. However, the important aspect of this figure is that it indicates how the different well data relates to the different geological structural elements. Another important aspect is that there is a poor overlap between the sample volumes of the core data (core plugs and probe data) and the conventional wireline logging tools. This gap ("the missing scale") causes some of the difficulties in estimating the petrophysical properties from different well data.

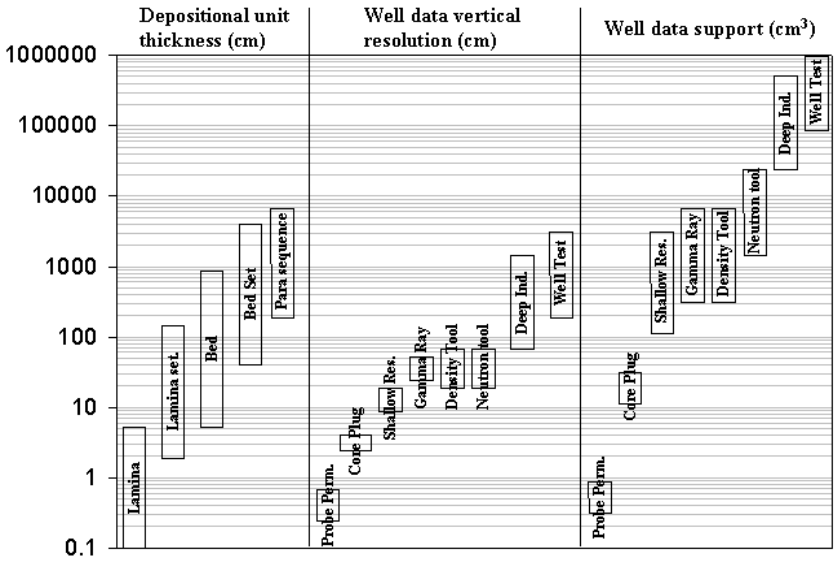

FIGURE 2.12 *Geological length scale in relation to well data support and vertical resolution. Left data set from Van Wagoner 1990. Middle and right data Serra (1984a), Ellis (1987) and Rider (1986).*

The most abundant core data available are the core plugs. Although this data set has a low sample volume it often "crosses" the scale between individual lamina and laminaset. Figure 2.13 shows what types of bias this data set may give in a deposit where the length scale of heterogeneity is below the size of the core plug. Even though standard industry practice is to sample core plugs with approximately 30 cm intervals, laboratory technical issues often prevents to sample some lithologies like

mud layers since the core plugs then often will break or split (figure 2.13a). There may also be some operator bias to preferentially sample high permeability zones or part of the core is damaged preventing particular zones to be sampled. Regardless of the reason, this will give a bias sample of the true population. This is an issue that will be extensively discussed in chapter 6. In deposits where the vertical scale of heterogeneity is shorter than the core plugs, permeability anisotropy may be difficult to estimate properly (figure 2.13b). The vertical and horizontal core plugs, although taken from the same depth, will sample different portions of the rock giving a biased estimate of the ratio between vertical and horizontal permeability (k_v/k_h ratio). Especially in tidal deposits, the horizontal correlation length of contrasting features may give an unrepresentative value of vertical permeability. Figure 2.13c, shows how mud layers (filled with horizontal lines), pinch out over relatively short distances. Vertical permeability measured from a core plug through this unit will then be dependent on where, in relation to the mud layer, it is taken.

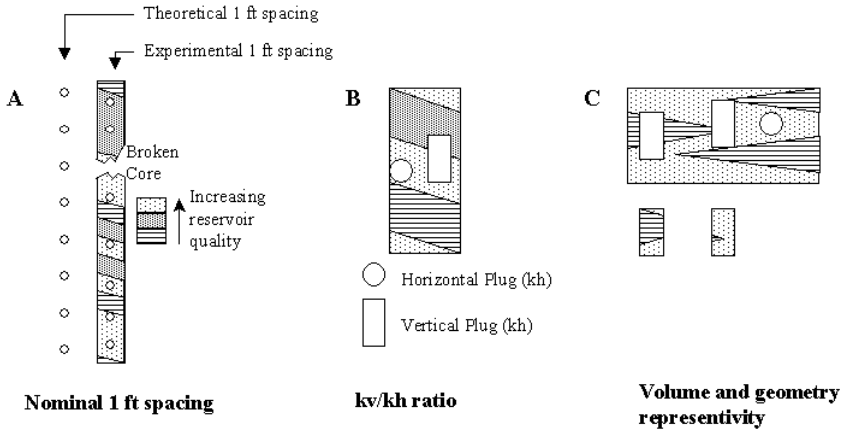

FIGURE 2.13 *Examples of biased core sampling. Modified after Corbett (1993).*

From the above discussion, we see that well data measurements have different volume supports. Given that the geological heterogeneity affects the petrophysical property, it is then clear that we should use well data that corresponds to the scale we are interested to characterize. Bear (1972, p. 124) have formulated this by stating: "*Alternating layers of different textures give rise to anisotropy. However, in order for a stratified formation of this kind to be qualified as an anisotropic homogeneous medium, the thickness of the individual layers should be much smaller than the length of interest. There is no use in attempting to determine the permeability of such a formation from a core whose size is smaller than the thickness of a*

single stratum". Although this may sound simple, several practical (and theoretical) issues make this difficult. Often core or wireline data measure at an intermediate scale with respect to geological heterogeneity, and the resulting value is an average of some kind of the constituting elements in the response volume. The geological control on petrophysical properties on many scales has been appreciated for several years, and one common question is why the averaged core data do not match the well test data (e.g. Dubrule and Halvorsen, 1986). In the next section, a few of the published methods to estimate porosity and permeability from core and wireline data will be reviewed. This will form a mean for comparison with the results in chapter 9. Following that, a review of methods for calculating effective permeability will be given, which then will be used to compare with the results in chapter 7 and 8.

2.3.4 Estimation of porosity and permeability from well data

Core data represent a direct measure of the reservoir properties at discrete locations under laboratory conditions. Wireline logs, on the other hand, represent a continuous, physiochemical signature of the rock at in situ conditions, which then have to be related to the petrophysical properties of interest. As a consequence, some assumptions have to be made either to correct the core data to in situ conditions, or to relate the tool response to porosity or permeability. However, as long as the measurement device is free of (systematic) error both data sets represent a measure of the true value of the device specific parameter. Whether this is a good estimate of for example porosity or permeability is another issue. In addition, the wireline tools generally measure a larger volume of rock compared to the core data. This means that both the physics of the measurement and the volume of investigation are different. One of the goals in petrophysics is to make use of both these data sets to give a correct as possible estimate of the parameters.

There is a tremendous amount of papers published on different aspects of core-log integration. There is no intention to give a comprehensive review here, but reviews and collection of articles of elements of these aspects can be found Hurst et al. (1990, 1992), Doveton (1992), Harvey and Lovell (1998) and Lovell and Parkinson (2003). However, a short summary of the main methods used to estimate porosity and permeability from core and wireline data will be given sufficient to understand the assumptions, challenges and shortcomings of these methods in very heterolithic reservoirs.

Since the well data, in general, have different measurement volumes, they are usually transferred to a common volume for comparison. Following the definition of

Corbett et al. (1998), the term up-scaling is "*the determination of an effective (or pseudo) property at a scale larger than that of the original measurement*", while cross-scaling is "*the determination of a relationship between two different physical properties*". The same notation, cross-scaling and up-scaling, will be used throughout this thesis.

To start at the smallest volume (or rather area), porosity and transport properties have been estimated from thin-sections in a variety of ways. Morphological analysis of the size and shape of pores (Ehrlich et al., 1984; Ehrlich et al. 1991a) have been related to pore throat size (McCreesh et al. 1991) calibrated with laboratory measurements of permeability (Ehrlich et al. 1991b), used as input to Kozeny-Carman relations (Berryman and Blair 1986, 1987; Liang et al. 1999) and as input to the effective medium theories (Koplik and Vermette, 1984, Doyen, 1988). Porosity and specific surface area of the rock has also been described by spatial correlation functions (Blair et al., 1996; Ioannidis et al., 1996), again as input to semi-empirical relations (variants of the Kozeny-Carman equation). Most of the studies have considered only two dimensions, but Koplik and Vermette (1984) and Liang et al. (1999) used serial sectioning and a Fourier transform, respectively to construct a three dimensional model of the pore network. Although the permeability estimators developed are quite complex mathematically, they either assumes that the Kozeny-Carman relation satisfactorily describes permeability or use another simplified model of the pore network. Nevertheless, these types of studies provide useful insight into those aspects of the micro-geoemtry that dominate the rock properties. As mentioned in section 2.1.3, theoretical models developed to calculate permeability contain some factors both difficult to relate to specific aspects of the pore geometry and that need laboratory measurements to be determined. As also noted by Doyen (1988), the Kozeny-Carman breaks down in the presence of inhomogeneity in the pore geometry. Interesting to note is that in some of the works, predictive relationships between resistivity and permeability are obtained (Koplik and Vermette, 1984; Doyen, 1988; Schwartz et al. 1993). This is in the end a result of the homogeneity and isotropy of the samples, as also pointed out by Jackson et al. (1994), and the relation will break down in more complex situations. Most of the models derived from micro-geometry use either sandstones that are well-sorted and homogeneous or artificial made samples. Realistic reservoir rocks are in general more complex and typically shows inhomogeneity and anisotropy at the lamina scale.

A more common approach to use is to develop relations between the core plug measurements and the wireline log responses. A critical point in this procedure is the depth matching of the two data sets where the wireline data and core data are adjusted so that they represent the same depth in the wellbore. For comparison,

either the core data have to be upscaled to the wireline resolution, or the response from the wireline tool has to be enhanced. The latter can be done through deconvolution of the original signal, although this is both theoretically and practically difficult for several of the tools (i.e. the nonlinear response of the resistivity tool or the stochastic nature of the nuclear tools) (Doveton and Prensky, 1992). More common practice is to calculate a (weighted) running average of the core plug data to match the vertical resolution of the wireline tool that it should be integrated with. The lateral variability is with such a running mean not taken into account. Following the smoothing of the core data, a regression is performed between the core data and the wireline response. If unsmoothed core data had been used, a larger scatter in the data set would be observed (e.g. Worthington, 1997). In the case of porosity estimation, density, neutron or sonic travel time are much used. The choice of regression line is not trivial, and depends on the assumptions about the two data sets (Williams, 1983; Doveton, 1994). However, the result is a prediction equation of the general form:

$$\varphi = a + bX \qquad \textbf{[2-21]}$$

where a and b are constants from the regression analysis and X is the log response. Moss (1997) has discussed such statistical procedures extensively. It is worth mention here that although there is obtained a good fit with a regression line (high correlation coefficient), there is not necessarily a casual relationship between the variables in question. This makes such predictive equations site specific that have to be reevaluated in new zones or other reservoirs. Since errors are associated with both the core and the wireline measurements, equation 2-21 can be re-written as a functional relation (here with density) of physical mixture of the components present:

$$\varphi = \frac{\rho_{ma} - \rho_b}{\rho_{ma} - \rho_f} \qquad \textbf{[2-22]}$$

where ρ_{ma}, ρ_b and ρ_f is the matrix, bulk (measured) and fluid density respectively. The intercept ($a = \rho_{ma}/(\rho_{ma} - \rho_f)$) and slope ($b = 1/(\rho_{ma} - \rho_f)$) can then be constrained by other independent analysis of fluid and matrix densities. The wireline response can for simplicity be regarded as a volume average of the different components present.

The inevitably assumption in this approach is that the core plug porosity represents the (1 foot) interval that it is sampled from. We noticed above that the core plug is one of many possible outcomes in the available core volume. However, if the core

plug represents an unbiased sample of the reservoir rock, then the density tool response, since it close related to the bulk density and since porosity is an additive property (section 2.1.4), is a good estimator for the porosity of the rock.

Although the estimation of porosity is relatively straightforward, the estimation of permeability is in general more difficult. At present, none of the conventional wireline tools measure permeability directly. As a consequence, models have been developed that relate permeability to other properties of the medium (see also section 2.1.3). But, like the Kozeny-Carman relation, these equations contain parameters (e.g. specific surface area, tortuosity) that also are difficult to estimate from the wireline measurements. In addition, there are some simplifying assumptions (about the porous medium) inherent in these types of equations.

The most common method to estimate permeability from logs that has been used is from empirical equations relating porosity and permeability:

$$\log k = a\varphi + b \qquad \textbf{[2-23]}$$

where a and b are constants determined from core measurements and applied to the wireline log estimate of porosity. Again, an implicit assumption is that the core plugs are representative of the volume of rock investigated by the wireline tool. Cross-plotting porosity and permeability generally produces a wide scatter, where permeability may vary by several orders of magnitude for a single porosity value (e.g. Brayshaw, 1996). Over the years, several methods have been proposed to improve the permeability predictor by including more wireline logs in multiple linear regression techniques (Wendt et al., 1986), non-linear regression (Yan, 2002), improved averaging methods of core data (Wong, 1999), fuzzy rule-based systems (Finol and Jing, 2002) or application of neural net methods (Rogers et al., 1992).

Characterizing the whole reservoir with one ϕ-k relationship will in general result in a poor prediction of permeability. One approach that takes into account that different lithofacies show different petrophysical properties have therefore been proposed (Ebanks, 1987; Amaefule et al. 1993; Jian et al., 1994; Cunha et al. 2001). Each lithofacies is a result of a particular depositional process resulting in a specific grain size distribution, sorting, amount and type of clay material and later modifications through diagenesis. A flow unit is therefore a volume of rock that is subdivided according to geological and petrophysical properties that influence the flow characteristics of the unit and Jian et al. (1994) called this a genetic approach. Corbett et al. (2003) distinguish between a flow unit that is a large-scale reservoir unit and a hydraulic unit that is based on classification of core plugs. Amaefule et al. (1993) developed a quantitative method, based on the Kozeny-Carman equation, to

subdivide the reservoir into hydraulic units. They divided eq. 2-10, by the effective porosity (ϕ_e) and took the square root of both sides and obtained

$$\sqrt{\frac{k}{\varphi}} = \left[\frac{\varphi_e}{1-\varphi_e}\right]\left[\frac{1}{\sqrt{F_s}\cdot\tau\cdot S_s}\right] \quad \textbf{[2-24]}$$

where k is expressed in μm^2 and the shape factor F_s is the same as c_0. The first term on the right-hand side is the void ratio also denoted ε by Prasad (2003). Further Amaefule et al. (1993) defined a Reservoir Quality Index (RQI):

$$RQI = 0{,}0314\sqrt{\frac{k}{\varphi_e}} \quad \textbf{[2-25]}$$

where k is expressed in mD. A Flow Zone Index (FZI) is then defined as;

$$FZI = \frac{1}{\sqrt{F_s}\cdot\tau\cdot S_s} = \frac{RQI}{\varepsilon} = \frac{0{,}0314}{\varepsilon}\sqrt{\frac{k}{\varphi_e}} \quad \textbf{[2-26]}$$

The FZI can then be calculated from a set of measured laboratory data on porosity and permeability. By plotting the log RQI against log ε, all values with similar FZI will follow a straight line. Data from other hydraulic units will then fall on parallel lines. The terms in equation 2-26 can be understood as the relation between the volume of void space (ε) and its geometric distribution (RQI) (Prasad, 2003). The method has proven valuable in several case studies (Amaefule et al. 1993; Corbett et al. 2003; Prasad, 2003).

In un-cored intervals, various techniques are proposed to divide the reservoir interval into lithofacies from wireline logs and some recent examples are Coll et al. (1999), Ye and Rabiller (2000) and Gupta and Johnson (2001). Each unit is then assigned a single ϕ-k relationship based on core data (e.g. Hook et al. 1994; Jian et al. 1994; Yan, 2002). The validation of these studies is often presented with a high correlation coefficient between the core permeability and the predicted permeability from the wireline logs in the cored interval. This correlation is of less importance if the core plugs do not measure the same amount of heterogeneity as the wireline log.

A basic assumption in the Hydraulic unit approach, as also pointed out by Corbett et al. (2003), is that the hydraulic elements are larger than the conventional core plugs. This seems as a fair assumption in most clastic reservoirs. They also implicitly assume that the core plugs represent the true petrophysical distribution of a par-

ticular hydraulic unit in a satisfying way. However, in tidal deposits (see chapter 3 and 5), the defined lithofacies may contain heterogeneities affecting flow properties at a scale smaller than the core plugs. In that case the core plugs may not always be representative for the petrophysical property of the lithofacies. This has also been noted by Ringrose et al. (1999a) in fluvio-deltaic deposits. In addition, biased sampling of core plugs may influence the petrophysical distribution (see figure 2.13). As will be clear in chapter 6, the core plugs for the studied interval in this thesis show very low petrophysical contrast between the defined lithofacies and a large internal variability. The wireline logs in this formation also show a low contrast between lithofacies as also noted by Berg et al. (1999). The above-mentioned problems are especially relevant for permeability. Porosity on the other hand, can be predicted through careful integration of core and wireline data even in these heterolithic deposits (Fløl o et al., 2000).

Since there is not available any direct measurement of permeability at several volume supports in the subsurface, one have to use certain surrogates, and porosity have been used extensively as described above. Theoretical studies have related resistivity and permeability (Koplik and Vermette, 1984; Katz and Thompson, 1987; Doyen, 1988; Schwartz et al. 1993) and showed that the correlation is best if the media is homogeneous and analysed at the same support. The advent of high-resolution resistivity tools has therefore resulted in several studies that estimate permeability through cross-scaling with resistivity. Jackson et al. (1994) found a strong correlation between probe resistivity and permeability at the lamina scale in an aeolian sample. Ball et al. (1994) using a fluvial sandstone, obtained a good match between averaged probe data and a shallow, high-resolution resistivity tool. They then used arithmetic, harmonic and geometric averages for different zones to match the production data. Finally, Thomas et al. (1996, 1997) used an electrical image log to predict permeability anisotropy at the lamina scale, and found that the ratio between harmonic and arithmetic average compared well with the larger scale dynamic measurements. These studies show that a good predictive algorithm can be established if both physics and sample volume are taken into consideration.

Although the cross-scaling of porosity and permeability from core plugs is a valid procedure (since same sample support), the use of the resulting regression equation on a larger support is not necessarily correct if the assumption of homogeneity is not satisfied. Worthington (1997) has shown that the coefficients of the empirical equations relating porosity and permeability are scale dependent, but becomes nearly constant at larger scales. For example, porosity can be estimated both from resistivity measurements (Archie equation) and density. Worthington (1994) showed that using the resistivity approach was dependent on the upscaling procedure (physical law or empirical relation), while using the density data was indepen-

dent of the upscaling method. This may be related to the fact that density is as additive property while resistivity is a non-additive property.

Deterministic (2D and 3D) modelling of sedimentary structures (*geopseudo approach)* (Corbett et al., 1992a) has been done to explore the lamina to bed-scale influence on permeability (Pickup et al. 1995, 1999, 2000; Pickup and Carruthers, 1996). Although the main focus has been on multiphase flow, single phase results have also been reported. In addition, focus has been on cross-stratified structures in fluvio-deltaic deposits (Pickup and Carruthers, 1996; Pickup et al. 1995; Ringrose et al. 1999), aeolian deposits (Pickup et al. 1999) and one case from the tidal deltaic environment (Pickup et al. 2000). If the sedimentary structures induce cross-flow, single-phase permeability need to be represented by a full tensor (Pickup et al. 1994). However, if cross-flow is negligible, only the diagonal elements of the permeability tensor is required. Pickup et al. (1995) found that the off-diagonal terms are needed if the laminae have a high angle with respect to the pressure gradient, if there is a large permeability contrast between the lamina or if the sedimentary structures are asymmetric. The diagonal permeability values are sufficient if the bottomset permeability is low, or if permeability increases upward along the foreset. Even if cross-flow can be significant at the lamina scale, Ringrose et al. (1999a) showed that at the bedding scale, the effect of the smaller scale laminae were masked by the effect of the approximately layered bed scale architecture. Detailed numerical models of small-scale structures can be difficult to make, but Pickup et al. (1999) found that a simpler, schematic model may be sufficient as long as the internal architecture (frequency and thickness of lamina) is representative.

2.3.5 Estimation of effective permeability

Some of the above mentioned methods were classified as an upscaling procedure where permeability or porosity values measured at a small support volume were “averaged” in order to obtain a value that was representative for a larger support volume (e.g. core plugs were upscaled to the wireline tool resolution). For all additive properties, the average value of a volume is simply the arithmetic average of all the values present in that volume. Since not “all” the possible core plugs are sampled, the traditional methods assume that the core plugs represent the complete volume. For non-additive properties (e.g. permeability), even if all the small-support values were available, an average would not equate to the large scale effective permeability. This is because it is the spatial distribution of the permeability values and the boundary conditions that determine the larger support value.

Renard and Marsily (1997) use the term *equivalent* permeability for a constant permeability tensor that represents a heterogeneous medium under the same boundary conditions. *Effective* permeability is on the other hand defined by these authors as the permeability of a medium that is statistically homogeneous on the large scale and that is independent on the macroscopic boundary conditions. This means that the spatial correlation lengths of the heterogeneities must be smaller than the domain. The effective permeability is thus an intrinsic property of the media. The equivalent permeability for a finite-size block, where the correlation lengths are on the order of the block-size, is denoted block-permeability. The block-permeability is dependent on the boundary conditions and is a function of the block size (Rubin et al. 1991).This notation is also used by Durlofsky (1991). Other authors (e.g. Pickup et al., 1995; Journel et al., 1986) use the term *effective* permeability for both effective and equivalent permeability as defined by Renard and Marsily (1997). In this thesis, the term effective permeability will be used for all upscaled permeabilities regardless of the independency of the boundary conditions.

Methods for calculating effective permeability are then often divided into three groups; deterministic, stochastic and heuristic (Renard and Marsily, 1997). The first one assumes that the permeability distribution is exactly known, the second treats the distribution as a random function in space, while the heuristic methods propose rules for calculating plausible effective permeabilities. For each of these groups, both numerical and analytical techniques can be used to calculate the permeability value. The analytical techniques will give an exact solution but require some model assumptions. The numerical techniques can be applied in more general cases, but the results are approximate. In addition, the numerical approach is more time consuming. By using a numerical approach, it is hoped to give insight into the factors affecting effective permeability and guiding the development of an analytical model. In the same way, a numerical model is often used to validate a proposed analytical model.

The methods described below will be used both to classify the upscaling method employed in this thesis and for comparison with the results in chapters 7 and 8. Methods for distributing geological elements and petrophysical properties in space will be reviewed in section 4.1.

2.3.5.1 Inequalities and heuristic methods

A simple technique that already has been described is *sampling*. This method assigns to the larger support volume the value measured at its centre. The obvious advantage is that it is a simple and fast method. The disadvantages concern the

assumption of homogeneity of the block and the representativity of the centre value.

For a system consisting of plane layers and where the flow is uniform, Scheidegger (1974) and Dagan (1989) have shown that arithmetic and harmonic averages of the individual permeability layers is equal to the effective permeability parallel and perpendicular to the layers, respectively. This fundamental *inequality*, also called the Wiener bounds, can then be expressed as:

$$\mu_a = \frac{\sum_{i=1}^{n} k_i t_i}{\sum_{i=1}^{n} t_i} \leq K_{eff} \leq \left[\frac{\sum_{i=1}^{n} t_i / k_i}{\sum_{i=1}^{n} t_i} \right]^{-1} = \mu_h \qquad \textbf{[2-27]}$$

where μ_a and μ_h are the arithmetic and harmonic averages, respectively, i=1,2,...n is the number of layers and t_i and k_i are the thickness and permeability if the ith layer.

By assuming an isotropic and binary media, Hashin and Shtrikman (1963) developed an inequality that is somewhat narrower than the bounds above;

$$\mu_a - \frac{f_1 f_0 (k_1 - k_0)^2}{(D - f_0)k_0 + f_1 k_1} \leq K_{eff} \leq \mu_a - \frac{f_1 f_0 (k_1 - k_0)^2}{(D - f_1)k_1 + f_0 k_0} \qquad \textbf{[2-28]}$$

where f_0 and f_1 are the fractions of the high permeability k_1 and the low permeability k_0 respectively[1]. D is the space dimension. The arithmetic average, μ_a, is given by $\mu_a = f_0 k_0 + f_1 k_1$. Figure 2.14 shows graphically equation 2-27 and 2-28 in the three dimensional space (D=3).

Heuristic approaches use various combinations of these inequalities to obtain a narrower set of bounds. Matheron (1967) uses a weighted average of the harmonic and arithmetic average:

$$k_{eff} = \mu_a^{\alpha} \cdot \mu_h^{1-\alpha} \qquad \textbf{[2-29]}$$

1. A mud permeability equal to 0.01 mD is used here. The effect of varying this parameter is considered in Chapter 8.

where $\alpha = \frac{D-1}{D}$, which applies for a statistical homogeneous and isotropic medium

.

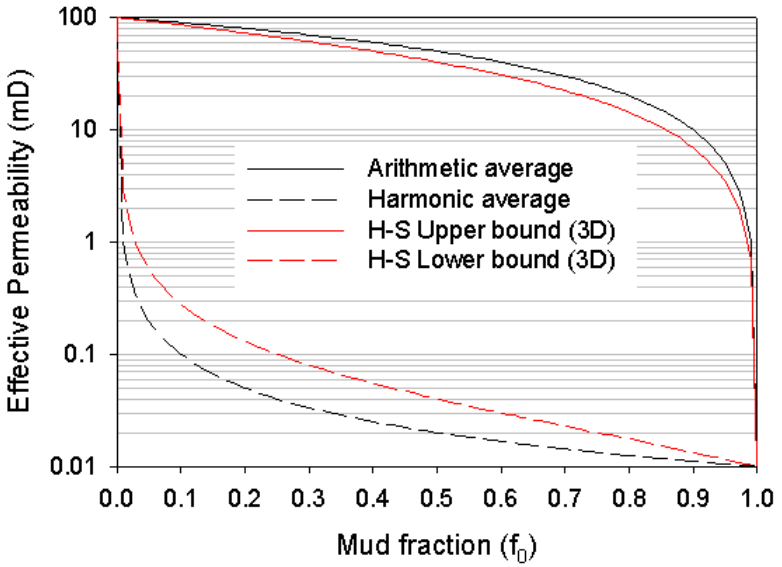

FIGURE 2.14 *Comparison between the arithmetic, harmonic and the upper and lower bound of Hashin and Shtrikman (1963).*

Ababou (1995) extend this to anisotropic, statistical homogeneous medium by changing the exponent to $\alpha_i = \frac{D - l_h / l_i}{D}$. The parameters l_i and l_h represents the correlation length in the relevant direction and the harmonic mean of the correlation lengths in the principal directions of anisotropy. Figure 2.15 shows the behaviour of equation 2-29 for different values of α.

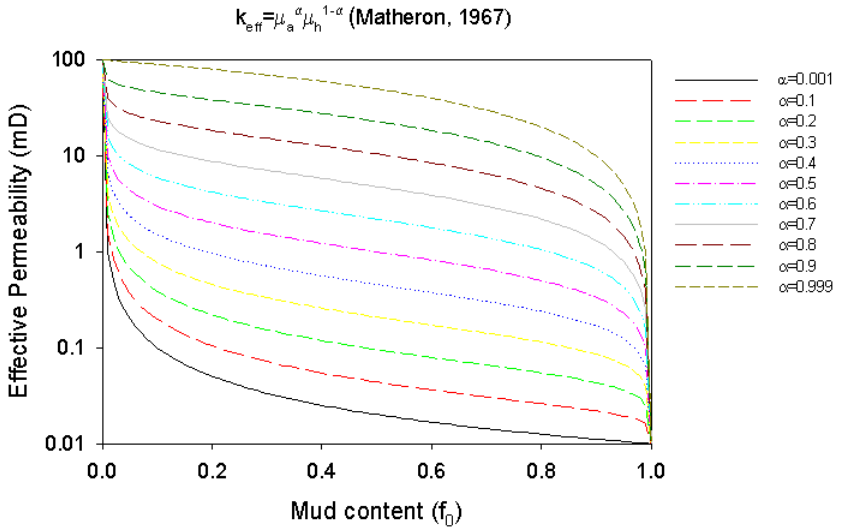

FIGURE 2.15 *Average of means (Matheron, 1967)*

Another heuristic approach to estimate the effective permeability is by taking the power average of the individual components. The general power averaging equation is given by (Journel et al. 1986):

$$\mu_p = \langle k^p \rangle^{1/p} = \left(\frac{1}{V} \int_V k(x)^p dV \right)^{1/p} \quad \textbf{[2-30]}$$

which for a binary medium becomes

$$k_{eff} = [f_0 k_0^p + f_1 k_1^p]^{1/p} \quad \textbf{[2-31]}$$

The arithmetic and harmonic average is obtained with p=1 and p=-1, respectively and the geometric average as $p \to 0$. Journel et al. (1986) found that a p-value of 0.57 matched the horizontal permeability in a anisotropic, correlated binary sand/shale model, while a p-value of 0.12 was appropriate for the vertical permeability. Deutsch (1989) used a model with randomly allocated ellipsoid shale bodies and found that p=0.73 and p=0.17 for horizontal and vertical flow, respectively. However, he only considered cases with a low fraction of shale (< 40%). For a statisti-

cally homogeneous and isotropic media $p = 1 - 2/D$, (Noettinger, 1994). Figure 2.16 shows the power average approach (eq.2-31) for different values of α, where $p = 2\alpha - 1$. Note that this method behaves quite differently for intermediate values of α compared with figure 2.15.

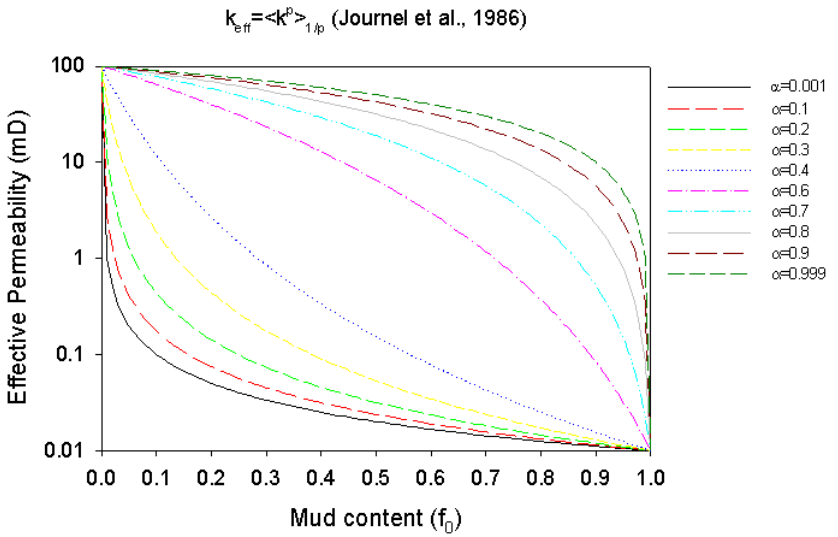

FIGURE 2.16 *Power average (Journel et al., 1986)*

The various methods described here have been used extensively in the literature. Although the equations have limited applicability, they have proven to be valuable as a quick and easy estimate for effective permeability. However, except for cases with simple geometries (e.g. plane layers), numerical experiments must be performed to establish the correct exponents. These methods also constrain the uncertainty envelope by defining the upper and lower bounds.

2.3.5.2 Deterministic methods

The permeability field and boundary conditions are assumed to be completely known for the deterministic methods (Renard and Marsily, 1997). When the geometry is simple, exact analytical results can be found. Otherwise, methods that give approximate results must be used.

Percolation theory is a mathematical model for connectivity. A basic assumption is that the media contain two types of components; one conducting (permeable) and

one non-conducting (impermeable). Percolation theory then evaluates how the flow properties of the media change with the fraction of the conducting component, p. Commonly, an infinite square lattice is used. The conducting elements (sites) are then distributed randomly onto the grid. As p increases, larger clusters are developed and at a certain fraction one cluster dominates and extends (percolates) through the lattice. This fraction is called the percolating threshold, p_c. This value will change for different grid shapes, dimensionality of the grid and the distribution process of the conducting elements (see e.g. Stauffner and Aharony, 1992, for an introduction to percolation theory). For a regular, square grid and site percolation, p_c is equal to 0.593 in 2 dimensions, while for a simple cubic network in three dimensions, p_c=0.312. An alternative approach to site percolation is bond percolation. Site and bond systems have slightly different properties.

A set of exponents can be defined that describes the behaviour of such a system. The exponent, β, is related to the probability that an occupied site belongs to the percolating cluster which is defined as P_∞ (p) (where the infinity symbols means that the lattice is infinitely large). Below the p_c, P_∞ =0, but then rises rapidly at $p>p_c$, and can be described as a power law relationship;

$$P_\infty \propto (p - p_c)^\beta \qquad \textbf{[2-32]}$$

The exponent β is called the connectivity exponent (Kirkpatrick, 1973). Further, a correlation function, g(r) can be defined as the probability that a cell a distance r away is occupied and belonging to the same and largest cluster. The connectivity length ζ, is then defined as;

$$\zeta = \left(\sum_r r^2 g(r)\right) \Big/ \left(\sum_r g(r)\right). \qquad \textbf{[2-33]}$$

The correlation length scales with the form:

$$\zeta \propto |p - p_c|^{-\nu} \qquad \textbf{[2-34]}$$

where ν is the correlation length exponent. Since the non-occupied cells are non-conducting, the conductivity below the percolating threshold is zero. Above p_c, the relation between conductivity (Σ) and the fraction of occupied cells takes the form;

$$\Sigma = (p - p_c)^\mu \qquad \textbf{[2-35]}$$

Here, μ is the conductivity exponent. Stauffer and Aharony (1992) gives following values for these exponents:

Exponent	2D	3D
β	5/36	0.4
ν	4/3	0.84
μ	1.3	1.9

TABLE 2.1 Critical exponents in percolation theory

These exponents are universal and only dependent on the dimension. The latter statement is however only true if the model size (L) is much larger than the correlation length ζ (i.e. $L \gg \zeta$). In the case of a finite size domain and where ζ is approaches L, conductivity can be expressed as (Stauffer and Aharony, 1992):

$$\Sigma \propto L^{-\mu/\nu} \qquad \textbf{[2-36]}$$

The form of equation 2-32 and 2-35 above the percolating threshold is quite different as noted by both Kirkpatrick (1973) and Stauffer and Aharony (1992) (figure 2.17). Since not all the cells in the percolating cluster are relevant for conductivity ("dead-end" cells), the conductivity tends to increase more slowly above the percolation threshold than P(p). Kirkpatrick (1973) used effective medium theory to model the behaviour of conductivity (in a resistor network) above p_c. In the case of infinite model domain, p_c is sharply defined (although it varies with model assumptions). In the finite size case, the observed threshold is less clear and tends to be smeared out in a transition zone (King, 1990).

The equations above are valid if the conducting elements are distributed randomly in the non-conducting background. This assumption is not always realistic especially in real sedimentary systems. Napiorkowski and Hemmer (1980) crated a square 2D lattice were the each cell was occupied with a repulsion to the next neighbour, thus giving a higher percolating threshold. However, this is not more geological realistic than the random assumption.

Deutsch (1989) investigated numerically the effect of anisotropy on the coefficients of equation 2-35. As expected, he found that p_c for horizontal permeability increased with increasing horizontal correlation length of the non-conducting element while this was opposite for the vertical percolating threshold. He also noticed

a dependency of the proportionality factor and the exponent μ on anisotropy, although no physical explanation could be given for the observed variation.

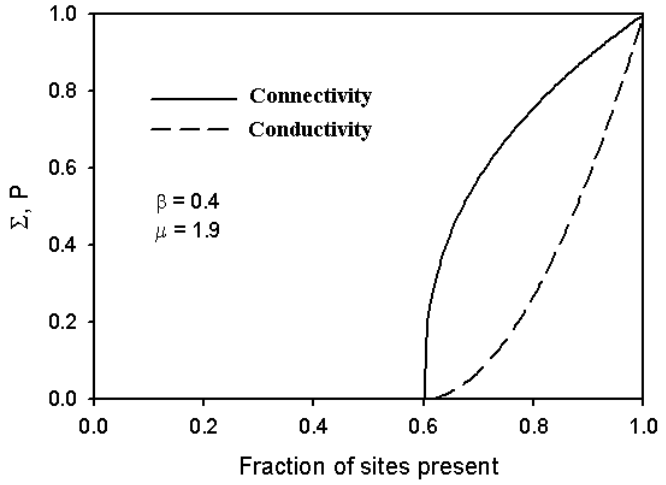

FIGURE 2.17 *Difference between connectivity of conducting cells and conductivity of the 3D system. The exponents are the same as in table 2.1.*

A criticism of percolation theory is that geological variables tend not to be distributed randomly in space, that the classification into permeable/non-permeable can be too simple and that the equations are only strictly accurate near the critical threshold. For spatially correlated heterogeneities in 3D percolation systems, clear findings are not yet established. Although several studies indicate that natural media can be explained by percolation theory (King, 1990, King et al., 2001; Deutsch, 1989), Deutsch (1989) point out that the percolation model has three adjustable coefficients compared to the power average method (only one). Hence, he recommends a power law approach. Despite this, percolating phenomena are often observed and an advantage with respect to the power average method is that the equations can be understood from a physical connectivity point of view.

Effective medium theory (EMT) or the self-consistent approach is based on the idea of replacing the inhomogeneous medium (consisting of a multiphase of homogeneous blocks) by an effective homogeneous medium of permeability k_{eff} such that if a single inclusion of a different permeability is introduced then the mean pressure fluctuation caused by the inclusion is zero (Kirkpatrick, 1973; Dagan, 1979; King,

1989). For spherical inclusions Dagan (1979) proposed the following expression for the effective permeability.

$$k_{eff} = \frac{1}{D}\left[\int_0^{\infty} \frac{f(k)dk}{k(D-1)+k_{eff}}\right]. \qquad \textbf{[2-37]}$$

Here, $f(k)$ is the probability density function of the permeability and D is space dimension as before. The relation then has to be solved iteratively for k_{eff}. For the binary permeability distribution in three dimensions, the relation reduces to

$$k_{eff} = \frac{1}{3}\left[\frac{f_1}{2k_{eff}+k_1} + \frac{f_0}{2k_{eff}+k_0}\right]. \qquad \textbf{[2-38]}$$

Since the inclusions are spherical the resulting effective permeability is isotropic. The main approximations with this method are (Dagan, 1979): 1) The heterogeneous matrix surrounding the inclusion is assumed can be replaced with a homogeneous matrix of unknown permeability, 2) the inclusion is spherical (Dagan 1989 p. 198, gives the expression for elliptic inclusion which gives the anisotropic permeability tensor), and 3) the averaging volume is large compared to the inclusion. The latter assumption implies that the heterogeneity is on a much smaller scale then the domain of interest. Equation 2-38 will be used in chapter 8 for comparison with the numerical results.

There exist other approximate deterministic methods to estimate effective permeability like streamlines (e.g. Haldorsen and Lake, 1982) and renormalization (e.g. King, 1989). Since these approaches will not be used in this thesis, detailed descriptions of these methods will not be given here (see e.g. Mansoori, 1994; Renard and Marsily, 1997).

An approach that in principle is more general consists in solving numerically the diffusion equation. There are several methods to solve the partial differential equation, but a finite-difference scheme is often used. Given constant head boundaries between the two sides (in the direction of flow) of the block and no-flow boundaries perpendicular to the mean flow direction (permeameter type flow), the numerical simulation gives the steady-state, single-phase flow rate over each basic cell. The total volumetric flux (Q) is then obtained by adding together the elementary flow rates and the block permeability is found by Darcy law (eq. 2-6). By rotating the boundary conditions, a directional permeability in each of the principal directions can be calculated (diagonal elements of the permeability tensor). This method is often called a sealed sided pressure solver. By using periodic boundary condi-

tions, Durlofsky (1991) and Pickup et al. (1994) calculated the full permeability tensor.

For a simple system of plane layers, the analytical solution of the diffusion equation gives of course the arithmetic and harmonic averages in equation 2-27. For such a simple system, Kasap and Lake (1990) also found an analytical expression for the off-diagonal terms in the permeability tensor.

2.3.5.3 Stochastic methods

In the deterministic methods described above, the spatial permeability distribution is assumed to be known at a given scale of heterogeneity. In the probabilistic approach, the permeability field is modeled as a random variable with a known joint probability distribution that defines its spatial structure (Renard and Marsily, 1997). The resulting effective permeability is thus also a random variable characterized with a probability density function (pdf). With the numerical methods, the entire pdf can be described as the number of simulations approaches infinity. An analytical method gives a few of the parameters describing the pdf of the random variable (e.g. mean and standard deviation). One exact analytical result is given by Matheron (1969), where for a two-dimensional isotropic, log-normal uncorrelated media, he found that the effective permeability was equal to the geometric mean. Warren and Price (1961) found, by numerical simulation, that the geometric mean provided the best estimate of effective permeability for a wide range of univariate distributions given that there was no spatial correlation. In three dimensions, an approximate analytical results is given with the assumption of low variance of the log-normal permeability distribution ($\sigma_{\ln k}^2$) (Gutjar et al. 1978):

$$k_{eff} = \mu_g \left[1 + \frac{\sigma_{\ln k}^2}{6} \right]. \qquad \textbf{[2-39]}$$

Anisotropy has been invoked in equation 2-39 by Ababou (1995). The geometric average, which lies between the arithmetic and harmonic average, is often used in the industry to calculate the effective permeability if the geometry is assumed to be random. These conventional averages will be used in chapter 7 and 8 for comparison with the effective permeability values calculated there.

In summary, section 2.3.5 has given several methods to estimate the effective permeability with some knowledge of the spatial distribution, either a complete knowledge as in the deterministic methods or a probabilistic knowledge as in the

stochastic methods. Both these methods can be solved by either numerical or analytical techniques. The analytical solutions are interesting since they give an exact value and that are fast to calculate. However, the limitations are related to the assumptions of the models, either with the geometry (plane layers, isotropic media etc.) or with the size of the heterogeneity with respect the to model size. The numerical methods are in principle more general and can be used on any permeability field, but they are more time consuming.

CHAPTER 3

Tidal cycles and tide-influenced deposits

The tide is the periodic rise and fall of the sea level caused by the variation in gravitational forces that occur in the earth-moon-sun rotational system. These vertical movements create horizontal water movements, the tidal currents. The periodic variation in the strength of this current will impact on the sedimentological record. The reasons for including this chapter are 1) the Tilje Formation is interpreted to have been deposited under tidal influence (Dreyer, 1992; Martinius et al. 2001), 2) periodic variation in current strength and thus depositional conditions will influence the petrophysical properties of the resulting sediments, and 3) an understanding of these processes is necessary when using a process-oriented tool to model tidal bedforms.

3.1 Tidal cycles

The tide in the oceans is controlled by Newton's law of gravitation, which states that the attractive force between two bodies is proportional to the product of their masses and inversely proportional to the square of the distance between them. The centrifugal force, as a result of the motion around a common mass centre, balances the attractive force. While the centrifugal force is equal for all particles on a revolving body, the gravitational force depends on the position on that body. In the case of the earth and the moon, the particles closest to the moon on the earth experience a larger gravity force then that needed to maintain the orbit (larger than the centrifugal force). At the same time, on the opposite side of the earth, the centrifugal force

is larger than the gravitational force (figure 3.1a). This difference generates the tide and is referred to as the tide-generating force (Werner, 1992). The influence of the sun, which is 0.44 times that of the moon, can then be superimposed on the effect of the moon. In tidal theory one often evaluates the equilibrium tide (Macmillian, 1966). This is the tide that would exist in a hypothetical, deep ocean that covered the earth uniformly and whose surface was always in equilibrium with the gravitational and centrifugal forces. In the following, the main tidal cycles, starting with the shorter ones, will be outlined. A more theoretical outline can be found in Macmillian (1966), Pugh (1987) or Werner (1992). Kvale et al. (1999), Archer et al. (1991) and Allen (1985) have given a comprehensive review of tidal theory with focus on the implications on the sedimentological record.

The earth rotates around its own axis in 24 hours (mean solar day), and the attractive forces in the earth-moon-sun system will produce oceanic bulges on each side of the earth. An observer at point P in figure 3.1a will then experience two periods with high water level as the bulges pass, and two periods with low water level. The vertical difference between the low and high water level is the tidal range. This type of tide is called semi-diurnal since the period of oscillation repeats approximately two times in a day. However, since the moon orbits around the earth with a period of approximately 27.32 days, the two highs and two lows happen about every 24.84 h (a lunar day). Moreover, the declination of the moon relative to the equator changes from a position northerly to a southerly position and back (figure 3.1b) in 27.32 days and modifies the tidal bulge. This period is called the tropical lunar month. In a semi-diurnal tide system this effect results in the diurnal inequality, which means that one of the daily high waters is higher than the other. When the moon passes the equator this effect is minimized. Another modification arises from the changing earth-moon distance during the lunar orbit. The orbital path of the moon is slightly elliptic and carries the moon from the closest position to the earth (perigee) to the farthest position (apogee) and back in 27.55 days (figure 3.1c). This period is called the anomalistic month and produces a fortnightly inequality between the perigee spring and apogee spring. Another important period to consider is the synodic month with a period of 29.53 days (figure 3.1d). When the moon orbits the earth in this period, the sun, moon and the earth are twice nearly aligned (syzygy) and there is either full or new moon. In two instances the moon and the sun form a right angle relative to the earth (quadrature). In syzygy the attractive forces from the sun and the moon reinforce (synodic spring) and the tidal height increases while in the quadrature the forces work in a right angle and the tidal height is a minimum (synodic neap). The sun also affects the tide through the axial tilt of the earth. The declination to the sun is largest in the solstices and least in the equinoxes, and the present day period of this cycle is 182.62 days. Like the moons elliptic path around the earth, the earth has an elliptic path around the sun on

a yearly time scale. In the position nearest the sun (perihelion; winter solstice) the gravitational force from the sun is stronger than in the position farthest away (aphelion; summer solstice). The positions between these extremes are called the autumnal and vernal equinoxes.

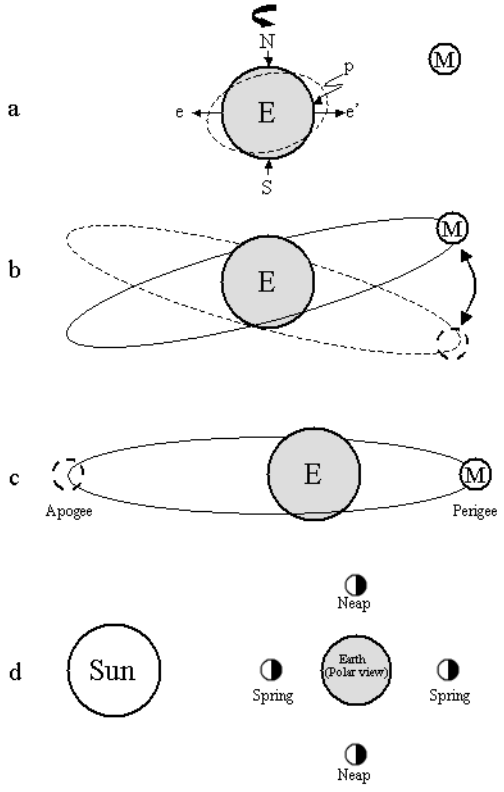

FIGURE 3.1 *Modification of the tidal bulge due to attractive forces between the earth (E), moon (M) and the sun (a). Variation in the declination of the moon in the lunar tropical month (b). The anomalistic cycle related to perigee and apogee position of the moon in relation to the earth (c). The moon phases in the Synodic month (d)*

The synodic, tropical and anomalistic periods have slightly different values. Twice a year these periods constructively amplify each other during which time the tidal forces reach a maximum. This amplification has a period of 183.29 days and is in part related to the latitude (Kvale et al. 1999). At a longer time scale, the angle of declination of the moon varies with $\pm 5°$ and this gives a lunar nodal cycle of 18.6 years, and the rotation of the moon's perigee with a period of 8.85 years (lunar apsides cycle). Figure 3.2 summarize the periods discussed so far in addition to some longer period ($<10^3$ years) astronomical cycles not considered further here.

The above-described periods relate to the equilibrium tide generated by the earth-moon-sun rotational system. Pugh (1987) considered this system as a set of satellites that each generates a tidal signal component (a tidal constituent) and that all the components together form the observed tide. The equilibrium tide consists of two symmetrical tidal bulges (figure 3.1a) directly under or directly opposite the sun or the moon. The maximum tidal range at equatorial latitude would then be approximately 0.5 m and the bulge would rotate around the earth as a uniform wave. The observed tide has however a more complicated pattern since 1) the ocean is not uniformly deep and 2) the continents disturb the wave propagation (see also discussion in Pugh, 1987, p. 143-144). Further, the various ocean basins have their individual natural mode of oscillation (resonance frequency) which influence their response to the tide generating force. When the tidal wave approaches the coast, shoaling will also amplify the tidal height. Thus the destruction (damping) or amplification of certain tidal constituents in each tidal basin determines whether or not the specific astronomical periods can be detected (Kvale et al. 1999). Harmonic analysis have been used to resolve the observed, complex, resultant tide into a discrete spectrum of sinusoidal constituents (e.g. Pugh 1987).

Most modern oceans are in near resonance with the semi-diurnal tidal frequency suppressing the diurnal component (figure 3.3a). Other basins however, amplify the diurnal component which results in a tide that reaches maximum and minimum elevation only one time in a day (figure 3.3c). In these basins, the tropical period is the main control on the neap-spring cycle, and a tropical neap-spring cycle is shorter than the synodic neap-spring cycle. All other tidal systems are intermediate between the semi-diurnal and diurnal end members depending on the relative importance of the semi-diurnal and diurnal components of the tides and upon the resonance with the specific basin (figure 3.3b). Although the equilibrium tide is a simplification of the real situation, many of the features predicted by the theory can be observed in the real tide

.

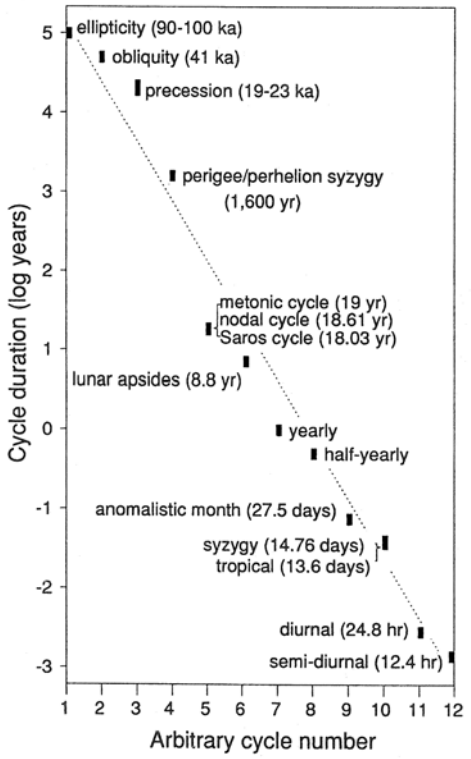

FIGURE 3.2 *Selection of periodicities in the earth-moon-sun orbital system. Semi-diurnal up to nodal cycles have been observed in the sedimentological record. From Archer 1996.*

Other, non-tidal components may modify the pure tidal signal. Seasonal variability in discharge from rivers, wind-speed and -direction, climatic variability and changes in the atmospheric pressure are just a few factors that will influence on the observed water level and induced currents (e.g. Archer et al., 1991; Kvale et al., 1994).

Another modification of the equilibrium tide is the Kelvin wave (e.g. Werner, 1992). Due to the rotation of the earth and the coriolis force, the tidal wave will rotate in an open embayment so that the incoming (flood) and outgoing (ebb) current will dominate each part of the bay. The tide appears to rotate (counterclock-

wise in the northern hemisphere) about a nodal point (amphidromic point), which has essential zero displacement.

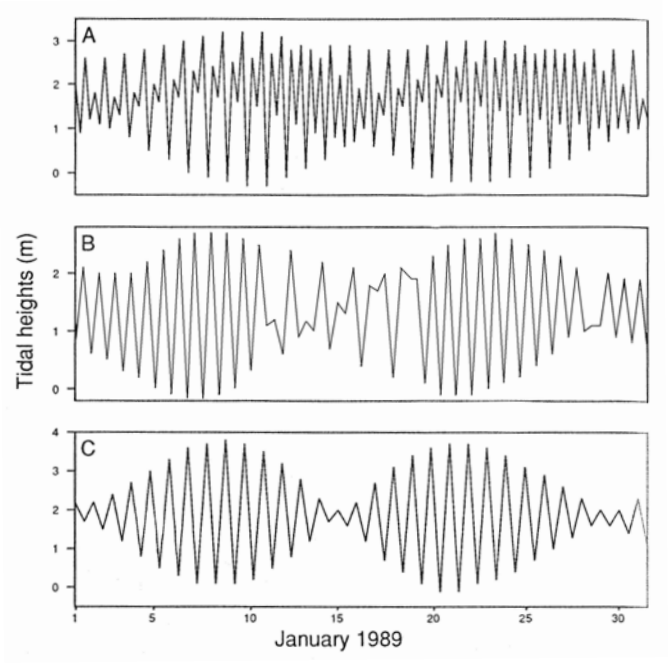

FIGURE 3.3 *Predicted tidal pattern from modern equatorial stations. A: Predominantly semidiurnal system., B: Mixed predominantly diurnal system. C: predominantly diurnal system. From Archer et al. (1991)*

The orbital speed and distance between the earth, moon and the sun has slightly changed during the last billion years. Although the actual duration of the solar year has not significantly changed in this period, the earth's axial spin has decreased owing to tidal friction and lunar retreat. However, both lunar and solar semi-diurnal period changes have been largely commensurate (Sonett et al. 1988; Archer and Johnson, 1997) giving only a slight decrease in the number of tidal days per neap-spring cycle. The effect of changing palaeogeography has however had a greater effect on the tidal pattern mainly through its influence on the resonance frequency of the basins.

3.2 Implications of tidal influence on the sedimentological record

The vertical difference between the high and low water level is called the tidal range. As the water level rises (flood) and falls (ebb) a horizontal current is induced and a larger tidal range normally gives a larger current speed (e.g. de Boer et al., 1989). From the tidal range a system can be classified as microtidal (<2 m tidal range), mesotidal (2-4 m), and macrotidal (>4 m) (Hayes, 1975). The depositional system can then further be divided into the sub-tidal zone below the mean low water level that in general is submerged at low tides, the supra-tidal zone above the mean high water level that is emerged for most of the spring tides, and the inter-tidal zone for the area between the sub-tidal and supra-tidal. Tide-influenced sedimentary deposits are found in many different depositional systems like the shelf environment, barrier and lagoon systems, deltas and estuaries. A comprehensive review of tidal influenced sedimentary systems is given in Ginsburg (1975), Klein (1977; 1979), Reading and Collinson (1996) and in the collection of papers in de Boer et al. (1988) and Smith et al. (1991).

In the sub-tidal environment there is, in theory, an infinitesimal time with still stand in the water movement between the flood and the ebb called “slack water”. In practice however, with regard to sediment transportation, this period is longer and is related to the entrainment velocity of the sediment present on the bed and on the current strength. Figure 3.4 shows a simplified asymmetrical flood-ebb cycle that can be divided into four different stages: the dominant current stage (from t_1 to t_4); the slack-water stage after the dominant current (from t_4 to t_5); the subordinate current stage (from t_5 to t_8); and the slack-water stage after the subordinate current (from t_8 to t_9). Allen (1985) assumed a bedload transport rate that was proportional to the cube of the difference between the current velocity (U(t)) and the entrainment velocity of the sand component (U_{ces}) and is indicated in figure 3.4 as the dotted area. The variation in the current speed will also influence on the ripple morphology (Oost and Baas, 1994), a result that will be further discussed in section 7.2.1.

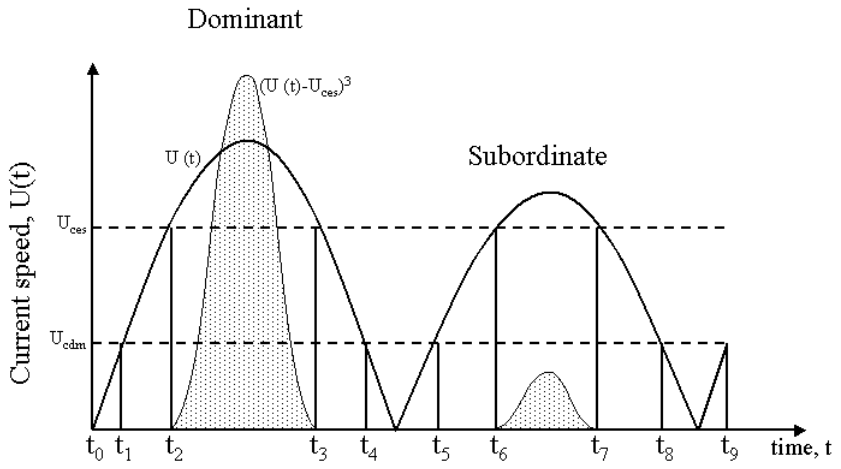

FIGURE 3.4 *Sand and mud transport/deposition during one tidal cycle. Modified from Allen (1985) and Nio and Yang (1991). U_{ces} is the entrainment velocity for sand and U_{cdm} is the critical threshold for mud deposition. Total sand transport is proportional to the stippled area under the curve $(U(t)-U_{ces})^3$.*

Cyclic variation in current speed (figure 3.4) has implications on the depositional process. The result of the four stages of daily deposition have been found and described in larger scale bars and dunes (e.g. Visser, 1980; Allen, 1981; Homewood and Allen, 1981; Boersma and Terwindt, 1981; Kreisa and Moiola, 1986) and in smaller scale planar and ripple cross-laminated bedforms (e.g. Kvale et al., 1989; Williams, 1989; Martino and Sanderson, 1992; Oost et al., 1993; Miller and Eriksson, 1997; Adkins and Eriksson, 1998; Brettle et al., 2002). For intercalations of ripple laminated sand and mud Reineck and Wunderlich (1968) proposed a descriptive classification that was based on the amount and appearance of the mud fraction (figure 3.5). Terwindt and Breusers (1972) gave a quantitative explanation based on the critical current velocity for movement of mud for these bedding types. Reineck and Wunderlich (1968) emphasized that the origin of these bedding types were not indicative of any particular depositional environment but that they are more common in tidal deposits. As an example, Bhattacharya (1997) and Martin (2000) have described flaser and wavy bedded units in fluvial and ephemeral streams, respectively.

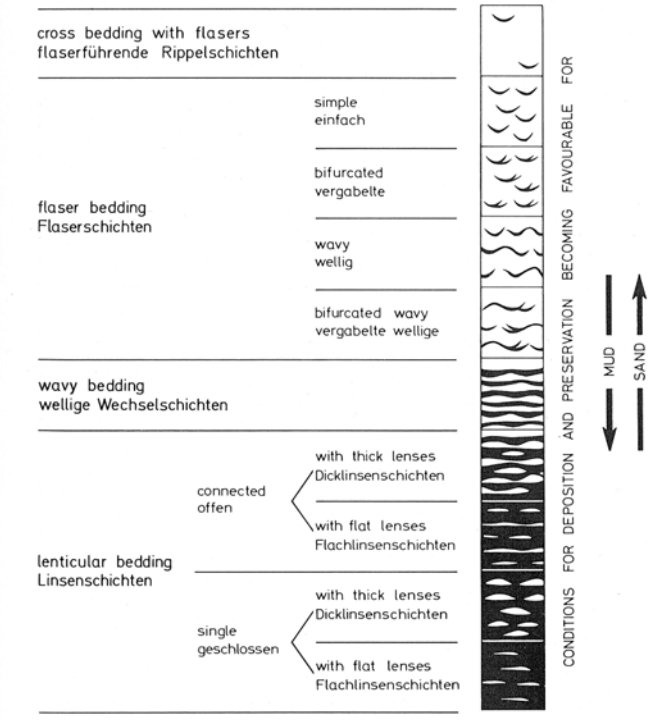

FIGURE 3.5 *Classification of flaser-, wavy- and lenticular bedding based on the amount and organization of sand and mud. From Reineck and* Wunderlich *(1968).*

The deposition of mud, expressed as the settling flux, is the product of the concentration and the settling velocity (Dyer, 1995) and below a current velocity of 0.2 cm/s, the deposition of mud from suspension is considerable (Einstein and Krone, 1962). The degree of flocculation of mud particles, which also is dependent on the concentration, influence on the settling velocity and can be correlated with the salinity of the water, electrical characteristics of the particles and turbulent shear in the water column among other factors (Dyer, 1995). Terwindt and Breusers (1972) did experimental studies on the maximum thickness of a mud layer in one tidal cycle. They found that with a near bed concentration of mud of 1 cm^3/l and a settling velocity of 0.04 cm/s, a 0.3 cm mud layer could be deposited in 2 hours. This mud layer will however have a high volumetric water content and go through a

phase with initial consolidation and further compaction during burial. Based on this, they concluded that deposition from suspension during one slack-water period only could produce a 2-3 mm freshly deposited mud layer. Wolanski et al. (1988) and McCave (1970) operates with slightly higher values for mud concentration, fall velocity and slack water time giving a thicker mud layer. Wunderlich (1978, cited in Reineck and Singh, 1980) observed that centimetre thick mud layers could be deposited during a short period of slack water. McCave (1970) has further proposed a quasi-continuous depositional model related to the existence of a viscous sub-layer near the bottom in which mud can be trapped but not ejected back into the overlying water. The process is believed to be valid in low velocity regions, and can explain, according to McCave (1970) some of the thicker mud layers encountered in flaser and wavy bedded offshore deposits.

The preservation potential of such a slack-water deposited mud layer depends on the rate of initial consolidation and the erosive power of the next current event. Increasing consolidation will increase the force needed to erode the surface. The erosion of a surface with both sand and mud exposed is however complex, and Terwindt et al. (1968) found from experiments that the critical shear stress for erosion was in the range of the mud and not the sand. Terwindt and Breusers (1972) found further that in a freshly deposited mud, the initial consolidation can be rather quick and after 3-4 hours the entrainment velocity increased markedly.

Mud deposition can also be related to high concentration near-bed slurries often referred to as fluidized muds. At high tidal energy levels, fine-grained sediments are mixed in the water column forming a homogeneous suspension. If the mud concentration is high enough (> 500 mg/l) and the energy level decreases, the fine material begins to settle and a lutocline forms based on concentration differences (Kirby and Parker, 1983; Kirby, 1991). As the energy level continue to diminish, the suspended material settles to form a dense near-bed mobile layer of high mud concentration. These layers can be transported by tidal currents and subsequently deposited during low energy periods (e.g. during a neap period). At increasing tidal ranges (towards spring), they usually become re-mobilized but can in some occasions consolidate and form a bed deposit. Kirby (1991) found that such processes created massive, centimetre thick units usually with a sharp base and top. Above the massive units, sub millimetre silt and clay alternations were deposited by conventional bottom traction of the silt layers and vertical slack water settling of the clay layers in a lower concentration regime (< 500 mg/l). The fluidization process of the mud can be attributed to wave action on already present mud (e.g. Ross and Mehta, 1991), through an increased influx of fine sediments during storm periods from the nearby offshore regions (Bartholdy and Anthony, 1998; Andersen and Pejrup, 2001) or as a result of varying water depth between flood and ebb tide

(Wolanski et al., 1988). As a result, initiation and deposition of fluidized muds occur most often episodically, but they can be related to both seasonal and tidal cycles that can give a regular sedimentation pattern.

The regular variations in strength and direction of the daily tide and its impact on the sedimentological record were described above. Also the longer tidal cycles explained in section 3.1 will influence on the depositional process. During a spring-neap-spring cycle, the tidal range and hence the current speed and the length of a slack water period varies in a systematic manner. Many authors have studied how the sedimentary deposits respond to such a variation. At spring time the current speed is at a maximum and the slack water period is shortest. Less mud is deposited and preserved during this period. The synodic neap-spring cycle have been reported from both larger scale bedforms (e.g. Visser, 1980; Boersma and Terwindt, 1981) and in planar laminated rhythmites (e.g. Brown et al., 1990; Kvale et al., 1989). Tessier (1993) found that there was a variation from spring deposited flaser bedding to neap deposited wavy to lenticular bedding. In thick sections, also the monthly (perigee-apogee) (e.g. Adkins and Eriksson, 1998), the semi-annual cycle (e.g. Williams, 1989; Kvale et al., 1999) and the 18.6-year nodal cycle (Oost et al., 1993; Miller and Eriksson, 1997) have been observed in finely laminated rhythmites. Figure 3.6 shows an idealized representation of how different orders of cyclicity can be present in tidal rhythmites. In addition, non-tidal, but relatively regular fluctuations like seasonal variation in river discharge, have been observed in planar laminated deposits (Kvale et al., 1994; Chan et al., 1994).

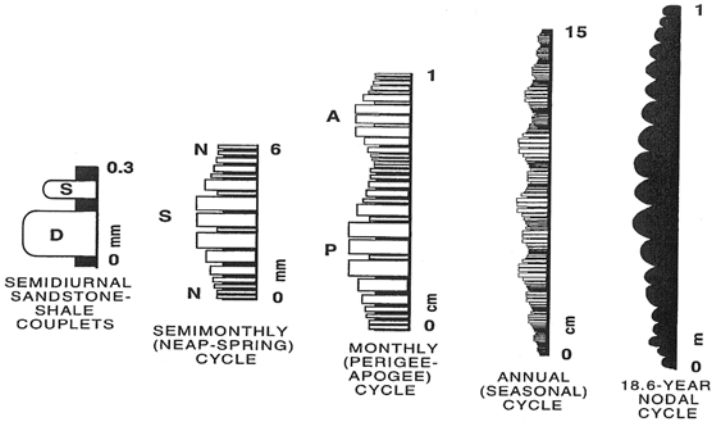

FIGURE 3.6 *Idealized sketch of five orders of cyclicity in tidal rhythmites. From Miller and Eriksson (1997).*

Several attempts have been made to find diagnostic criteria for recognition of tidal influence in the sedimentary record and more specifically to distinguish between sub-tidal and intertidal facies. (e.g. Klein, 1970; Ginsburg, 1975; Clifton, 1983; Terwindt, 1988). The presence of certain oysters in growth position was considered to be diagnostic for a sub-tidal environment while certain plant remnants were highly indicative of an intertidal environment (Clifton, 1983). The presence of clay-draped couplets were used by Visser (1980) and many later authors as a diagnostic criteria for sub-tidal deposits, while Fenies et al. (1999) have reported similar structures from the intertidal environment. Even though the establishment of diagnostic criteria is debatable, several criteria have been published to be characteristic of a tidal setting. This means that their presence suggest, rather than require, tidal influence or dominance and that an association of several characteristic criteria strongly indicates a tidal origin. Nio and Yang (1991) reviewed diagnostic criteria for tidal deposits and concluded that the presence of several orders of cyclicities, and their correlation with different orders of tidal cyclicities, were an unique criteria for recognition of tidal dominance.

An estuary, defined as *the seaward portion of a drowned valley system which receives sediment from both fluvial and marine sources and which contains facies influenced by tide, wave and fluvial processes* (Dalrymple et al. 1992), can be developed during transgression and is favorable with respect to preservation of tide-influenced deposits. This geologically-oriented definition has however been criticized by Perillo (1995) for being too restrictive. As the tidal wave approaches the shore, some of its energy is dissipated by friction but this effect is usually offset by the amplification caused by shoaling. In addition, estuaries in general have a funnel shaped morphology that further amplifies the tidal wave giving a stronger imprint on the sedimentary deposits. Tide-influenced estuarine facies have been reported by e.g. Terwindt (1971), Clifton (1982), Kohsiek et al. (1988), Pejrup et al. (1988), Allen (1991), Dalrymple and Rhodes (1995) and Wells (1995) while Dalrymple et al. (1991), and Perillo (1995) have proposed different classification schemes for estuaries. The lower part of the Tilje Formation is envisaged to have been deposited in an estuarine system (see chapter 5). From a modelling perspective, tide-influenced lithofacies in estuaries are difficult to characterize because of the complex array of sedimentary heterogeneities. More specific, the presence of mud on different scales ranging from centimetres (e.g. flasers) to tens of meter (e.g. fluidized mud deposits) makes the division into representative flow units difficult. Yoshida et al. (2001) proposed a hierarchy of heterogeneities in estuaries (figure 3.7) and the main focus in this thesis corresponds to Yoshida et al.'s small-scale where the heterogeneities ranges from a few centimetre to a few tens of centimetre.

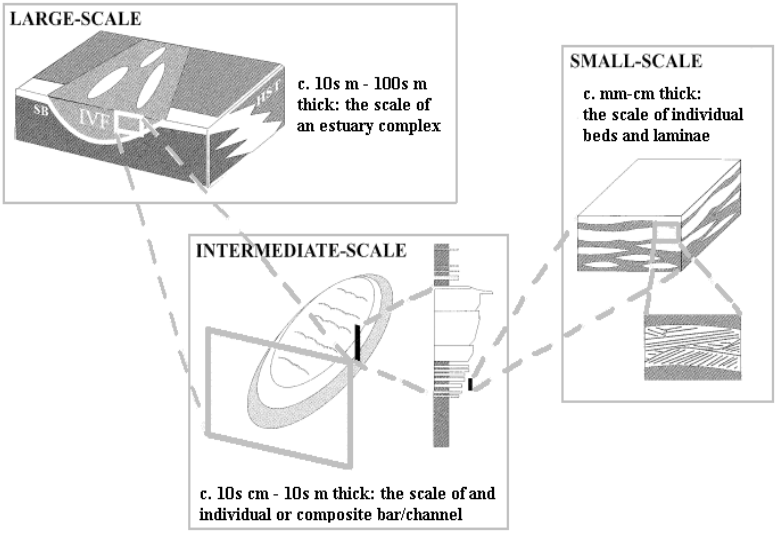

FIGURE 3.7 *Scales of heterogeneity in an estuary. The focus in this thesis will be on the small-scale bedding heterogeneities. From Yoshida et al. (2001).*

This chapter has given an overview of tidal theory, how the tide influence on the sedimentary record and that recognition of several orders of cyclicity is one of the few diagnostic criteria for identifying tidal influence (Nio and Yang, 1991). In contrast to planar rhythmites and larger scale bedforms, considerably less material is published on the cyclicity in ripple-laminated deposits (one notably exception is the study by Martino and Sanderson, 1993). The theory reviewed here will be used in subsequent chapters to better understand the process-based modeling tool that will be used in this thesis, interpret tidal influence in a ripple-laminated lithofacies in the Tilje Formation and to form a better basis for evaluating the petrophysical properties of this formation.

CHAPTER 4 *Near wellbore modelling tool*

In this thesis, a recently commercialized modelling tool, SBED[1] will be used to create a detailed near wellbore model[2] of the lower Tilje Formation in Heidrun (chapter 5 and 6). This *earth model* is then used for reconciling well data and to evaluate petrophysical variability with sample support for some ripple laminated tidal facies. To put the near wellbore modelling tool in a general geomodelling framework, a short review of the most frequently used methods to model geological and petrophysical properties will be given in section 4.1. In section 4.2 and 4.3 the main input parameters to SBED, the deterministic input and the parameters representing spatial variability, respectively, will be described. The principal output parameters or the simulation results will be listed in section 4.4 and some advantages, limitations and challenges of the modelling tool are given in section 4.5.

The user guide for SBED gives only a short and technical introduction to the different input parameters. The main concern for the user is however, 1) how can the parameters be controlled in order to build a particular bedform and 2) how can these parameters be obtained from the sedimentological record. From a petrophysical point of view it is also important to understand which parameters control the effective petrophysical properties. The spatial distribution of the mud layers will

1. SBED™ is trademark software developed by Geomodeling Technology Corp.
2. See section 5.3.1 for definition of the term ‘near wellbore model’

influence on the vertical and horizontal permeability (e.g. Jackson et al. 1999; 2003). This is then intimately linked with the geometrical input parameters. From a scientific point of view it is also important to show that the user has an understanding of the relation between the input and the output and not turn the modelling tool into a “black-box” tool, using only the default parameters. As a consequence, section 4.6 shows the results from a study aimed at increasing the knowledge of the input parameters and to give some practical guidelines for using the modelling tool. This workflow will be used in chapter 5 to construct a detailed model of a selected interval of the Tilje Formation and in chapter 7 when developing a parameter set for general tidal models based on flume tank studies.

4.1 Review of geomodelling methods

Petrophysical properties vary through space as a result of the complex geological processes through which a reservoir evolves (section 2.2). Numerical models that solve flow equations (described in section 2.3.5) require a map or cube of the spatial distribution of the relevant properties (e.g. porosity and permeability). Several methods have been developed during the last decades that use different data to create a realistic as possible representation of the subsurface. Haldorsen and Damsleth (1990), Bryant and Flint (1993), Srivastava (1994) and Koltermann and Gorelick (1996) have reviewed some of the different models that have been used for modelling subsurface flow. Koltermann and Gorelick (1996) divide the map generation into three types: structure imitating, process-imitating and descriptive. The structure imitating and process imitating methods will be briefly described below. The process of making an image usually contains two steps: creation of the geometry of the geology and linking the petrophysical properties to the geometrical image. In some methods however, the first step is omitted and a map of petrophysical properties is made directly that may reflect geological structure.

4.1.1 Structure imitating methods

Structure imitating methods rely on correlated spatial statistics, probabilistic rules or deterministic constraints developed from facies relations to create an image of the reservoir. This model group can be further divided into spatial statistical algorithms and sedimentation pattern imitation methods (Koltermann and Gorelick, 1996).

Reviews of spatial statistical models can be found in Srivastava (1994) and Haldorsen and Damsleth (1990). These models create many equally probable images (realizations) of the reservoir and this model class can be further divided into dis-

crete or object based models and continuous or pixel based models. In the first one objects representing geological units are distributed randomly in space. Rules can be used that control the degree of overlap or erosion into each other and the attraction or repulsion of objects. Petrophysical properties must be populated in the objects subsequently. In continuous models, petrophysical properties are simulated at each point in the reservoir space directly without first specifying a geological geometry. A model of the spatial variability is used to distribute the petrophysical values. Other modelling techniques included in the spatial statistical model class are simulated annealing and indicator-based methods. A combination of these modelling methods can be used where discrete objects are distributed in space within which variations of reservoir properties are modelled with a continuous method (e.g. Damsleth et al., 1990). The main drawback of this modelling class is that sedimentary geometry can be reproduced without addressing the mechanism by which the sedimentary deposits form giving unreasonable images unless quality checked. One of the strengths is that models created by spatial statistical methods can be conditioned to local values (e.g. well observations).

Sedimentation pattern-imitating methods predict the geometry and lithology of sedimentary deposits using rules derived from conceptual depositional models (Koltermann and Gorelick, 1996). These methods have been used both on the basin scale and at the scale of small sedimentary bedforms. The so-called random walk method has been used to model network of channels or braided streams (e.g. Webb, 1994) while modelling of avulsion has been used to create images of meandering streams (e.g. Bridge and Leeder, 1979). Analytical sedimentation pattern methods produce cross-sectional models of sedimentary features ranging the from basin scale (Paola et al., 1992) to aeolian cross-stratified bedforms (Cox et al., 1994). Although a model of sedimentary structures is made, fluid flow and sediment transport and erosion is not simulated explicitly.

4.1.2 Process imitating methods

Process-imitating methods construct models of heterogeneity through mathematical models of either subsurface flow or the geological processes governing sedimentary basin formation and filling (Koltermann and Gorelick, 1996). One sub-class of this modelling method uses measured data (e.g. hydraulic head), solve the equations for fluid flow to estimate a relation to unknown parameters (e.g. permeability or transmissivity). Traditionally, such models are calibrated through trial-and-adjustment processes (history matching). Geological process methods model the evolution of a deposit in time with depositional, tectonic or climatic processes. Unlike the sedimentation pattern methods described above, fluid flow equations

and mass conservation of sediment are used to model sediment entrainment, sediment transport and depositional rate or erosion. This model class then considers erosion, transport and deposition by wind, water and mass movements by using the equations to distribute sediments over an area and predict the sedimentological structures produced by the flow and sediment type. This method then gives the opportunity to evaluate the relation between permeability structure and the processes that formed the deposit. Pioneering work was done by Bonham-Carter and Sutherland (1968) working with deltaic deposits. Tetzlaff and Harbaugh (1989) developed a code that simulated braided stream deposits while Anderson and Haff (1988) simulate saltation in an aeolian environment. The challenges with process models are that they are constrained by our ability to represent geological processes mathematically and that they only can condition to measured values through trial-and-adjustment of input.

4.1.3 Sedimentary BEDing tool (SBED)

4.1.3.1 Background

Modelling of small scale (cm-dm) sedimentological bedforms has been done by several authors and has in part been driven by the development of probe data measurements providing petrophysical values at the lamina scale. A pioneering work on synthetic modelling of bedforms was done by Rubin (1988) who used variations of the equations from earlier work by Allen (1968) (see section 2.2.2.3). The difficulty of relating surface forms to the resulting (cross-) laminated deposit has been discussed by several authors and Rubin (1988) states that "*...instantaneous observation of bedforms gives a detailed view of morphologic properties such as height, spacing, asymmetry, crestline sinuosity, and trough profile, but gives no indication of changes through time in bedform morphology or of transport related characteristics such as the relative migration speeds of the main bedforms, spurs, or scour pits. In contrast, cross-bedding commonly contains less information about the morphology of bedforms that existed at any one time but contains more information about morphologic history and transport-related behavior of bedforms.*" The code developed by Rubin (1988) uses sine curves that are displaced in time and space to mimic the migration of lamina surfaces. The SBED method developed by Wen et al. (1998) makes a significant step towards a petrophysical useful method by combining sedimentation pattern imitation methods, in part related to the Rubin (1988) code, and stochastic methods. In this way, the stochastic components model the natural variability. In addition, Wen et al. (1998) included 3D property modelling and by using a sealed sided pressure solver, the effective permeability of the bedding models could be calculated. The Rubin (1988) code has also been used in petro-

physical modelling by Cox et al. (1994), but neither the stochastic variability or the petrophysical modelling was included in the same manner as in SBED.

Early versions of the SBED (then called TBED for Tidal BEDding) were in part developed at the Statoil Research Centre in cooperation with Geomodeling Technology Corp. Since 2000, the SBED tool pack has been further developed in a Joint Industry Project (JIP) between several major oil companies and the first commercial version was released in 2002.

4.1.3.2 Modelling concept

The method used in SBED is based on manipulation of the following surface function (Wen et al. 1998):

$$z(x,y)^t = A\sin\left(\frac{x}{L_x} + \theta_x\right) + B\sin\left(\frac{y}{L_y} + \theta_y\right) + g(x,y) \qquad \textbf{[4-1]}$$

where x and y are spatial coordinates, t is a nominal time increment, A and B are amplitudes of the bedform in the current (x) and crest (y) directions, L_x and L_y are wavelengths of the bedform in the current and crest directions, θ_x and θ_y are initial phase angles (radians) and g(x,y) is a 2D gaussian random function. These surfaces are displaced by vectors to simulated migration of bedforms. The displacement creates a 3D volume separated by the surfaces giving a simulated lamina (see figure 4.1). Correlated random variables are added to each of the control variables (see below). After a sequence of surfaces, $z(x,y)^{t=n}$, a hiatus is simulated and erosion by a new time series is possible. In this way, creation of laminaset, bed and bedset can be simulated. The final geometrical grid consists of cells at the lamina scale (the volume between two surfaces) which is populated with porosity and permeability drawn from a 2D gaussian field. A more recent description of the modelling method is given by Ringrose et al. (2003, 2004).

This geomodelling method can be classified as a sedimentation pattern imitation method by Koltermann and Gorelick (1996). However, the method is here referred to as a process-*oriented* method, since the migration and deposition of sedimentological components are mimiced.

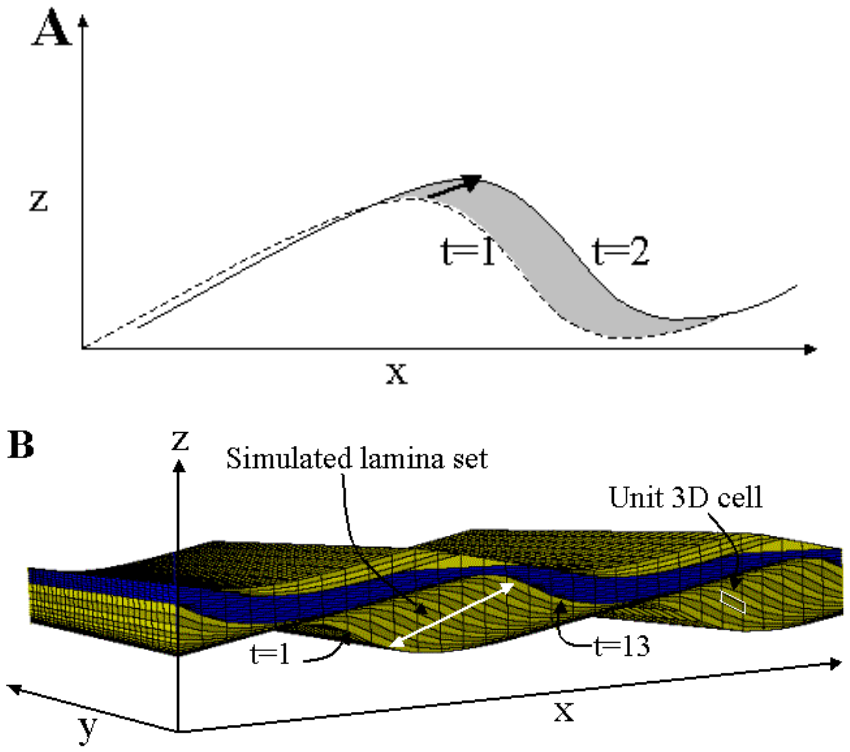

FIGURE 4.1 *A: Schematic sketch of the generation of lamina surfaces in SBED between the t=1 and t=2 in the time series of equation 4-1. The grey area is the preserved lamina and the arrow indicates the migration direction and speed (length of the arrow). Note that the y-direction is not shown in the figure and that the preserved lamina is a 3D volume. B: Simulated 3D sand and mud laminaset in SBED.*

On the final grid, with assigned permeability values, a directional flow is simulated numerically by imposing constant head gradient between two opposite sides of the block and no-flow on the perpendicular sides (permeameter-type boundary condition). The single-phase steady state flow equation is then solved by a finite-difference method for the head at each grid node. The total flow rate crossing the medium is found by adding the elementary flow rates giving the directional permeability from Darcy's law (equation 2-6). By rotating the boundary conditions and

repeating the flow simulation, the permeability for the three orthogonal directions is found.

Some terms used here need to be defined specifically. SBED uses a set of control parameters (further described in the following sections). These parameters define a *template*. By running the code, several *realizations* that are equally probable are made (simulated) due to the stochastic components. In short, and when there can be no confusion the term *model* will be used to describe the realizations created with a given parameter set. Given the seed number of the simulation, the same realizations can be re-made giving a possibility to check and reproduce the results.

The term net-to-gross (N/G or NTG) has been used in the literature with different meanings and is recently reviewed by Worthington (2003b). In this thesis, using SBED as a simulation tool, three different lamina types, mud lamina and two (possibly petrophysically contrasting) sand lamina, will be considered, which also will be referred to as (lithological) components. The net-to-gross is then used here as the ratio between the volume (or area in 2D) of the two sand components to the total volume (area) (i.e. the net sand to the gross interval). More often, the terms mud fraction/content or sand fraction/content will be used to denote the fraction of mud or the fraction of the two sand components respectively. Naturally, these two fractions will sum up to 1.

4.2 Deterministic input parameters

Most of the input parameters are given with a mean value (or a mean value and a standard deviation) with a possibility to add linear trends, periodic variation or random fluctuations. The former represents the mean value of the parameters that together describe the bedform, while the latter three add different forms of deterministic and stochastic variability to the mean pattern.

There are several different types of bedforms that can be simulated, but focus will here be on the tidal bedding models. Many of the parameter sets are however equal between the different bedding models, but where there are discrepancies these will be briefly described.

4.2.1 Cell and model size

Basic to the understanding of SBED is that each cell represents both a compositional element (different sand types or mud) and a homogeneous and isotropic petrophysical property. The spatial distribution of these cells is controlled by the

input parameters and constitutes a particular sedimentary bedform. Figure 4.2 shows the General tab in SBED where the cell size, number of cells and the units are chosen by the user.

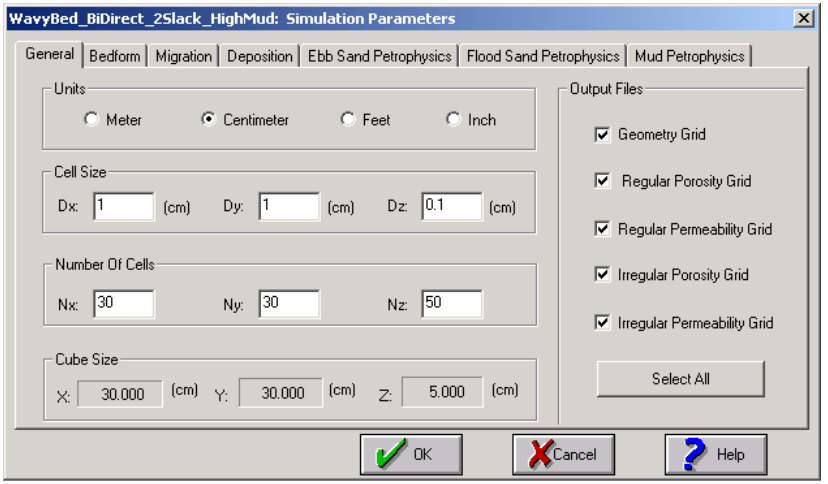

FIGURE 4.2 *The General tab in SBED where the cell size, model size and output files are specified.*

The cell size is initially dimensionless, and the user decides what length scale the cell should have (meter, centimeter, feet or inch). There are two possible options with respect to the grid cell shape in the petrophysical output; regular grid or irregular grid. In the regular grid the cell size is equal for all cells although the dimensions in each direction can be different. In order to capture geometrical details, a large number of regular grid cells have to be produced. Variation over short distances is particular pronounced in the vertical direction and the irregular grid adapts to this variation producing a smaller number of vertical cells compared to the regular grid if the same amount of detail should be captured. Hence, the grid size in the plane (D_x and D_y) is similar for both grid types but the vertical cell (D_z) has to be specified in the regular grid. The geometrical models are only created with irregular grids. The product of the cell size and the number of cells in each direction (N_x, N_y, N_z) then gives the model size (X, Y, Z). Figure 4.3 shows the concept of the regular and irregular grid. This thesis will use irregular grids with the cell dimensions in centimeter and $D_x = D_y = 1$cm unless otherwise stated.

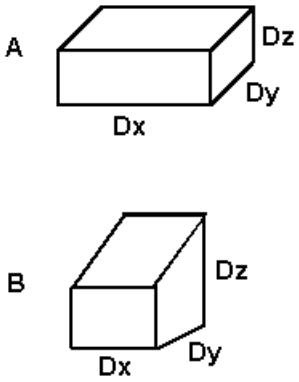

FIGURE 4.3 *A: Regular grid cell where* $Dx = Dy \geq Dz$ *and constant. B: Irregular grid where* $Dx = Dy$ *and where Dz varies.*

4.2.2 Bedform parameters

The bedform parameter tab for cross-bedding and tidal bedforms (figure 4.4) specifies the bedform shape both parallel and perpendicular to the current direction.

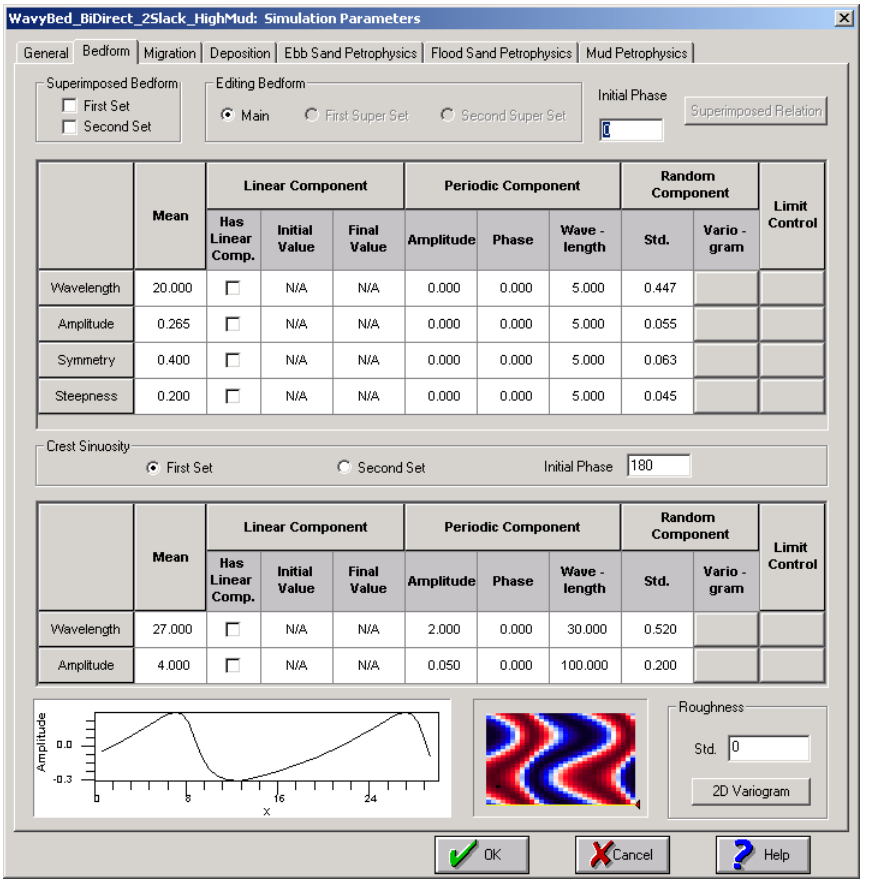

FIGURE 4.4 *The Bedform parameter tab for tidal bedforms. The upper table specifies the bedform shape in cross-section and the lower table in plan view.*

The shape of the bedform (e.g. ripple or dune) is given by a sine curve (figure 4.4). The wavelength and amplitude (half the bedform height) are then related to the number of cells in the particular direction. Symmetry (value between 0 and 1 where 0 is symmetric) and steepness can be used to modify the basic sine curve shape. Symmetry in SBED is expressed differently from that defined in Reineck and Singh

(1980) and McKee (1965) (see section 2.2.2.2). Roughness on the bedform can be modelled by a standard deviation and a 2 D variogram. A sine curve is also used to express the plan form shape of the bedform (lower part of figure 4.4) with a wavelength and amplitude. In addition to the main bedform, superimposed bedforms can be included. This is necessary in order to model out-of-phase ripples (see figure. 2.7), by letting the main and superposed bedforms have a 90° phase difference in the planview.

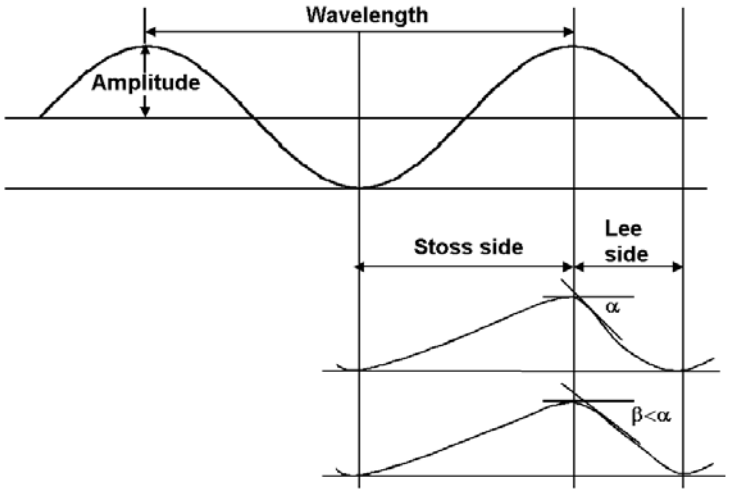

FIGURE 4.5 *Upper part: Symmetric sine curve with terminology used in SBED. Lower part: Asymmetric bedform resembling ripples with different steepness parameter.*

The parallel laminated sand and hummocky cross-stratification models have slightly different bedform tabs compared to cross-bedding and tidal bedforms. The parallel lamina parameter set is composed of a lamina thickness parameter for sand and mud, dip and azimuth to the xy-plane (for both components) and a possibility to include mud layers either regularly or with a Markov transition probability. The hummocky cross-stratification models are defined with a wavelength and amplitude in the x and y direction and the number and thickness variation of sand lamina per laminaset.

4.2.3 Migration parameters

Figure 4.6 shows the tab with the input parameters related to bedform migration. Logically, the migration parameters only apply to the sine curves resembling the migration of the traction bedforms and not the mud laminae. The mud laminae can only “migrate” vertically with a thickness related to the depositional rate (see below).

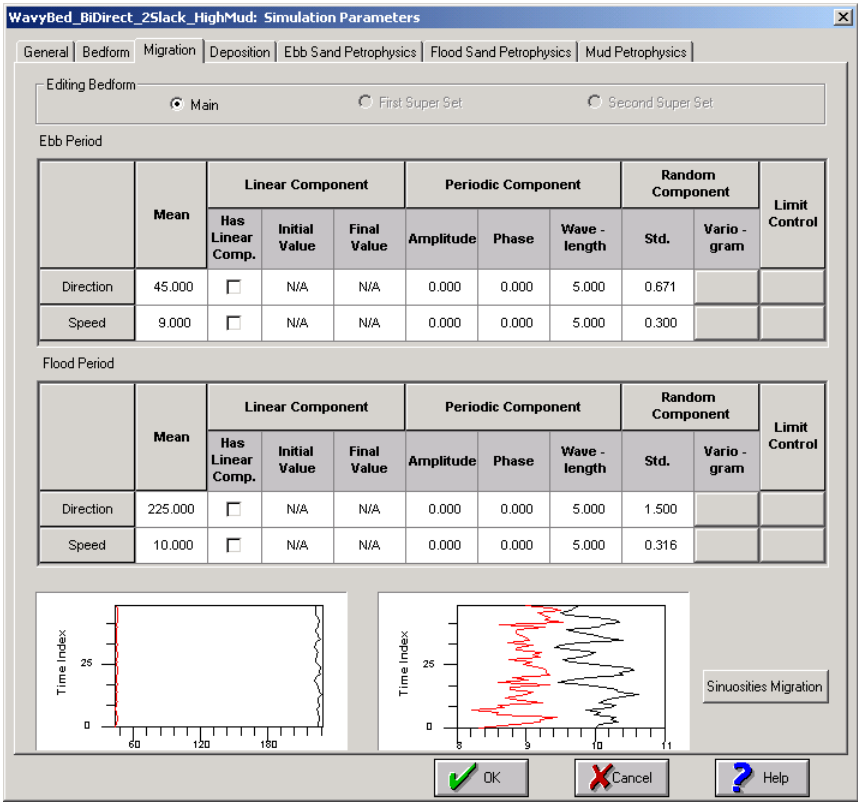

FIGURE 4.6 *The Migration input parameters to SBED tidal bedforms*

In general, there is little information available about bedform migration speed in the literature since it is an un-steady and difficult process to observe (Reineck and Singh, 1980). In the natural environment bedform migration is assumed to take

place in pulses (Allen, 1965, 1970b; Jopling, 1966, section 2.2.2.3). As described above, SBED simulates bedform movement and creation of (sand) lamina as a successive displacement of sine curves in a time series. Based on geometrical considerations, Allen (1970a) and Rubin and Hunter (1982) expressed the bedform migration by a vector V that has a vertical (V_z) and a horizontal (V_x) component (the angle of the vector is labeled ζ in figure 2.10). The equation for the tangent of the angle of climb was then given as:

$$\tan\zeta = \frac{V_z}{V_x} \qquad \textbf{[4-2]}$$

V_z is then the net deposition, while V_x is the rate of bedform migration across the sediment surface (see also equation. 2-17). The migration speed parameter in SBED is related to this vector and defines the displacement direction and magnitude. However, the depositional rate of sand will also influence on the lamina thickness (see below). As it will be shown, for a constant depositional rate, a low migration speed gives steeper angle of climb, thinner lamina and deposition on the stoss side. This is consistent with the super- or sub critical cross-stratification (see page 32). The displacement vector in SBED can however not have a negative angle with respect to the xy-plane and consequently an overall erosional situation (as in figure 2.17 c) cannot be simulated.

Migration direction (figure 4.6) controls the direction of bedform movement relative to the x-axis. Default for tidal bedding templates are that the flood and the ebb sand laminaset migrate in opposite directions (180° phase difference). In some tidal settings, this might not be the case and the parameters can then be adjusted according to the interpreted current pattern.

The same simulation concept is applied for migration of hummocks although the migration characteristics have to be given in x and y direction. The migration process for plane and near horizontal bedforms in the upper flow regime is complex and debatable (e.g. Smith, 1971; Cheel, 1990; Best and Bridge, 1992). There are no parameters for migration of parallel sand lamina and the laminasets are simulated as plane layers stacked upon each other.

4.2.4 Depositional parameters

Figure 4.7 shows the parameter tab with input parameters related to depositional rate and length for the tidal bedding models. Different parameters can be given for

the flood- and the ebb-deposited sand components, but it is not possible to distinguish between the two sand components (laminae) in each laminaset. The depositional rate controls along with the migration speed the thickness of the lamina and the degree of deposition on the stoss side (super critical climbing). It is observed that the specification of depositional length only is necessary when mud is deposited between the migrating stages. It is also observed that when the length parameter is set to unity, five displacements of the sine curve are simulated (i.e. five timesteps are simulated with the length parameter set to 1). With some modifications, the sand and mud laminaset thickness can be calculated as the product of depositional rate and length (see section 4.6).

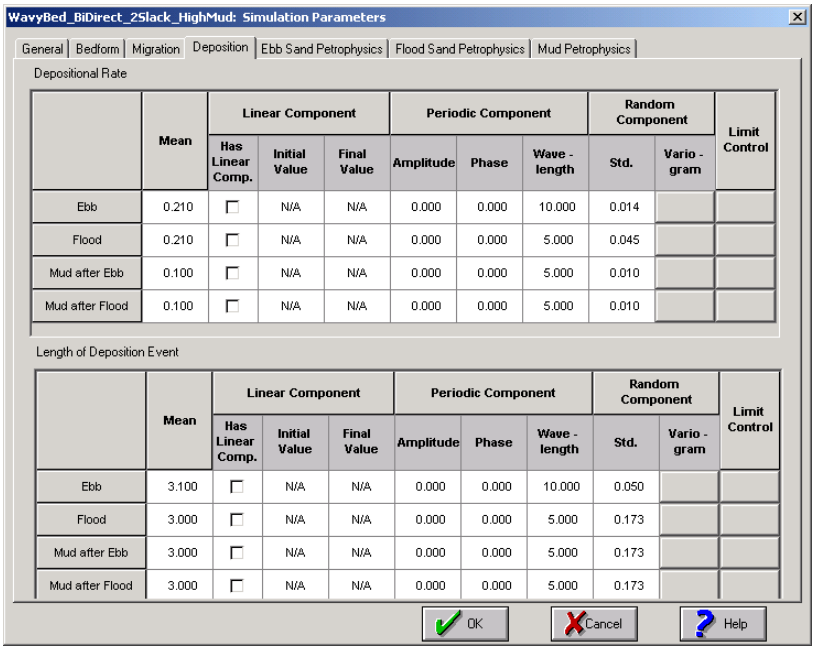

FIGURE 4.7 *The Depositional input parameters to tidal bedforms where the upper part specifies the depositional rate and the lower part the depositional length of the three lithological components.*

4.2.5 Petrophysical parameters

For tidal bedforms, six depositional components can be specified: two “sand” components for both the flood and ebb migrating stage and a mud component deposited after the flood and the ebb. In this study, no evidence was found for having different petrophysical properties for the flood and the ebb sand or the mud. This might, however, be the case in other situations. Consequently, three components are considered here: contrasting sand lamina equal for flood and ebb migrating stages and a mud component. The parameter tab with the petrophysical parameters for the ebb migrating stage are shown in figure 4.8. The parameter tabs for the flood migrating stage and the mud component are similar to this.

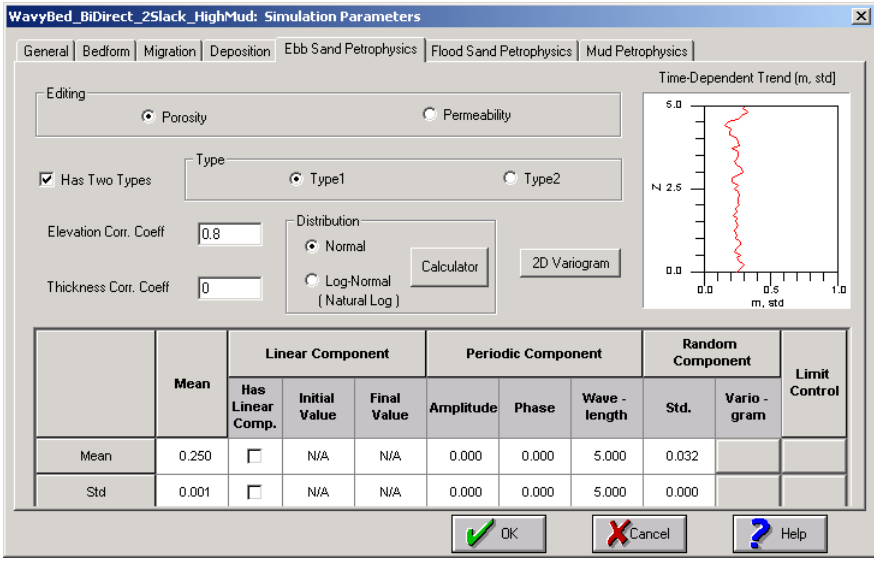

FIGURE 4.8 *The Petrophysical input parameters for the ebb-migrating stage. The tab for the flood migrating stage and the mud is similar.*

Porosity is specified with a mean and a standard deviation for the different components used. The distribution can either be normal or log-normal. The normal distribution is used for porosity. As discussed in section 2.2.2.3 the depositional process of grains on a bedform leeside may influence on the texture and consequently on porosity and permeability. This variation can be simulated with the elevation coefficient. Increasing porosity up-slope is achieved with a higher correlation coefficient.

The opposite trend, as might be the case with lower flow velocities or lower sediment concentration in suspension (Allen, 1965), is not possible to simulate. The height coefficient can be used if it is assumed that the petrophysical property varies with the size of the bedform.

The porosity input parameter given by the user can be either connected or total porosity depending on the data available. The calculated porosity type is then dependant on the input porosity type.

As for porosity, permeability has to be specified with a mean, a standard deviation and a distribution type. Unless otherwise is stated, the log normal distribution is used here. The value of each cell is a homogeneous and isotropic value. Campbell (1967) defines a lamina to be uniform in composition and texture. This implies that the lamina scale permeability is homogeneous, but not necessarily isotropic. Since different trends can be given both along the lamina surface and perpendicular to the lamina, the probable limitation with isotropic cell values is assumed to be of minor importance.

If a correlation between porosity and permeability is found from e.g. core plugs, the correlation coefficient can be specified. As discussed in section 2.3.4 this correlation may be highly scale dependent and should be used with caution.

4.3 Stochastic, linear and periodic components

In the section above, the mean values (m) of the parameters are described. These mean values can be modified to have a linear or periodic trend, or a random component in the direction perpendicular to the simulation surface. This is not directly the vertical direction but is related to the migration vector. Variation in the simulation parameter, V(t), is then modelled as a linear combination of these components. The linear component is modelled as

$$V_L = at + b \qquad \textbf{[4-3]}$$

where V is the parameter considered (e.g. steepness, migration speed or depositional rate), t is the time increment and a and b are constants. When a linear trend is used, the mean value is not specified. The periodic component is modelled by a sine function:

$$V_P = \sin(t) \qquad \textbf{[4-4]}$$

The random component (V_R) is modelled by a one-dimensional Gaussian random function with a mean of zero. A variogram can specify such a function. Each of the parameters described in section 4.2 can then be simulated as a time dependent variable V(t):

$$V(t) = \begin{matrix} m + V_P + V_R \\ V_L + V_P + V_R \end{matrix}. \quad \textbf{[4-5]}$$

The upper equation applies for the case without a linear component while the lower for the case where there is a linear component.

A 2D variogram can be used to specify the spatial correlation structure in each lamina surface. The sill value is taken from the mean standard deviation parameter.

In this thesis, the periodic component is used to model the vertical variation in sand and mud content due to the tidal influence (chapter 5), and the random components (1D and 2D) are used to add (natural) variability.

4.4 Output parameters

The deterministic input parameters specify the time series and determine the bedform shape and evolution with time in addition to the petrophysical properties. The stochastic component then gives the possibility to generate equally possible realizations. Depending on the output-files selected in the General tab (figure 4.2), a realization of the geometry, porosity and permeability is obtained. These represent then one realization of the near wellbore model. The geometry grid where each cell represents one of the components will herein be refered to as the geometrical or sedimentological model.

4.4.1 Geometry Grid

Figure 4.9 shows a realization of the geometry grid of a SBED model. The flood and ebb migrating bedforms with mud (dark grey) in-between are clearly visible. The flood and the ebb sand laminasets are composed of two sand lamina types (different grey shadings). The grid lines are removed for clarity, but as described above they are irregular in vertical direction and follow the lamina surfaces.

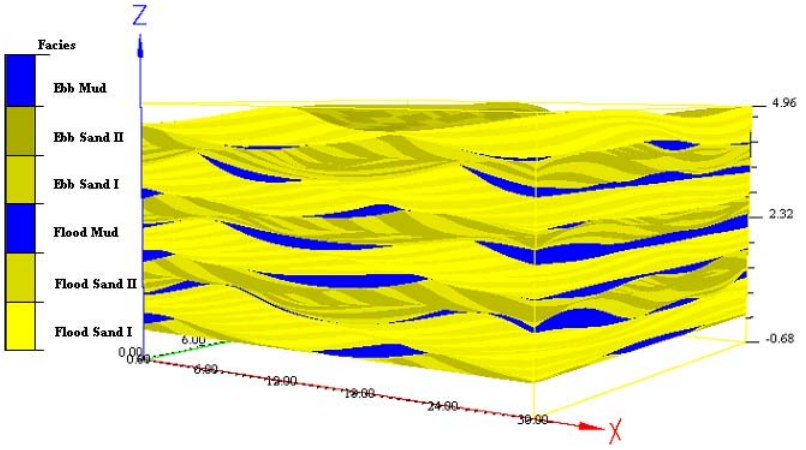

FIGURE 4.9 *An example of one realization of the geometry. The model dimensions are: x=30 cm, y=30 cm and z=5cm. The vertical scale is exaggerated three times*

This particular realization consists of 283500 cells (approximately 30 by 30 by 5 cm), which is a low number compared to the models generated in this study. This high number of cells both indicates an advantage and a limitation with the modelling tool: to capture the variability present, a large number of cells are required, but many cells also take up large disc space and can be time consuming to simulate. To illustrate this, figure 4.10 shows the disc-space required for a similar model as in figure 4.9 as a function of the model size (number of cells: $N_x * N_y * N_z$).

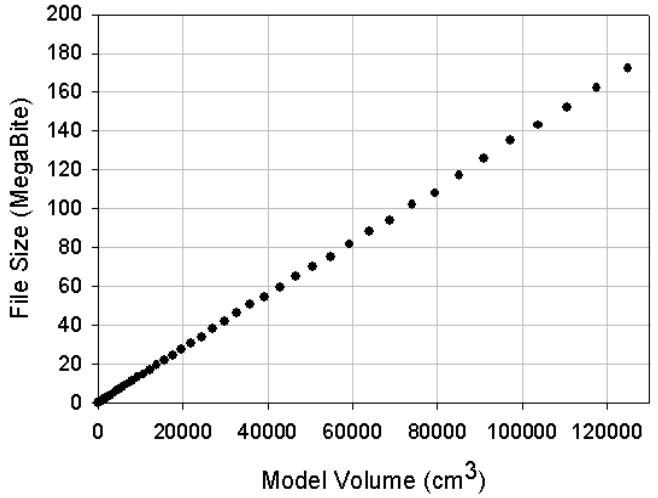

FIGURE 4.10 *An Illustration of the required disc-space with increasing model size (increasing number of cells in the realization).*

4.4.2 Porosity and Permeability grids

Porosity and permeability grids can be either regular or irregular. Figure 4.11 shows the porosity realization and figure 4.12 the permeability realization of figure 4.9. We can see that the irregular grid captures the details of the lamina better. An elevation coefficient[1] equal to 0.8 has been given, and the effect is that both porosity and permeability are higher at the crest of the bedform.

1. The elevation coefficient ($\varepsilon[0,1]$) specifies the relationship between the relative height of the bedform and porosity. With a high correlation coefficient there will be higher porosity at the crest of the bedform compared to the trough.

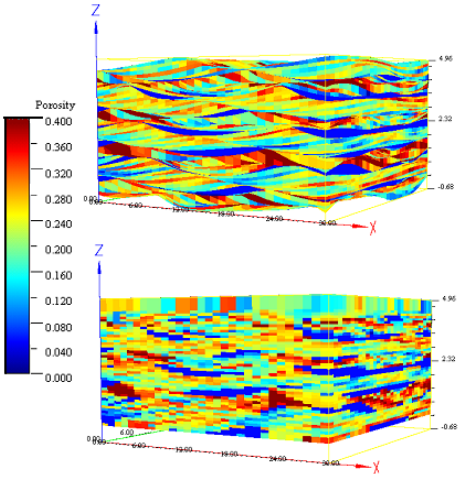

FIGURE 4.11 *Porosity distribution of figure 4.9.Upper grid is irregular while the lower gird is regular. Note the difference in capturing lamina geometries and the effect of the elevation coefficient*

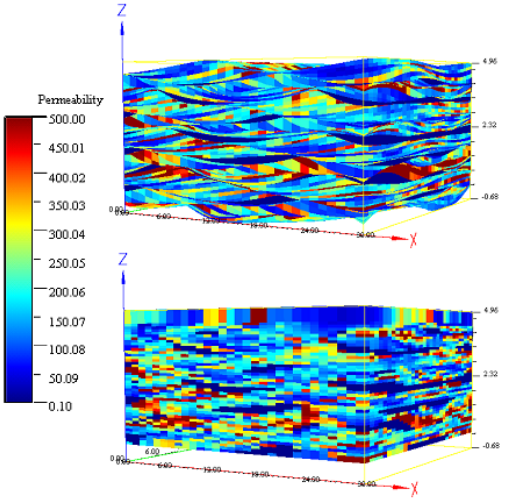

FIGURE 4.12 *Permeability distribution of figure 4.9. Upper grid is irregular while the lower gird is regular. Note the difference in capturing lamina geometries and the effect of the elevation coefficient.*

Figure 4.13 shows a histogram of the porosity output values (all grid cells) and the input (normal) distribution. This confirms that the input distribution is equal to the output, however, due to the stochastic parameters, some variations are expected between realizations. The same cell values are plotted in figure 4.14 for permeability. The random component described above, is then used to describe the variability of the mean and standard deviation of the input curves.

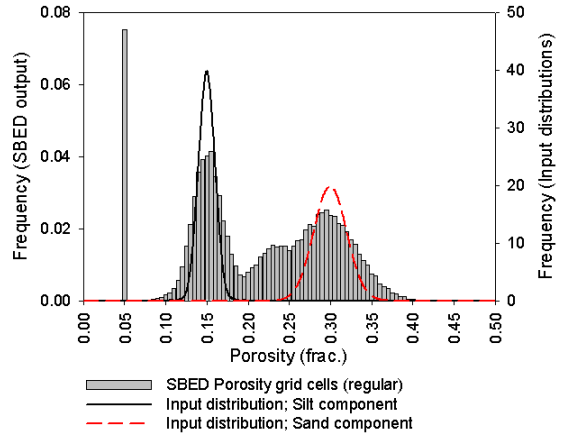

FIGURE 4.13 *Comparison of porosity input and output distributions from figure 4.11 (regular grid). The mud porosity was set to a constant value of 0.05*

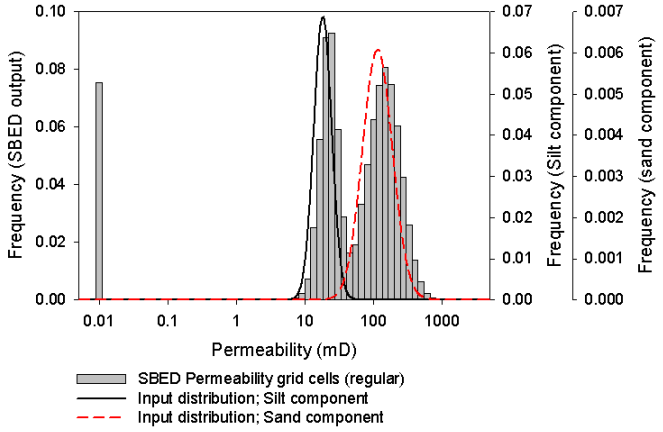

FIGURE 4.14 .*Comparison of permeability input and output distributions from figure 4.12 (regular grid). The mud permeability was set to a constant value of 0.01 mD*

4.4.3 Effective petrophysical properties

Built into SBED is a code to calculate effective petrophysical properties. However, the petrophysical grids can be exported to other simulation programs for evaluation (e.g. Eclipse). The built-in simulator uses a sealed sided pressure solver (Renard and Marsily, 1997) (see also section 2.3.5.2 for a discussion). The result gives the diagonal terms of the permeability tensor (k_{xx}, k_{yy} and k_{zz} hereafter labeled k_x, k_y and k_z). The porosity of the realizations is calculated as the arithmetic average of cell values. As discussed in section 2.3.5, there are a few cases were the effective permeability can be calculated exactly. For plane, infinite layers the arithmetic average is equal to the effective horizontal permeability while the harmonic average is equal to the vertical permeability. Figure 4.15 shows that the sealed sided pressure solver gives the correct effective permeability in this case.

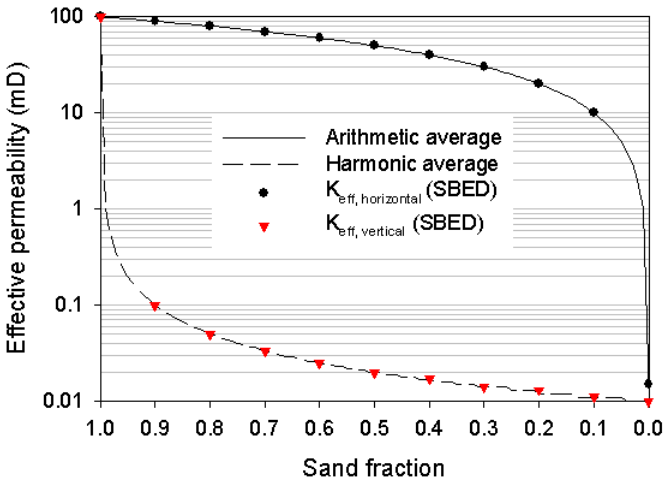

FIGURE 4.15 *Comparison between calculated permeability (arithmetic and harmonic average) and the result from SBED in the case of plane layers.*

The routines incorporated in the SBED code for calculation of effective permeability is well known to give good results in many cases. It is also known that when the correlation lengths approaches the size of the model domain, no-flow boundaries can influence on the calculation. Periodic boundary conditions are shown to give more exact results in such cases (Pickup et al., 1994; Durlofsky, 1991). Such a code was not available in this study. Therefore, only the built-in simulator is used.

The time consumed for the calculation of effective permeability (upscaled permeability) increases with number of grid cells (figure 4.16), and it seems to increases when larger fractions of low permeable components are present (not shown). Because of limitations in the computer power, this will limit the size of the model (i.e. the number of cells in the model) that can be evaluated.

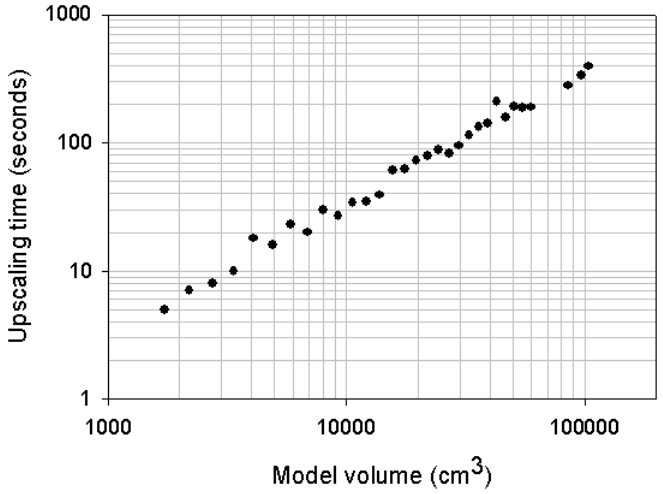

FIGURE 4.16 *The time used to calculate an effective permeability (upscaling time) as a function the number of cells in the grid (model volume).*

4.4.4 Sub-grid

A useful option in the tool is to sample or extract smaller parts of the full grid. These are called sub-grids and will be used extensively in chapter 7 when evaluating how porosity and permeability vary with sample volume. The size of the sub-grid is necessarily related to the dimensions of the grid-cells. Figure 4.17 shows two sub-grids and the full size realization.

I

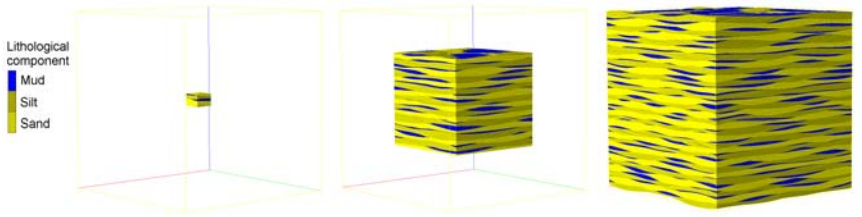

FIGURE 4.17 *Illustration of sub-grids from a realization.*

4.5 Discussion of the SBED tool

A review of different geomodelling methods was given in 4.1. There exist few, if any other, commercially available modelling tools that are designed to specifically model the bedform scale in the near wellbore region. It is therefore difficult to compare SBED with other modelling methods. Nevertheless, there are both advantages and limitations with this tool as will be discussed below. From a practical point of view, there are also some challenges when trying to use the code to model real sedimentary structures with a given distribution of porosity and permeability.

4.5.1 Advantages

The first and obvious advantage with SBED is that it considers sedimentary structures in a way few other modelling tools do. It should be clear from the discussion in section 2.3 that sedimentary structures and the petrophysical distribution at this scale affect the effective properties at a larger scale. The distribution of the different components and their petrophysical properties are given by a spatial correlation structure and the deterministic parameters, and are thus not a result of a random process. This assumption is reasonable for a sedimentologist that regards sedimentation processes as a, in theory, predictable process. The link between the sedimentary structure and the petrophysical property is regarded as an advantage since this has been observed using high-resolution probe-permeameter measurements (see 2.2.2.4). The possibility to evaluate different portions of the model with respect to effective properties is also considered an advantage. Finally, although the generated models can demand large disc-space and can be time consuming to upscale, one can generate many realizations of a range of different bedding structures much easier

than using real outcrop or core data. This, of course, assumes that the synthetic models, within certain limits, are representative of the real rock.

All the parameters controlling the bedform shape and evolution in time and the petrophysical properties have to be specified by the user. This means that the modelling tool is no “black-box” that generates structures or petrophysical distributions not specified by the user. As will be shown in the next sections, the input parameters and their effect on the output are well understood and can be used to generate realistic models of sedimentary structures.

4.5.2 Limitations

The main limitation of SBED is that it approximates the depositional process with displacement of a sine curve. This means that the actual deposition and migration process, as discussed in section 2.2.2.3, is not simulated and that sedimentological unrealistic structures easily can be generated. It is also quite clear that modelling a real bedform in space and time with a sine curve has to be an approximation. Although the overall shape can be resembled with this method, all the natural variability is difficult to incorporate with the stochastic component described above. Following are some ripple types and situations that are difficult to simulate with the SBED code; 1) isolated ripples (formsets) in lanes in a muddy background, 2) splitting and re-joining of the ripple crests, 3) ripples with migration vector below or parallel the horizontal plane and 4) depositional rate and length cannot be specified for the two lamina types (e.g. silt and sand) but only for the flood or ebb migrating stages. In general, it can be stated that there is a tendency to create too simple structures compared to the real situation.

Both the isotropic petrophysical distribution and the limitations with the upscaling method are discussed above.

Other factors that yet cannot be simulated directly in this tool are: 1) compaction, 2) diagenesis and 3) fractures. These factors will influence the petrophysical properties. However, compaction and some diagenetic effects can be included implicitly through the petrophysical input distribution and correlation structure.

4.5.3 Challenges

The geometrical input parameters to SBED mimics the bedform shape and evolution with time. When using core data to create a near wellbore model, the result of the depositional process is observed. Consequently, the largest challenge when

using a modelling tool like SBED is to obtain the input parameters. The core has to be parameterized in a way that enables the user to ensure that the models made are realistic. With a realistic model, it is meant a model that resembles the natural deposit. In the next section, a set of plots is shown that enables the user to select a set of input parameters based on core observations.

Although there is a good knowledge about the different input parameters, some additional adjustments often have to be made. Some understanding of sedimentary structures is then needed. The approach used in this thesis will be to measure assumed relevant geometrical statistics on the core and with the help of the plots in the next section, find the correct input parameters. Chapter 5 will give more details about this approach and how it was used to develop bedding models for the selected interval of the Tilje Formation.

The permeability and porosity values (mean, standard deviation and correlation structure) are specified for each lamina type. Unless probe-permeameter equipment is available (that has a tip size less than the lamina thickness), it is challenging to obtain the input distribution for porosity and permeability. The core plugs represent an average of all these three components and in chapter 6 a method will be used that takes this into account when finding the input parameters for porosity and permeability at the lamina scale.

4.6 Sensitivity study of model parameters and practical transformations

From a scientific, and a practical, point of view it is important to have a good understanding of the input parameters and their effect on the output files. The user guide for this modelling tool gives a short and technical description of the model parameters and these were described in section 4.2 to 4.4. However, only limited information is given about how these parameters can be obtained (e.g. from cores or outcrops) and how the different parameters affect the bedding and lamina geometry (e.g. shape and thickness of lamina and laminaset).

4.6.1 Method

It can be assumed from percolation concepts that the geometry of the sand and mud laminasets controls the petrophysical properties and especially the k_v/k_h ratio at the bedding scale in tidal deposits. It is therefore important to evaluate which parameters affect the geometry and distribution of the mud layers. Naturally, also the petrophysical input parameters will affect the effective properties, and this will be

explored in chapter 8. Here, focus will be on understanding the geometrical input parameters in general and especially with respect to the continuity of the mud layers.

There are more than 200 geometrical input parameters that can be specified in SBED. Evaluating all these parameters at 3 levels, in a standard experimental design, would require more than 10^{100} experiments. Even if only the 64 mean components are evaluated, about 10^{30} different experiments have to be performed in order to use every possible combination of the three levels. This is of course impossible to do, and a selection of the parameters that will be evaluated has to be done. The selection is based on some experience with the modelling tool. The study is by no means meant to be exhaustive and can be a subject for further investigation. It is further assumed that the following results are detailed enough to understand the parameters that control lamina, laminaset and bed geometry with emphasis on continuity of the mud layers, and to develop the interval specific models in chapter 5 and the general tidal bedding models in chapter 7.

Two base case models will be used: one for a cross-laminated sand and one where mud is present between bi-directional sand laminaset. The first model will be used to explore the parameters control on the geometry of the sand layers and the lamina, while the other base case model will explore the factors influencing the continuity of the mud layers. The base case models are invariable in the y-direction and with no stochastic component. It is appreciated that the base case models are simplified compared to real sedimentary deposits. Simple models are, however, valuable when evaluating the effect of parameter changes. The relations found below will still be useful when building more complex bedding models in chapter 5.

4.6.2 Results

The results from the analysis of the cross-laminated models are meant to give an understanding of the parameters that control the geometry and internal characteristics of the sand laminaset.

The *wavelength* of the bedform is straightforward to understand and denotes the horizontal number of cells of one bedform surface. Figure 4.18 shows four different realizations of models with different wavelengths, where all the other parameters are constant. The *symmetry* of the bedform is given by a value between 0 and 1 where 0 denotes a symmetrical bedform. This is in the opposite sense to that proposed by Reineck and Singh (1980). Figure 4.19 shows the results for models with different symmetry value. The *amplitude* parameter gives half the bedform height,

and when the wavelength is kept constant, decreasing amplitude decreases the lee side slope (lee side lamina tend to be longer and more tangential) for a constant wavelength. The steepness parameter changes the slope of the upper part of the lee side lamina. Figure 4.20 shows the effect of changing the amplitude and the steepness simultaneously.

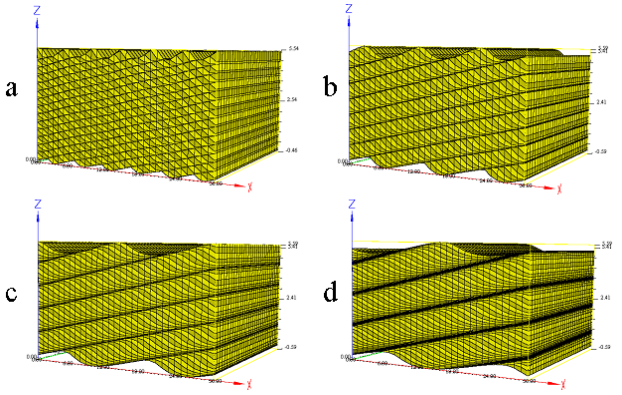

FIGURE 4.18 *Effect of varying the wavelength (WL) of main bedform in SBED. a) WL=5, b) WL=10, c) WL=15 (base case) and c) WL=20.*

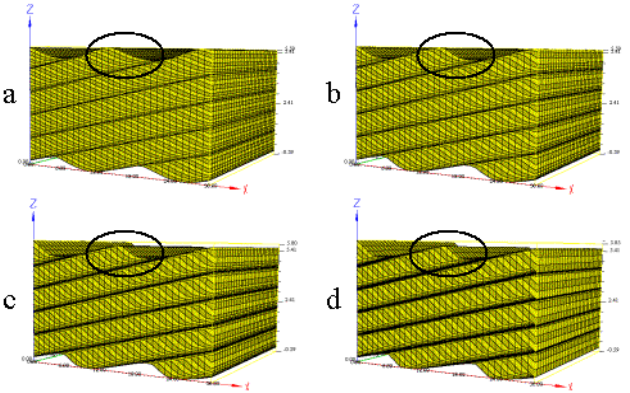

FIGURE 4.19 *Effect of varying the symmetry parameter (SY) of main bedform in SBED. a) SY=0 b) SY=0.4 (base case), c) SY=0.6 and c) SY=0.8.*

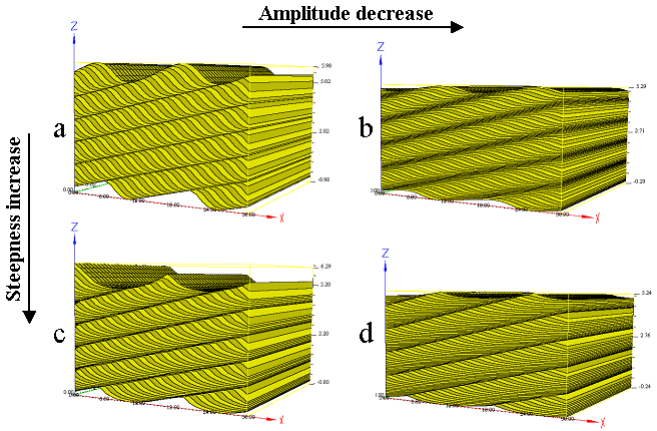

FIGURE 4.20 *Effect of varying the amplitude (A) and steepness (ST) parameters. a) A=0.5, ST=0, b) A=0.15, ST=0, c) A=0.5, ST=1, d) A=0.15, ST=1*

From a sedimentological point of view, these parameters will, in general, be correlated, especially the amplitude and the wavelength. The steepness will depend on the depositional process on the lee side (see section 2.2.2.3) and the symmetry on the prevailing current patterns.

The migration speed denotes the direction and magnitude of the displacement vector for the sine curves. Figure 4.21 shows the effect of increasing the migration speed, keeping the other parameters constant. A decreasing migration speed increases the amount of simulated sediment deposited on the stoss side (and hence increase the angle of climb) as well as decreasing the lee side lamina thickness. Also an increase in depositional rate on the sand component increases the lamina thickness and increases the angle of climb (more deposition on the stoss-side) (figure 4.22). This means that the aggradation rate is simulated with these parameters. Figures 4.23 and 4.24 show the relation between lamina thickness (observed on a simulated bedding model) and migration speed and depositional rate, respectively. Figures 4.25 and 4.26 give the relation between sand laminaset thickness and the migration speed and depositional rate of sand, respectively, while figure 4.27 shows that the angle of bedform climb also is related to the this input parameter.

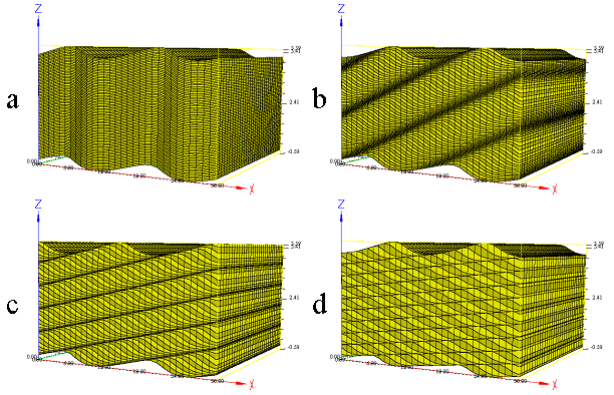

FIGURE 4.21 *Migration speed increasing from a to d.*

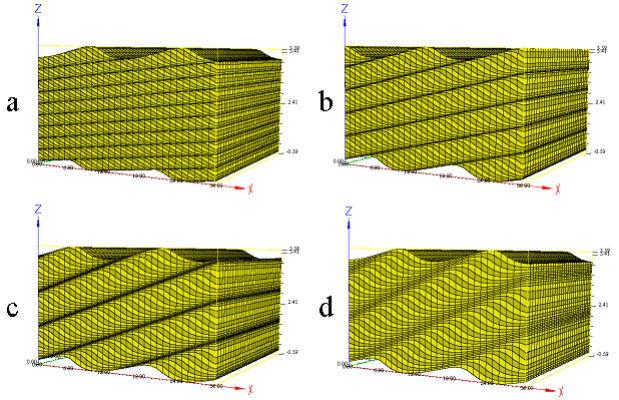

FIGURE 4.22 *Depositional rate increasing from a to d.*

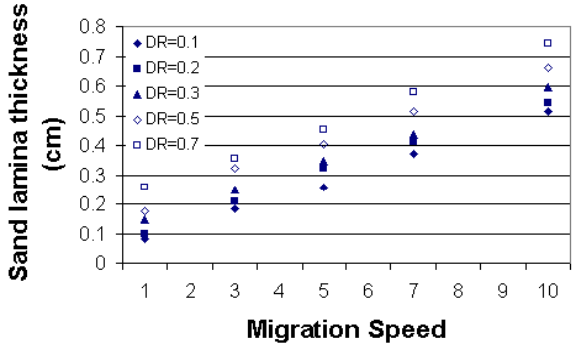

FIGURE 4.23 *The observed relation between migration speed and sand lamina thickness for different depositional rates (DR).*

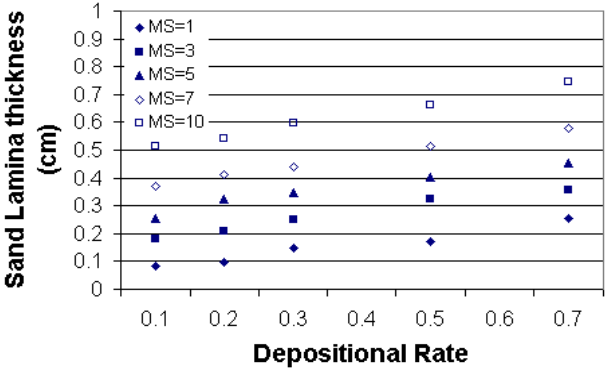

FIGURE 4.24 *The observed relation between depositional rate and sand lamina thickness for different migrations speeds (MS).*

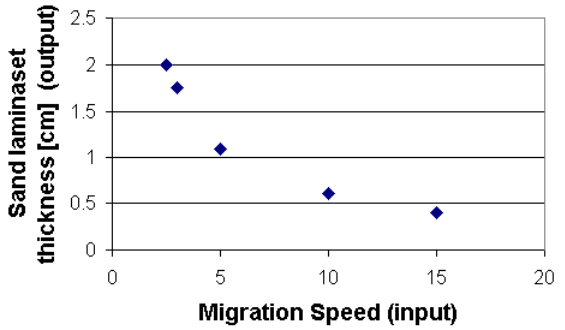

FIGURE 4.25 *The observed relation between migration speed and sand laminaset thickness.*

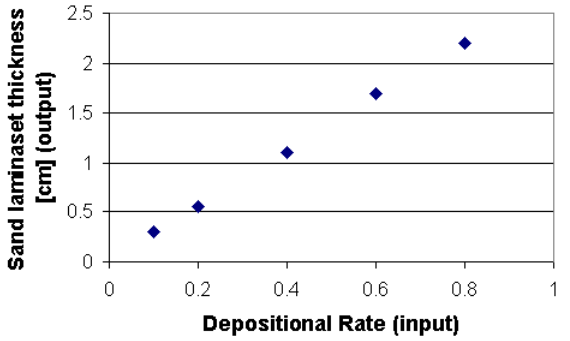

FIGURE 4.26 *The observed relation between depositional rate (sand) and sand laminaset thickness when the migration speed is constant.*

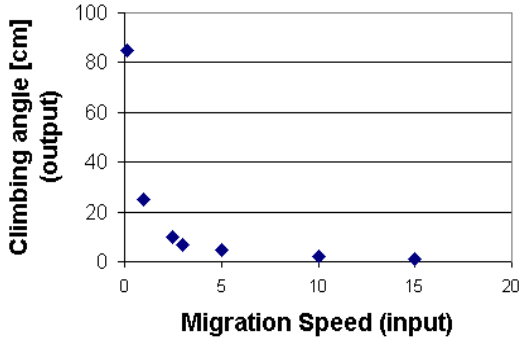

FIGURE 4.27 *The observed relation between migration speed and the angle of bedform climb.*

When mud is present between bi-directional migrating sand laminasets, the depositional length (of sand and mud) gives the number of lamina deposited in each migrating stage. The lamina thickness is unaffected. A depositional time of 1 results in five displacements of the sine curve and hence five lamina. Both an increase in depositional rate and length of sand will given an increase in the sand laminaset thickness (figure 4.28). When increasing the depositional rate, lamina thickness increases in addition to more deposition on the stoss side. Increasing the depositional length produces bedforms that climb, whether super- or sub-critical depending on the depositional rate, with a constant lamina thickness.

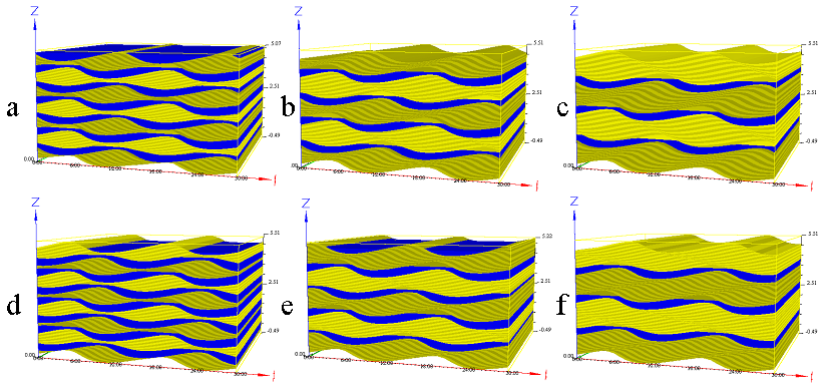

FIGURE 4.28 *Effect of increasing depositional rate (a-c) or length (d-f). In the first case only the sand lamina thickness increases, while in d-f, climbing bedforms are produced. The choice of control parameter to adjust sand laminaset thickness should reflect the observed or interpreted pattern from core or outcrop.*

Having reviewed some of the control parameters and explored how they affect the bedding models gives basis to set up a workflow that can be used in a modelling study. From a core (photo) one can, depending on core quality and orientation, observe and quantify the following features: 1) sand lamina thickness 2) sand laminaset thickness and vertical variation, 3) sand lamina geometry (e.g. angle and shape of lee side lamina), 4) climbing angle for sand laminaset and 5) mud laminaset thickness and vertical variation. In addition, an interpretation of the bedding type can be done which implies some information about the bedform three-dimensionality. To create models based on such core statistics, one then has to relate the observed parameters to the input parameters. From the results above, some conceptual relations between the input parameters and sand lamina thickness, sand laminaset thickness and mud laminaset thickness can be given:

$$SandLaminaThickness = f(MigrationSpeed_{Sand}; DepositionalRate_{Sand})$$

$$SandLaminaSetThickness = f(MigrationSpeed_{Sand}; DepositionalRate_{Sand} \quad DepositionalLenght_{sand}) \quad \textbf{[4-6]}$$

$$MudLaminaSetThickness = f(DepositionalRate_{Mud}; DepositionalLength_{Mud})$$

The following workflow is proposed for modelling tidal bedforms in SBED; 1) Set the mean migration speed for sand constant, 2) Calculate the depositional rate parameter from observed sand lamina thickness (figure 4.24), 3) Calculate depositional length of sand from observed sand laminaset thickness (figure 4.29), 4) from observed mud laminaset thickness calculate depositional rate and length of mud (figure 4.30), 5) use periodic variation on migration speed to simulate lamina thickness variations in each sand laminaset and 6) use periodic variation on depositional length for sand and mud to model vertical variation in sand laminaset and mud laminaset thickness.

The following plots can be used to relate the observed statistics to input parameters. Figure 4.29 shows how the depositional length of sand can be used to simulate the sand laminaset thickness for different depositional rates (that determines the sand lamina thickness; figure 4.24). The simulated thickness of mud is simply the product of the depositional rate and the depositional length of mud. However, as new bedforms migrate over previously deposited mud layers, some of the simulated surfaces are removed (see section 4.1.3.2). Thus the resulting (observed) mud laminasets are thinner than the calculated thickness (figure 4.30).

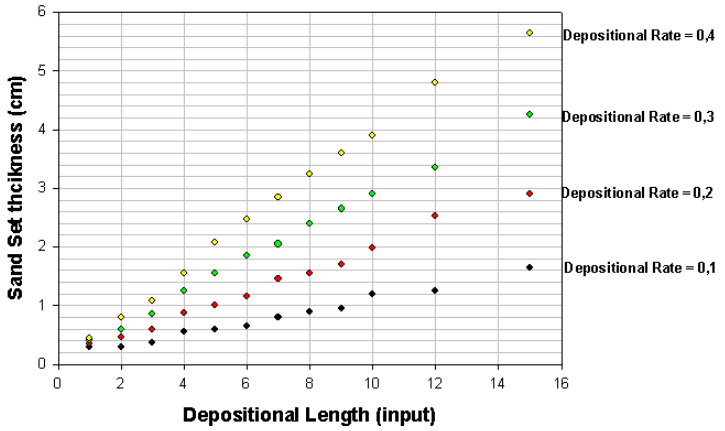

FIGURE 4.29 *Determination of input depositional length for different sand laminaset thickness (for different sand depositional rates).*

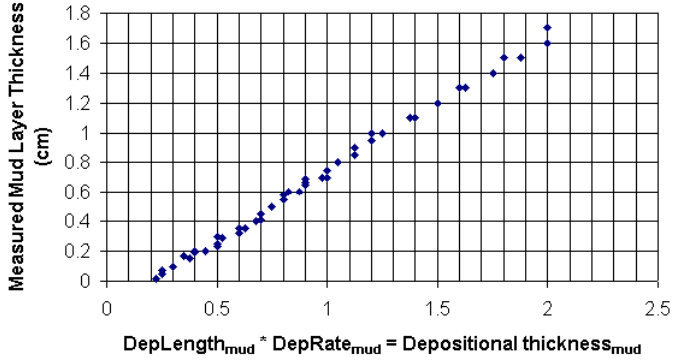

FIGURE 4.30 *The product of depositional rate and length for the mud component gives the observed mud laminaset thickness corrected for "erosion". Note that mud laminaset thinner than 0.2 (mm with the specified dimensions) is not preserved.*

4.6.3 Implications for modelling workflow

Using sine curves, flat surfaces and gaussian distributions will inevitably be an approximation for modelling the observed, complex sedimentary structures. However, the overall geometry and to some extent the lamina characteristics, can be captured adequately. The SBED modelling tool consists of a large number of parameters and even though it is well known what each parameter controls, interactions between them are less studied. It will always be important to use sedimentological knowledge when judging the output files since the code can create unrealistic sedimentary structures.

Specific modelling of the near wellbore volume based on core are in general difficult due to several aspects:

1) the observations are in 2D while the parameters are in 3D

2) some parameters required are difficult to measure from the core that also might influence on the effective permeability (e.g. crest sinuosity)

3) validating the simulated 3D models is not straight forward from 2D data.

Some constraints on the control parameters can be obtained from good outcrops or flume tank studies, particular regarding lateral variability. This will still be a source of uncertainty that will be discussed more in chapter 5 and 6. Consequently, using core data to produce a near wellbore model of tide-influenced deposits, focus should be on sand and mud fraction and their spatial correlation and connectivity. This implies in part an interpretation step, but should be based on measured data.

CHAPTER 5

Near wellbore sedimentological model of lower Tilje Formation

The lower part of the Tilje Formation in a well in the Heidrun field is selected as an interval for detailed analysis in this thesis. Here, a workflow is proposed on how to create and validate a near wellbore model of the bedding types encountered in this interval based on the results from chapter 4. An outcome of the detailed analysis was a revised interpretation of some sedimentary structures in one of the lithofacies.

5.1 Sedimentological description of selected interval

The late Pliensbachian to early Toarcian Tilje Formation (Dalland et al., 1988) subcrops on the Halten Terrace offshore mid-Norway and contains several large hydrocarbon fields (figure 5.1). Focus in this thesis will be on the Heidrun field since the Tilje formation is relatively shallow buried (~2500m) and not severely affected by diagenesis. The formation has previously been interpreted to be deposited in a shallow marine setting with varying degree of tidal influence (Gjelberg et al., 1987; Pedersen et al., 1987; Dreyer, 1992, 1993). More recently, Martinius et al. (2001) interpreted the lower part of the Tilje formation (Tilje 1.2 and most of Tilje 2) to have been deposited in an estuarine system while the upper part (Tilje 2 to Tilje 6) in a tide- and fluvial-dominated delta-like system. Martinius et al. (2001) divided the Tilje Formation into ten facies associations (figure 5.2) of which four of them will be in focus here: Facies association 1, Facies association 3, Facies association 4 and Facies association 7.

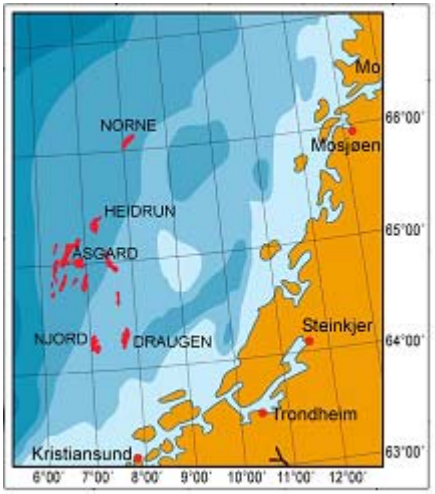

FIGURE 5.1 *Location of the Heidrun field off shore mid-Norway on the Halten Terrace. From Martinius et al. (2001).*

The main focus here is to evaluate the influence of sedimentary heterogeneities on the petrophysical properties and especially on the k_v/k_h ratio. The lithofacies defined for the Tilje Formation by Martinius et al. (2001) were developed to be generally applicable for the Tilje Formation on the Halten Terrace. Occasionally these lithofacies contain additional, smaller sedimentary features that possible can affect k_v/k_h and that should be included in a detailed analysis as here. It is thus focused on the elements that influence on the petrophysical properties, and in tidal deposits, the thickness, lateral correlation, and spatial distribution of the mud layers are of significance at the bedding scale (Martinius et al., 1999).

The following description and interpretation of lithofacies is taken from Martinius et al. (2001). Where necessary, these are subdivided into bedding types that here is termed subfacies. Each such subfacies is then modelled separately and labeled by the lithofacies number and an abbreviated descriptive term of the bedding type. Figure 5.3 shows the sedimentological log of the selected interval with the lithofacies boundaries, and figure 5.9 a table of the lithofacies and the subfacies modelled in this study (see section 5.3). The selected interval consists of the stratigraphic units Tilje 1.1 - 2.1 and focus will be on the interval between 2594.7 m and 2619 m (core depth). The selected well is an exploration well and drilled nearly vertical.

.

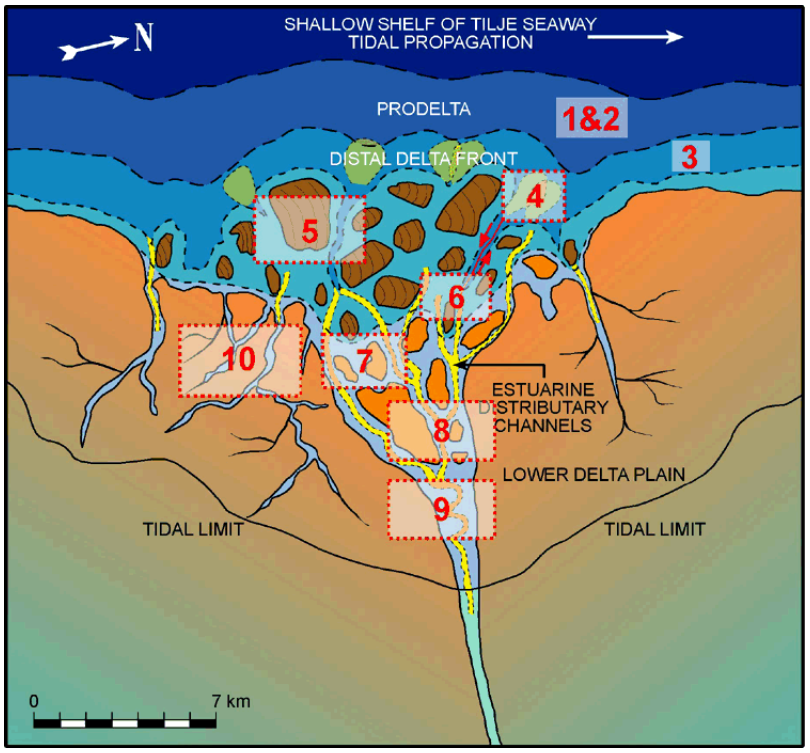

FIGURE 5.2 *Sketch of the conceptual depositional model for the studied interval of the Tilje Formation. The boxes and the numbers indicate the position of the different facies association (FA's). Focus here will be on FA 1, FA 3, FA 4 and FA 7. From Martinius et al. (2001)*

Facies Association 1: Storm-influenced prodelta facies

This facies association (FA1) consists in general of three lithofacies (LF): 1.1 Distal shoreface, 1.2 Storm beds and 1.3 Hummocky (Martinius et al., 2001) and is present in the Tilje 1.1 in the Heidrun field. Lithofacies 1.1, which is a muddy, very fine-grained, strongly bioturbated sandstone is not present in the studied interval.

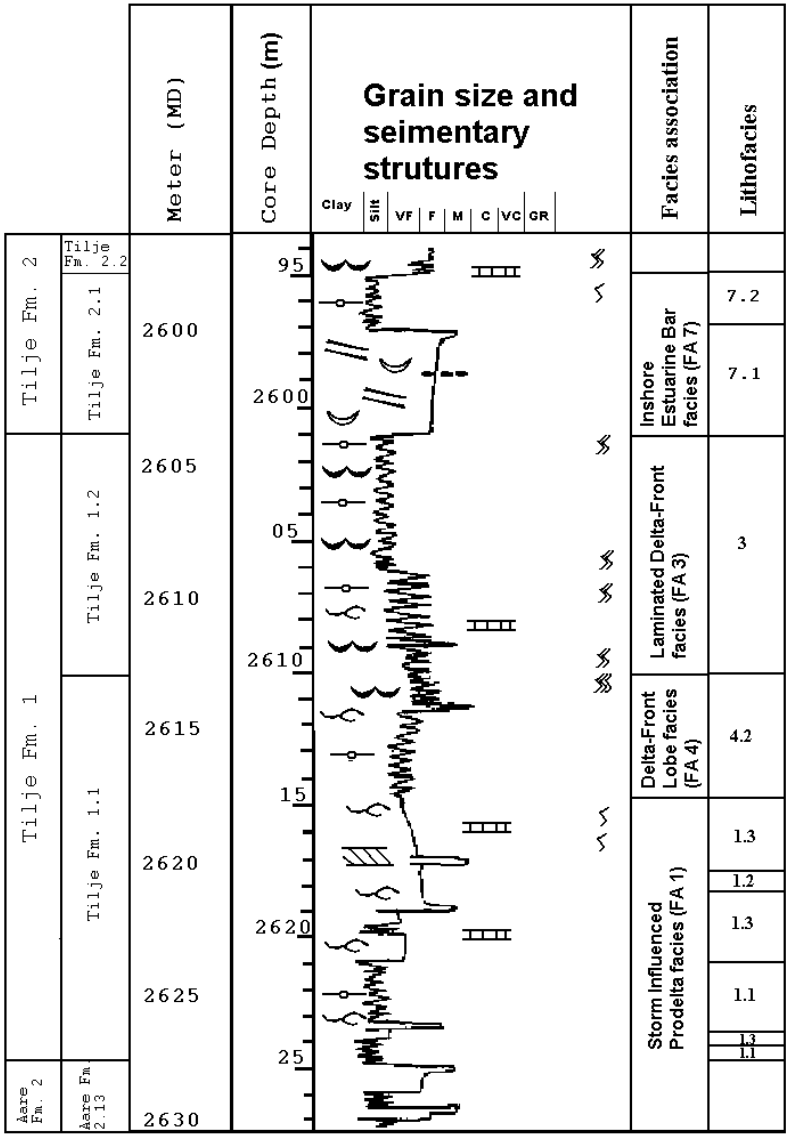

FIGURE 5.3 *Sedimentological log of the selected interval in the lower part of the Tilje Formation (Heidrun Field).*

LF 1.3 is a moderately to well-sorted homogeneous and fine-grained sandstone often showing hummocky cross-stratification. LF 1.2 is characterized by a well-sorted, medium- to fine-grained sandstone sets with a sharp, parallel-laminated base and ripple-laminated top and found interbedded with LF1.3. Martinius et al. (2001) have interpreted LF1.2 as proximal storm beds whereas amalgamation of hummocky cross-stratified sets are interpreted to represent deposition during episodic storm events on the lower shoreface. Facies association 1 is interpreted to have been deposited in a prodelta setting between storm wave base and fair-weather wave base.

In the selected interval, FA1 is 4.25 m and dominated by LF1.3 (92%). LF1.3 is here further divided into three subfacies: one with lithological clean hummocky cross-stratified sand (LF1.3_HCS), one with relatively thick mud layers between the HCS sets (LF1.3_HCS_Mud) and one that are moderately bioturbated (LF1.3_HCS_Bio). These features are assumed to influence on the petrophysical properties and hence need to be represented explicitly. The lamina thickness of the cross-stratified sand are between 0.1 and 0.3 mm and the set thickness vary between 5 and 25 cm. Figure 5.4 shows some examples of the subfacies defined here.

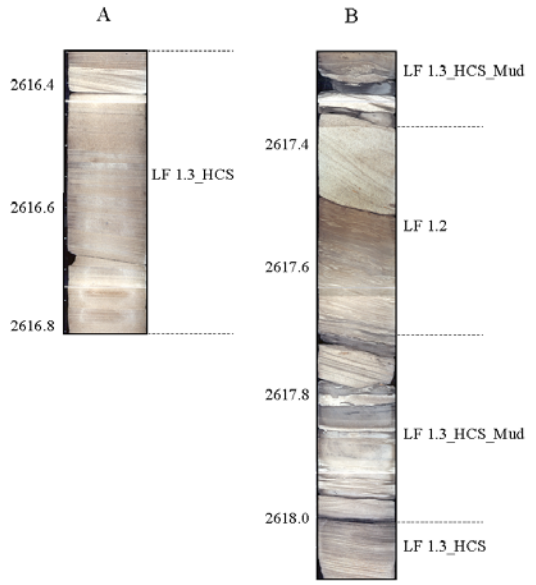

FIGURE 5.4 *Core photo of facies association 1 in the selected interval showing subfacies LF1.3_HCS, LF1.3_HCS_Mud and LF1.2.*

Facies association 4: Delta-front lobe facies

Facies association 4 is found above FA1 in the studied interval and is typified by interbedded fine- to medium-grained sand and mud layers forming a heterolithic deposit. The facies association is divided into two lithofacies based on the thickness and frequency of the mud layers: lithofacies 4.1 with thin and irregular mud layers and lithofacies 4.2 with thicker and more regular interbedding of sand and mud stone layers. Only lithofacies 4.2 is present in the studied interval. The thick mud layers are interpreted to be a result of high-suspended sediment concentrations during one slack-water period, or from amalgamation of mud layers formed during several slack-water periods (Martinius et al., 2001). The sand layers are fine-grained forming wave and current ripples with some indications of tidal influence. Facies association 4 is inferred to have been deposited on low-relief delta-front barforms where LF 4.2 is the distal equivalent of LF4.1.

In the studied interval, LF4.2 is 3.05 m thick and it is divided into three subfacies based on its inferred influence on the petrophysical properties. At the base, two intervals are more mud rich and lenticular to wavy bedded (LF4.2_LTW) while towards the top the sand layers become thicker, the mud fraction is lower and a wavy to flaser bedding is present (LF4.2_WSF). Interbedded these heterolithic bedding types are clean, fine-grained sandstone layers with low angle, plane stratification similar to the hummocky cross-stratified sand layers in the lithofacies below and termed LF4.2_HCS. Descriptive statistics of the heterolithic bedding are found in section 5.3. Figure 5.5 shows some examples of the different subfacies found in this lithofacies.

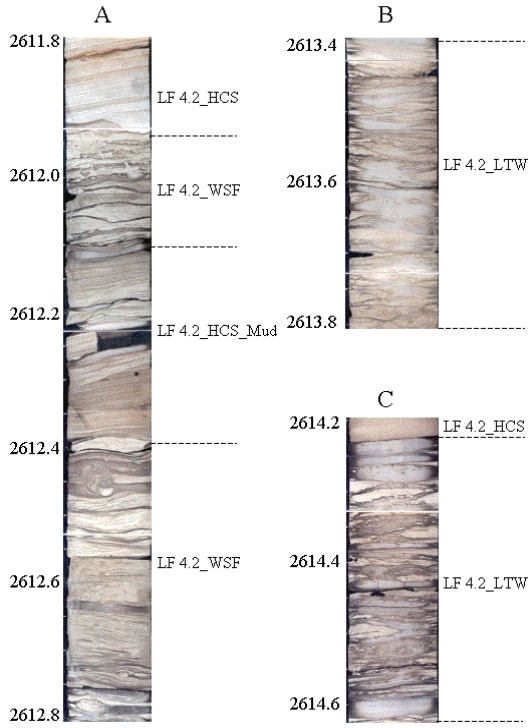

FIGURE 5.5 *Core photo of lithofacies 4.2 in the selected interval showing subfacies LF4.2_WSF, LF4.2_LTW, LF4.2_HCS and LF4.2_HCS_Mud.*

Facies association 3: Laminated delta-front facies

Martinius et al. (2001) recognize one lithofacies for this facies association. That lithofacies is characterized by persistent wavy bedding, with fine-grained sandstone interbedded with approximately equal thick mud layers. Mud layers usually cover single sandstone sets. Both wave and current ripples are present suggesting relatively low energy conditions during deposition. Minor storm events resulting in relatively clean, sharp-based sandstone layers can be present. Couplets are often found in LF3, although Martinius et al. (2001) found no direct evidence of daily tidal cyclicity. It was however assumed that longer-term cyclicities dominate the het-

erolithic bedding structure. This issue will be extensively discussed in section 5.2. Lithofacies 3 is interpreted to have been deposited in a quite-water, mud-rich delta front environment with slow deposition from suspension and sand deposition by traction current. Tidal influence and possible seasonal variability are assumed to be the main influence on the sedimentation pattern.

In the selected interval, LF 3 is 11.1 m thick and consists of a lenticular to wavy bedded unit (LF3_LTW). Beside a minor unit with a hummocky cross-stratified sandstone, further division of the lithofacies is done based on the degree of bioturbation due to its assumed influence on the petrophysical properties. (Unfortunately, using models with bioturbation in a stacked sequence (see chapter 9) is not yet possible. These subfacies are however separated here giving the possibility for inclusion in a later modelling work.) The sand laminasets usually have a sharp boundary to the mud at the base. Occasionally, a transitional boundary is found between the sand laminaset and the succeeding mud. A non-bioturbated interval of LF 3 is used to evaluate the tidal influence. These results will be given in section 5.2. Figure 5.6 shows some examples of the subfacies in LF3 defined here.

Facies association 7: Inshore estuarine facies

A sharp, erosive surface, interpreted to be a sequence boundary by Martinius et al. (2001) separates LF 3 from the above facies association 7. The facies association is divided into a lower lithofacies 7.1 and an upper lithofacies 7.2. LF 7.1 consists of relatively well-sorted, fine-grained, simple flaser-bedded sandstone. It is assumed that both wave and tidal-current process were operating during deposition. LF 7.2 is composed of fine- to coarse-grained sandstone layers interbedded with thicker mud layers forming a wavy bedded heterolithic facies. Occasionally, erosional surfaces with lag deposits are found. The facies association is interpreted by Martinius et al. (2001) to represent the regressive infill of the inshore part of a relatively large but shallow estuary. LF 7.1 represents then the deposits from the deeper, sub-tidal parts of the channel while LF7.2 is interpreted to be inclined, laterally accreted point bars where run-off channels, draining the intertidal flats, created the erosive surfaces with the associated lag deposits.

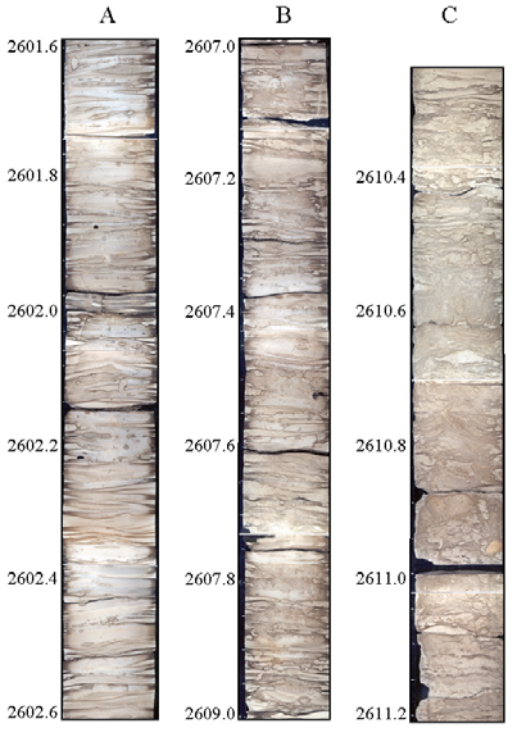

FIGURE 5.6 *Core photo of lithofacies 3 in the selected interval showing A: Non-bioturbated; B: Moderately bioturbated and C: Very bioturbated. All examples of subfacies LF3_LTW with varying degree of bioturbation. However, only the un-bioturbated case (A) is modelled because of limitations in the code (see text).*

The total thickness of facies association 7 is 5.9 m in the selected well where LF 7.1 is 3.4 m. LF 7.1 is further divided into two subfacies where the first reflects the wavy to simple flaser-bedded deposits described above (LF7.1_WSF) and the second a fine- to medium-grained, planar stratified deposits (LF7.1_PPL). A further interpretation of the latter bedding type is not given, but it is assumed that is was deposited in the upper flow regime, and it will be shown that some cyclicity is present in this subfacies. LF7.1_WSF is dominated by thin, (< 2 mm) mud drapes that occasionally cover the ripple crest (e.g. 2598.88) but most often they are only preserved in the ripple troughs (e.g. 2598.65-2598.80). Thicker mud layers (< 1

cm) appear to be irregular spaced (see section 5.3 for statistics) which can be interpreted as fluidized mud deposits.

FIGURE 5.7 *Core photo of lithofacies 7.1 in the selected interval showing subfacies LF7.1_WSF and LF7.1_PPL.*

Lithofacies LF7.2 is divided into a lenticular-bedded subfacies (LF7.2_LTW) and a wavy bedded subfacies (LF7.2_WB) in addition to the coarse (medium to lower coarse) lag deposits (LF7.2_RunOffSand). A 7 cm thick, cemented layer that is assumed to be lateral persistent in the near wellbore volume, is identified and modelled separately (LF7.2_Cement). LF7.2_WB consists of cm thick sand layers that internally show some low angle stratification. The boundaries to the mud layers, that cover individual sand sets are usually sharp, but can be transitional in the top. The sand laminasets in the muddier LF7.2_LTW appears to have the same grain size and sorting as LF7.2_WB. The bedding types in LF7.2 resemble LF3 although the internal stratification in the sand component and the grain size is different. Figures 5.7 and 5.8 show some representative intervals from these two lithofacies.

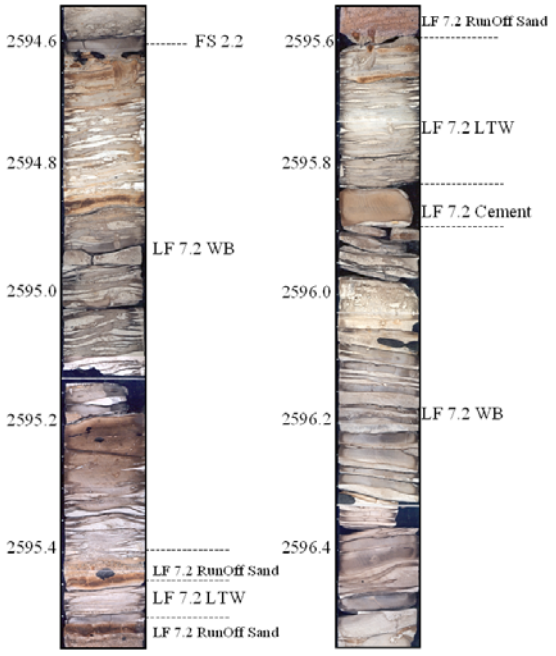

FIGURE 5.8 *Core photo of lithofacies 7.2 in the selected interval showing subfacies LF7.2_WB and LF7.2_LTW in addition to a cemented layer and a coarse sand lag possible deposited in a run-off channel.*

This section has described the sedimentological features of the selected interval in the Tilje Formation in the example well. The interpretation proposed by Martinius et al. (2001) is kept but it was necessary to further divide the lithofacies into subfacies due to its assumed influence on the petrophysical properties. Although the geometrical characteristics (bedding geometry) can be similar for some of the subfacies (e.g. LF4.2_LTW, LF3_LTW and LF7.2_LTW), the petrophysical properties can be different. Based on the description and interpretation here and further quantification of critical parameters (especially mud- and sand-laminaset statistics), near wellbore models are created in section 5.3.

	Top (m)		2594.7
	Base (m)		2619
	Thickness (m)		24.3

Stratigraphy	Top	Base	Thickness (cm)	Sub facies modelled in SBED™	Lithofacies (Martinius et al., 2001)
T2.1	2594.7	2595.4	70	LF7.2_Wavy Bedding	Inshore Estuarine Bar - Heterolithic tidal point bar (LF 7.2)
	2595.4	2595.45	5	LF7.2_"RunOff" Sand	
	2595.45	2595.5	5	LF7.2_LenticularBedding	
	2595.5	2595.63	13	LF7.2_"RunOff" Sand	
	2595.63	2595.83	20	LF7.2_LenticularBedding	
	2595.83	2595.9	7	LF7.2_Cement	
	2595.9	2597.2	130	LF7.2_Wavy Bedding	
	2597.2	2597.75	55	LF7.1_WavyToSimpleFlaser	Inshore Estuarine Bar - Accretionary channel bank (LF 7.1)
	2597.75	2598.6	85	LF7.1_PlaneParalellLamination	
	2598.6	2599.85	125	LF7.1_WavyToSimpleFlaser	
	2599.85	2600.1	25	LF7.1_PlaneParalellLamination	
	2600.1	2600.6	50	LF7.1_WavyToSimpleFlaser	
T1.2	2600.6	2601.15	55	LF3_Lenticular to wavy (moderately bioturbated)	Laminated delta front (LF 3)
	2601.15	2605	385	LF3_Lenticular to wavy (no bioturbation)	
	2605	2608	300	LF3_Lenticular to wavy (moderately bioturbated)	
	2608	2608.9	90	LF3_Lenticular to wavy (no bioturbation)	
	2608.9	2609.25	35	LF4.2_HCS_Mud	
	2609.25	2610.1	85	LF3_Lenticular to wavy (moderately bioturbated)	
	2610.1	2611.7	160	LF3_Lenticular to wavy (very bioturbated)	
T1.1	2611.7	2611.95	25	LF4.2_HCS	Distal delta front lobe (LF 4.2)
	2611.95	2612.1	15	LF4.2_WavyToFlaser	
	2612.1	2612.4	30	LF4.2_HCS_Mud	
	2612.4	2612.9	50	LF4.2_WavyToFlaser	
	2612.9	2613	10	LF4.2_HCS	
	2613	2613.3	30	LF4.2_WavyToFlaser	
	2613.3	2613.95	65	LF4.2_LenticularToWavy	
	2613.95	2614.25	30	LF4.2_HCS	
	2614.25	2614.75	50	LF4.2_LenticularToWavy	
	2614.75	2615.7	95	LF1-3_HCS	Hummocky (LF 1.3)
	2615.7	2615.8	10	LF1-3_HCS_Bio	
	2615.8	2616.15	35	LF1-3_HCS	
	2616.15	2616.25	10	LF1-3_HCS_Bio	
	2616.25	2617.2	95	LF1-3_HCS	
	2617.2	2617.35	15	LF1-3_HCS_Mud	
	2617.35	2617.5	15	LF1.2_LargeScaleX-bed	Storm beds (LF 1.2)
	2617.5	2617.7	20	LF1.2_SmallScaleX-bed	
	2617.7	2618	30	LF1-3_HCS_Mud	Hummocky (LF 1.3)
	2618	2619	100	LF1-3_HCS	
		Total Thickness	2430		

FIGURE 5.9 *Selected interval divided into lithofacies (Martinius et al. 2001) and subfacies modelled in this study.*

5.2 Tidal signatures in Lower Tilje Formation, Heidrun Field

One of the few diagnostic criteria for recognizing tidal deposits is the presence of different orders of cyclicities (Nio and Yang, 1991). To reveal if such multi-order cyclicity is present in the interval, two time series techniques have been used on data describing the sand and mud laminaset thickness and the sand-fraction in LF3.

The Tilje Formation has been interpreted to be influenced by tidal processes. For the lower part of the formation, Martinius et al. (2001) have shown qualitatively that there was some variation in the sand/mud laminaset thickness and attributed this to long-period tidal cycles and stated that daily tidal variations were difficult to recognize. Dreyer (1992) analysed a section of the Tilje Formation in a stratigraphic higher location than the one studied here. He concluded that each sand laminaset was a result of one of the current stages (flood or ebb) and the mud draping the sand laminaset was deposited in the slack-water period between the current stages. The resulting, extremely high sedimentation rate was explained by the episodic variation in accommodation space. Focus will here be on the wavy-bedded LF3 since published quantitative studies on such ripple bedded deposits are sparse, the tidal influence is unclear, and that longer intervals are required for application of time series analysis. However, sand and mud laminaset thickness are measured in most of the other heterolithic facies for constraining the input parameters when constructing the near wellbore models.

5.2.1 Method and Measurements

For simplicity, the terms sand layer and mud layer are used for sand laminaset and mud laminaset respectively. The sand layers in LF3 usually consist of two lithological components with assumed different grain size: a light coloured fine-grained sand and a darker coloured lamina composed of silt or finer sized particles. This contrast enhances the internal stratification. The sand layers in LF3 can either be form-sets, sets or co-sets, but dominated by the first. The sand layers are bounded above and below by mud layers and the sand can show faint lamination in the upper part at the transition to the overlying mud layer and commonly a sharp lower boundary. Depending on the bedding type, the sand or mud layers may or may not be continuous in the core width.

Figure 5.10 shows the method used to measure the thickness of the sand and mud layers in selected subfacies of the interval. Core photographs were used and care was taken to ensure that colour changes in the photograph represented actual lithological changes. However, as heterolithic facies are clearly differentiable, this was a

minor problem. With 2 mm resolution, it was then determined whether a sand component (1) or a mud component (0) was present (dominant within the 2 mm interval). Similar measurements were performed on three parallel lines along the core; left, centre and right of the core photo. In some cases the sand or mud layers were extremely thin and discontinuous making their recognition a matter of judgement. The ripple bedding obviously causes lateral variability in sand layer thickness. In addition, burrowing, although relatively sparse, causes changes in the original sand layer thickness and continuity of the mud layers in some intervals. Amalgamation of sand or mud layers can also add noise to the data. However, by measuring the thickness along three lines gave a better basis for evaluating the statistics and periodicities since local irregularities were averaged out.

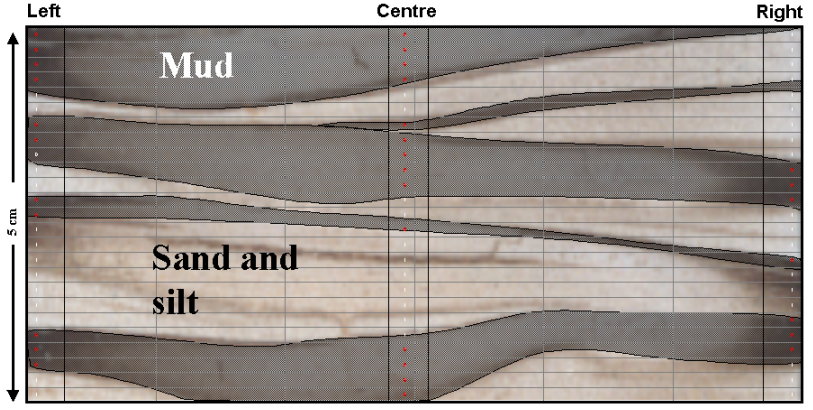

FIGURE 5.10 *The method used for measuring the sand and mud layer thickness. The darker laminae in the sand layers are silt components that here are included in the sand component. The three parallel lines along which the measurements were taken are indicated in the figure.*

The recorded binary data gave two different data sets: 1) sand and mud layer thickness along each line and 2) the sand or mud fraction at each depth. The first data set was used to evaluate the number of layers per cycle for interpretation of the tidal influence in addition to constrain the input parameters to get the correct layer thickness and variation. The second data set, obtained by taking the arithmetic average of the measurements at each depth and then taking a running average down the core made it possible to validate the mud fraction in the generated models. In addition it

was used to find the wavelength of the periodic component on the input parameters that determined the vertical variation of sand and mud layer thickness.

Time series analysis to reveal tidal cyclicities has mainly been done on either large-scale cross-bedding or on finely, laminated successions of sand and silt/mud often referred to as rhythmites (section 3.2). Considerable fewer studies are published on heterolithic, ripple laminated flaser-, wavy- or lenticular bedding. One notably exception is the study by Martino and Sanderson (1993). In this section, a 3.28 m interval of LF3 is studied in more detail to see if there are some periodicities present that can be related to tidal influence.

The autocorrelation function (ACF) measures the degree of self-similarity between observations separated by a distance called lag (h). Inference based on this function is called an analysis in the time domain. Commonly, the autocorrelation is calculated for lags from 0 to n/4 were n is the number of measurements and displayed as a plot against the lag (autocorrelogram). To perform this operation the time series must have certain characteristics (Yang and Nio, 1985): it must consist of a sequence of observations of a variable measured continuously at successive and constants instants in time or space. The first data set consists of variables describing the sand and mud layer thickness (in mm). It is for the moment assumed that each sand and mud layer is deposited in the same period of time and that there has been continuous sedimentation and no erosion. For the second data set, the variable is a number between 0 (mud component) and 1 (sand component) and it is measured at constant intervals in space (2 mm). If there is cyclicity present at a certain lag, then this will be evident as higher correlation coefficient at this lag. Increased correlation will also be present at multiples of that lag. A slight departure from a periodic signal will influence on the ACF. However, if a cyclic component in an autocorrelogram appears, it is probably a significant element (Jensen et al. 1997).

Spectral analysis considers the frequency properties of a time series. The spectral density function partitions the variation in a time series into components according to the duration or length of the intervals within which the variation occurs (Chatfield, 1996). As for the ACF analysis, it is assumed that the observed variable is either measured at a constant space interval or represents a constant period of time. Spectral analysis is based on the idea that the time series is composed of several orthogonal (statistical independent) simpler sine curves (harmonics). Estimation of this function is called spectral analysis and inference based on such a method is an analysis in the frequency domain. Since the time series can be regarded as a sum of many sinusoidal functions, the variance of the time series must be composed of the sum of the variance of the individual harmonics. The result is usually plotted as a line spectrum of the frequency (or the reciprocal period) against the variance (or

power) of frequencies, called a periodogram. The software package SPSS version 11 (SPSS inc. software) has been used to calculate the autocorrelation function and the periodogram. Further information on these analysis methods can be found in Chatfield (1996) or Davis (1986).

A basic requirement of analysis of time series is that the series is stationary. This means qualitatively that there exists no significant trends in the data. Strict stationarity means that all moments are invariant under translation. Often a weak stationarity is assumed where the mean is constant and the covariance only depends on the separation distance (lag) (for a further discussion on the concept of stationarity, see section 7.4). Trends must then be removed from the data set before the time series analysis can be performed. No trends were, however, found in the studied interval. A running, un-weighted (arithmetic) average was used to smooth high frequency noise.

Table 5.1 gives the intervals that are measured with the method described above. Some of the sections were too short to perform time series analysis. However, these data still form an important basis for building realistic models in section 5.3.

Subfacies	Depth interval (m)	Number of counted sand layers (total)	Analysis
LF4.2_LTW	2614.22-2614.58	87	Desc.Stat
LF4.2_WSF	2612.00-2612.90 (not continuous)	62	Desc.Stat
LF3	2601.25-2604.532	780	Desc.Stat, ACF, Spectral
LF7.1_PPL	2598.251-2598.412	121	Desc.Stat, ACF
LF7.2_WB and LF7.2_LTW	2594.7-2596.46 (not continuous)	229	Desc.Stat

TABLE 5.1 Subfacies measured with the method in figure 5.10.

5.2.2 Results

The method described in section 5.2.1 was used to evaluate if there were any significant periodic components in the sand laminaset thickness in LF3. The measurements are taken from a 3.28 m, non-bioturbated interval (table 5.1). If deposition of sand and mud is only influenced by the tidal cyclicity, the sand and mud layer thickness will coincide (Allen, 1985). There are, however, no clear trend between a

sand laminaset thickness and the succeeding mud laminaset thickness in this interval. An absent of such a trend in tidal rhythmites was also noted by Stupples (2002). Nevertheless, they show approximately the same periodic variations as the sand laminaset (figure 5.11 to 5.16). Because of time constraints, the time-series analysis is only performed on the sand laminaset thickness data.

To reduce high frequency noise, a 5-point running average was performed on the raw data. Figures 5.11 to 5.16 show plots of the smoothed data sets and visual inspection suggests some periodicities, possible of several orders. Table 5.2 gives some estimated statistical parameters from the data set and figure 5.17 shows the histogram for the sand and mud laminaset thickness. Both components show an approximately log normal distribution with a sand fraction of 0.47.

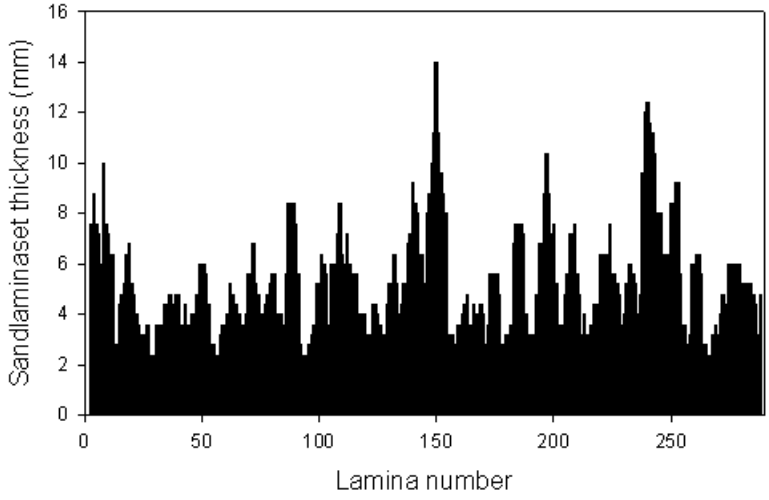

FIGURE 5.11 *Sand laminaset thickness along the left line of the core. The raw data set has been smoothed with a 5 point running average.*

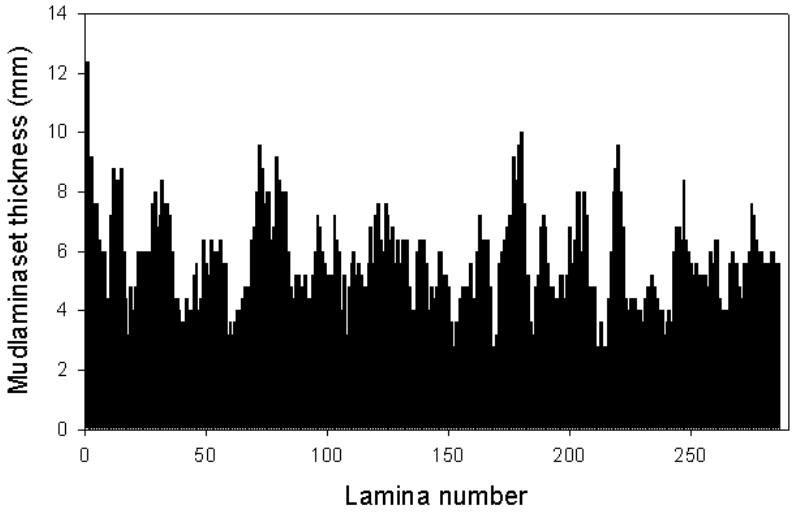

FIGURE 5.12 *Mud laminaset thickness along the left line of the core. The raw data set has been smoothed with a 5 point running average.*

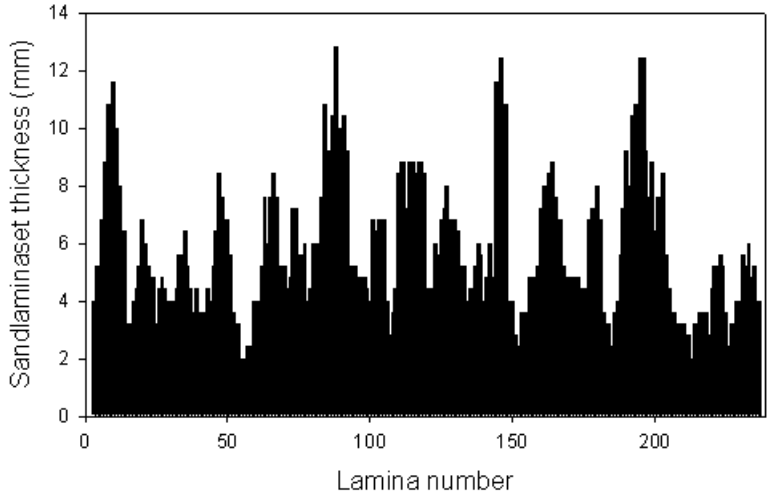

FIGURE 5.13 *Sand laminaset thickness along the centre line of the core. The raw data set has been smoothed with a 5 point running average.*

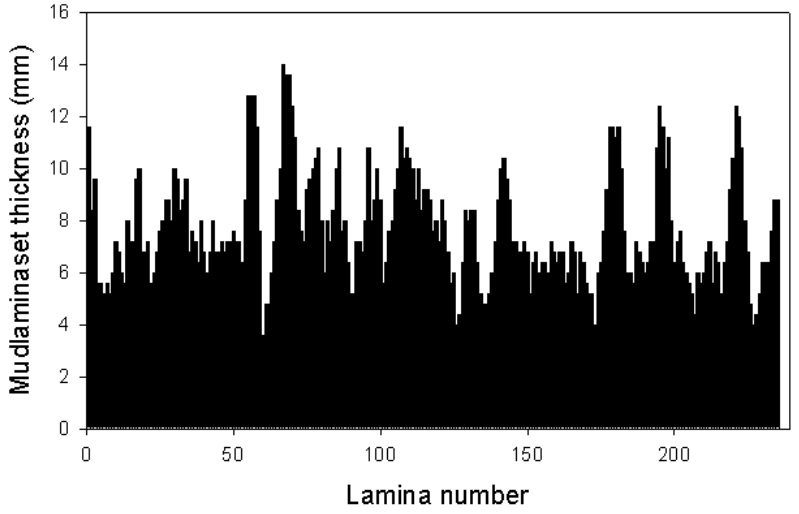

FIGURE 5.14 *Mud laminaset thickness along the centre line of the core. The raw data set has been smoothed with a 5 point running average.*

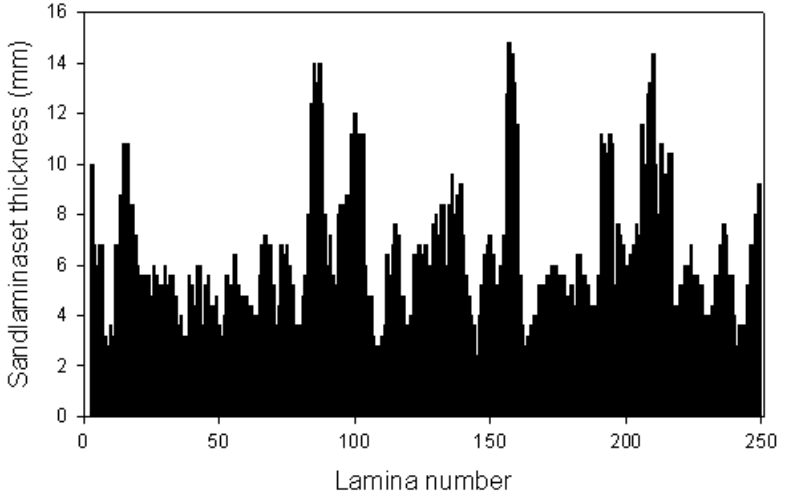

FIGURE 5.15 *Sand laminaset thickness along the right line of the core. The raw data set has been smoothed with a 5 point running average.*

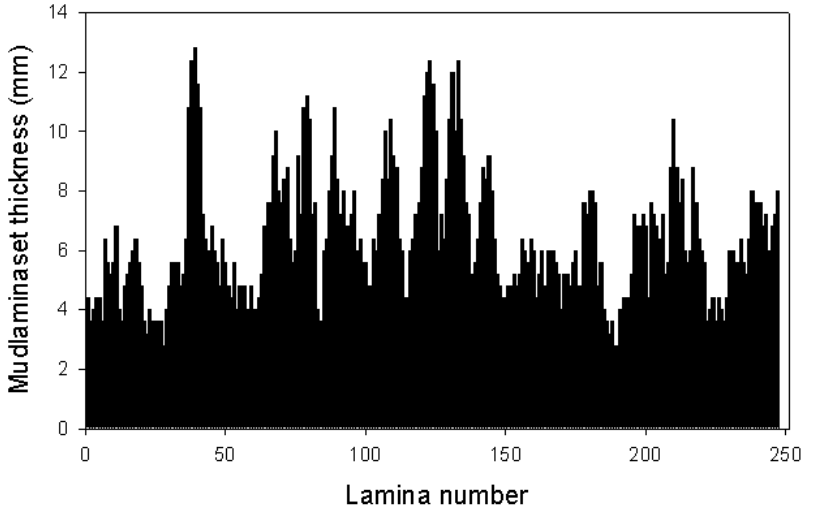

FIGURE 5.16 *Mud laminaset thickness along the right line of the core. The raw data set has been smoothed with a 5 point running average.*

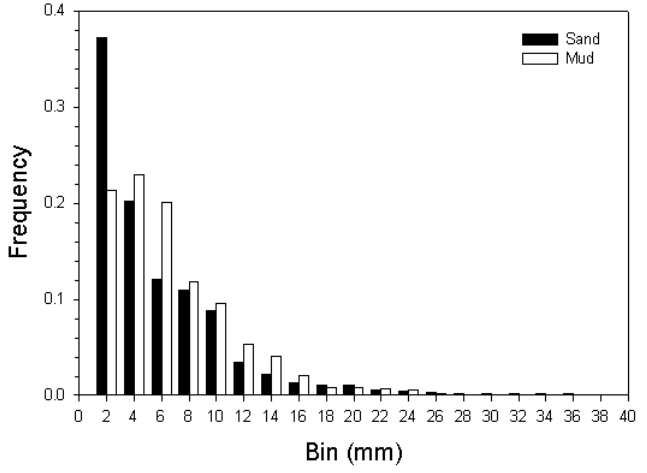

FIGURE 5.17 *Histogram for sand and mud laminaset thickness (sand = black and mud = white) for LF3. The distribution is calculated based on all the three parallel lines along the core.*

	Sand	Mud
n (number of laminaset)	780	780
Arithmetic average	5.83	6.58
Standard Deviation	4.90	4.36
Median	4	6
Mode	2	4
Minimum value	2	2
Maximum value	36	26
Total mm	4544	5132
Sand fraction	0.47	

TABLE 5.2 Descriptive statistics for the thickness of sand and mud lamina set in LF3. Measurements are in millimeters and are based on all the three lines along the core.

On the smoothed data set, ACF analysis and spectral analysis were performed. The autocorrelogram for the three parallel lines are shown in figures 5.18 to 5.20 and the results from the spectral analysis are shown in figures 5.21 to 5.23.

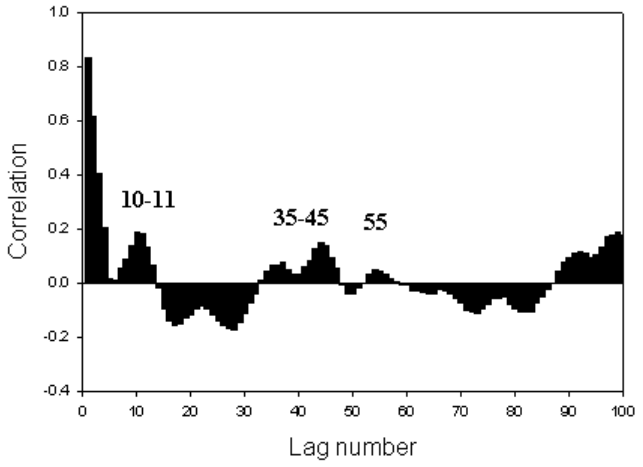

FIGURE 5.18 *Autocorrelation function estimated on the sand laminaset thickness along the left line of the core (the data in figure 5.11).*

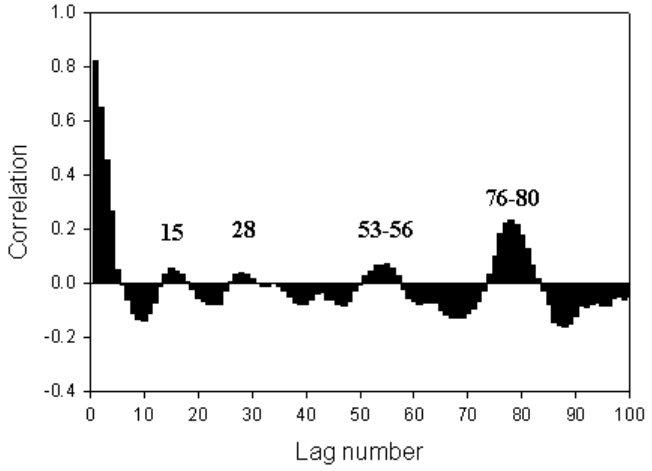

FIGURE 5.19 *Autocorrelation function estimated on the sand laminaset thickness along the centre line of the core (the data in figure 5.13).*

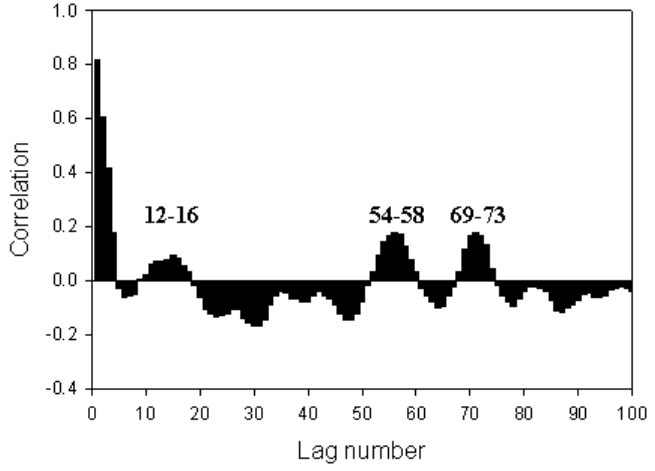

FIGURE 5.20 *Autocorrelation function estimated on the sand laminaset thickness along the right line of the core (the data in figure 5.15).*

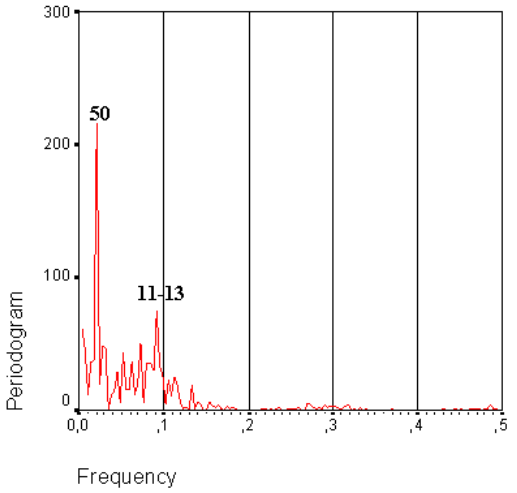

FIGURE 5.21 *Spectral analysis on the sand laminaset thickness along the left line of the core (the data in figure 5.11).*

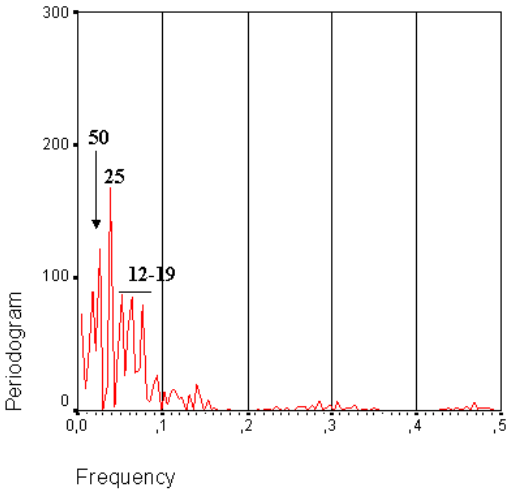

FIGURE 5.22 *Spectral analysis on the sand laminaset thickness along the centre line of the core (the data in figure 5.13).*

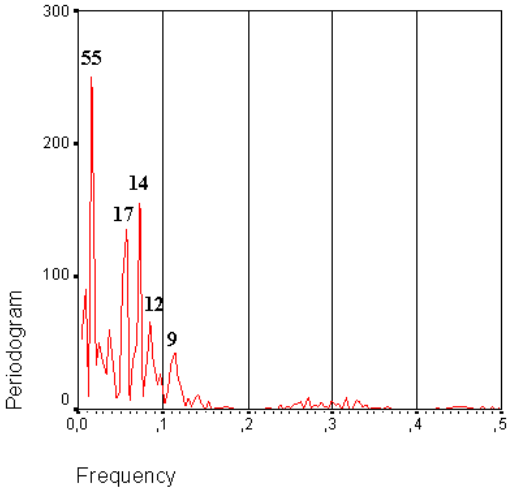

FIGURE 5.23 *Spectral analysis on the sand laminaset thickness along the right line of the core (the data in figure 5.15).*

Given the highly variable data set even in core width, the results from the time series analysis of the three parallel lines are quite consistent. Both the analysis in the time domain and the frequency domain show a few prominent ranges of periodicities indicating that these are significantly present. High frequency variation (short wavelength or lag) is smoothed out due to the running average. The period with the shortest wavelength present is approximately between 11 and 16 sand layers. All three lines also show a periodic component with a wavelength around 55. Intermediate wavelengths are also present, but these appear to be less prominent. Table 5.3 gives all the periodicities found in the studied interval.

For completeness, the time series analysis of the sand fraction curve is given below. This gives an image of how the sand fraction in such a deposits can vary over relatively short distances. Figure 5.24 shows the data set with a 5 cm running average, figure 5.25 the result from the autocorrelation analysis and figure 5.26 the result from the spectral analysis. Table 5.3 lists the periodic components found in this data set. The shortest wavelength (14-18 cm) will be used as input for modelling vertical variability in sand fraction. The 40-45 cm period apparent in figure 5.25 are probable a multiple of the shortest wavelength, while the longest wavelength (~65 cm), possibly corresponds to the periodic component found by Dreyer (1992).

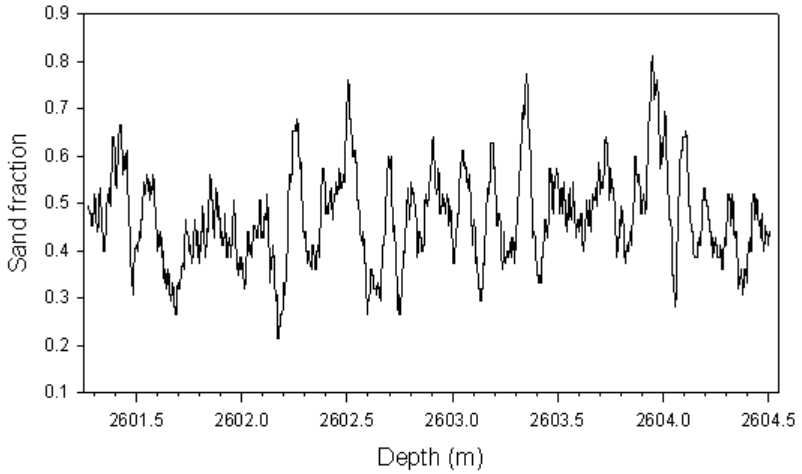

FIGURE 5.24 *Measured sand fraction curve with a 2 mm resolution and smoothed with a 5 cm running average.*

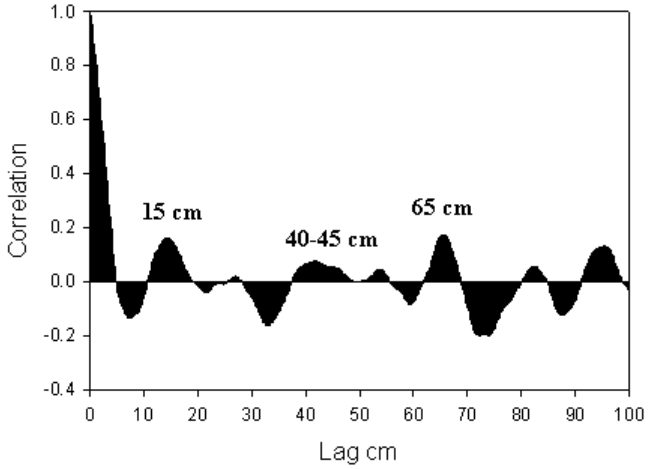

FIGURE 5.25 *Autocorrelation analysis on the data from figure 5.24.*

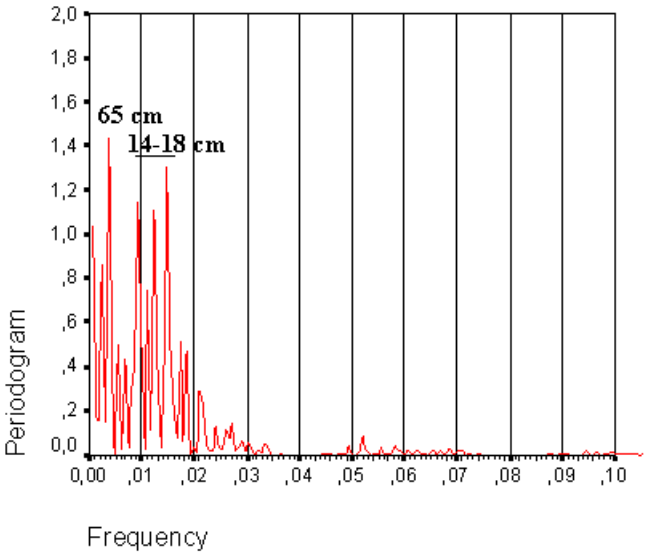

FIGURE 5.26 *Spectral analysis of the data in figure 5.24.*

	Spectral analysis		ACF analysis
Parameter	Frequency (f)	Period (1/f)	Lag (# of sand lamina sets)
Sand layer left profile	0.09-0.08	11-12.5	10-11
	0.02	50	44
			54
Sand layer centre profile	0.078	12.8	15
	0.062	16.1	28
	0.051	19.6	55
	0.04	25	78
	0.02	50	
Sand layer right profile	0.11	9.1	12-16
	0.084	11.9	54-58
	0.071	14.1	69-73
	0.059	17	
	0.018	55.6	
Sand fraction	0.018	55.6 (11.1 cm)	15 cm
	0.015	66.7 (13.3 cm)	40-45 cm
	0.012	83.33 (16.7 cm)	65 cm
	0.009	111.1 (22.2 cm)	
	0.003	333.3 (66.7 cm)	

TABLE 5.3 Periodic components from ACF and spectral analysis for both the analysis on the sand laminaset thickness, giving the number of sand laminaset per cycle, and the continuous measurement of sand fraction.

5.2.3 Interpretation, discussion and implications for modelling

With respect to their bedding characteristics, that is successive sand and mud laminaset and vertical evolution, each sand layer can be interpreted to be a result of one current stage (flood or ebb) and that the overlying mud layer a result of the deposition during the following slack-water period. The shortest periodicity recorded (10-16 sand layers) would then be a neap-spring cycle in a mixed tidal system. In a

stratigraphic higher but a sedimentological similar interval of the Tilje Formation, Dreyer (1992) proposed such an interpretation. There are however some problems with this interpretation: 1) The majority of the mud laminasets are too thick to have been formed in just one slack water period, 2) the internal stratification of the sand laminaset and the transition between the sand and the mud indicate deposition over a longer time interval than one flood or ebb current. Besides Martino and Sanderson (1993), there are few studies that have focused on periodic components in heterolithic, ripple-laminated deposits which gives, in general, a noisier data set than in the more studied planar laminated deposits.

The deposition of mud in tidal systems was discussed in section 3.2 (page 69). Even though extremely high sedimentation rates have been reported (Reineck and Singh, 1980), a literature search indicates that a *freshly* deposited mud layer thicker than 5-10 mm seems unlikely to result from one slack water period (McCave, 1970; Terwindt and Breusers, 1972; 1982). Deposition of fluidized mud can however result in thicker mud layers (Kirby, 1991). Even though a detailed compaction curve for the mud in LF3 is not available (burial depth ~ 2500 m in the Heidrun field), it is assumed that a measured mud layer thickness in the core of more than 4 mm could not have been deposited from suspension during one tidal slack period. From figure 5.17 we see that c. 55% of the mud layers measured in the selected interval are more than 4 mm thick. This seems like an conservative limit since only the initial consolidation has been shown to reduce the thickness with about 50% (Terwindt and Breusers, 1972) and that further compaction will reduce the thickness even more.

The daily tidal variation and its influence on the sedimentological record was discussed in section 3.2 (figure 3.4). In large barforms and in planar laminated rhythmites, the daily cyclicity was found in addition to longer tidal periodicities (e.g. semi-monthly, monthly, semi-annual and lunar nodal cycle). Another type of ripple cyclicity less encountered in the literature is the Type II ripple of Tessier (1993). Figure 5.27 shows this ripple type. It is composed of a set of three-dimensional small-scale climbing ripples. The internal structure of the ripple is composed of sand laminae and thin mud drapes. At the base, the laminations mould the underlying ripple morphology. Upwards, the laminae thicken, the slope angle of the lee side increases and the mud content decreases, before, towards the top, the angle again decreases and the mud content increases. Tessier (1993) denotes a sand lamina and its succeeding mud drape a tidal couplet indicating that each sand lamina was deposited in a flood or ebb cycle. It thus resembles the geometry often recorded in much larger scale tidal dunes or mega-ripples (e.g. Visser, 1980; Kreisa and Moiola, 1986). Oost and Baas (1994) explained, with their empirical flow model, why the ripples developed with linguoid crest lines even though the flow

velocity during deposition was low. Similar rippled bedforms have also been described in the ancient rock record by Kvale and Archer (1990,1991), Leithold and Bourgeois (1984), Lanier et al. (1993), Tessier et al. (1995) and Lanier and Tessier (1998). The examples described have been from intertidal areas although Kvale and Archer (1990) assumed that some of the structures were deposited subtidally. Molgat and Arnott (2001) described a lithofacies from the Upper Jurassic Swift Formation with 0.3-2cm thick sand layers showing the same internal stratification as the Type II ripple, bounded by less than 1 cm thick mud drapes and forming persistent wavy to lenticular bedded deposit. They interpreted this lithofacies to have been deposited in a low energy, bedload sediment starved, marine setting and that the internal stratification was formed by low-energy combined-flow ripples (tide- and wave-induced currents, Arnott and Southard, 1990). The ripples migrated episodically between periods of mud deposition from suspension. Even though they noted the variation in lamina angle and qualitatively related that to a neap-spring cycle, they did not perform time series analysis to reveal possible influence of longer tidal cycles.

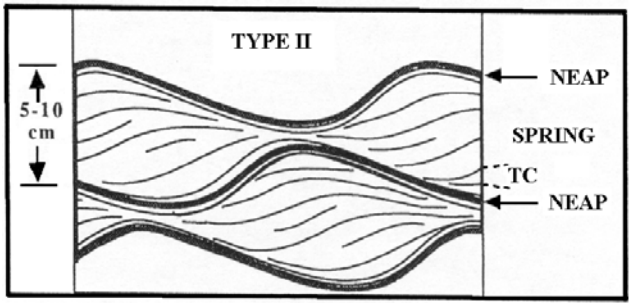

FIGURE 5.27 *Ripple type II (Tessier, 1993). The thickness of each sand laminaset are one order of magnitude larger than observed in here.*

Figures 5.28 to 5.31 show detailed core photos of some of the laminated sand layers found in the studied interval. Internally, these sand layers consist of lamina that are either sub horizontal (figure 5.30) or that have a cross-laminated appearance (figure 5.28, 5.29 and 5.31). The lighter laminae are slightly coarser than the darker laminae, which accentuate the internal lamination pattern. The contrasting laminae show variability in both thickness and slope of the lee angle. In the centre of the cross-laminated sand layer, the sand laminae are thicker, have a higher angle on the lee side and the mud drapes are generally thinner or absent. It has not been possible

to discover whether, in their most complete form, they contain a specific number of dark and light laminae. Where visible, the sand laminaset grades into the overlying mud laminaset in a transition zone giving a faint lamination at the base of the mud laminaset (e.g. figure 5.30). On the other hand, the boundary between a mud laminaset and the succeeding sand laminaset is most often sharp (e.g. figure 5.28), although mm-scale load casts can be found (figure 5.30). The climbing ripples described in Kvale and Archer (1991) were slightly thicker at the crest and they found mm-scale reverse ripple cross-lamination indicating bi-directional currents. Molgat and Arnott (2001) reported reactivation surfaces on the lee-side. Such features were not found in the studied interval, and no grading is observed in the individual lamina. This can indicate that the sub-ordinate currents are too weak to erode and transport the previously deposited sand (strongly asymmetrical tide) or that only one of the tidal currents dominate in this part of the basin.

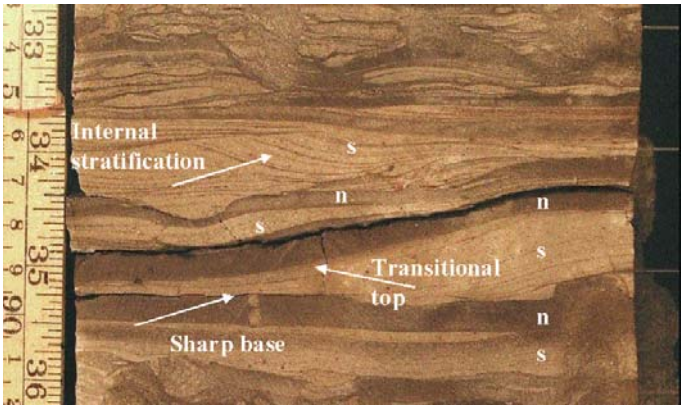

FIGURE 5.28 *Core photo of the interval between 2603.80-2603.90 showing sand laminaset equal to the Type II ripple and the transitions between the sand and mud layers (n=neap and s=spring)*

FIGURE 5.29 *Core photo of the interval between 2604.93-2604.98 showing a sand laminaset with internal stratification resembling the Type II ripple.*

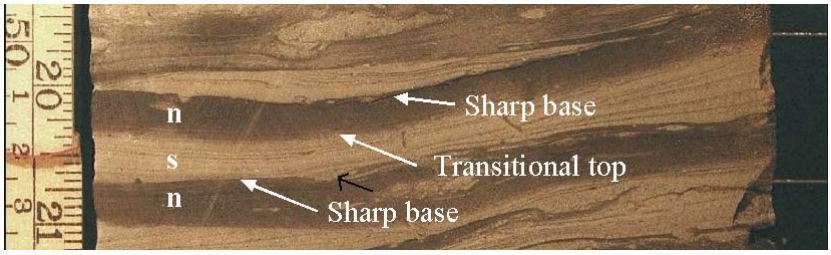

FIGURE 5.30 *Core photo of the interval between 2604.47-2604.51. Showing good examples of the transitions zones. The black arrow indicate a small load cast.*

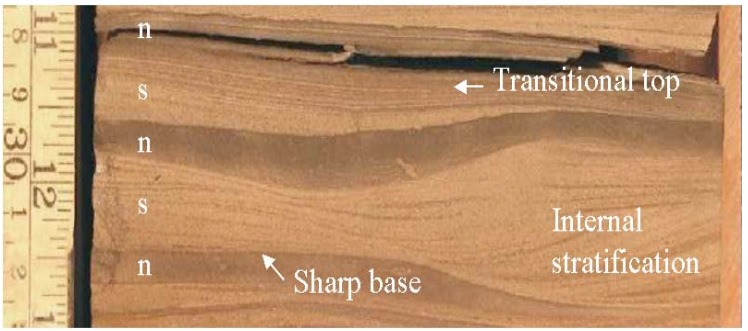

FIGURE 5.31 *Core photo of the interval between 2602.24-2602.29 showing the characteristic internal stratification and the transitional zones.*

Although not proven here by observations in the nature or in a flume tank, the following tentative explanation of the depositional process is put forward. The interpretation is based on the above observation of the internal structure of the sand layers, the boundaries between the sand and the mud, that the thickness of the mud in general opposing deposition during only one slack water period and the recorded periodic components.

The entrainment velocity for fine-grained sand (U_{ces}) is found to be slightly above 0.2 m/s (Miller et al., 1977) while the deposition of mud starts considerably below 0.2 m/s (U_{cdm}) (Einstein and Krone, 1962). It is therefore assumed here that the entrainment velocity for the fine sand/silt fraction is higher than the threshold velocity where mud starts to fall out of suspension. Terwindt et al. (1968) investigated experimentally bed erosion in the complex situation of alternating sand and mud and found that resistance to erosion was depending more on the properties of the mud than the sand. In cohesive mud deposits, this value commonly exceeds that of sand. As the tidal range varies through a spring-neap-spring cycle (figure 5.32), the current velocity and the time the current is above U_{ces} and below U_{cdm} varies with the same period. In the proposed depositional process, resulting in the lenticular to wavy bedded unit analysed above, the dominant and subordinate (if present) maximum current speed is both below U_{ces}, and the threshold for mud erosion around neap time. These currents are also possible below the U_{cdm} (solid line in figure 5.32 denotes this case and the dashed line the case were the maximum current speed is above U_{cdm}). The (semi-) continuous deposition of mud around neap time creates an amalgamation of thin mud laminae that, after settlement, undergo

initial consolidation. Terwind and Breusers (1972) found experimentally, that a freshly deposited mud layer could bear a 0.5 cm sand layer and give a sharp boundary to the underlying mud after about 4 h. of consolidation. In the proposed model described here (see also figure 5.32), most of the deposited mud has a consolidation time of several hours (days). As the tidal range and maximum current speed increases towards spring, the threshold for sand movement is passed. Some of the most recently deposited mud can be removed if the current speed exceeds that of mud erosion, but the deposited sand will in general have a sharp boundary to the underlying, initially consolidated mud. Occasionally, however, soft sedimentation deformation in the form of small load-casts occurs (e.g. figure 5.30) as also reported in the study by Molgat and Arnott (2001). Small, three-dimensional bedforms develop equal to the type II climbing ripples of Tessier (1993). They are however about one order of magnitude smaller than found in this reference but on the same scale as in Molgat and Arnott (2001). Around spring time, the current velocity is largest and the thickest sand/silt laminae are deposited (approximately proportional to $(U(t) - U_{ces})^3$). There is, as mentioned above, not measured if there is a specific number of lamina in the ripples although a number less than 28 is expected if only the dominant current is present. As the tidal range decreases towards the following neap, successive smaller components of the current velocity are above the threshold for sand movement. This gives a faint lamination between traction deposited sand and suspension deposited mud in a transitional zone to the overlying neap-deposited, amalgamated mud. Similar upper and lower boundaries were also found in Baker et al. (1995) in the sub-tidal deposits although they did not attribute the observation to a specific tidal influence but by general lowering of the energy level (a possible combined tide and wave influence). Regular alternation of the current speed related to a spring-neap-spring cycle can therefore explain these alternating bedforms.

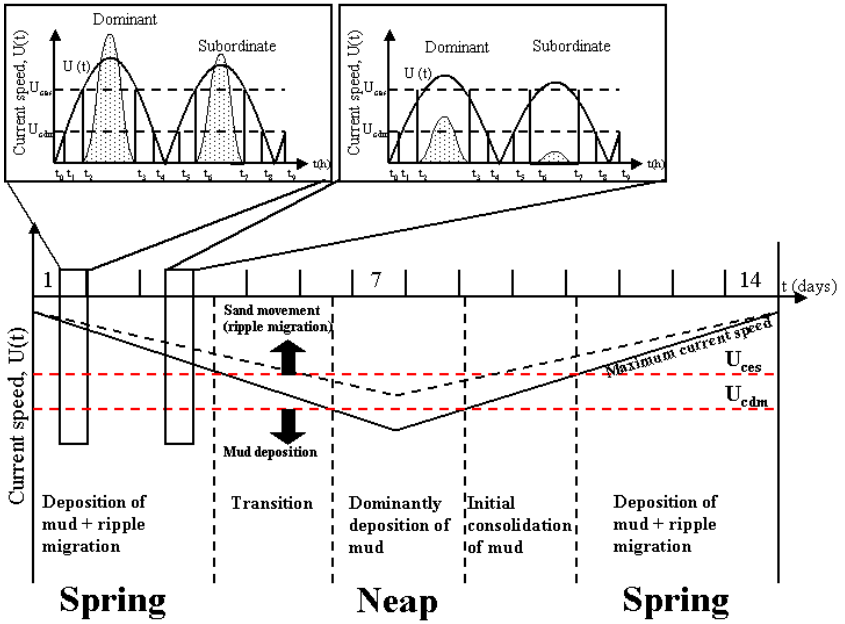

FIGURE 5.32 *The proposed cyclic behaviour in current speed resulting in the observed laminaset characteristics in LF3. The blown-up sections are in principal equal to figure 3.4 but with a less asymmetrical tide. The degree of asymmetry (diurnal inequality) is however not a requirement of the proposed depositional process.*

Other non-tidal factors like wave action, seasonal fluctuation in river discharge, and episodic storm events can be superposed on this sequence. Some of the mud layers show a sharp upper and lower boundary and have a massive appearance indicating that they can be deposits of the fluidized muds described by Kirby (1991). Some of the mud layers are thin and can have been deposited in one slack water period. Few examples of reversing ripple migration support however that one of the current stages are weaker than the other and not able to transport a significant amount of sand. In addition, sand layers, somewhat coarser, above average thickness and with erosional base can be interpreted as sand deposited during storm periods.

Even though the data set is noisy, both the autocorrelation and the spectral analysis have detected a few significant periodicities. The shortest period consists of 10-16 sand layers. Both the sun's declination to the earth and the constructive interference

of the tropical, anomalistic and synodic month has a period at the semi-annual time scale with 182.62 days and 183.29 days, respectively. Given that each sand layer is deposited in a neap-spring cycle, each semi-annual cycle would then be composed of approximately 13 spring deposits (13 fortnightly periods during a half year). It is not considered whether the neap-spring cycle is of a synodic or tropical origin. Similar semi-annual periods are observed in finely laminated sediments by Kvale et al. (1994, 1999) who in addition related them to seasonal variation in rainfall and discharge. Also Williams (1989), Miller and Eriksson (1997) and Stupples (2002) have found records of cyclicity of around 13 neap-spring deposits and interpreted those as a semi-annual cycle.

The longest period recorded in all the data sets are 50-60 sand layers. About 3 to 4 cycles with this wavelength are recorded in the interval and represents some of the thicker sand layers encountered (figures 5.11 to 5.15). By inspection of the core, it is, however, not evident that these layers have a different texture or structure than the majority of the other, thinner sand layers. If there was continuous sedimentation, this period would reflect a modified 2 yearly cycle, but no clear interpretation is suggested for this period. The studied interval has both non-tidal, but possible cyclic components like seasonal variations and most probably diastems not recognized in the core. Such components will influence on the periodic signal and complicate the interpretation.

In summary, the high mud content and the presence of small-scale ripples suggest deposition during overall low energy conditions. Alternations of sand/silt and mud laminasets suggest further that the energy level fluctuated. The internal structure, resembling the Type II ripple, visible in many of the sand laminasets indicate that the current varied regularly in strength. Since the internal sand/silt laminations are interpreted as tidal couplets, the wave energy level must have been low. Also supporting a low wave influence is that higher energy wave-generated structures like hummocky cross-stratification is rather uncommon in this lithofacies. Reversing cross-laminations or reactivations surfaces are not common features. However, strongly rectilinear or highly elliptical rotary tidal currents in semi-enclosed basins are often observed giving a predominantly unidirectional current pattern (e.g. Oost and Baas, 1994). A weak current, dominantly tidal but with a possible weak wave component, combined with the interpreted low ripple migration speed suggest that the depositional area was relatively starved of bedload sediment. Fine-grained sediments can have been brought into the pro-delta area by hyperpycnal plumes or by longshore currents, which subsequently was modified by the weak currents into the observed rippled bedforms. The apparent low wave energy conditions favoured a stronger imprint from the tidal current and that the semi-annual tidal cyclicity could be recorded in the deposits. Although the semi-annual solar tide is rather weak (8%

weaker than the principal lunar semi diurnal component (Werner, 1992)), Williams (1989) suggested that the semi-annual signal was amplified by the constructive interference of the synodic, tropical and anomalistic periods.

The present interpretation of LF 3 as a quiet-water, mud-rich delta-front facies (Martinius et al., 2001) fits well with the re-interpretation of the delicate, small-scale structures described above. However, the tidal influence has been quantified through the recognition of several orders of cyclicity.

Important for modelling of the near wellbore volume is also that a periodic variation in the sand fraction will influence the petrophysical properties. This was also noted by Dreyer (1992). It is thus essential to incorporate such a variation in the input parameter set. The observed 14-18 cm period is used, in a transformed fashion, as input to the depositional length in the modelling tool. This will thus resemble the variation in the time available for ripple migration. The periodic component is acting parallel the migration vector (section 4.2.3) and the input wavelength needs thus to be found that corresponds to a vertical wavelength of approximately 15 cm. In this case a wavelength of 150 (i.e. 150 time steps, see eq. 4-1) was used on the depositional rate and length.

5.3 Sedimentological models in SBED

One goal of this thesis was to build a detailed near wellbore model of the lower part of the Tilje Formation in an example well from the Heidrun field using the SBED modelling code. It was then assumed that some of the models created could be used in other wells from the same stratigraphic interval in the Heidrun field.

The SBED tool was described in chapter 4 and a set of graphs illustrated the relation between the input parameters and the simulated bedforms. These graphs are used here to build detailed models of the subfacies described above. Sand and mud laminaset thickness statistics, measured in all the heterolithic facies were used to obtain the input parameters along with the sedimentological interpretation. When focus is to create a sedimentological and petrophysical model that can be used to evaluate the petrophysical variability (e.g. the k_v/k_h) in the near wellbore region, the parameters that influence such properties should naturally be considered. For the tide influenced, heterolithic deposits in the selected interval, the amount and spatial distribution of the sand and mud laminasets will be important parameters. Since the 3-D models are based on core data, a method that in part can be used to verify the numerical models is proposed. However, the degree of realism must also

be based on a sedimentological understanding and evaluation and is difficult to quantify exactly.

5.3.1 Modelling of subfacies

It was argued above that the lithofacies defined by Martinius et al. (2001) could be divided into subfacies based in its inferred influence on the petrophysical properties. This means that characteristics at the bedding scale are the main focus when parameterization the core. The aim here is to model the *near wellbore* region. The near wellbore model is here defined as *a numerical representation of the sedimentological components and petrophysical properties in a rectangular shaped volume along the wellbore with a lateral dimension on the scale of the conventional wireline tool resolution*[1]. This also approximately corresponds to the lateral correlation lengths of the sedimentological and petrophysical elements at the small scale of Yoshida et al. (2001) (see figure 3.7). It is thus assumed that subfacies defined in this interval are persistent in the near wellbore region.

The three-dimensional models built are based on observations from the core. With respect to the facies encountered in this interval, the core can be regarded as an 1 dimensional observation. Although some lateral variability can be observed, the width is limited with respect to the lateral extension of the sedimentological features (e.g. wavelength of the bedforms) giving only a partial measurement of the lateral variability. In other words, the horizontal correlation lengths of the sedimentological and petrophysical components are often longer than the core width and hence the core is a less than a 2-D observation. One principal problem then is how to use data from a lower dimension to create a model in three dimensions and also to verify that the created model is realistic in sedimentological and petrophysical terms. Using standard formulations of stereology, Geehan and Underwood (1993) showed that going from a 2-D distribution to a 3-D (or 1-D to 2-D) the relative frequency of a particular length class would decrease in proportion to its length, assuming an isotropic shape. For a non-isotropic shape the product of length and width is the relevant parameter. Geehan and Underwood (1993) also discuss partial measured mud layers and mud layers extending across the measurable area (unlimited mud layers). In the part of the Tilje Formation studied here, the dominant type is both the partial and unlimited mud layer. However, at the bedding scale in tidal

1. The lateral dimension of the near wellbore model is defined by the depth of investigation of the wireline tool that is used in that particular well. It should however, also have a lateral scale large enough to capture a representative amount of sedimentological and petrophysical heterogeneity around the wellbore.

facies there is, in general, a correlation between the lateral extension of the mud layers and the size of the migrating bedforms: longer bedforms will give longer mud layers with otherwise similar conditions. Quantifying sedimentary bedforms in 3D are inherently difficult. Yoshida et al. (2001) photographed and digitized representative areas of outcrop samples (blocks) with tide-influenced deposits and with a serial sectioning technique re-constructed the three-dimensional bedforms. They used this method on two facies: a mud-rich lenticular to wavy bedded facies and a more sand rich flaser to wavy bedded facies. At the scale of a core plug, the sand and the mud layers had higher lateral continuity than on the scale of the model (~40cm). Further, the sand layers in the mud rich facies appeared discontinuous in 2-D although they were connected in 3-D. Similar, the thin mud layers in the sand rich facies were laterally persistent in 2-D at the model scale but in the third dimension they were discontinuous. This observation emphasises the importance of a good three-dimensional understanding of the sedimentary architecture at the bedding scale. Such knowledge can in part be based on a good understanding of the depositional process and its lateral variability.

As discussed in chapter 4, the bedding models are created based on successive displacement of sine curves to mimic bedform migration. The underlying structure is deterministic, but stochastic (and periodic) components can be added to several parameters. Still, an exact re-creation of the nature with all its variability is impossible with such an approach. Pickup et al. (1999) showed, using a complex aeolian dune as an example that only the main features affecting flow had to be included in the model when evaluating effective properties. In that case, the simpler, schematic models had to have realistic values of the frequency and thickness of the contrasting lamina of the system to be representative with respect to flow properties.

The mean and standard deviation of the sand and mud laminaset thickness is not directly used as input to SBED. Instead, parameters describing the depositional rate and length, migration speed and bedform morphology combined determine the bedform geometry and thickness distributions. Some relations between the input parameters and bedform characteristics (e.g. lamina and laminaset thickness) were shown in section 4.6. These relations are used here to build the models for the individual subfacies described in section 5.1. Table 5.4 gives some statistics for sand and mud laminaset measured with the method described in section 5.2.1.

Most of the subfacies show an approximately log-normal distribution of sand and mud layer thickness. The sand fraction varies form about 0.30 in the lenticular-bedded units to above 0.70 in the flaser bedded subfacies. Focus has been on the most heterolithic subfacies and such detailed measurements have not been performed on the lithological cleaner hummocky cross-stratified facies or the cross-stratified

units in LF1.2. The reference parameters for the individual bedding models are given in Appendix A.1.

Component	Parameter	7.2_WB	7.2_LTW	7.1_WSF	7.1_PPL	4.2_LTW	4.2_WSF
Sand	n	211	75	11	121	87	62
	Arit.Avg	6.48	3.92	20.14	1.3	5.03	19.39
	StDev	5.35	2.66	18.64	0.5	3.37	21.02
	Median	4	2	15.9	1.14	4	14
	Mode	2	2	N/A	1.14	2	2
	Min	2	2	2	0.57	2	2
	Max	32	12	59.2	3.43	16	82
	Tot. mm	1368	294	2215	157.7	438	1202
Mud	n	213	79	11		88	59
	Arit.Avg	7.46	7.29	0.68		6.32	6.27
	StDev	5.85	4.18	0.35		3.11	4.11
	Median	6	6	0.8		6	6
	Mode	2	4	0.8		4	4
	Min	2	2	0.1		2	2
	Max	36	18	1.2		14	20
	Tot. mm	1590	576	75		556	370
Sand fraction		0.462	0.338	0.967 (*4.8)	1	0.441	0.765

TABLE 5.4 Descriptive statistics for selected subfacies. Based on measurements from three parallel lines along the core. *For the subfacies LF_7.1_WSF, the number of thick mud layers per meter is the most relevant parameter to consider. The data for this particular subfacies are given in cm.

5.3.2 Validation of subfacies models

Models based on a truly process based simulation code are difficult to verify (Anderson, 1996). The simulation code in SBED is however composed of both deterministic components, including the periodic components, and random components giving variability superposed on the underlying structure. It should thus be possible to at least verify that the models created are correct with respect to some aspects of the core-derived parameters.

From the simulated models, sub-grids (see section 4.4.4) are extracted that have the same width as the core (10 cm), a thickness of 1 cm and length related to the length of the subfacies in the interval. Sub-grids both perpendicular and parallel to the migration direction are evaluated. For each of the heterolithic models, five realizations are simulated. From each realization, two orthogonal sub-grids are taken and on these sub-grids three, equally spaced, parallel lines along the model length are evaluated with respect to the frequency distribution of the sand and mud laminasets. This method thus resembles the method used to derive the input parameters. As discussed above, there are some principal problems using 1-D data to create 3-D models. By using orthogonal “cores” from the model, it is assumed that some of the 3-D variability is captured. Oblique sub-grids would be valuable but are currently not possible to extract from the model. The underlying assumption by using this approach is that the real core also is cutting the facies perpendicular or parallel the depositional direction. The limitations of the validation procedure are recognized. Since the 3-D connectivity is assumed to be one of the most important parameter when calculating effective permeability, a method that could evaluate the sand/mud connectivity and thickness distribution of the simulated models would be of great value but such an analysis is not performed. The proposed method is here used, combined with a visual inspection of the models, to ensure that the models are realistic with respect to the subfacies described in section 5.1. Table 5.5 gives the thickness distribution of the sand and mud laminasets measured on the simulated models. This table can then be compared with table 5.4.

Component	Parameter	7.2_WB	7.2_LTW	7.1_WSF	7.1_PPL	3_LTW	4.2_LTW	4.2_WSF
Sand	n	1405	1330	117	383	8545	1499	457
	Arit.Avg	4.70	3.65	21.1	1.30	4.57	4.34	24.58
	StDev	2.88	2.11	1.98	0.43	3.39	3.59	6.52
	Median	4	3	21	1.3	4	3	24
	Mode	4	2	21	1.3	2	2	24
	Min	1	1	20.5	0.3	1	1	11
	Max	22	16	42.2	2.3	40	32	70
	Tot. mm	6605	4851	24684	499.7	39045	6500	11234
Mud	n	1413	1346	117		8526	1502	430
	Arit.Avg	5.91	7.53	0.421		5.85	5.65	8.76
	StDev	3.00	4.12	0.18		3.87	4.08	3.39
	Median	6	7	0.4		5	5	9
	Mode	6	7	0.5		5	4	9
	Min	1	1	0.1		1	1	1
	Max	25	40	0.9		50	40	18
	Tot. mm	8355	10139	492		49898	8482	3766
Sand fraction		0.442	0.324	0.98 (*4.6)	1	0.44	0.434	0.749

TABLE 5.5 Descriptive statistics for selected subfacies modelled in SBED. Based on measurements from three parallel lines along two orthogonal, 10 cm wide subgrids of 5 realizations. *For the subfacies LF_7.1_WSF, the number of thick mud layers per meter is the most relevant parameter to consider. To be compared with table 5.4.

To give a visual comparison between the simulated and the measured sand and mud laminaset thickness, the following histograms are shown (figure 5.33 to 5.37). Subfacies LF7.1_WSF has only 11 recorded mud/sand laminaset and a stable histogram was not possible to be produced. The important parameter is however the number of mud layers per meter. From table 5.4 and 5.5 we see that this statistic is in well agreement between the core and the realizations.

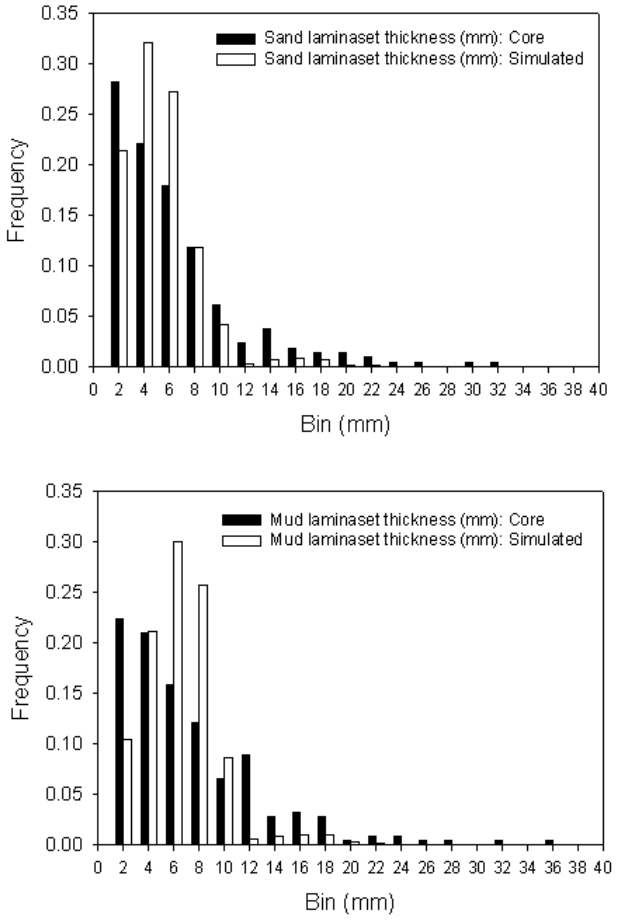

FIGURE 5.33 *Simulated laminaset thickness for mud and sand from the core and the simulated subfacies (Subfacies LF 7.2_WB).*

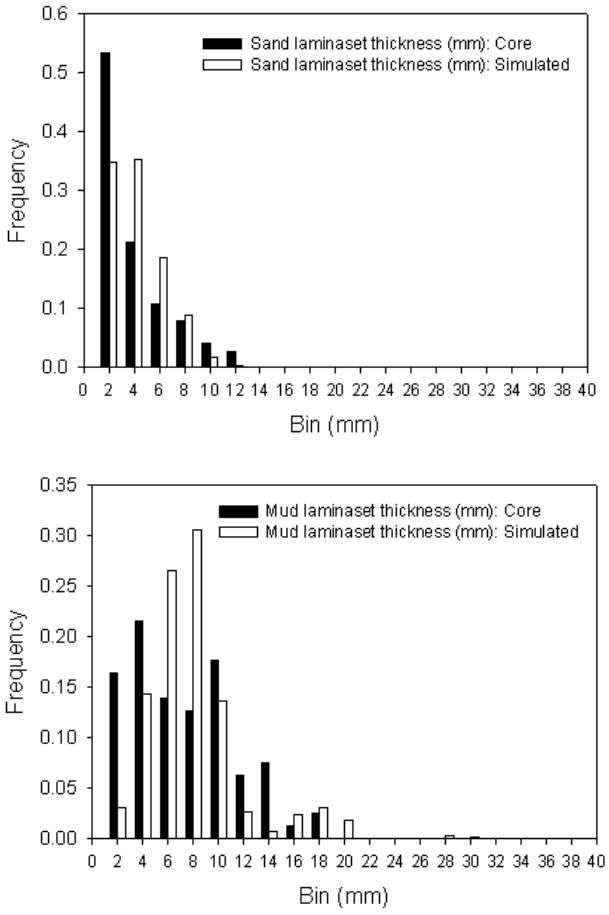

FIGURE 5.34 *Simulated laminaset thickness for mud and sand from the core and the simulated subfacies (Subfacies LF 7.2_LTW).*

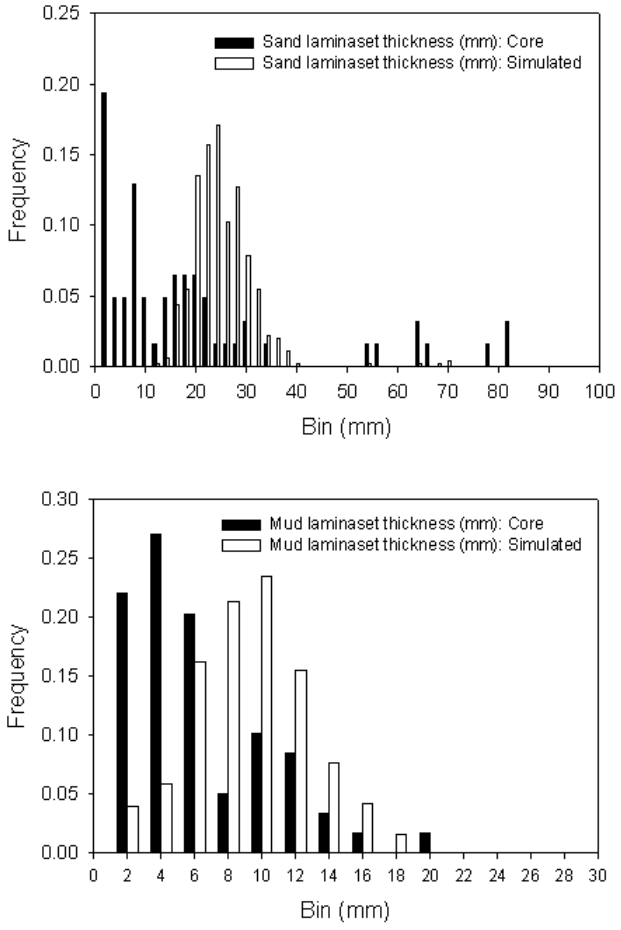

FIGURE 5.35 *Simulated laminaset thickness for mud and sand from the core and the simulated subfacies (Subfacies LF 4.2_WSF).*

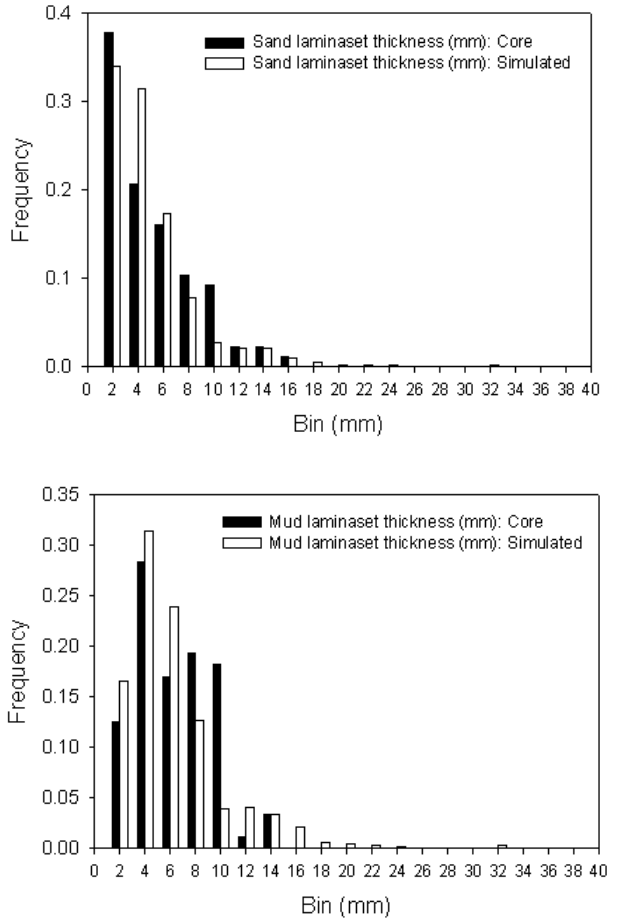

FIGURE 5.36 *Simulated laminaset thickness for mud and sand from the core and the simulated subfacies (Subfacies LF 4.2_LTW).*

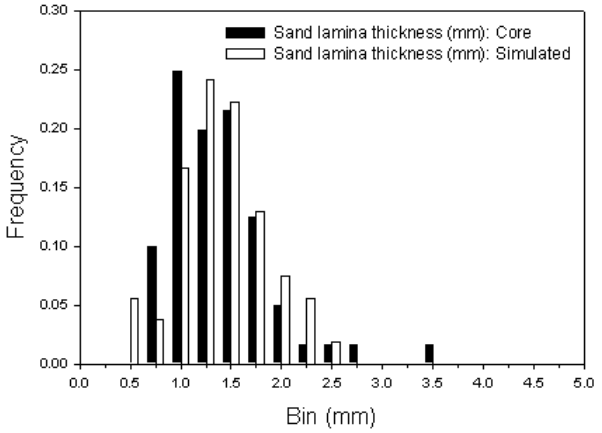

FIGURE 5.37 *Simulated lamina thickness for sand from the core (black) and the simulated (white) subfacies (Subfacies LF 7.1_PPL)*

For a statistical comparison of the simulated and measured distributions, F-test and t-test could have been calculated on log-transformed data sets to check if the variability and the mean, respectively, were similar. The measurements on the core had a resolution of 2 mm, while the vertical cell size (regular) in the simulated models was 1 mm. Due to difference in resolution between the core measurements and the simulations, t- and F-test cannot be used to test the degree of similarity between the two data sets. However, the histograms with, except for LF7.1_PPL, a bin size of 2 mm are used, in addition to the reported statistics, to validate the models and it is fair to state that the simulated models are similar to the observed subfacies.

The lamina thickness in LF7.1_PPL showed a possible periodic component. Figure 5.38 shows the ACF results of the core measurements and the simulated models. Both show a periodic component at lag 14. A tentative interpretation of this periodicity can be that it reflects a neap-spring cyclicity in a diurnal system or in a mixed to semi-diurnal system where the sub-ordinate current are too weak to transport sediments. Reineck and Singh (1980, p. 120-121) observed that similar structures formed on beaches owing to swash and back-swash of waves and that during one tidal phase, 6-16 lamina were produced. They also discussed alternative depositional processes. Regardless of the interpretation, the periodic component is

observed and incorporated in the simulation parameters giving a fine scale vertical variation in petrophysical properties in this subfacies.

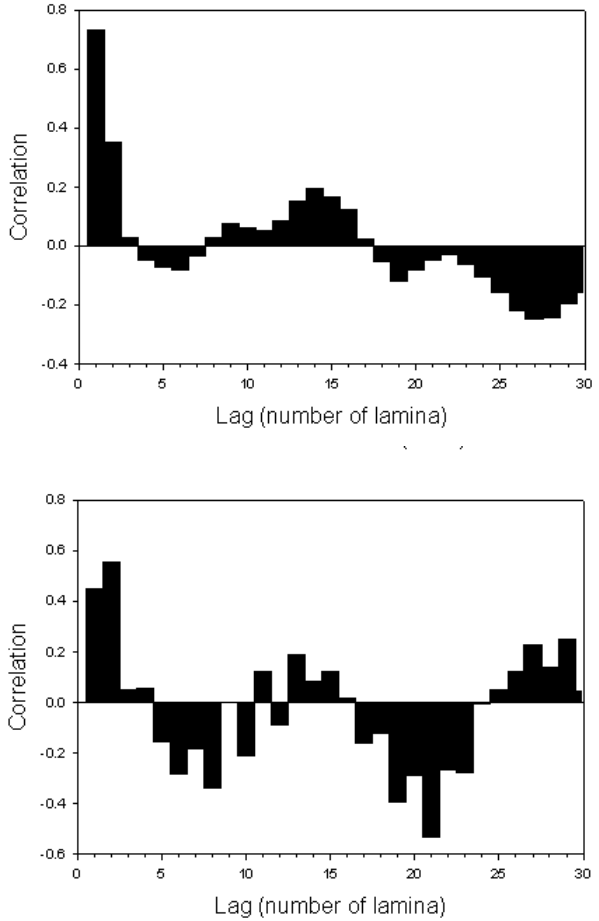

FIGURE 5.38 *Comparison of periodicities in LF 7.1_PPL between core measurements (top) and resulting periodicity from the simulation (base). Both measurements show increased correlation at the 13-15 lamina lag. The data are smoothed with a 3-point running average.*

The periodic components in LF3 were extensively discussed above. The shortest wavelength, prominent in all the measured lines and in both the ACF and the spectral analysis, were interpreted to represent a semi-annual tidal influence. The results

showed that approximately 15 sand layers constitute one cycle. This corresponded to approximately 15 cm cyclicity in the sand fraction (figure 5.25 and 5.26). A vertical periodic component was thus included in the simulation parameters. Figure 5.39 shows the histograms for the sand and mud laminaset thickness in the core and from the simulations and the statistics are given in table 5.2 and 5.5.

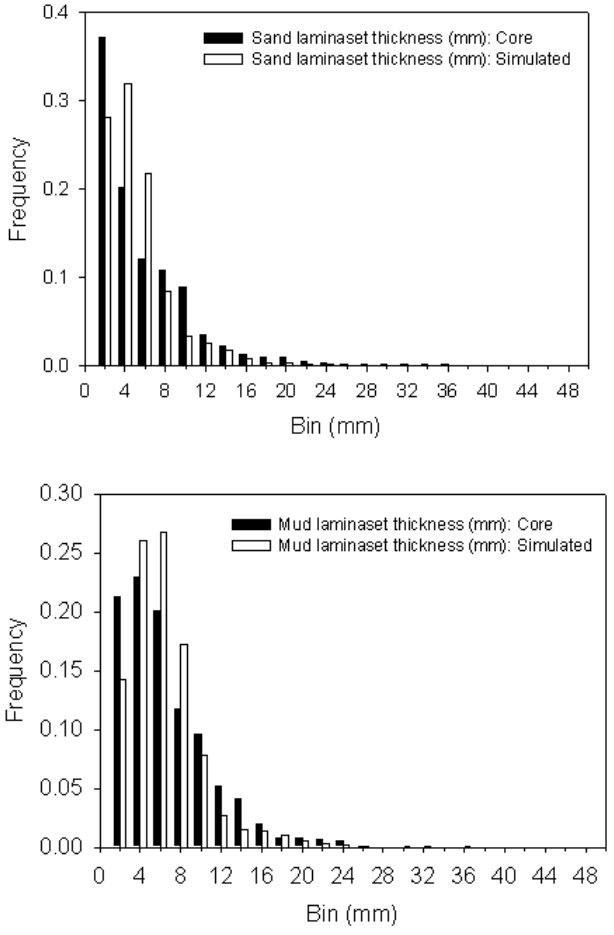

FIGURE 5.39 *Histograms of sand and mud laminaset thickness in LF3 from core and simulations.*

To test that the periodicity observed was simulated correctly, four realizations were analysed with the ACF and the spectral method. Figure 5.40 shows the results from the ACF analysis and figure 5.41 the results from the spectral analysis of the sand laminaset thickness. Figure 5.42 shows similar results for the sand fraction curve. The results are also reported in table 5.6. In the ACF plot, some of the increased correlations at longer lags represent multiples of a shorter period. There is, however, a reasonable good match between the observations and the simulations which, with the limitations discussed above, verify that the models are realistic with respect to this parameter.

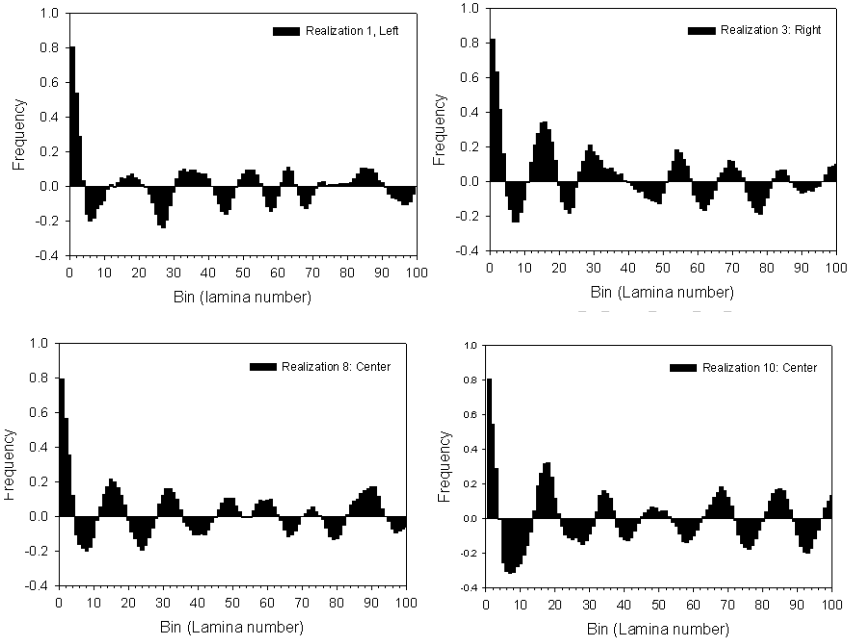

FIGURE 5.40 *ACF results on the sand laminaset thickness from the simulations on LF3. One line from 4 realizations are shown. The simulated periodicities are good agreement with the observed periodicity from the core measurements. The other realizations show similar result. The raw data are smoothed with a five-point running average before the analysis.*

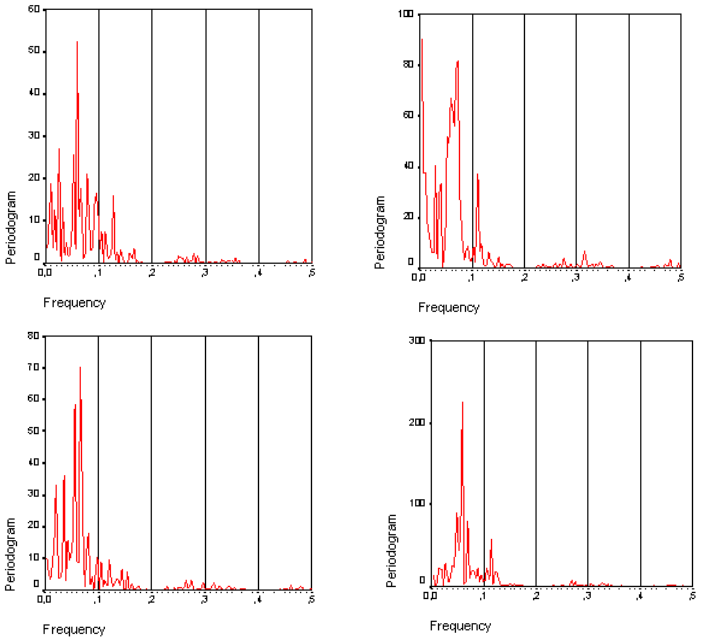

FIGURE 5.41 *Spectral results on the same data set as in figure 5.40. The results are in agreement with the measured periodicities (figure 5.21 to 5.23 and table 5.3) from the core validating this parameter.*

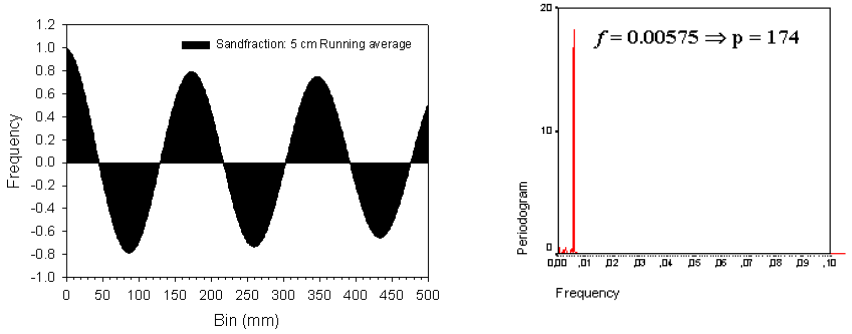

FIGURE 5.42 *ACF and spectral results from the sand fraction curve. The data used is an arithmetic average of the 10 sub-grids (5 realizations) and with a 5 cm running average taken down core subsequently. The calculated periodicity of 17 cm is in well agreement with the observation of a 14-18 cm periodic components from the core (figure 5.25 and 5.26).*

	Spectral analysis		ACF analysis
	Frequency (f)	Period (1/f)	Lag
Realization 1	0.126	7.9	15-19
	0.095	10.5	32-36
	0.078	12.8	50-54
	0.058	17.2	63
	0.025	40	
Realization 3	0.11	9.1	14-17
	0.072	13.9	28-30
	0.05-0.07	14.3-18.2	53-56
	0.03	33.3	68-71
Realization 8	0.08	12.5	13-18
	0.069	14.5	30-33
	0.057	17.5	87-91
	0.03	33.3	
	0.02	50	
Realization 10	0.11-0.1	9-10	15-19
	0.07	14.3	33-35
	0.06-0.05		67-69
			83-86
Sand fraction	0.00575	174 (17.4 cm)	173 (17.3 cm)

TABLE 5.6 Periodic components from ACF and spectral analysis of the simulated templates (compare with table 5.3).

This chapter has, based on the work of Martinius et al. (2001), described the lower part of the Tilje Formation in the Heidrun field and showed how realistic near wellbore models of the lithofacies present can be made. The near wellbore models created here, which contain information about the geometry and distribution of the major lithological components, will in the next chapter be populated with petrophysical properties giving basis for evaluating the flow properties of these heterolithic lithofacies. This chapter has also used time-series analysis methods on a ripple-laminated lithofacies and suggested a depositional model that explains the tidal cyclicity observed.

CHAPTER 6

Petrophysical distributions in tidal facies

In chapter 5, models of the sedimentological components, their geometry and distribution in space were created for a specific interval of the lower Tilje Formation. In this chapter, these models are populated with petrophysical properties from core plugs. Besides suggesting a simple and practical iterative procedure to populate the models with core plug properties, an additional outcome of this work is that the petrophysical properties of the lamina can be evaluated and related to the facies it represents. The result is a better understanding of where and how the variability varies with measurement method. Correct population of the geometrical models with petrophysical properties is also an important step in creating a realistic numerical model of the near wellbore region. All the petrophysical input distributions reported in this chapter are given in Appendix A.2.

The decrease in sample variance with increasing sample support is well known (e.g. Journel and Huijbregts, 1989; Armstrong, 1998). Haldorsen (1986), Ringrose et al. (1999a), Ball et al. (1997), Panda et al. (2001) and Worthington (2003a) amongst others, have shown this with well data from different sample volumes. This chapter will cover a short petrophysical description of the selected interval showing the high variability within lithofacies, the decrease in variance with increasing sample volume and some effects of biased sampling (section 6.1). An iterative procedure is described in section 6.2 that can be used to obtain input parameters for modelling (e.g. with SBED). The results are given in section 6.3.

The petrophysical input parameters for bedding modelling require lamina scale data (chapter 4). Ideally, one would then prefer measurements of the individual lamina. This can be obtained with a well-designed probe permeameter study. Probe permeameter data are not routinely taken, in contrast to core plug samples that are taken with regular spacing in most cored intervals. If, however, there is lithological variability below the core plug scale, these measurements represent an average of these components (see discussion in section 2.3.3). Further, the input permeability is usually given as a scalar value such that permeability anisotropy at the lamina scale is not included. Campbell (1967) defined a lamina to be uniform in composition and texture, which however implies that it can be anisotropic with respect to permeability. At present, in the SBED program, the input permeability variable must be given with the assumption that it is isotropic at the lamina scale and that anisotropy at the bedding scale arise because of contrast between lamina.

Permeability values can span several orders of magnitude in value and the standard deviation usually increases as the mean increases. A useful measure of permeability dispersion, called the Coefficient of Variation (C_V) is defined as (e.g. Jensen et al., 1997):

$$C_V = \frac{\sqrt{Var(k)}}{E(k)} \qquad \textbf{[6-1]}$$

where Var (k) and E(k) is the variance and the expected value of k, respectively. An estimator for C_V is:

$$\hat{C}_V = \frac{\hat{s}}{\overline{k}_A} \qquad \textbf{[6-2]}$$

where $\hat{s}$ is the estimate of standard deviation and $\overline{k}_A$ the arithmetic average of the samples. The coefficient takes into account that the mean and standard deviation tend to change together: the standard deviation usually increases as the mean increases. The C_V can thus be used to compare variability between sample sets with different arithmetic average and standard deviation. For small samples (N<10) a correction factor of $\left[1 + \frac{1}{4(N-1)}\right]$ needs to be multiplied to the C_V estimate. Based on a large published data set, Corbett and Jensen (1992c) defined heterogeneity classes from the C_V:

$0.0 < C_V < 0.5$	Homogeneous
$0.5 < C_V < 1.0$	Heterogeneous
$1.0 < C_V$	Very heterogeneous

TABLE 6.1 Heterogeneity classes based on C_V (Corbett and Jensen, 1992c).

When $C_V < 0.5$ the permeability distribution is approximately normal and can be considered to be effectively homogeneous and not affecting the flow properties. As C_V increases, the distribution becomes increasingly more skewed and thus more heterogeneous. The N_0 method (Hurst and Rossvoll, 1991) can further be used to find the optimum number of samples to best describe the media:

$$N_0 = (10C_V)^2 \quad \textbf{[6-3]}$$

Corbett and Jensen (1992b), showed that this sample number gives an arithmetic average within 20% of the true value. When evaluating C_V of media that constitute of several components it is important to bear in mind that this statistic is not an additive property (Jensen et al. 1997). The total C_V for this mixture is not, in general, the weighted average of the present C_V's.

6.1 Petrophysical description of Lower Tilje Formation, Heidrun Field

Available petrophysical well data for this interval were horizontal and vertical core plugs and a suite of conventional wireline logs. In addition, a 10x10 cm grid with high-resolution probe permeameter data in LF7.1_WSF was available. The core plugs are Klinkenberg and overburden corrected (only horizontal core plugs). A Statoil wireline based estimator of permeability (KLOGH) and porosity were given. These estimates are based on several wireline logs along with a calibration to core data. Figure 6.1 shows both the core data and a selection of the wireline log curves in the interval with the lithofacies zonation defined by Martinius et al. (2001). It is clear from this figure that there is, in general, a mis-match between the core data and the wireline logs. It is also clear that there is a large variability within each lithofacies and, beside LF 7.1, the variability, or contrast, between the lithofacies is low. However, from the core description in chapter 5, it was evident that there were lithological variations affecting k_v/k_h both internally in each lithofacies and also

between the lithofacies. This indicates that the lithofacies are not well characterized with the available well data.

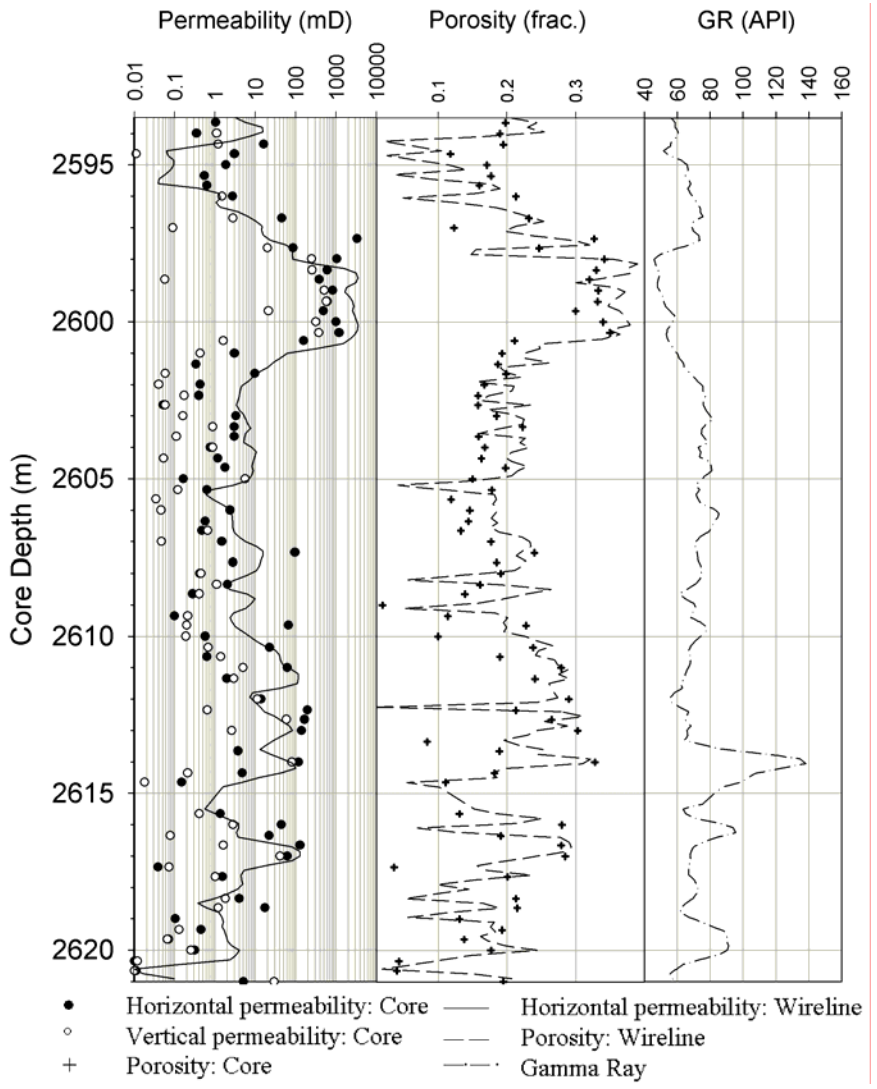

FIGURE 6.1 *Core and wireline interpreted properties from the studied interval. Note that there is a large variability in the data in each lithofacies (right) and that the petrophysical contrast between the lithofacies is low.*

To quantify the variability in petrophysical properties, the values for C_V for the different lithofacies have been calculated from different data sources representing different sample support. Equation 6-3 has also been applied to see if there were a sufficient number of samples from the lithofacies. The results are reported in table 6.2 to 6.6 (for the lithofacies code see section 5.1).

Interval/ lithofacies	N	Arit. Avg.	Min	Max	Median	StDev	C_V	N_0
T1.1-2.1	65	169.6	0.04	3355.19	3.01	482.63	2.86	817
LF 7.2	6	8.98	0.54	45.15	2.27	17.75	2.08	431
LF 7.1	11	887.2	86.24	3355.19	609.48	893.04	1.03	107
LF 3	30	9.53	0.05	95.92	1.32	22.86	2.42	586
LF 4.2	8	80.36	0.15	196.85	65.58	83.13	1.07	115
LF 1	10	28.09	0.04	128.61	10.59	41.15	1.51	227

TABLE 6.2 Descriptive statistics for horizontal core plugs (KLHOB)

Interval/ lithofacies	N	Arit. Avg.	Min	Max	Median	StDev	C_V	N_0
T1.1-2.1	56	45.44	0.01	576	0.78	124.31	2.75	756
LF 7.2	4	1.1	0.01	2.8	0.8	1.32	1.3	17
LF 7.1	10	231.5	0.06	576	249.5	215.52	0.96	92
LF 3	26	0.84	0.03	5.6	0.21	1.44	1.74	303
LF 4.2	7	21.95	0.02	80	2.6	33.24	1.58	249
LF 1	9	5.56	0.07	41.10	1.20	13.36	2.48	614

TABLE 6.3 Descriptive statistics for vertical core plugs (KLV)

Interval/ lithofacies	N	Arit. Avg.	Min	Max	Median	StDev	C_V	N_0
T1.1-2.1	69	0.2	0.02	0.35	0.19	0.08	0.37	14
LF 7.2	7	0.17	0.12	0.23	0.17	0.04	0.26	7
LF 7.1	11	0.31	0.21	0.35	0.33	0.04	0.14	2
LF 3	32	0.17	0.02	0.28	0.17	0.05	0.29	8
LF 4.2	9	0.22	0.08	0.33	0.21	0.09	0.40	17
LF 1	10	0.2	0.04	0.29	0.21	0.08	0.42	18

TABLE 6.4 Descriptive statistics for core porosity

	N	Arit	Min	Max	Median	StDev	C_V	N_0
T1.1-2.1	160	300.23	0.04	3540.01	8.34	835.16	2.79	778
LF 7.2	17	3.26	0.04	14.57	1.06	5.04	1.57	247
LF 7.1	23	1903	15.7	3540.01	2246.99	1337.95	0.71	51
LF 3	74	40.32	0.58	1523.54	6.54	180.09	4.48	2010
LF 4.2	20	35.50	4.91	101.18	26.67	29.06	0.83	69
LF 1	26	19.25	0.37	127.37	3.70	38.19	2.00	402

TABLE 6.5 Descriptive statistics for wireline estimate of permeability (KLOGH)

	N	Arit	Min	Max	Median	StDev	C_V	N_0
T1.1-2.1	156	0.22	0.01	0.39	0.21	0.08	0.37	14
LF 7.2	16	0.15	0.03	0.25	0.17	0.07	0.48	24
LF 7.1	23	0.33	0.15	0.39	0.35	0.07	0.20	4
LF 3	73	0.20	0.04	0.29	0.21	0.05	0.23	6
LF 4.2	19	0.23	0.01	0.32	0.24	0.08	0.36	14
LF 1	25	0.17	0.05	0.29	0.16	0.07	0.42	18

TABLE 6.6 Descriptive statistics for wireline estimated porosity (PHIF)

Except for vertical core plug permeability in LF 7.1, all the core plug permeability data are very heterogeneous (> 1) and they are in general under sampled (using the N_0 method). For KLHOB and KLV, the C_V for the whole interval (T1.1-T2.1) is higher than for the individual components. Comparing C_V for horizontal permeability from core plug and the wireline estimate, there is a general decrease. One notability exception is in LF 3 where C_V increases from 2.42 to 4.48. As discussed in section 2.3.3 and further below, there is a tendency for the core plugs to be taken from the more sand rich intervals, avoiding the mud layers giving a biased data set. The wireline log estimate, although often calibrated to the core plug measurements, is a less-biased data set since it is a continuous record against depth. The increase in C_V with sample volume may thus be related to the under-sampling of the mud layers by the core plugs. If the core plugs are un-biased, the calibrated log should reproduce the core-sample mean (Jennings, 1999). For horizontal permeability this is in general not the case, further indicating that the core plugs are biased.There might also be some errors in the depth matching and the “shoulder effect” from over- and underlying facies, but this effect is assumed to be minor relative to the sampling bias.

In contrast to the vertical and horizontal permeability core plug data, the porosity measurements from the core plugs data set are more homogeneous (C_V<0.5). In addition, there is in general no large variation between the core plug and the wireline-estimated porosity indicating that there are not much bias in the core sample set (Jennings, 1999). It appears that although the samples have some bias with respect to permeability, porosity is less affected and that porosity measured at the core plug scale have almost the same mean and variance as the wireline based estimate. This can in part be related to the additive property of porosity.

6.2 Method

Since only a limited number of probe-data were available in this interval, the core plug data were the only generally available measurements of porosity and permeability. These measurements represent, however, an average of all the components present and cannot be used directly as input parameters to the modelling tool. A simple, straightforward procedure was therefore used in order to find the PDF’s for the individual lithological components present in the core plugs. The following numerical experiments can thus give some initial guidelines to the ‘true’ or underlying distribution for the lamina petrophysical properties. The assumptions and limitations of the procedure are discussed in section 6.4.

6.2.1 Simulating the core plug process

Horizontal core plugs are conventionally taken every foot in cored sections while vertical core plugs usually are taken less frequently. Ideally, the sampling program should be adjusted according to the heterogeneity level of the lithofacies by using the N_0-rule as guideline, but this is seldom done in the industry. To simulate the process of taking core plugs, 3 m long intervals of the models representing the different subfacies (chapter 5) were created. From the simulated model, a rectangular sub-model was extracted every 30 cm along the model. The sub-model had the dimension 3cm by 2 cm by 2 cm in the x, y and z-directions respectively. This sample volume (12 cm^3) is approximately the same as a conventional core plug. In the following, these core plug sized sub-models will be called ‘simulated core plugs’. It is important to note that there is no bias in this sampling program. Due to time constraints, only core plugs with longest axis in the x-direction were simulated. The correlation lengths of the different components, especially the mud layers, are usually longer then the sub-model domain and it is therefore assumed that there will be no large variation for simulated core plugs with the longest axis in the y-direction. For the vertical direction, the correlation lengths of the mud layers are usually shorter than 2 cm and it is therefore assumed that calculating the effective vertical permeability of the simulated horizontal core plugs approximates an expression for the vertical permeability at the core plug scale. However, this is not strictly true, and if the procedure should be applied routinely, these assumptions should be checked further.

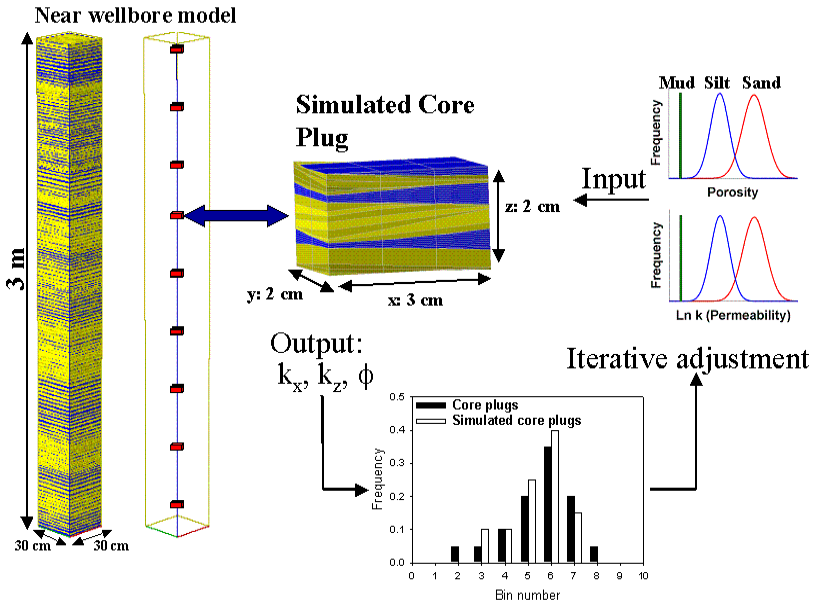

FIGURE 6.2 *Method used for simulation of core plugs. The core plug sized sub-grids are upscaled and compared with the real core plug distribution. If a mis-match is present the input distribution is changed.Yellow and brown is sand (two types, representing contrasting lamina) and blue is mud.*

All the described subfacies in chapter 5 that had core plugs were subject to this procedure. The natural logarithm of the measured values from the core plugs was used as a starting point. By iterative adjustment of the input value, the upscaled simulated core plugs were compared with the real core plug distribution. When a satisfactory match was obtained between the two data set the input properties (porosity and permeability) were regarded as a property of the individual lithological components present. The near wellbore model, the simulated core plugs and the iterative adjustment of the petrophysical input parameters are illustrated in figure 6.2.

6.3 Results: Simulated lamina properties and its relation to bedding type

Using the procedure described above, an attempt was made to determine the input porosity and permeability distributions that produced an upscaled distribution simi-

lar to the core plugs. Statistical similarity between these data sets would give, in part, a validation of the simulated near wellbore models for the different subfacies. In addition, it gives a possibility to evaluate if there is some relationship between the lamina properties and the upscaled (averaged) distribution at the core plug scale.

Arithmetic and harmonic averages are often used to calculate horizontal and vertical permeability for infinite layers. A first guess could then be that the respective average of the individual lithological components would approach the observed distribution at the core plug scale. The petrophysical properties of the components are given as a normal and log-normal distribution for porosity and permeability respectively, which are completely specified with the mean (μ) and standard deviation (σ). Equations 6-4 and 6-5 give the expressions for these distributions.

$$f(x;\sigma,\mu) = \frac{1}{\sqrt{2\pi\sigma^2}} e^{\left[-\frac{1}{2}\left(\frac{x-\mu}{\sigma}\right)^2\right]} \quad \text{Normal distribution} \qquad \textbf{[6-4]}$$

$$f(x;\sigma_{\ln x},\mu_{\ln x}) = \frac{1}{x\cdot\sigma_{\ln x}\cdot\sqrt{2\pi}} e^{\left[-\frac{1}{2}\left(\frac{\ln x-\mu_{\ln x}}{\sigma_{\ln x}}\right)^2\right]} \quad \text{Log normal distribution} \qquad \textbf{[6-5]}$$

As discussed previously, in the models made here there are three lithological components each described with a random normal variable: sand ($Y_1 \sim N(\mu_1, {\sigma_1}^2)$), silt ($Y_2 \sim N(\mu_2, {\sigma_2}^2)$) and mud ($Y_3 \sim N(\mu_3, {\sigma_3}^2)$). Assuming that these components are independent, and with a sand fraction equal to b/2, silt fraction equal to b/2 and a mud fraction of (1-b), the arithmetic average is (see table 5.4 for values of b for the subfacies):

$$\bar{Y}_{Arithmetic} = \frac{b}{2}Y_1 + \frac{b}{2}Y_2 + (1-b)Y_3 \qquad \textbf{[6-6]}$$

which is normally distributed with the parameters

$$\bar{Y}_{Arithmetic} \sim N\left[\left(\frac{b}{2}\mu_1 + \frac{b}{2}\mu_2 + (1-b)\mu_3\right), \left(\left(\frac{b}{2}\right)^2{\sigma_1}^2 + \left(\frac{b}{2}\right)^2{\sigma_2}^2 + (1-b)^2{\sigma_3}^2\right)\right] \qquad \textbf{[6-7]}$$

Equations 6-7, 6-4 and 6-5 are thus used to calculate the arithmetic average of the input distributions for comparison with the upscaled distribution to see if the simulated horizontal core plug distribution and porosity could be estimated with a simple linear combination of random variables. Harmonic average of random variables, to estimate the vertical permeability, cannot be done analytically, but can be found by e.g. Monte Carlo simulations. Such a simulation is not performed here.

To compare the simulated and the observed core plug distributions, both t-test and F-test statistics were taken on the two data sets. The t-test is used to test the hypothesis that the *means* of the two distributions are similar at a certain confidence level. The F-test is used to test if the *variances* of the two distributions are statistically similar. A basic assumption is that the data are independent and normal distributed. For the permeability data a log-normal transformation is thus applied. The results from these tests are reported in the sections below. The p-value, which is the lowest level of significance at which the observed value of the test statistic is significant, is given for each test. For values larger than 0.05, the difference is insignificant (at this significance level). For further explanation of these statistical tests, see Jensen et al. (1997) or Walpole et al. (1998).

The petrophysical properties, and especially the permeability of the mud components is difficult to assess from a laboratory perspective. This thesis has used a constant and low value for both porosity and permeability of mud using values of 0.05 and 0.01 mD, respectively. The effect of varying the mud permeability at certain (critical) mud fractions will be presented in chapter 8.

Subfacies LF4.2_LTW has few core plugs. However, the bedding type, including the grain size, resembles subfacies LF3_LTW (see table 5.2 and table 5.4). It is assumed that the petrophysical properties of these two units are the same and they are combined in the further analysis.

6.3.1 Horizontal Permeability

Figure 6.3 shows the results from the simulations and table 6.7 gives the mean and standard deviation of the log-transformed data sets in addition to the p-value from the t- and F-tests.

The arithmetic means of the simulated core plugs are generally statistically equal to the observed core plug distribution. The variance is, however, in general not equal. This is true even though the visual fit between these two distributions is good.

The modelled facies have different bedding geometry and different mud fraction (see table 5.5). Figure 6.3 shows that there is a shift of the input distribution of the sand components towards lower values as the mud content increases. In figure 6.3 (A) and 6.3 (D) the mud fraction is 0.45-0.5 and the sand and silt distributions are located around the mean horizontal permeability of the core plugs. As the mud content decreases (figure 6.3 E, C, B and F) the core plug values are gradually shifted to the upper tail of the sand and silt component distributions. In the HCS (figure 6.3 F) there are however some cemented core plugs that disturb this trend. As the mud content decreases, the arithmetic average of the three (or two) components present approaches the distribution at the core plug scale. At high mud contents, the arithmetic average is considerably below the core plug distribution and the variance is very low. One reason for this is that the mud permeability used is a low and constant value giving a low variance also influencing the mean value. An additional cause can be that the horizontal permeability is less affected by the mud layers. In the case of the latter, the arithmetic average of the sand and silt components could have given a better match to the core plug distribution. This observation will be discussed in a broader context in section 8.4 were different flow-regimes will be quantified.

In subfacies LF7.1_WSF there was available a grid of closely (2mm) spaced probe permeameter data. The absolute values of these measurements are higher than the Klinkenberg corrected and overburden corrected core plug data. In figure 6.3 (C), these data can be seen to be close to the mean input permeability and showing that the variance of the probe data are on the same order as the input variance at the lamina scale. This observation shows the potential for using probe data as input parameter for near wellbore modelling.

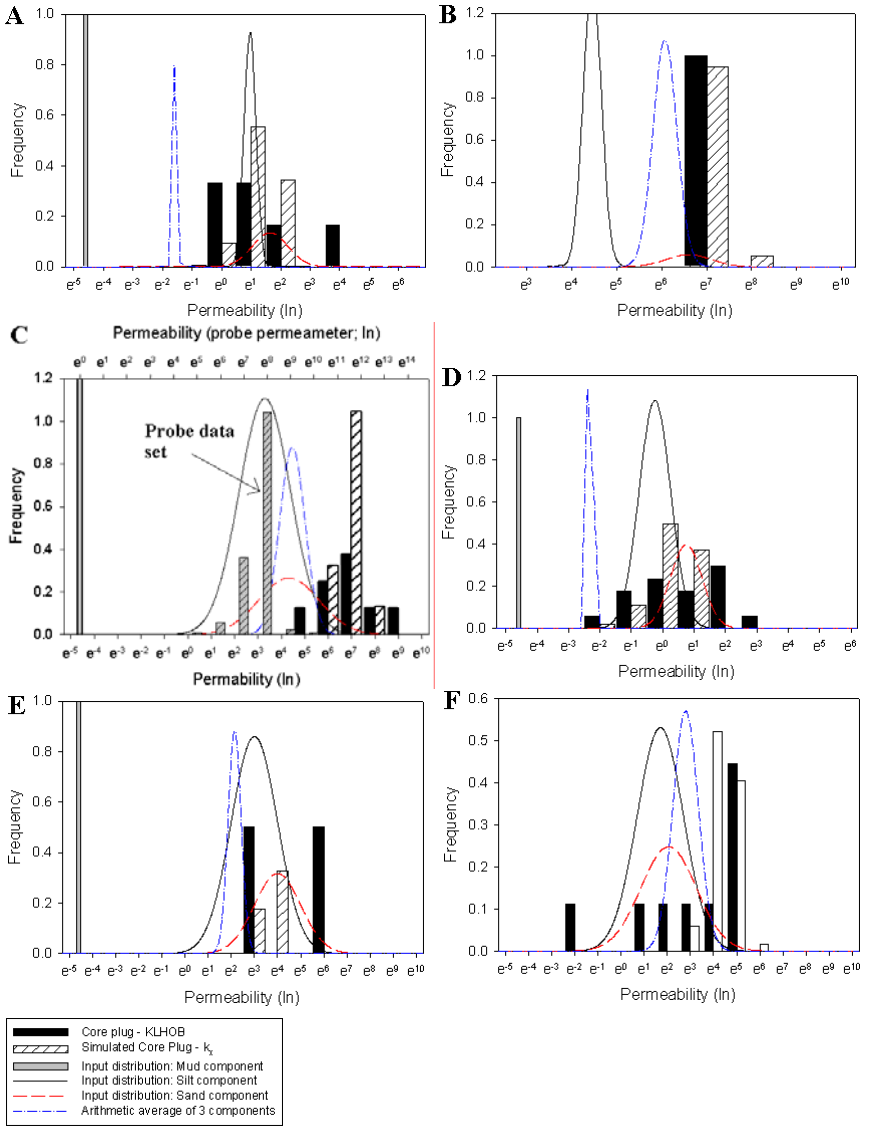

FIGURE 6.3 *Horizontal permeability (k_x). Comparison of observed and simulated core plugs. A: 7.2_WB, B: 7.1_PPL, C: 7.1_WSF, D: 3_4.2_LTW, E: 4.2_WSF, F: 1.3_HCS. Note that the x-values for the probe-data is indicated on top in C.*

Although there are relatively few core plugs in some of the subfacies, it appears that there is a relationship between the permeability distribution of the lithological components (input distribution), the upscaled distribution (at the core plug scale) and the bedding type. At low mud contents, the permeability distribution at the core plug scale is mostly dominated by high permeability values (streaks) since the observed core plug distribution is located in the upper tail of the input distribution. At higher mud contents, the geometry and property of the mud layers also influence on the core plug distribution. This will be further discussed in section 6.4.

	Core plug			SBED simulated core plug			F-test	t-test
SBED model	N	A.Avg (ln)	Var (ln)	N	A.Avg (ln)	Var (ln)	P	P
7.2_WB	6	0.91	2.55	171	0.72	0.30	3.4E-7	**0.79**
7.1_WSF	8	6.25	1.31	171	6.38	0.25	1.6E-5	**0.76**
7.1_PPL	3	6.76	0.09	171	6.7	0.03	**0.05**	**0.78**
LTW	17	-0.02	1.97	171	-0.25	0.40	2.5E-8	**0.50**
4.2_WSF	2	6.76	0.09	171	6.70	0.03	0.002	**0.71**
HCS	9	2.75	6.17	171	3.86	0.32	1.5E-20	**0.22**

TABLE 6.7 Descriptive statistics and results from F and t-test comparing horizontal permeability for core plugs from the different subfacies with the simulated core plugs for the same subfacies. Bold values indicate that the two data sets are statistically similar (larger or equal to 0.05).

6.3.2 Vertical Permeability

The results from the simulation of vertical permeability (k_z) are reported graphically in figure 6.4 and summarized in table 6.8. There are in general fewer vertical core plugs than horizontal giving the iterative process few values to condition on. The t-test results indicate that the mean of the two distributions are similar for all the models but that the variance (as for horizontal core plugs) is more difficult to match.

In contrast to permeability in the x-direction, there is no clear relation between the input distribution for the lithological components, the distribution at the core plug scale and the bedding type. The input permeabilities for the sand and silt components in the more mud-rich models have higher mean values than the upscaled per-

meabilities at the core plug scale (figure 6.4 A and D). This indicates, as expected, that the vertical permeability is more dependent on the amount, geometry and

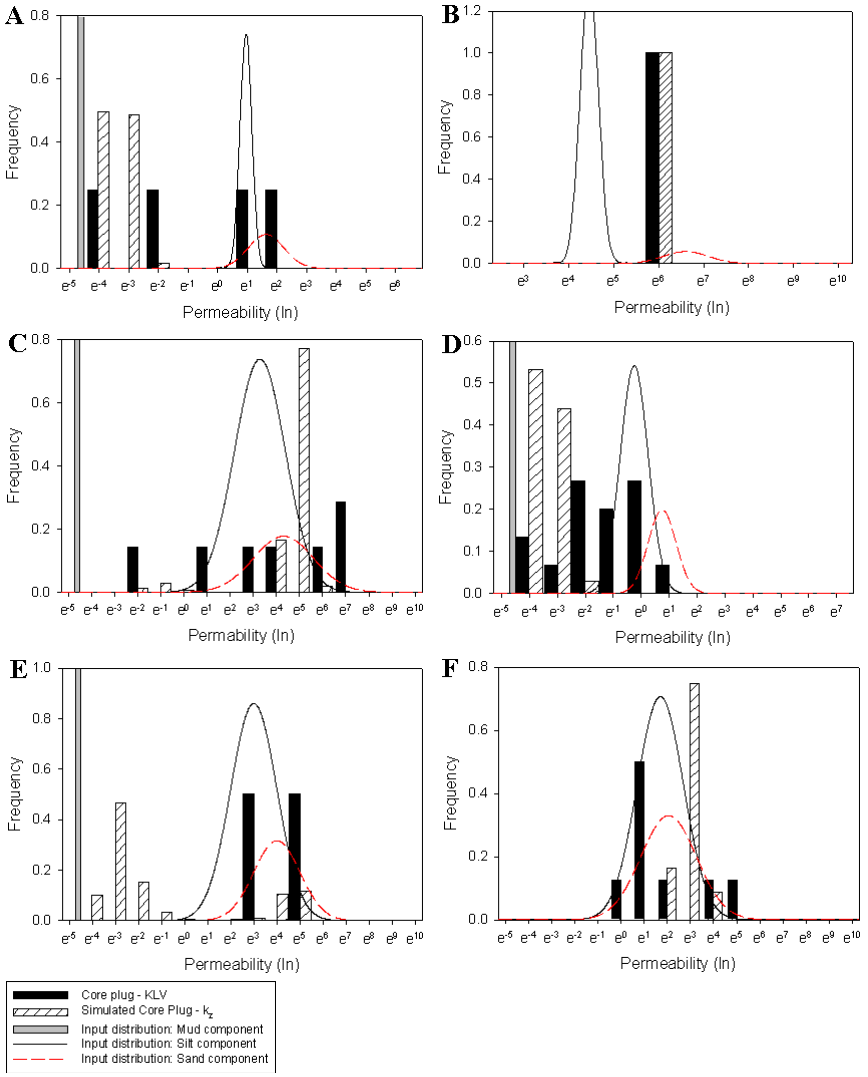

FIGURE 6.4 *Comparison of simulated and observed core plugs for vertical permeability (kv). A: 7.2_WB, B: 7.1_PPL, C: 7.1_WSF, D: 3_4.2_LTW, E: 4.2_WSF, F: 1.3_HCS.*

the petrophysical properties of the mud layers than the silt and sand components. From the core plug distribution we also see the effect of biased sampling. A large number of the observed vertical permeabilities are high and close to the sand and silt values even though the thickness of the sand layers are on average smaller than the length of the vertical core plugs. This indicates that the vertical core plugs are taken from the more sand-rich intervals and thereby represent a biased sample. In the iterative procedure that is used here, such core plugs are given less weight since they probably are unrepresentative.

	Core plug			SBED simulated core plug			F-test	t-test
SBED model	N	A.Avg (ln)	Var (ln)	N	A.Avg (ln)	Var (ln)	P	P
7.2_WB	4	-1.37	6.62	171	-3.93	0.13	4.3E-23	**0.14**
7.1_WSF	7	3.16	11.8	171	4.05	1.70	1.3E-06	**0.52**
7.1_PPL	3	5.60	0.02	171	5.47	0.006	0.042	**0.25**
LTW	15	-1.98	2.07	171	-3.93	0.15	9.2E-22	1.3E-4
4.2_WSF	2	3.25	1.36	171	-1.64	9.7	**0.30**	**0.11**
HCS	8	1.30	3.25	171	2.43	0.18	3.4E-18	**0.12**

TABLE 6.8 Descriptive statistics and results from F and t-test comparing vertical permeability for core plugs from the different subfacies with the simulated core plugs for the same subfacies. Bold values indicate that the two data sets are statistically similar (larger or equal to 0.05).

6.3.3 Porosity

The results from the simulation of the porosity core plugs are given in figure 6.5 and table 6.9. The t-and F-test indicates that the simulated core plugs are statistically similar to the core plug distribution in all the facies except for subfacies LTW (6.9 D).

The arithmetic average of the three (or two) components are, in all facies, close to the observed and simulated core plug distributions. This indicates that an additive property like porosity can be well estimated with a simple arithmetic average of the input distributions. The low, constant value of the mud porosity gives however a very low variance in the mud-rich models (A, D and E). The variance of the input distributions had to be set considerably larger then the core plug distribution, mean-

ing that a large fraction of the variability in porosity at the lamina scale is removed at the core plug scale.

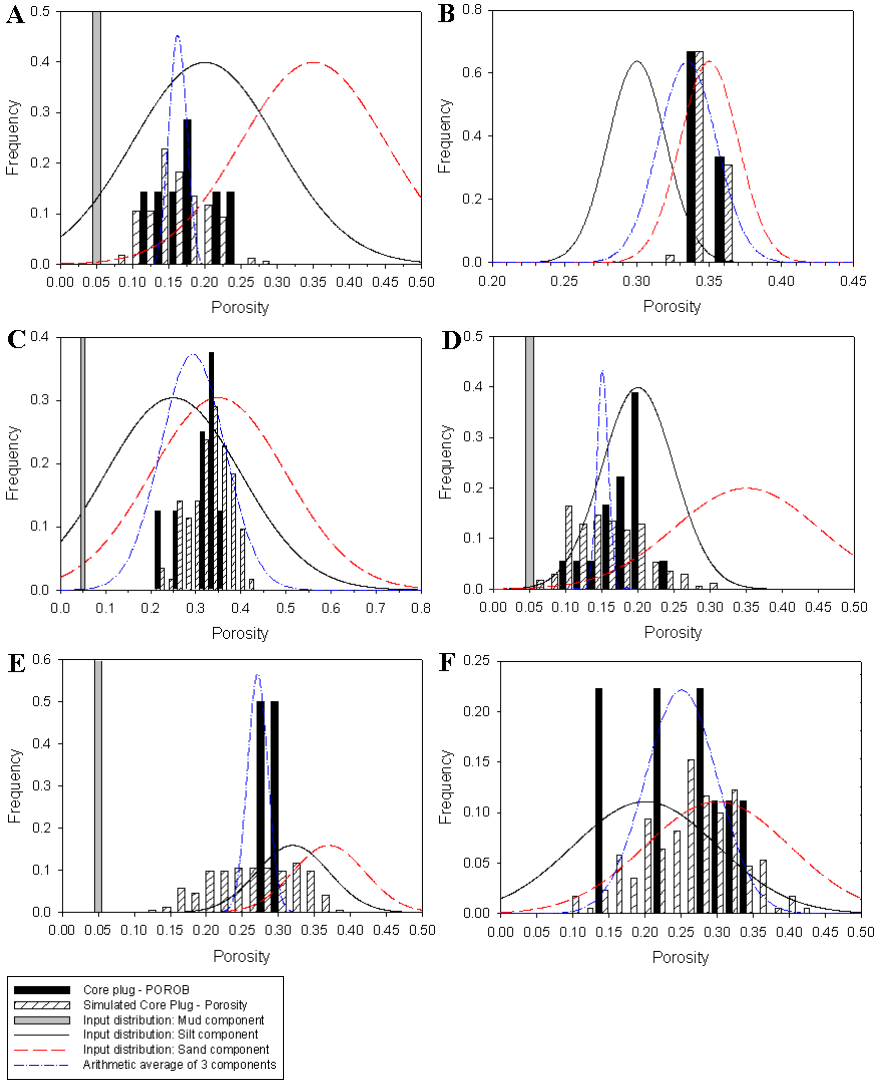

FIGURE 6.5 *Porosity (frac.). A: 7.2_WB, B: 7.1_PPL, C: 7.1_WSF, D: 3_4.2_LTW, E: 4.2_WSF, F: 1.3_HCS. See text for discussion.*

	Core plug			SBED simulated core plug			F-test	t-test
SBED model	N	A.Avg (ln)	Var (ln)	N	A.Avg (ln)	Var (ln)	P	P
7.2_WB	7	0.17	0.002	171	0.15	0.001	**0.31**	**0.22**
7.1_WSF	8	0.304	0.002	171	0.32	0.002	**0.33**	**0.34**
7.1_PPL	3	0.34	4E-5	171	0.34	5.4E-5	**0.53**	**0.79**
LTW	18	0.17	0.001	171	0.15	0.002	0.03	0.02
4.2_WSF	2	0.28	3E-4	171	0.25	0.003	**0.24**	**0.31**
HCS	9	0.24	0.005	171	0.25	0.004	**0.28**	**0.64**

TABLE 6.9 Descriptive statistics and results from F and t-test comparing porosity for core plugs from the different subfacies with the simulated core plugs for the same subfacies. Bold values indicate that the two data sets are statistically similar (larger or equal to 0.05).

6.4 Discussion

The primary aim of this chapter was to obtain a set of input parameters describing the petrophysical properties of the subfacies in the interval hence giving a realistic as possible representation of the near wellbore region in the selected interval. Core plugs were the only direct source of porosity and permeability. Since these represent an average of several lithological components, an iterative procedure was used to find the distributions for the individual components. More core plugs from the same interval in nearby wells would give a better basis for finding the lamina scale petrophysical properties. The intention of this chapter was however not to produce a set of input parameters valid for the whole field, but to develop a general method applicable for using core plugs as input to a near wellbore model and to test the method on the available data set.

Although there were few core plugs from each subfacies, and the N_0-rule generally indicate that permeability is under-sampled, it is assumed that the method can be used in general were core plugs are the primary source of petrophysical properties. It should be clear that probe data are favorable since they measure at a scale that approaches the lamina scale. Such measurements give however not porosity, and the method used by Fløl o et al. (2000) where the porosity-permeability relationship

derived at the core plug scale is used to calculate a mini-porosity can be difficult to apply here due the biased sampling and sub-core plug heterogeneities.

For horizontal permeability there were a possible relation between the input distribution, the core plug distribution and the bedding geometry and the presence of higher than average permeability lamina is used as a possible explanation. Such laminae have been reported by Atkins and Bride (1992), Bryant et al. (1993) and Robertson and Caudle (1971). These studies found that larger pore throats often exists in adjacent pairs and that they are not distributed randomly. Such an organizations of pore throats will then give lamina that can influence the flow properties significantly on the larger scale. From a geostatistical point of view, Isaaks and Srivastava (1989) showed that the degree of spatial continuity of the parameter of interest affected the averaging process. The effect of support on the averaging volume was greatest in un-correlated (homogeneous) data, while correlated (heterogeneous) data sets will be dominated by the extreme values. In SBED, a 2D variogram with a range on the order of 5 cm have been used to simulate a correlation structure in permeability and porosity. As the results above indicate, when the sand part of the core plug dominates the flow, the core plug distribution is located in the upper, higher permeability tail of the input distribution. In these low mud content facies, the mud layers have a small influence on the horizontal permeability. This influence will be further explored and discussed in section 8.3.3 and 8.4.

Vertical permeability in tidal deposits is more affected by the mud layers and their properties. The biased sampling along with the low and constant mud permeability that has been used, made a less good match between the simulated core plugs and the observed core plugs. An additional source to the mis-match is that permeability not always follows a perfect log-normal distribution as noted by Tidewell and Wilson (2000). At present only normal or log-normal distribution can be used as input to SBED.

There was in general a better match between the simulated core plug porosity and the observed core plug porosity. In contrast to permeability, that has to be matched in two directions (vertical and horizontal), the scalar porosity is easier to adjust. The weakness is obviously that the solution is not unique. The same upscaled results can be obtained by simultaneously changing the three (two) input distributions.

There are several subfacies described in chapter 5 that were not sampled with core plugs. These units are assumed to have the same petrophysical properties at the lamina scale as nearby subfacies. For example 7.2_LTW is assumed to have the same porosity and permeability distribution as 7.2_WB. The facies without core

plugs are volumetric less important than the subfacies that are modelled here, but they can still affect the near wellbore petrophysical properties. Further sampling, preferably with probe permeameter, must be done to assess the true lamina petrophysical properties of these subfacies.

The algorithm used to calculate the effective permeability (see chapter 4) produces only the diagonal elements of the permeability tensor. This means that an induced cross-flow is not satisfactorily taken into account. Pickup et al. (1994, 1995) have studied the amount of cross-flow in cross-laminated sedimentary structures. When the cross-terms are larger than 10%, a full tensor representation of permeability is needed. In cases where the angle of the lamina is small, the contrast between the lamina is low or the permeability of the bottomset laminae is low, cross-flow was found to be small and only the diagonal elements was needed. Further, in symmetrical bedforms, as the hummocky cross-stratification can be, no cross-terms are needed. In the tide-influenced subfacies studied here, the mean contrast between the sand and silt lamina (the cross-laminated components), varies from 0.1 in 7.1_PPL, 0.18 in 7.2_WB and between 0.3 and 0.37 for the remaining models (see Appendix A.2 for the petrophysical input parameters). According to Pickup et al. (1995), a contrast below 0.4 between the low and high permeability laminae give significantly (> 10%) cross-flow. Hence, some cross-flow is expected in the structures modelled here and an alternative algorithm with periodic boundary conditions (Durlofsky, 1991; Pickup et al., 1992) should be used. However, Ringrose et al. (1999) found that the amount of cross-flow was scale dependent. In a model with several ripple laminated sets (bed set), the off-diagonal terms were negligible since, at that scale, the flow pattern was dominated by the geometry of the laminasets and not the internal lamina structure.

As a final comment, the results from this chapter verifies that the geometrical and petrophysical near wellbore model created of the interval is relatively realistic and that it captures the main heterogeneities affecting the petrophysical properties. The models can thus be regarded as representative for some of the lithofacies encountered in the lower part of the Tilje Formation in the Heidrun field. This near wellbore model will be used in chapter 9 to forward model porosity and permeability at various sample volumes giving a mean for comparison with the currently used estimators.

CHAPTER 7

Petrophysical variation and sample support

It was discussed in section 2.1 that calculation of permeability at the pore scale is challenging due to the complex pore geometry. A common approach is instead to evaluate the porous media in a statistical sense. Fundamental to this approach, the continuum approach, is to determine how much of the rock volume that needs to be statistically averaged to give a representative value. This chapter will evaluate numerically how the dispersion of porosity and permeability varies as a function of sample support. Moreover, focus will be on the influence of spatial distribution and correlations of the sedimentological components (connectivity of sand and shale). Evaluation of the petrophysical influence of contrasting lamina will be explored in chapter 8. The results will be used in chapter 9 to give a better and more accurate estimate of the k_v/k_h ratio in the selected interval.

Since the studied interval contains only some of the possible tidal bedding types that can be encountered in a reservoir and since it is of interest to evaluate petrophysical variability with sample support from a general point of view, published flume tank studies are used to create a range of realistic tidal bedding models.

7.1 The continuum approach and representative elementary volume

The continuum approach has been described qualitatively in section 2.1. Essential to the concept of a continuum is the notation of a Representative Elementary Volume (REV). Bear (1972) was one of the first to thoroughly discuss the REV con-

cept. Following the arguments of Bear (1972), a REV can be defined as follows: a mathematical point P is situated in a porous medium. A volume ΔV_i much larger than the pores or grains has P as a centroid. For this volume the ratio

$$\varphi_i = \varphi_i(\Delta V_i) = \left[\frac{(\Delta V_p)_i}{\Delta V_i}\right] \quad \textbf{[7-1]}$$

can be determined where $(\Delta V_p)_i$ is the volume of pore space within ΔV_i. By gradually decreasing ΔV_i around P ($\Delta V_1 > \Delta V_2 > \Delta V_3 \ldots$) a sequence of values $\varphi_i(\Delta V_i)$, $i = 1, 2, 3 \ldots$ may be obtained. A schematic graph of the relationship between φ_i and ΔV_i is showed in figure 7.1. In an inhomogeneous medium, φ_i may undergo gradual changes as ΔV_i decreases. Below a certain value of ΔV_i these fluctuations are reduced leaving a near constant value of φ_i. Further reducing ΔV_i will lead to large fluctuations in φ_i and as ΔV_i converges on the mathematical point P, φ_i will either take the value zero or one depending on whether P is inside a pore or a solid grain. Bear (1972) then defined the volumetric porosity as the limit of the ratio φ_i as $\Delta V_i \rightarrow \Delta V_0$:

$$\varphi(P) = \lim_{\Delta V_i \rightarrow \Delta V_0} \varphi_i\{\Delta V_i(P)\} = \lim_{\Delta V_i \rightarrow \Delta V_0} \frac{(\Delta V)_i(P)}{\Delta V_i}. \quad \textbf{[7-2]}$$

For volumes below ΔV_0 the individual pores must be considered and no single value can represent the porosity at P. Bear (1972) defined the volume ΔV_0 as the Representative Elementary Volume (REV) of the mathematical point P. Such a volume is characterized by the property that adding or subtracting a small number of pores will not change the porosity value. Stated qualitatively, a REV, if it exists, must be much smaller than the entire flow domain since it should represent the property at P, and it should include a sufficient number of pores to permit a meaningful statistical average. By introduction of the REV concept, the actual porous medium is replaced by a fictitious continuum representing the property at the point P.

In an inhomogeneous medium, an upper limit of REV, in this case for porosity, can be defined with a characteristic length L

$$L = \frac{\varphi}{\partial\varphi/\partial l} \quad \text{[7-3]}$$

that in cartesian coordinates becomes

$$L_x = \frac{\varphi}{\partial\varphi/\partial x} \quad L_y = \frac{\varphi}{\partial\varphi/\partial y} \quad L_z = \frac{\varphi}{\partial\varphi/\partial z} \quad \text{[7-4]}$$

which indicate the rate at with changes in porosity take place. The volume $L_x L_y L_z$ then serves as the upper limit of the range from which we may choose the REV for porosity. The lower limit is given by ΔV_0.

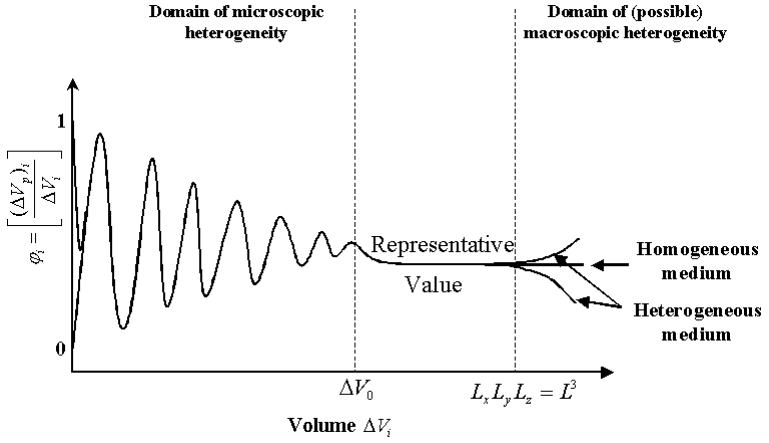

FIGURE 7.1 *Schematic REV graph with the characteristic lengths defining the size of the REV. Modified from Bear (1972).*

The upper and lower limits are closely related to the geostatistical terms local homogeneity and local stationarity (Anguy et al. 1994). Homogeneity is defined qualitative as a characteristic denoting that physical properties between elemental volumes of a material have the same value regardless of their locations (Olea, 1991). Local homogeneity is attained at that scale where the local fabric or microstructure is either random or quasi-periodic. This is the same as the condition where a measured property is relatively insensitive to small changes in volume or location. Local stationarity occurs when two or more mutually adjacent, locally homogeneous samples yield similar value of the property of interest. Strict stationarity requires that all the moments of the spatial distribution function are invariant under

translation (Journel and Huijbregts, 1978, p. 32). Usually only a condition of weak stationarity is required where the first two moments are invariant. That is, that the mean is constant and that the variance between two samples is only are dependent on the distance between them. As pointed out by Anguy et al. (1994), without local (weak) stationarity the physical property of the sample has little bearing on the properties of the large volume of the porous medium. In fact, they define a lamina or bed as an interval in which local stationarity exists. It should be clear from this discussion, that a representative petrophysical value should be measured at a volume that is locally homogeneous and locally stationary. The volume of a measurement is termed the sample support volume (section 2.3.3) and ideally this should be coincident with the REV.

The same line of arguments can be made for other properties of the porous media (e.g. permeability) and Bear and Braester (1972) were one of the first to note that the REV can be different for different petrophysical properties. If different properties have different REV, then a common volume, if it exists, should be chosen as a representative volume.

Bear (1972) focused mainly on the pore scale REV: how many pores and grains must be sampled to obtain a representative value at point P. In a natural sedimentary depositional system, it can be assumed that there exist several REV's related to the different scales (section 2.3.3 and 3.2). Norris and Lewis (1991) introduced the notation of "scale n REV" to extend the concept beyond the pore scale. The pore level $REV^{n=1}$ will then be at the pore to the lamina scale. This chapter will focus on the lamina to bed scale $REV^{n=2}$ (dm-m scale). Figure 7.2 shows conceptually how a nested structure of scales can give different REV's. In the following, the n=2 notation is implied and not explicitly written.

Another way of illustrating the variance reduction with volume is with the additive relation of Krige (e.g. Armstrong, 1998):

$$\sigma^2(v|V') = \sigma^2(v|V) + \sigma^2(V|V') \qquad \textbf{[7-5]}$$

where $v < V < V'$. This means that the variance of v within V´ is equal to the variance of v within V plus the variance of V within V´. Although a simple relation much used in the mining industry, it only applies to properties that can be averaged arithmetically (Isaaks and Srivastava, 1989). Hence, variance reduction of permeability can not in general be estimated with this relation, but Dubrule and Haldorsen (1986) gave an approximation to equation 7-5 using a logarithmic transformation of permeability.

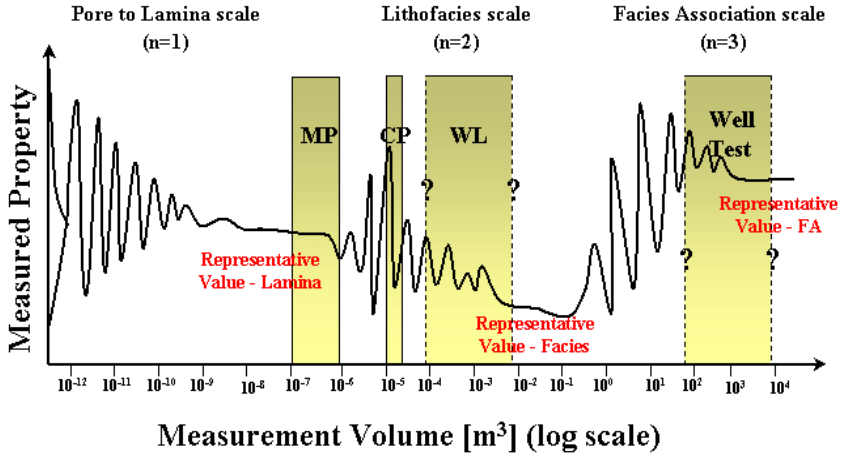

FIGURE 7.2 *A conceptual sketch of different possible scales (n=1,2,3) of REV related to sedimentological heterogeneities. Also indicated are the approximate measurement volumes of some well data types. MP = mini-permeameter, CP = core plug and WL = wireline log measurement.*

The REV concept has been discussed in relation to calculation of effective petrophysical properties in reservoir evaluation in many publications (e.g. Hassanizadeh and Gray, 1983; Haldorsen, 1986; Hurst, 1993; Nottinger, 1994). The operational significance of the continuum hypothesis has been reviewed by Bavey and Sposito (1984) who concluded that the REV concept was unnecessarily restrictive and that the application was difficult since experimental verification was challenging.

Experimental evaluation of the existence and size of the REV has been limited. Tidwell and Wilson (2000) and Corbett et al. (1999) have used a multi support probe (MSP) permeameter to investigate the pore scale REV. The first paper used a cross-stratified sandstone and found that the variance decreased with increasing sample support (increasing inner tip radius). Corbett et al. (1999) used both a homogeneous sandstone sample and heterogeneous carbonate samples. They found that in the homogeneous case the traditional averaging techniques (of the probe data) matched the larger scale measurements (Hassler cell), while for the anisotropic sample the harmonic and arithmetic averages match the perpendicular and parallel permeabilities, respectively, adequately. They questioned however if the MSP gave sufficient sample support in the carbonate samples. Although not directly addressing the REV concept, Henriette et al. (1989) divided a sandstone and a lime-

stone block (15*15*150 cm) successively into smaller samples measuring the permeability at each step both by flooding and numerically. Different averaging schemes were tried to upscale the smallest samples to the full block sample. The arithmetic average was found to give the best estimate in all cases. Jackson et al. (1999; 2003) divided two heterolithic rock cubes (~17000 cm^3) with different sand fractions (0.93 and 0.445) with a serial sectioning technique and reconstructed the architecture of the samples. The effective permeability was then calculated numerically at different sample volumes. The REV concept was to some extent validated and they reported that the core plugs represented a volume considerably below the REV. The error introduced by using different averages (arithmetic, geometric and harmonic) of the core plug data were evaluated and they found that the error was negligible for horizontal permeability but that it could be significant for vertical permeability. Norris and Lewis (1991) investigated tidal heterolithic facies in 2D where they digitized a photo into binary values (sand and mud) and calculated the effective permeability with a renormalization technique. Consequently, they examined the two-dimensional sand (or mud) connectivity. The representative elementary area (REA) was found to be equally large (around 20000 cm^2) for both vertical and horizontal permeability and for different fractions of mud (bedding types). The representative value was argued to be independent of location by observing that expansion of the averaging area with different starting points approached the same permeability value. They did not take into consideration that these areas eventually became overlapping (see discussion below).

The concept and existence of a REV at the bedding scale might seem intuitive and obvious. The references cited above have given some indications that there exists such a volume for different lithofacies. However, numerical experiments on a range of heterogeneous systems in three-dimensions have not been reported. The study presented here involving multiple simulations of heterolithic tidal deposits thus provides a new insight into REV.

7.2 Method

A range of flume-tank constrained numerical tidal bedding models were made and then upscaled to different support volumes. This will then form a basis for evaluation of how porosity and permeability varies as a function of sample support and to the discussion of the REV and scaling issues in complex, heterolithic tidal facies.

7.2.1 Flume tank constrained models

Relations between planform morphology, cross-section geometry and flow characteristics have been discussed in section 2.2.2.2. Baas (1994) studied the development of ripple morphology under unidirectional flow using flume tank experiments. He found that ripples approached an equilibrium size and shape with either increasing current velocity or depositional time. Given enough time, all ripples will evolve into an equilibrium size (height and wavelength) with linguoid planform, but increasing current velocity reduces the time before equilibrium is reached. Figure 7.3 shows the development of ripple wavelength and amplitude for a given grain size (0.095 mm) and current velocity (0.7 m/s) as a function of time, while figure 7.4 shows the evolution of the plan form morphology.

In depositional environments where tidal currents are present, the current velocity is typical unsteady with a cyclic variation related to the flood and ebb periods (section 3.2). Based on flume tank experiments, Oost and Baas (1994) observed that the ripple size and plan shape were related to the length and strength of the current. Figure 7.5 shows the flow velocity curves they used. Run T3 produced non-equilibrium ripples while run T1 created equilibrium ripples.

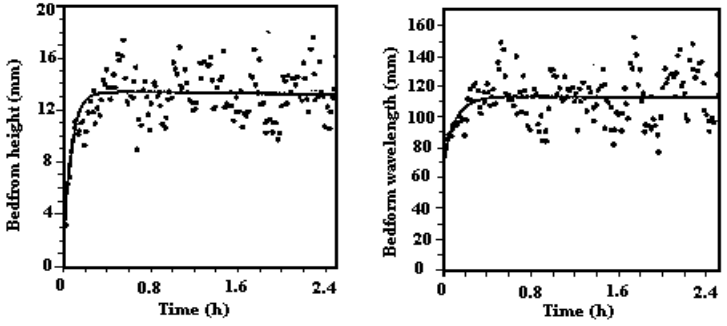

FIGURE 7.3 *Experimental flume-tank data of the bedform amplitude and wavelength as a function of time. From Baas (1994)*

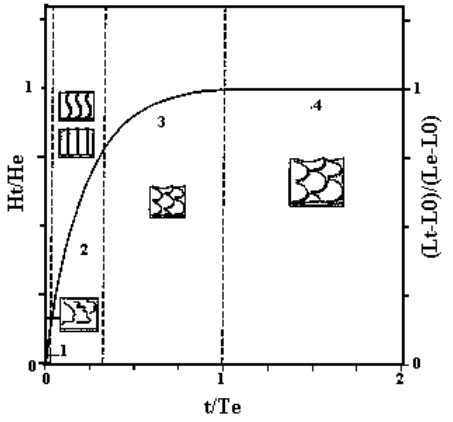

FIGURE 7.4 *Development of plan form morphology as a function of time. From Baas (1994).*

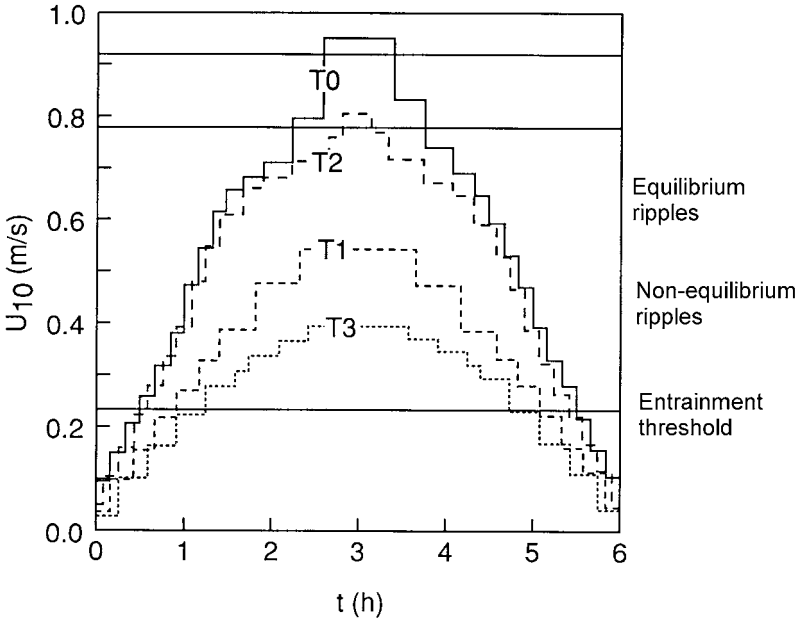

FIGURE 7.5 *A figure from Oost and Baas (1994) showing the velocity variation in the flume-tank resembling one tidal period (flood or ebb current). Compare this with figure 3.4.*

The results from Baas (1994) and Oost and Baas (1994) are used with some assumptions to create a set of bedding models that range from mud-rich lenticular bedding to sand-rich flaser bedding.

The following assumptions are used:

1) It is the depositional time above the entrainment threshold that controls the amount of sand deposited with respect to mud. This means that the bedding type is assumed to be related to the area between the different runs in figure 7.5 and the threshold velocity (Allen, 1985) (see also section 3.2).
2) Current velocity is proportional to flow strength (see discussion in section 2.2.2.1).
3) Increased flow strength does not increase erosion (out of the system) of sand significantly. This means that increasing the current velocity from below T3 to just above T1 in figure 7.5 will only increase the amount of sand deposited and the morphology and size of the deposited ripple.
4) Current velocity (and flow strength) are always in the lower flow regime.

Based on these assumptions, the following arguments are used to suggest that the time-axis in figure 7.3 and 7.4 can be replaced with increasing sand fraction. The amount of sand with respect to mud deposited in one cycle (flood or ebb period) is related to the area between the flow velocity curve and the entrainment threshold. Significant amounts of mud are only deposited from suspension at velocities below the entrainment velocity for sand grains (see also figure 3.4). A hypothetical curve below T3 will give a short period with sand deposition and consequently a longer period with mud deposition. Curves at or above T1 will then give a more sand rich deposit where only a short time period was available for deposition of mud. The bedform wavelength and amplitude produced for velocity curves around T3 and lower are in non-equilibrium due to shorter depositional time (figure 7.3).

The input parameters describing the bedform shape (mainly bedform wavelength and bedform amplitude) should then be related to the bedding type: the more sand rich deposit, the more close to the equilibrium state the ripples become. The input parameters for bedform wavelength (figure 7.6) and amplitude (figure 7.7) can then be expressed as a function of sand fraction (pseudo-time variable). The solid line and the error bars in these figures denote the mean and one standard deviation on the input parameter respectively. The standard deviation specifies the stochastic variability that gives different realizations of the model. The numerical input parameters are given in Appendix A.3. The overall shape of these two curves resembles the curves in figure 7.3, but the time axis is replaced with a sand fraction axis. The equilibrium wavelength and amplitude of the simulated ripples are here

chosen to be 20 and 0.2 respectively. The absolute values are not to be compared with the numerical values in figure 7.3, since the input values in SBED are dimensionless and only related to the number of cells in the model. The important aspect is thus the evolution of the mean and the variance with increasing sand fraction. However, these values will, together with the model-size, control correlation lengths of the individual components (sand and mud), as will be discussed below.

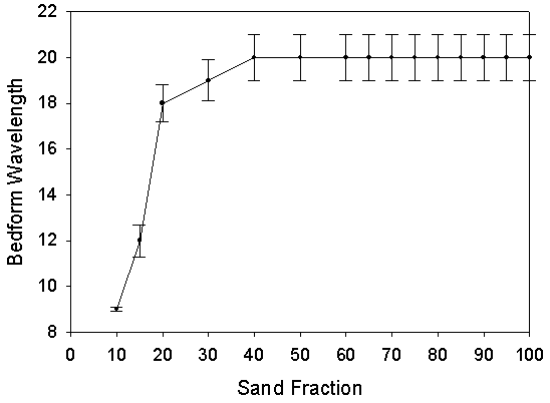

FIGURE 7.6 *The bedding model input parameter describing the bedform wavelength. The solid line is the mean value and the error bars denote one standard deviation.*

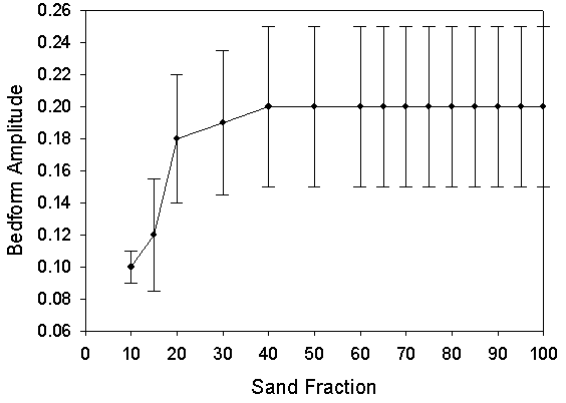

FIGURE 7.7 *The bedding model input parameter describing the bedform amplitude. The solid line is the mean value and the error bars denote one standard deviation.*

The planform shape of the bedforms in SBED is mainly simulated with a wavelength and an amplitude of the ripple crest (section 4.2.2). According to the arguments above, ripples deposited in mud rich deposits (lenticular bedding) will be straighter than ripples deposited in a flaser bedding (since the latter ripples have been deposited during longer time and hence are closer to equilibrium shape). It is currently not possible to explicitly model linguoid planforms and consequently, an equilibrium planform shape is here simulated to be a sinuous crest with wavelength equal to 20 and amplitude equal to 5. Straighter ripples will then have a lower amplitude and longer wavelength. These input parameters are plotted as a function of sand fraction in figure 7.8 and can be compared to figure 7.4.

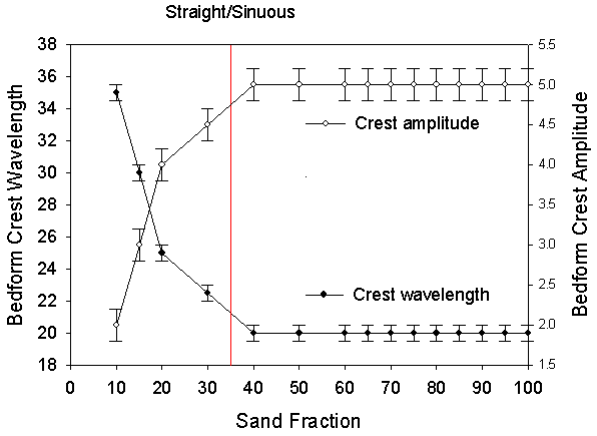

FIGURE 7.8 *The bedding model input parameters controlling the planform shape of the ripples. The solid lines are the mean values and the error bars denote one standard deviation of the input parameters.*

The simulated sand fraction is controlled by the depositional rate and length of both sand and mud (chapter 4). The input depositional rate and length for the two components are given in figure 7.9 and 7.10. Some adjustments from linearity had to be made due to numerical limitations in the program. Using these input curves, sand fraction specific, realistic bedding models can easily be generated. Thus we have selected mean and variance input parameters in such a way as to mimic as closely as possible the observed geometries of flume tank experiments performed by Baas (1994) and Oost and Baas (1994).

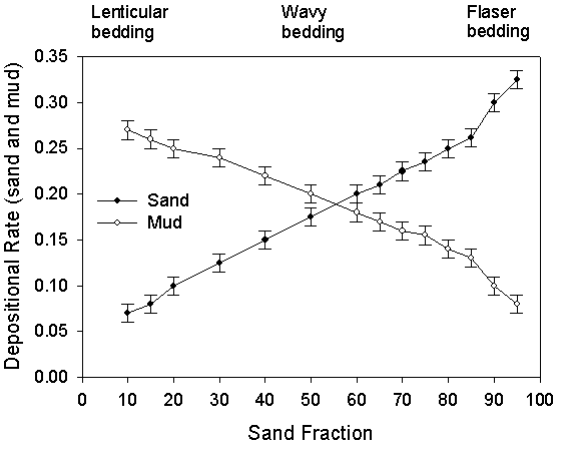

FIGURE 7.9 *The bedding model input depositional rate for sand and mud for the different sand fraction templates. The solid lines are the mean values and the error bars denote one standard deviation of the input parameters.*

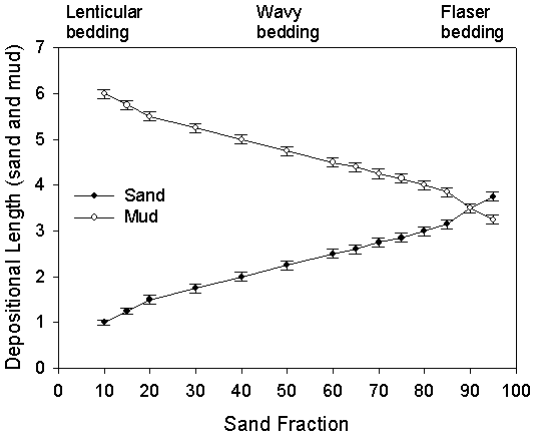

FIGURE 7.10 *The bedding model input parameters describing the depositional length for sand and mud for the different templates. The solid lines are the mean values and the error bars denote one standard deviation of the input parameters.*

Some of the assumptions regarding the use of the empirically observed data were outlined above. In addition, there are some limitations to this parameter set.

1) The curves found by Baas (1994) were valid for a specific grain size class (mean of 0.095 mm). It can, however, be assumed that the grain size in sand rich sediments are more coarse grained than in the mud rich deposits due to higher depositional energy in the former. This effect is not simulated in these bedding models but can to some extent be included in the petrophysical parameters (e.g. higher permeability for coarse-grained facies).
2) There is no simulated relation between the angle and shape of the lee side lamina and the current speed as discussed in section 2.2.2.3. However, as shown is chapter 4, these parameters will not have a large influence on the sand/mud connectivity.
3) Some adjustments to the depositional rate and length from linearity had to be made. This was particularly the case in the high mud fraction models since the numerical code tends to give long and continuous lamina even at a small depositional rate and length. The connectivity of the sand lenses would consequently have been too high if the adjustments not had been done. However, it was not possible to reduce the connectivity perpendicular to the depositional direction (y-direction) due to the straightness of the ripple crest (i.e. splitting and re-joining of crests is not simulated). As a result, only the component parallel depositional direction is used in the following flow simulation analysis (x-direction).

In this chapter, twelve models representing a range of bedding types are used to evaluate the variation in porosity and permeability with sample volume. It is assumed that the petrophysical variance and spatial correlation structure will influence this relationship. Of more fundamental interest is to see the effect of the bedding type. To isolate the effect of sand and mud connectivity, the petrophysical properties are set to constant values. Further, the petrophysical contrast between the two sand components (contrasting lamina) is set to one. In chapter 8, the effect of changing the contrast between these laminae and the effect of varying the petrophysical properties of the mud component will be evaluated. Here, the sand porosity is set to 0.25 and the mud porosity is set to 0.05. The permeability of the sand and mud are 100 mD and 0.01 mD. The permeability contrast is thus 10^4.

7.2.2 Serial upscaling of sub-grids

The sub-grid function (section 4.4.4) was used to create progressively larger samples of the same realization. The smallest number of cells used was 2^3 which corresponds to 8 cm^3 with the chosen units. A smaller cube was not possible to upscale

due to numerical limitations. The largest cube was 30^3 cm^3 and consists of 0.6-1.4*10^6 irregular cells. Ideally, the largest cube should have somewhat larger dimensions (see discussion in 7.4), but the size used was a compromise since larger grids are both time consuming to upscale and require large disc-space.

The subgrid size was increased in a cubic series (figure 7.11) to allow an even increment in the x, y and z direction. This ensures that the variability in each direction is captured in each volume step.

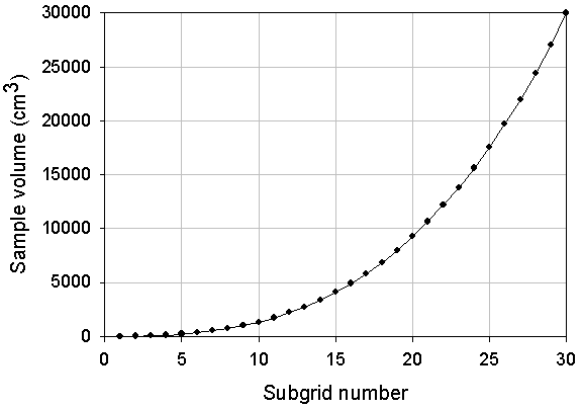

FIGURE 7.11 *Graph showing how the sample volume is increased in a cubic series.*

No dependency was observed on the evolution of the upscaled values as a function of sample volume with the location of the centre point of the increasing cube. Figure 7.12 shows the result of five different starting points (denoted by the x, y and z coordinates of the centre point) in the same realization of a model with 20% mud fraction. The C_V of the measured properties at each sub-grid volume is calculated for vertical and horizontal permeability, as well as the standard deviation for porosity. It is assumed that the other models behave in a similar manner. This figure will be further discussed in section 7.4.

.

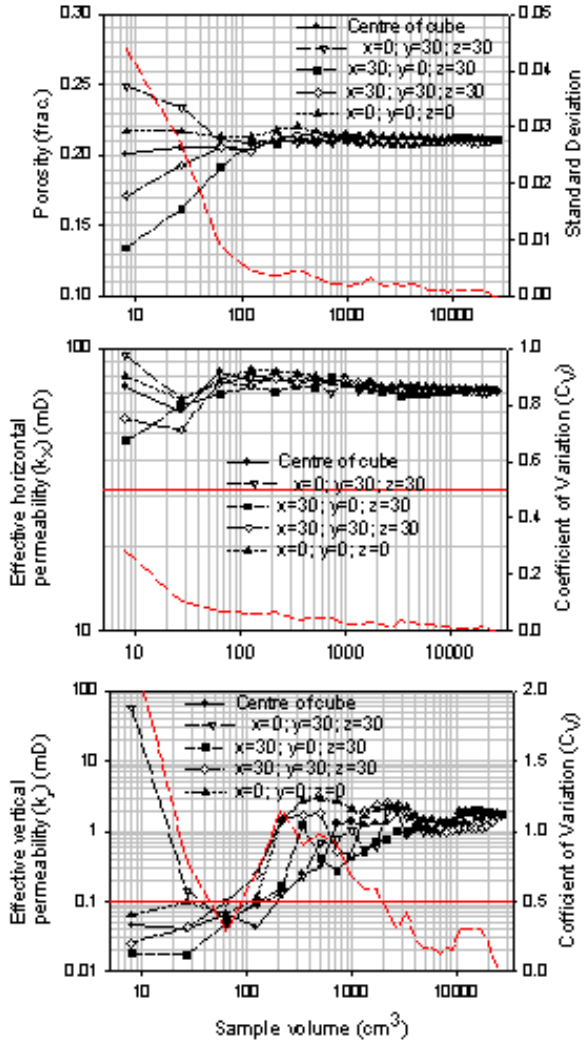

FIGURE 7.12 *Figure showing the same realization (seed no.: 105489792) evaluated as a function of sub-grid size: Porosity (top), k_x (center) and k_z (base). The center-point of the expansion is however varied (given by the x, y and z coordinates in the figure). The dashed line is the CV of the different starting-points. There appears to be no relation between the starting-point and the degree of variability.*

7.3 Results: Petrophysical properties as a function of sample support

Ten realizations of the 12 bedding models were made each with 29 subgrids which give 3480 subgrids in total. Each of these sub samples were upscaled numerically with the built-in algorithm giving single-phase permeability in x, y and z-direction. The seed numbers are given in Appendix A.4. The results are shown graphically in section 7.3.1 to 7.3.3.

The aim in performing these experiments was to see if the variability in porosity and permeability changes with sample support. Each realization will thus express the variability as a function of sample volume and can be compared with figure 7.1. The ten realizations will approach an expression of the variability of a particular bedding type (i.e. sand or mud fraction). The coefficient of variation (C_V) is used to describe the variability at a particular sample volume between the ten realizations. For permeability (horizontal and vertical) the C_V is plotted as a function of sample support and the 0.5 level (upper limit for effectively homogeneous media) is indicated. It is then assumed that when the C_V remains in the homogeneous range, a representative effective property is calculated and that the corresponding sample volume approximates a Representative Elementary Volume (REV). This assumption will be further discussed in section 7.4. Since porosity for sand and mud is set to a constant value, these curves follow the same trend as the sand fraction curves. The standard deviation for porosity is used as a measure on the variability at each sample support and different limits can be used to assign a volume were the measured bulk porosity is locally homogeneous and where the corresponding sample volume approximates a REV (see figure 7.33 and 7.34).

7.3.1 Vertical permeability

Figures 7.13 to 7.16 show the variability in vertical permeability (k_v) for different bedding types (defined by sand fractions) in relation to sample volume. The solid lines represent the individual realizations while the dashed line represents the C_V curve calculated from these realizations. In general, for all the bedding types, there is variability between the realizations for small sample volumes. This is indicative that local homogeneity is not achieved and this is reflected in the C_V which in general are higher in this region. At larger sample volumes, the variability between the realizations is minimized and the C_V decreases and eventually remains in the homogeneous region. Vertical permeability is then less sensitive to small variations in sample volume and, in terms of the continuum theory, a (locally) homogeneous value is approached. Occasionally a low value of C_V can be observed at several

smaller volumes, but only the volume where the C_V remains below 0.5 for larger samples is relevant here.

The C_V curves from the 12 bedding models are plotted together in figure 7.17. There appears to be a relationship between the size of a locally homogeneous value and the bedding type. For low mud fraction models (mud fraction below approximately 0.35) there is a steady increase in this volume. Bedding types with higher mud fractions are nearly always in the homogeneous range which means that only small sample volumes are necessary in order to capture a representative amount of heterogeneity affecting the vertical permeability. The (volume) point where the C_V curve remains in the homogeneous region is plotted against the sand fraction of the models in figure 7.18. It is proposed here that there is a relationship between the size of this locally homogeneous sample and the correlation length of the mud layers in the x and y directions. This can conceptually be expressed as

$$V_{C_V < 0{,}5,\, k_v} \sim f(\lambda_{x,\, mud}/D_x, \lambda_{y,\, mud}/D_y) \qquad \textbf{[7-6]}$$

where $\lambda_{x,mud}$ and $\lambda_{y,mud}$ are the correlation lengths of mud in x and y direction and D_x and D_y are the model dimensions in those directions. λ/D is a dimensionless correlation coefficient. When $\frac{\lambda_{x,\, mud}}{D_x} \geq 1$ and $\frac{\lambda_{y,\, mud}}{D_y} \geq 1$ then a continuous mud layer percolates through the model and the vertical permeability is drastically reduced. The trend seen in figure 7.18 is then a result of the increasing dimensionless correlation lengths in x and y direction. Above approximately 35% mud content, the variability is reduced significantly since some mud layers percolate the model and in order to capture the vertical variability only one sand and one mud layer have to be sampled. As a result the volume where a locally homogeneous value is obtained is significantly lower.

This finding will be discussed in section 7.4 after the results of horizontal permeability and porosity are presented.

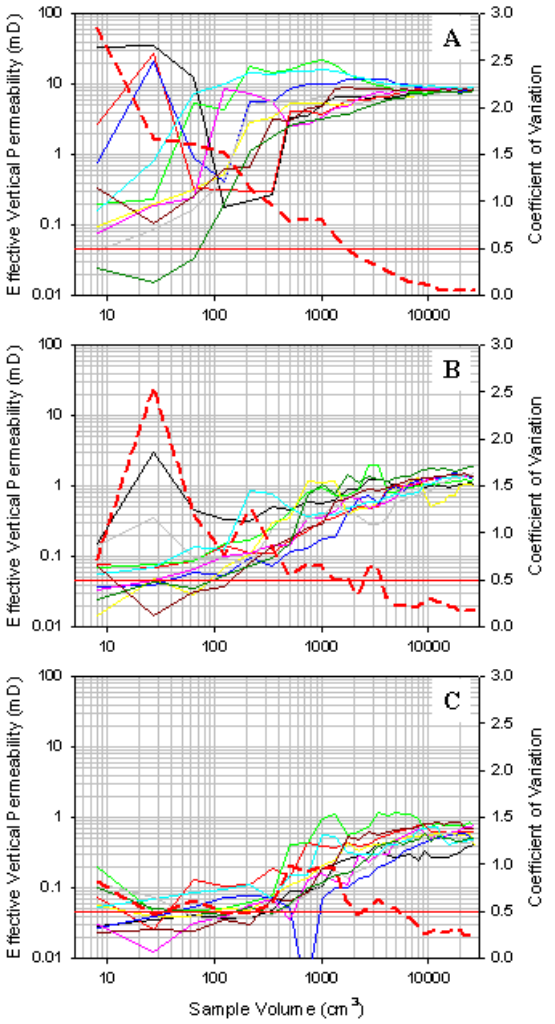

FIGURE 7.13 *Variation of vertical permeability with sample volume. A) Sand fraction =0.90, B) Sand fraction = 0.80 and C) Sand fraction = 0.75.*

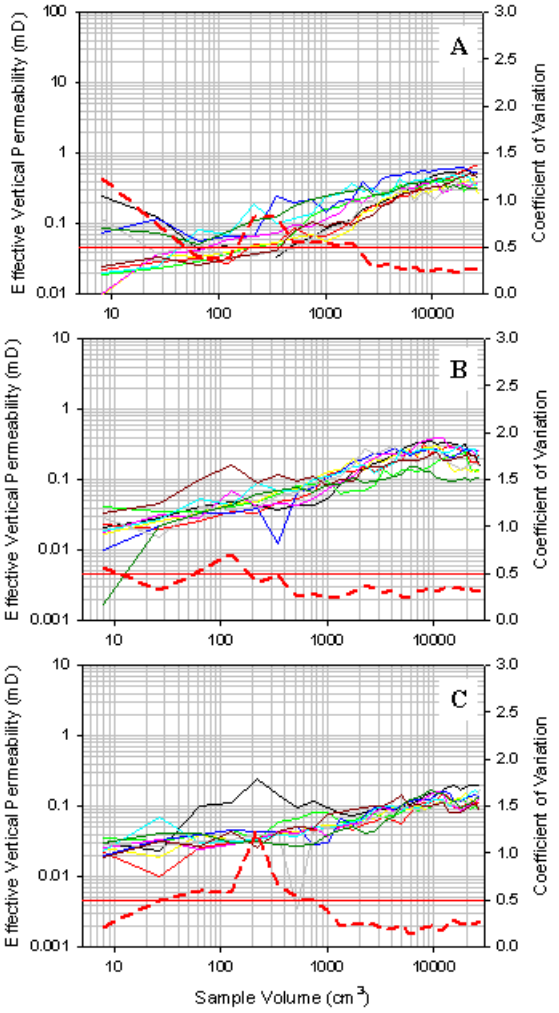

FIGURE 7.14 *Variation of vertical permeability with sample volume. A) Sand fraction =0.70, B) Sand fraction = 0.65 and C) Sand fraction = 0.60.*

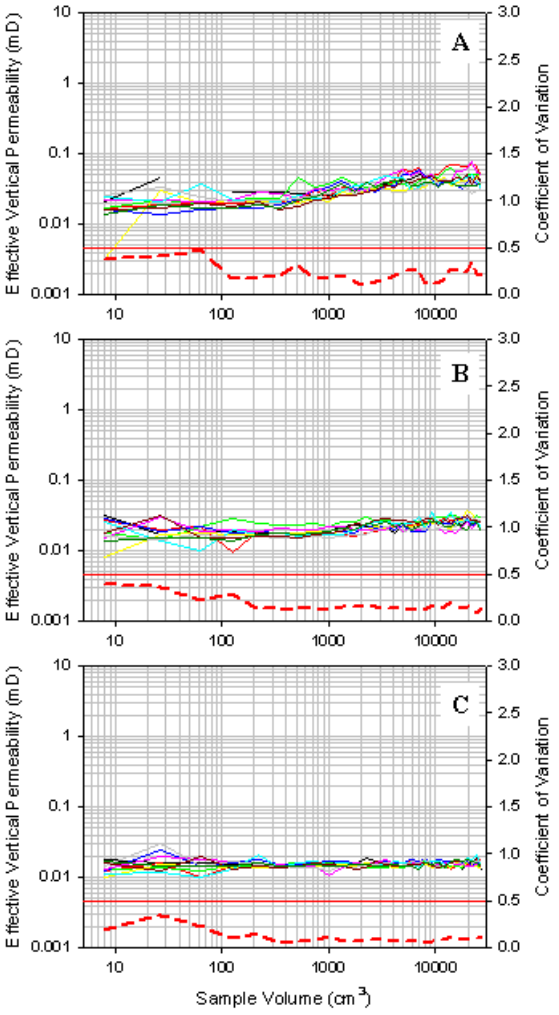

FIGURE 7.15 *Variation of vertical permeability with sample volume. A) Sand fraction =0.50, B) Sand fraction = 0.40 and C) Sand fraction = 0.30.*

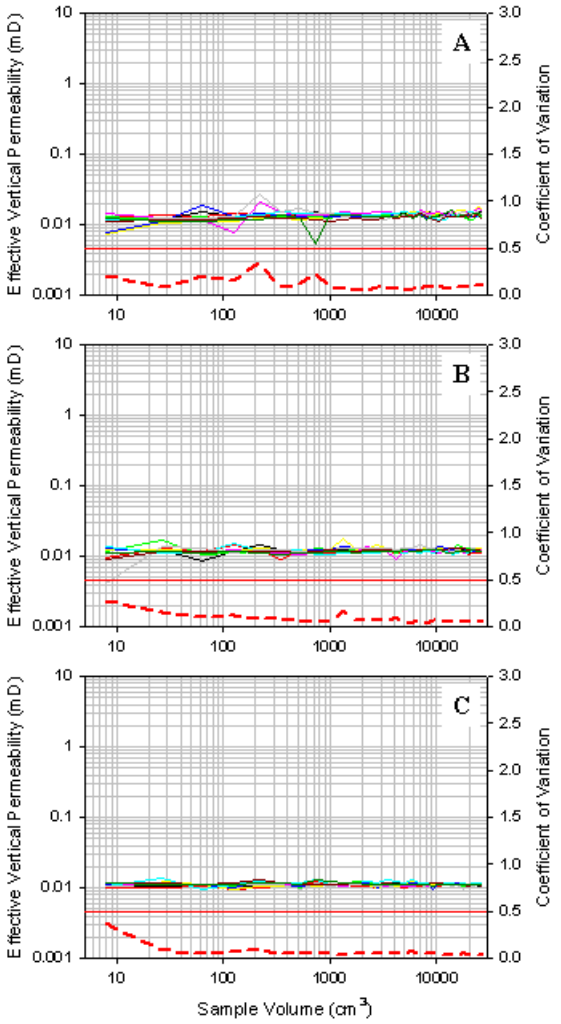

FIGURE 7.16 *Variation of vertical permeability with sample volume. A) Sand fraction =0.20, B) Sand fraction = 0.15 and C) Sand fraction = 0.10.*

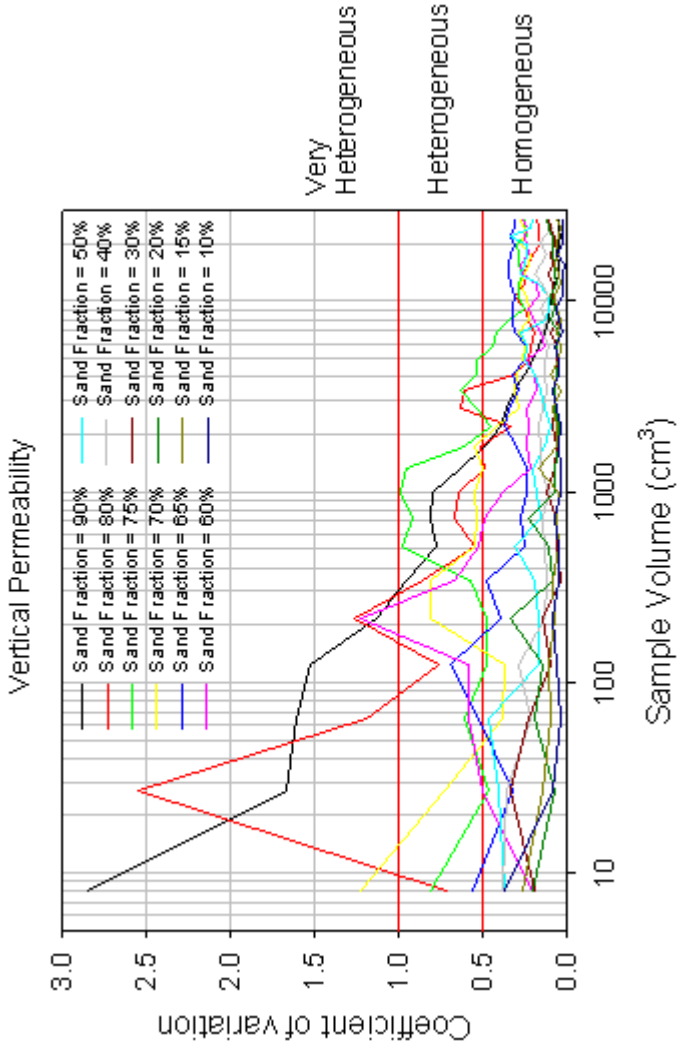

FIGURE 7.17 *All the C_V-curves for vertical permeability (k_z). Based on figure 7.13 to 7.16*

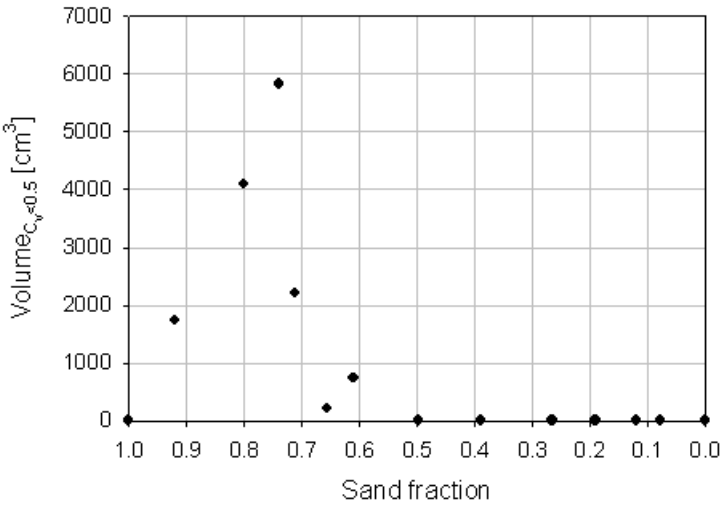

FIGURE 7.18 *Experimental result of size of locally homogeneous sample for different sand fractions (bedding types). The data is based on figure 7.17. Note that there is a trend in the high sand fraction region (sand fraction > 0.75) that drops to zero below a critical sand fraction (percolating threshold of a mud laminaset).*

7.3.2 Horizontal Permeability

While the size of a locally homogeneous sample for vertical permeability was dependent on the correlation length of the mud layers (in x and y-direction), the sand continuity is intuitively more important for horizontal permeability. Sedimentologically, the continuity perpendicular to the bedform migration direction (y-direction in the simulated models) is higher then parallel to it (x-direction in the simulated models). In addition, as discussed above, the code cannot for example simulate splitting or rejoining along the crest, which gives a higher then expected connectivity in the y-direction. To explore the percolating behaviour of the simulated sand lamina-sets, only the effective permeability in the x-direction (k_x) is considered below. As for vertical permeability, the evolution of k_x with sample volume is studied. Figures 7.19 to 7.22 show the results for each sand fraction model (i.e. bedding types). The solid line in each plot represents one realization, and the dashed line is the C_V curve based on these ten realizations. Figure 7.23 shows all the C_V curves for horizontal permeability and figure 7.24 the point where the C_V

curve remains in the homogeneous region similar to figure 7.18. Although the trend is less clear than for vertical permeability, there appears to be a relationship between the size of the sample that is locally homogeneous and the bedding type. At low and intermediate mud fractions, low C_V values are obtained at small sample volumes. At higher mud fractions, where the sand lenses starts to disconnect in the plane, larger C_V values are calculated. This can again be expressed conceptually in terms of the correlation lengths of the conducting (sand) component.

$$V_{C_V < 0{,}5,\, k_x} \sim f(\lambda_{x,\, sand} / D_x, \lambda_{y,\, sand} / D_y) \qquad \textbf{[7-7]}$$

where $\lambda_{x,sand}$ and $\lambda_{y,sand}$ are the correlation lengths of sand in x and y direction and D_x and D_y are the model dimensions in those directions. When $\frac{\lambda_{x,\, sand}}{D_x} \geq 1$ and $\frac{\lambda_{y,\, sand}}{D_y} \geq 1$ then a sand layer (plane) percolates through the model and the horizontal permeability is increased significantly.

Alternatively, since the horizontal permeability has two components (k_x and k_y), the locally homogeneous sample volume may be expressed as a function of the mud correlation length:

$$V_{C_V < 0{,}5,\, k_x} \sim f(\lambda_{y,\, mud} / D_y, \lambda_{z,\, mud} / D_z) \qquad \textbf{[7-8]}$$

in the x-direction and

$$V_{C_V < 0{,}5,\, k_y} \sim f(\lambda_{x,\, mud} / D_x, \lambda_{z,\, mud} / D_z) \qquad \textbf{[7-9]}$$

in the y-direction.

These results will be discussed in more depth in section 7.4.

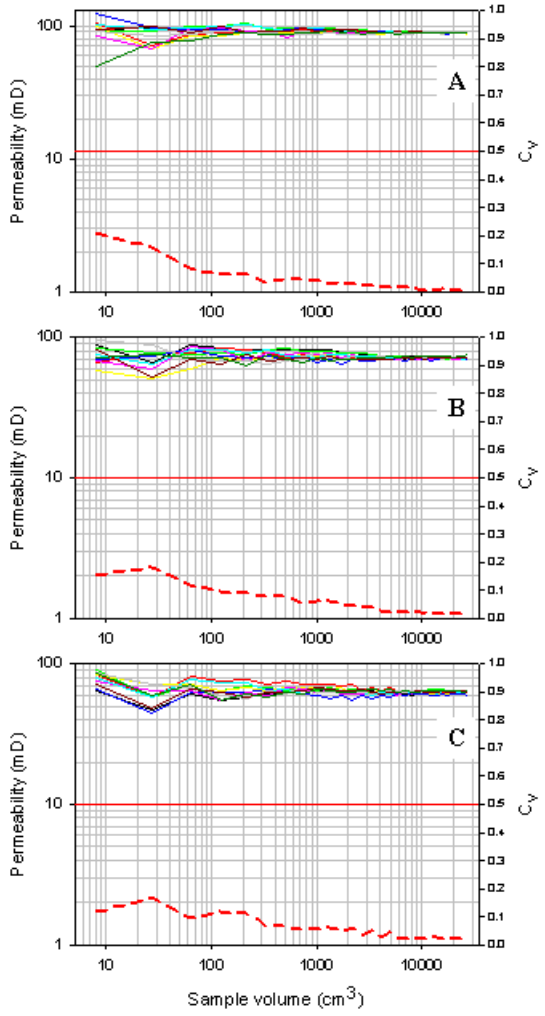

FIGURE 7.19 *Variation of horizontal permeability with sample volume. A) Sand fraction =0.90, B) Sand fraction = 0.80 and C) Sand fraction = 0.75.*

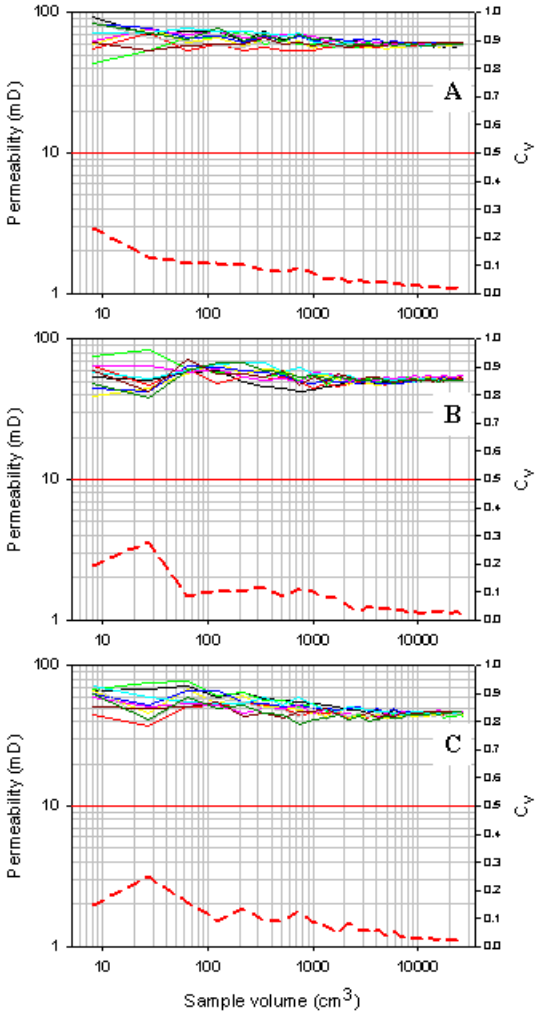

FIGURE 7.20 *Variation of horizontal permeability with sample volume. A) Sand fraction =0.70, B) Sand fraction = 0.65 and C) Sand fraction = 0.60.*

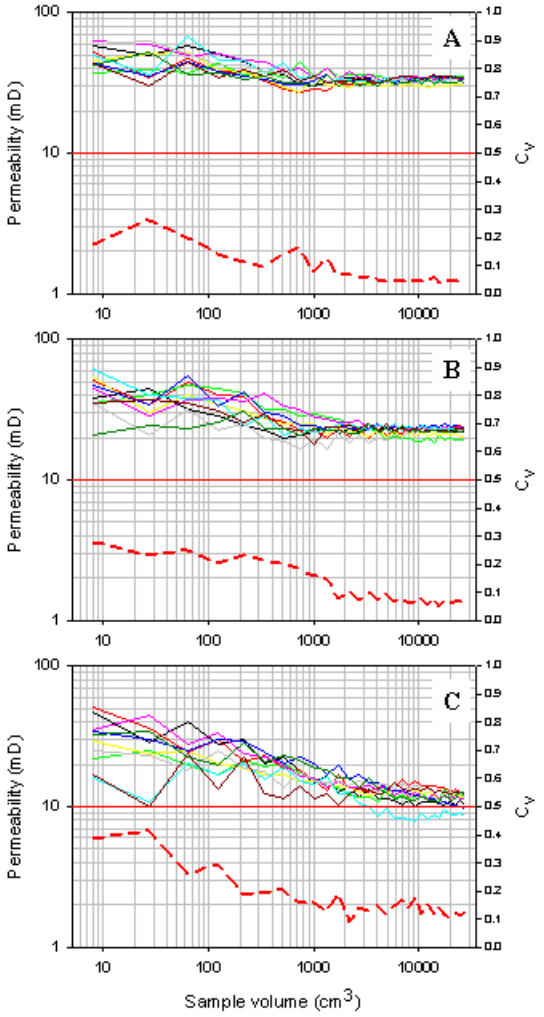

FIGURE 7.21 *Variation of horizontal permeability with sample volume. A) Sand fraction =0.50, B) Sand fraction = 0.40 and C) Sand fraction = 0.30.*

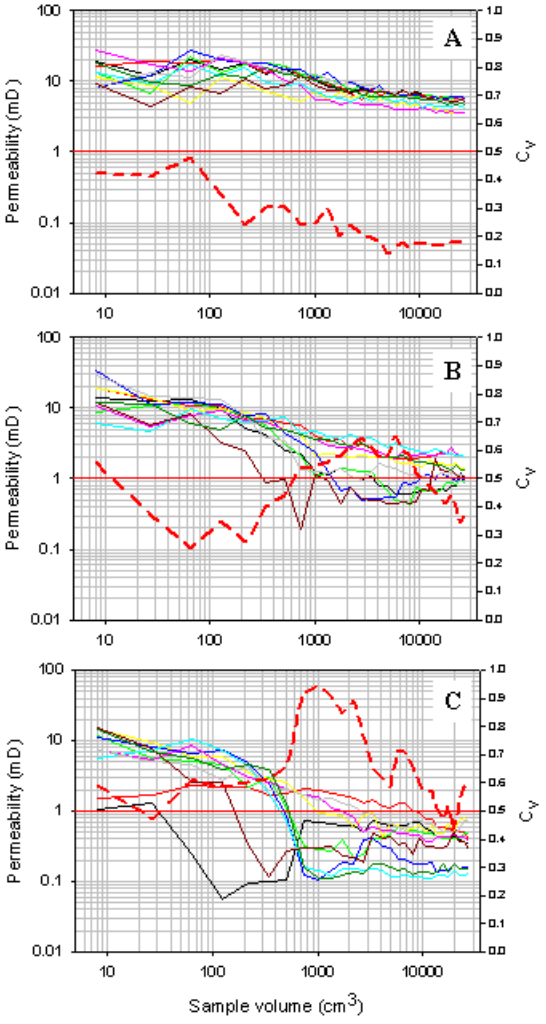

FIGURE 7.22 *Variation of horizontal permeability with sample volume. A) Sand fraction =0.20, B) Sand fraction = 0.15 and C) Sand fraction = 0.10.*

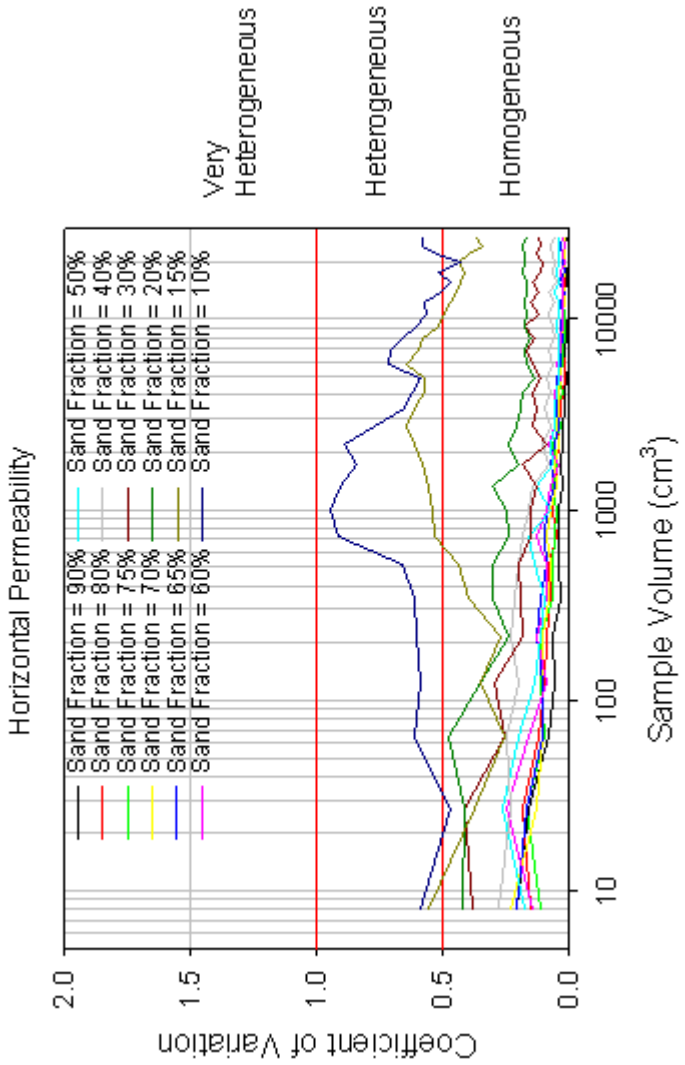

FIGURE 7.23 *All the C_V -curves for horizontal permeability (k_x). Based on figure 7.19 to 7.22.*

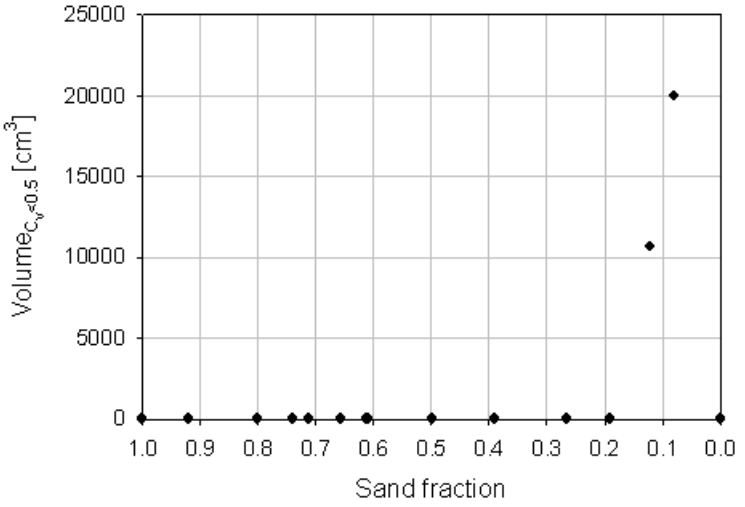

FIGURE 7.24 *Experimental result of size of locally homogeneous sample for different sand fraction (bedding types). Based on figure 7.23.*

7.3.3 Porosity and Sand/Mud fraction

Since each component is given a constant porosity value, the relation between porosity and sand fraction is linear. For completeness both the sand fraction (figure 7.25 - 7.28) and porosity (figure 7.29 - 7.32) variability with sample volume are shown. If variable porosity fields were used for each laminaset more variability would be observed but this is not expected to be large as porosity does not typically vary much within laminasets.

The porosity (and sand/mud fraction) can be understood with simple mixture rules where their upscaled value is only dependent on the amount of each component and not on their distribution. The mean value for porosity decreases with increasing mud content (i.e. bedding model) while the standard deviation, calculated between the realizations, is approximately the same. As a result, the C_V will not give a good picture of the variability in porosity with sample volume for different mud fractions. The standard deviation is instead used alone. As for permeability, there is observed a decrease in the standard deviation with sample volume, consistent with

the REV concept. There is however no observed difference between the different bedding models in contrast to permeability (figure 7.33 and 7.34).

.

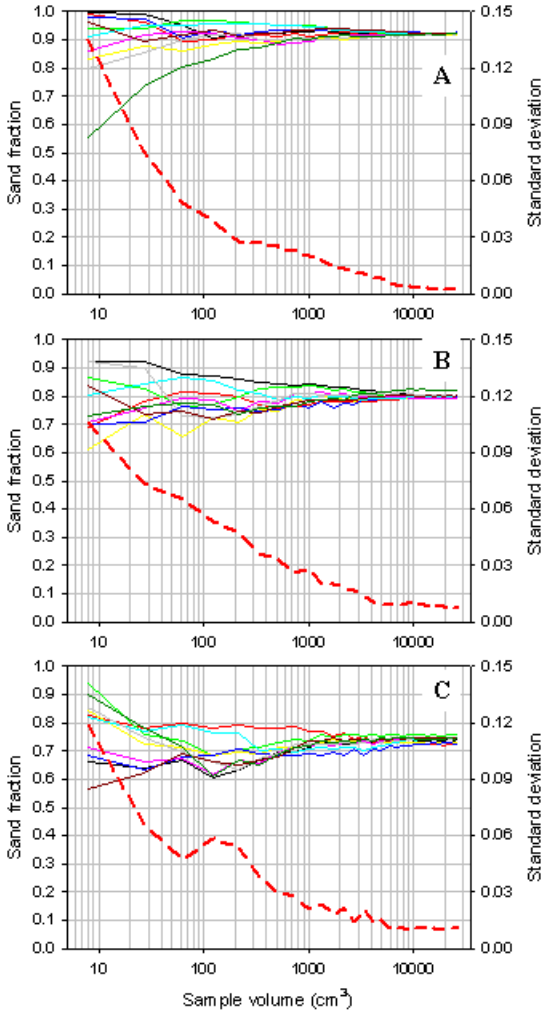

FIGURE 7.25 *Variation of sand fraction with sample volume. A) Sand fraction = 0.90, B) Sand fraction = 0.80 and C) Sand fraction = 0.75.*

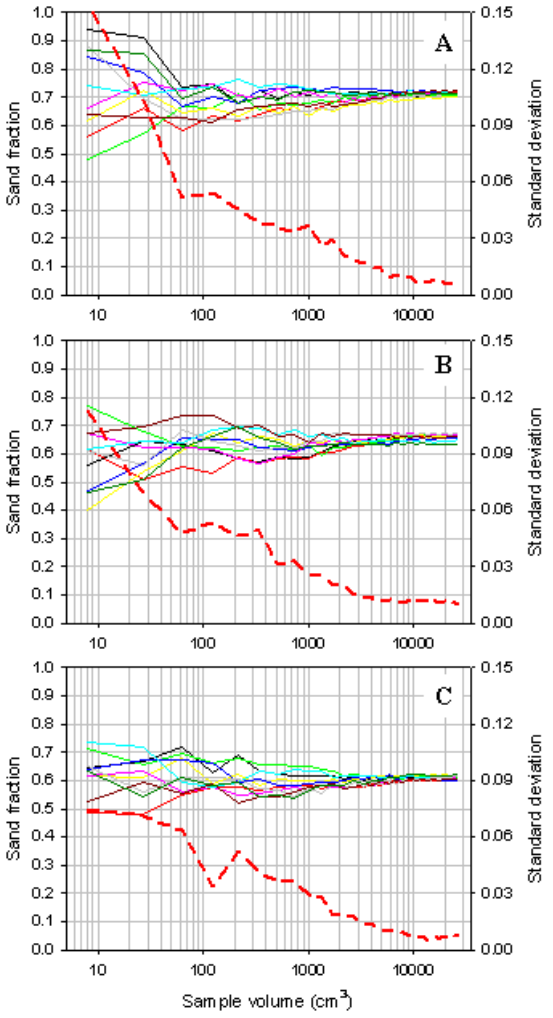

FIGURE 7.26 *Variation of sand fraction with sample volume. A) Sand fraction =0. 70, B) Sand fraction = 0.65 and C) Sand fraction = 0.60.*

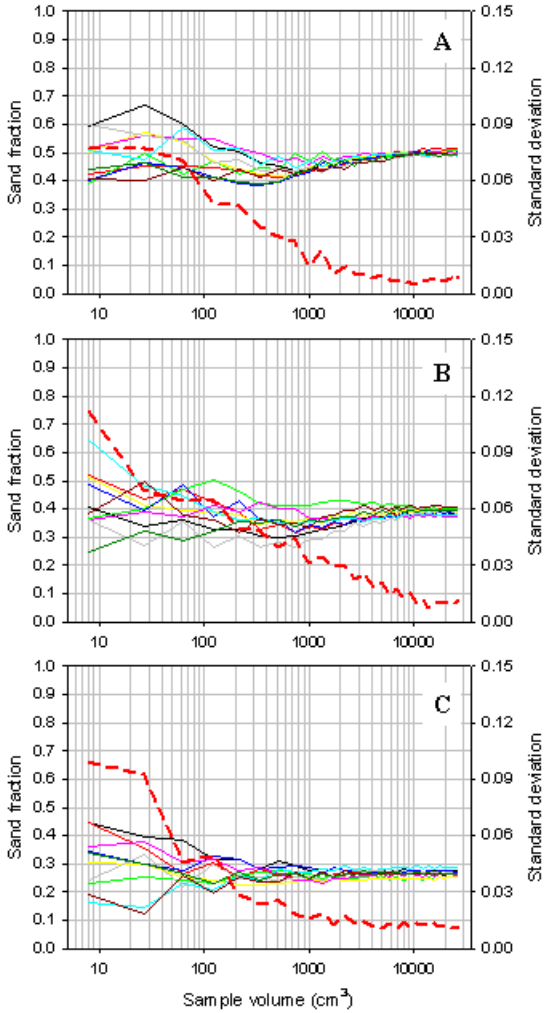

FIGURE 7.27 *Variation of sand fraction with sample volume. A) Sand fraction = 0.50, B) Sand fraction = 0.40 and C) Sand fraction = 0.30.*

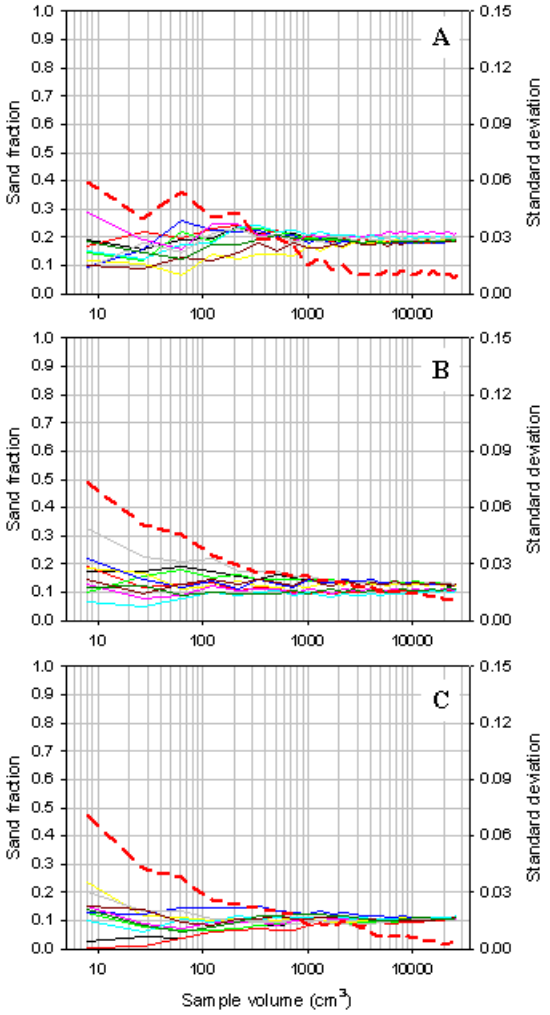

FIGURE 7.28 *Variation of sand fraction with sample volume. A) Sand fraction = 0.20, B) Sand fraction = 0.15 and C) Sand fraction = 0.10.*

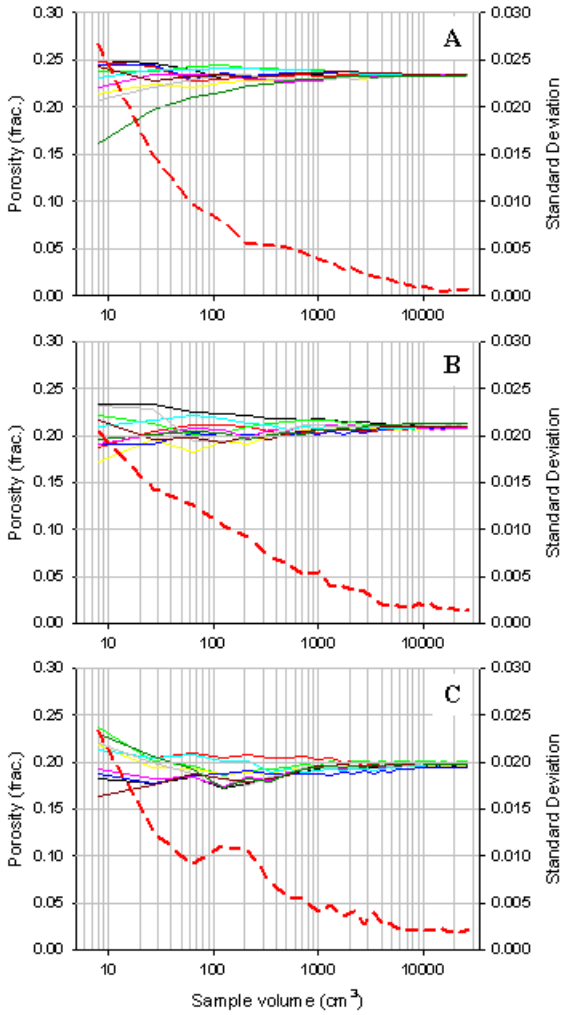

FIGURE 7.29 *Variation of porosity with sample volume. A) Sand fraction = 0.90, B) Sand fraction = 0.80 and C) Sand fraction = 0.75.*

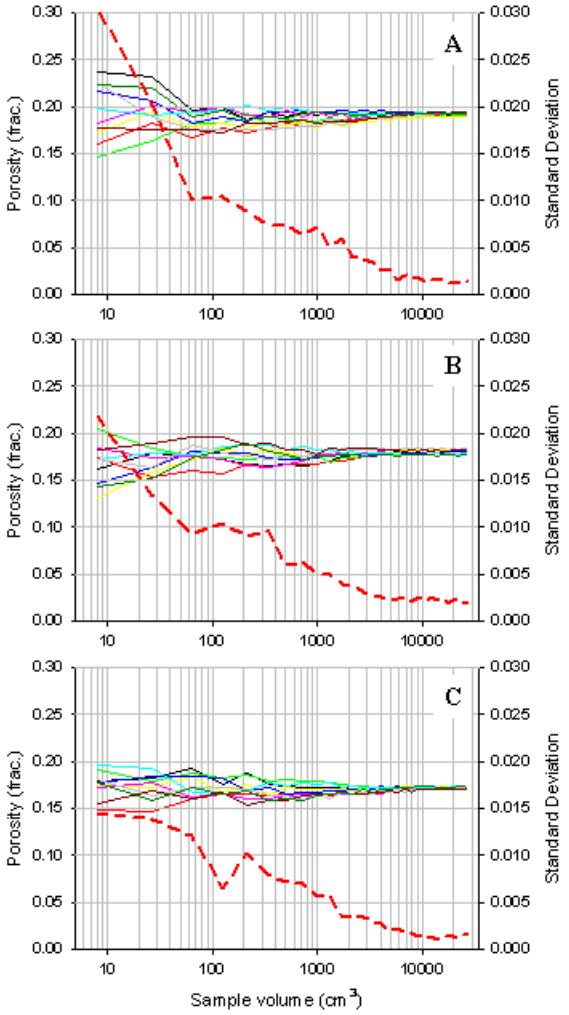

FIGURE 7.30 *Variation of porosity with sample volume. A) Sand fraction = 0.70, B) Sand fraction = 0.65 and C) Sand fraction = 0.60.*

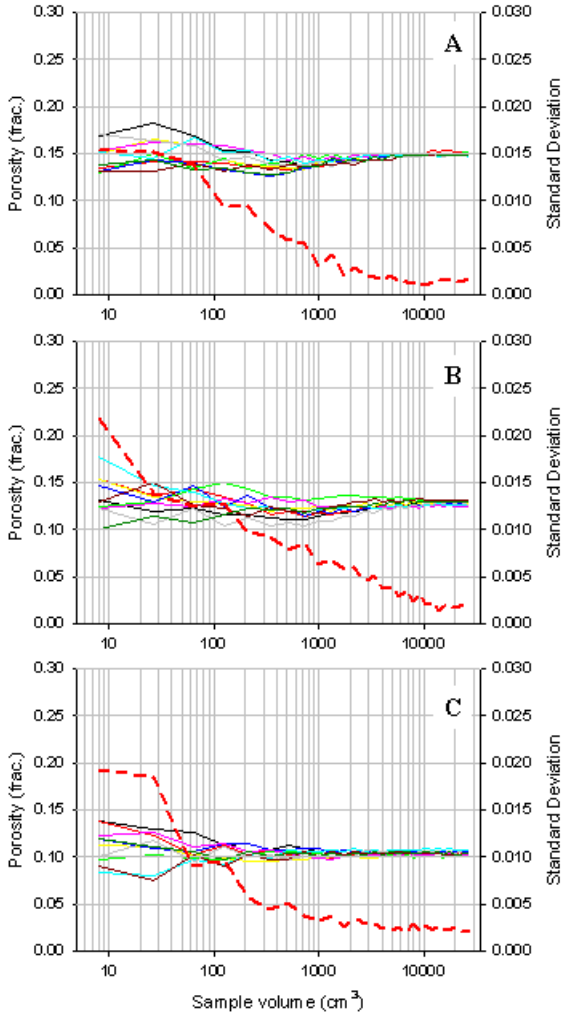

FIGURE 7.31 *Variation of porosity with sample volume. A) Sand fraction = 0.50, B) Sand fraction = 0.40 and C) Sand fraction = 0.30.*

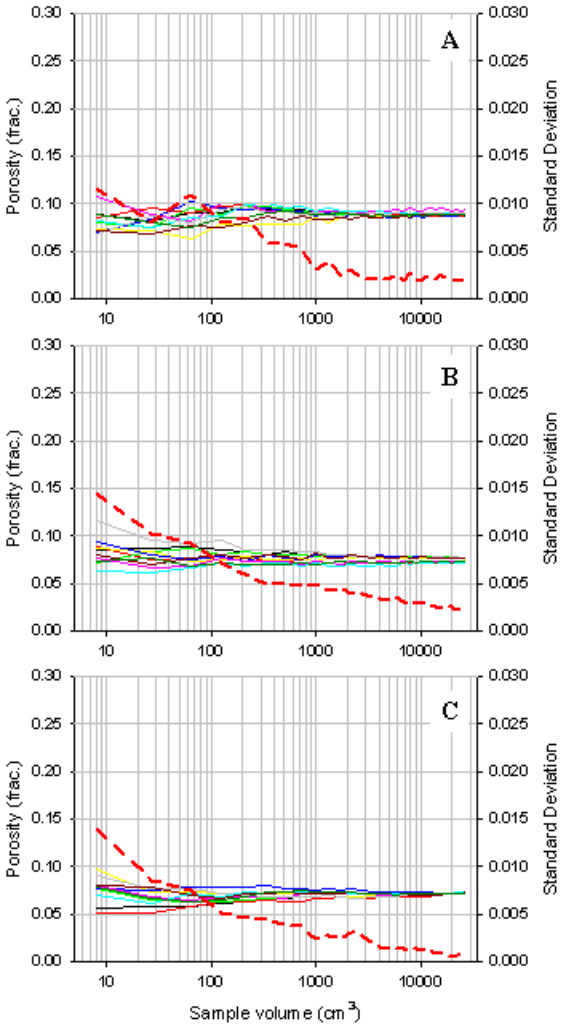

FIGURE 7.32 *Variation of porosity with sample volume. A) Sand fraction = 0.20, B) Sand fraction = 0.15 and C) Sand fraction = 0.10.*

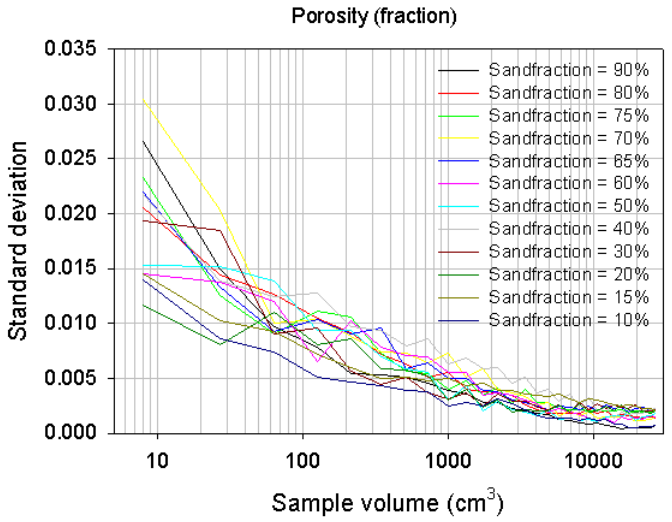

FIGURE 7.33 *Standard deviation for porosity of the12 bedding models with increasing sub-grid volume. The standard deviation is based on 10 realizations. Based on figure 7.29 to 7.32.*

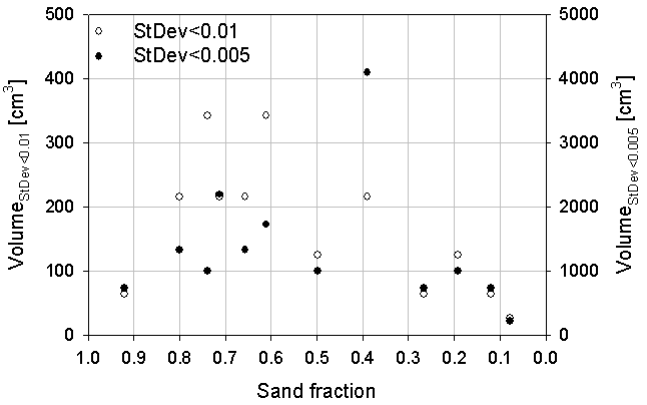

FIGURE 7.34 *Variability of locally homogeneous sample in relation to cube size for porosity. Compare with figure 7.18 and 7.24 which shows a relation to the sand fraction. Two limits for determining the size of the locally homogenous sample are used: when the standard deviation is below 0.01 (white circles) and below 0.005 (black circles)*

7.4 Discussion

In section 2.3.5 the difference between block permeability and effective permeability was reviewed. Effective permeability was in contrast to block permeability shown to be independent of the boundary condition, and hence is an intrinsic property of the medium. A basic requirement for an effective permeability to occur was that the correlation length was much smaller than the model domain. In the general tidal models described above, and in some of the models discussed in chapter 5, the scales of heterogeneity are on the same order as the model size although the petrophysical properties for the individual components have a shorter correlation length (on the order of a few centimeters; see chapter 6). Figure 7.35 shows some examples of the tidal bedding models used here. It is clear that the correlation length of the mud layers varies and that, at some point, approaches (figure 7.35 C) and becomes larger (figure 7.35 D) than the model size. The numerical upscaling method used in this work, a sealed sided pressure solver, can produce non-unique results (i.e. depending of the boundary conditions applied) when the scale of the heterogeneity approaches the model size (e.g. Gomez-Hernandez and Journel, 1990). A periodic boundary condition would give a better estimate of the effective permeability (Pickup et al., 1994; Durlofsky, 1991). Also, in the case of an impermeable component (e.g. zero mud permeability), the pressure solver algorithm has been shown to give incorrect result (Begg et al. 1987). In this thesis, finite mud permeability has been used (in general equal to 0.01 mD, but sensitivity to this parameter is considered in Chapter 8) to avoid this limitation.

Assuming that the calculated permeability tensor with diagonal terms only is approximately correct, the main aim of this chapter is to evaluate how the dispersion in porosity and permeability varies with sub-grid size, to find a representative value at an appropriate support and to relate this to bedding type (i.e. the correlation lengths of the components present).

.

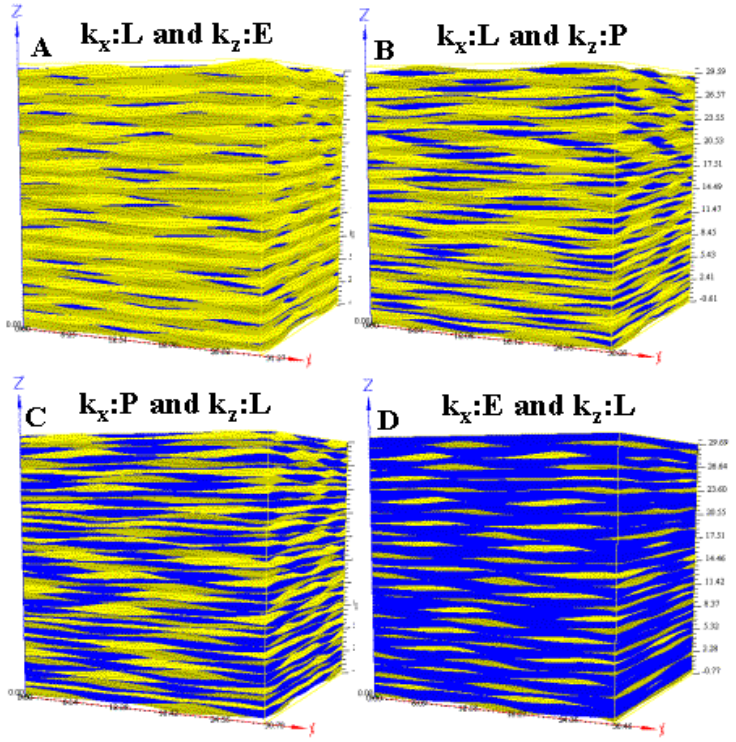

FIGURE 7.35 *One realization of four different bedding models with different mud fractions showing visually the correlation structure for the sand (light) and mud (dark) components and its relation to the mud fraction (bedding type). Realization A, B, C and D have a mud fraction of 0.07, 0.25, 0.49 and 0.78 respectively. The headings for the different models indicate the flow regimes and will be explained further below.*

If one takes one of the realizations in the figures in the previous sections (figures 7.13 to 7.16, figures 7.19 to 7.22 or figures 7.25 to 7.32), it is clear that there are fluctuations at small model volumes and that these fluctuations are minimized at larger model volumes. This resembles the behaviour shown in figure 7.1 and suggest, based on numerical experiments, that the tidal system modelled here shows a behaviour corresponding to the conceptual REV sketch. The challenge then is to decide if a REV exists according to certain published statistical criteria and how to estimate this volume from the numerical data presented above. It should be remem-

bered that the models above have constant petrophysical properties for the two components. This means that only the geometry (i.e. the spatial distribution of the components) is considered. If a REV is found, then this would represent a REV for connectivity (i.e. a 'geometrical REV') and it is further assumed that this will be a minimum REV since including petrophysical variability most likely will increase the representative volume (as also shown by Norris and Lewis, 1991, for two dimensions).

Theoretically, homogeneity and stationarity should be present to achieve a representative property measured at a representative elementary volume (e.g. Baveye and Spositio, 1984). Local homogeneity is achieved, as described in section 7.1, when a measured property from different elemental volumes has the same value regardless of location (Olea, 1991). Corbett et al. (1999) stated that an appropriate sample volume is considered to be the volume where the measured property is relatively insensitive to small changes in volume or location and that stationarity in the data can be evaluated by the observation of how the mean and variance vary with location. Anguy et al. (1994) used a Fourier transformation (at the pore-scale) to show that they had attained local homogeneity and that mutually adjacent samples gave the same measured value which they used to argue for the presence of local stationarity.

By evaluating the figures above, showing the evolution of the realizations with increasing sub-grid size (figures 7.13 to 7.16, figures 7.19 to 7.22 or figures 7.25 to 7.32), the following observation can be made:

1) The individual realizations have relatively large fluctuations at small sub-grid sizes and the variation is reduced as the averaging volume increases
2) The variance between the ten realizations is large at small sub-grid sizes and become small at large sample volumes.

The variability between the ten realizations was, for permeability, expressed by the C_V. When the variation for a single realization is minimized, this corresponds to a locally homogeneous sample according to the criteria above. Relatively similar mean values between different realizations suggests that the data are ergodic (Davis, 1986; Jensen et al., 1997; Olea, 1991). Dagan (1990) also assumed that the ergodic hypothesis was satisfied when the C_V was negligible. Deciding whether stationarity is achieved is difficult to assess especially since some authors (Journel and Huijbregts, 1989; Olea, 1991) state that stationarity is a property of the model and not the data. However, by using the criteria of Anguy et al. (1994) where local stationarity occurs when two or more mutually adjacent, locally homogenous samples give the same value, the procedure used in figure 7.12 could have been used.

Using the same realization, and evaluating the measured properties between mutually adjacent sub-grids could have addressed the presence of local stationarity. Unfortunately, the model sizes (figure 7.12) were too small to give locally homogeneous samples without having overlapping sub-grids. To achieve this, the model would have needed to be at least twice as large in the x, y and z direction, and preferentially larger than this to give more than two adjacent, locally homogeneous samples. Such a large model gives too many cells to be tractable with the available computer. However, at the largest support, the measured porosity and permeability values show a small variance (both individual realizations and between realizations) which implies a locally homogeneous value according to Anguy et al. (1994) and an 'appropriate' volume according to Corbett et al. (1999). Based on this and by using the C_V as a measure of variability between realizations, the lower limit for a REV has been set as the corresponding (smallest) volume were the C_V between the realizations remains below 0.5. Obviously, since only the bedding scale heterogeneity is simulated here, the upper limit of the $REV^{n=2}$, cannot be found (see figure 7.1 and 7.2). It should further be noted that the REV found here is valid with the sealed sided pressure solver, and that the numerical value of REV and the representative property may be different with other boundary conditions. It should also be realized that calculation and even the existence of local homogeneity and stationarity on this data set is difficult especially where the heterogeneity approaches the scale of the model domain.

Before discussing the relation between the size of the REV and the bedding type, a comment on the correlation length, its relation to the bedding type and the size of the model domain is needed. The effects of block-size relative to scale of heterogeneity have been discussed by many authors (e.g. Begg et al. 1987; Desbarats, 1987; Deutsch, 1989; Rubin et al., 1991). In these references, the distribution of the mud was random and anisotropy invoked by using different correlation lengths in the vertical and horizontal plane. They then studied the effect of the model size (and grid size) on the effective properties for increasing mud content, keeping the anisotropy ratio constant. Spatially correlated mud elements are added until the specified target volume of mud is met. In such a system, the percolation threshold is related to the anisotropy ratio where higher anisotropy gives a higher horizontal percolating threshold and a lower vertical percolating threshold (Deutsch, 1989). In the tidal bedding models simulated here the situation is more complex. First, the mud is not distributed randomly but its location and shape is determined by the bedform morphology (e.g. wavelength and amplitude of the migrating bedforms). Second, as the mud content increases so does its correlation length relative to the model size. Figure 7.35 shows visually how the correlation length of the mud increases as the mud content increases for some of the simulated tidal bedding models.

Increasing correlation length relative to the model domain clearly suggests that the system exhibits a percolating behaviour. To show this clearer, the experimental, effective permeability data from above (3480 points), representing different sub-grid sizes are plotted against the mud fraction (figure 7.36). It is evident from this figure that there is a large scatter (more than 2 orders of magnitude) in certain ranges, namely between 40% to 20% mud content for vertical permeability and above 70% mud content for horizontal permeability. This indicates that the effective permeability is dependent, to a large extent, on the averaging volume in these regions. As suggested with equations 7-6 and 7-7, the size of the sample volume needed to give a representative value is dependent on the correlation length of both the sand and the mud component. As the correlation length approaches the size of the model (without taking the complicating and limiting factors already discussed into account) the size of a representative volume also increases.

In figure 7.36, the results of the whole model calculations are separated out (dark points), and there is apparently a functional relationship between the effective permeability and the mud content. Different equations will be fitted to these data points in chapter 8, where also the effect of contrasting sand lamina will be studied.

A relation between the size of the REV, based on the C_V, and mud content (bedding type) was shown in figure 7.18 and 7.24 for vertical and horizontal permeability respectively. As the mud content increases from a pure sand model, the mud layers increase in size and, at some mud content, they extend throughout the model. This will correspond to the percolation threshold for vertical permeability. Increasing the mud content even more will eventually give isolated sand lenses and this denotes the percolation threshold for horizontal permeability. Based on figure 7.36 it is thus argued that the percolation threshold for vertical permeability is in the range 30-50% mud while the percolating threshold for horizontal permeability is in the range 70-90% mud.

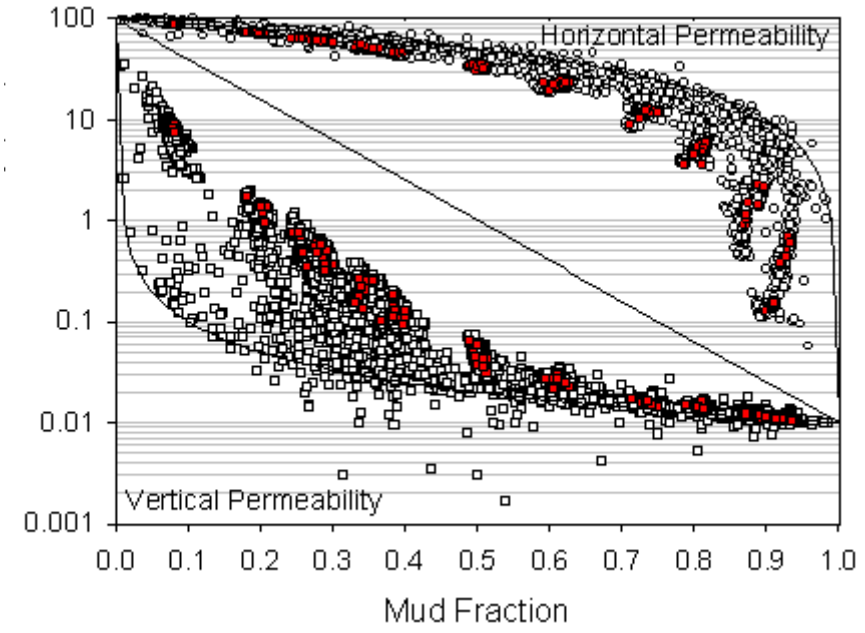

FIGURE 7.36 *Plot of all the experimental data (3480 data points) representing different sample volumes and different mud fractions. Note that there is a large scatter in some regions and that there is a functional relation between the data measured on the whole model (dark squares) and the mud content and that this relation deviates from the arithmetic and harmonic averages. A few data points fall outside the theoretical upper (arithmetic) and lower (harmonic) limits and this is because of numerical errors in the upscaling code.*

Jackson et al. (2003) noted that the vertical permeability increased with sample volume while the horizontal permeability generally decreased and explained this observation with reference to the correlation length of the sand and the mud. At small sample volumes both the sand and the mud layers were likely to be continuous across the sample but became more discontinuous as the volume increased. The results presented here support those findings. Jackson et al. (2003) studied two real rock blocks with different bedding types (a flaser bedded model with a sand fraction of 0.93 and a lenticular to wavy bedded model with a sand fraction of 0.445). In this chapter, a wide range of numerical bedding types have been used. From figure 7.13 to 7.16 and 7.19 to 7.22 it is clear that the vertical permeability generally increases with sample volume but that this effect is largest for low mud contents

while horizontal permeability in general is constant at low mud fractions and decreases as the mud fraction increases. The argument for this behaviour is the same as in Jackson et al. (2003), but with a wider range of models it was possible here to evaluate that trend as a function of mud content.

As discussed above, calculation of an affective permeability is dependent on the model size and the correlation length on the heterogeneity. Generally, for applying an effective medium theory for estimation of effective permeability, the size of heterogeneity should be much smaller than the model domain (this is discussed extensively in relation to the REV theory in Bear, 1972). Deutsch (1989) found that the block size should be at least three times longer than the shale length to filter out the influence of the grid size. Other, more conservative estimates have been given by Ababou et al. (1989) who suggest a value of 5 times the longest correlation length. Due to this, the estimation of an effective permeability in these highly correlated bedding models must be divided into different regions that require different estimation method for effective permeability. The flow regimes proposed by Ringrose et al. (2003) are used here and the results presented above support and extend their results. At low mud contents, the correlation length (both horizontal and vertical) of the mud is in general short with respect to the model size, and the vertical permeability can be estimated with an effective medium approximation. Approaching the volume fraction of mud for the vertical permeability percolation threshold, a percolation model should be used, since the assumptions in the effective medium theory breaks down. At mud contents above the percolation threshold, the vertical permeability seems to follow the harmonic average that is theoretically correct for flow perpendicular to infinite plane layers. (It should be noted that using an average is also an effective medium approach. There is, however, a distinction between the regions where the correlations lengths are smaller than the model domain and where the traditional averages will, in general, give a wrong estimate of the effective properties and the regions which can be treated as a layered system.) For horizontal permeability, the data are less clear, but the data suggest a horizontal percolation threshold around 70-90% mud content and that an effective medium approximation can be used above this content (sand correlation length in vertical and horizontal direction is smaller than the model size). Above the percolation threshold, most of the sand layers extend through the model and horizontal permeability approaches the arithmetic average although with some deviation. Figure 7.37 shows these domains superposed on the experimental data (figure 7.18 and figure 7.24). The flow regimes are also indicated in figure 7.35 which shows a SBED model for each of the flow regimes. Both the data and the conceptual equations (equation 7-6 and 7-7), suggest that a relation exists between the size of the REV and the bedding type which contradicts the findings in Norris and Lewis (1991). Based on the data, a linear trend between the size of the REV and the mud

content is assumed in the range where the effective medium theory is valid. Approaching the percolation threshold (both vertical and horizontal), this curve rises asymptotically to infinity. The exact shape of these curves are not known and it is possible that the assumed linear parts in fact are non-linear. Above the percolation threshold, the size of the REV is constant and small only related to the thickness of the components. Some of the points in figure 7.37 clearly fall off this pattern: 1) k_z for a value slightly below a mud fraction of 0.3 and 2) k_x for a value around a mud fraction 0.9. The first case is a result of a few mud layers present that do not percolate (in the x-y-plane) throughout the model while the latter represents a few isolated sand layers shorter than the horizontal model dimension. This highlights the difficulty in calculation of a representative volume in this critical, percolating region.

This study is the first to thoroughly address these issues experimentally in 3D for a range of complex, heterolithic tidal bedding models. Furthermore, these numerical model are closely matched to flume tank experimental data on this sedimentary system. More experiments that include an independent analysis of the percolation threshold, could give more insight into this relation. The presented results, possibly supported by additional experiments, can then guide the development of an analytical solution. Such a solution must in any case be cross-checked with numerical results.

Estimation of a REV for porosity (and for the sand/mud fraction) was based on the standard deviation, and a decreasing trend was observed for increasing sample volume. Following the same argumentation as for permeability, the data indicate that a representative value is approached that corresponds to a REV for porosity. The selection of a lower limit for the REV based only on the standard deviation can be somewhat arbitrary (in contrast to the limit based on $C_V<0.5$). In figure 7.33, two limits have been used: below a standard deviation of 0.01 and 0.005. Porosity and sand/mud content is a scalar property and only the amount and not the spatial distribution of the different components are important. As a consequence, there is no apparent relation between bedding type and the size of the REV. In addition, a locally homogeneous sample is obtained at a lower sample volume compared to permeability.

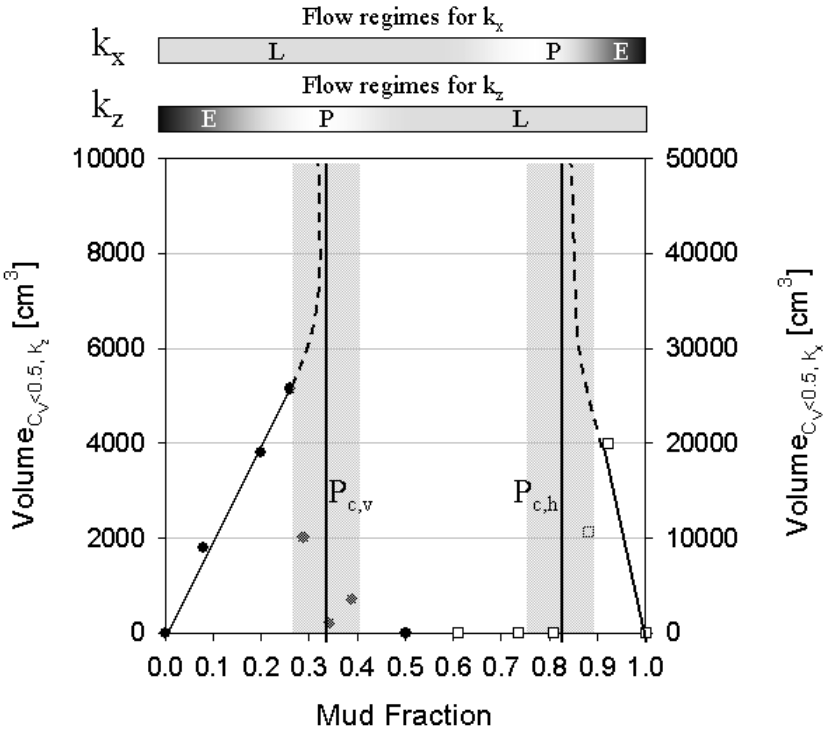

FIGURE 7.37 *Conceptual sketch of the relation between the mud fraction and the smallest size of a locally homogeneous sample. The experimental data (black and white markers) are the same as in figure 7.18 and 7.24. The solid lines are based on these data while the dashed lines are extrapolations into regions not possible to simulate correctly. The three flow regimes are indicated on the top of the figure: L = Layered system where the traditional averaging schemes are applicable, P = close to the percolation threshold ($P_{c,v}$ and $P_{c,h}$ is the vertical and horizontal percolation threshold, respectively) and E = discontinuous sand or mud layers that requires an effective medium approach. Figure 7.35 shows visually these flow regimes.*

The existence of a REV and the fact that this volume in general appears to be larger than the core plug scale (~ 10-20 cm^3) gives a way to quantify the error associated with traditional averaging schemes and for establishing relations between data with different sample support (e.g. core and wireline data). From figure 7.36, a large scatter was observed in certain regions indicating a high dependency on the sample volume. In these regions, the use of values derived from small sample volumes (e.g.

core plugs) will vary greatly and give a high uncertainty for estimation of an effective permeability. Evaluating figure 7.13 to 7.16 in more detail shows that the effective vertical permeability tends to increase with increasing sample volume giving a general underestimation if an estimate is made on a small sample volume. This is also clear from figure 7.36, were the representative values (dark points) deviated from the traditional averaging schemes. Figure 7.38 shows the ratio between the effective (representative) permeability values and their respective, traditional averaging methods (arithmetic average for horizontal permeability and harmonic average for vertical permeability). The use of these averages carries with them an assumption of plane and infinite layers that are not met in the tidal bedding models used here. This will consequently give an underestimation of vertical permeability and an overestimation of horizontal permeability, but the effect is largest for k_v.

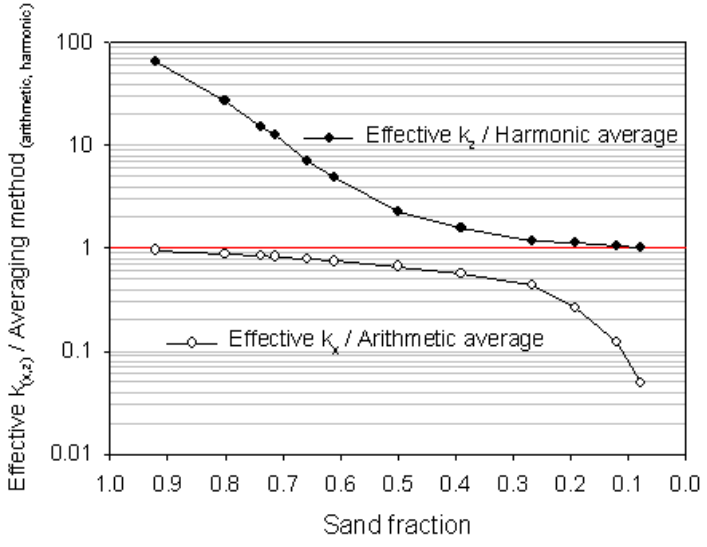

FIGURE 7.38 *The ratio between simulated permeability and the traditional average showing a large deviation in certain regions. See also figure 7.36. Note that the pure sand and mud models are excluded. These models have a k_v/k_h ratio close to 1.*

CHAPTER 8

Effect of petrophysical contrast on effective properties

8.1 Introduction

A set of conceptual tidal bedding models was used to evaluate how porosity and permeability varied with sample support in chapter 7. At some sample volume all the realizations approached a constant value. The permeability measured at such a volume was regarded as a representative permeability value for that particular bedding type. Figure 7.36 shows that these representative values follow a trend when plotted against the mud fraction. The trend occurs since there is apparently a relationship between the volume fraction of mud, and the effective permeability. Calculation of effective permeability in sand/mud system has been a focus in many previous studies (see section 2.3). Often these studies have focused on two components (sand and mud), possibly with anisotropic shapes, distributed randomly in space. Less work has been done on the estimation of effective permeability in a three component system.

In this chapter, the results from section 7.3 will be extended with 10 additional realizations at the locally homogeneous scale (C_V<0.5). These results, representing a two component system, can then be compared with analytical methods for calculating the effective permeability. Next, by introducing contrasting sand laminae the system is made more complex, and the effect of anisotropy within sand lamina are taken into account. Finally, the petrophysical properties of the mud layers which are uncertain, are tested using different mud properties. Together, these more com-

plex cases will give a better picture of how the effective permeability is dependent on the bedding type and how the permeability of the components influence the effective properties for different mud fractions.

8.2 Method

The same flume tank constrained models developed in chapter 7 are used here. Two additional models are included: one with no mud (only the two sand components) and one with approximately 5% mud. The latter bedding model is included since the vertical permeability trend in the low mud fraction regions is not linear in log-linear space.

The SBED program can simulate five different laminasets: mud, flood sand and ebb sand, where the latter two can have alternating lamina with contrasting petrophysical properties (sand type 1 and sand type 2). These two lamina types are often present in real sedimentary deposits as finer and coarser lamina and are in part the reason why we can observe inclined lamination in the laminaset. They may have different texture and fabric (as discussed in section 2.2.1) and consequently they can have different petrophysical properties. These properties are not easily resolved with core plugs, but they can, with some assumptions, be estimated (chapter 6). To simulate petrophysically contrasting lamina and their effect on the effective permeability and porosity, the input parameters for the two sand components were varied systematically (table 8.1 and table 8.2). As in chapter 7, the porosity and permeability values are constant. Furthermore, the porosity and permeability values were chosen to have a nearly linear relationship in log-linear space. From these models (same geometrical parameters but with different porosity and permeability values) 20 realizations were made. All the models have a model size of 30*30*300 regular cells which in all the cases should produce a homogenous porosity and permeability value (chapter 7) with the exception of k_x in the very high mud content region (figure 7.23).

Case	Sand component	Silt component	Mud component
Sand-Silt contrast 1:1	100 mD	100 mD	0.01 mD
Sand-Silt contrast 1:2	100 mD	50 mD	0.01 mD
Sand-Silt contrast 1:5	100 mD	20 mD	0.01 mD
Sand-Silt contrast 1:10	100 mD	10 mD	0.01 mD
Sand-Silt contrast 1:100	100 mD	1 mD	0.01 mD

TABLE 8.1 Input permeability values used to simulate contrast between sand lamina

Case	Sand component	Silt component	Mud component
Sand-Silt contrast 1:1	0.25	0.25	0.05
Sand-Silt contrast 1:2	0.25	0.225	0.05
Sand-Silt contrast 1:5	0.25	0.2	0.05
Sand-Silt contrast 1:10	0.25	0.175	0.05
Sand-Silt contrast 1:100	0.25	0.1	0.05

TABLE 8.2 Input porosity values used to simulate contrast between sand lamina

8.3 Results

The results from the two component system (sand and mud with constant permeability) are first compared with published studies and the relevant parameters are fitted to the numerical data (section 8.3.1). Then, the effect of varying the contrast between the two sand components is explored in section 8.3.2. Finally, the influence of mud permeability is evaluated in the two component system (section 8.3.3).

8.3.1 Effective permeability in a two-component system

The results from chapter 7 are extended with ten additional realizations to get a better data set at the scale where the effective permeability (k_z and k_x) is homogenized. Figure 8.1 shows a scatter plot of the simulation results. The arithmetic and harmonic averages are shown for comparison. Note that k_y and k_x diverge at high mud

fractions which is a result of the higher connectivity perpendicular the depositional direction. It is assumed that the connectivity in the y-direction is in general higher in the simulated models than in reality due to limitations in the code as discussed in section 4.5.2. Because of this and for consistency with the results from chapter 6 and chapter 7, only k_z and k_x will be used in the following analysis. A degree of validation of the synthetic bedding models used here is achieved by comparing the simulations with the effective permeabilities obtained from two outcrop samples (Jackson et al., 2003)

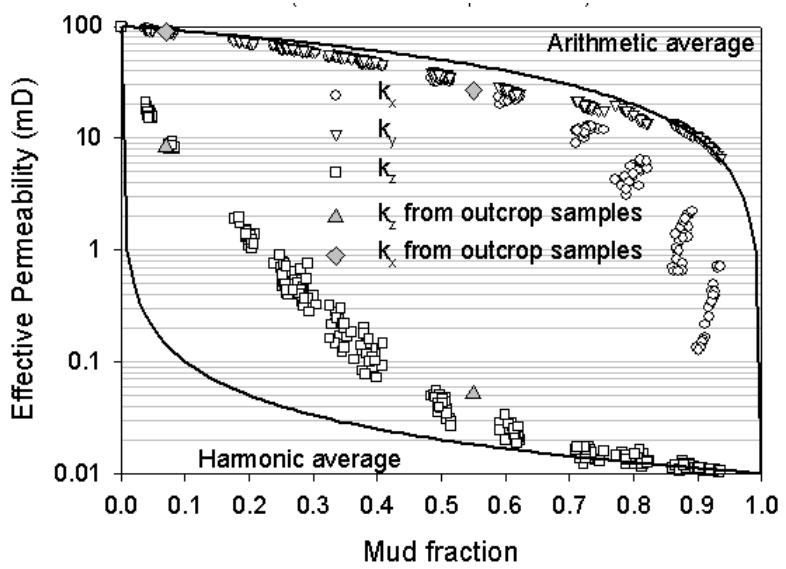

FIGURE 8.1 *All the simulated results for vertical (k_z), and horizontal (k_x and k_y) permeability and the effective permeability values derived from two outcrop samples (Jackson et al., 2003).*

From the numerical experiments, a clear functional relation is observed. A similar relation is reported in many other studies, and different methods have been used to fit curves through such data. Below, a selection of these proposed methods will be applied to the data in figure 8.1. Many of the reported relations have been limited to the low mud content region (e.g. Deutsch, 1989; Cuthiell et al., 1991; Begg and King, 1985). The various studies have also used different methods in the generation of the permeability field, giving implications for the relation between the correlations length and the mud content (see the discussion on page 227). In the following, an arithmetic average is taken for each bedding model giving an average mud fraction that corresponds to an average effective permeability.

An often used heuristic method is to take a power average of order p to get an estimate for the effective permeability (see section 2.3.5.1 and equation 2-30). A power average is an empirical approach and makes no reference to the equations of continuity or motion governing fluid flow at the scale of the averaged quantity. Hence, the use of this equation requires a set of experimental data for the estimation of the exponent p. Although lacking a physical basis, the method has been used in many studies with success. Table 8.3 gives some of these published p-values for horizontal and vertical flow. Using regression analysis, equation 2-31 was fitted to the data in figure 8.1. A p-value of 0.65 for horizontal permeability and -0.32 for vertical permeability gave a $R^2 > 0.99$, and these curves are plotted in figure 8.2. For vertical permeability at intermediate mud fractions (approximately between 0.1 and 0.4) there appears to be a linear relation in log-linear space which is indicated with the stippled line in figure 8.2. Extrapolating this trend to zero mud fraction, gives a too low vertical permeability. Although the power average method gives a correct estimate at zero mud fraction and the correlation coefficient is high, the linear trend is not well captured.

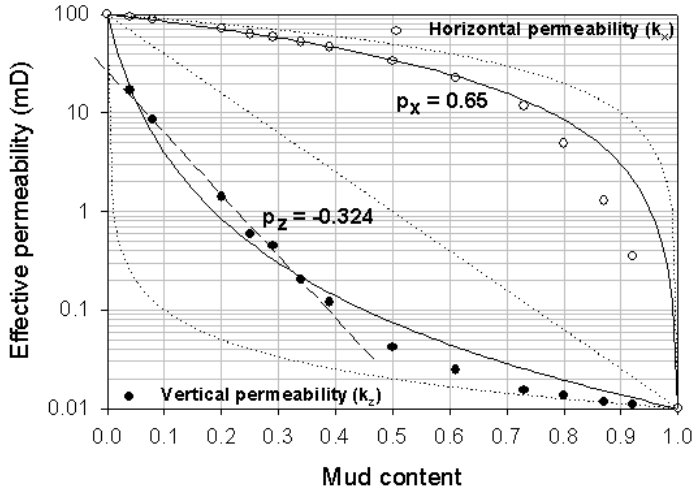

FIGURE 8.2 *Averaged experimental data and a fitted power average using equation 2-31. The stippled lines denote the arithmetic (upper), geometric (middle) and harmonic (lower) averages, respectively.*

Reference	$P_{horizontal}$	$P_{vertical}$	Comment
Cuthiell et al. (1991)	0.574	0.260	Digitized shale clast geometry
			2 D simulations
			Contrast: 1:1000
Deutsch (1989)	0.73	0.17	Indicator simulation with varying correlation lengths
			3 D simulations
			Contrast 1:100 000
Journel et al. (1986)	0.57	0.12	Indicator simulation with varying correlation lengths
			3D simulations
			Contrast 1:1 000 000
Desbarats (1992)	0.59	-0.33	Indicator simulation with varying correlation lengths
			2D and 3D simulations
			Contrast vary from 1:10 to 1:000
This study	0.650	-0.324	Process oriented modelling of tidal bedforms
			3D simulations
			Contrast 1:10000

TABLE 8.3 Published power-average exponents (p-values) for different sand/mud model systems compared with the results in this thesis.

Another heuristic method was proposed by Matheron (1967) (see section 2.3.5.1 and equation 2-29) which is a weighted average of the Wiener bounds. For a statistically homogeneous and isotropic medium, the exponent, α, is only dependent on the space dimension and for 3D it is 2/3. This equation was fitted to the simulation results and the best value of α was found to be 0.66 for k_z and 0.984 for k_x. Figure 8.3 shows the equation with the best exponent for the experimental data. For mud fractions higher than 0.1 the fit to vertical permeability is clearly poor. The estimator for horizontal permeability, being very close to the arithmetic average, fits the data reasonably well up to a mud fraction of 0.6.

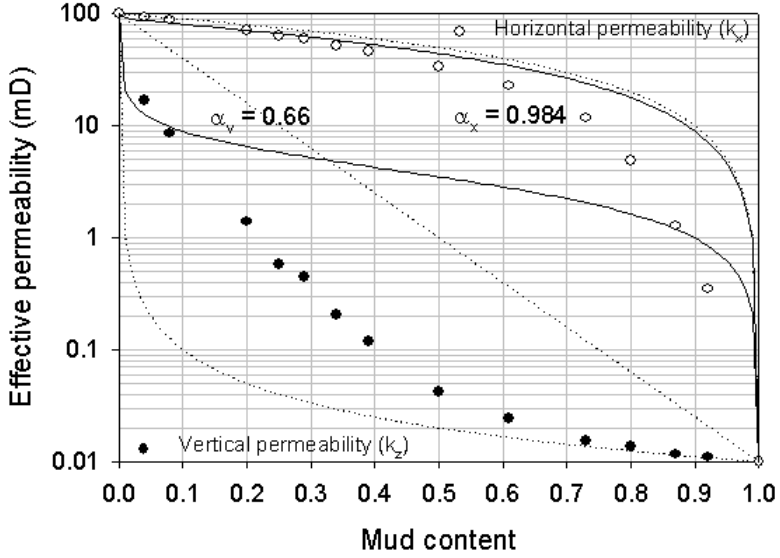

FIGURE 8.3 *Weighted average of the Wiener bounds as proposed by Matheron (1967) (see equation 2-29)*

Dagan (1979) used a self-consistent approach (effective medium theory) to derive an expression for effective permeability for a medium with spherical inclusions (equation 2-37). Analytical methods are intuitively appealing since they are quick to use and do not need experiments for calibration of empirical parameters. For a two-component system equation 2-37 reduces to equation 2-38 which was solved iteratively. The result is showed in figure 8.4. The equation does not contain any information regarding spatial correlation structure and thus gives the same results for isotropic permeability fields with zero and non-zero integral ranges. Desbarats (1987) showed, using numerical experiments, that in a permeability field with an isotropic spatial covariance structure, there was a good match when the mud content was below 0.6. Figure 8.4 shows that there is a reasonable fit between k_x and the analytical model at mud contents below 0.5. This suggests that the shape of the mud component, which has a more complex geometry in the models used here, is of minor importance with respect to k_x and that an approximation to spherical inclusion is justifiable. At higher mud contents, the deviation is however large, which is a result of the correlated structure in the simulated models giving a higher horizontal continuity deviating significantly from a spherical shape.

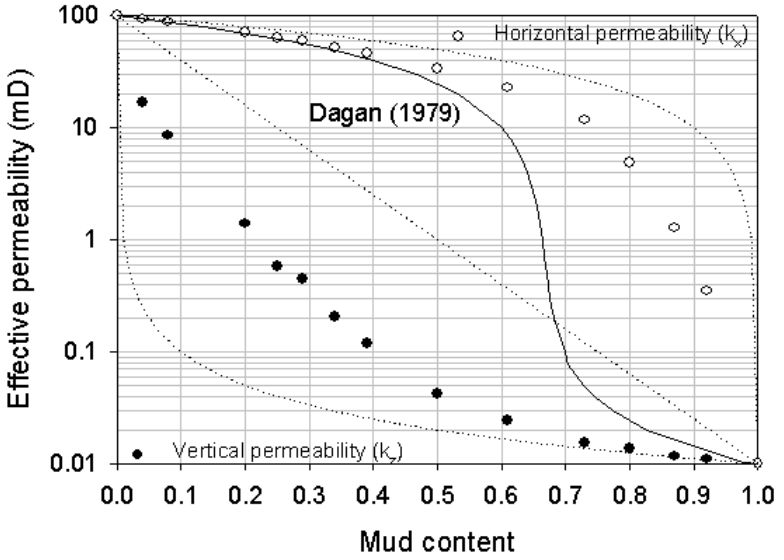

FIGURE 8.4 *An analytical, effective medium method published by Dagan (1979) describes k_x reasonably well at low mud fractions.*

Percolation theory was, in addition to the effective medium theory, classified as a deterministic method (Renard and Marsily, 1997) and the basic concept was reviewed in section 2.3.5.2. For effective permeability, equation 2-35 can be written as (Kirkpatrick, 1973; Deutsch, 1989):

$$k_{eff} = k_s \cdot c \cdot (V_{m,c} - V_m)^t \qquad V_m < V_{m,c} \qquad \textbf{[8-1]}$$

where k_s is the sand permeability, V_m and $V_{m,c}$ are the mud fraction and critical mud fraction respectively, and c and t are coefficients to be adjusted. Note that the mud permeability is not a factor in this equation since it is set to zero permeability and that only the connectivity of the conducting component is considered. Deutsch (1989) did a sensitivity analysis of the parameters as a function of the anisotropy ratio. He suggested that the exponent t was relatively constant around 1.71 for vertical flow and varying from 1.71 to 1.25 for horizontal flow. The proportionality constant varied from 2.6 for vertical flow to 1.2 for horizontal flow for high anisot-

ropy ratios. Deutsch (1989) gave no physical interpretation of these two parameters which might have given a better basis for adjusting the parameters.

The percolation threshold is a defined physical constant. For infinite grid-sizes and some special configurations, the critical threshold can be predicted with percolation theory. For finite-size models, the threshold tends to be smeared out into a transition zone (King, 1990) rather than a clearly defined mud fraction. Nevertheless, since the critical threshold is a physical quantity, this parameter must first be established before regression analysis is used to fit the remaining two parameters. Estimation of these parameters based on the experimental data is however complicated because the estimate of one parameter will influence on the choice of the other. Figure 8.5 shows the best fit of equation 8-1. Although Deutsch (1989) obtained a reasonable match with vertical permeability in the presence of anisotropic shales, no such match could be done here since k_z drops too quickly at very low mud fractions. The critical mud fraction for horizontal permeability is not clearly defined in the simulated model, in part as a result of the limitations in the code. Based on figure 7.37 a mud fraction 0.8 was chosen and a good match was found (R^2>0.99) for a t-value of 1.30 and c-value of 1.34. These values are in agreement with the findings in Deutsch (1989; his figure 9) for large anisotropy ratios.

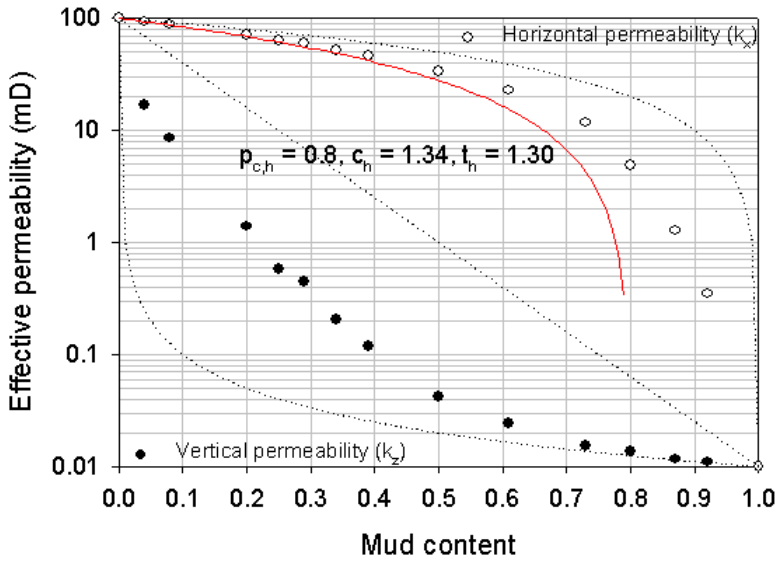

FIGURE 8.5 *Percolation model with adjusted parameters to fit the experimental data. Note that only horizontal permeability is calculated with this method.*

8.3.2 Effective permeability in a three component system

The porosity and permeability values were changed as specified in table 8.1 and 8.2. For each of the 14 bedding model types, 20 realizations were made and upscaled numerically. The results are shown in figure 8.6 along with the traditional averages.

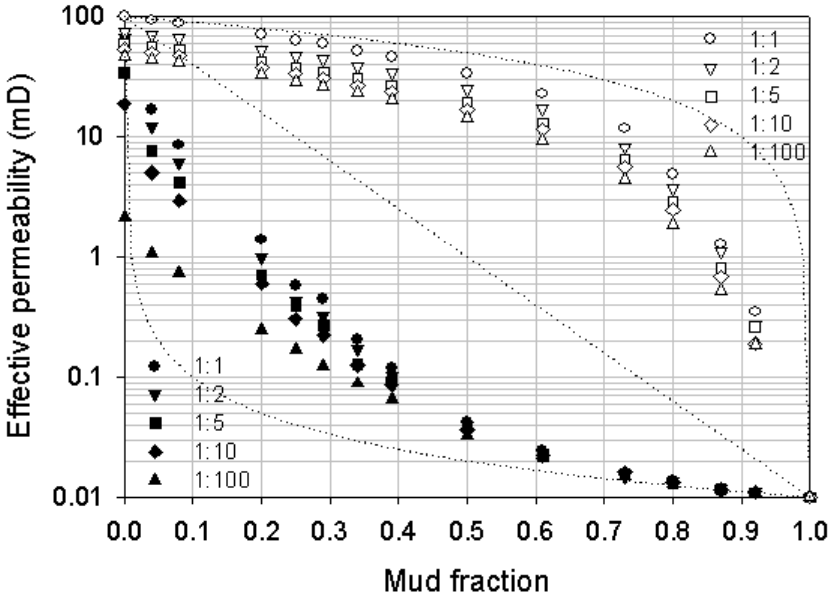

FIGURE 8.6 *Scatter plot of effective permeability (k_z=filled symbols and k_x=open symbols) with varying permeability contrast between the sand components. Note that only the arithmetic, geometric and harmonic averages for the two-component system are shown (dotted lines).*

The first thing to notice is that the percolation behaviour of the system becomes clearer. At low mud fractions the effective permeability is dependent on the permeability contrast between the sand components. As the mud content increases, the connectivity aspect of the sand layers become more critical. For vertical permeability, the effect of permeability contrast between the sand components becomes insignificant at around a mud fraction of 0.5. For permeability in the x-direction, the trend is less clear, but above mud fraction 0.8 it is difficult to separate the different cases, indicating that the k_x is less dependent on the sand permeability contrast. These values indicate a percolation threshold for the k_z and k_x.

In chapter 7, the onset of a percolating regime (figure 7.37) was set to a mud fraction of 0.35 for vertical permeability, which is somewhat lower than the threshold used here. Figure 7.37 was based on the size of the REV. The fact that the percolation behaviour was controlled by the majority of the mud laminasets gave an increasing (to infinity) REV approaching the critical mud fraction. Even though the majority of the mud laminasets show a percolation behaviour, there will still be some vertical, although tortuous, paths that give an effective permeability depending on the permeability contrast between the sand lamina. When the mud fraction is increased further (from 0.35 towards 0.5), there will eventually be mud layers that cover the xy-plane completely at one or more levels in the model giving, as observed in figure 8.6, an independency of the permeability contrast between the sand lamina. This issue will be further elaborated in section 8.4. In the following, a critical mud fraction is set at 0.5 for vertical permeability and to 0.8 for horizontal permeability.

Introducing a contrast between the sand components makes the situation both more realistic and more complex to handle, since an anisotropy in the sand component will affect the horizontal and vertical permeability differently. Beside the power average, there are no published methods (e.g. percolation equations or effective medium theories) that explicitly take into account a three-component system. Assuming that there are equal amounts of the two sand components each with a volume fraction of $(1 - V_m/2)$ the power average equation becomes:

$$k_{eff} = \left[(V_m \cdot k_m^p) + \left(1 - \frac{V_m}{2}\right) \cdot k_{s,1}^p + \left(1 - \frac{V_m}{2}\right) \cdot k_{s,2}^p \right]^{1/p} . \qquad \textbf{[8-2]}$$

The exponent p in equation 8-2 can be adjusted to give a best match. Figure 8.7 shows the result of using equation 8-2 on the data from figure 8.6.

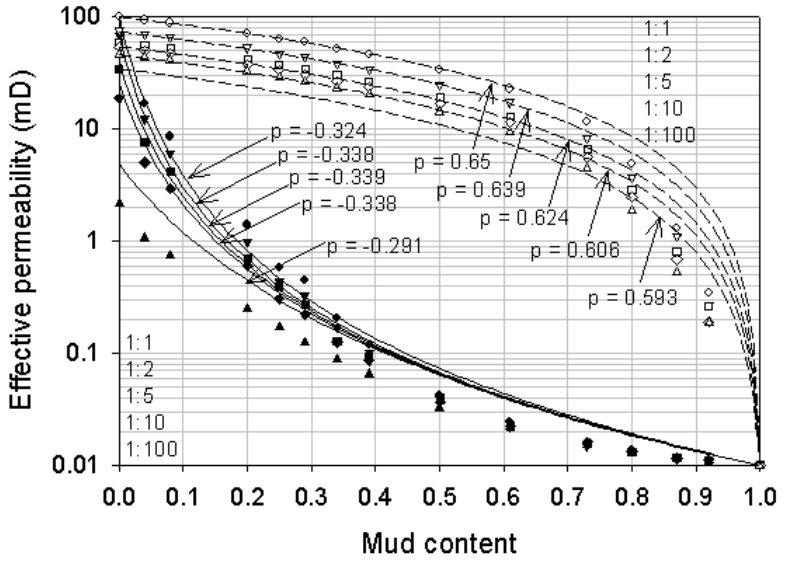

FIGURE 8.7 *The result of adjusting a three-component power average to the experimental data. The p-values are listed in the figure.*

As discussed above, the power average method is easy to match with only one parameter, but has no relation to the physical characteristics of the system and thus needs experimental data to find the exponent. Ringrose et al. (2003), using similar numerical models, proposed a modified geometric ($p \to 0$) and arithmetic mean ($p = 1$), for vertical and horizontal permeability respectively, to take into account the percolation threshold. Their equation for vertical permeability was

$$k_v = k_s * \left(\frac{k_m}{k_s *}\right)^{\left(\frac{V_m}{V_{m,c}}\right)} \qquad (V_m < V_{m,c}) \qquad \textbf{[8-3]}$$

where k_s^* is the sand permeability modified by a factor to account for internal sand laminaset anisotropy (to be discussed below). Their expression for horizontal permeability was

$$k_h = \frac{V_m}{V_{m,c}} k_m + \left(1 - \frac{V_m}{V_{m,c}}\right) k_s^* \qquad (V_m < V_{m,c}) \qquad \textbf{[8-4]}$$

Their argument for using the geometric mean as a basis for vertical flow was based on the log-linear trend in k_z for mud fractions between 0.1 and 0.5. This trend is also evident here in figure 8.6 for different contrast cases. Changing the contrast between the sand components is thus expressed with the anisotropy factor in k_s^*. As also noted by Ringrose et al. (2003), at very low mud fractions (V_m<0.05) the observed k_z values deviate from the linear trend. Extrapolating the linear trend to V_m=0 will give a too low vertical permeability for a clean (two-component) sand model (the dashed line in figure 8.2). The exact reason for this behaviour is not understood but it can partly be a numerical effect or an additional flow effect of thin mud lenses at low mud fraction (Ringrose et al. 2003).

In contrast to the power average method, equation 8-3 and 8-4 contains two adjustable parameters (implicitly assuming that $p \to 0$ for k_z and $p = 1$ for k_x): the critical mud content and the anisotropy factor. The critical mud fraction is a clearly defined physical quantity while the anisotropy ratio is based on the permeability contrast between the sand components that can be obtained by e.g. probe permeameter measurements. Ringrose et al. (2003) used an arithmetic average of the sand components in equation 8-4 and 0.3 times the harmonic average in equation 8-3 to fit their data set.

Figure 8.8 shows the experimental data from figure 8.6 and the estimators defined in equation 8-3 and 8-4. As a first approximation, the harmonic (for k_z) and arithmetic (for k_x) averages of the sand permeabilities are used as an anisotropy factor and the percolation threshold is set at 0.5 for k_z and 0.8 for k_x. The correlation coefficient is in all cases above 0.95 and highest for the 1:100 permeability contrast case. Given that the parameters used are based on properties that can be evaluated independently or based on knowledge of the system and not an arbitrary adjustment of a parameter, the correlation is good. The use the harmonic average as modifying factor in 8-3 was done deliberately since this is an estimate that can be found without numerical experiments. It is likely that the match would have been better if the parameter was allowed to be adjusted.

To better reproduce the non-linear trend at low mud fractions, and base the expression on some physical measures, a modified power average can be used:

$$k = \left[\frac{V_m}{V_{m,c}} k_m^p + \left(1 - \frac{V_m}{V_{m,c}}\right) {k_s}^{*p}\right] \quad (V_m < V_{m,c}) \qquad \textbf{[8-5]}$$

Although this equation, a heuristic extension of the power average, will honour the percolating behaviour it needs some experimental data to find the exponent and is thus, in essence, no better than the equations above. The best fit of equation 8-5 is shown in figure 8.9.

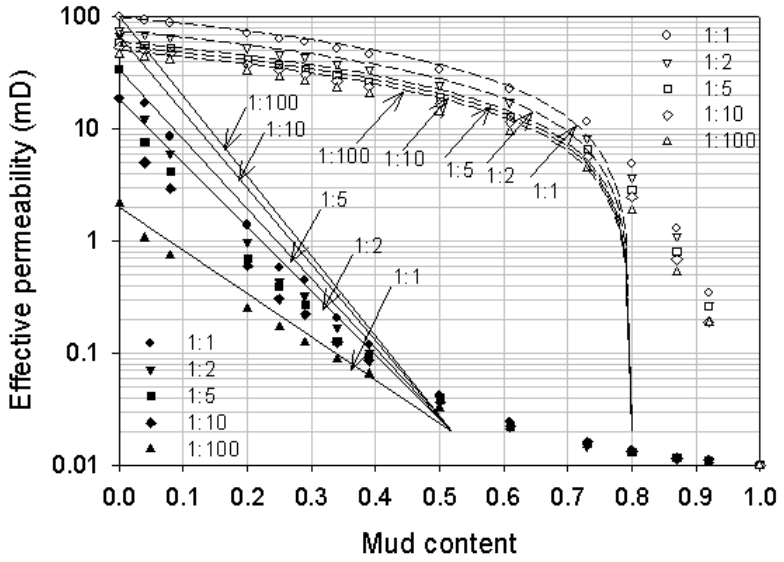

FIGURE 8.8 *Re-scaled geometric average for vertical permeability and an accelerated arithmetic average for horizontal permeability. Based on the equations from Ringrose et al. (2003).*

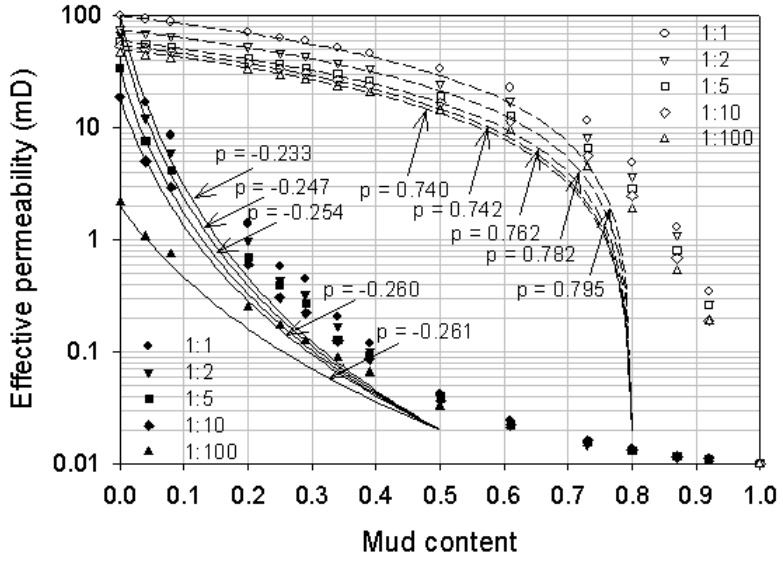

FIGURE 8.9 *Modified power average scaled to the percolation threshold. The p-values that gave the best fit are listed in the figure. This figure can be compared with figure 8.7.*

Although the main focus here has been on permeability, the bulk porosity of the simulated models has also been calculated. The porosity values were changed according to table 8.2 to give a log-linear plot with permeability. Figure 8.10 shows the simulated porosity values as a function of the mud content. As expected, porosity, being an additive property, is well estimated with a weighted arithmetic average of its constituent parts.

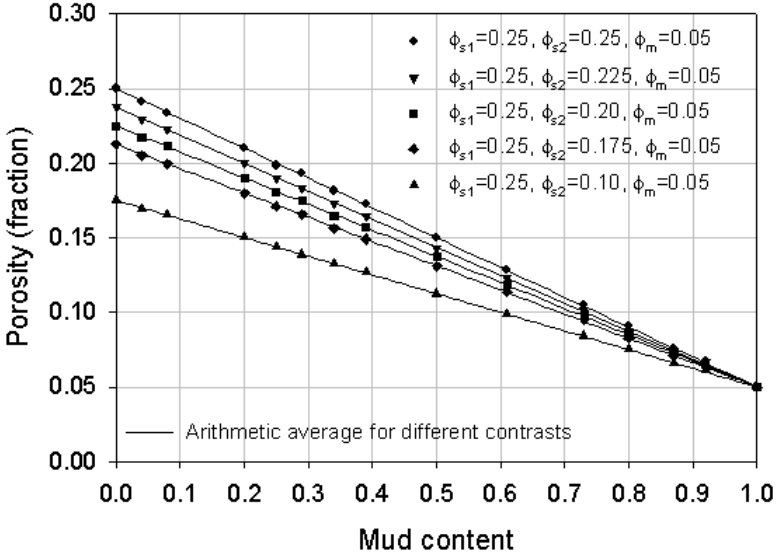

FIGURE 8.10 *Simulated bulk porosity estimated with a weighted arithmetic average of the three components.*

8.3.3 Effect of petrophysical contrast between sand and mud

The petrophysical properties of the mud component are, as discussed earlier, uncertain. A limited data set (Ringrose et al. 2004) suggests that the mud components on the Haltenbanken area have values in the range 10^{-6} to 10^{-3} mD. From visual inspection, some of the mud laminasets in the studied interval are silt-rich and can consequently have higher permeability and (effective) porosity. Table 8.4 gives the different mud permeabilities that were used in this section.

Case	Sand component	Silt component	Mud component
Sand-Mud contrast 10^2	100 mD	100 mD	1 mD
Sand-Mud contrast 10^3	100 mD	100 mD	0.1 mD
Sand-Mud contrast 10^4	100 mD	100 mD	0.01 mD
Sand-Mud contrast 10^5	100 mD	100 mD	0.001 mD
Sand-Mud contrast 10^6	100 mD	100 mD	0.0001mD
Sand-Mud contrast 10^7	100 mD	100 mD	0.00001 mD

TABLE 8.4 Varying the mud permeability with a 1:1 contrast between the sand and the silt component to evaluate the influence of contrast between the sand laminasets and the mud laminasets.

Based on the results above, a few selected bedding models were chosen for evaluation on the influence of varying mud permeability. The first model is a sand rich bedding type with a mud fraction of approximately 0.1 and both the vertical and the horizontal permeability is assumed to be mostly dominated by the sand properties. The second model type has a mud content of 0.35 and is close to the percolation threshold for vertical permeability (see figure 7.37). The last bedding model is close to the percolation threshold for horizontal permeability (mud fraction of 0.85). These three bedding models will thus reveal key characteristics of the flow properties and their dependency on the mud permeability. To complete the picture, the results from section 8.3.2 are inserted in the following figures. Figures 8.11 and 8.12 show the results for vertical and horizontal permeability in the low mud content case. Figures 8.13 and 8.14 show the results for the case near the vertical percolating threshold, while figures 8.15 and 8.16 give the results for the case near the horizontal percolating threshold.

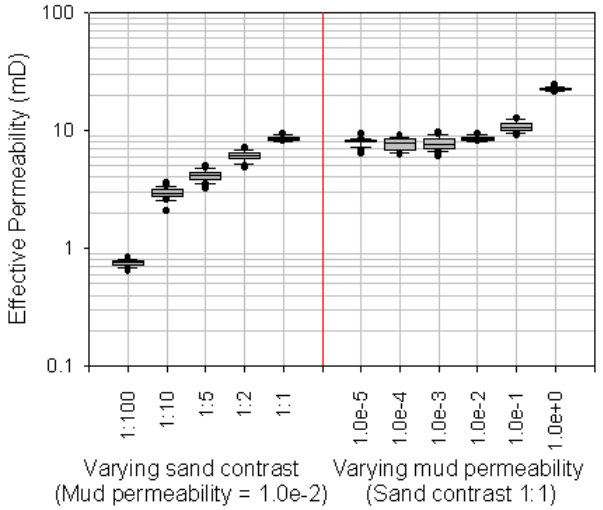

FIGURE 8.11 *Variation in k_z when the sand lamina contrast and the mud permeability are varied. The model has a mud fraction of 0.10.*

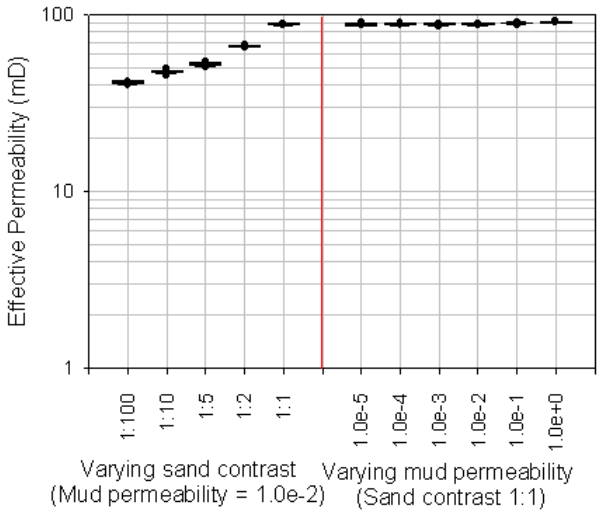

FIGURE 8.12 *Variation in k_x when the sand lamina contrast and the mud permeability are varied. The model has a mud fraction of 0.10.*

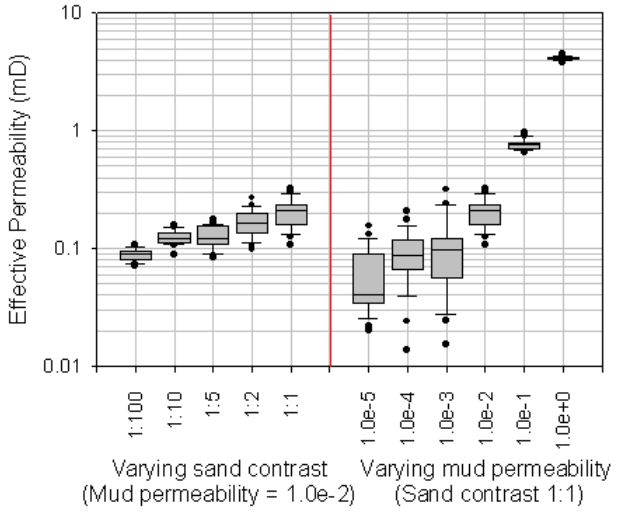

FIGURE 8.13 *Variation in k_z when the sand lamina contrast and the mud permeability are varied. The model has a mud fraction of 0.35.*

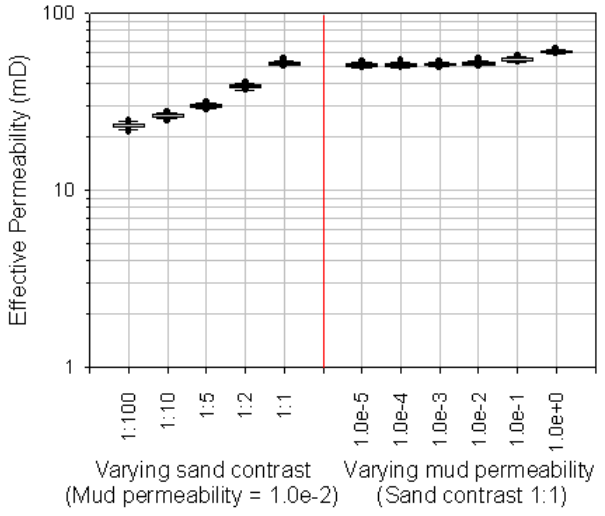

FIGURE 8.14 *Variation in k_x when the sand lamina contrast and the mud permeability are varied. The model has a mud fraction of 0.35.*

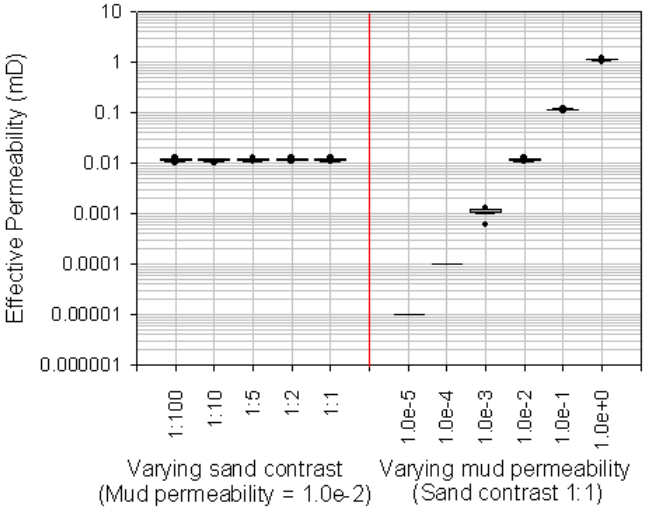

FIGURE 8.15 *Variation in k_z when the sand lamina contrast and the mud permeability are varied. The model has a mud fraction of 0.85.*

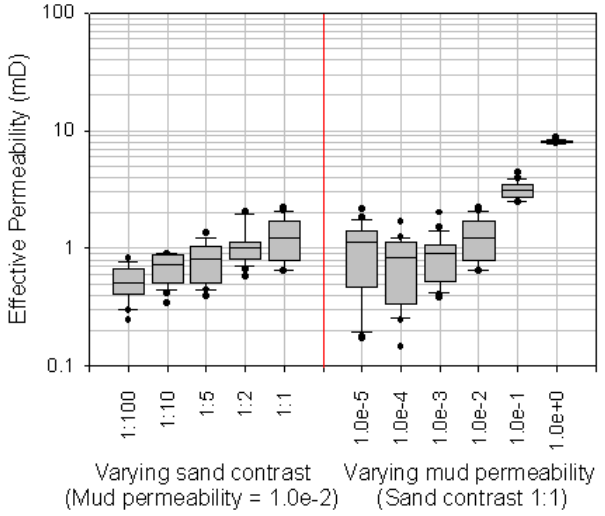

FIGURE 8.16 *Variation in k_x when the sand lamina contrast and the mud permeability are varied. The model has a mud fraction of 0.85.*

In the low mud fraction case (figure 8.11 and 8.12), both the horizontal and the vertical permeability are dominated by the connectivity of the sand. Changing the permeability contrast between the sand components by 2 orders of magnitude gives about an order of magnitude difference in effective k_z. The effect of changing the mud permeability by 5 orders of magnitude gives only a minor effect on the vertical permeability. The effect on horizontal permeability is minor in both cases and least when varying the mud properties.

Near the critical mud fraction for vertical permeability (figure 8.13 and 8.14), changing the mud properties gives a larger effect with almost two orders of magnitude variation in k_z. The effect of varying the sand permeability contrast on k_z is slightly lower than for the sand rich case (figure 8.11). For k_x, the effect of permeability contrast between the sand components and the mud/sand permeability contrast are comparable with the low mud fraction case, indicating that k_x is dominated by flow in the sand at this mud fraction. From figure 8.13 it is also clear the there is a large variability in k_z for each mud permeability case, especially when k_m is below 10^{-3}. The C_V values in these cases are larger than 0.5 even though, as was shown in chapter 7, with a k_m equal to 0.01 the model is statistically homogeneous with a C_V of 0.3. This may indicate:

1) the model is too small to produce a local homogeneous property with a very low k_m even though the REV is assumed to be related only to the spatial distribution of the sand and the mud,
2) too few realizations were made and that more will give a $C_V<0.5$ or
3) a numerical error due to the low mud permeability not giving an accurate effective vertical permeability in these cases.

At present, this inconsistency is not further exploited but figure 8.13 shows, nevertheless, that the vertical permeability close to the percolation threshold shows a high dependency on the mud permeability, meaning that the properties of the mud layers become increasingly important.

At very high mud fractions (figure 8.15 and 8.16), the sand starts to disconnect in the x-direction. The effect of varying the permeability contrast between the sand components has a small but noticeable effect on k_x and no effect on k_z. Since the vertical permeability is completely dependent on the mud properties, a linear relation between the mud permeability and k_z is observed. As for k_z at 35% mud fraction, k_x at 15% mud fraction shows an almost 2 orders of magnitude variation when increasing the mud permeability. As discussed above, it seems that the size of a

locally homogeneous sample increases with decreasing mud permeability. Whether this is an effect of the model size, number of realizations or numerical errors is unclear. A general decreasing trend in figure 8.16 is however present, suggesting as expected a dependency to the mud properties close the percolating threshold for k_x.

8.4 Discussion

A clear functional relationship has been observed between the effective permeability and the mud content (figure 8.2 and 8.6). Similar relations have been found by Desbarats (1987), Deutsch (1989), Cuthiell et al. (1991) and Norris and Lewis (1992) by using different types of models (i.e. different distribution of the components). Ringrose et al. (1999b; 2003; 2004) and Martinius et al. (2001) used the same modelling method to generate tidal bedding models and found similar relations as here. Such trends are empirically observed and not analytically derived. As a result, it is of interest to describe this relation with models that can be used in the absence of experimental data.

Some sort of power averaging scheme is intuitively appropriate since the effective permeability must be a value between the harmonic and arithmetic average. Although this method is heuristic, making no reference to geometric features like the percolation threshold, the p-value must contain some information about the spatial distribution of the components. Deutsch (1989) showed that the p-value increased and decreased with increasing anisotropy ratio for horizontal and vertical flow respectively. However the correlation length of the mud was set independently of the mud fraction. In addition, as shown in figure 8.7, increasing the number of components with contrasting permeabilities also influences on the p-value. Figure 8.17 shows the relation between the p-values and the permeability contrast, and it appears that for the bedding models and the upscaling method used here, increasing the contrast above 1:10 only has a minor influence on the power exponent.

A percolation-based model seems better since the system shows a percolation behaviour. The critical mud content can be found by independent measures, but the constant and the exponent in the equation need experimental data to be matched properly. Deutsch (1989) found no physical explanation for these parameters. To evaluate equation 8-1, figure 8.18 shows the case where the critical mud fraction and the exponent t are kept fixed and the constant c is varied. Figure 8.19 shows how the equation behaves as the exponent t is varied and the other parameters are kept constant. It is evident from these figures that the constant merely shifts the curve vertically (the overall shape of the curves are similar), while the exponent influences the behaviour (i.e. shape of the curve) for the intermediate mud frac-

tions. In the system used above, the permeability of clean sand model ($V_{mud} = 0$) is known. As a result, the constant parameter can be used to adjust the curve to get correct effective permeability in the pure sand case, while the exponent can be used to change the shape of the curve to a best fit with the data. Figure 8.20 shows equation 8-1 with a fixed critical mud fraction of 0.75, varying the exponent (t) and adjusting the constant (c) to the known sand permeability.

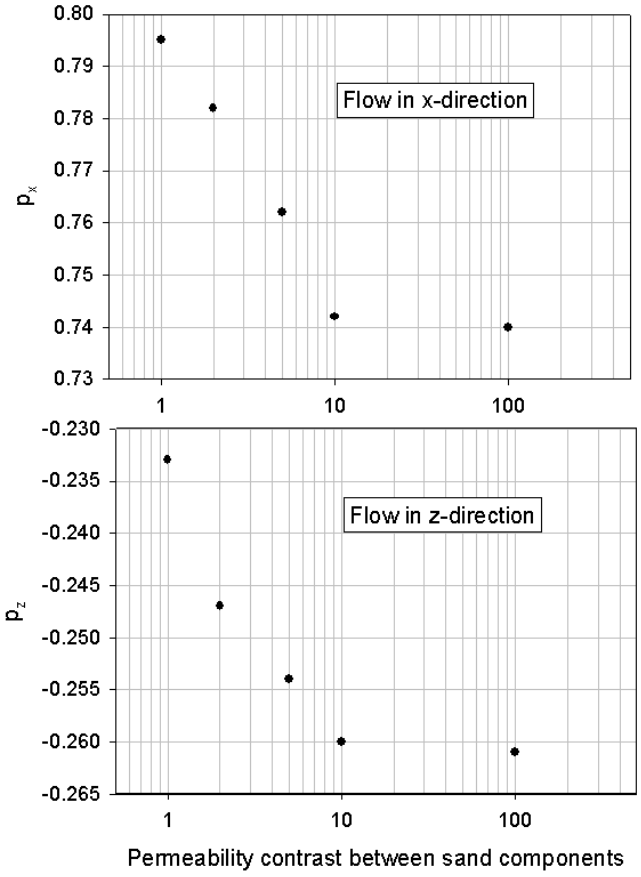

FIGURE 8.17 *Variation of the p-exponent in the power average equation for different contrasts between the sand components. The data is based on figure 8.7. Although sparse data, the plot indicates that a contrast larger than 1:10 only has a minor influence on the p-value.*

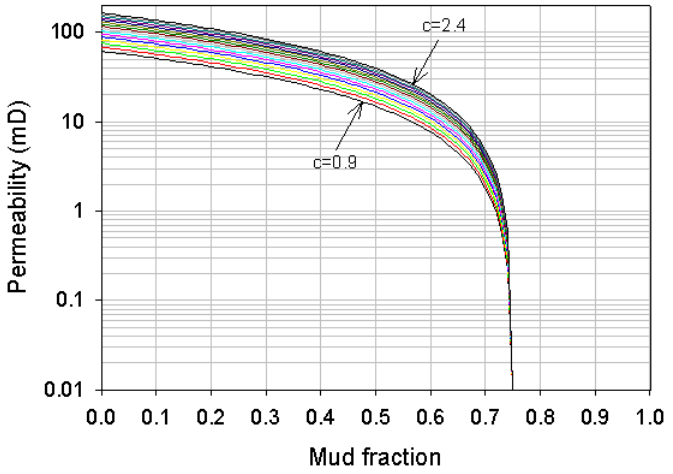

FIGURE 8.18 *The constant c (equation 8-1) is varied in equal steps of 0.1 from 0.9 to 2.4. The percolation threshold is at V_m=0.75. Note that the constant only shifts the curves vertically.*

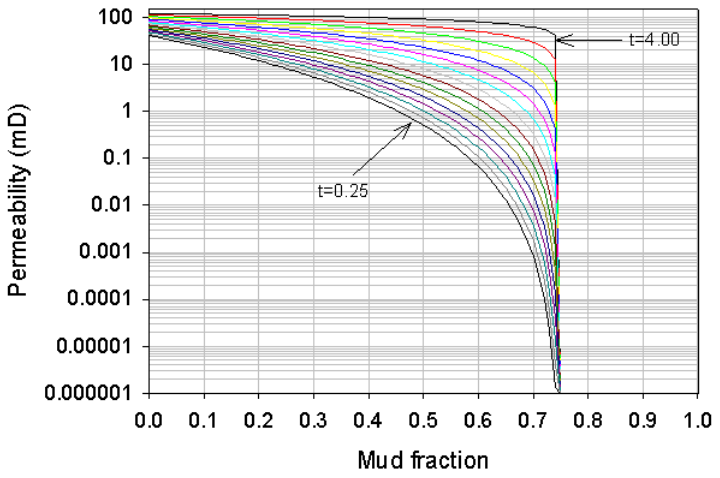

FIGURE 8.19 *The exponent t (equation 8-1) is varied in equal steps of 0.25 from 0.25 to 4.0. The percolation threshold is at V_m=0.75. Note that the exponent mainly influences on the shape of the curve for intermediate mud fractions.*

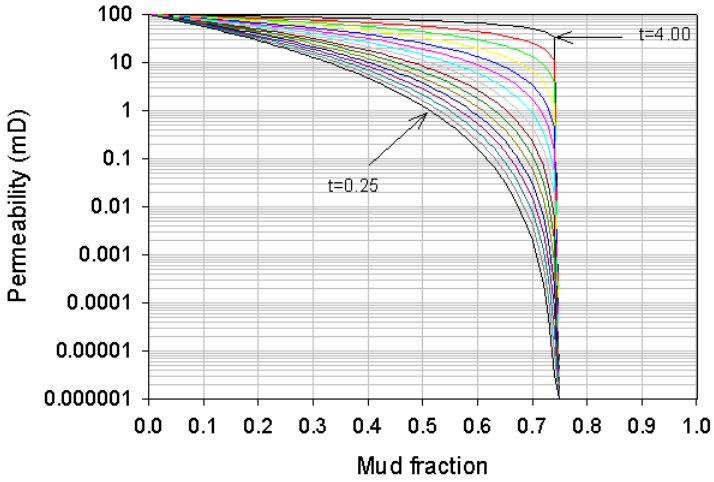

FIGURE 8.20 *The exponent t (equation 8-1) is varied in equal steps of 0.25 from 0.25 to 4.0 while the constant is adjusted to match a k_{eff}=100 mD for V_m=0. The percolation threshold is at V_m=0.75.*

Although not explicitly stated in the in the method, the exponent t contains information about the correlation structure (connectivity of the conductive component). If such information is available, a preliminary estimate of the exponent can made. The exact relation between the (dimension less) correlation length and the t-value is not clear, and requires further work. Care should however be taken since high values of the exponent can give an effective permeability larger than the arithmetic average.

Much analysis, both theoretical and experimental, has been done on the percolating threshold. For 2D bond percolation on a square lattice, the exact percolation threshold is equal to 0.5 (see Kirkpatrick, 1973 or Stauffer and Aharony, 1992). For more complex geometries (and lattices), numerical estimates have been obtained. The threshold, expressed as the amount of conducting component and not as mud fraction as above, has been observed to decrease going from 2D to 3D (e.g. Desbarats, 1987; Deutsch, 1989; Kirkpatrick, 1973). Introducing a correlation structure on one of the components significantly influences the critical threshold giving a lower threshold for horizontal flow and a higher for vertical flow.

The thresholds above are found to be in agreement with other studies. The exact value is however difficult to define. From figure 7.37 a range was proposed based on the relation between the size of the REV and the mud content. From figure 8.6

the value for the vertical threshold appeared to be at a higher mud content based on a criterion of independency of the permeability contrast between the sand components. In the latter case, this will correspond to a mud content that gives a persistent mud layer in the xy-plane. This should be the most restrictive critical threshold, and was used to calculate the parameters of the estimators in figure 8.8 and figure 8.9. From the point of view of analytically calculating the effective permeability on a finite model with correlation lengths approaching the model size, the range proposed in figure 7.37 is more relevant. Above a mud fraction of 0.35, the effective medium methods will fail and the use of a percolation model is more correct. The estimates of the critical threshold from the models used here can be improved by an independent analysis of the connectivity of the conducting components. It should however be noted that there is a distinction between the connectivity and the conductivity of this system, since not necessarily all the connected parts contribute to the conductivity (figure 2.17).

Ringrose et al. (2003) used the same modelling tool as in this thesis (although the input parameters describing the geometry of the sand and mud component were slightly different). Their results are similar to those shown in figure 8.1. They did not, however, consider explicitly how k_x and k_z varied with model size, so it is not possible to evaluate whether their models behave similarly at smaller sample volumes. At the larger volume, the results are similar suggesting that the degree of detail as incorporated in the input parameters here (section 7.2.1) is of minor importance for single phase calculations. For multiphase flow, the effect can be larger. Equation 8-3 and 8-4 were proposed by Ringrose et al. (2003) to describe this type of system and the equations were fitted to the data in this thesis in figure 8.8. This equation is better than the power average method since the parameters are physically well defined and need, in theory, no numerical experiments for adjustment. Compared to the percolation model, this method gives a better expression for the vertical permeability, can be used for more than one component and does not require an impermeable mud. The implicit assumption in the equations is that a p-value corresponding to the geometric and arithmetic averages can be used. In the low mud content region, a non-linear trend in simulated vertical permeability is not well captured. Based on this, a modified power average was proposed that fits the data better in this region (equation 8-5). The obvious disadvantage is that some numerical experiments must be performed to find the proper p-values.

In section 3.2 the sedimentological terms flaser, wavy and lenticular were explained qualitatively. Ringrose et al. (2003) proposed that these terms can be quantified in terms of connectivity and defined three flow-regimes based on the mud fraction:

1) low mud fraction were the flow is dominated by flow through the sand and with a flow path distortion effect caused by the isolated mud lamina,

2) intermediate mud fraction close to the percolation threshold for critical flow phenomena, and
3) high mud fraction regime were the flow is dominated by flow through mud with a flow distortion effect caused by isolated sand lamina.

They stated further that regime 1 and 3 should be described by an effective media theory (e.g. self consistent), while regime 2 should be described with percolation theory. This classification scheme also appears to apply to the data presented in this thesis, and the division is here further supported by figure 7.37 (where the geometry of the sand and the mud component were considered) and figure 8.6 and figure 8.11 to 8.16 (where the permeability contrast between the sand components and the mud permeability were evaluated).

Figure 8.6 shows that the effective permeabilities deviate from the traditional averaging methods often used. To clearly see the difference, figure 8.21 shows the ratio between the respective traditional (weighted) averaging scheme and the calculated effective properties. For k_z the effect is greatest in the low mud content region, but is reduced as the permeability contrast between the sand lamina increases. This is expected since the permeability of the second lamina type is decreased by two orders of magnitudes. For k_x the effect is less, but the deviation is about one order of magnitude for high mud contents. The influence of the permeability contrast between the lamina is surprisingly not very large.

Varying the mud permeability was noted to have an influence as the mud content approached, and exceeded, the percolating threshold. Jackson et al. (2003), by analysing two real heterolithic rock cubes with a sand fractions of 0.93 and 0.445, found that the mud permeability influenced significantly the vertical permeability but that the effect on horizontal permeability was minor, supporting the results presented here.

The results presented in this chapter suggest that the focus in data collection can be adjusted according to the mud content. In the low mud content region, the petrophysical properties of the sand lamina are the most important parameter and the use of a probe permeameter device or thin sections, can provide the necessary data. This applies in particular for the estimation of vertical permeability since the horizontal permeability appears to be less influenced. As the mud content increases, the mud property becomes naturally more important. However, since the percolation threshold is very different for k_x and k_z, the sand contrast is the most important parameter to consider when focusing on k_x even for rather high mud fractions. In flow regime 2 (i.e. close to the percolation threshold), the mud properties are

important and figure 8.13 and 8.16 showed that the effective permeability can vary several orders of magnitude depending on the permeability value chosen. Especially for the vertical permeability at intermediate mud fractions, this can be important since many of the reservoirs on the Haltenbanken consist of such lithofacies. The results presented here can also be helpful to better decide on a cut-off on the V_{mud} log. It should be clear from the above that such a cut-off depends on the property of interest (e.g. vertical or horizontal permeability).

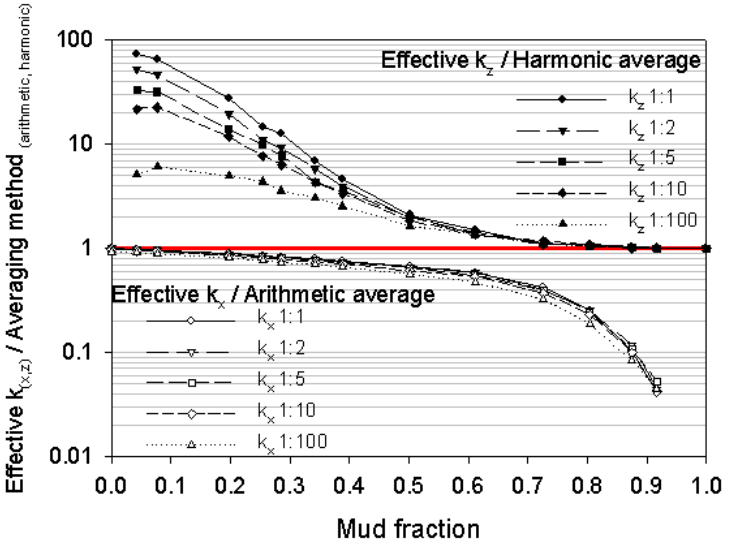

FIGURE 8.21 *The ratio between the effective permeability and the respective conventional applied averaging schemes. Note the different effect on vertical and horizontal permeability of increasing the permeability contrast between the sand components.*

As also discussed at the end of chapter 6, the permeability contrast between the sand and between the sand and the mud influence the amount of cross-flow (the off-diagonal terms in the permeability tensor). Pickup et al. (1995) showed that when the contrast between the low and the high permeable lamina became higher than 0.4, the cross-terms became significant. In the models used here the contrast vary from 0.5 to 0.01 (calculated from table 8.1) suggesting that periodic boundary conditions should have been used to estimate the effective permeability. However, the arrangement of several sand laminasets separated by the low permeability mud

laminaset can be used as an argument that the cross-flow is of less importance (Ringrose et al., 1999).

It is hoped that the numerical results presented here have provided some insight into the factors controlling the effective permeability and that they can form the basis for the development of an analytical solution that can be used for calculation of effective permeability in these complex models. It is felt that an analytical method describing this system probably needs some form of expression of the correlations lengths of the components and that the permeability of the mud component should be taken into account explicitly.

CHAPTER 9 *Application of results*

One of the practical goals of this thesis was to give a better estimate for horizontal and vertical permeability that better takes into account the sedimentological and petrophysical variability present in the interval. As described in the preceding chapters, there have been made fine-scale sedimentological and petrophysical models of the interval, and the petrophysical variability with sample support and the effect of permeability contrast between the lithological components has been evaluated. These results will be used here to give a rescaled estimate of porosity and permeability that integrates core and wireline data better and gives an opportunity to address the uncertainty associated with estimators based on traditional core-log integration. Some of these results have also been reported in Nordahl et al. (2003; 2004, see Appendix B and Appendix D) and Ringrose et al. (2004).

9.1 Introduction

The general challenge with estimation of porosity and permeability from core and wireline data is that the two data sources measure different physical parameters and that they represent different sample volumes. The former is a subject of cross-scaling while the latter is an upscaling issue (Corbett et al. 1997). In heterolithic units, the sampling bias can also be an important issue. It should nevertheless be clear that the measurements themselves, whether measured in the laboratory or by a downhole device, would, under favorable conditions and experimental experience, produce an accurate measure (Lovell et al. 1998) of the parameter the device was

designed to measure (e.g. flow rate in a Hassler cell or the attenuation of gamma-rays in the density tool). The wireline tools do not record the parameters porosity and permeability directly but have to be interpreted (see section 2.3.4) and the degree to which the interpreted values are accurate (close to the true value) is more difficult to quantify. The basic question then is what is the uncertainty or error associated with 1) the use of the measured wireline recorded parameter(s) as surrogates for the parameters of interest and 2) the dependency of the parameters on differences in sample support.

In this chapter, two different methods will be used to give a better, more reliable estimate of porosity and permeability based on the core data (both sedimentological and petrophysical). The first method (section 9.2), being the most time consuming, uses the results from chapter 4 to 6 to forward model the porosity and permeability values. Using this method, the individual lithofacies models can be studied and a moving window averaging technique can be used to forward model a continuous porosity and permeability log-curve for comparison with the currently used interpretations. The second method (section 9.3) uses the results from chapter 7 and 8 and estimates effective permeability based on the apparent relation between the volume fraction of mud and the effective permeability. Porosity will not be estimated with this method since there is a 1:1 relation between the mud fraction and the porosity (figure 8.10).

9.2 Method 1: Forward modelling of porosity and permeability.

The numerical near wellbore model, created in chapter 5 and 6, will be used in the following to forward model porosity and permeability. This model, based on sedimentological and petrophysical core data, is then used to give re-scaled properties that can be compared with the wireline based estimators. This method is the most time consuming to perform on regular basis since detailed core analysis is necessary. It is assumed that this method will give the most accurate estimate, but as the results will show, capturing all the natural variability is nevertheless challenging.

First an evaluation of the individual lithofacies models is done. With this method, biased core data, variance reduction with sample volume and comparison with a value measured at the REV can be addressed. Three of the models from chapter 5 and 6 are used as examples: LF7.2_WB, LF7.1_WSF and LF3_LTW. These models represent different bedding types and mud fractions, and are relatively thick compared to the vertical resolution of conventional wireline tools. The latter is important to measure a value that is less affected by the over- and underlying lithofacies. Some ‘shoulder-effects’ will however be present in the wireline data set.

Figures 9.1, 9.3 and 9.2 show the results for horizontal permeability, the k_z/k_x-ratio and porosity for each of the three bedding models. These figures show the results from chapter 6 compared to the wireline log interpretation (from the Statoil database) and a value measured on the synthetic bedding models at a representative volume (labeled "REV" in the figures).

If the core plug data were unbiased, a reduction in the variance would be expected when comparing with measures taken on a larger sample. This tendency will be dependent on the degree of bias in the core data, as discussed in chapter 6. For horizontal permeability (figure 9.1) a similarity between the simulated core plug data and the real core plug data is observed and there is in general a decrease in variance when the property is estimated from the wireline log. Since the simulated core plugs are un-biased (section 6.2.1), this indicates that either 1) the measured core plug data is not very biased or 2) that the bias in the core plug data is of minor importance when estimating horizontal permeability. Based on the detailed analysis of the core plugs in chapter 6, it was shown that there was some bias in the data. However, as shown in chapter 7 and 8, for mud fractions below the percolation threshold for horizontal flow ($p_{c,h}$), the connectivity of the sand layers and the permeability properties of the sand and silt components influence more on horizontal permeability than the mud permeability. The three bedding models used here have mud fractions below $p_{c,h}$. The independency of mud permeability on horizontal permeability for similar bedding types was also observed by Jackson et al. (2003). The evaluation of variation in porosity with measurement volume is given in figure 9.2. As discussed in chapter 6, there is a fairly good match between the simulated and measured core plug data although the effect of biased sampling become evident as the mud fraction increases (see also table 6.9 and figure 9.1C).

Comparing with the wireline based estimates of porosity and horizontal permeability there are, in general, a decrease in variance because of the larger measurement volume. Note, however, that the large variance in the wireline data seen in figure 9.1 B and 9.2 B most likely is a result of the 'shoulder-bed' effect. Comparing with the value of k_x (or porosity) calculated at the REV there is a clear reduction in variance and in most cases the mean of the core plug data and the wireline data matches the REV value quite well. Where a mis-match is found, for example in figure 9.1 C or figure 9.2 C, this can, in part, be related to the fact that not all the features affecting the porosity or horizontal permeability are satisfactory included in the model (e.g. diagenetic features and bioturbation) as will be further discussed below.

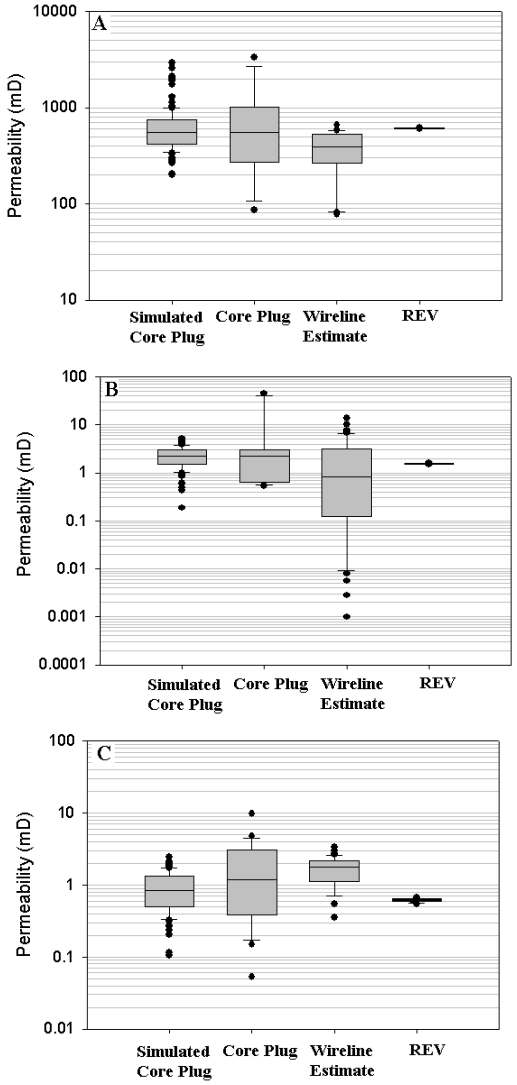

FIGURE 9.1 *Comparison of k_x derived from different sources and sample volumes.The lower and upper limit of the box indicate the 25th and the 75th percentile while the whiskers represent the 10th and 90th percentile. The solid line is the median and the black dots are the outliers. A: Model LF7.1_WSF, B: Model LF7.2_WB and C: Model LF3_LTW.*

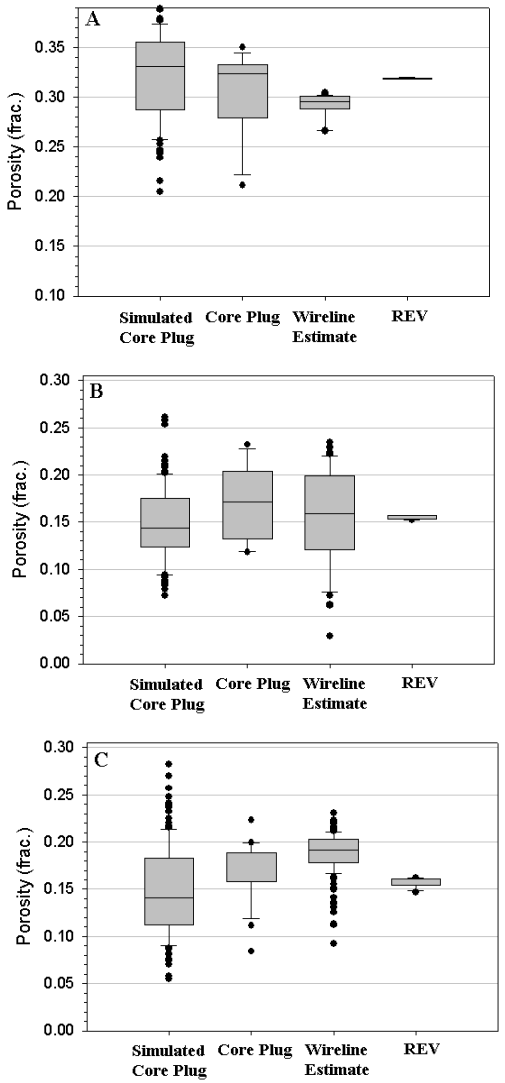

FIGURE 9.2 *Comparison of porosity derived from different sources and sample volumes.The lower and upper limit of the box indicate the 25th and the 75th percentile while the whiskers represent the 10th and 90th percentile. The solid line is the median and the black dots are the outliers. A: Model LF7.1_WSF, B: Model LF7.2_WB and C: Model LF3_LTW.*

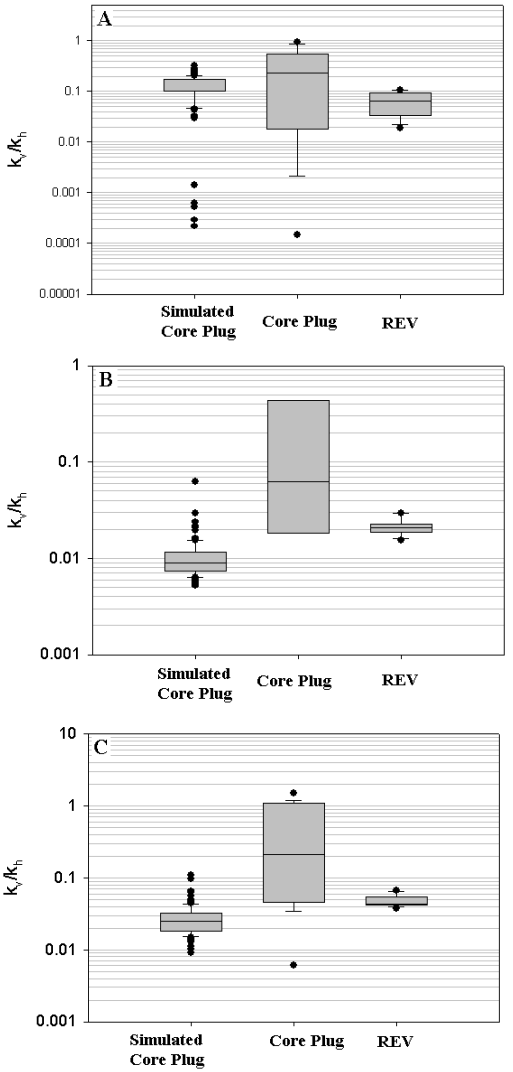

FIGURE 9.3 *Comparison of k_V/k_X-ratio derived from different sources and sample volumes.The lower and upper limit of the box indicate the 25th and the 75th percentile while the whiskers represent the 10th and 90th percentile. The solid line is the median and the black dots are the outliers. A: Model LF7.1_WSF, B: Model LF7.2_WB and C: Model LF3_LTW.*

For the k_z/k_x-ratio there exists currently no wireline based estimate in this interval. As shown in chapter 6, statistical similarity between the simulated and measured core plugs is difficult to obtain especially because the vertical core plugs are very biased often taken from the more sand rich intervals. As a result the k_v/k_h -ratio based on the core plugs will be significantly larger than the simulated k_z/k_x, particularly for intermediate mud fractions (figure 9.3 B and C). For these mud fractions the properties of the mud component becomes increasingly important (section 8.3.3). Going to a value calculated at the REV, the variance is clearly reduced and it is observed that the value for the intermediate mud fractions (figure 9.3 B and C) show a slightly higher value than the simulated plug mean. This is consistent with the results on the conceptual bedding models (section 7.3 and the discussion on page 229) and indicates that the connectivity issue in 3D is of importance and can result in higher k_v than observed from the core plugs (Yoshida et al., 2001; Jackson et al., 2003).

The method described above is useful where a particular lithofacies is important for the overall flow properties and needs to be evaluated in detail, especially when biased core data is assumed to be present. In other cases, a continuous estimate of a sequence of lithofacies models resembling the wireline recording is more interesting. In this case the forward modelled curves can be used to evaluate the interpreted wireline estimate of porosity and permeability. The models described in chapter 5 and 6 are stacked (in the model) according to the observed stacking pattern in the interval (figure 5.9) and ten realizations were created. On this stacked model, a portion specified by a window length is upscaled. Then the centre of the window is moved upward, according to the step length, before an upscaled value again is calculated. Figure 9.4 shows one realization of a stacked model and the window and step lengths.

The window length corresponds to the vertical resolution of the wireline tool. This parameter should be chosen based on the tool that is used to interpret the porosity or permeability. The density tool is the primary source for the interpretation of porosity and permeability in the selected interval. The vertical resolution for this tool is commonly set to 1 foot (approximately 30 cm) and a measurement is recorded every 6 inch (approximately 15 cm) (figure 2.12). The depth of investigation varies according to lithology and fluid properties but can be assumed to be around 10-15 cm. With the chosen cell dimension, each cell has a length of one centimeter in x- and y-direction (section 4.2.1). To approach the depth of investigation of the density tool, the number of cells in the plane is set to 10*10 giving a 3000 cm^3 volume of investigation. In addition, a model set is created with a 30*30 cm^2 area in the

plane for which a representative upscaled value can be calculated (a volume of 27000 cm^3).

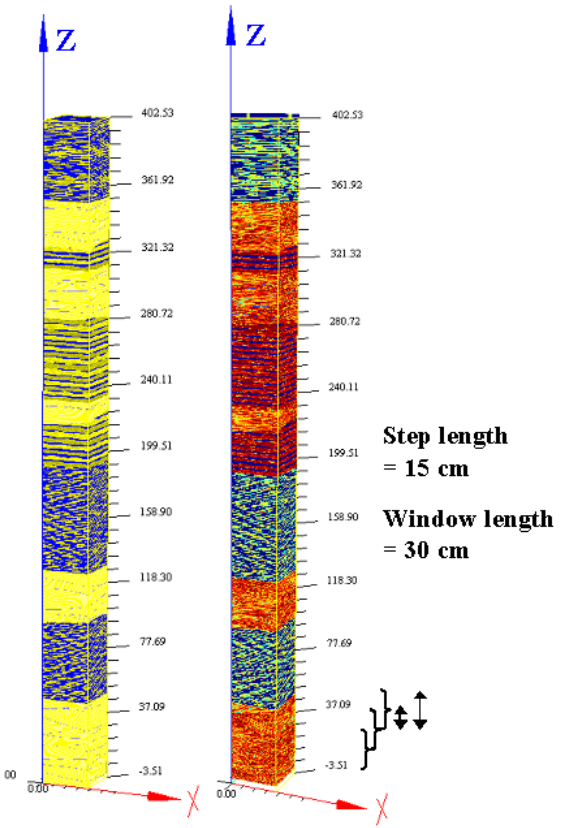

FIGURE 9.4 *One realization of a stacked model (the interval between 2611.2 m and 2615.25 m).Left stack is the geometry grid and the right stack is the permeability realization (white indicate high permeability and dark color indicate low permeability). The brackets and arrows indicate the window length and the step length.*

Figure 9.5 to 9.8 show the result of forward modelling the permeability, porosity and sand fraction from 10 realizations of the near wellbore model. The error bars denote one standard deviation and are calculated from the ten realizations of the stacked model.

In addition to the detailed (2 mm-resolution) measurements of sand/mud content reported in chapter 5, a visual estimate (at approximately 30 cm resolution to match the density tool vertical resolution) was made of the sand fraction in the core. This semi-quantitative curve is compared with the forward modelled sand fraction curve (in figure 9.5) for which input parameters were based on the detailed measurements of selected parts of the individual lithofacies. It is evident that the two curves are fairly similar and some of the difference can be explained by the 2D-3D effect, discussed in chapter 5. The visual estimate is used in the following since it is performed over the whole core length and has the same vertical resolution as the density log recording. Figure 9.6 shows the forward modelled vertical permeability in addition to the vertical core plugs. Also plotted is the visual estimate of the sand fraction (there exists no wireline based estimate for this property). It is evident that the biased core plugs give a mis-leading picture of the vertical permeability especially for lower sand fractions. It is also noted that the largest error-bars are present in the upper, sand rich part of the interval. The horizontal permeability (figure 9.7) shows, in contrast, slightly higher variability in the high mud content intervals although the overall variability is significantly lower than the variations seen in the interpreted wireline based estimate (KLOGH). The general pattern is, however, quite similar with high permeability recorded in Tilje 2.1, lower permeability in Tilje 1.2 and variable in Tilje 1.1. The forward modelled porosity (figure 9.8), shows lower variability compared to both the core plug data and the wireline based estimates although the general trend is similar.

To evaluate this more in detail where the simulated variability is largest and the effect of sample volume is most significant, figure 9.9 shows the calculated C_V from the stacked model with 10x10 cells and 30x30 cells in the xy-plane along with the visual estimate of sand fraction. The C_V is based on the upscaled values taken at each depth from the ten realizations. The vertical permeability shows the highest variation in the most sand rich intervals (mud fraction below 0.2) as in the upper interval between 2596 m and 2600 m. This is in agreement with the results from chapter 7 (figure 7.37). Also in agreement with those results, is the observation that the horizontal permeability shows largest variability in the mud rich models (e.g. between 2601 m and 2611 m). It should be noted that a high C_V also could arise at the boundary between two petrophysical contrasting lithofacies. Contrasting bedding types will affect the REV as also noted by Bear and Bachmat (1990, p.232-236). For porosity there is, as expected (see figure 7.34), no clear relation between the degree of variability and the bedding type, and the occasionally larger standard deviation can be attributed to the shoulder effect. Also as expected, the variability is reduced going from the smallest (10x10) to the largest model (30x30) for both k_x, k_z and porosity.

The construction of a detailed near wellbore model, based on quantities measured at the lamina scale, organized in a sedimentological reasonable way and validated at the scale where the measurements were taken, is assumed to give a better basis for estimation of porosity and permeability compared to the available wireline based estimate. There are, however, several factors that are not included in the model and that could significantly affect the petrophysical properties. Most important are diagenetic effects, bioturbation and fractures. It is thus assumed that the variability in the model would be larger if these effects were included. The same was noted in chapter 6 where the simulated variance at the core plug scale was found to be lower than the observed variance, although some of the discrepancy was attributed to the biased sampling. The Heidrun field is, however, relatively unaffected by diagnesis compared to other more deeply buried field in the Haltenbanken region. Using this method in those more complex fields will thus require a model that can capture the diagenetic issues. If some other independent in situ measure of permeability had been available (e.g. well test or MDT measurements), these could be used to quantify the influence from the different factors. In a similar study on a different formation, Elfenbein et al. (2003) used the results from a well test and a similar near wellbore model to differentiate between the effect of primary sedimentary structures and calcite cementation. More recently, Zhang et al. (2004), compared models developed in this thesis to another Heidrun well where well test permeability estimates were available and obtained a good match with the near wellbore model.

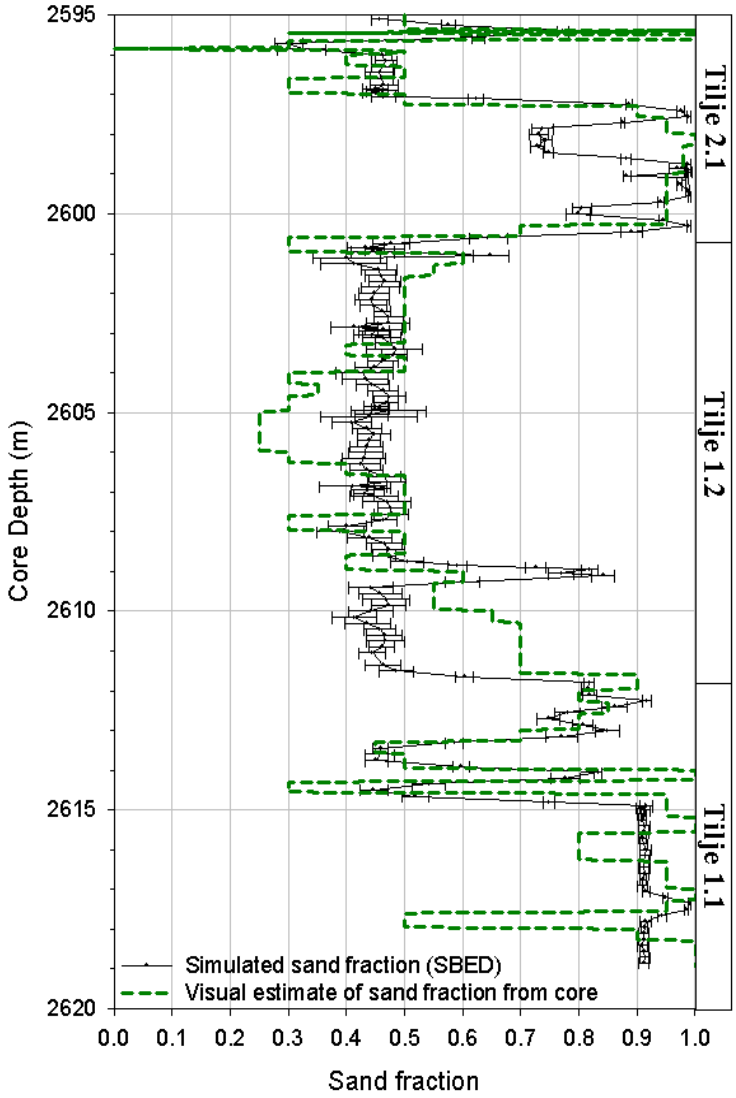

FIGURE 9.5 *Comparison between simulated and measured sand fraction.The error bars represent one standard deviation calculated from the 10 realizations.*

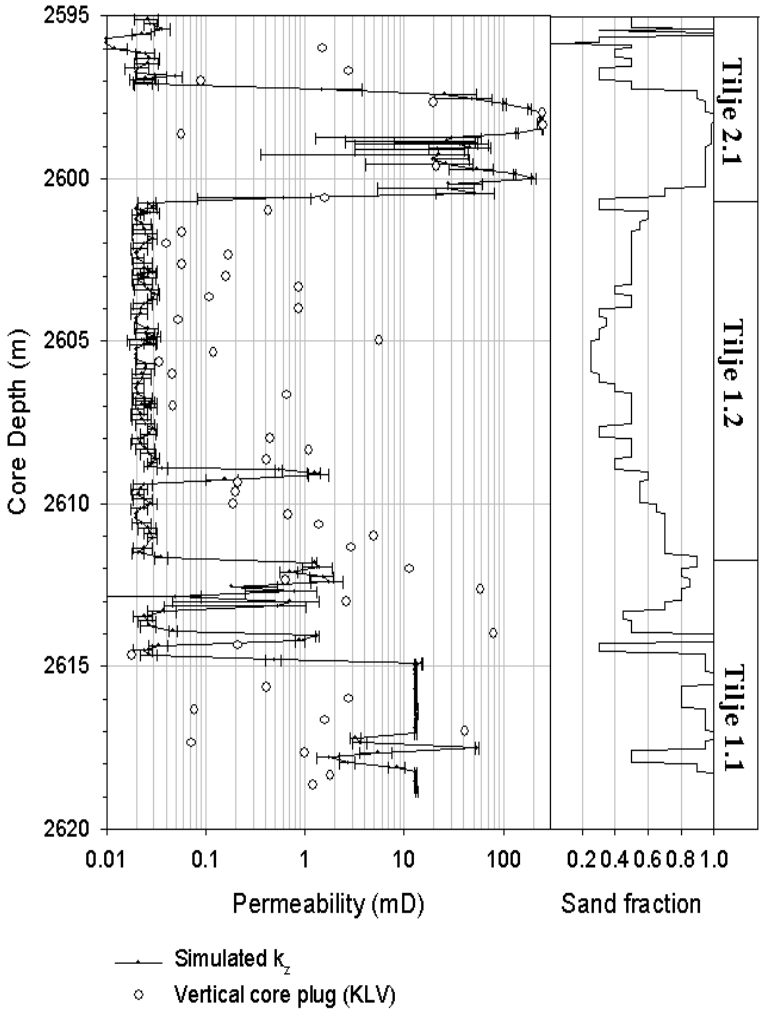

FIGURE 9.6 *Comparison between simulated vertical permeability (using the 10x10x30 cm^3 model) and measured vertical permeability from core plugs. The error bars represent one standard deviation calculated from the 10 realizations*

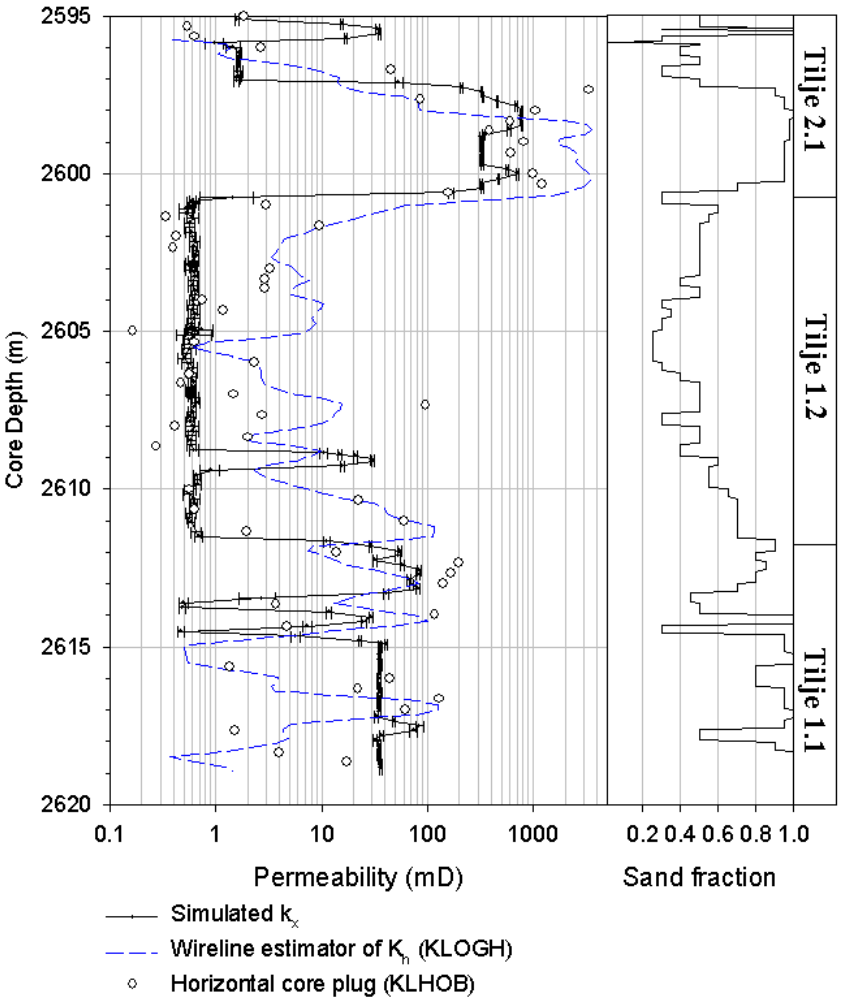

FIGURE 9.7 *Comparison between simulated horizontal permeability (using the 10x10x30 cm^3 model), the standard wireline based permeability estimator (KLOGH) and permeability from horizontal core plugs. The error bars represent one standard deviation calculated from the 10 realizations*

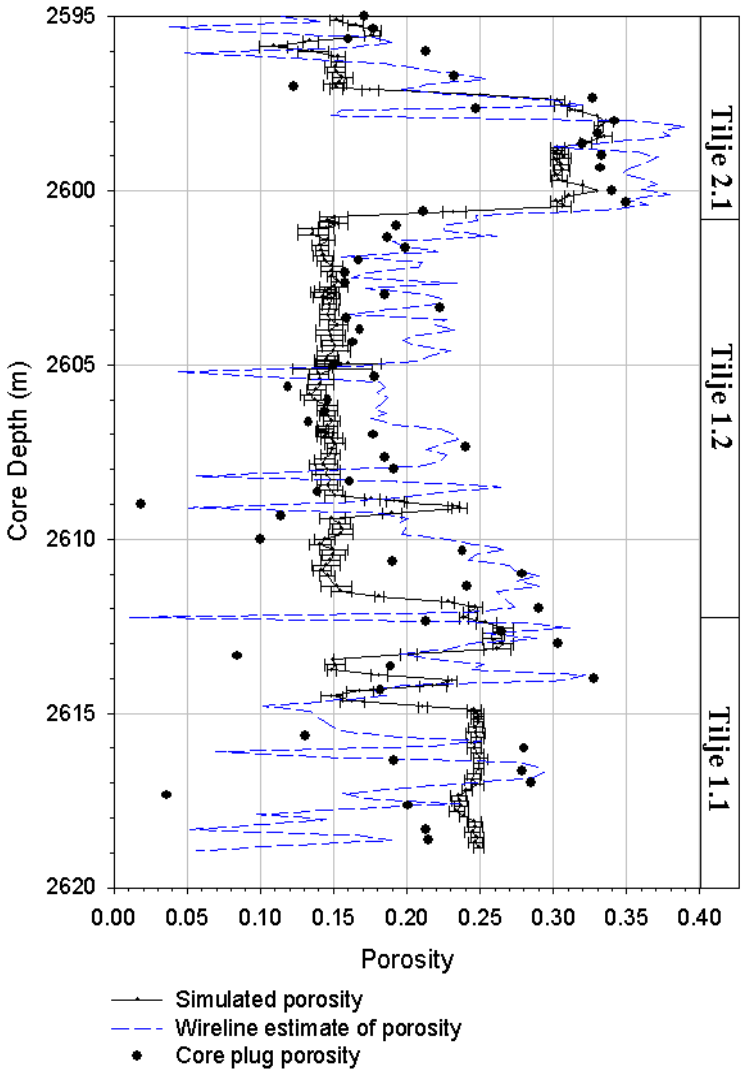

FIGURE 9.8 *Comparison between simulated porosity (using the 10x10x30 cm^3 model), wireline based porosity estimate and core plug porosity data. The error bars represent one standard deviation calculated from the 10 realizations*

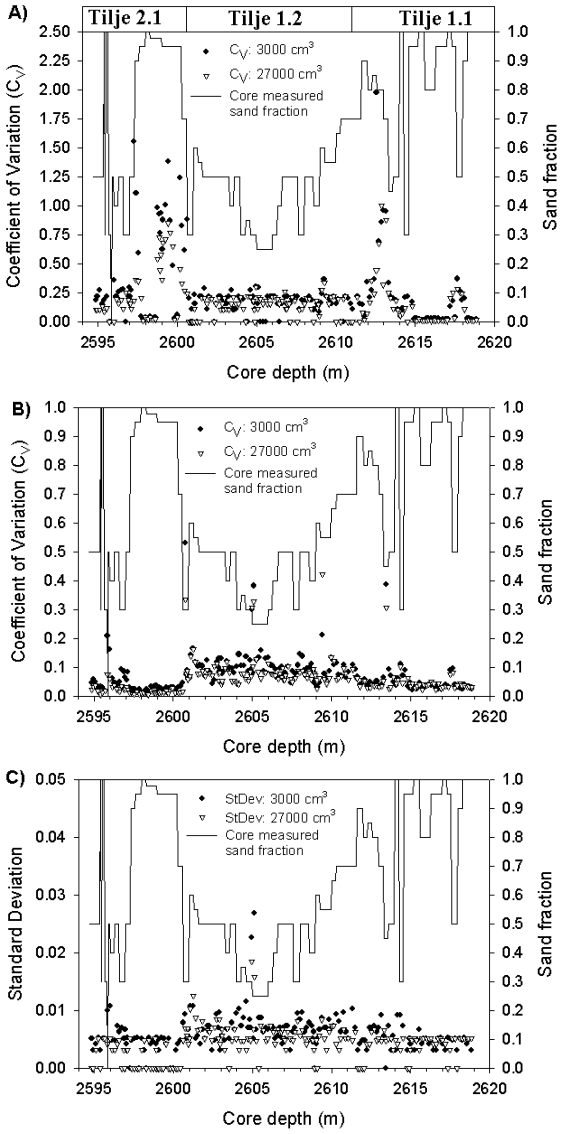

FIGURE 9.9 *Comparison of the C_V calculated from the smallest scale (10x10x30 cm^3) and the largest scale (30x30x30 cm^3) numerical models; for A) k_z, B) k_x and C) porosity. The k_z varies most in the sand-rich intervals while k_x varies most in the mud-rich intervals. Variation in porosity is independent of bedding type. See top figure for stratigraphy.*

9.3 Method 2: Functional relation between mud fraction and effective permeability

The results from chapter 7 and 8 will be used in this section to give a continuous estimate of horizontal and vertical permeability. It was found that there was a functional relation between the mud fraction and the effective permeability and several different curves were fitted to the experimental data. Similar relations are also found in earlier work (e.g. Journel et al., 1986; Deutsch, 1989; Cuthiell et al., 1991) for sand-mud systems with other characteristics than the models used here. Martinius et al. (1999) and Ringrose et al. (1999) have used results from SBED simulations to estimate an expression, denoted a ”type curve”, for the relation between the bedding type and the effective permeability. In contrast to simulation of the full near wellbore model, the petrophysical variability in the different lithological components are not taken explicitly into account. Only the variation in effective permeability related to the spatial distribution of the lithological components is considered.

Commonly, a combination of neutron and/or density log curves, calibrated to the core plugs, is used to give a wireline based estimate of the porosity. At the core plug scale a relation is found between porosity and horizontal permeability. This relation is then used to predict horizontal permeability from the wireline based porosity estimate, implicitly assuming that the relation from the core plug scale is valid at the wireline scale (section 2.3.4). It has been shown in chapter 7 that there can be significantly variation, especially for horizontal and vertical permeability, at volume supports larger than the core plug. Appreciating that the core plugs also can be biased, the relation is further weakened.

The relation observed in figure 8.1 and 8.6 is between data measured (numerically) at a representative sample volume. To estimate the effective vertical or horizontal permeability along the wellbore, a continuous estimate of a mud fraction is needed. Whether or not this estimate is representative will be discussed below. By evaluating the available log curves, it appeared that in this particular interval the density log could be used as a sand fraction estimator. In other intervals, different wireline tools may provide a better estimate of the mud fraction (e.g. the gamma ray tool). The following relation was used to calibrate the density curve to the visual estimate of sand fraction,

$$SandFraction = \frac{\rho_{mud} - \rho_b}{\rho_{mud} - \rho_{sand}} \qquad \textbf{[9-1]}$$

where ρ_b is the wireline recorded density. Since the grain size varies between the facies associations in the interval, different values were used for ρ_{sand} and ρ_{mud} in the different zones (table 9.1). These values are within expected limits (Serra, 1986; Rider, 1996), although the mud density and sand density appears to be quite high and low, respectively. The values may be changed after more detailed analysis, but for practical purposes here they are satisfactory.

Facies association (FA)	ρ_{mud} (g/cm^3)	ρ_{sand} (g/cm^3)	k_{mud} (mD)	k_{sand} (mD)
FA 7	2.70	2.10	0.01	3500
FA 3 and FA 4	2.70	2.05	0.01	50
FA 1	2.80	2.25	0.01	100

TABLE 9.1 Density values used in equation 9-1 to calibrate the density curve to the core derived sand fraction and the end-member permeabilities used to constrain the functional relations (see below). Note that the densities for "sand" and "mud" include porosity.

Figure 9.10 shows the visual estimate of the core sand fraction and the calibrated density curve. Except for the lower 5 m where the hummocky cross-stratified units often are partly cemented, the density-log estimated sand fraction matches the visual sand fraction estimate quite well. The next step is the choice of which equation to use from the selection presented in chapter 8 and to assign permeability values to the end-members (lithologically clean sand and mud). The core plug values were used as guidelines for assigning the clean sand permeability while the mud permeability was assumed to be low and constant for all the facies (and equal to the value used in chapter 7). Because of the lithological differences between the facies associations, different values were chosen for the different zones (see table 9.1). For the upper interval (FA 7), a small probe-permeameter data set was available and used as a guideline for the value of k_{sand}. The probe-permeameter measurements are in general seen as favourable compared to the core plugs as they approach the lamina-scale permeability value. Again, the value of the mud permeability is uncertain, but the results from chapter 8 can be used as an indication of which parameter is critical for which lithofacies. Figures 9.11 and 9.12 show the vertical and horizontal permeability, respectively, calculated with three different equations. The solid line represents an estimate based on equation 2-30 which is the two-component power average and with the p-values from table 8.3. The two other curves shows equation 8-5 which is a power law equation modified with an anisotropy factor and re-scaled to the percolating threshold. In one case the permeability contrast between the sand components was set to 1:10 and in the other case it was 1:1 implying a two-component system resembling equation 2-30 but with the percolating

threshold. The percolating threshold used here is the same as in chapter 8 (V_m=0.5 for k_z and V_m=0.8 for k_x) and the p-values for the relevant permeability contrasts are given in figure 8.9. Ringrose et al. (2004) using the same mud fraction estima-

tors as here, used equation 8-3 and 8-4 to give a continuous expression of the k_v/k_h-ratio.

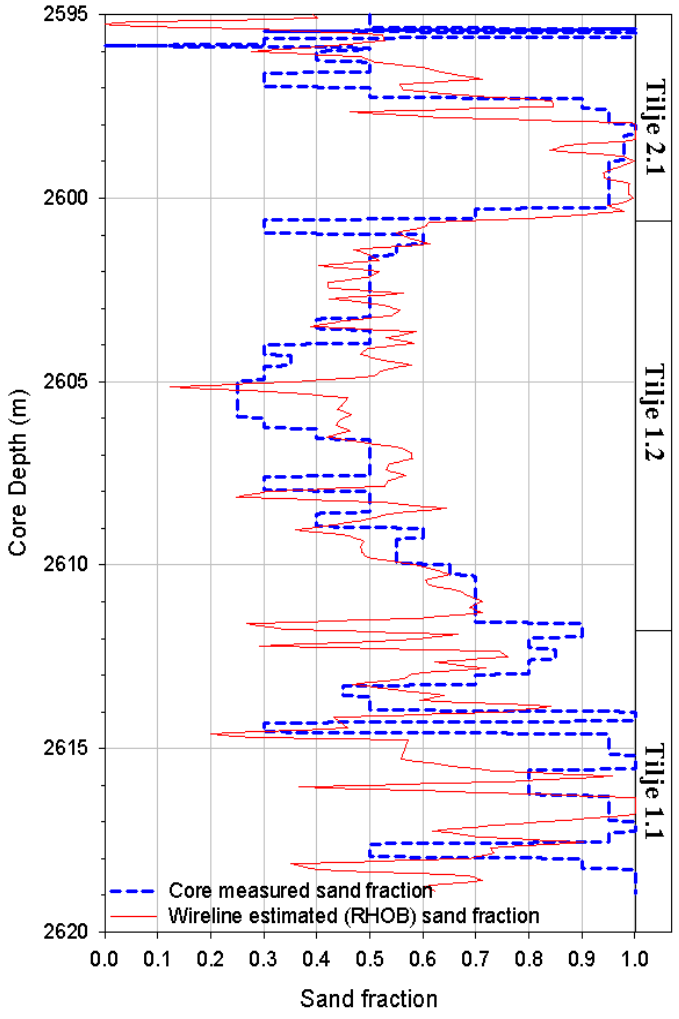

FIGURE 9.10 *RHOB estimate of sand fraction (mud content) and the core measured sand fraction (the same curve as in figure 9.5). A fairly good match indicates that the density log can be used as a V_{mud}-log in this particular interval.*

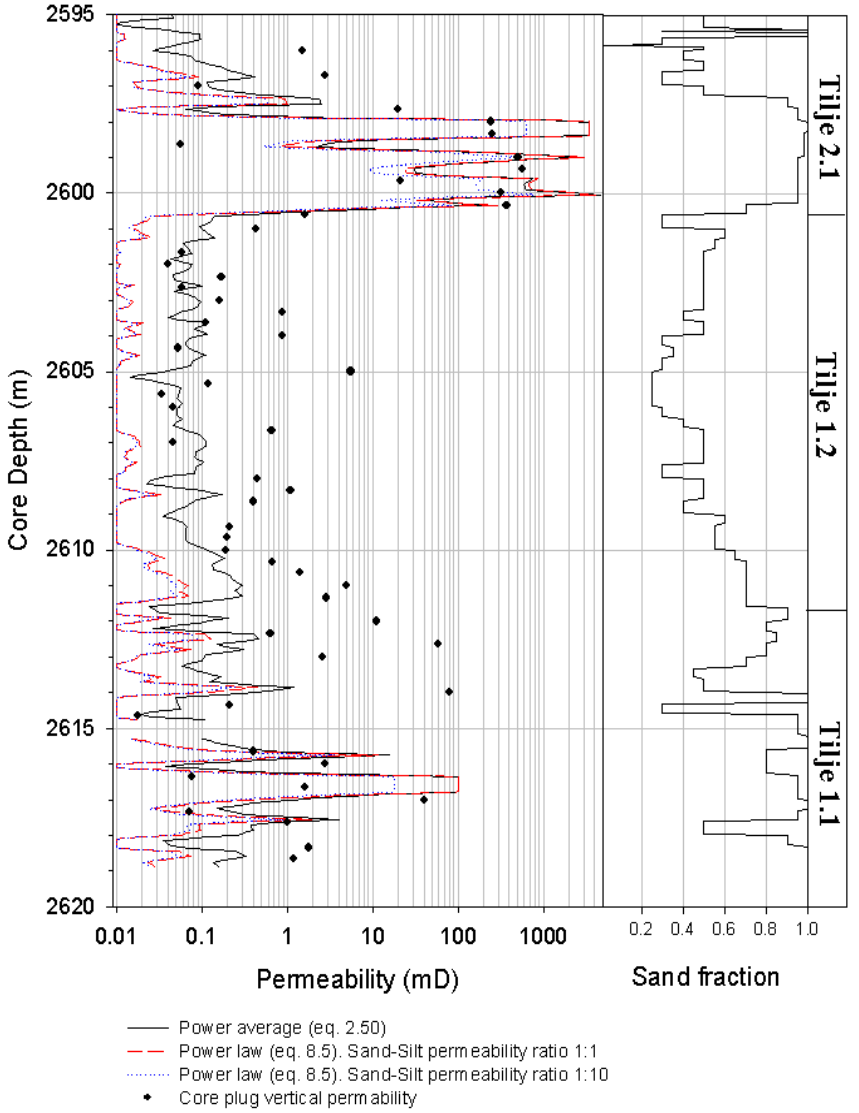

FIGURE 9.11 *Continuos estimate of vertical permeability in the selected interval. The core plugs show an overall higher permeability than the continuos estimate mainly due to biased sampling.*

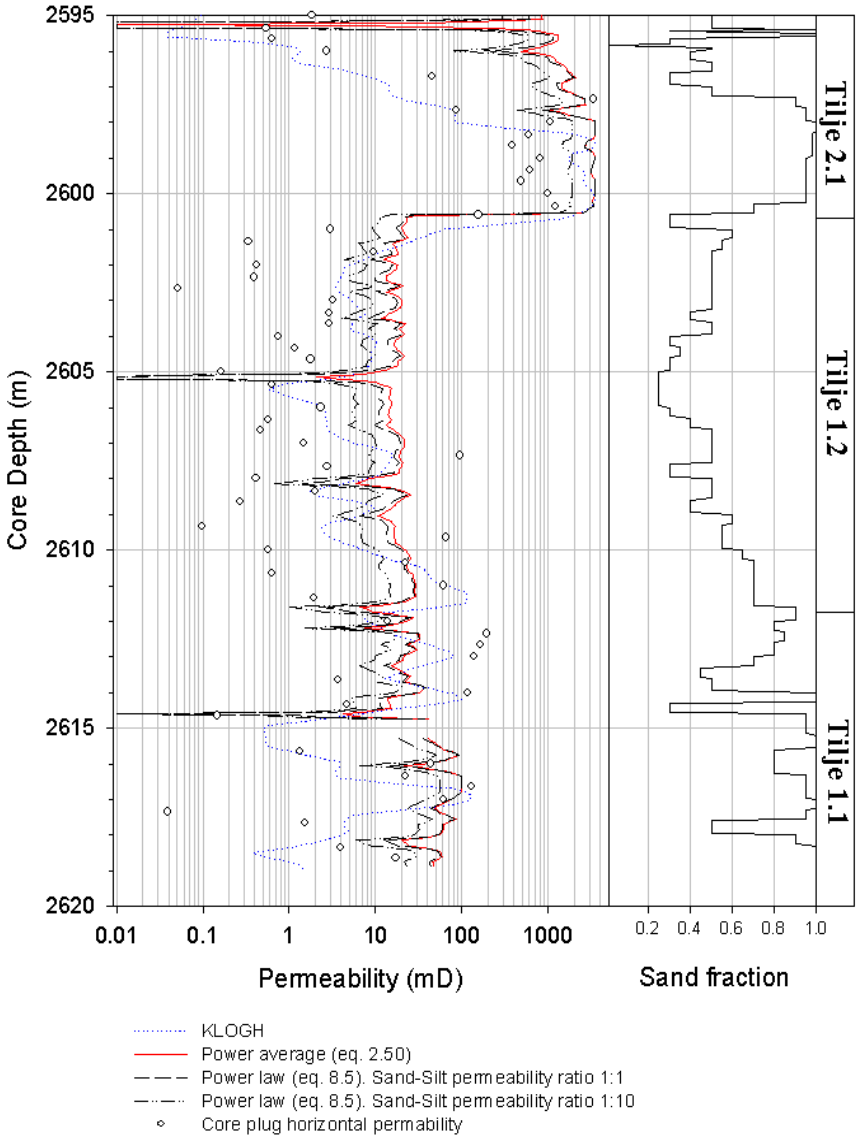

FIGURE 9.12 *Continuos estimate of horizontal permeability. The KLOGH-curve is the estimator based on traditional integration of core and wireline data.*

As expected from the results in chapter 8, the two-component vertical and horizontal permeability estimators are similar at low mud contents and deviate more approaching and exceeding the respective percolating thresholds. The effect of permeability contrast expressed as an anisotropy factor is, in contrast, largest at low mud fractions since the flow is dominated by flow through the sand component. Note that the term “low mud fraction” denotes a mud fraction less than the critical mud fraction and is significantly different for vertical and horizontal flow.

Method 2 (using type curves) clearly differs from the more traditional approach since a relation between the variables (mud fraction and permeability) is expressed at a representative sample volume. One then needs a representative measure of the mud fraction, and an estimate based on the density log was used here. The exact volume of investigation for this tool will always be uncertain, but a volume of about $3\text{-}10*10^3$ cm^3 is a common assumption (see figure 2.12). It was found in chapter 7 that a representative value for mud fraction was measured at or below this sample volume for all the bedding types indicating that the density estimate of mud fraction can be regarded as close to representative. In contrast, the representative volume for horizontal and vertical permeability is dependent on the bedding type and in some cases it is larger than the representative volume for mud fraction and the volume of investigation for the density tool. The following line of argument is therefore used to validate the use of the type curve as a permeability estimator. The type curve used is based on data measured at a representative volume. Assume that the bedding type under consideration is larger than the REV for k_z and k_x. Let us further assume that the sample volume of the density tool is approximately fixed and larger than the REV for mud fraction but smaller than the REV for k_z and k_x. In this situation (assumed to be common), a representative permeability value can still be estimated from the type curve since the independent parameter (mud fraction) is representative. The converse is, however, not true (although using permeability as a regressor variable may be regarded as a hypothetical case).

Defining a REV and the corresponding representative value across contrasting units (e.g. permeability contrast between bedding types) is challenging since the requirement of linear variation in the macroscopic quantity over the REV is not satisfied (Bear and Bachmat, 1990, p. 232-236). Figure 9.13 illustrates this problem were the actual variation in the property in every region of transition must be replaced by an idealized boundary in the form of a surface across which an abrupt change in that property takes place. The continuum approach is thus applicable to each subdomain up to the boundary surface. In the case were a particular unit (bedding type) is smaller than the REV for permeability but a representative mud fraction estimate is made, the estimated permeability from the type-curve will not be representative. For thin units, below the vertical resolution of the density tool, a true density value

will not be recorded and consequently the conditions for representative measurements are not satisfied. From a continuous estimated mud fraction in an interval with rapidly alternating, contrasting bedding types, the estimation of representative values will be difficult with the approach outlined here. On the other hand, the results from chapter 7 and 8 can in these instances be used to give an uncertainty band around the mean estimate (e.g. based on the C_V). Both the uncertainty related to the bedding thickness and to the uncertainty related to the volume of investigation of the wireline measurement can, with these results, be quantified. As noted earlier, the REV found in chapter 7 was only related to the spatial distribution of sand and mud and did not take into account that the variability in the petrophysical properties. The uncertainty in the estimated permeability value is thus the minimum variability. The assumptions and limitations with Method 2 will be further discussed in the next section.

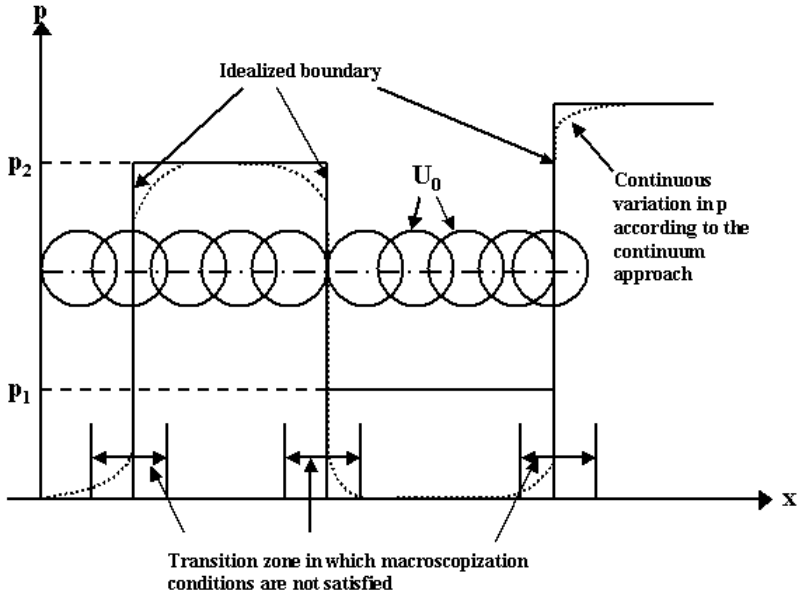

FIGURE 9.13 *Principal sketch for a situation with contrasting units (with respect to property p) where the conditions for defining a REV (U_0) is not met. Modified from Bear and Bachmat (1990). See text for discussion.*

9.4 Discussion

This chapter has described two different methods based on the results from chapter 4 to 8 to estimate permeability in the studied interval. Method 1 used a very detailed near wellbore model and forward modelled directly porosity and permeability at any scale. The input data was, as far as possible, validated at the scale they were taken ensuring that a rescaled estimate honoured the underlying variability. Two cases were evaluated where a realization of the stacked model was upscaled at approximately the volume of investigation equivalent to the density tool (10x10x30 cm^3) while the other to a volume approaching a representative elementary volume (30x30x30 cm^3). Estimating porosity, being the most straightforward from the density recording, was then expected to have the same mean and variance as the forward modelled porosity curve with the smallest upscaling volume. As figure 9.8 shows, the simulated porosity curve shows a smaller variability than the wireline estimate, and there are several possible reasons that can explain this. The shape of the sample volume of the density tool is not known exactly but it is commonly assumed to be hemispherical. Using a rectangular shaped volume as we have done here will thus give a larger upscaling volume, reducing the variance with an unknown factor. Comparing the forward modelled horizontal permeability (k_x) and the wireline estimate (KLOGH) the difference can also be attributed to this factor. In addition, KLOGH is predicted from the porosity estimate using a regression equation established at the core plug scale. A linear expression relating porosity to the logarithm of permeability at the core plug scale is not likely the same at the wireline log scale. Equally important is the fact that capturing all the features influencing the density tool in the near wellbore model is challenging. As indicated earlier, diagenesis and bioturbation are both present in the studied interval but it was not possible to include these aspects in the stacked model. By using core plugs measured in the laboratory, that need to be corrected to in situ conditions, errors can be introduced to the input parameters. In addition, the geometrical model is only validated in 2D and there is a possibility that the true 3D variability is not properly simulated. Finally, there are limitations in the code making it difficult to simulate large variability without losing the realism in the models as discussed in section 4.5. In this respect, there exists no measure here that can be used to evaluate how good the simulated horizontal permeability is. Other, independent and preferably in situ measures should be used for such an evaluation. Elfenbein et al. (2003) and Zhang et al. (2004) considered well test results and found that carefully calibrated SBED models did indeed reproduce these in situ measurements.

The advantage of Method 2 compared to Method 1 is that once the type curve is established, it can easily be adjusted to other intervals with similar bedding types

given that there is a reliable estimate of mud fraction, potentially including non-cored wells. In contrast to simulation of the full near wellbore model, the petrophysical variability in the sand components is not taken explicit into account. Only the variation in effective permeability related to the spatial distribution of the two components is considered. Although the bedding models used to find the type curve were conceptual, the input parameters were based on flume tank experiments and thus assumed to be realistic.

Porosity is commonly used as a regressor variable to predict permeability, but a large variation in permeability for individual porosity values are often observed. In the heterolithic, tide-influenced deposits studied here, the amount and arrangement of the sand and mud components are more important. One can initially assume that a static, additive property like mud fraction is less useful for prediction of a non-additive, tensorial property like permeability. However, because of the close correspondence between the amount of mud and how it is organized in the lithofacies, the static mud fraction contains information that influences permeability. This can be one of the reasons why mud fraction is a better regressor variable than porosity in these deposits.

The type curve then gives a relation between the mud fraction and permeability at a volume where both the properties were shown to be representative. This method then clearly differs from the more traditional approach since a relation is expressed directly at the representative volume avoiding the necessary upscaling of a relation found at the core plug scale. The type-curve approach has also been used in other deposits that, although tide-influenced, represents larger scale bed forms. Elfenbein et al. (2003) found that larger migrating shallow marine bars also could be analysed with Method 2. This indicates that there is potential for a wider application of this method at least in lithofacies where the spatial distribution of contrasting lithologies is the dominant factor controlling effective permeability. It is however essential to be aware of the limitations caused by the presence of thin (relative to the vertical resolution of the wireline estimator of mud fraction) units and the proximity of boundaries between petrophysically contrasting bedding types.

The density log calibrated to match a visual estimate of mud fraction was used here as a V_{mud}-log. Using core plugs as calibration points will necessarily introduce the problem of biased sampling. Likewise, the use of the density log directly to find the values in table 9.1 will give a value that represents the average of several components. It is however assumed that estimation of mud fraction is more practicable than the direct estimation of permeability from the wireline logs, and there was no intention here to propose general method estimating V_{mud} from the wireline logs.

There exits of course many other published methods that have been used to estimate permeability and porosity from well data. Some of these have been mentioned in section 2.3.4 but it would be impossible to evaluate all these methods to see if they perform any better then the two methods used here. However, one of the methods, Hydraulic (Flow) Units (HU's) originally described by Amaefule et al. (1993), is based on fundamental concepts and is easy to use (see section 2.3.4 and equations 2-24 to 2-26). Following the approach of Corbett et al. (2003), equation 2-26 was rearranged with respect to permeability and by varying systematically the FZI-value, boundaries separating the different HU's were calculated. Although the values for FZI were chosen arbitrarily, Corbett et al. (2003) assumed that there can be a relation between the grain size classes and HU's. Figure 9.14 shows the calculated boundaries and the core plug data from the intervals.

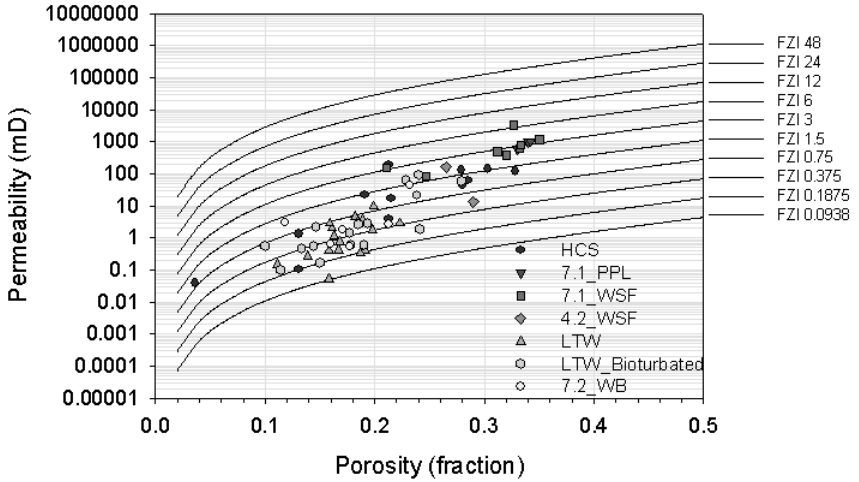

FIGURE 9.14 *Scatter plot of core plug porosity and horizontal permeability sorted on the subfacies modelled in this study. The solid lines represents constant FZI-values giving the boundaries between the HU's.*

The core data was sorted according to the bedding types that have been used here. Except for facies LF7.1_PPL and LF7.1_WSF which follows the line with an FZI equal to 3, the other bedding types are scattered and can not be described sufficiently with a constant FZI (i.e. does not represent the same HU). This can indicate that the detailed subdivision into different bedding types is less important or that the subdivision is incorrect with respect to the flow properties. However, it is assumed that the defined bedding types represent different flow properties and that the main reason for the scatter is the inadequacy of the core plugs to capture the het-

erogeneity (dominantly below the core plug scale in these deposits) and the general high degree of bias in the data that disrupt the trend.

In similar reservoir types the two methods have potential to be applied more generally. The near wellbore model (method 1) can be used for detailed calibration to the core and for better understanding of what is the net reservoir and quantification of the effect of different cut-offs in reservoir description (Worthington et al., 2003b). This is a critical issue often difficult to address with conventional methods. Another application of the near wellbore model is to better understand the wireline tool responses in these heterolithic reservoir types. Simulation of tool responses (e.g. resistivity, acoustic) can then form a better basis for interpreting these wireline logs and is topic for further research. The type-curve approach (method 2), has a large potential for systematic mapping of horizontal and vertical permeability into the reservoir volume as outlined by Elfenbein et al. (2003). Extending this method to other depositional environments is also a topic for further research. In general, the introduction of an integrated near wellbore model, common to both the sedimentologist, petrophysicist and the reservoir engineer will be an important step towards better characterization of the reservoir, particularly in those reservoirs where traditional methods become uncertain.

CHAPTER 10 *Summary and conclusions*

The material presented in chapter 4 to chapter 9 is summarized below along with the main conclusions from this thesis. At the end, some recommendations for further work are given.

1. A process-oriented geomodeling tool is used to simulate clastic, sedimentary bedding types. Based on a sensitivity study of the input parameters and their effect on the resulting bedding model, a workflow is proposed that translates core observations into a set of input parameters that can be used in a modelling study.
2. The selected interval of the Tilje Formation was described, based upon the interpretation given by Martinius et al. (2001). These lithofacies were further divided into subfacies that were assumed to influence the petrophysical properties in the near wellbore volume. A method was used that parameterized the core giving a data set describing the distribution of the sand and the mud components. The proposed workflow was shown to give good match between the core and the simulated bedding models. The validation procedure did in part take into consideration the dimensionality problem in these data sets. It is thus concluded that for heterolithic deposits, as studied here, it is possible to create realistic near wellbore models based on core information with this modelling approach .

3. The Tilje Formation has been interpreted to be influenced by tidal processes but time series analysis has only occasionally been performed to reveal the degree of influence. In addition, quantitative detection of cyclicity in ripple laminated heterolithic deposits has been reported less frequent in the literature. Due to the need for relatively long intervals for time series analysis, only one of the lithofacies could be analysed in detail: LF3 (Laminated Delta Front facies). The autocorrelation method (time domain) and the spectral analysis method (frequency domain) revealed two orders of cyclicity: one with approximately 11-16 sand laminaset per cycle and one with approximately 50-60 sand laminaset per cycle. Equally important was that the internal stratification suggested that these were similar to the Type II ripple of Tessier (1993) and that many of the sand laminaset showed a sharp lower boundary and a transitional upper boundary to the preceding and succeeding mud laminaset. Furthermore, the thickness of the mudlayers in general opposes deposition during only one slack water period. A depositional model was proposed that explained these sedimentary structures. The shortest cycle observed was then related to a semi-annual cycle implying that a sand laminaset and the succeeding mud laminaset was deposited during a fortnightly period. The observed 11-16 period was then attributed to the semi-annual constructively interference of the synodic, anomalistic and tropical cycles with a small component from the semi-annual tidal solar period. The longest cycle would in this setting denote an approximately two-yearly cycle. Other non-tidal, but possible periodic components like seasonal driven mudflows, hyperpycnal plumes and storms can also influence on the observed variability. Incorporating vertical, periodic variation in mud fraction will have implications on the reservoir properties and is thus important to incorporate in the near wellbore model.
4. The porosity and permeability from core and wireline estimates shows that the lower part of the Tilje Formation is heterogeneous and in general under-sampled. By a iterative procedure, the lamina petrophysical properties (porosity and permeability) were found from the core plugs. The procedure was verified by a probe permeameter data set. There is, as expected, a general decrease in variance between the input distribution and the upscaled distribution at the core plug scale. For horizontal permeability there was a possible relation between the input distribution, the core plug distribution and the bedding geometry. For vertical permeability, the amount and geometry of the mud layers was important. The effect of biased sampling was quantified by comparing the observed core plugs with the un-biased simulated core plugs. It is concluded that in the absence of high-resolution (at the lamina scale) measurements of porosity and permeability, the proposed iterative procedure can be used to estimate lamina-scale properties using the more generally available core plugs.

5. A set of general tidal bedding models with a wide range of mud fractions have been developed based on published flume tank studies. The original time axis was replaced by a pseudo-sandfraction axis. This study shows that the amount of mud deposited is correlated with the correlationlength of the sand and the mud component: as the mud component increases, the correlation length of the mud laminaset increases.
6. The numerical models have been upscaled at several sample supports. The results showed that the upscaled property varied with the sample volume and that the variability was dependent on the property and bedding type. To some extent, the concept of Representative Elementary Volume (REV) has been experimentally verified in these synthetic bedding models. Single realizations show a large variability at small sample volumes but the variability is reduced as the sample volume increases. Published criteria for defining REV have been reviewed. The variability between different realizations, expressed with the C_V, decreases with increasing model size (sample support). An REV is defined here by plotting the C_V as a function of sample volume and determining the volume where the C_V remains in the homogeneous regions (C_V<0.5).

   For horizontal and vertical permeability, the size of the REV depends on the bedding type. The relation was explained by the correlation lengths relative to the model size of the two components present. The amount and geometry of the mud layers control the vertical permeability while the amount and geometry of the sand layers control the horizontal permeability. The conceptual equations (eq. 7-6 and eq. 7-7) were verified by the experiments and summarized in figure 7.37. Based on these results, three flow-regimes were identified that each require a different method to estimate effective permeability: 1) Layered system where the arithmetic and harmonic averages are appropriate, 2) Close to the percolation threshold where a percolation model should be used and 3) Discontinuous system where an effective medium method provides the best estimate of permeability. The division into flow-regimes are different for vertical and horizontal permeability. The critical mud content for vertical flow is found to be between 0.35 and 0.5 while for horizontal flow around 0.8. It is appreciated that calculation of effective permeability in highly correlated systems where the correlation lengths approache the model size, inherently is difficult. It is however concluded that at the bedding scale there exist a volume that is necessary for capturing a representative amount of heterogeneity, and that this volume is dependent on the property of interest and the bedding type. As long as the correlation lengths at the bedding scale are larger than a few centimetres, the use of core plugs for estimation of permeability will, in general, be incorrect. These

results are then used to quantify the error in the core to log integration process.

7. Additional models and realizations were used to improve the functional relation between effective permeability and mud fraction at a representative sample volume. The permeability contrast between the sand lamina was varied, giving a three-component system. The functional relation was quantified by fitting equations (denoted type curves) to the two- and three-component systems. Several of the equations gave a good fit to the experimental data, but it is felt that incorporating some physical constraints, like the percolation threshold, strengthen the use of such curves by making them more general and less dependent on numerical experiments. The most challenging region to describe is the non-linear part in k_z for low mud fractions. Depending on the region of interest (i.e. bedding types), time available and initial knowledge about the system, different type curves can be used.

   Using the type curve as means to estimate permeability differs from the traditional core-log integration method since a relation is found at the representative volume and mud fraction is used as a regressor variable. The mud fraction, although scalar, contains in these particular deposits some information about the spatial distribution of mud, which is a major control on the effective permeability.

8. The effect of changing the petrophysical contrast between the two sand components and between the sand and the mud was explored for selected models that represented different flow regimes. At a mud fraction below the critical threshold for vertical flow, the sand properties have most influence on k_z and to some extent on k_x. The mud property has only a minor influence on k_z and an insignificant influence on k_x. Close to $P_{c,v}$, the mud property becomes increasingly important for calculation of k_z which at the same time shows a reducing dependency on the sand contrast. The horizontal permeability shows similar behaviour as in the low mud fraction case since the system still behaves as a layered system with respect to this parameter. Close to $P_{c,h}$, k_z is controlled exclusively by the mud property and independent on the sand contrast. The horizontal permeability is dependent on both the mud property and the sand contrast (similar to the situation for k_z close to $P_{c,v}$). These results give guidelines for data collection that depends on the bedding type under consideration. The sand contrast is important below the percolation threshold, while the mud properties become important approaching and exceeding the percolation threshold.

9. The results are applied to a 25 m interval of the Lower Tilje Formation on the Haltenbanken. Two methods are used. 1) Direct simulation of permeability and porosity on the near wellbore model created in chapter 5 and 6 and 2) by the use of the results from chapter 7 and 8 (type curves). The first method, being the most time consuming, gives the possibility to study individual subfacies in the well and, through upscaling to different sample volumes with a moving window averaging, to compare with the current wireline-based estimates. It seems that it is difficult to incorporate all the natural variability in the near wellbore model, but the earth model provides a better basis for integration of available welldata. The second method utilizing a functional relation between mud fraction and effective permeability is potentially a simple and powerful method to be applied on routine basis, also in un-cored wells. The advantage of this method is that it is fairly general in tidal influenced deposits and can applied to other (un-cored) wells with only local adjustment of sand and mud permeability values. The method also has the ability to quantify the errors associated with traditional core-log integration methods.

This thesis has only considered some of the many aspects of the general objective of reconciliation of well data for better estimation of reservoir performance and use of the possibilities that a shared earth model can provide. In the future, the following tasks are considered to be important for further developments in this area:

- There could be improvements in the construction of synthetic bedding models of these tidal bedding types. The three-dimensionality of the sedimentary structures, influencing on the spatial distribution and continuity of the mud layers, could be better understood through detailed analysis of outcrops or from recent depositional environments. A further development of the simulation code that gives a better ability to model more complex bedforms, will be an improvement (e.g. splitting and rejoining of crests, isolated ripples and catenary and linguiod crest lines).
- The same analysis as here, should be performed on bedding types with different characteristics. The extension to bedding types where the distribution of mud fraction is a critical parameter is natural, but also to sedimentary bedding types where other factors are more important. Development of type curves for different sedimentary environment can greatly improve the understanding of the system and the estimation of reservoir performance. These curves are, however, scale-dependent and should be established at a representative volume.
- The analysis of scaling issues of the bedding models can be improved by an independent evaluation of connectivity of both the conducting and non-conduct-

ing components. Such an evaluation can be used to develop analytical models for calculation of effective permeability, establishing the percolation threshold quantitatively and evaluate scaling issues around the percolation threshold, which is difficult.

- In un-cored intervals, a type curve method is the most suitable. We see, however, the potential in using image logs for obtaining critical input parameters. This data type can also give additional information about the correlation structure wider than the core (across the borehole).
- A significant step forward would be to use the near wellbore model to simulate various tool responses, as for example resistivity and acoustics. The results could then help improving the understanding of the wireline recordings in these heterolithic deposits, and to improve the petrophysical interpretation models giving better reconciliation of core and wireline data. Such an approach would require that the simulation code could incorporate the relevant physical parameters.
- Only single-phase permeability has been calculated in this thesis. Evaluation of multiphase flow on such realistic bedding models should also be a topic for further research. In addition, since there have been indications that cross-flow can be significant, calculation of effective permeability with other boundary conditions will provide a more correct estimate of the permeability field. The outcome of such a calculation can be an improved estimate of the REV, although it is assumed that the dependency to the correlation lengths in the sedimentary structure found in this thesis will be approximately the same.

References

Ababou, R. 1995. Random porous media flow on large 3-D grids: numerics, performance, and application to homogenization. *In*: Wheeler, M. F. (ed.), IMA volumes in Mathematics and its Applications, "*Environmental studies: Mathematical, Computational and Statistical Analysis*", p. 1-25.

Ababou, R., McLaughlin, D., Gelhar, L. W. and Tompson, A. F. B. 1989. Numerical simulation of three-dimensional saturated flow in randomly heterogeneous porous media. *Transport in Porous Media*, Vol. **4**, No. 6, p. 549-565.

Adkins, R. M. and Eriksson, K. A. 1998. Rhythmic sedimentation in a mid-Pennsylvanian delta-front succession, Magoffin Member (Four Corners Formation, Breathitt Group), Eastern Kentucky: a near-complete record of daily, semi-monthly, and monthly tidal periodicities. In: Alexander, C. R, Davis, R. A., and Henry, V. J. (eds.), *Tidalites: Processes and Products*, SEPM Special Publication **No. 61**, p. 85-94.

Ahmed, U., Crary, S. F. and Coates, G. R. 1991. Permeability estimation: The various sources and their interrelationships. *Journal of Petroleum Technology*, May, p. 578-587.

Allen, G. P. 1971. Relationship between grain size parameter distribution and current patterns in the Gironde Estuary (France). *Journal of Sedimentary Petrology*, Vol. **41**, No. 1, p. 74-88.

Allen, G. P. 1991. Sedimentary processes and facies in the Gironde estuary: a recent model for macrotidal estuarine systems. *In*: Smith, D. G., Reinson, G. E., Zaitlin, B. A. and Rahmani, R. A. (eds.) *Clastic Tidal Sedimentology.* Canadian Society of Petroleum Geologist, Memoir **16**.

Allen, J. R. L. 1963. The classification of cross-stratified units, with notes on their origin. *Sedimentology*, **2**, p. 93-114.

Allen, J. R. L. 1965. Sedimentation to the lee of small underwater sand waves: An experimental study. *Journal of Geology*, Vol. **73**, p. 95-115.

Allen, J. R. L. 1968. *Current Ripples. Their relation to patterns of water and sediment motion*. North-Holland Publishing Company, Amsterdam.

Allen, J. R. L. 1969. On the geometry of current ripples in relation to stability of fluid flow. *Geografiske Annaler*, **51A**, 1-2, p. 61-96.

Allen, J. R. L. 1970a. A quantitative model of climbing ripples and their cross-laminated deposits. *Sedimentology*, **14**, p. 5-26.

Allen, J. R. L. 1970b. *Physical Processes of Sedimentation*. An Introduction. London, George Allen & Unwin Ltd.

Allen, J. R. L. 1977. The plan shape of current ripples in relation to flow conditions. *Sedimentology*, **24**, p. 53-62.

Allen, J. R. L. 1981. Palaeotidal speeds and ranges estimated from cross-bedding sets with mud drapes. *Nature*, Vol. **293**, p. 579-581.

Allen, J. R. L. 1982a. *Sedimentary Structures: Their character and physical basis. Volume I*. Developments in Sedimentology 30A. Elsevier Scientific Publishing Company.

Allen, J. R. L. 1982b. *Sedimentary Structures: Their character and physical basis. Volume II*. Developments in Sedimentology 30B. Elsevier Scientific Publishing Company.

Allen, J. R. L. 1985. *Principles of physical sedimentology.* London, George Allen & Unwin Ltd.

Amaefule, J. O., Altunbay, M., Tiab, D., Kersey, D. G. and Keelan, D. K.1993. SPE 26436. Enhanced reservoir description: using core and log data to identify hydraulic (flow) units and predict permeability in uncored intervals/wells. Presented at the 68th SPE Annual Technical Conference and Exhibition, p. 205-220.

Andersen, T. J. and Pejrup, M. 2001. Suspended sediment transport on a temperate, micro-tidal mudflat, the Danish Wadden Sea. *Marine Geology*, **173**, p. 69-85.

Anderson, G. 1975. *Coring and core analysis handbook*. PennWell Books, Tulsa, U.S.A. ISBN: 0-87814-058-1.

Anderson, M. P. 1996. Characterization of geological heterogeneity. *In*: Neuman, S. and Dagan, G. (eds.), *Stochastic Subsurface Hydrology*, Cambridge University Press, New York, p. 23-43.

Anderson, R. S. and Haff, P. K. 1988. Simulation of eolian saltation. *Science*, **241**, p. 820-823.

Anderton, R. 1985. Clastic facies models and facies analysis. *In*: Brenchley, P. J. and Williams, B. P. J. (eds.), *Sedimentology: Recent advances and applied aspects*, Geological Society Special Publication No. **18**. Blackwell Scientific Publications, p. 31-47.

Anguy, Y, M., Ehrlich, R., Prince, C. M., Riggert, V. L., and Bernard, D. 1994. The sample support problem for permeability assessment in sandstone reservoir. *In*: Yarus, J. M. and Chambers, R. L. (eds.), *Stochastic Modelling in Geostatistics: principles, methods, and case studies*, AAPG Computer Applications in Geology, No. **3**, p. 37-54.

Anthony, D. and Bartholdy, J.1998. Variability of fine-grained sediment concentrations in a back-barrier channel during calm weather conditions. *In*: Alexander, C. R, Davis, R. A., and Henry, V. J. (eds.), *Tidalites: Processes and Products*, SEPM Special Publication No. **61**, p. 53-58.

API: *Recommended practice for core analysis*. 1998. American Petroleum Institute RP 40.

Archer, A. W. 1995. Modeling of cyclic tidal rhythmites based on a range of diurnal to semidiurnal tidal-station data. *Marine Geology*, Vol. **123**, p. 1-10.

Archer, A. W. 1996. Reliability of lunar orbital periods extracted from ancient cyclic tidal rhythmites. *Earth and Planetary Science Letters* **141**, p. 1-10.

Archer, A. W. 1998. Hierarchy of controls on cyclic rhythmite deposition: Carboniferous basin of Eastern and Mid-Continental U.S.A. *In*: Alexander, C. R, Davis, R. A., and Henry, V. J. (eds.), *Tidalites: Processes and Products*, SEPM Special Publication No. **61**, p. 59-68.

Archer, A. W., Kvale, E. P. and Johnson, H. R. 1991.Analysis of modern equatorial tidal periodicities as a test of information encoded in ancient tidal rhythmites. *In*: Smith, D. G., Reinson, G. E., Zaitlin, B. A. and Rahmani, R. A. (eds.), Clastic Tidal Sedimentology, Canadian Society of Petroleum Geologists Memoir **16**, 189-196.

Archer, A. W. Kuecher, G. J. and Kvale, E. P. 1995. The role if tidal-velocity asymmetries in the deposition of silty tidal rhythmites (Carboniferous, Eastern Interior

Coal Basin, U. S. A.). *Journal of Sedimentary Petrology*, Vol. **A65**, No. 2, p. 408-416.

Archer, A. W. and Johnson, T. W. 1997. Modelling of cyclic tidal rhythmites (Carboniferous of Indiana and Kansas, Precambrian of Utah, USA) as a basis for reconstruction of intertidal positioning and palaeotidal regimes. *Sedimentology*, **44**, p. 991-1010.

Armstrong, A. 1998. *Basic Linear Geostatistics*. Springer-Verlag Berlin Heidelberg.

Arnott, R. W. C. and Southard, J. B. 1990. Exploratory flowduct experiments on combined-flow bed configurations, and some implications for interpreting storm-event stratification. *Journal of Sedimentary Petrology*, Vol. **60**, p. 211-219.

Ashely, G. M., Southard, J. B. and Boothroyd, J. C. 1982. Deposition of climbing-ripple beds: a flume simulation. *Sedimentology*, Vol. **29**, p. 67-79.

Ashley, G. M. 1990. Classification of large-scale subaqueous bedforms: a new look at an old problem. SEPM Bedforms and Bedding Structures. Jo*urnal of Sedimentary Petrology*, Vol. **60**, No. 1, p. 160-172.

Atkins, J. E. and McBride, E. F. 1992. Porosity and packing of Holocene river, dune, and beach sands. *AAPG Bulletin*, Vol. **76**, No. 3, p. 339-335.

Atwater, B. F. 1984. Periodic floods from glacial Lake Missoula into the sanpoil arm of glacial Lake Columbia, northwestern Washington. *Geology*, Vol. **12**, p. 464-467.

Baas, J. H. 1993. *Dimensional analysis of current ripples in recent and ancient depositional environments*. Geological Ultraiectina No. **106**.

Baas, J. H. 1994. A flume study on the development and equilibrium morphology of current ripples in very fine sand. *Sedimentology*, **41**,p. 185-209.

Baker, E. K., Harris, P. T., Keene, J. B. and Short, S. A. 1995. Patterns of sedimentation in the macrotidal Fly River delta, Papua New Guinea. *In*: Flemming, B. W. and Bartholomä (eds.), *Tidal Signatures in Modern and Ancient Sediments*. Spec. Publ. Int. Assoc. Sedimentol., **24**, p. 193-211.

Ball, L. D., Corbett, P. W. M., Jensen, J. L. and Lewis, J. J. M. 1994. The role of geology in the behaviuor and choice of permeability predictors. *SPE Formation Evaluation*, Vol. **12**, p. 32-39.

Banks, N. L. and Collinson, J. D. 1975. The size and shape of small-scale current ripples: an experimental study using medium sand. *Sedimentology,* **22**, p. 583-599.

Barret, P. J. 1980. The shape of rock particles, a critical review. *Sedimentology,* **27**, p. 291-303.

Bartholdy, J. and Anthony, D. 1998. Tidal dynamics and seasonal dependent import and export of fine-grained sediment through a back-barrier tidal channel of the Danish Wadden Sea. *In*: Alexander, C. R, Davis, R. A., and Henry, V. J. (eds.), *Tidalites: Processes and Products*, SEPM Special Publication No. **61**, p. 43-52.

Baveye, P. and Sposito, G. 1984. The operational significance of the continuum hypothesis in the theory of water movement through soils and aquifers. *Water Resources Research*, Vol **20**, No. 5, p. 521-530.

Bear, J. 1972. *Dynamics of fluids in porous media*. American Elsevier.

Bear, J. 1988. *Dynamics of fluids in porous media*. Dover Public Inc.

Bear, J. and Braester, C. 1972. On the flow of two immiscible fluids in fractured porous media. *In*: International Symposium on the Fundamentals of Transport Phenomena in Porous Media, Developments in soil science **2**. Elsevier, p. 177-202.

Bear, J. and Bachmat, Y. 1990. *Introduction to modelling of transport phenomena in porous media*. Kluwer Academic Publishers Group.

Beard, D. C. and Weyl, P. K. 1973. Influence of texture on porosity and permeability of unconsolidated sand. *AAPG Bulletin*, Vol. **57**, No. 2, p. 349-369.

Begg, S. H. and King, P. R. 1985. Modelling the effects of shales on reservoir performance: Calculation of effective vertical permeability. SPE 13529, *Society of Petroleum Engineers*.

Begg, S. H., Carter, R. R. and Dranfield, P. 1987. Assigning effective values to simulator grid-lock parameters heterogeneous reservoirs. Paper SPE 16754, presented at the 62nd Annual Technical Conference and Exhibition of Society of Petroleum Engineers.

Berg, F. K., Martinius, A. W. and Johnsen, S. O. 1999. Application of discriminant analysis in characterization and prediction of heterolithic deposits in the Early Jurassic Tilje Formation, offshore mid-Norway. *In*: Lippard, S. J., Næss, A, and Sinding-Larsen, R. (eds.) *Proceedings of the 5th Annual Conference of the International Association of Mathematical Geology (IAMG)*, Trondheim, p. 729-734, p. 127-133.

Bernasconi, J. 1974. Conduction in anisotropic disordered systems: Effective-medium theory. *Physical Review B*, Vol. **9**, No. 10, p. 4575-4579.

Berrymann, J. G. and Blair, S. C. 1986. Use of digital image analysis to estimate fluid permeability of porous materials: Application of two-point correlation functions. *Journal of Applied Physics*, Vol. **60**, No. 15, p. 1930-1938.

Berrymann, J. G. and Blair, S. C. 1987. Kozeny-Carman relations and image processing methods for estimating Darcy's constant. *Journal of Applied Physics*, Vol. **62**, 2221-2228.

Best, J. 1992. On the entrainment of sediment and initiation of bed defects: insights from recent developments within turbulent boundary layer research. *Sedimentology*, **39**, p. 797-811.

Best, J. and Bridge, J. 1992. The morphology and dynamics of low amplitude bedwaves upon upper stage plane beds and the preservation of planar laminae. *Sedimentology*, **39**, p. 737-752.

Bhattacharya, A. 1997. On the origin of non-tidal flaser bedding in point bar deposits of the river Ajay, Bihar and West Bengal, NE India. *Sedimentology*, **44**, p. 973-975.

Blair, S. C., Berge, P. A. and Berrymann, J. G. 1996. Using two-point correlation functions to characterize microgeometry and estimate permeabilities of sandstone and porous glass. *Journal of Geophysical Research*, Vol. **101**, No. B9, p. 20359-20375.

Blackbourn, G. A. 1990. *Cores and core logging for geologists*. Whitless Publishing, ISBN: 1-870325--25-7.

Boersma, J. R. and Terwindt, J. H. T. 1981. Neap-spring tide sequences of intertidal shoal deposits in a mesotidal estuary. *Sedimentology*, Vol. **28**, p. 151-170.

Boguchwal, L. A. and Southard, J. B. 1990. Bed configurations in steady unidirectional water flows. Part 1. Scale model study using fine sands. *Journal of Sedimentary Petrology*, Vol. **60**, No. 5, p. 649-657.

Bonham-Carter, G. and Sutherland, A. J. 1968. Mathematical model and Fortran IV program for computer simulation of deltaic sedimentation. *Computer Contributions*, Vol. **24**. Kansas Geological Survey, Lawrence, p. 1-54.

Bourdet, D., Ayoub, J. A. and Pirard, Y. M. 1989. Use of pressure derivate in well-test interpretation. *SPE Formation Evaluation*, **June**, p. 293-302.

Brandsæter, I., Wist, H. T., Næss, A., Lia, O., Arntzen, O. J., Ringrose, P. S., Martinius, A. W. and Lerdal, T. R. 2001. Ranking of stochastic realizations of complex tidal reservoirs using streamline simulation criteria. *Spec. Publ. Petrol. Geoscience*, **7**, S53-S63.

Brayshaw, A. C., Davies, G. W. and Corbett, P. W. M. 1996. Depositional controls on primary permeability and porosity at the bedform scale in fluvial reservoir sandstone. *In*: Carling. P. A. and Dawson, M. R. (eds.) *Advances in Fluvial Dynamics and Stratigraphy*, p. 373-394.

Bridge, J. S. 1975. Computer simulation of sedimentation in meandring streams. *Sedimentology*, **22**, p. 3-43.

Bridge, J. S. and Leeder, M. R. 1979. A simulation model of alluvial stratigraphy. *Sedimentology*, **26**, p. 617-644.

Brendsdal, A. and Halvorsen, C. 1993. Quantification of permeability variations across thin laminae in cross-bedded sandstone. *In*: Worthington, P. F., *Advances in Core Evaluation Accuracy and Prediction III*. Gordon and Breach, London.

Brettle, M. J., McIlroy, D., Elliot, T., Davies, S. J. and Waters, C. N. 2002. Identifying cryptic tidal influence within deltaic successions: an example from the Marsdenian (Namurian) interval of the Pennine Basin, UK. *Journal of the Geological Society*, London, Vol. **159**, p. 379-391.

Briggs, L. I. and Middleton, G. V. 1965. Hydrodynamical principles of sediment structure formation. *In*: Middleton (ed.), *Primary sedimentary structures and their hydrodynamic interpretation*, Society of Economic Paleontologists and Mineralogists Special Publication No. **12**, p. 5-16.

Brown, M. A., Archer, A. W. and Kvale, E. P. 1990. Neap-spring tidal cyclicity in laminated carbonate channel-fill deposits and its implications: Salem Limestone (Mississippian), south-central Indiana, U.S.A. *Journal of Sedimentary Petrology*, Vol. **60**, p. 152-159.

Bruggemann, D. A. G. 1935. Berechnung verschiedener physikalischer Konstanten von heterogenen Substanzen. *Annl. Phys*. (Leipzig), **24**.

Brush, L. M. Jr. 1965. Sediment sorting in alluvial channels. *In*: Middleton (ed.), *Primary sedimentary structures and their hydrodynamic interpretation*, Society of Economic Paleontologists and Mineralogists Special Publication No. **12**, p. 25-33.

Bryant, S. Cade, C. and Mellor, D. 1993. Permeability prediction from geological models. *AAPG Bulletin* Vol. **77**, No. 8, p. 1338-1350.

Bryant, I. D. and Flint, S. S. 1993. Quantitative clastic reservoir geological modelling: problems and perspective. *SEPM Special Publication* No. **15**, p. 3-20.

Campbell, C. V. 1967. Lamina, laminaset and bedset. *Sedimentology*, **8**, p. 7-26.

Carman, P. C. 1937. Fluid flow through a granular bed. *Transactions of the Institute of Chemical Engineers*, London, vol. **15**, no. 2.

Chan, M. A., Kvale, E. P., Arscher, A. W., and Sonett, C. P. 1994. Oldest direct evidence of lunar-solar tidal forcing encoded in sedimentary rhythmites, Proterozoic Big Cottonwood Formation, central Utah. *Geology*, vol. **22**, p. 791-794.

Chatfield, C. 1996. *The analysis of time series. An introduction*. 5th edition. Chapman & Hall. ISBN 0 412 71640 2.

Cheel, R. J. 1990. Horizontal lamination and the sequence of bed phases and stratification under upper-flow-regime conditions. *Sedimentology*, **37**, p. 517-529.

Choi, K. S., Kim, B. O., and Park, Y. A. 2001. Late Pleistocene rhythmites in Kyunggi Bay, west coast of Korea: A comparison with simulated rhythmites based on modern tides and implications for intertidal positioning. *Journal of Sedimentary Petrology*, Vol. **71**, No. 5, p. 680-691.

Clemetsen, R., Hurst, A. R., Knarud, R., and Omre, H. 1990. A computer program for evaluation of fluvial reservoirs. *In*: Buller, A. T., Berg, E. and Hjelmeland, O.

North Sea Oil and Gas Reservoirs II, proceedings from the 2nd North Sea Oil and Gas Reservoirs conference, Trondheim, Norway, p. 373-385.

Clennel, M. B. 1997. Tortuosity: a guide through the maze. *In*: Harvey, M. A. and Lovell, P. K. (eds.), *Developments in petrophysics*, Geological Society Special Publication No. **122**, p. 299-344.

Clifton, H. E. Estuarine Deposits. 1982. *In*: Scholle, P. A. and Spearing, D. (eds.) *Sandstone deposits and environments*. American Association of petroleum Geologists, Memoir **31**, p. 179-189.

Clifton, H. E. 1983. Discrimination between subtidal and intertidal facies in Pleistocene deposits, Willapa Bay, Washington. *Journal of Sedimentary Petrology*, Vol. **53**, No. 2, p. 353-369.

Coelman, J. M. and Gagliano, S. H. 1965. Sedimentary structures: Mississippi river deltaic plain. *In*: Middleton (ed.), *Primary sedimentary structures and their hydrodynamic interpretation*, Society of Economic Paleontologists and Mineralogists Special Publication No. **12**, p. 133-148.

Coll, C., Jing, X. D. and Muggeridge, A. H. 1999. Integration of core and log information to improve the representation of small/medium scale heterogeneity. Presented at the 1999 SPE Annual Technical Conference and Exhibition. *SPE 56804*.

Corbett, P. M. W., Ringrose, P. S., Jensen, J. L. and Sorbie, K. S. 1992a. Laminated Clastic Reservoirs; the Interplay of Capillary Pressure and Sedimentary Architecture. Presented at the 67th Annual Technical Conference and Exhibition of the Society of Petroleum Engineers, *SPE 24699*.

Corbett, P. W. M. and Jensen, J. L. 1992b. Variation of reservoir statistics according to sample spacing and measurement type for some intervals in the Lower Brent Group. *The Log Analyst*, January-February, p. 22-41.

Corbett, P. W. M. and Jensen, J. L. 1992c. Estimating the mean permeability: how many measurements do we need?. *First Break*, Vol. **10**, No. 3.

Corbett, P. 1993. *Reservoir characterisation of a laminated sediment. The Rannoch Formation Middle Jurassic, North Sea*. Unpubl. PhD thesis, Heriot-Watt University, Edinburgh.

Corbett, P. W. M. and Jensen, J. L. 1993. Application of probe permeametry to the prediction of two-phase flow performance in laminated sandstones (lower Brent Group, North Sea). *Marine and Petroleum Geology*, Vol. **10**, August, p. 335-346.

Corbett, P. W. M., Stromberg, S. G., Brenchley, P. J. and Geehan, G. 1994. Laminaset geometries in fine grained shallow marine sequences: core data from the Rannoch Formation (North Sea) and from outcrop data from the Kennilworth Member (Utah, USA) and the Bencliff Grit (Dorset, UK). *Sedimentology*, **41**, p. 729-745.

Corbett, P. W. M., Jensen, J. L. and Sorbie, K. S. 1998. A review of up-scaling and cross-scaling issues in core and log data interpretation and prediction. *In*: Harvey, P. K. and Lovell, M. A. (eds.), *Core-Log Integration*, Geological Society Special Publication No. 136, London, p. 9-16.

Corbett, P., Anggraeni, S. and Bowen, D. 1999. The use of the probe permeameter in carbonates - addressing the problems of permeability support and stationarity. *The Log Analyst*, Vol. **40**, No. 5, p. 316-326.

Corbett, P., Ellabad, Y., Mohammed, K. and Pososyaev, A. 2003. Global hydraulic elements - elementary petrophysics for reduced reservoir modelling. Presented at the 65th EAGE Conference and Exhibition, paper **F-26**.

Cowan, E. A., Seramur, K. C., Cai, J., and Powell, R. D. 1999. Cyclic sedimentation produced by fluctuations in meltwater discharge, tides and marine productivity in Alaskan fjord. *Sedimentology*, Vol. **46**, p. 1109-1126.

Cox, D. L., Lindquist, S. J., Bargas, C. L., Havholm, K. G., and Srivastava, R. M. 1994. Integrated modelling for optimum management of a giant gas condensate reservoir, Jurassic Eolian Nugget Sandstone, Anschutz Ranch East Field, Utah Overthrust (U.S.A.). *In*: Yarus, J. M. and Chambers, R. L. (eds.), *Stochastic Modelling in Geostatistics: principles, methods, and case studies*. AAPG Computer Applications in Geology, No. **3**, p. 287-321.

Cunha, L. B., Barroso, A. S., Romeu, R. K., Sombra, C. L., Cortez, M. M., Backheuser, Y., Lopes, M. F., Schwerdesky, G., Bruhn, C. H., Souza, R. S. and Becker, M. R. 2001. A multi-scale approach to improve reservoir characterization and forecasting: the Albacora Field (deep-water offshore Brazile) study. *Petroleum Geoscience*, Vol. **7**, p. S17-S23.

Cushman, J. H. 1986. On measurement, scale and scaling. *Water Resources Research*, Vol. **22**, No. 2, p. 129-134.

Cuthiell, D. L., Bachu, S., Kramers, J. W. and Yuan, L-P. 1991. Characterizing shale clast heterogeneities and their effect on fluid flow. *In*: Lake, L. W., Carroll, H. B. and Wesson, T. C. (eds.) *Reservoir Characterization II*. Academic Press, San Diego, p. 226-250.

Dagan, G. 1979. Models of groundwater flow in statistically homogeneous porous formations. *Water Resources Research*, **15**, No. 1, 47-63.

Dagan, G. 1986. Statistical theory of groundwater flow and transport: pore to laboratory, laboratory to formation and formation to regional scale. *Water Resources Research*, Vol. **22**, No. 9, p. 120S-134S.

Dagan, G. 1989. *Flow and Transport in Porous Formations*. Springer-Verlag. ISBN: 3-540-51602-6.

Dagan, G. 1990. Transport in heterogeneous porous formations: spatial moments, ergodicity, and effective dispersion. *Water Resources Research*, Vol. **26**, No. 6, p. 1281-1290.

Dalland, A., Worsley, D., and Ofstad, K. 1988. A lithostratigraphic scheme for the Mesozoic and Cenozoic succession offshore mid- and norther Norway. *Norwegian Pet. Direct. Bull*., **4**, 1-65.

Dalrymple, R. W., Makino, Y. and Zaitlin, B. A. 1991. Temporal and spatial patterns of rhythmite deposition on the mud flats in the macrotidal Cobequid Bay-Salmon River estuary, Bay of Fundy, Canada. *In*: Smith, D. G., Reinson, G. E., Zaitlin, B. A. and Rahmani, R. A. (eds.) *Clastic Tidal Sedimentology.* Canadian Society of Petroleum Geologist, Memoir 16, p. 137-160.

Dalrymple, R. W., Zaitlin, B. A. and Boys, R. 1992. Estuarine facies models: conceptual basis and stratigraphic implications. *Journal of Sedimentary Research*, Vol. **62**, No. 5, p. 1130-1146.

Dalrymple, R. W. and Rhodes, R. N. 1995. Estuarine dunes and bars. *In*: Perillo, G. M. E. (ed.) *Geomorphology and Sedimentology of Estuaries*. Developments in Sedimentology 53. Elsevier Science B. V, p. 359-422

Damsleth, E.,Tjølsen, C. B., Omre, K. H. and Haldorsen, H. H. 1990, A two-stage stochastic model applied to a North Sea reservoir. *SPE 20605*.

Damsleth, E. and Tjølsen, C. B. 1992. Scale consistency from cores to geologic description. *SPE Formation Evaluation*, **December**, p. 295-299, *SPE 24700*.

Davis, J. C. 1986. *Statistics and Data Analysis in Geology.* Second edition. John Wiley & Sons.

Daws, J. A., and Prosser, D. J. 1992. Scales of permeability heterogeneity within the Brent Group. *Journal of Petroleum Geology*, Vol. **15**, No. 4, p. 397-418.

De Boer, P. L., van Gelder, A. and Nio, S. D. (eds.). 1988. *Tide-influenced sedimentary environments and facies*. Extended version of papers presented on Clastic Tidal Deposits, Aug. 1985, Utrecht, Netherlands. D. Reidel Publ. Co.

De Boer, P. L., Oost, A. P. and Visser, M. J. 1989. The diurnal inequality of the tide as a parameter for recognizing tidal influence. *Journal of Sedimentary Petrology*, Vol. **59**, No. 6, p. 912-921.

Desbarats, A. J. 1987. Numerical estimation of effective permeability in sand-shale formations. *Water Resources Research*, **23**, No. 2, 273-286.

Desbarats, A. 1989. Support effects and the spatial averaging of transport properties. *Mathematical Geology*, Vol. **21**, No. 3, p. 383-389.

Desbarats, A. J. and Dimitrakopoulos, R. 1990. Geostatistical modelling of transmissibility for 2D reservoir studies. *SPE Formation Evaluation*, **December**, p. 437-443, *SPE 19355*.

Desbarats, A. J. 1992. Spatial averaging of hydraulic conductivity in three-dimensional heterogeneous porous media. *Mathematical Geology*, Vol. **24**, No. 3, p. 249-267.

Deutch, C. 1989. Calculating effective absolute permeability in sandstone/shale sequences. *SPE Formation Evaluation*, Vol. **4**, No. 3, 343-348.

Dewan, J. T. 1983. *Essential of modern open-hole log interpretation*, PennWell, Tulsa.

Doucette, J. S. 2002. Geometry and grain-size sorting of ripples on low-energy sandy beaches: field observations and model prediction. *Sedimentology*, **49**, p. 483-503.

Doveton, J. H. and Presnky, S. E. 1992. Geological applications of wireline logs - a synopsis of developments and trends. *The Log Analysts*, **May-June**, p. 286-303.

Doveton, J. H. 1994. *Geological log analysis using computer methods*. AAPG Computer Applications in Geology, No. **2**.

Doyen, P. M. 1988. Permeability, conductivity and pore geometry of sandstone. *Journal of Geophysical Research*, Vol. **93**, No. B7, p. 7729-7740.

Dreyer, T. Scheie, Å. and Walderhaug, O. 1990. Minipermeameter-based study of permeability trends in channel sand bodies. *The American of Petroleum Geologist Bulletin*, Vol. **74**, p. 359-374.

Dreyer, T. 1992. Significance if tidal cyclicity for modelling of reservoir heterogeneities in the Lower Jurassic Tilje Formation, mid-Norwegian shelf. *Norsk Geologisk Tidsskrift*, Vol. **72**, p. 159-170.

Dreyer, T. 1993. Geometry and facies of large-scale flow units in fluvial-dominated fan-delta-front sequences. *In*: Ashton, M. (ed.), *Advances in Reservoir Geology*, Geological Society Special Publication No. **69**, p. 135-174.

Dubrule, O. and Haldorsen, H. H. 1986. Geostatistics for permeability estimation. *In*: Lake, L. W. and Caroll, H. B. (eds) *Reservoir Characterization*. Academic Press, Orlando, p. 223-247.

Dubrule, O. 1998. *Geostatistics In Petroleum Geology.* AAPG Continuing Education Course Note Series # 38.

Dullien, F. A. L. 1992. *Porous media. Fluid transport and pore structure*. Second Edition. Academic Press Inc.

Durlofsky, L. J. and Chung, E. Y. 1990. Effective Permeability of heterogeneous reservoir regions. *In*: Guérillot, D. and Guillon, O. (eds.) 2nd European Conference on the Mathematics of Oil Recovery, Paris, Edition Technip., p. 57-64.

Durlofsky, L. J. 1991. Numerical calculation of equivalent grid block permeability tensors for heterogeneous porous media. *Water Resources Research*, Vol. **27**, No. 5, p. 699-708.

Durlofsky, L. J. 1992. Representation of grid block permeability in coarse scale models of randomly heterogeneous porous media. *Water Resources Research*, Vol. **28**, No. 7, p. 1791-1800.

Dyer, K. R. 1995. Sediment transport processes in estuaries. *In*: Perillo, G. M. E. (ed.) *Geomorphology and Sedimentology of Estuaries*. Developments in Sedimentology 53. Elsevier Science B. V.

Ebanks, W. J. 1987. Geology in enhanced oil recovery. *In*: Tillman, R. W. and Weber, K. J. (eds.), *Reservoir sedimentology*, SEPM Special Publication No. **40**, p. 1-14.

Ehrlich, R., Crabtree, S. J., Kennedy, S. K. and Cannon, R. L. 1984. Petrographic image analysis, I. Analysis of reservoir pore complexes. *Journal of Sedimentary Petrology*, Vol. **54**, No. 4, p. 1365-1378.

Ehrlich, R., Crabtree, S. J., Horkowitz, K. O., and Horkowitz, J. P. 1991a. Petrography and reservoir physics I: objective classification of reservoir porosity. *AAPG Bulletin*, Vol. **75**, No. 10, p. 1547-1562.

Ehrlich, R., Etris, E. L., Brumfield, D., Yuan, L. P. and Crabtree, S. J. 1991b. Petropgraphy and reservoir physics III: Physical models for permeability and formation factor. *AAPG Bulletin*, Vol. **75**, No. 10, p. 1579-1592.

Einstein, H. A. and Krone, R. B. 1962. Experiments to determine modes of cohesive sediment transport in salt water. *Journal of Geophysical Research*, Vol. **67**, No. 4, p. 1451-1461.

Ejipe, R. and Weber, K. J. 1971. Mini-permeameters for consolidated rock and unconsolidated sand. *AAPG Bulletin*, Vol. **55**, No. 2, p. 307-309.

Elfenbein, C., Husby, Ø, and Ringrose, P. S. 2003. Geologically-based estimation of kv/kh ratios: an example from the Garn Formation, Tyrihans Field, mid-Norway. *Proceedings of the 6th Petroleum Geology Conference: North West Europe and global perspectives*. The Geological Society of London.

Ellis, D. W. 1987. *Well logging for earth scientists*. Elsevier, New York. ISBN:0-444-01180-3.

Enderlin, M. B., Hansen, D. K. T. and Hoyt, B. R. 1991. Rock volumes: considerations for relating well log and core data. *In*: Lake, L. W., Carroll, H. B. and Wes-

son, T. C. (eds.) *Reservoir Characterization II*. Academic Press, San Diego, p. 277-288.

Etherridge, D. W. and Kemp, P. H. 1978. Velocity measurements downstream of rearward-facing steps, with reference to bed instability. *Journal of Hydraulic Research*, Vol. **17**, p. 107-119.

Fan, D. and Li, C. 2002. Rhythmic deposition on mudflats in the mesotidal Changjiang Estuary, China. *Journal of Sedimentary Petrology*, Vol. **72**, No. 4, p. 543-551.

Fenies, H., de Resseguier, A. and Tastet, J-P. 1999. Intertidal clay-drape couplets (Gironde estuary, France). *Sedimentology*, **46**, p. 1-15.

Finol, J. and Jing, X-D. D. 2002. Permeability prediction in shaly formations: The fuzzy modelling approach. *Geophysics*, Vol. **67**, No. 3, p. 817-829.

Flemming, B. W. 1988. Process and pattern of sediment mixing in a macrotidal coastal lagoon along the west coast of South Africa. *In*: de Boer, P. L., van Gelder, A and Nio, S. D. (eds.), *Tide-influenced Sedimentary Environments and Facies*, D. Reidel Publishing Company.

Fløl0, L. H., Kjærefjord, J. M., Arnesen, D. M., Menard, W. P. and Weissenburger, K. W. 2000. Revealing the petrophysical properties of a thin-bedded rock in a Norwegian Sea reservoir with logs, core and miniperm data. *SPE Reservoir Evaluation and Engineer*, Vol. **3**, p. 249-255.

Forrester, W, D. 1992. Tides. In: Nierenberg, W. A. (ed.), *Encyclopedia of Earth System Science*, Academic Press Inc., San Diego, California.

Fraser, H. J. 1935. Experimental study of porosity and permeability of clastic sediments. *Journal of Geology*, **43**, p. 910-1010.

Frykman, P. 2001. Spatial variability in petrophysical properties in Upper Maastrichtian chalk outcrops at Stevens Klint, Denmark. *Marine and Petroleum Geology*, Vol. **18**, p. 1041-1062.

Geehan, G. and Underwood, J. 1993. The use of length distributions in geological modelling. *Special Publications International Association of Sedimentologist*, **15**, p. 205-212.

Gelhar, L. W. and Axness, C. L. 1983. Three-dimensional stochastic analysis of macrodispersion in aquifers. *Water Resources Research*, Vol. **19**, No. 1, p. 161-180.

Gibbons, K., Halvorsen, C. and Siring, E. 1993. Vertical and horizontal permeability variation within a sandstone reservoir based on minipermeameter measurements. *Marine and Petroleum Geology*, p. Vol. **10**, August, p. 325-334.

Ginsburg, R. N. 1975. *Tidal Deposits*. New York, Heidelberg, Berlin: Verlag.

Gjelberg, J., Dreyer, T., Høie, A., Tjelland, T., and Lilleng, T. 1987. Late Triassic to Mid-Jurassic sandbody development on the Barents and mid-Norwegian shelf. *In*: Brooks, J. and Glennie, K. W. (eds.), *Petroleum Geology of North West Europe*, p. 1105-1129.

Goggin, D. J., Thrasher, R. L. and Lake, L. W. 1988. A theoretical and experimental analysis of minipermeameter response including gas-slippage and high-velocity flow effects. *In Situ*, **12**, p. 79-116.

Goggin, D. J., Chandler, M. A., Kocurek, G. and LAke, L. W. 1988. Patterns of permeability in eaolian deposits: Page Sandstone (Jurassic), Northeastern Arizona. *SPE Formation Evaluation*, **June**.

Gomez-Hernandez, J. J. and Journel, A. G. 1990. Stochastic characterization of grid-block permeabilities: from point values to block tensors. *In*: Guérillot, D. and Guillon, O. (eds.) *2nd European Conference on the Mathematics of Oil Recovery*, Paris, Edition Technip.

Grafton, L. C. and Fraser, H. J. 1935. Systematic packing of spheres with particular relation to porosity and permeability. *Journal of Geology*, **43**, p. 785-909.

Grebb, S. F. and Archer, A. W. 1995. Rhythmitic sedimentation in a mixed tide and wave deposit, Hazel patch Sandstone (Pennsylvanian), Eastern Kentucky Coal Field. *Journal of Sedimentary Research*, Vol. **B65**, No. 1, p. 96-106.

Grebb, S. F. and Archer, A. W. 1998.Annual sedimentation cycles in rhythmites of Carboniferous tidal channels. *In*: Alexander, C. R, Davis, R. A., and Henry, V. J. (eds.), *Tidalites: Processes and Products*, SEPM Special Publication No. **61**, p. 75-83.

Gupta, R. and Johnson, H. D. 2001. Characterization of heterolithic deposits using electrofacies analysis in tide-dominated Lower Jurassic Cook Formation (Gullfaks field, offshore Norway). *Petroleum geoscience,* Vol. **7**, p. 321-330.

Gutjar, A. L., Gelhar, L. W., Bakr, A. A., and McMillan, J. R. 1978. Stochastic analysis of spatial variability in subsurface flow2: Evaluation and application. *Water Resources Research,* Vol. **14**, No. 5.

Haldorsen, H. H. and Lake, L. W. 1982. A new approach to shale management in field scale simulation models. *SPE 10976.*

Haldorsen, H. H. 1986. Simulator parameter assignments and the problem of scale in reservoir engineering, *In*: Lake, L. W. and Caroll, H. B. (eds) *Reservoir Characterization*. Academic Press, Orlando, p. 293-340.

Haldorsen, H. H. and Chang, D. M. 1986. Notes on stochastic shales; from outcrop to simulation model. *In*: Lake, L. W. and Caroll, H. B. (eds) *Reservoir Characterization*. Academic Press, Orlando, p. 445-485.

Haldorsen, H- H. and Damsleth, E. 1990. Stochastic modelling. *Journal of Petroleum Technology,* Vol. **42**, No. 4, p. 404-412.

Halvorsen C. and Hurst, A. 1990. Principles practice and applications of laboratory minipermeametry. *In*: Worthington (ed), *Advances in Core Evaluation,* p. 521-549.

Halvorsen, C. 1993. Probe permeametry applied to a highly laminated sandstone reservoir. *Marine and Petroleum Geology,* Vol. **10**, August, p. 347-351.

Harms, J. C. and Fahnestock, R. K. 1965. Stratification, bedforms, and flow phenomena (with example from the Rio Grande). *In*: Middleton (ed.), *Primary sedimentary structures and their hydrodynamic interpretation*, Society of Economic Paleontologists and Mineralogists Special Publication No. 12, p. 84-115.

Harms, J. C. 1969. Hydraulic significance of some sand ripples. *Geological Society of America Bulletin*, Vol. **80**, p. 363-396.

Hartkamp-Bakker, C. A. and Donselaar, M. E. 1993a. Permeability patterns in point bar deposits: Tertiary Loranca Basin, central Spain. *In*: Flint, S. and Bryant, I. D. *The geological modelling of hydrocarbon reservoirs and outcrop analogues*, Special Publication Number **15** of the International Association of Sedimentologist, p. 157-168.

Hartkamp-Bakker, C. A., Arribas, J. and Tortosa, A. 1993b. Grain size, composition, porosity and permeability contrasts within cross-bedded sandstone in Tertiary fluvial deposits, central Spain. *Sedimentology,* Vol. **40**, p. 787-799.

Harvey, P. K. and Lovell, M. A. (eds.). 1998. *Core-log Integration*. Geological Society Special Publication No. **136**.

Hashin, Z. and Shtrikman, S. 1962. A variational approach to the theory of the effective magnetic permeability of multiphase materials. *Journal of Applied Physics*, Vol. **33**, No. 10, p. 3125-3131.

Hassanizadeh, M. and Gray, W. G. 1983. General conservation equations for multiphase systems: 1. Averaging procedure. *In*: Pinder, G. F. (ed.) *Flow through porous media, Recent Developments*. A Computational Mechanics Publication Publications, ISBN 0 905451 06 6, p. 1-16.

Hayes, M. O. 1975. Morphology and sand accumulation in estuaries: an introduction to the symposium. *In*: L. E. Cronin (ed.), *Estuarine Research, Vol. II Geology and engineering*, p. 3-22, Academic Press, London.

Hearn, C. L., Ebanks, W. J., Tye, R. S. and Ranganathan, V. 1984. Geological factors influencing reservoir performance of the Hartzog Draw Field, Wyoming. *Journal of Petroleum Technology,* **August**, p. 1335-1344.

Heller, P- L- and Paola, C. 1996. Downstream changes in alluvial architecture: an exploration of controls on channel-stacking patterns. Journal of Sedimentary Research, Vol. 66, No. 2.

Henriette, A. and Jacquin, C. G. 1989. The effective permeability of heterogeneous porous media. *PhysioChemical Hydrodynamics* Vol. **11**, No. 1, p. 63-80.

Homewood, P. and Allen, P. 1981. Wave-, tide-, and current-controlled sandbodies of Miocene Molasse, Western Switzerland. *The American Association of Petroleum Geologists Bulletin*, Vol. **65**, No. 12, p. 2534-2545.

Hook, J. R. 2003. An introduction to porosity. *Petrophysics*, **May-June**, p. 205-212.

Hook, J. R., Nieto, J. A., Kalkomey, C. T. and Ellis, D. 1994. Facies and permeability prediction from wireline log and core - a North Sea case study. Presented at the *35th SPWLA Annual Logging Symposium*, **paper AA**.

Hunter, R. E. 1977. Terminology of cross-stratified sedimentary layers and climbing ripple structures. *Journal of Sedimentary Petrology*, Vol. **47**, p. 697-706.

Hurst, A., Lovell, M. A. and Morton, A. C. 1990. Geological applications of wireline logs, Special Publications of Geological Society, No. 48, Geological Society, London.

Hurst, A. and Rosvoll, K. 1991. Permeability variations in sandstone and their relationship to sedimentary structures. *In*: Lake, L. W., Carroll, H. B. and Wesson, T. C. (eds.) *Reservoir Characterization II*. Academic Press, San Diego, p. 166-196.

Hurst, A., Griffiths, C. M. and Worthington, P. F. (eds.). 1992. *Geological applications of wireline logs II*. Special Publications of Geological Society, No. **65**, Geological Society, London.

Hurst, A. 1993. Sedimentary flow units in hydrocarbon reservoirs: some shortcomings and a case for high-resolution permeability data. *In*: Flint, S. and Bryant, I. D. *The geological modelling of hydrocarbon reservoirs and outcrop analogues*, Special Publication Number **15** of the International Association of Sedimentologists, p. 191-204.

Imbrie, J. and Buchanan, H. 1965. Sedimentary structures in the modern carbonate sands of the Bahamas. *In*: Middleton (ed.), *Primary sedimentary structures and their hydrodynamic interpretation*, Society of Economic Paleontologists and Mineralogists Special Publication No. **12**, p. 149-172.

Ioannidis, M. A., Kwiecien, M. J. and Chatzis, I. 1996. Statistical analysis of the porous microstructure as a method for estimating reservoir permeability. *Journal of Petroleum Science and Engineering*, Vol. **16**, p. 251-261.

Isaaks, E. H. and Srivastava, R. M. 1989. *An introduction to applied geostatistics*. Oxford University Press. ISBN 0195959134.

Jackson, M. A., Bowen, D. G., Jensen, J. L. and Todd, A. C. 1994. Resistivity and permeability mapping at the lamina scale. Proceedings of the International Symposium of the Society of Core Analysts, Stavanger, *SCA-9415*.

Jackson, M. D., Yoshida, S., Johnson, D., Muggeridge, A. H., Næss, A. and Ringrose, P. 1999. Upscaling complex three-dimensional bedform-scale sedimentary structures within tidal sandstone reservoirs. *In*: Lippard, S. J., Næss, A, and Sind-

ing-Larsen, R. (eds.) *Proceedings of the 5th Annual Conference of the International Association of Mathematical Geology (IAMG)*, Trondheim, p. 729-734.

Jackson, M. D. and Muggeridge, A. H. 2000. Effect of discontinuous shales on reservoir performance during horizontal waterflooding. *SPE Journal*, Vol. **5**, No. 4.

Jackson, M. D., Muggeridge, A. H., Yoshida, S., and Johnson, H. D. 2003. Upscaling permeability measurements within complex heterolithic tidal sandstones. *Mathematical Geology*, Vol. 35, No. 5, p. 446-454.

Jackson, P. D., Harvey, P. K., Lovell, M. A., Gunn, D. A., Williams, C. G. and Flint, R. C. 1998. Measurement scale and formation heterogeneity: effects on the integration of resistivity data. *In*: Harvey, P. K. and Lovell, M. A. (eds.), *Core-Log Integration*, Geological Society Special Publication No. 136, London, p. 261-272.

Jacquin, C. G., Henriette, A., Guerillot, D. and Alder, P. M. 1991. Heterogeneity and effective permeability of porous rocks: experimental and numerical investigation. *In*: Lake, L. W., Carroll, H. B. and Wesson, T. C. (eds.) *Reservoir Characterization II*. Academic Press, San Diego, p. 662-664.

Jennings, J. W. 1999. How much core-sample variance should a well-log model reproduce. *SPE Reservoir Evaluation & Engineer*, Vol. **2** No. 5, p. 442-470.

Jensen, J. L. 1991. Use of the geometric average for effective permeability estimation. *Mathematical Geology*, Vol. **23**, No. 6, p. 833-840.

Jensen, J. L., Corbett, P. W. M., Pickup, G. E. and Ringrose, P. S. 1996. Permeability semivariograms, geological structure and flow performance. *Mathematical Geology*, Vol. **28**, No. 4, p. 419-435.

Jensen, J. L., Lake, L. W., Corbett, P. W. M. and Goggin, D. J. 1997. *Statistics for Petroleum Engineers and Geoscientists*. Prentice and Hall.

Jian, F. X., Chork, C. Y., Taggert, I. J., McKay, D. M. and Bartlett, R. M. 1994. A genetic approach to prediction of petrophysical properties. *Journal of Petroleum Geology*, Vol. **17**, No. 1, p. 71-88.

Jones, A., Doyle, J. Jacobsen, T. and Kjønsvik, D. 1995. Which sub-seismic heterogeneities influence waterflood performance? A case study of low net-to.-gross fluvial reservoir. *In*: Haan, H. J. (ed), *New developments in improved oil recovery*, Geological Society Special Publication No. **84**, p. 5-18.

Jopling, A. V. 1965a. Laboratory study of the distribution of grain sizes in cross-bedded deposits. *In*: Middleton (ed.), *Primary sedimentary structures and their hydrodynamic interpretation*, Society of Economic Paleontologists and Mineralogists Special Publication No. 12, p. 53-65.

Jopling, A. V. 1965b. Hydraulic factors controlling the shape of laminae in laboratory deltas. *Journal of Sedimentary Petrology*, Vol. **35**, No. 4, p. 777-791.

Jopling, A. V. 1966. Some principles and techniques used in reconstructing the hydraulic parameters of a paleo-flow regime. *Journal of Sedimentary Petrology*, Vol. **36**, No. 1, p. 5-49.

Jopling, A. V. 1967. Origin of laminae deposited by the movement of ripples along a streambed: a laboratory study. *Journal of Geology*, Vol. **75**, p. 287-305.

Jordan, R. and Campell, F. L. 1984. *Well logging B1, rock properties, borehole environment, mud and temperature logging*. SPE Monograph series Vol. **9**.

Journel, A. G., Deutsch, C., and A. J. Desbarats. 1986. Power averaging for block effective permeability. Presented at the 56th California Regional Meeting of the Society of Petroleum Engineers. *SPE 15128*, p. 329-334.

Journel, A. G. and Huijbregts, C. J. 1989. *Mining Geostatistics*. Academic Press, 600 p.

Karssenberg, D., Tornqvist, T. E. and Bridge, J. S. 2001. Conditioning a process-based model of sedimentary architecture to well data. *Journal of Sedimentary Research*, Vol. **71**, No. 6, p. 868-879.

Kasap, E. and Lake, L. W. 1990. Calculating the effective permeability tensor of a gridblock. *SPE Formation Evaluation*, **June**, *SPE 18434*, p. 192-200.

Katz, A. J. and Thompson, A. H. 1987. Prediction of rock electrical conductivity from mercury injection measurements. *Journal of Geophysical Research*, Vol. **92**, No. B1, p. 599-607.

King, P. R. 1989. The use of renormalization for calculating effective permeability. *Transport in Porous Media*, Vol. **4**, p. 37-58.

King, P. R. 1990. The connectivity and conductivity of overlapping sand bodies. *In*: Buller, A. T., Berg, E. and Hjelmeland, O. *North Sea Oil and Gas Reservoirs II*,

proceedings from the 2nd North Sea Oil and Gas Reservoirs conference, Trondheim, Norway, p. 353-362.

King, P. R., Buldyrev, S. V., Dokholyan, N. V., Havlin, S., Lee, Y., Paul, G., Stanley, H. E., and Vandesteeg, N. 2001. Predicting oil recovery using percolation theory. *Petroleum Geoscience*, Vol. **7**, p. S105-S107.

Kirby, R. and Parker, W. R. 1983. Distribution and behaviour of fine sediment in the Severn Estuary and the Inner Bristol channel, U.K. *Can. J. Fish. Aquat. Sci.*, **40**, p. 83-95.

Kirby, R. 1991. Distinguishing features of layered muds deposited from shallow water, high concentration suspension. *In*: Bennet, R. H., Bryant, W. R. and Hulbert, M. H., *Microstructure of Fine-grained Sediments: From mud to shale*. Springer Verlag, New York, p. 167-173.

Kirkpatric, S. 1973. Percolation and conduction. *Reviews of Modern Physics*, Vol. **45**, No. 4, p. 574-588.

Klein, G. V. 1963. Bay of Fundy intertidal zone sediments. *Journal of Sedimentary Petrology*, Vol. **33**, No. 4, p. 844-854.

Klein, G. V. 1965. Dynamic significance of primary structures in the Middle Jurassic Great Oolite series, Southern England. *In*: Middleton (ed.), *Primary sedimentary structures and their hydrodynamic interpretation*, Society of Economic Paleontologists and Mineralogists Special Publication No. **12**, p. 173-191.

Klein, G. V. 1970. Depositional and dispersal dynamics of intertidal sand bars. *Journal of Sedimentary Petrology*, Vol. **40**, No. 4. p. 1095-1127.

Klein, G. V. 1977. *Clastic Tidal Facies*. Continuing Education Publication Company. ISBN 0-89469-092-2

Kohsiek, L. H. M., Buist, H. J., Bloks, R., van den Berg, J. H., and Visser, J. 1988. Sedimentary processes on a sandy shoal in a mesotidal estuary (Oosterschelde, The Netherlands). *In*: de Boer, P. L., van Gelder, A and Nio, S. D. (eds.), *Tide-influenced Sedimentary Environments and Facies*, D. Reidel Publishing Company, p. 201-214.

Koltermann, C. E. and Gorelick, S. M. 1996. Heterogeneity in sedimentary deposits: A review of structure imitating, process-imitating and descriptive approaches. *Water Resources Research*, **32**, No. 9, p. 2617-2658.

Koplik, J. and Vermette, M. 1984. Conductivity and permeability from microgeometry. *Journal of Applied Physics*, Vol. **56**, No. 11, p. 3217-3131.

Korvin, G. 1982. Axiomatic characterization of the general mixture rule. *Geoexploration*, **19**, p. 267-276.

Kreisa, R. D. and Moiola, R. J. 1986. Sigmoidal tidal bundles and other tide-generated sedimentary structures of the Curtis Formation, Utah. *Geological Society of American Bulletin*, Vol. **97**, p. 381-387.

Krinsley, David H. Doornkamp, John C. 1973. *Atlas of Quartz and Surface Textures*. Cambridge Earth Science Series.

Krõgel, F. and Flemming, B. W. 1998. Evidence for temperature-adjusted sediment distributions in the back-barrier tidal flats of the East Frisian Sea (Souther North Sea). *In*: Alexander, C. R, Davis, R. A., and Henry, V. J. (eds.), *Tidalites: Processes and Products*, SEPM Special Publication No. **61**, 31-41.

Kvale, E. P., Archer, A. W. and Johnson, H. R. 1989. Daily, monthly, and yearly tidal cycles within laminated siltstone of the Mansfield Formation (Pennsylvanian) of Indiana. *Geology*, Vol. **17**, p. 365-368.

Kvale, E. P. and Archer, A. W. 1990. Tidal deposits associated with low-sulfur coals, Brazil FM. (Lower Pennsylvanian), Indiana. *Journal of Sedimentary Petrology*, Vol. **60**, No. 4. p. 563-574.

Kvale, E. P. and Archer, A. W. 1991. Characteristics of two. Pennsylvanian-age, semidiurnal tidal deposits in the Illinois Basin, U.S.A. *In*: Smith, D. G., Reinson, G. E., Zaitlin, B. A. and Rahmani, R. A. (eds.) *Clastic Tidal Sedimentology*. Canadian Society of Petroleum Geologist, Memoir **16**, p. 179-188.

Kvale, E. P., Fraser, G. S., Archer, A. W., Zawistoski, A., Kemp, N., and McGough, P. 1994. Evidence of seasonal precipitation in Pennsylvanian sediments of the Illinois basin. *Geology*, Vol. **22**, p. 331-334.

Kvale, E. P., Johnsson, H. W., Sonett, C. P., Archer, A. W. and Zawistoski, A. 1999. Calculating lunar retreat using tidal rhythmites. *Journal of Sedimentary Petrology*, Vol. **69**, p. 1154-1168.

Ladipo, K. O. 1988. Example of tidal current periodicities from Upper Cretaceous sandstone succession (Anambra Basin, S. E. Nigeria). 1988. *In*: de Boer, P. L., van Gelder, A and Nio, S. D. (eds.), *Tide-influenced Sedimentary Environments and Facies*, D. Reidel Publishing Company, p. 333-340.

Lake, L. W. 1988. The origin of anisotropy. *Journal of Petroleum Technology*, **April**, p. 395-396.

Lake, L. W. and Jensen, J. L. 1991. A review of heterogeneity measures used in reservoir characterization. *In Situ*, Vol. **15**, No. 4, p. 409-439.

Lanier, W. P. Feldmann, H. R. and Archer, A. W. 1993. Tidal sedimentation from a fluvial to estuarine transition, Douglas Group, Missourian-Virgillian, Kansas. *Journal of Sedimentary Petrology*, Vol. **63**, No. 5, p. 860-873.

Lanier, W. P. and Tessier, B. 1998. Climbing-ripple bedding in the fluvio-estuarine transition: a common feature associated with tidal dynamics (modern and ancient analogues). *In*: Alexander, C. R, Davis, R. A., and Henry, V. J. (eds.), *Tidalites: Processes and Products*, SEPM Special Publication No. **61**, p. 109-117.

Lasseter, T. J., Waggoner, J. R. and Lake, L. W. 1986. Reservoir heterogeneities and their influence on ultimate recovery. *In*: Lake, L. W. and Caroll, H. B. (eds) *Reservoir Characterization*. Academic Press, Orlando, p. 545-559.

Leclair, S. F. 2002. Preservation of cross-strata due to the migration of subaqueous dunes: an experimental investigation. *Sedimentology*, **49**, p. 1157-1180.

Leithold, E. L. and Bourgeois, J. 1984. Characteristics of coarse-grained sequences deposited in nearshore, wave-dominated environments - examples from the Miocene of South-west oregon. *Sedimentology*, **31**, p. 749-775.

Le Roux, J. P. 1998. Entrainment threshold of natural grains in liquids determined empirically from dimensionless settling velocities and other measures of grain size. *Sedimentary Geology*, **119**, p. 17-23.

Liang, Z. R., Pilippi, P. C., Fernandes, C. P. and Magnani, F. S. 1999. Prediction of permeability from the skeleton of three-dimensional pore structure. *SPE Reservoir Evaluation & Engineering*, Vol. **2**, No. 2, *SPE 56006*.

Harvey, P. K. and Lovell, M. A. 1998. *Core-Log Integration*, Geological Society Special Publication, No **136**, Geological Society, London.

Lofts, J. C. and Bristow, J. F. 1998. Aspects of core-log integration: an approach using high resolution images. *In*: Harvey, P. K. and Lovell, M. A. (eds.), *Core-Log Integration*, Geological Society Special Publication No. **136**, London, p. 273-283.

Lovell, M. and Parkinson, N. 2003. Geological applications of well logs. *AAPG Methods in Exploration*, No. **13**.

Lovell, M. A., Harvey, P. K., Jackson, P. D., Brewer, T. S., Williamson, G. and Williams, C. G. 1998. Interpretation of core and log data - integration or calibration. *In*: Harvey, P. K. and Lovell, M. A. (eds.) *Core-Log Integration*, Geological Society, London, Special Publication, 136, p. 39-51.

Macmillian, D. H. 1966. *Tides*. CR Books Limited, London, 240 p.

Mansoori, J. 1994. A review of basic upscaling procedures: advantages and disadvantages. *In*: Yarus, J. M. and Chambers, R. L. (eds.), *Stochastic Modelling in Geostatistics: principles, methods, and case studies*. AAPG Computer Applications in Geology, No. **3**, p. 65-74.

Martin, A. J. 2000. Flaser and wavy bedding in ephemeral streams: a modern and an ancient example. *Sedimentary Geology* **136**, p. 1-5.

Martinius, A. W., Ringrose, P. S., Næss, A. and Wen, R. 1999. Multi-scale characterization and modeling of heterolithic tidal systems, offshore Mid-Norway. GCSSEPM Foundation 19th Annual Research Conference advance Reservoir Characterization, Advanced Reservoir Characterization, p. 193-204.

Martinius, A. W., Kaas, I., Næss, A., Helgesen, G., Kjærefjord, J. M. and Leith, D. A. 2001. Sedimentology of the heterolithic and tide-dominated Tilje Formation (Early Jurassic, Halten Terrace, offshore mid-Norway). *In*: Martinsen, O. M. and Dreyer, T. (eds.) Sedimentary Environments Offshore Norway - Palaeozoic to Recent. NPF Special Publication **10**, p. 103-144, Elsevier Science B. V, Amsterdam.

Martino, R. L. and Sanderson, D. D. 1993. Fourier and autocorrelation analysis of estuarine tidal rhythmites, Lower Breathitt Formation (Pennsylvanian), eastern Kentucky, USA. *Journal of Sedimentary Petrology,* Vol. **63**, No. 1, p. 105-119.

Matheron, G. 1967. *Elements pour une Theorie des Milieux Poreux*. Masson, Paris.

Mavko, G. and Nur, A. 1997. The effect of percolation threshold in the Kozeny-Carman relation. *Geophysics*, Vol. **62**, No. 5, p. 1480-1482.

McCave, I. N. 1970. Deposition of fine-grained suspended sediment from tidal currents. *Journal of Geophysical Research*, Vol. **75**, No. 21, p. 4151-4159.

McCave, I. N. 1971. Wave effectiveness at the sea bed and its relationship to bedforms and deposition of mud. *Journal of Sedimentary Petrology,* Vol. **41**, No. 1, p. 89-96.

McCreesh, C. A., Ehrlich, R. and Crabree, S. J. 1991. Petropgraphy and reservoir physics II: Relating thin section porosity to capillary pressure, the association between pore types and throat size. *AAPG Bulletin*, Vol. **75**, No. 10, p. 1563-1578.

McKee, E. D. 1957. Flume experiments on the production of stratification and cross-stratification. *Journal of sedimentary Petrology,* Vol. **27**, No. 2, p. 129-134.

McKee, E. D. 1965. Experiments on ripple lamination. *In*: Middleton (ed.), *Primary sedimentary structures and their hydrodynamic interpretation*, Society of Economic Paleontologists and Mineralogists Special Publication No. **12**, p. 66-83.

McKee, E. D. and Weir, G. W. 1953. Terminology for stratification and cross-stratification in sedimentary rocks. *Bulletin of the Geological Society of America*, Vol. **64**, p. 381-389.

McLaren, P. and Bowles, D. 1985. The effects of sediment transport on grain-size distributions. *Journal of Sedimentary Petrology,* Vol. **55**, No. 4, p. 457-470.

Middleton, G. V. 1965a. Introduction. *In*: Middleton (ed.), *Primary sedimentary structures and their hydrodynamic interpretation*, Society of Economic Paleontologists and Mineralogists Special Publication No. **12**.

Middleton, G. V. (ed.). 1965b. *Primary sedimentary structures and their hydrodynamic interpretation*, Society of Economic Paleontologists and Mineralogists Special Publication No. **12**.

Middleton, G. V. 1976. Hydraulic interpretation of sand size distributions. *Journal of Geology*, Vol. **84**, p. 405-426.

Middleton, G. V. and Southard, J. B. 1977. *Mechanics of sediment movement*. Lecture notes SEPM Short course No. **3**.

Miller, D. J. and Eriksson, K. A. 1997. Late Mississippian prodeltaic rhythmites in the Appalachian basins: A hierarchical record of tidal and climatic periodicities. *Journal of Sedimentary Petrology*, Vol. **67**, No. 4, p. 653-660.

Miller, M. C., McCave, I. N., and Komar, P. D. 1977. Threshold of sediment motion under unidirectional currents. *Sedimentology*, **35**, p. 507-527.

Molgatt, M. and Arnott, R. W. C. 2001. Combined tide and wave influence on the sedimentation patterns in the Upper Jurassic Swift Formation, south-eastern Alberta. *Sedimentology*, **48**, p. 1353-1369.

Monicard, R. P. 1980. *Properties of reservoir rocks: Core analysis*. Institut Francais du Pétrole Publications, Editions Technip ISBN: 2-7108-0387-9.

Moss, B. P. 1997. The partitioning of petrophysical data: a review. *In*: Lovell, M. A. and Harvey, P. K. (eds.), *Developments in Petrophysics*, Geological Society Special Publication No. **122**, p. 181-252.

Munson. B. R., Young, D. F. and Okiishi, T. H. 1994. *Fundamentals of fluid mechanics*, 3. rd edition. Wiley, New York.

Napiorkowski, M. and Hemmer, P. C. 1980. Correlated percolation on quadratic lattice. *Physics Letters*, Vol. **76A**, No. 5,6, p. 359-361.

Narasimhan, T. N. A note on volume-averaging. 1983. *In*: Pinder, G. F. (ed.) *Flow through porous media, Recent Developments*. A Computational Mechanics Publication Publications, ISBN 0 905451 06 6, p. 46-50.

Nio, A-D. and Yang, C-S. 1991. Diagnostic attributes of clastic tidal deposits: a review. *In*: Smith, D. G., Reinson, G. E., Zaitlin, B. A. and Rahmani, R. A. (eds.) *Clastic Tidal Sedimentology.* Canadian Society of Petroleum Geologist, Memoir **16,** p. 3-28.

Norris, R. J. and Lewis, J. J. M. The geological modelling of effective permeability in complex heterolithic facies. Paper presented at the 66th Annual Technical Conference and Exhibition, Dallas October 6-9, p. 359-374, *SPE 22692*.

Nottinger, B. 1994. The effective permeability of a heterogeneous porous medium. *Transport in Porous Media*, Vol. **15**, p. 99-127.

Nutting, P. G. 1930. Physical analysis of oil sands. *Bulletin of the American Association of Petroeum Geology* **14**, p. 1337-1349.

Olea, R. A. 1991. *Geostatistical glossary and multilingual dictionary.* International Association for Mathematical Geology Studies in Mathematical Geology, No. **3**. Oxford University Press.

Olea, R. A. 1994. Fundamentals of semivariogram estimation, modelling and usage. *In*: Yarus, J. M. and Chambers, R. L. (eds.), *Stochastic Modelling in Geostatistics: principles, methods, and case studies.* AAPG Computer Applications in Geology, No. **3**, p. 27-35.

Oost, A. P., de Haas, H., van den Boogert, J. M. and de Boer, P. L. 1993. The 18.6 yr nodal cycle and its impact on tidal sedimentation. *Sedimentary Geology*, **87**, p. 1-11.

Oost, A. P. and Baas, J. H. 1994. The development of small scale bedforms in tidal environments: an empirical model for unsteady flow and its applications. *Sedimentology*, **41**, p. 883-903.

Panda, M. N. and Lake, L. W. 1994. Estimation of single phase permeability from parameters of particle-size distribution. *AAPG Bulletin*, Vol. **78**, p. 1028-1039.

Panda, M. N. and Lake, L. W. 1995. A physical model of cementation and its effects on single-phase permeability. *AAPG Bulletin*, Vol. **79**, p. 431-443.

Panda, M. N., Mosher, C. and Chopra, A. K. 2001. Reservoir modeling using scale-dependent data. *SPE Journal*, **June**, p. 157-170, *SPE 71311*.

Paola, C. and Borgman, L. 1991. Reconstructing random topography from preserved stratification. *Sedimentology*, **38**.

Paola, C., Heller, P. L., and Angevine, C. L. 1992. The large-scale dynamics of grain-size variation in alluvial basins, 1, Theory. *Basin Research*, Vol. **4**.

Pedersen, T., Harms, J. C., Harris, N. B., Mitchell, R. W. and Tooby, K. M. 1987. The role of correlation in generating the Heidrun Field geological model. *In*: Collinson, J. D. (ed.), *Correlation in Hydrocarbon Exploration*, proceedings of the conference Correlation in Hydrocarbon Exploration organized by the Norwegian Petroleum Society (NPF), Bergen, Norway, 3-5 October.

Pejrup, M. 1988. The triangular diagram used for classification of estuarine sediments: A new approach. *In*: de Boer, P. L., van Gelder, A and Nio, S. D. (eds.), *Tide-influenced Sedimentary Environments and Facies*, D. Reidel Publishing Company, p. 289-300.

Pejrup, M. 1991. The influence of flocculation on cohesive sediment transport in microtidal estuary. *In*: Smith, D. G., Reinson, G. E., Zaitlin, B. A. and Rahmani, R. A. (eds.) *Clastic Tidal Sedimentology.* Canadian Society of Petroleum Geologist, Memoir **16**, p. 283-290.

Perillo, G. M. E. 1995. Definitions and geomorphologic classifications of estuaries. *In*: Perillo, G. M. E. (ed.) *Geomorphology and Sedimentology of Estuaries*. Developments in Sedimentology **53**. Elsevier Science B. V.

Pettijohn, F. J., Potter, P. E. and Siever, R. 1972. *Sand and Sandstone*. Springer Verlag, New York. p. 618.

Pickup, G. E., Jensen, J. L., Ringrose, P. S, and sorbie, K. S. 1992. A method for calculating permeability tensors using perturbed boundary conditions. *Proceedings from the 3rd European Conference on the Mathematics of Oil Recovery*, Delft University Press.

Pickup, G. E., Ringrose, P. S., Jensen, J. L. and Sorbie, K. S. 1994. Permeability tensors for sedimentary structures. *Mathematical Geology*, Vol. **26**, No. 2. p. 227-250.

Pickup, G. E., Ringrose, P. S., Corbett, P. W. M., Jensen, J. L. and Sorbie, K. S. 1995. Geology, geometry and effective flow. *Petroleum Geoscience*, Vol. **1**, p. 37-42.

Pickup, G. E. and Carruthers, D. 1996. Effective flow parameters for 3D reservoir simulation. *Presented at the European 3-D Reservoir Modelling Conference*, Stavanger, Norway, p. 143-151, *SPE 35495*.

Pickup, G. E., Hern, C. Y., Ma, J., Gardiner, A. R. and Morgan, B. E. F. 1999. The effect of bounding surfaces and laminae on flow parameters in aeolian sequences. *In*: Lippard, S. J., Næss, A. and Sinding-Larsen, R. (eds.), *Proceedings IAMG*, Trondheim, p. 747-753.

Pickup, G. E., Ringrose, P. S. and Sharif, A. 2000. Steady-state upscaling: from lamina-scale to full-field model. *SPE Journal*, Vol. **5**, No. 2, p. 208-217.

Prasad, M. 2003. Velocity-Permeability relations within hydraulic units. *Geophysics*, Vol. **68**, No. 1, p. 108-117.

Pugh, D. T. 1987. *Tides, surges and mean sea-level*. John Wiley and Sons, Chichester: 472 pp.

Pryor, W. A. 1973. Permeability-Porosity patterns and variations in some Holocene sand bodies. *AAPG Bulletin*, Vol. **57**, No. 1, p. 162-189.

Reading, H. G. and Collinson, J. D. 1996. Clastic coasts. *In*: Reading, H. G. (ed.), *Sedimentary Environments, Processes, Facies and Stratigraphy*, 3 rd. edition, Blackwell Science.

Reineck, H-E. and Wunderlich, F. 1968. Classification and origin of flaser and lenticular bedding. *Sedimentology*, **11**, p. 99-104.

Reineck, H.-E. and Singh, I. B. 1980. *Depositional Sedimentary Environments. With reference to terrigenous clastics*. Second version. Springer-Verlag.

Renard, Ph. and de Marsily, G. 1997. Calculating equivalent permeability: a review. *Advances in Water Resources*, **20**, No. 5-6, p. 253-278.

Rider, M. 1996. *Geological Interpretation of Well Logs*. 2nd. edition. Whittles Publishing.

Ringrose, P. S., Pickup, G. E., Jensen, J. L, and Forrester, M. 1999a. The Ardoss reservoir gridblock analog: sedimentology, statistical representative and flow upsclaing. *In*: Schatzinger, R. and Jordan, J. (eds.), *Reservoir Characterization - recent Advances*, AAPG Memoir **71**, p. 265-276.

Ringrose, P., Sharif, A., Munkerud, P. K. and Næss, A. 1999b. Multi-scale assessment of gas/oil displacement in a thinly-layered (tidal) reservoir system. *Presented at the EAGE 61st Conference and Technical Exhibition*, Helsinki, Finland.

Ringrose, P. S., Skjetne, E. and Elfenbein, C. 2003. Permeability estimation functions based on forward modeling of sedimentary heterogeneity. Paper *SPE 84275* presented at the SPE Annual Technical Conference and Exhibition, Denver, Colorado, 5-8 October 2003.

Ringrose, P., Nordahl, K. and Wen, R. 2004. Vertical permeability estimation in tidal deltaic reservoir systems. *Submitted to Petroleum Geoscience*.

Roberson, G. M. and McPhee, C. A. 1990. High resolution probe permeability: an aid to reservoir description. *In*: Worthington (ed.), *Advances in core evaluation: accuracy and precision in reserves estimation*. Proceedings from the First Society of Core Analysts European Core Analysis Symposium, London, p. 495-520.

Robertson, R. W. and Caudle, B.H. 1971. Permeability continuity of laminae in the Calvin Sandstone. *Journal of Petroleum Technology*, **June**, p. 661-670.

Rogers, S. J., Fang, J. H., Karr, C. L., and Stanley, D. A. 1992. Determination of lithology from well logs using a neural network. *AAPG Bulletin*, **Vol**. 76, no. 5, p. 731-739.

Ross, M. A. and Mehta, A. J. 1991. Fluidization of soft estuarine mud by waves. *In*: Bennet, R. H., Bryant, W. R. and Hulbert, M. H., *Microstructure of Fine-grained Sediments: From mud to shale*. Springer Verlag, New York.

Rubin, D. M. and Hunter, R. E. 1982. Bedform climbing in theory and nature. *Sedimentology*, **29**, p. 121-138.

Rubin, D. M. 1987. *Cross-bedding, Bedforms, and Paleocurrents. Concepts in Sedimentology and Paleontology*, Volume 1, Society of Economic Paleotologists and Mineralogists (Special Publication).

Rubin, Y., Gomez-Hernandez, J. J. and Journel, A. G. 1991. Analysis of upscaling and effective properties in disordered media. *In*: Lake, L. W., Carroll, H. B. and Wesson, T. C. (eds.) *Reservoir Characterization II*. Academic Press, San Diego, p. 251-276.

Sahimi, M. 1995. Flow and transport in porous media and fractured rock. From classical methods to modern approaches. VCH Verlagsgesellschaft mbH, Weinheim. ISBN 3-527-29260-8

Schatzinger, R. A. and Tomutsa, L. 1999. Multiscale heterogeneity characterization of tidal channel, tidal delta, and foreshore facies, Almond Formation outcrops, Rock Springs Uplift, Wyoming. *In*: Schatzinger, R. A and Jordan, J. (eds.), *Reservoir Characterization - recent Advances*, AAPG Memoir **71**, p. 45-56.

Scheidegger, A. E. 1974. *The physics of flow through porous media*. Third Edition. University of Toronto Press

Schwartz, L. M., Martys, N., Bentz, D. P., Garboczi, E. J. and Torquato, S. 1993. Cross-porperty relations and permeability estimation in model porous media. *Physical Review E*, Vol. **48**, No. 6., p. 4584-4591.

Serra, O. 1984a. *Fundamentals of well-log interpretation, 1. The acquisition of logging data*. Elsevier.

Serra, O. 1984b. *Fundamentals of well-log interpretation, 2. The interpretation of logging data.* Elsevier.

Simons, D. B., Richardson, E. V., Nordin, C. F. Jr. 1965. Sedimentary structures generated by flow in alluvial channels. *In*: Middleton (ed.), *Primary sedimentary structures and their hydrodynamic interpretation*, Society of Economic Paleontologists and Mineralogists Special Publication No. **12**, p. 34-52.

Smith, D. G. 1988. Modern point bar deposits analogous to the Athabasca oil sands, Canada. *In*: de Boer, P. L., van Gelder, A and Nio, S. D. (eds.), *Tide-influenced Sedimentary Environments and Facies*, D. Reidel Publishing Company.

Smith, D. G., Reinson, G. E., Zaitlin, B. A., and Rahmani, R. A. (eds.) 1991. *Clastic tidal sedimentology*, Canadian Society of Petroleum Geologist Memoir **16**.

Smith, D. S. 1971. Pseudo-planar stratification produced by very low amplitude sand waves. *Journal of Sedimentary Petrology*, **41**, p. 69-73.

Smith, E. H. 1991. The influence of small-scale heterogeneity on average relative permeability. *In*: Lake, L. W., Carroll, H. B. and Wesson, T. C. (eds.) *Reservoir Characterization II*. Academic Press, San Diego. p. 52-76.

Smith, N. D. 1971. Transverse bars and braiding in the Lower Platte River, Nebraska. *Geological Society of America Bulletin*, Vol. **82**, p. 3407-3420.

Smith, N. D., Phillips, A. C., and Powell, R. D. 1990. Tidal drawdown: A mechanism for producing cyclic sediment laminations in glaciomarine deltas. *Geology*, Vol. **18**, p. 10-13.

Sonett, C. P., Finney, S. A., and Williams, C. R. 1988. The lunar orbit in the later Precambrian and the Elatina sandstone laminae. *Nature*, Vol. **335**, p. 806-808.

Southard, J. B. and Dingler, J. R. 1971. Flume study of ripple propagation behind mounds on flat sand beds. *Sedimentology*, **16**, p. 251-263.

Southard, J. B. and Boguchwal, L. A. 1973. Flume experiments on the transition from ripples to lower flat bed with increasing sand size. *Journal of Sedimentary Petrology*, Vol. **43**, No. 4, p. 1114-1121.

Southard, J. B and Boguchwal, L. A. 1990. Bed configurations in steady unidirectional water flows. Part 2. Synthesis of flume data. *Journal of Sedimentary Petrology*, Vol. **60**, No. 5, p. 658-679.

Sposito, G., Gupta, V. K. and Bhattacharya, R. N. 1983. Foundational theories of solute transport in porous media: a critical review. *In*: Pinder, G. F. (ed.) *Flow through porous media, Recent Developments*. A Computational Mechanics Publication Publications, ISBN 0 905451 06 6, p. 76-85.

Srivastava, R. M. 1994. An overview of stochastic methods for reservoir characterization. *In*: Yarus, J. M. and Chambers, R. L. (eds.), *Stochastic Modelling in Geostatistics: principles, methods, and case studies*. AAPG Computer Applications in Geology, No. **3**, p. 3-16.

Stalkup, F. I. 1986. Permeability variations observed at the faces of crossbedded sandstone outcrops. *In*: Lake, L. W. and Caroll, H. B. (eds) *Reservoir Characterization*. Academic Press, Orlando, p. 141-179.

Stauffer, D. and Aharony, A. 1992. Introduction to percolation theory. Second edition. Taylor & Francis Ltd. ISBN 0-7484-0027-3

Storms, J. E. A., van Dam, R. L. and Leclair, S. F. 1999. Preservation of cross-sets due to migration of current ripples over aggrading and non-aggrading beds: comparison of experimental data with theory. *Sedimentology*, **46**, p. 189-200.

Stride, A. H. 1965. Preservation of some marine current-bedding. *Nature*, Vol. **206**, p. 498.

Stupples, P. 2002. Tidal cycles preserved in late Holocene tidal rhythmites, the Wainway Channel, Romney Marsh, southeast England. *Marine Geology*, Vol. **182**, p. 231-246.

Sun, D., Bloemendal, J. Rea, D. K., Vandenberghe, J. Jiang, F., An, Z and Su, R. 2002. *Sedimentary Geology* **152**, p. 263-277.

Terwindt, J. H. J. 1971. Lithofacies of inshore estuarine and tidal inlet deposits. *Geologie en Mijnbouw*, Vol. **50** (3), p. 515-526.

Terwindt, J. H. J., Breusers, H. N. C. and Svasek, J. N. 1968. Experimental investigation on the erosion-sensitivity of a sand-clay lamination. *Sedimentology*, **11**, p. 105-114.

Terwindt, J. H. J and Breusers, H. N. C. 1972. Experiments on the origin of flaser, lenticular and sand-clay alternating bedding. *Sedimentology*, **19**, No. 1/2, p. 85-98.

Terwindt, J. H. J and Breusers, H. N. C. 1982. Discussion: Flume experiments on the origin of flaser bedding. *Sedimentology*, **29**, p. 903-907.

Terwindt, J. H.L. 1988. Palaeo-tidal reconstruction of inshore tidal depositional environments. *In*: de Boer, P. L., van Gelder, A and Nio, S. D. (eds.), *Tide-influenced Sedimentary Environments and Facies*, D. Reidel Publishing Company, p. 233-263.

Tessier, B. 1993. Upper intertidal rhythmites in the Mont-Saint-Michel Bay (NW France): Perspectives for paleoreconstruction. *Marine Geology*, **110**, p. 355-367.

Tessier, B. 1998. Tidal cycles: Annual versus semi-lunar records. *In*: Alexander, C. R, Davis, R. A., and Henry, V. J. (eds.), *Tidalites: Processes and Products*, SEPM Special Publication No. **61**, p. 69-74.

Tessier, B., Archer, A. W., Lanier, W. P. and Feldman, H. R. 1995. Comparison of ancient tidal rhythmites (Carbonifereous of Kansas and Indiana, USA) with modern analogues (the Bay of Mont-Saint-Michel, France). *In*: Flemming, B. W. and Bartholomã (eds.) *Tidal Signatures in Modern and Ancient Sediments*, Special Publication Number **24** of the International Association of Sedimentologists, p. 259-271.

Tessier, B. and Gigot, P. 1989. A vertical record of different tidal cyclicities: an example from the Miocene Marine Molasse of Digne (Haute Provence, France). *Sedimentology*, **36**, p. 767-776.

Tetzlaff, D. M. and Harbaugh, J. W. 1989. *Simulating clastic sedimentation*. Van Nostrand Reinhold, New York. 402 p.

Tetzlaff, D. M. 1991. The combined use of sedimentary process modelling and statistical simulation in reservoir characterization. *SPE 22759* presented at the 66th Annual Technical Conference and Exhibition of the Society of Petroleum Engineers, Dallas, p. 937-945.

Theys, P. 1999. *Log data acquisition and quality control*, 2nd edition. Editions Technip, France. ISBN: 2-7108-0748-3.

Thomas, S., Corbett, P. and Jensen, J. 1996. Permeability and permeability anisotropy characterisation in the near wellbore: a numerical model using the probe permeameter and micro-resistivity image data. *Presented at the 37th SPWLA Annual Logging Symposium*, paper **JJJ**.

Thomas, S. D., Corbett, P. and Jensen, J. 1997. Permeability, anisotropy estimation within the Sherwood Sandstone, Morecambed Bay gas field: a numerical approach using probe permeametry. *In*: Oakman, C. D., Martin, J. H. and Corbett, P. W. M (eds.), *Cores from the Northwest Hydrocarbon Province: An illustration of the geological applications from exploration to development*, p. 197-203.

Thorsæter, O. and Abrahi, M. 2000. *Experimental reservoir engineering laboratory workbook*. Department of Petroleum Engineering and Applied Petrophysics, Norwegian University of Science and Technology.

Tiab, D. and Donaldson, E. C. 1996. *Petrophysics: Theory and practice of measuring reservoir rock and fluid transport properties*. Gulf Publishing Company, Houston, Texas, ISBN: 0-88415-634-6.

Tidwell, V. C. and Wilson, J. L. 1999. Permeability upscaling measured on a block of Berea Sandstone: Results and interpretation. *Mathematical Geology*, Vol. **31**, No. 7, p. 749-769.

Tidwell, V. C. and Wilson, J. L. 2000. Heterogeneity, permeability patterns, and permeability upscaling: physical characterization of a block of Massillon Sandstone exhibiting nested scales of heterogeneity. *SPE Reservoir Evaluation and Engineering*, Vol. **3**, No. 4, p. 283-291.

Tittman, J 1986. *Geophysical well logging*. Academic Press, Orlando.

Troutman, B. M. and Williams, G. P. 1987. Fitting straight lines in the earth science. *In*: Size, W. B. (ed.), *Use and Abuse of Statistical Methods in the Earth Science*. International Association for Mathematical Geology Studies in Mathematical Geology No. 1. Oxford University Press, p. 107-128.

Uhlir, D. M., Akers, A., and Vondra, C. F. 1988. Tidal inlet sequence, Sundance Formation (Upper Jurassic), north-central Wyoming. *Sedimentology*, **35**, p. 739-752.

van den Berg, J. H. 1981. Rhythmic seasonal layering in a mesotidal channel fill sequence, Oosterschelde Mouth, the Netherlands. *In*: Nio, S. D., Schõttenhelm, R. T. E. and van Weering, Tj. C. E. (eds.) *Holocene marine sedimentation on the north sea basin*. Special Publication International Association of Sedimentologists Number **5**, p. 147-159.

van Wagooner, J. C., Mitchum, R. M., Campion, K. M. and Rahmanian, V. D. 1990. Siliciclastic sequence stratigraphy in Well Logs, Cores and Outcrops, *AAPG Methods in Exploration Series*, No. **7**, American Association of Petroleum Geologists, Tulsa, Oklahoma, 55p.

Visher, G. S. 1965. Fluvial processes as interpreted from ancient and recent fluvial deposits. *In*: Middleton (ed.), *Primary sedimentary structures and their hydrodynamic interpretation*, Society of Economic Paleontologists and Mineralogists Special Publication No. **12**, p. 116-132.

Visher, G. S. 1969. Grain size distributions and depositional processes. *Journal of Sedimentary Petrology*, Vol. **39**, No. 3., 1074-1106

Visser, M. J. 1980. Neap-spring cycles reflected in Holocene subtidal large-scale deposits: a preliminary note. *Geology*, Vol. **8**, p. 543-546.

Walker, R. G. 1984. General Introduction: Facies, Facies sequences and Facies models, *In*: Walker, R. G. (ed.), Facies Models, 2nd. edition, Geoscience Canada, Reprint Series 1, p. 1-9.

Wallbridge, S., Voulgaris, G., Tomlinson, B. N. and Collins, M. B. 1999. Initial motion and pivoting characteristics of sand particles in uniform and heterogeneous beds: experiments and modelling. *Sedimentology*, **46**, p. 17-32.

Walpole, R. E., Myers, R. H. and Myers, S. L. 1998. *Probability and Statistics for Engineers and Scientists*. Sixth edition. Prentice Hall International, Inc.

Warren, J. E. and Price, H. S. 1961. Flow in heterogeneous porous media. *Society of Petroleum Engineer Journal*, **1**, p. 153-169.

Weaver, C. E. 1989. *Clays, muds and shales*. Developments in Sedimentology **44**, Elsevier Amsterdam.

Webb, E. K. 1994. Simulating the three-dimensional distribution of sediment units in braided-stream deposits. *Journal of Sedimentary Research*, Vol. **62**, 2.

Weber, K. J. 1982. Influence of common sedimentary structures on fluid flow in reservoir models. *Journal of Petroleum technology*, Vol. 44, p. 665-672.

Weber, K. J. 1986. How heterogeneity affects oil recovery. *In*: Lake, L. W. and Caroll, H. B. (eds) *Reservoir Characterization*. Academic Press, Orlando, p. 487-544.

Wells, J. T. 1995. Tide-dominated estuaries and tidal bars. *In*: Perillo, G. M. E. (ed.) *Geomorphology and Sedimentology of Estuaries*. Developments in Sedimentology **53**, Elsevier Amsterdam.

Wen, R. Martinius, A. W., Næss, A. and Ringrose, P. 1998. Three-dimensional simulation of small-scale heterogeneity in tidal deposits - a process-based stochastic simulation method. *In*: Buccianti, A, Nardi, G. and Potenza, R. (eds.) *Proceedings of the 4th Annual Conference of the International Association of Mathematical Geology (IAMG)*, Ischia, p. 129-134.

Wendt, W. A, Sakurai, S. and Nelson, P. H. 1986. Permeability prediction from well logs using multiple regression. *In*: Lake, L. W. and Caroll, H. B. (eds) *Reservoir Characterization*. Academic Press, Orlando, p. 181-221.

Werner, F. E. 1992. Tidal Hydrodynamics, Quantitative Aspects. *In*: Nierenberg, W. A. (ed.), *Encyclopedia of Earth System Science*, Academic Press, Inc., San Diego, California.

Williams, G. E. 1989. Late Precambrian tidal rhythmites in South Australia and the history of the Earth's rotation. *Journal of the Geological Science*, London, Vol. **146**, p. 97-111.

Williams, G. E. 1991. Upper Proterozoic tidal rhythmites, South Australia: sedimentary features, deposition, and implications for the Earth's paleorotation. *In*: Smith, D. G., Reinson, G. E., Zaitlin, B. A. and Rahmani, R. A. (eds.) *Clastic Tidal Sedimentology.* Canadian Society of Petroleum Geologist, Memoir **16**, p. 161-178.

Williams, G. P. 1983. Improper use of regression equations in earth science. *Geology*, Vol. **11**, 195-197.

Williams, N. H., Gardiner, A. R. and Jensen, J. L. 1999. Inter-relationship between measurement scale, sampling rate and sedimentary heterogeneity in fluvio-aeolian succession permeability variograms. *In*: Lippard, S. J., Næss, A, and Sinding-Larsen, R. (eds.) *Proceedings of the 5th Annual Conference of the International Association of Mathematical Geology (IAMG)*, Trondheim.

Wolanski, E., Chappell, J., Ridd, P. and Vertessy, R. 1988. Fluidization of mud in estuaries. *Journel of Geophysical Research*, Vol. **93**, No. C3, p. 2351-2361.

Wong, P. M. 1999. Permeability prediction from well logs using an improved windowing technique. *Journal of Petroleum Geology*, Vol. **22**, No. 2, p. 215-226.

Worthington, P. F. 1991. Reservoir characterization at the mesoscopic scale. *In*: Lake, L. W., Carroll, H. B. and Wesson, T. C. (eds.) *Reservoir Characterization II*. Academic Press, San Diego, p. 123-165.

Worthington, P. F. 1994. Effective integration of core and log data. *Marine and Petroleum Geology*, Vol. **11**, No. 4, p. 457-466.

Worthington, P. F. 1997. Petrophysical estimation of permeability as a function of scale. *In*: Lovell, M. A. and Harvey, P. K. (eds.) *Developments in Petrophysics*, Geological Special Publication No. **122**, p. 159-168.

Worthington, P. F. 1998. Conjunctive interpretation of core and log data through association of the effective and total porosity models. *In*: Harvey, P. K. and Lovell, M. A. (eds.), *Core-Log Integration*, Geological Society Special Publication No. **136**, London, p. 213-223.

Worthington, P. F. 2003a. The effect of scale on the petrophysical estimation of intergranular permeability. *Presented at the 44th SPWLA Annual Logging Symposium*, Paper **A**.

Worthington, P. F. 2003b. The role of cut-offs in integrated reservoir studies. *SPE 84387* presented at the SPE Annual Technical Conference and Exhibition, Denver, Colorado, 5-8 October 2003.

Yan, J. 2002. Reservoir parameters estimation from well log and core data: a case study from the North Sea. *Petroleum Geoscience*, Vol. **8**.,p. 63-69.

Yang, C-S. and Nio, S-W. 1985. The estimation of palaehydrodynamic processes from subtidal deposits using time series analysis methods. *Sedimentology*, **32**, p. 41-57.

Yang, C. T. 1996. *Sediment Transport. Theory and Practice*. The McGraw-Hill Companies, Inc. ISBN: 0-07-114882-5

Ye, S-H. and Rabiller, P. 2000. A new tool for electro-facies analysis: milt-resolution graph-based clustering. *Presented at SPWLA 41st Annual Logging Symposium*, paper **PP**.

Yoshida, S., Johnson, H. D., Jackson, M. D., and Martinius, A. W. 1999. Quantification of heterogeneities within tidal sandstone outcrops: analogue study for subsurface reservoir characterization. *In*: Lippard, S. J., Næss, A, and Sinding-Larsen, R. (eds.) *Proceedings of the 5th Annual Conference of the International Association of Mathematical Geology (IAMG)*, Trondheim, p. 127-133.

Yoshida, S., Jackson, M. D., Johnson, H. D., Muggeridge, A. H. and Martinius, A. W. 2001. Outcrop studies of tidal sandstones for reservoir characterization (Lower Cretaceous Vectis Formation, Isle of Wight, southern England). *In*: Martinsen, O. M. and Dreyer, T. (eds.) *Sedimentary Environments Offshore Norway - Palaeozoic to Recent*. NPF Special Publication **10**, p. 103-144, Elsevier Science B. V, Amsterdam.

Zhang, P., Ringrose, P., Langeland, H., Nordahl, K., Elfenbein, C., Næss, A. 2004. Permeability rescaling and near-wellbore modeling of heterogeneities in the Lower Jurassic tidal-influenced Tilje Formation, Heidrun Field. To be presented at the SPWLA 45th Annual Logging Symposium, June 6-9.

Appendix A Reference Parameters

The following tables list the control parameters that were used to create the near well-bore models in this thesis.

A.1 Geometrical reference parameters

Control parameter	Sub-facies model	LF7.2_WB	LF7.2_LTW	LF_7.2_RunOffSand	LF7.1_WSF	LF7.1_PPL
Bedform_1_Wavelength/X-dir (HCS)	Mean (StDev)	20 (1)	19 (0.9)	20 (0.2)	20 (1)	
Bedform_1_Amplitude/X-dir (HCS)	Mean (StDev)	0.2 (0.05)	0.19 (0.045)	0.4 (0.01)	0.2 (0.05)	
Bedform_1_Symmetry	Mean (StDev)	0.4 (0.05)	0.4 (0.045)	0.4 (0.01)	0.4 (0.05)	
Bedform_1_Steepness	Mean (StDev)	0.2 (0.05)	0.2 (0.045)	0.2 (0.01)	0.2 (0.05)	
CrestSinuosity_1_1_Wavelength	Mean (StDev)	20 (0.5)	22.5 (0.5)	20 (0.5)	20 (0.5)	
CrestSinuosity_1_1_Amplitude	Mean (StDev)	5 (0.2)	4.5 (0.2)	5 (0.2)	5 (0.2)	
CrestSinuosity_1_2_Wavelength	Mean (StDev)	30 (0.6)	32.5 (0.6)		30 (0.6)	
CrestSinuosity_1_2_Amplitude	Mean (StDev)	3 (0.1)	2.75 (0.1)		3 (0.1)	
Migration Speed_1_Ebb/Sand:x-bed	Mean (StDev)	5 (0.5)	5 (0.5)	5 (0.5)	5 (0.5)	
Migration_Direction_1_Ebb/Sand:x-bed	Mean (StDev)	0 (5)	0 (5)	0 (10)	0 (5)	
Migration Speed_1_Flood/X-dir (HCS)	Mean (StDev)	5 (0.5)	5 (0.5)		5 (0.5)	
Migration_Direction_1_Flood	Mean (StDev)	180 (5)	180 (5)		180 (5)	
Bedform_2_Wavelength/Y-dir (HCS)	Mean (StDev)	18 (0.5)	17 (0.45)	18 (0)	18 (0.5)	
Bedfrom_2_Amplitude/Y-dir (HCS)	Mean (StDev)	0.18 (0.05)	0.17 (0.045)	0.3 (0)	0.18 (0.05)	
Bedform_2_Symmetry	Mean (StDev)	0.4 (0.05)	0.4 (0.045)	0.4 (0)	0.4 (0.05)	
Bedform_2_Steepness	Mean (StDev)	0.2 (0.05)	0.2 (0.045)	0.2 (0)	0.2 (0.05)	
CrestSinuosity_2_1_Wavelength	Mean (StDev)	20 (0.5)	22.5 (0.5)	18 (0.5)	20 (0.5)	
CrestSinuosity_2_1_Amplitude	Mean (StDev)	5 (0.2)	4.5 (0.2)	4 (0.2)	5 (0.2)	
CrestSinuosity_2_2_Wavelength	Mean (StDev)					
CrestSinuosity_2_2_Amplitude	Mean (StDev)					
Migration Speed_2_Ebb/Sand:x-bed	Mean (StDev)	4 (0.5)	4 (0.5)	4 (0.4)	4 (0.5)	
Migration_Direction_2_Ebb/Sand:x-bed	Mean (StDev)	0 (5)	0 (5)	0 (5)	0 (5)	
Migration Speed_2_Flood/Y-dir (HCS)	Mean (StDev)	4 (0.5)	4 (0.5)		4 (0.5)	
Migration_Direction_2_Flood	Mean (StDev)	180 (5)	180 (5)		180 (5)	
Number of Lamina (HCS)	Mean (StDev)					
Crest Thickness (HCS)	Mean (StDev)					
Trough Thickness (HCS)	Mean (StDev)					0.13 (0.05;0.1 82;0.025)
Sand Lamina thickness (parallel bedding)	Mean (Amp;Phase;WL;StDev)					0.05 (0;0;0;0)
Mud Lamina thickness (parallel bedding)	Mean (Amp;Phase;WL;StDev)					
Depositional Rate Sand	Mean (Amp;Phase;WL;StDev)	0.165 (0.01)	0.14 (0.01)	0.4 (0.1)	0.3	
Depositional Rate Mud	Mean (Amp;Phase;WL;StDev)	0.21 (0.01)	0.23 (0.1)		0.1	
Depositional Length Sand	Mean (Amp;Phase;WL;StDev)	2.15 (0.1)	1.8 (0.1)	3 (1)	70 (0.1)	
Depositional Length Mud	Mean (Amp;Phase;WL;StDev)	4.76 (0.1)	4.8 (0.1)		7.5 (1)	

FIGURE A.1 *Control parameters describing the geometry of the bedforms of the selected interval.*

Control parameter	Sub facies model	LF3_LTW	LF42_LTW	LF42_WSF	LF4.2_HCS (and LF4.2_HCS_Mud)	LF1.2	LF1.3_HCS (and LF1.3_HCS_Mud)
Bedform_1_Wavelength/X-dir (HCS)	Mean (StDev)	20 (1)	15 (1)	15 (1)	100 (5)	100 (5)	100 (5)
Bedform_1_Amplitude/X-dir (HCS)	Mean (StDev)	0.2 (0.05)	0.2 (0.05)	0.25 (0.05)	2 (0.5)	3 (0.5)	2 (0.5)
Bedform_1_Symmetry	Mean (StDev)	0.4 (0.05)	0.4 (0.05)	0.4 (0.05)		0.5 (0.01)	
Bedform_1_Steepness	Mean (StDev)	0.2 (0.05)	0.2 (0.05)	0.2 (0.05)		0.4 (0.01)	
CrestSinuosity_1_1_Wavelength	Mean (StDev)	20 (0.5)	20 (0.5)	20 (0.5)		100 (10)	
CrestSinuosity_1_1_Amplitude	Mean (StDev)	5 (0.2)	0.5 (0.2)	0.5 (0.2)		5 (0.5)	
CrestSinuosity_1_2_Wavelength	Mean (StDev)	30 (0.6)	30 (0.6)	30 (0.6)			
CrestSinuosity_1_2_Amplitude	Mean (StDev)	3 (0.1)	3 (0.1)	3 (0.1)			
Migration Speed_1_Ebb/Sand:x-bed	Mean (StDev)	5 (0.5)	5 (0.5)	5 (0.5)		5 (0.2)	
Migration_Direction_1_Ebb/Sand:x-bed	Mean (StDev)	0 (5)	0 (5)	0 (5)		0 (0)	
Migration Speed_1_Flood/X-dir (HCS)	Mean (StDev)	5 (0.5)	5 (0.5)	5 (0.5)	10 (1)		10 (1)
Migration_Direction_1_Flood	Mean (StDev)	180 (5)	180 (5)	180 (5)			
Bedform_2_Wavelength/Y-dir (HCS)	Mean (StDev)	18 (0.5)	13 (0.5)	14 (0.5)	100 (5)		100 (5)
Bedfrom_2_Amplitude/Y-dir (HCS)	Mean (StDev)	0.18 (0.05)	0.18 (0.05)	0.23 (0.05)	2 (0.5)		2 (0.5)
Bedform_2_Symmetry	Mean (StDev)	0.4 (0.05)	0.4 (0.05)	0.4 (0.05)			
Bedform_2_Steepness	Mean (StDev)	0.2 (0.05)	0.2 (0.05)	0.2 (0.05)			
CrestSinuosity_2_1_Wavelength	Mean (StDev)	20 (0.5)	20 (0.5)	20 (0.5)			
CrestSinuosity_2_1_Amplitude	Mean (StDev)	5 (0.2)	5 (0.2)	5 (0.2)			
CrestSinuosity_2_2_Wavelength	Mean (StDev)						
CrestSinuosity_2_2_Amplitude	Mean (StDev)						
Migration Speed_2_Ebb/Sand:x-bed	Mean (StDev)	4 (0.5)	4 (0.5)	4 (0.5)			
Migration_Direction_2_Ebb/Sand:x-bed	Mean (StDev)	0 (5)	0 (5)	0 (5)			
Migration Speed_2_Flood/Y-dir (HCS)	Mean (StDev)	4 (0.5)	4 (0.5)	4 (0.5)	10 (1)		10 (1)
Migration_Direction_2_Flood	Mean (StDev)	180 (5)	180 (5)	180 (5)			
Number of Lamina (HCS)	Mean (StDev)				100 (5)		100 (5)
Crest Thickness (HCS)	Mean (StDev)				0.1		0.1
Trough Thickness (HCS)	Mean (StDev)				0.2		0.2
Sand Lamina thickness (parallel bedding)	Mean (Amp;Phase;WL;StDev)						
Mud Lamina thickness (parallel bedding)	Mean (Amp;Phase;WL;StDev)						
Depositional Rate Sand	Mean (Amp;Phase;WL;StDev)	0.1 (0.05;180;150;0.02)	0.1 (0.01)	0.2 (0.01)		0.4 (0.02)	
Depositional Rate Mud	Mean (Amp;Phase;WL;StDev)	0.2 (0.05;0;150;0.04)	0.22 (0.02)	0.23 (0.015)			
Depositional Length Sand	Mean (Amp;Phase;WL;StDev)	3 (2;180;150;0.5)	2 (0.1)	12 (1)			
Depositional Length Mud	Mean (Amp;Phase;WL;StDev)	5 (0;0;0.5)	4.3 (0.1)	6.3 (0.5)			

FIGURE A.2 *Control parameters describing the geometry of the bedforms of the selected interval.*

A.2 Petrophysical reference parameters

		Porosity			Permeability (ln)		
Model		Sand type 1	Sand type 2	Mud	Sand type 1	Sand type 2	Mud
LF7.2_WB	Mean	0.35	0.2	0.05	2	1	-4.6
	StDev	0.1	0.1	0	0.6	0.2	0
LF7.2_RunOffSand	Mean	0.25	0.2		5	3	
	StDev	0.1	0.1		0.3	0.2	
LF7.2_LTW	Mean	0.35	0.2	0.05	2	1	-4.6
	StDev	0.1	0.1	0	0.6	0.2	0
LF7.1_WSF	Mean	0.25	0.35	0.05	6	1.3	-4.6
	StDev	0.15	0.15	0	4.5	1.1	0
LF7.1_PPL	Mean	0.35	0.3		6.85	4.5	
	StDev	0.02	0.02		0.5	0.2	
LF3_LTW	Mean	0.35	0.2	0.05	1	0	-4.6
	StDev	0.1	0.1	0	0.5	0.5	0
LF4.2_WSF	Mean	0.37	0.32	0.05	5	4	-4.6
	StDev	0.05	0.05	0	1	1	0
LF4.2_LTW	Mean	0.37	0.32	0.05	5	4	-4.6
	StDev	0.05	0.05	0	1	1	0
LF1.3_HCS	Mean	0.3	0.2		3.5	2.7	
	StDev	0.1	0.1		1.2	1	
LF1.3_HCS_Mud	Mean	0.3	0.2	0.05	3.5	2.7	-4.6
	StDev	0.1	0.1	0	1.2	1	0
LF1.2	Mean	0.25	0.2		5	3	
	StDev	0.1	0.1		0.3	0.2	

FIGURE A.3 *Porosity and permeability input data obtained in chapter 6. Note that the permeability values are given as log normal values.*

A.3 Geometrical reference parameterts for conceptual tidal bedding models

Control parameter	Simulated Sand Fraction (mean)	1	0.957102	0.922061			0.9834	0.744	0.716165	0.658466	0.611788	0.499634	0.391054	0.27727	0.198	0.125	0.091364
	Simulated Sand Fraction (ebb/e)	0	0.003099	0.002083			0.007047	0.008145	0.030176	0.010266	0.008974	0.003665	0.000985	0.011098	0.013766	0.008995	0.010318
	Model Name	SF=1	SF=0.95	SF=0.9	SF=0.85	SF=0.80	SF=0.75	SF=0.70	SF=0.65	SF=0.60	SF=0.55	SF=0.50	SF=0.40	SF=0.30	SF=0.20	SF=0.15	SF=0.10
Bedform_1 Wavelength	Mean	20	20	20	20	20	20	20	20	20	20	20	20	20	18	12	9
	StDev	1	1	1	1	1	1	1	1	1	1	1	1	1	1	1	1
Bedform_1_Amplitude	Mean	0.2	0.2	0.2	0.2	0.2	0.2	0.2	0.2	0.2	0.2	0.2	0.2	0.19	0.18	0.17	0.1
	StDev	0.05	0.05	0.05	0.05	0.05	0.05	0.05	0.05	0.05	0.05	0.05	0.05	0.045	0.04	0.035	0.001
Bedform_1_Symmetry	Mean	0.4	0.4	0.4	0.4	0.4	0.4	0.4	0.4	0.4	0.4	0.4	0.4	0.4	0.4	0.4	0.4
	StDev	0.05	0.05	0.05	0.05	0.05	0.05	0.05	0.05	0.05	0.05	0.05	0.05	0.045	0.04	0.035	0.01
Bedform_1_Steepness	Mean	0.2	0.2	0.2	0.2	0.2	0.2	0.2	0.2	0.2	0.2	0.2	0.2	0.2	0.2	0	0
	StDev	0.05	0.05	0.05	0.05	0.05	0.05	0.05	0.05	0.05	0.05	0.05	0.05	0.045	0.04	0.035	0.01
CrestSinuosity_1_1_Wavelength	Mean	20	20	20	20	20	20	20	20	20	20	20	20	22.5	25	30	35
	StDev	0.5	0.5	0.5	0.5	0.5	0.5	0.5	0.5	0.5	0.5	0.5	0.5	0.5	0.5	0.5	0.5
CrestSinuosity_1_1_Amplitude	Mean	5	5	5	5	5	5	5	5	5	5	5	5	4.5	4	3	2
	StDev	0.2	0.2	0.2	0.2	0.2	0.2	0.2	0.2	0.2	0.2	0.2	0.2	0.2	0.2	0.2	0.2
CrestSinuosity_1_2_Wavelength	Mean	30	30	30	30	30	30	30	30	30	30	30	30	32.5	35	37.5	40
	StDev	0.6	0.6	0.6	0.6	0.6	0.6	0.6	0.6	0.6	0.6	0.6	0.6	0.6	0.6	0.6	0.6
CrestSinuosity_1_2_Amplitude	Mean	3	3	3	3	3	3	3	3	3	3	3	3	2.75	2.5	2	1.5
	StDev	0.1	0.1	0.1	0.1	0.1	0.1	0.1	0.1	0.1	0.1	0.1	0.1	0.1	0.1	0.1	0.1
Migration Speed_1_Ebb	Mean	5	5	5	5	5	5	5	5	5	5	5	5	5	5	5	5
	StDev	0.5	0.5	0.5	0.5	0.5	0.5	0.5	0.5	0.5	0.5	0.5	0.5	0.5	0.5	0.5	0.5
Migration_Direction_1_Ebb	Mean	0	0	0	0	0	0	0	0	0	0	0	0	0	0	0	0
	StDev	5	5	5	5	5	5	5	5	5	5	5	5	5	5	5	5
Migration Speed_1_Flood	Mean	5	5	5	5	5	5	5	5	5	5	5	5	5	5	5	5
	StDev	0.5	0.5	0.5	0.5	0.5	0.5	0.5	0.5	0.5	0.5	0.5	0.5	0.5	0.5	0.5	0.5
Migration_Direction_1_Flood	Mean	180	180	180	180	180	180	180	180	180	180	180	180	180	180	180	180
	StDev	5	5	5	5	5	5	5	5	5	5	5	5	5	5	5	5
Bedform_2_Wavelength	Mean	18	18	18	18	18	18	18	18	18	18	18	18	17	15	10	8
	StDev	0.5	0.5	0.5	0.5	0.5	0.5	0.5	0.5	0.5	0.5	0.5	0.5	0.45	0.4	0.035	0.035
Bedform_2_Amplitude	Mean	0.18	0.18	0.18	0.18	0.18	0.18	0.18	0.18	0.18	0.18	0.18	0.18	0.17	0.15	0.1	0.09
	StDev	0.05	0.05	0.05	0.05	0.05	0.05	0.05	0.05	0.05	0.05	0.05	0.05	0.045	0.04	0.035	0.001
Bedform_2_Symmetry	Mean	0.4	0.4	0.4	0.4	0.4	0.4	0.4	0.4	0.4	0.4	0.4	0.4	0.4	0.4	0.4	0
	StDev	0.05	0.05	0.05	0.05	0.05	0.05	0.05	0.05	0.05	0.05	0.05	0.05	0.045	0.04	0.035	0.01
Bedform_2_Steepness	Mean	0.2	0.2	0.2	0.2	0.2	0.2	0.2	0.2	0.2	0.2	0.2	0.2	0.2	0.2	0.2	0
	StDev	0.05	0.05	0.05	0.05	0.05	0.05	0.05	0.05	0.05	0.05	0.05	0.05	0.045	0.04	0.035	0.01
CrestSinuosity_2_1_Wavelength	Mean	20	20	20	20	20	20	20	20	20	20	20	20	22.5	25	30	35
	StDev	0.5	0.5	0.5	0.5	0.5	0.5	0.5	0.5	0.5	0.5	0.5	0.5	0.5	0.5	0.5	0.5
CrestSinuosity_2_1_Amplitude	Mean	5	5	5	5	5	5	5	5	5	5	5	5	4.5	4	3	2
	StDev	0.2	0.2	0.2	0.2	0.2	0.2	0.2	0.2	0.2	0.2	0.2	0.2	0.2	0.2	0.2	0.2
CrestSinuosity_2_2_Wavelength	Mean	0	0	0	0	0	0	0	0	0	0	0	0	0	0	0	0
	StDev	0	0	0	0	0	0	0	0	0	0	0	0	0	0	0	0
CrestSinuosity_2_2_Amplitude	Mean	0	0	0	0	0	0	0	0	0	0	0	0	0	0	0	0
	StDev	0	0	0	0	0	0	0	0	0	0	0	0	0	0	0	0
Migration Speed_2_Ebb	Mean	4	4	4	4	4	4	4	4	4	4	4	4	4	4	4	4
	StDev	0.5	0.5	0.5	0.5	0.5	0.5	0.5	0.5	0.5	0.5	0.5	0.5	0.5	0.5	0.5	0.5
Migration_Direction_2_Ebb	Mean	0	0	0	0	0	0	0	0	0	0	0	0	0	0	0	0
	StDev	5	5	5	5	5	5	5	5	5	5	5	5	5	5	5	5
Migration Speed_2_Flood	Mean	4	4	4	4	4	4	4	4	4	4	4	4	4	4	4	4
	StDev	0.5	0.5	0.5	0.5	0.5	0.5	0.5	0.5	0.5	0.5	0.5	0.5	0.5	0.5	0.5	0.5
Migration_Direction_2_Flood	Mean	180	180	180	180	180	180	180	180	180	180	180	180	180	180	180	180
	StDev	5	5	5	5	5	5	5	5	5	5	5	5	5	5	5	5
Depositional Rate Sand	Mean	0.3	0.305	0.3	0.262	0.25	0.235	0.225	0.21	0.2	0.175	0.15	0.125	0.1	0.09	0.07
	StDev	0.01	0.01	0.01	0.01	0.01	0.01	0.01	0.01	0.01	0.01	0.01	0.01	0.01	0.01	0.01
Depositional Rate Mud	Mean	0	0.08	0.1	0.13	0.14	0.155	0.16	0.17	0.18	0.2	0.22	0.24	0.25	0.26	0.27
	StDev	0	0.01	0.01	0.01	0.01	0.01	0.01	0.01	0.01	0.01	0.01	0.01	0.01	0.01	0.01
Depositional Length Sand	Mean	4	3.75	3.5	3.15	3	2.85	2.75	2.6	2.5	2.25	2	1.75	1.5	1.25	1
	StDev	0.1	0.1	0.1	0.1	0.1	0.1	0.1	0.1	0.1	0.1	0.1	0.1	0.1	0.075	0.05
Depositional Length Mud	Mean	0	3.25	3.5	3.85	4	4.15	4.25	4.4	4.5	4.75	5	5.25	5.5	5.75	6
	StDev	0	0.1	0.1	0.1	0.1	0.1	0.1	0.1	0.1	0.1	0.1	0.1	0.1	0.1	0.1

FIGURE A.4 *Control parameters for the concetual tidal bedding models. The petrophysical properties are listen in table 8.1 and 8.2.*

A.4 Seed numbers

Contrast	SandFraction	Real_1	Real_2	Real_3	Real_4	Real_5	Real_6	Real_7	Real_8	Real_9	Real_10
1:1	100	1055570724	2097067268	624790122	510044318	918453414	1074000303	661998886	2076419658	1813546087	1004702267
1:1	95	1235598586	1690912209	319494001	762954534	1490470336	270398260	1406950374	487095086	1327488506	1401216330
1:1	90	*1054915211*	*1688039839*	*558682835*	*2092364177*	*1206113002*	*394036938*	*458840222*	*1382025544*	*242362157*	*1135946036*
1:1	80	*1054926986*	*1482100474*	*222496900*	*1120141698*	*637780907*	*202538311*	*664020575*	*1930742506*	*2022466330*	*1536166252*
1:1	75	*1054966807*	*1401276317*	*1934553063*	*449277602*	*2080258789*	*764830699*	*1780382051*	*212996933*	*691913485*	*1860381159*
1:1	70	*1054977188*	*1674248593*	*1648407653*	*957391337*	*1614999052*	*1096485550*	*527240974*	*2073260821*	*427971807*	*1057327710*
1:1	65	*1029860577*	*1404052018*	*340251588*	*1968878978*	*1624567790*	*48099961*	*1976416803*	*1321949274*	*386252578*	*1719486673*
1:1	60	*1056141085*	*1792863444*	*1214524736*	*1474497711*	*1414484501*	*461002557*	*1111371221*	*1784768341*	*149509481*	*828444152*
1:1	50	*1056153730*	*1159373022*	*777188863*	*1382543746*	*1305822335*	*90777940*	*2123415290*	*1418522373*	*1095977463*	*426292816*
1:1	40	*1055225178*	*1193880901*	*804793019*	*1265948955*	*1520007234*	*655788997*	*1590814504*	*1236181251*	*864566620*	*680965817*
1:1	30	*1055244364*	*484219598*	*633879395*	*1826957130*	*913779794*	*1359430955*	*292309343*	*480222507*	*1611033975*	*487730944*
1:1	20	*1055309950*	*967058550*	*832271048*	*1440166239*	*1700398648*	*605332333*	*373030363*	*640149316*	*1186971664*	*1648112912*
1:1	15	*1056333511*	*163242444*	*1152200085*	*335266471*	*959691674*	*195795045*	*999987606*	*1984618696*	*2060845185*	*562879715*
1:1	10	*1055396164*	*1379257261*	*929044483*	*1571106194*	*1792671921*	*1045380018*	*951588418*	*690967892*	*1901470133*	*1582284848*
1:2	100	2097067268	1055746985	2097067268	2006378505	844565837	272574613	5292993	1552254964	1151560784	961169778
1:2	95	1359815724	1243394380	441043551	49649061	407705040	224336120	803986657	116032608	733380963	372805686
1:2	90	782962760	1333260204	447746619	1931969633	1623311955	1288969945	1215162839	475958766	1108581901	247026922
1:2	80	1605136024	668675129	203493466	27412547	458064726	34496263	669340374	450794623	1762669435	242530129
1:2	75	364343629	1459575393	1338436929	1268094500	1262548042	1515682676	1340476661	1379102643	1377638906	1559200362
1:2	70	777829416	764870564	1233273908	222751384	583689537	173117628	140530000	865307344	838209394	1462000999
1:2	65	501260724	851223296	1746128363	656088695	1483064955	2091473146	1329752598	145095459	809943015	186664805
1:2	60	1055596416	1055597255	865325405	571236279	512985268	2028968234	12966273	1993702200	139427117	623670350
1:2	50	2090142333	892908243	654741663	1183679538	798831926	1297860866	595737703	598940860	892725592	807684645
1:2	40	668847390	1203727170	1049904414	423251960	208080469	1869656255	213537346	396533341	1633126228	1202867290
1:2	30	1547010505	277536324	752163505	1904912752	1772413171	113939992	690160499	413505727	1490149961	1783790928
1:2	20	1098076291	372007736	385426776	588476955	423890542	681889931	251921090	163695250	1251829801	205883523
1:2	15	1907456191	1605797498	603309103	1100254316	1101420200	1192294681	1960492641	1386120095	657867290	95770246
1:2	10	444769929	713809508	2078647852	2068561576	959280244	1831503581	307053744	741726661	1658337222	1403633228
1:5	100	2097067268	1055760677	1542934829	5300200	1061695019	646358634	428262437	577901158	752379487	412774198
1:5	95	1359815724	984532512	1855962629	591812900	1274244786	1882703137	1730911253	359884263	388488142	106237973
1:5	90	853512200	990272485	1243544083	1801780769	1492241907	2005817805	567082953	544662102	845474244	718411730
1:5	80	1020977884	1302918874	1694688276	2101114640	251318281	1062884707	1604184163	201748312	1688640726	1968044849
1:5	75	341120589	1460771146	811295122	525655917	114186328	1449405669	104369253	2100341843	263585797	889410303
1:5	70	1181999704	316715048	1232362458	1836306173	1206822226	369256543	426239629	1636407568	1767056373	157370506
1:5	65	1516112845	2002110481	1477673911	1033668986	394951216	1395938564	1920422489	744731980	783592528	1481170626
1:5	60	1035918621	1055778960	1822864714	592442134	1456218137	524928070	369256820	227579271	127083931	1549023320
1:5	50	1616204303	969779367	2061525370	429286563	479691002	647460053	347496224	969046651	2016497838	1848652199
1:5	40	823409643	2080249682	251965035	77739320	1137276292	718218703	788706544	1734587279	2081676646	357733716
1:5	30	2092081377	1046157829	1699223686	1349958369	1486743195	1764487477	1048382259	1867380599	444846755	1461076538
1:5	20	189030932	449043979	1152105033	1147341276	1869846638	1892263937	2129652378	1390580883	1031708191	765227201
1:5	15	727991189	301297100	1491578330	22408305	535768020	376894921	1762171101	720181052	639701190	1767362325
1:5	10	843613553	670965915	667187066	965907299	1259003869	2126274028	1938311698	512429484	808277633	515722318
1:10	100	2097067268	1055773410	2097067268	879273707	217656749	2097211101	430936594	1669787106	952511878	587246868
1:10	95	1046088259	716447583	1678693232	643796845	1738458425	319675995	784805423	681922755	446640201	827002771
1:10	90	209873205O	815129842	11975147	954675418	121279100	1539342706	1916140683	347041315	125085823	26055462
1:10	80	188138953	237231178	1274660902	637802228	2107730781	915034779	1059669948	1553552991	895166439	1504442109
1:10	75	1555942677	1443613539	1156433891	1868975687	124896648	1491575171	868471386	1546712911	1356822015	1920404379
1:10	70	945218981	1765846888	1699387700	1900822413	1928009748	799533249	783640296	1692236935	972129352	1276122484
1:10	65	1208294417	631249606	697069881	1986176817	1133038684	1275496833	1747375939	2011095960	1667992936	2036270210
1:10	60	1792863444	1055852883	90436408	1950959735	2118373411	58715799	1067025262	113153920	619257119	1771317058
1:10	50	573575112	867708356	566349378	1241441598	309848331	1992915641	1768001561	2077005225	1881155835	83731209
1:10	40	992592825	304965432	1357182634	455821740	1383038138	1379534596	698614583	1405109065	870628900	479703051
1:10	30	316765439	1149739875	536428238	1462763023	490547440	2130414120	1386046025	999804313	1062945154	1698317582
1:10	20	257835744	2010506762	980624896	1734248711	288277369	1048348588	109675142	300862521	147385470	2036919563
1:10	15	1895070536	1017725082	1834075643	298668262	153857542	1309147332	767774427	1944217666	644670537	1105527618
1:10	10	1737182118	1111377342	645810359	129675145	71595659	1703483572	1214875989	1562257367	2146852412	1235188759
1:100	100	1201026129	1055837820	2097067268	624790122	510044318	918453414	1074000303	661998886	2076419658	1813546087
1:100	95	462712876	366234874	2030994296	937159718	2038039321	461014796	1264760130	2114082873	1063936959	971798765
1:100	90	1676872781	898954744	869824889	1001632021	1367339578	777206622	1494598061	1221307243	2011918449	516399666
1:100	80	901246013	2014363514	1961052172	1805352315	953509809	865227293	546921519	1284991103	875283101	680703709
1:100	75	1493648068	1739937125	1525710245	1349425005	1377080505	1519920406	814369435	105821094	1190648119	1657587192
1:100	70	713241233	203300769	1676708392	800011663	1631301885	1811321810	802384232	469736518	421175467	1307346862
1:100	65	1074694129	231011146	1656434102	2016777964	408735357	594294371	1383882011	1344600291	1081932096	984052130
1:100	60	1325796085	1055056305	1792863444	1214524736	1474497711	1414484501	461002557	1111371221	1784768341	149509481
1:100	50	1290113467	845700397	1073319395	934548049	1482267269	2129095330	678442814	989913607	519523275	1742154041
1:100	40	2068181957	1697612551	201282692	1869585778	1673422093	1292642234	1292312039	38343824	757320774	1136686318
1:100	30	1495408755	189121140	642348733	93363074	1883740715	443053918	435587557	1844953913	1610869506	1910997296
1:100	20	1374396945	1405632698	1957813902	1639812671	335853573	245583313	608201507	656317635	1185786104	1381850120
1:100	15	1230970079	828630759	1055985223	445634705	834195457	1680034985	38039472	2014036912	704999807	1336013640
1:100	10	767243373	268744701	1060064812	268011494	1980339988	651074465	543736859	776218508	2110997801	1662009039

FIGURE A.5 *Seed number for realization 1 to 10 of the conceptual tidal bedding models used in chapter 8. The seed numbers in italic were used in chapter 7.*

Contrast	SandFraction	Real_11	Real_12	Real_13	Real_14	Real_15	Real_16	Real_17	Real_18	Real_19	Real_20
1:1	100	1457606506	289861068	2043781298	2062710737	554999361	1789513022	778420973	1641928802	1538484885	366234874
1:1	95	1104963671	993931827	1288460583	2119242707	673780808	2111809877	541650132	1051493964	167220166	280913211
1:1	90	1431998219	1055573657	1688039839	558682835	2092364177	1206113002	394036938	458840222	1382025544	242362157
1:1	80	1135946036	1906775393	187050105	367540993	1018342924	1460709090	576566251	381074529	1782583979	1780963494
1:1	75	431628237	954546596	1431471209	105179834	237855645	15453984	1095959148	1351735504	1769005821	1642939725
1:1	70	956951776	1211769395	1322130511	1971026338	138163348	899177420	978604622	123994779	1257679607	527223546
1:1	65	1055577688	639380284	554046661	409258890	731288805	1685949267	255120308	1205416424	560098846	789785890
1:1	60	265600311	1244931526	1891038408	2014734604	504285231	1554067706	384760125	1905938609	1750204300	444254398
1:1	50	2147152814	307506253	1434084249	687530225	580777412	2070597538	302176101	248405803	688504575	1255129553
1:1	40	1127970004	261154095	187750470	590339179	868381388	1716694730	1970013014	1781286747	1498159905	189547707
1:1	30	1727235665	1130824088	478539181	789671821	1980685575	1124597922	841180752	135893826	7136080	1823391145
1:1	20	820283210	1775158711	103574920	783902528	1036023870	879912626	2045436263	567126121	102595293	766009152
1:1	15	1772984381	420771559	1988101477	1053271800	1588900439	21734040	1696888344	234827539	667450300	1419381977
1:1	10	2112999977	1802789758	1984886157	2092040005	2073310540	1812713027	1674426365	1800429429	595201032	1108575225
1:2	100	6477195	1711752730	1952736016	1632500343	1099303452	1072635281	1018568609	800283353	1412121772	27271637
1:2	95	1267632629	439689934	1306747901	39189662	1261343436	1213595972	37674297	1109689207	1538425520	1642969163
1:2	90	1472086481	1993763865	1588669601	2028353434	1263560951	938204866	1359009926	1228275269	180844426	1015496476
1:2	80	302908098	1070120695	1449232263	1918275779	1067272430	1253149116	1328373483	1462914264	1483398354	169341453
1:2	75	2142611809	274864045	1001507139	454344411	1881406009	38995033	1955407792	986016572	2071276655	786539154
1:2	70	1899317332	1211380154	1212965367	1163531220	636075156	207656425	100378994	2088622641	55320299	1539920780
1:2	65	416819433	346790825	1484651688	888135853	343009543	107140256	1444052674	318973874	1340683520	1599982644
1:2	60	480534782	950514114	1398443747	1234332800	54501480	629406512	1525852398	1540391100	1691262402	1966231426
1:2	50	1001905054	1911777903	1920895111	373840606	627715576	1176098424	762925742	1434116840	1293688794	949309694
1:2	40	1350176452	1314627155	1137269032	1043986323	1389099515	56778986	1098585417	518147666	1072625904	1755803909
1:2	30	937204896	391155157	515582561	1358817526	917389401	619559444	239445657	1147601148	1800975882	591386816
1:2	20	1965236092	849784921	558545774	1949678349	1150277270	1395594535	1380393055	1194644801	555832971	2143465790
1:2	15	1039344921	1782741183	298506608	1446558359	501799010	1266965839	1895275170	1185304022	558483931	1419646315
1:2	10	346483565	1819605871	1951813133	1819998929	1363430344	182021966	757427786	1358359690	1985008961	101173579
1:5	100	730704022	983247271	1727440921	238466730	1089497067	295125334	1934527301	278852227	92361401	190393572
1:5	95	354609316	1818656047	552209823	2079724695	712175787	1309968630	425284606	970086725	882411919	1232734259
1:5	90	1484968641	1636193477	579869694	18959809	546787383	768838922	1088232898	871212988	483261355	1155861844
1:5	80	1891803329	1432300374	775446776	1173309408	241081233	12224102	312899620	527207260	859683705	1371992288
1:5	75	1793303793	89118750	1093815696	671280613	10539266	1533952279	1866045631	564385739	1078568327	1628042907
1:5	70	2096848160	1953080381	1841496692	16137014	742511510	763146724	1088865216	950860378	1269311650	1456949733
1:5	65	501683528	1628310905	250484826	1722898208	1884779810	1129732745	993336328	1857439611	1494621516	1980969967
1:5	60	1440530282	1570978472	476559268	1988715141	1738903164	1971643208	1714279029	123850402	1563646572	2045548330
1:5	50	1523322285	1505557277	12875956	1322488770	991959061	1168901949	1053449838	1908314359	937015582	1374459134
1:5	40	1880787941	970099817	1151706644	1602434478	1918194989	1801817411	738056565	1209618036	276385313	2017851460
1:5	30	32567673	342044217	931605649	1889939171	2091183057	673682737	618944613	2141026476	1886224332	219099353
1:5	20	1380303893	65549524	1286310235	96402336	1410628986	1337734760	1678567583	75359546	988559510	29666698
1:5	15	74860145	585794870	216888171	1857375195	570803794	1368012546	99389318	1348697577	1510326120	10226072
1:5	10	1050008519	1460030324	1621304639	524405508	378718162	1942615042	1863513738	607374766	1085067289	536049199
1:10	100	1451192565	2066028578	337164870	918727894	1772871332	844617417	2068879919	1207041568	1482687043	472282079
1:10	95	1944843084	701185400	2037384836	643052357	445607100	525686157	394262116	876398803	417137368	71708784
1:10	90	738486277	200770444	1854984545	553391021	462664932	1157016472	1863919714	295309764	1484381539	1065774520
1:10	80	242874001	1010624948	1056926934	1366884240	1796992472	8723773	2035017314	1457700611	310765731	1411952264
1:10	75	1685885887	2141960032	204184561	744794910	1411166461	1532809457	1958841719	1606450563	631355386	963665258
1:10	70	1772688017	918531751	1124122243	2096377284	835289928	568604452	700538420	410725990	475627705	846306943
1:10	65	1646800182	386189543	1788854224	2005433000	1119561753	1739503314	952013545	1296228068	513882065	260335135
1:10	60	1735584565	1203342633	1809781190	608485304	1039093031	1487799981	2046668974	68006644	1164844650	1888175148
1:10	50	1798439732	1673217659	33140359	763363903	1064558866	246259744	121086978	733910753	1318902184	1843494562
1:10	40	1471346121	602292553	950693224	2087389742	506805041	761937623	938481418	380587801	1824383083	1455032608
1:10	30	373351379	1249147263	1575967528	1614415244	205886222	798833310	474383201	937155282	2077178243	1270466393
1:10	20	10705524	421811142	1033229175	1293686766	107247815	1210495796	1224489080	2007259540	706161881	1756783107
1:10	15	1394809063	123870550	849206058	1111195054	1309790848	1336522709	237425542	166373863	1270096625	1191636590
1:10	10	2030312426	807070762	1233796823	1822222907	1593411225	1176773051	2043044456	1987847549	775044660	873157358
1:100	100	1004702267	1457606506	289861068	2043781298	2062710737	554999361	1789513022	778420973	1641928802	1538484885
1:100	95	578358502	1976739781	176079637	112732445	1526799195	1744632061	1554214826	510001337	1255212534	959483577
1:100	90	438048622	916367115	1198536700	866060151	1364670051	364662322	1878509640	1198983760	93381661	514346549
1:100	80	362590997	707882059	78797922	1491389151	1010092866	2078016336	89287871	1112275715	701165147	1899674576
1:100	75	2012581469	373013530	1143066503	1301280897	1633759641	1742984569	1036092099	1250018817	309771692	1580504388
1:100	70	691086815	1585901369	2063682304	903593936	1782181967	710627603	48409140	1408410794	546789285	1689270491
1:100	65	826053815	1348857500	1661352733	1404311510	1684081054	1817279126	351268476	667463722	2100802794	529610038
1:100	60	828444152	1800802198	1180449013	478450897	1609286844	1410874891	1362019909	1575181024	1859343341	2141558034
1:100	50	196268554	696533076	89274232	911467269	1245552511	2057492626	108956103	876586609	989035575	23762641
1:100	40	1101262228	1878279753	1542480439	45272159	761187113	546830140	1250960743	1301622584	1248922595	726182993
1:100	30	502935297	685589988	681290050	291569837	1949428065	1678322977	931154357	871181082	1406011140	438488076
1:100	20	706616717	1461955989	2057416780	727634033	1147128509	153931197	821701505	527902798	1255905719	896034165
1:100	15	1459556706	596340780	1166572781	1733341202	107085207	813670960	90017228	845296474	1023254954	640549103
1:100	10	1345688403	1904046388	185956251	607226735	1596981272	600106156	287417361	1402039807	907473560	463562641

FIGURE A.6 *Seed number for realization 11 to 20 of the conceptual tidal bedding models used in chapter 8.*

Appendix B Paper 1

Extended abstract presented at the 65th EAGE Conference & Exhibition - Stavanger, Norway, 2-5 June, 2003.

1

F-25 Petrophysical variation as a function of scale and implications for core-log integration

KJETIL NORDAHL[1], PHILIP RINGROSE[2], AND RENJUN WEN[3]

[1] Norwegian University of Science and Technology, Department of Geology and Mineral Resources Engineering, N-7491 Trondheim, Norway, [2] Statoil Research Centre, [3] Geomodeling Technology Corp.

Abstract

We have used a process oriented modelling tool, SBED™, to evaluate how petrophysical properties vary as a function of scale in the near well-bore region of a highly heterogeneous reservoir interval. A 25 m interval of the Tilje formation, offshore mid-Norway, is studied in detail and core parameters are extracted which can be used to create a realistic sedimentological and petrophysical model of the near well-bore region. When integrating core and wireline data there is usually a problem with sample support, and we show how the core plug distribution is related to the "true" petrophysical distributions. By using the concept of representative element volume we give an estimate of the error related to traditional upscaling or averaging techniques.

Introduction

Petrophysical characterisation of heterogeneous reservoirs involves challenges. Many of the parameters measured or estimated are scale dependent and this will affect the integration and subsequent upscaling of the data. In tide-influenced deposits, like the Tilje formation offshore mid-Norway, the main scale of heterogeneity affecting the reservoir performance is at the mm-cm scale. At this scale, intercalations of sand, silt and mud, which is the result of fluctuating hydrodynamic conditions during deposition gives variability in petrophysical properties below the core plug scale. To model this heterogeneous interval, we used the SBED™ tool, which simulates the depositional process through migration of sine curves in space and time (forward modelling) (Wen et al. 1998). The petrophysical properties are distributed stochastically for each lamina, but linked to the simulated bedform. The result is a detailed (sub-mm) model with a realistic sedimentological geometry and small-scale petrophysical properties. The simulated cubes can be evaluated at different volume scales.

Representative Element Volume

The concept of Representative Element Volume (REV) (Bear, 1988) can be used to evaluate how the petrophysical properties vary with sample volume. In heterogeneous media, a measured property will depend on the scale the property was measured. Mud layers that appear continuous at the core width may be discontinuous at some larger scale, and a measure of porosity and permeability will most likely be different. Figure 1 shows a plot of an example facies with 20 % mud content and the variation of horizontal permeability as a function of volume scale is clear. At small sample volumes, the measured property varies greatly since its value strongly depends on sample position. At some scale, the REV, the variation is minimized and the sample is effective homogeneous. In the studied formation

there is, in addition to the clear difference between sand and mud, a variation within the sand; one relatively clean lamina and one silty. The core plug values are therefore an average of these three components. Since the plug scale is below the representative element volume, the plug samples are generally un-representative. This highlights the uncertainty associated with using the petrophysical distribution obtained directly from core plugs in upscaling and log integration.

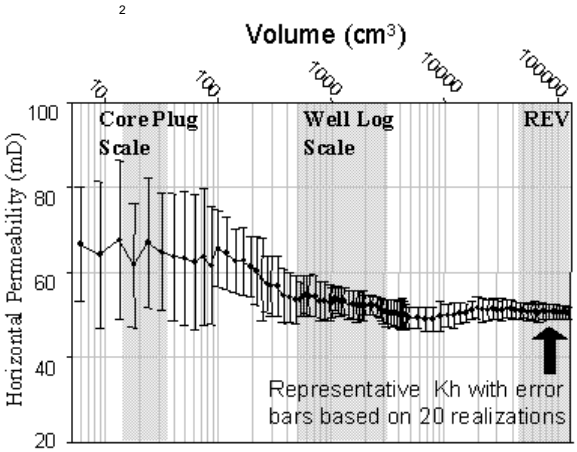

Figure 1: Variation of horizontal permeability as a function of sample scale. Note that both the core plug and the wireline log measures at an inappropriate scale to give a representative value.

Results

From the studied interval, we selected two facies. Facies 1 is a wavy to flaser bedded unit (3 components) where the cm thick mud-layers are spaced with 10's of centimetre. Facies 2 is a hummocky cross-stratified unit where the sand lamina has varying degree of contrast (2 components). By varying the distribution of the components present in each facies, we simulated core plug samples that matched the core plug distribution from the well. In figure 2 (facies 1) and figure 3 (facies 2) the distribution of the different components in these two facies is plotted along with the resulting simulated and observed core plug distribution. A match with the measured core plug distribution is a validation of the model, in addition to showing how the underlying distributions of the components are changed with increasing scale. We also made models at the REV scale in order to estimate the error associated with upscaling based on core plugs. In both facies, the observed porosity distribution can be obtained by a larger than observed variance on the different components and the mean is a result of simple volume averaging. This is the case because porosity is an additive property. Even so, we see that the representative value in facies 1 is lower than the core plug average (figure 2). The core plugs often do not sample the thin mud layers and this results in an overestimation of porosity. At a larger scale these layers are included in the sample volume and a lower effective porosity is measured. Permeability however, is more complex since it is non-additive property. Thin, high permeability streaks may affect the overall permeability. As a result, the underling distributions are skewed towards lower values with tails into the high permeability regions. Using the core plug values directly will, in this case, give an overestimation of the horizontal permeability. In facies 2 there is a mis-match between the core plug average and the representative value of horizontal permeability (figure 3). This unit consists of both high and low contrast sand sets and biased sampling has given an underestimation of the overall permeability field.

Conclusion

The relationship between the petrophysical variability at the lamina scale and the core plug scale are explored by using a process oriented modelling tool. In these systems, the variability is a function of scale and assuming that the core plug distribution is a representative measure may be misleading. The increased variance and shift of the mean towards lower values for the

individual components can be used to give a better estimate of the representative value at a larger scale through upscaling. These detailed analysis of a heterogeneous well interval provide basis for improved calibration of wireline logs, well test, and production data in intervals that often show major inconsistency between data types.

References

Bear, J., 1988, Dynamics of fluids in porous media, Elsevier, New York

Wen, R., A. W. Martinius, A. Næss and P. S. Ringrose, 1998, Three dimensional simulation of small-scale heterogeneity of tidal deposits – a process based stochastic simulation method, in Bucianti, A., G. Nardy and R. Potenza, eds, Proceeding of the 4th Annual Conference International Association of Mathematics, Ischia, p. 119-124.

SBED™ is trademark software developed Geomodeling Technology Corp.

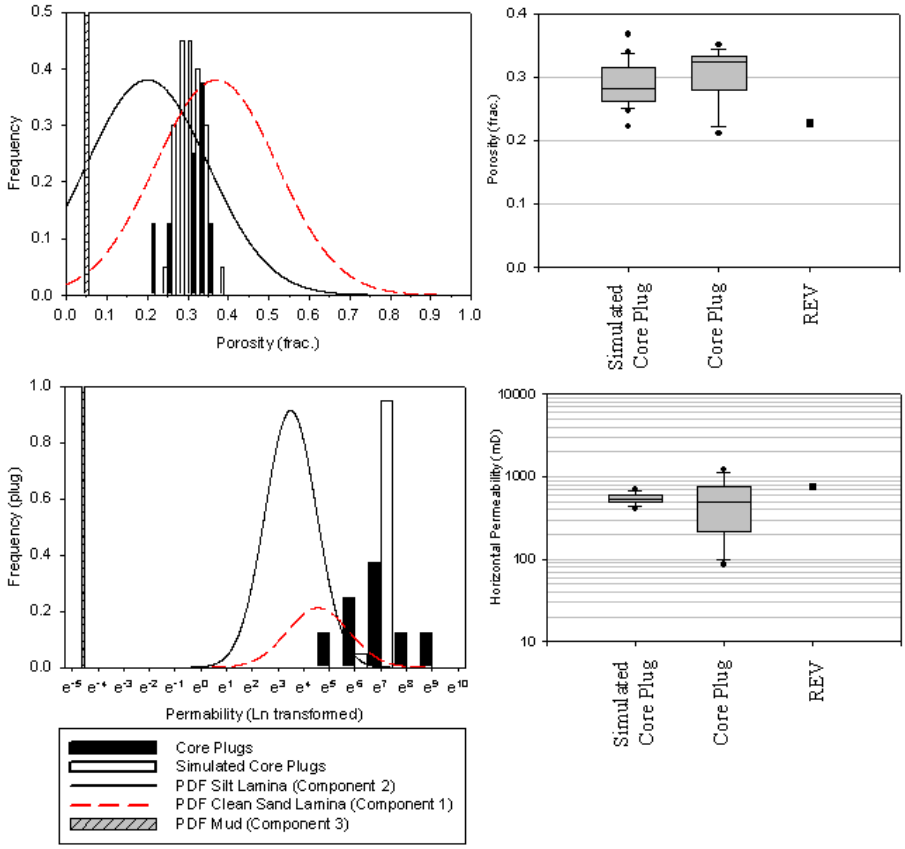

Figure 2. Wavy to flaser bedded facies. Left: Porosity (top) and permeability (base) distribution of the individual components (laminas) and the corresponding distribution at the core plug scale. Right: Box-plot of the variation of the simulated and measured core plugs along with the effective (representative) value measured at the REV. Note the difference between the core plug average and the representative value for porosity and the shift of the underlying permeability distributions towards lower permeability values.

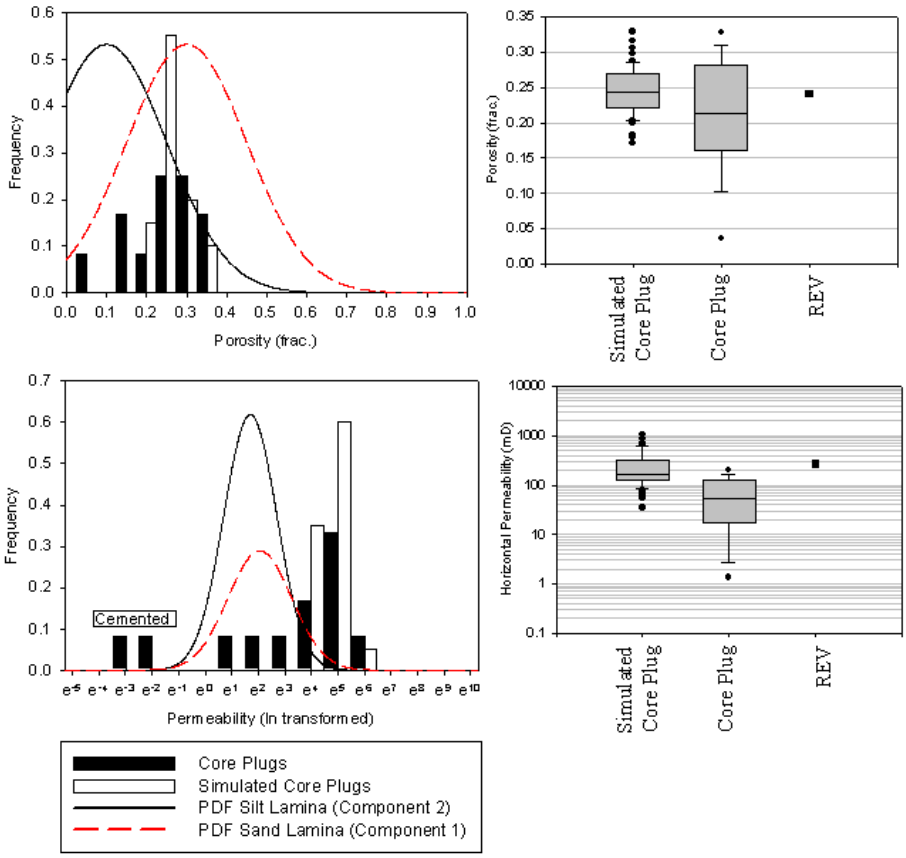

Figure 3. Hummocky cross-stratified facies. Left: Porosity (top) and permeability (base) distribution of the individual components (laminas) and the corresponding distribution at the core plug scale. Right: Box-plot of the variation of the simulated and measured core plugs along with the effective (representative) value measured at the REV. Note the difference between core plug average and the representative value for horizontal permeability.

Appendix C Paper 2

This extended abstract is submitted and accepted for oral presentation at the 6th International Conference on Tidal Sedimentology August 2-5, 2004, Coopenhagen, Denmark.

Identifying tidal influence in the lower Tilje Formation, Heidrun Field, offshore Mid-Norway: Time-series analysis on ripple-laminated deposits and implications for reservoir modelling.

Kjetil Nordahl[1] and Allard W. Martinius[2]

[1] *Department of Geology and Mineral Resources Engineering, Norwegian University of Science and Technology. Present address: Statoil Research Centre, Rotvoll, Trondheim N-7005, Norway. E-mail: KJN@statoil.com*
[2] *Statoil Research Centre, Rotvoll, Trondheim N-7005*

Introduction

The late Pliensbachian to early Toarcian Tilje Formation is found on the Halten terrace offshore mid-Norway and contains several large hydrocarbon fields. The lower part of the Tilje Formation has been interpreted to be deposited in an estuarine system influenced by tidal processes (Martinius et al., 2001). One of the few diagnostic criteria for recognizing tidal deposits is the presence of different orders of cyclicities (Nio and Yang, 1991). Time series analysis to reveal tidal cyclicities have mainly been carried out on either large-scale cross-bedding or on finely laminated successions of sand and silt/mud often referred to as rhythmites. Considerable fewer studies are published on heterolithic, ripple laminated flaser-, wavy- or lenticular bedding (but see Martino and Sanderson, 1993). Here, focus will be on a ripple laminated wavy-bedded heterolithic lithofacies interpreted to be a laminated shallow water deltafront deposit underlaying the estuarine deposits. These are of considerable lateral extent (up to 10 km at least). Two time series techniques have been used on data describing the sand and mud lamina set thickness and the mud-fraction at each depth. The lithofacies is chosen because 1) it is preserved in a long section in the selected well (a request for using time series analysis), 2) the tidal influence on this lithofacies is not proven, and 3) a vertical variation in mud fraction as a result of tidal influence is important to take into account when analyzing well data for hydrocarbon flow studies.

Method

On a selected 3.28 m long core interval (~2600 m depth), the thickness of sand and mud lamina sets was measured with 2 mm resolution. The measurements were performed on three parallel lines along the core; left, center and right. The recorded binary data gave two different data sets: 1) sand and mud layer thickness along each line and 2) the sand or mud fraction at each depth. The first data set was used to evaluate the number of layers per cycle for interpretation of the tidal influence. The second data set, obtained by taking the arithmetic average of the measurements at each depth and then taking a running average down the core, made it possible to validate the vertical variation in mud fraction which will influence on the vertical variability in bulk petrophysical properties. On these two data sets, the autocorrelation function (ACF) and the periodogram is calculated.

Description and Interpretation

The lithofacies is characterized by persistent wavy to lenticular bedding, with fine-grained sandstone interbedded with approximately equal thick mud layers. The sand lamina sets can either be form-sets, sets or co-sets, but are dominated by the first. They are bounded above and below by mud layers that can show faint lamination in the upper part at the transition to

the overlying mud layer and commonly have a sharp lower boundary. Each sand layer can be interpreted to be a result of one current stage (flood or ebb) and the overlying mud layer a result of deposition during the following slack-water period. However, two problems appear: 1) The majority of the mud lamina sets are too thick to have been formed in just one slack water period, 2) the internal stratification of the sand lamina set and the transition between the sand and the mud lamina indicate deposition over longer time intervals than one flood or ebb current. McCave (1970) and Terwindt and Breusers (1972) have indicated that a freshly deposited mud layer thicker than 5-10 mm seems unlikely to result from one slack water period and it is thus assumed that a measured mud layer thickness of more than 4 mm could not have been deposited from suspension during one tidal slack period. In the measured section, c. 55% of the mud layers are more than 4 mm thick. The internal stratification of the sand lamina sets resembles the Type II ripple of Tessier (1993) (figure 1). It is composed of 3D small-scale climbing ripples where the laminations at the base mould the underlying ripple morphology. Upwards, the laminae thicken, the slope angel of the lee side increases and the mud content decreases, before, towards the top, the angel again decreases and the mud content increases.

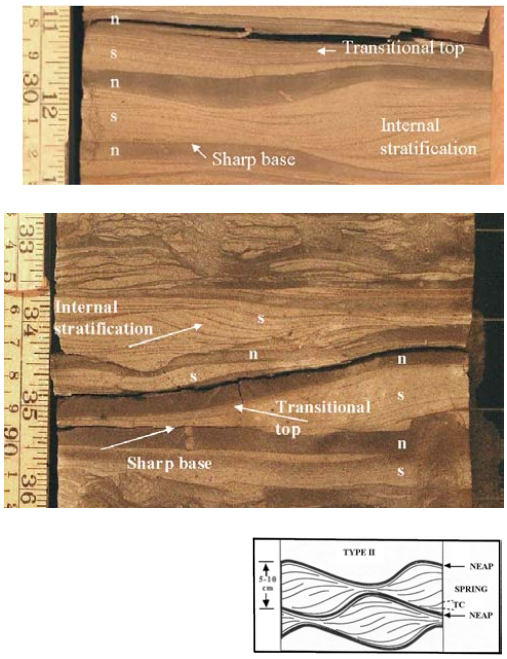

Figure 1: Top and Middle: Examples of Type II ripples from the studied interval showing a characteristic internal stratification and a sharp base and transitional top (n=neap and s=spring). Base: A schematic sketch of the Type II ripple (Tessier, 1993).

A depositional model for the observed ripple laminated deposits is proposed (Figure 2). It is assumed that the entrainment velocity of the sand (U_{ces}) is higher than the threshold velocity where mud starts to fall out of suspension (U_{cdm}). As the tidal range varies through a spring-neap-spring cycle, the current velocity and the time the current is above U_{ces} and below U_{cdm} varies with the same period. It is proposed that both the dominant and subordinate (if present) maximum current speed are below U_{ces}, around neap time. The (semi-) continuous deposition of mud around neap time creates an amalgamation of thin mud lamina that after settlement undergoes initial consolidation. As the tidal range and maximum current speed increases towards spring, the threshold for sand movement is passed. Some of the most recently deposited mud laminae can be removed if the current speed exceeds that required for mud erosion, but the deposited sand laminae will in general have a sharp boundary to the underlying, initially consolidated mud. Small, three-dimensional bedforms develop equal to the type II climbing ripples. Around spring time, the current velocity is largest and the

thickest sand/silt laminae are deposited. As the tidal range decreases towards the following neap, successive smaller components of the current velocity are above the threshold for sand movement. This results in a faint lamination between traction deposited sand and suspension deposited mud in a transitional zone to the overlying neap-deposited, amalgamated mud.

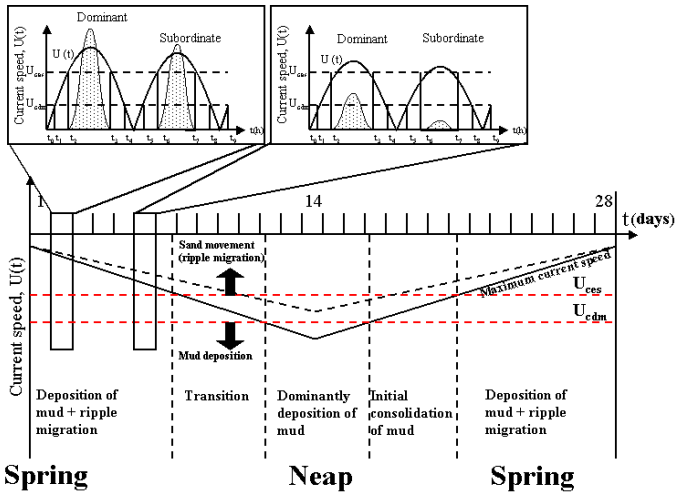

Figure 2: Proposed depositional process for the wave to lenticular bedded lithofacies. Periodic variation on current strength and the slack-water period. U_{ces}=critical threshold for sand movement and U_{cdm}=the critical threshold for mud deposition from suspension.

Figure 3 shows a bar plot of the sand lamina set thickness and the ACF and spectral analysis results. Prior to the analysis, the raw data was smoothed with a three-point running average. Although the data are noisy, a few prominent periodicities are recorded both in the time domain and the frequency domain: 10-13 sand layers and approximately 50 sand layers per cycle. The 13 spring deposits correspond to the shortest period recorded in the data. Both the sun's declination to the earth and the constructive interference of the tropical, anomalistic and synodic month has a period at the semi-annual time scale with 182.62 days and 183.29 days, respectively. Similar semi-annual periods are observed by for example Kvale et al. (1999), Miller and Eriksson (1997) and Stupples (2002).

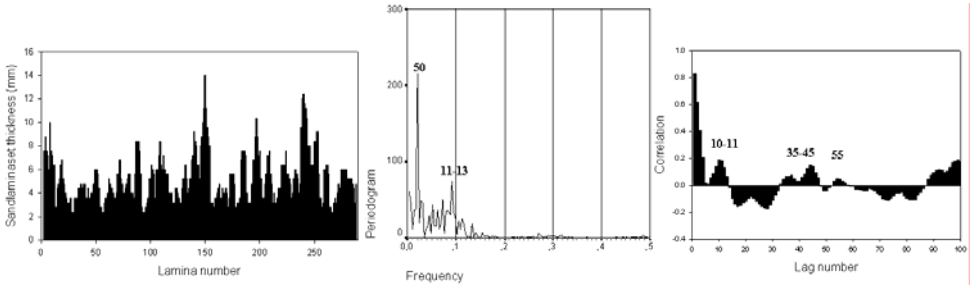

Figure 3: Left: Bar plot of the sand lamina set thickness (smoothed with a three-point running average). Middle: Spectral analysis of the smoothed data set showing two prominent periodic components. Right: The ACF function of the same data set.

In summary, the high mud content and the presence of small scale ripples suggest deposition during overall low energy conditions. A weak current, dominantly tidal but with a possible small wave component, combined with the interpreted low ripple migration speed suggest that the depositional area was relatively starved of bedload sediment. Fine-grained sediments can have been brought into the pro-delta area by hyperpycnal plumes or by longshore currents that subsequently were modified by the weak currents into the observed rippled bedforms. The

apparent low wave energy conditions favoured 1) a stronger imprint from the tidal current and 2) recording of the semi-annual tidal cyclicity.

Reservoir Modelling

In addition to the sand and mud lamina set thickness data, a continuous, vertical record of mud fraction is obtained. Figure 4 shows how the mud fraction varies along the core and the results from the ACF and spectral analysis. Important for reservoir modelling is also that periodic variation in the mud fraction will influence petrophysical properties. For example, Ringrose et al. (2003) have shown how the effective permeability in the vertical and horizontal direction is related to the mud content in tidal deposits. To model this observation we have used a process-oriented modelling tool, SBED (Wen et al., 1998) that creates near wellbore numerical models that subsequently are populated with petrophysical properties. A common Earth model that has the ability to incorporate detailed sedimentological information and that is used by the sedimentologist, petrophysicist and reservoir engineer has proven particularly valuable for reconciling well data with different sample support (Elfenbein et al., 2003).

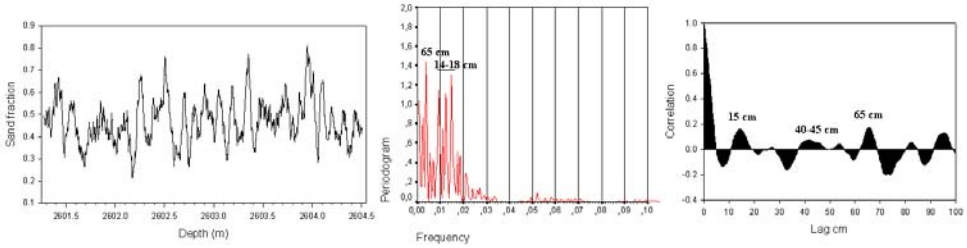

Figure 4: Left: A continuous record of mud fraction along the analysed lithofacies (smoothed with a 5 cm running average). Middle and Right shows respectively the spectral and ACF results on the same data set indicating a few prominent periodic components.

References

Dreyer, T. 1992. Significance if tidal cyclicity for modelling of reservoir heterogeneities in the Lower Jurassic Tilje Formation, mid-Norwegian shelf. Norsk Geologisk Tidsskrift, Vol. 72, p. 159-170.

Elfenbein, C., Husby, Ø. And Ringrose, P. 2003. Geologically-based estimation of k_v/k_h ratios: an example from the Garn Formation, Tyrihans Field, Mid-Norway. Presented at the 6th Petroleum Geology Conference: North West Europe & Global Perspectives. 7-9 October 2003. The Geological Society of London, The Institute of Petroleum & The PESGB (Petroleum Exploration Society of Great Britain)

Kvale, E. P., Johnsson, H. W., Sonett, C. P., Archer, A. W. and Zawistoski, A. 1999. Calculating lunar retreat using tidal rhythmites. Journal of Sedimentary Petrology, Vol. 69, Vol. 69, p. 1154-1168.

Martinius, A. W., Kaas, I., Næss, A., Helgesen, G., Kjærefjord, J. M. and Leith, D. A. 2001. Sedimentology of the heterolithic and tide-dominated Tilje Formation (Early Jurassic, Halten Terrace, offshore mid-Norway). In: Martinsen, O. M. and Dreyer, T. (eds.) Sedimentary Environments Offshore Norway - Palaeozoic to Recent. NPF Special Publication 10, 103-144, Elsevier Science B. V, Amsterdam.

Martino, R. L. and Sanderson, D. D. 1993. Fourier and autocorrelation analysis of estuarine tidal rhythmites, Lower Breathitt Formation (Pennsylvanian), eastern Kentucky, USA. Journal of Sedimentary Petrology, Vol. 63, No. 1, p. 105-119.

McCave, I. N. 1970. Deposition of fine-grained suspended sediment from tidal currents. Journal of Geophysical Research, Vol. 75, No. 21.

Miller, D. J. and Eriksson, K. A. 1997. Late Mississippian prodeltaic rhythmites in the Appalachian basins: A hierarchical record of tidal and climatic periodicities. Journal of Sedimentary Petrology, Vol.67, No. 4, p. 653-660.

Nio, A-D. and Yang, C-S. 1991. Diagnostic attributes of clastic tidal deposits: a review. *In*: Smith, D. G., Reinson, G. E., Zaitlin, B. A. and Rahmani, R. A. (eds.) *Clastic Tidal Sedimentology*. Canadian Society of Petroleum Geologist, Memoir 16.

Ringrose, P. S., Skjetne, E. and Elfenbein, C. 2003. Permeability estimation functions based on forward modeling of sedimentary heterogeneity. Paper SPE 84275 presented at the SPE Annual Technical Conference and Exhibition, Denver, Colorado, 5-8 October 2003.

Stupples, P. 2002. Tidal cycles preserved in late Holocene tidal rhythmites, the Wainway Channel, Romney Marsh, southeast England. Marine Geology, Vol. 182, p. 231-246.

Terwindt, J. H. J and Breusers, H. N. C. 1972. Experiments on the origin of flaser, lenticular and sand-clay alternating bedding. Sedimentology, Vol. 19, No. 1/2.

Tessier, B. 1993. Upper intertidal rhythmites in the Mont-Saint-Michel Bay (NW France): Perspectives for paleoreconstruction. Marine Geology, 110, p. 355-367.

Wen, R. Martinius, A. W., Næss, A. and Ringrose, P. 1998. Three-dimensional simulation of small-scale heterogeneity in tidal deposits - a process-based stochastic simulation method. In: Buccianti, A, Nardi, G. and Potenza, R. (eds.) Proceedings of the 4th Annual Conference of the International Association of Mathematical Geology (IAMG), Ischia, 129-134.

Appendix D Paper 3

Accepted for publication in Petroleum Geoscience as of 24. Spetember 2004.

Nordahl, K., Ringrose, P. S. and Wen, R.
Accepted for publication in Petroleum Geoscience as of 19 September 2004

Petrophysical characterisation of a heterolithic tidal reservoir interval using a process-based modelling tool

Kjetil Nordahl[1], Philip S. Ringrose[2], and Renjun Wen[3]
[1]Norwegian University of Science and Technology, Department of Mineral Resources and Engineering, Trondheim N-7491, Norway. Present address: Statoil Research Centre, Rotvoll, Trondheim N-7005, Norway.
[2]Statoil ASA, Exploration and Production, N-7501 Stjørdal, Norway.
[3]Geomodeling Technology Corp., Suite 230, 633 6th Avenue S.W. Calgary, Alberta, T2P 2Y5, Canada.

Abstract

Heterolithic lithofacies in the Jurassic Tilje Formation, offshore mid-Norway, consist of three components: sand, silt and mud intercalated at the cm scale, and are generally difficult to characterise petrophysically with core and wireline data. A near well-bore model of the lower part of the Tilje Formation in the Heidrun field is constructed to illustrate the application of these results to formation evaluation studies. The sedimentological model is developed by detailed parameterisation of a cored well interval and the petrophysical properties are based on core plug data, taking into account sampling bias and length scale. The variation in petrophysical properties as a function of sample volume is examined by calculating the representative elementary volume. The sensitivity of the representative permeability values to the contrast between the three components is studied and gives a better understanding of the flow behaviour of this system. These results are used to rescale the core plug data to a representative value and thereby quantify the uncertainty associated with the wireline-based estimates of porosity and horizontal permeability and to given an improved estimate of the k_v/k_h ratio.

Key words: *petrophysics, permeability, porosity, heterolithic sandstone.*

Introduction

Sedimentary architecture causes heterogeneity at many scales, which can affect reservoir performance (e.g. Haldorsen, 1986). At the bedding (sub-metre) scale, primary sedimentary structures can significantly influence the flow properties, as has been shown for a range of sedimentary systems (Weber, 1982; Corbett and Jensen, 1993; Hartkamp-Bakker and Donselaar, 1993; Hurst and Rosvoll, 1991). These studies show that porosity and permeability are strongly controlled by depositional processes through their influence on grain size, sorting, and fabric. Because of computational limits on the number of grid-cells in reservoir simulation, small-scale sedimentary structures cannot be included explicitly, but have to be represented by effective or representative values.

The problem of integrating data with different sample support in heterogeneous reservoirs has also been widely appreciated (Haldorsen, 1986; Enderlin et al., 1991; Worthington, 1994; Corbett et al.,

1998). In particular, the integration between core data (usually represented by discrete core plugs) with continuous wireline data is challenging since heterogeneities are often on the same scale as the measurement resolution. To integrate the two data sets, the normal approach is to upscale the measurements with the smallest sample support to the scale of the larger.

Methods for generating numerical models of the subsurface domain are reviewed by Koltermann and Gorelick (1996). Population of these models with petrophysical properties and calculating the effective flow properties at a larger scale can be done in a variety of ways (Renard and Marsily, 1997). For simple geometries (e.g. a stratified medium) exact analytical solutions can be found. In more complex cases, numerical methods can be used to estimate effective properties. Usually, only two component systems (sand and mud) are evaluated (Begg and King, 1985; Desbarats, 1987; Deutsch, 1989; Durlofsky and Chung, 1990).

Regardless of the upscaling technique, the question remains as to what scale the measurements should be rescaled to. Bear (1972) introduced the concept of Representative Elementary Volume (REV). This is based on effective medium theory, which assumes that the correlation lengths are shorter than the model domain. If the sample support is small compared to the length scale of the heterogeneity, the measured value will vary with a change in the support since varying degree of heterogeneity is included in the sample volume. At some scale (the REV), the fluctuations are minimized and a representative amount of heterogeneity can be measured (Figure 1).

The tidal deltaic Tilje formation (Martinius et al., this volume), is particularly heterogeneous and exhibits variability at many scales. Brandsæter et al. (2001) showed that the ratio between vertical and horizontal permeability (k_v/k_h ratio) was one of the most important parameters influencing oil recovery in this formation. At the bedding scale, thin intercalations of mudstone and sandstone layers have a strong influence on the flow properties (these two lithological components are hereafter referred to as sand and mud). These facies are dominated by heterolithic current ripple bedforms which have been described as flaser, wavy or lenticular bedding (Reineck and Wunderlich, 1968). Flaser and lenticular

bedding represent end-members of a range of tidal bedding types, with discontinuous mud lamina and discontinuous sand ripples, respectively. Wavy bedding describes more regular interbedding with approximately equal amounts of sand and mud. These mm to cm scale heterogeneities are not well characterised by the core plug or the wireline log measurements. Core plug measurements are at a volume scale below the characteristic length scale of the heterogeneity and the wireline logs tend to average out the responses from the different lithological components present. Integration between these two data sets is thus problematic. Figure 2 shows the studied interval of well H1 from the lower part of the Tilje formation in the Heidrun Field. This figure shows that the petrophysical variability is high, both within and between the different facies associations, such that there is in general a mis-match between the core and the wireline values.

This paper considers these problems using a process-based stochastic modelling tool (SBED™) (Wen et al., 1998). With this method, a realistic near wellbore model is created. The near wellbore model is defined here as a numerical representation of the sedimentological components and petrophysical properties in a rectangular shaped volume along the wellbore with a lateral dimension on the scale of the conventional wireline tool resolution. This also approximately corresponds to the lateral correlation lengths of the sedimentological and petrophysical elements in tidal facies. To be able to evaluate the tidal bedding system in general, a range of bedding models with different mud contents were created. Permeability is shown to vary with the sample volume and the REV can be calculated on these models. Furthermore, the sensitivity of flow behaviour to the permeability contrast between the different lithological components is explored. Finally, the near wellbore model is used to quantify the uncertainty associated with traditional averaging of core and wireline data to give improved estimates of the petrophysical properties in the studied interval.

The near wellbore model

Modelling of small-scale (cm-dm) sedimentological bedforms has been widely studied, and pioneering work on synthetic bedform modelling was published by Rubin (1988). The SBED™ method was

developed by Wen et al. (1998) and makes a significant step towards a petrophysically useful method by extending the approach of Rubin (1988) to include stochastic elements and 3D property modelling. The method used in SBED is based on manipulation of the following surface function:

$$z(x,y)^t = A\sin\left(\frac{x}{L_x} + \Theta_x\right) + B\sin\left(\frac{y}{L_y} + \Theta_y\right) + g(x,y) \qquad (1)$$

where x and y are spatial coordinates, t is a nominal time increment, A and B are amplitudes of the bedform in the current (x) and crest (y) directions, L_x and L_y are wavelengths of the bedform in the current and crest directions, Θ_x and Θ_y are initial phase angels (radians) and g(x,y) is a 2D gaussian random function. The input parameters to the program describe the bedform morphology in cross-section and plan-view (by a sine-function) and also how the surfaces move in space and time by vectors to mimic bedform migration (Figure 3A). The displacement creates a 3D volume separated by the surfaces giving a simulated lamina (Figure 3B). After a sequence of surfaces representing a lamina set, $z(x,y)^{t=n}$, a hiatus is simulated and erosion by a new time series is initiated (i.e. a new lamina set). The migration of bedforms, that in nature is a result of periodic avalanching and suspension fallout on the bedform lee- and stoss-side, is here simulated by displacement of successive sine curves. This is a simpler approach than process-based methods in which grain deposition is simulated. The input parameter set comprises a set of values to give a particular type of sedimentary bedform. The stochastic elements of the code reflect the natural variability in the deposits and ensure that a number of equiprobable realizations of the bedform model can be generated. Figure 3C shows an example of a realization of a geometry model. Statistical parameterisation of the sedimentological observations from core gives us the opportunity to determine the mean value of the deterministic part of the code while allowing the natural variability to be included in the stochastic elements. Table 1 gives some of the sedimentological parameters considered for this interval. The key parameters are the geometry, thickness variation and frequency of the mud layers, since these will have a strong influence on the vertical and horizontal permeability. Also listed in Table 1 are the main input parameter groups that are used to mimic the depositional process.

Within this geometrical bedding framework, petrophysical properties (porosity and permeability) are simulated using correlated 2D gaussian random fields. On the resulting permeability grid (Figure 3D), directional flow is simulated numerically by imposing a constant head gradient between opposite sides of the model and no-flow boundaries on the perpendicular sides. The single-phase steady state flow equation is then solved by a finite-difference method (described by Warren and Price 1961, White and Horne 1987, and Renard and Marsily 1997). By rotating the boundary condition setup, and repeating the flow simulation, the diagonal elements of the permeability tensor are found (denoted here as k_x, k_y and k_z,). Since porosity is an additive property (Narasimhan, 1983), the bulk porosity of the bedding model is simply found by taking the arithmetic average of the individual grid-cell values.

In this study only single-phase flow has been considered. However, where sedimentary structures have a significant effect on single-phase permeability, the multiphase effect on permeability is likely to be even greater. Multiphase flow aspects also need to be considered in reservoir studies and Pickup et al. (2000) performed two-phase upscaling on similar synthetic tidal bedding models as used here.

Bedding geometry model

The geometrical model represents the sedimentological features observed in the core such as the lamina and lamina set characteristics (Table 1). After dividing the core into lithofacies, a detailed log of mud content and lamina set thickness distribution within the cored interval was made, and these statistics were then used to develop the bedding models. To illustrate the modelling method, lithofacies 7.1 from the upper part of Figure 2 was selected. Ringrose et al. (this volume) consider the entire interval in Figure 2 for estimation of vertical permeability. The selected lithofacies is interpreted as an accretionary channel bank deposit (Martinius et al. 2001) and is dominated by flaser bedded deposits separated by thicker mud layers. The number and thickness of the mud and sand lamina sets (Table 2) were considered to have an important control on effective permeability. In order to ensure

that the near wellbore model of this lithofacies is realistic, the same parameters were measured on the numerical model. A realistic model is obtained when the two data sets are statistically similar (Table 2). Figure 4 shows part of this interval with one realization of the near wellbore model. Table 4 gives the geometrical input parameters while Table 3 gives the petrophysical parameters for this specific facies.

The petrophysical model

Each grid-cell in the model has a constant lateral dimension (1 by 1 cm) and a vertical dimension related to the lamina thickness (usually on the mm-scale, see Figure 3), and is by definition an isotropic and homogeneous petrophysical element. The model dimensions are 0.3 m by 0.3 m by 0.3 m and consist of c. one million cells. The grid cell scale is approximately the scale of the probe-permeameter device, c. 2-5mm (Halvorsen and Hurst, 1990, Ringrose et al., this volume). One detailed probe-permeability grid was available in the selected lithofacies. The main direct measurement of porosity and permeability are however the core plugs. In order to constrain the petrophysical model to data, we simulated the process of taking core plugs with 30cm spacing from the SBED™ model. The input petrophysical properties were then adjusted until a match was obtained between the real core plug data set and the simulated core plug data set. The simulated core plugs have the same dimension and orientation as the real core plugs and consist of approximately 600-800 grid-cells depending on the lamina thickness. There are limitations to this approach. Firstly, there should be a sufficient number of real core plugs from each facies to produce a stable histogram. Secondly, the real core plugs are often taken from the more sand rich zones avoiding the mud layers (see Figure 4), but the simulated core plugs are unbiased. Thirdly, several solutions are possible by changing the mean or variance of the input distribution (i.e. the solution is not unique). This is especially the case for porosity. The input permeability has to match both the upscaled vertical and horizontal core plug distributions giving a better constraint to the options available. Figure 5A and 5B show the results of this method for horizontal permeability and porosity, respectively, for the selected facies in the interval. There is a good match between the simulated and the real core plug data set, both validating

the petrophysical model and giving the three-component distribution of porosity and (isotropic) permeability. Figure 5A also show the available probe permeameter data and the distribution is similar to the distribution to the sand and silt components. Table 3 gives the petrophysical parameters for these curves and Figure 4 shows a realization of the final bedding model for the selected facies.

Even though there is an acceptable match between the core plug values and the model results, the latter tend to have slightly lower variability than the former. This is mainly because it is not possible to include all natural variability in geometry and petrophysics. For example, diagenetic features and fractures are not included in the synthetic bedding models. Although the Tilje Formation in the Heidrun Field is not severely affected by diagenesis, in other cases diagenesis could be equally important as the influence of the primary sedimentary structures. However, it is considered that the near wellbore model created here captures the most important features affecting the bedding-scale petrophysical properties.

There are few reported measurements on the mud component from these intercalated bedding types, but Ringrose et al. (this volume) discuss plausible values for mud permeability. A constant value of 0.01 mD is chosen here and then the sensitivity to this parameter on effective vertical and horizontal permeability is evaluated. Although 0.01 mD may be a rather high permeability for mud, for single-phase simulation, it is the contrast between the lithological elements that is most important.

Petrophysical variability with sample support

Several theories have been developed to estimate effective properties of heterogeneous media. In simple geometrical cases exact solutions exist, and for infinite, continuous parallel layers the horizontal and vertical effective permeability is given by the arithmetic and harmonic averages, respectively. In the case of a random, uncorrelated, isotropic lognormal permeability distribution, the geometric average has been shown to give a good estimate (Warren and Price, 1961). Although these estimates are useful, they do not generally apply to real sedimentary deposits, which often show more

complex geometry and variability. Effective media theories assume that the heterogeneity can be modelled as an inclusion embedded in a homogeneous matrix. If the inclusion has a simple form, analytical expressions for permeability can be calculated (e.g. Dagan, 1979). In percolation theory, assuming two components where one is non-permeable and the components are distributed randomly in space, the threshold for flow can be evaluated as a function of the conducting component (e.g. Begg and King, 1985). Randomly dispersed shales in a sandstone medium were evaluated numerically by Desbarats (1987), who showed that the effective permeability depends on the shale volume fraction, the spatial correlation structure and the dimensionality of the flow system. Deterministic modelling of sedimentary structures has also been performed (e.g. Corbett et al., 1992; Pickup et al., 1995; Ringrose et al., 1999), where the main focus was on fluvial and aeolian deposits. In these previous studies, only two components (sand and shale or two types of sand) were considered. The assumption of a two-component system is a simplification of tidal deposits since the sand lamina set consists of both sand and silt sized particles organized as cross-stratification in addition to the mud component. In addition, both the sand and the mud components are highly spatial correlated in these tidal deposits.

When the correlation lengths of the different components are smaller than the model domain, a property measured on a sub domain will depend on the size, position and orientation of this sub domain. Bear (1972) showed that at some sample support (the REV), the variability is minimized and a representative property could be measured (Figure 1). Norris and Lewis (1991) calculated in 2D the representative elementary area (REA) for a range of tidal facies based on binary images of an outcrop sample and found that for horizontal permeability the same REA applied regardless of the mud content. Jackson et al. (2003), dividing heterolithic rock cubes into smaller samples, showed that the effective property in 3D could be estimated with simple averaging schemes and that the choice of estimator depended on bedding type.

In order to evaluate the fundamental properties of the heterolithic bedding system, a set of models with different mud fraction was developed ranging from sand-dominated flaser bedding to mud-dominated lenticular bedding. Baas (1994) studied the development of ripple morphology in unidirectional flow

using flume tank experiments and found that ripples approached an equilibrium size and shape with either increasing current velocity or depositional time. Oost and Baas (1994) also evaluated the effect of unsteady flow (common with tidal currents) in the bedform morphology development. These experimental results have been used to constrain the input parameters for our numerical model thereby obtaining realistic geometries. The geometrical input parameters for these general tidal bedforms are found in Table 4.

Firstly, to evaluate how the petrophysical properties vary with sample support, and to isolate the effect of geometry and mud fraction, a two-component system (sand and mud) was used where the petrophysical contrast between the components was constant and equal to 10^4 (sand permeability of 100 mD and mud permeability of 0.01 mD). Smaller sub-models were then extracted from the larger scale model in a systematic manner, where the sub-grid size (i.e. sample volume) is increased in a cubic series (in 30 steps) from the smallest sample in the centre of the realization to the full size (0.3^3 m^3). There was no observed dependency on the location of the centre point of the sub grids. The effective permeability for each sub grid was then calculated for the vertical direction (k_z) and in the horizontal direction along the migration direction for the ripples (k_x). A total of 12 different bedding models (with 10 realizations of each) with varying mud content were used and Figure 6 shows all the results from the simulation where each square represents a specific mud content and sample volume. Note that there is a larger spread in upscaled permeability (more than 2 orders of magnitude) for certain ranges, namely below 40% mud fraction for vertical permeability and above 70% mud fraction for horizontal permeability. This indicates that the effective permeability is dependent on the sample size in these mud fraction ranges. Figure 7 shows the effective vertical permeability vs. sample volume for one of these models; a flaser bedded model with 10% mud fraction where the mud occurs as isolated lenses between the sand lamina sets. Each solid line represents one realization. This example clearly shows that the largest variability occurs at small sample volumes and that the fluctuations are minimized at large scales, consistent with the REV concept outlined above. For each sub-gird size, the coefficient of variation (C_v) was calculated between the realizations (see Jensen et al., 1997, for fuller discussion of use of C_v for petrophysical analysis). As proposed by Corbett and

Jensen (1992), a C_v below 0.5 indicates a statistically homogenous medium, while above 1 the samples can be considered very heterogeneous. It is observed (Figure 7) that the C_v decreases as the sample size (sub-grid size) increases, indicating that the effective property approaches the REV. Note that this REV is related only to geometrical heterogeneity and that spatial correlation in permeability will be likely to increase the absolute size of the representative volume. Similar curves as in Figure 7 were obtained for all the other 11 tidal bedding models and the results for vertical permeability are shown in Figure 8, where it can be seen that the sample volume (for $C_v < 0.5$) varies with mud content (this is in contrast to conclusion of Norris and Lewis, 1991). For vertical permeability (figure 8) there is a steady increase of this inflection point with increasing mud content, but above 40% mud, all the C_v curves lies in the homogeneous region. This behaviour is related to percolation theory, which predicts the point at which one component will start to connect across the model domain. The change in variability expressed with the C_v curve is related to the change in correlation lengths of sand and mud lenses with respect to the model domain. Further analysis of porosity and horizontal permeability is given in Nordahl (2004) where the issues of stationarity, correlation lengths, percolating thresholds and how to define REV on these bedding models are discussed. The permeability values measured at the REV are indicated in Figure 6 by black squares. It is clear that the representative effective permeability trends deviate significantly from the commonly used arithmetic and harmonic averages, which only are correct in the case of a perfectly stratified medium. The effective permeability of the more realistic and complex models used here can thus not be properly estimated with these estimates. Ringrose et al. (2003; this volume) discuss different methods that can be used to describe this trend.

Effect of petrophysical contrast in a three-component system

The previous results were for a two-component system (sand and mud), and the variability observed as a function of sample support was a result only of the geometry of the two components. As mentioned above, most of the sand lamina sets in the Tilje Formation consists of (at least) two different grain size classes. Petrophysically, these facies can then be treated as a three-component system. In this section,

the effect of changing the petrophysical contrast between the two sand components (contrasting lamina) is evaluated and then, keeping this contrast constant, the effect of different permeability of the mud layers is assessed.

Effect of contrast between sand components

The effect of varying the petrophysical contrast within each sand lamina set (Table 3) is evaluated by keeping the permeability of one of the sand components constant and equal to 100 mD and decreasing the permeability of the other component (the silty component). In this case the largest sample volume for each realization was used, such that in all cases the REV has been reached ($C_v < 0.5$). In Figure 9, the effective vertical and horizontal permeability is plotted against the mud fraction for the different contrast cases. In the low mud range, effective permeability is closely related to mud fraction and follows clear separate trends for each contrast case. For vertical permeability there is a change at around 40-50% mud content where the different cases merge towards one curve. The data for horizontal permeability have similar characteristics; however, the convergence of the five contrast cases occurs at around 80% mud fraction. This is again related to the percolation threshold and will be discussed below. Desbarats (1987) found similar threshold values using a markedly different two-component model.

Effect of contrast between sand and mud

The petrophysical properties of the mud layers, and especially the permeability, are difficult to measure and represent a large uncertainty. To evaluate this uncertainty we kept the contrast between the sand and silt component constant (and equal to 1) and varied the mud permeability from 10^{-5} to 10^{0} in six steps (Table 3). The models with mud content of 10%, 35% and 85% are used to evaluate the effects in different flow regimes. The results are plotted in Figure 10 A-D, along with a summary of the study of varying the contrast within sand lamina set (from Figure 9). In the case with only 10% mud, the vertical permeability is dominated by the magnitude of the contrast between the sand components and almost unaffected by varying the mud permeability (Figure 10A) meaning that the

mud lenses only act as weak baffles to the vertical flow. The same was found for horizontal permeability (not shown). Near the percolation threshold for vertical flow (35% mud), vertical permeability shows a strong dependency on the mud permeability (Figure 10B), while horizontal permeability is only weakly affected by the contrast between the sand components (Figure 10C). However, at higher mud contents (85%, Figure 10D), the sand ripples start to disconnect in the horizontal plane meaning that the percolation threshold for horizontal flow is reached. This gives a higher sensitivity to mud properties and less to the variation in permeability contrast within sand lamina set. The results above clearly show how effective permeability in complex, heterolithic deposits can be understood with respect to connectivity of sand and mud laminasets. That is, concepts from both effective medium theory and percolation theory must be used to properly assess this system. These results also indicate that the data collection should be linked with the bedding type. For example, close to and below the percolation thresholds, which are very different for vertical and horizontal flow, mud properties have most influence on effective permeability while the contrast between the cross-stratified components are more important above the percolating threshold.

Error associated with wireline estimates

An important application of these results is that the uncertainty associated with the wireline estimates of porosity and horizontal permeability can be evaluated. Porosity is usually estimated by using a neutron or density wireline log with a calibration to the core porosity. Although porosity is not an extensive property, it is volume-normalised and consequently additive (Narasimhan, 1983). Since the wireline tool physically measures quantities closely related to the total porosity (e.g. Hook, 2003), the integration between core porosity and the wireline tools often is quite reliable. However, in heterolithic deposits, the core plugs tend to be a biased sample (see Figure 4) since the mud layers are only occasionally sampled and this may adversely influence the integration. A traditional method to estimate horizontal permeability is to establish a regression equation between core porosity and core permeability and use this to estimate wireline permeability from the wireline estimate of porosity or by the use of some semi-empirical equations (e.g. Kozeny-Carman). Permeability being an intensive,

non-additive property will, in general, not be predictable with respect to porosity. This is especially the case when the sample support is very different, as in the case of core plugs and wireline tools, and when the scale of heterogeneity is between these two volume scales. With the SBED™ tool, porosity and permeability input distributions are taken directly from core plugs, probe permeameter measurements or thin sections, and assigned for each lamina and then rescaled to the scale of interest with a realistic bedding model. We thus have a method to address the uncertainty in the wireline estimate.

To illustrate this, models of lithofacies 7.1 have been used. This facies is from the upper part of the studied interval, which is a dominantly flaser-bedded facies with some thicker mud layers separating the different sets (see also Figure 2 and 4 and Table 2). The near wellbore model of this facies was evaluated at a scale large enough for representative properties to be obtained (in this case 10^6 cm^3). Figure 4 shows the core photo with the positions of the core plugs and the thicker mud layers characteristic of this facies indicated. Note that the core plugs in general miss the mud layers giving a biased dataset.

Although porosity is an easier parameter to estimate, the bias in the core plug data set towards sand properties will influence on the calibration process with the wireline tool. Figure 11A shows the distribution of the core plugs, the wireline estimate and a data set measured on a representative scale from the near wellbore model. In accordance with the REV concept, a reduction in the variance is observed when going from the measures representing the smallest volume to the largest. However, due to under-sampling of the mud layers, the correct and representative porosity value is somewhat lower. In this case, the error is not large compared to the wireline estimate, but it illustrates well the problem with biased sampling.

Figure 11B shows the result for horizontal permeability. In such a low-mud content facies, the dependency of the mud properties on horizontal permeability is small (see also figure 10C). However,

by using the estimate made at a representative scale we see that the variance in the data set is reduced, thereby giving a less uncertain estimate of this property.

The ratio between vertical and horizontal permeability (k_v/k_h) is both a difficult property to measure and an important property in reservoir simulation (Brandsæter et al., 2001). This parameter is particular sensitive to the geometry and the petrophysical properties of the mud layers. There is no wireline estimate for this property, and estimates from production data are often uncertain. However, by using the near wellbore model, a representative value for k_v/k_h for this facies can be found. Figure 11C shows that this estimate is lower than the estimate from core plug data, which is expected because of the bias in this data set. The minimum value of the simulated k_v/k_h ratio is higher than the minimum value from core plugs. This is because the few mud layers sampled (by the core plugs) are continuous in the sample but are discontinuous at the scale of the model. This difference in mud layer continuity from core plugs to a larger-scale 3D model has also been noted by Jackson et al. (2003). The k_v/k_h ratio will be very dependent on the chosen mud permeability, but even with the rather high value used here (0.01 mD), the difference to the core plug estimate is significant.

There are still issues that have to be addressed in the future to further reduce uncertainty. The true properties of the different components and especially the mud properties will be critical, and the probe permeameter data can play an important role to assess the sand lamina set variability. To be able to directly simulate the wireline tool responses on the near wellbore model would greatly advance the basis for an improved integration. Since some of the sedimentological elements models have correlation lengths that approach the model size, it would be useful to use more advanced upscaling techniques (e.g. periodic boundary conditions; Durlofsky, 1991) to calculate the effective properties. In addition, the effect of multiphase flow in this heterogeneous system is not considered here and should be investigated. As a result, much more work is still required to properly characterise these heterolithic deposits. However, the introduction of the near wellbore model, common to the

sedimentologist, the petrophysicist and the reservoir engineer, is an important step towards a better and fully integrated characterisation of these reservoirs.

Conclusion

Estimation of petrophysical properties in reservoirs where there are large petrophysical variations at the scale of core plugs and wireline logs is challenging. A key element of this paper is that in these heterogeneous reservoir intervals, the core plug values cannot be used directly in calibration and integration with wireline data since they represent measurements from a different sample support and a biased sample.

A process-based numerical modelling tool has been used to evaluate the near wellbore region of a tide influenced and heterogeneous reservoir interval in the Heidrun field in the Haltenbanken area, offshore mid-Norway. A method for parameterisation of the core data useful for this modelling tool has been proposed and successfully used to create realistic facies models from the interval. Also a method to establish the underlying distributions of a three-component sedimentary system from simulation of core plugs is outlined. The near wellbore model is used to rescale the core plug data to the scale of interest giving a better basis for comparing with other well data.

The variation of effective properties as a function of sample support has been evaluated. It is found that the variability is reduced at some sample volume and that the size of this volume was dependent on the mud content. The trends observed between representative permeability values and mud fraction are related to the percolation thresholds. By changing the contrast between the sand components and between the sand and the mud, different sensitivity to these contrasts were identified and this should guide the data collection in the well.

The results were also used to evaluate the uncertainty associated with the wireline estimates. The k_v/k_h ratio is often the most difficult parameter to estimate from available well data, and we have shown

how a better and less uncertain estimate can be made. Ringrose et al. (this volume) discuss the estimation of vertical permeability both in the Heidrun field and in the deeper buried and more complex Smørbukk field.

Acknowledgement

The first author will thank the Formation Evaluation Project at Norwegian University of Science and Technology for financial support. Comments from Inge Brandsæter, Arve Næss, Allard Martinius and Sverre Ola Johnsen during the work are appreciated. The comments from two anonymous reviewers are gratefully acknowledged. Simulations were performed using the SBED™ software package (Geomodeling Technology Corp.).We thank Statoil ASA for permission to publish the data.

References

Baas, J. H. 1994. A flume study on the development and equilibrium morphology of current ripples in very fine sand. *Sedimentology*, **41**, 185-209.

Bear, J. 1972. Dynamics of fluids in porous media. American Elsevier, New York.

Begg, S. H. and King, P. R. 1985. Modelling the effects of shales on reservoir performance: Calculation of effective vertical permeability. Paper SPE 13529 presented at the 1985 SPE Symposium on Reservoir Simulation, Dallas, TX, Feb. 10-13.

Brandsæter, I. Wist, H. T., Næss, A. et al. 2001. Ranking of stochastic realizations of complex tidal reservoirs using streamline simulation criteria. *Petroleum Geoscience*, **7**, S53-S63.

Corbett, P. W. M., Ringrose, P. S., Jensen, J. L. and Sorbie, K. S. 1992. Laminated clastic reservoirs: the interplay of capillary pressure and sedimentary architecture. Paper SPE 24699 presented at the 67th SPE Annual Technical Conference and Exhibition.

Corbett. P. W. K. and Jensen, J. L. 1992. Estimating the mean permeability: how many measurements do you need? *First Break*, **10**, 89-94.

Corbett, P. W. M. and Jensen, J. L. 1993. Application of probe permeametry to the prediction of two-phase flow performance in laminated sandstones (lower Brent Group, North Sea). *Marine and Petroleum Geology*, **10**, 335-346.

Corbett, P. W. M., Jensen, J. L. and Sorbie, K. S. 1998. A review of upscaling and cross-scaling issues in core and log data interpretation and prediction. *In*: Harvey, P. K. and Lovell, M. A. (eds.) *Core-Log Integration*, Geological Society, London, Special Publications, **136**, 9-16.

Dagan, G. 1979. Models of groundwater flow in statistically homogeneous porous formations. *Water Resources Research*, **15**, No. 1, 47-63.

Desbarats, A. J. 1987. Numerical estimation of effective permeability in sand-shale formations. *Water Resources Research*, **23**, No. 2, 273-286.

Deutsch, C. 1989. Calculating effective absolute permeability in sandstone/shale sequences. *SPE Formation Evaluation*, **4**, No. 3, 343-348.

Durlofsky, L. J. and Chung, E. Y. 1990. Effective Permeability of heterogeneous reservoir regions. *In*: Guérillot, D. and Guillon, O. (eds.) *2nd European Conference on the Mathematics of Oil Recovery*, Paris, 57-64.

Durlofsky, L. J. 1991. Numerical calculation of equivalent grid block permeability tensors for heterogeneous porous media. *Water Resources Research*, **27**, 699-708.

Enderlin, M. B., Hansen, D. K. T. and Hoyt, B. R. 1991. Rock volumes: Considerations for relating well log and core data. *In*: Lake, L. W., Carroll, H. B. and Wesson, T. C. (eds.) *Reservoir Characterization II*, Academic Press, San Diego, 277-288.

Haldorsen, H. H. 1986. Simulator parameter assignment and the problem of scale in reservoir engineering. *In*: Lake, L. W. and Carroll, H. B. (eds.) *Reservoir Characterization*, Academic Press, Orlando, 293-340.

Halvorsen, C. and Hurst, A. 1990. Principles, practice and applications of laboratory mini-permeametry. *In*: Worthington, P. F. (ed.) *Advances in Core Evaluation: Accuracy and Precision in Reserves Estimation*, *Reviewed proceedings of the First Society of Core Analysts European Core Analysis Symposium,* London. Gordon and Breach Science Publishers, 521-549.

Hartkamp-Bakker, C. A. and Donselaar, M. E. 1993. Permeability patterns in point bar deposits: Tertiary Loranca Basin, central Spain. *In*: Flint, S. S. and Bryant, I. D. (eds.) *The Geological modelling of hydrocarbon reservoirs and outcrop analogues,* Special Publication of the International Association of Sedimentologist, **15**, 157-168.

Hook, J. R. 2003. An introduction to porosity. *Petrophysics*, **44**, No. 3, 205-212.

Hurst, A. and Rosvoll, K. 1991. Permeability variations in sandstone and their relationship to sedimentary structures. *In*: Lake, L. W., Carroll, H. B. and Wesson, T. C. (eds.) *Reservoir Characterization II*, Academic Press, San Diego, 166-196.

Jackson, M. D., Muggeridge, A. H., Yoshida, S. and Johnson, D. 2003. Upscaling permeability measurements within complex heterolithic tidal sandstones. *Mathematical Geology*, **35**, No. 5, 499-519.

Jensen, J. L., Lake, L. W., Corbett, P. W. M. and Goggin, D. J. 1997. *Statistics for Petroleum Engineers and Geoscientists*. Prentice Hall PTR, New Jersey.

Koltermann, C. E. and Gorelick, S. M. 1996. Heterogeneity in sedimentary deposits: A review of structure imitating, process-imitating and descriptive approaches. *Water Resources Research*, **32**, No. 9, 2617-2658.

Martinius, A. W., Kaas, I., Næss, A., Helgensen, G., Kjærefjord, J. M. and Leith, D. A. 2001. Sedimentology of the heterolithic and tide-dominated Tilje Formation (Early Jurassic, Halten Terrace, offshore mid-Norway). *In*: Martinsen, O. M. and Dreyer, T. (eds.) *Sedimentary Environments Offshore Norway – Palaeozoic to Recent*. NPF Special Publication **10**, 103-144, Elsevier Science B. V, Amsterdam.

Martinius, A. W., Ringrose, P. S., Brostrøm, C., Elfenbein, C., Næss, A. and Ringås, J. E. (this volume). Reservoir challenges of heterolithic tidal hydrocarbon fields (Halten Terrace, Mid Norway).

Narasimhan, T. N. A note on volume-averaging. 1983. *In*: Pinder, G. F. (ed.) *Flow through porous media*. A Computational Mechanics Publication, CML Publications, 46-50.

Nordahl, K. 2004. *A petrophysical evaluation of tidal heterolithic deposits: application of a near wellbore model for reconciliation of scale dependent well data*. PhD thesis, Norwegian University of Science and Technology, Trondheim, Norway.

Norris, R. J. and Lewis, J. J. M. 1991. The geological modelling of effective permeability in complex heterolithic facies. Paper SPE 22692 presented at the 66th Annual Technical Conference and Exhibition, Dallas October 6-9, 359-374.

Oost, A. P. and Baas, J. H. 1994. The development of small scale bedforms in tidal environments: an empirical model for unsteady flow and its applications. *Sedimentology*, **41**, 883-903.

Pickup, G. E., Ringrose, P. S., Corbett, P. W. M., Jensen, J. L. and Sorbie, K. A. 1995. Geology, geometry and effective flow. *Petroleum geoscience*, **1**, 37-42.

Pickup, G., Ringrose, P. S. and Sharif, A. 2000. Steady-state upscaling: from lamina-scale to full-field model. *SPE Journal*, **5**, No. 2, 208-217.

Nordahl, K., Ringrose, P. S. and Wen, R.
Accepted for publication in Petroleum Geoscience as of 19 September 2004

Reineck, H-E. and Wunderlich, F. 1968. Classification and origin of flaser, and lenticular bedding. *Sedimentology*, **11**, 99-104.

Renard, Ph. and de Marsily, G. 1997. Calculating equivalent permeability: a review. *Advances in Water Resources*, **20**, No. 5-6, 253-278.

Ringrose, P. S., Pickup, G. E., Jensen, J. L. and Forrester, M. 1999. The Ardoss reservoir gridblock analogue: Sedimentology, statistical representivity and flow upscaling. *In*: Schatzinger, R. and Jordan, J. (eds.), *Reservoir Characterization – Recent Advances*, AAPG Memoir **71**, 265-276.

Ringrose, P. S., Skjetne, E. and Elfenbein, C. 2003. Permeability estimation functions based on forward modeling of sedimentary heterogeneity. Paper SPE 84275 presented at the SPE Annual Technical Conference and Exhibition, Denver, Colorado, 5-8 October 2003.

Ringrose , P., Nordahl, K. and Wen, R. (this volume). Vertical permeability estimation in tidal deltaic reservoir systems. Rubin, D. M. 1987. Cross-bedding, Bedforms, and Paleocurrents. *Concepts in Sedimentology and Paleontology*, *Volume 1*, Society of Economic Paleotologists and Mineralogists Special Publication.

Rubin, D. M. 1988. Cross-bedding, bedforms, and palaeocurrents. *Concepts in Sedimentology and Paleontology, Volume 1*, Society of Economic Palaeontologists and Mineralogists Special Publication.

Warren, J. E. and Price, H. S. 1961. Flow in heterogeneous porous media. *Society of Petroleum Engineer Journal*, **1**, 153-169.

Weber, K. J. 1982. Influence of common sedimentary structures on fluid flow in reservoir models. *Journal of Petroleum Technology*, **34**, 665-672.

Wen, R., Martinius, A. W., Næss, A. and Ringrose, P. 1998. Three-dimensional simulation of small-scale heterogeneity in tidal deposits – a process-based stochastic simulation method. *In*: Buccianti, A, Nardi, G. and Potenza, R. (eds.) *Proceedings of the 4th Annual Conference of the International Association of Mathematical Geology (IAMG)*, Ischia, 129-134.

White, C. D. and Horne, R. N. 1987. Computing absolute transmissibility in the presence of fine-scale heterogeneity. SPE Paper 16011, Presented at the 9th SPE Symposium on Reservoir Simulation, San Antonio, TX, February 1-4, 209-220.

Worthington, P. F. 1994. Effective integration of core and wireline data. *Marine and Petroleum Geology*, **11**, No. 4, 457-466.

Figure 1: Concept of Representative Elementary Volume (REV). In this paper, the microscopic domain refers to the scale from lamina to bed set, while the macroscopic domain to a scale larger than the lithofacies. Modified after Bear (1972).

Figure 2: Core data and wireline estimate from the studied interval in the Tilje Formation. The facies associations are from Martinius et al. (2001).

Figure 3: A: Schematic sketch of the generation of lamina surfaces in SBED between the t=1 and t=2 in the time series of equation 1. The grey area is the preserved lamina and the arrow indicates the vector that displaces the surface to mimic bedform migration. Note that the y-direction is not shown and that the preserved lamina is a 3D volume. B: Simulated 3D sand and mud laminaset in SBED. C: A realization of a sedimentological model. The three different lithological components present in the geometrical model can be clearly seen; sand (grey), silt (dark grey) and mud (black). D: A realization of a permeability model. The model size in C and D is 30 by 30 by 10 cm.

Figure 4: Core photo and 3D near wellbore model of the selected lithofacies 7.1 (see Figure 2 and Table 4). The cylinders indicate the positions of the vertical and horizontal core plugs and the arrows indicate the thick mud layers. Note that the core plugs do not generally sample the mud layers (biased samples).

Figure 5: Comparison between the core plug data (black bars) and the simulated core plugs (crosshatched bars) for horizontal permeability (A) and porosity (B). The solid (silt) and dashed (sand) curves show the input distributions that were used to obtain the simulated core plug distribution. The input porosity distribution was truncated at 50% porosity. The mud component was given a low and constant value (grey bar). Inserted in Figure 5A is also the probe-permeameter distribution, which has approximately the same variability as the input sand and silt curves.

Figure 6: Simulated horizontal (k_x, white circles) and vertical (k_z, white squares) permeability representing different sample volumes and mud contents (total of 3600 data points). The values measured at the REV are marked by black squares (k_z) and circles (k_x). The solid lines represent the harmonic, geometric and arithmetic averages.

Figure 7: Example of variation in vertical permeability with sample volume in a low mud content (10%) flaser bedded model. Each solid line represents one realization and the dashed line is the C_V curve calculated between the ten realizations at each volume step. At volumes larger than about 2000 cm^3, the C_V value becomes lower than 0.5.

Figure 8: The C_V curve for vertical permeability for 12 different tidal bedding models with varying mud fraction. Each C_V - line is based on similar calculations as Figure 7.

Figure 9: Effective vertical (white) and horizontal (grey) permeability with varying contrast between the sand and silt component (constant mud permeability). The plot is based on 240 realizations all at a REV scale. See table 3 for petrophysical input parameters.

Figure 10: Effect of changing the mud permeability. Inserted are also the relevant results from Figure 9.Three mud fraction models are used: A) low mud content case (10%), B) and C) near the percolating threshold for vertical flow (35%), and D) a high mud content (85%) lenticular bedded model near the percolation threshold for horizontal flow. See table 3 for petrophysical input parameters.

Figure 11: Comparison of porosity (A), horizontal permeability (B) and kv/kh-ratio (C) estimated or measured from different sources and sample volumes. The lower and upper limits of the box indicate the 25^{th} and the 75^{th} percentile while the whiskers represent the 10^{th} and the 90^{th} percentile. The solid line is the median and the black dots are the outliers. The values at the REV are measured on the bedding model at a representative scale and the distribution is based on ten realizations. There exist no wireline estimate for the kv/kh-ratio.

Table 1: Recorded sedimentological core data (left) and main input parameter groups in SBED™ (right).

Core Parameters	Geometrical input parameters
Lamina thickness (mean and standard deviation)	Bedform morphology (plan form and cross-section)
Sand/Mud laminaset thickness (mean and standard deviation)	Migration speed and direction
Periodic components (wavelength and amplitude)	Depositional rate and length for sand and mud
Bedding type (i.e. geometry of mud layers)	

Table 2: Core statistics for of sand and mud lamina set thickness in the selected lithofacies 7.1.

Component	Parameter	Core	Simulation
Sand lamina set	n	11	117
	Arithmetic average	20.14	21.1
	Standard deviation	18.64	1.98
	Median	15.9	21
	Mode	N/A	21
	Minimum	2	20.5
	Maximum	59.2	42.2
	Total cm	221.5	2468.4
Mud lamina set	n	11	117
	Arithmetic average	0.68	0.421
	Standard deviation	0.35	0.18
	Median	0.8	0.4
	Mode	0.8	0.5
	Minimum	0.1	0.1
	Maximum	1.2	0.9
	Total cm	7.5	49.2
Sand fraction		0.967	0.98
Number of mud layers per meter		4.8	4.65

Table 3: Petrophysical input parameters used; mean (standard deviation). The upper part relates to Figure 6-10.

	Sand Component	Silt Component	Mud Component
Sand-Silt Contrast 1:1	100 mD	100 mD	0.01 mD
Sand-Silt Contrast 1:2	100 mD	50 mD	0.01 mD
Sand-Silt Contrast 1:5	100 mD	20 mD	0.01 mD
Sand-Silt Contrast 1:10	100 mD	10 mD	0.01 mD
Sand-Silt Contrast 1:100	100 mD	1 mD	0.01 mD
Sand-Mud Contrast 10^{0}	100 mD	100 mD	1 mD
Sand-Mud Contrast 10^{-1}	100 mD	100 mD	0.1 mD
Sand-Mud Contrast 10^{-2}	100 mD	100 mD	0.01 mD
Sand-Mud Contrast 10^{-3}	100 mD	100 mD	0.001 mD
Sand-Mud Contrast 10^{-4}	100 mD	100 mD	0.0001 mD
Sand-Mud Contrast 10^{-5}	100 mD	100 mD	0.00001 mD
Lithofacies 7.1 (fig. 4, 5 and 11)	Mean ln 6 (0.2) StDev ln 1.2 (0)	Mean ln 4.5 (0.2) StDev ln 1 (0)	0.01 mD (0)

Table 4: Input geometrical parameters for the tidal bedding models; mean (standard deviation). The bedform morphology parameters have dimensions in centimetre, while the depositional parameters are relative length and rate. The variability were modelled with a spherical variogram with range = 3 cm for all the parameters. MF = Mud Fraction.

Control parameter	MF_0	MF_0.1	MF_0.2	MF_0.25	MF_0.3	MF_0.35	MF_0.4	MF_0.5	MF_0.6	MF_0.7	MF_0.8	MF_0.85	MF_0.9	Example facies (fig. 4 and 11)
Bedform_1 Wavelength	20 (1)	20 (1)	20 (1)	20 (1)	20 (1)	20 (1)	20 (1)	20 (1)	20 (1)	19 (0.9)	18 (0.8)	12 (0.7)	9 (0.1)	20 (1)
Bedform_1 Amplitude	0.2 (0.05)	0.2 (0.05)	0.2 (0.05)	0.2 (0.05)	0.2 (0.05)	0.2 (0.05)	0.2 (0.05)	0.2 (0.05)	0.2 (0.05)	0.19 (0.045)	0.18 (0.04)	0.12 (0.035)	0.1 (0.01)	0.2 (0.05)
Bedform_2 Wavelength	18 (0.5)	18 (0.5)	18 (0.5)	18 (0.5)	18 (0.5)	18 (0.5)	18 (0.5)	18 (0.5)	18 (0.5)	17 (0.45)	15 (0.4)	10 (0.035)	8 (0.03)	18 (0.5)
Bedform_2 Amplitude	0.18 (0.05)	0.18 (0.05)	0.18 (0.05)	0.18 (0.05)	0.18 (0.05)	0.18 (0.05)	0.18 (0.05)	0.18 (0.05)	0.18 (0.05)	0.17 (0.045)	0.15 (0.04)	0.1 (0.035)	0.09 (0.001)	0.18 (0.05)
Crest Sinousity_1 Wavelength	20 (0.5)	20 (0.5)	20 (0.5)	20 (0.5)	20 (0.5)	20 (0.5)	20 (0.5)	20 (0.5)	20 (0.5)	22.5 (0.5)	25 (0.5)	30 (0.5)	35 (0.5)	20 (0.2)
Crest Sinousity_1 Amplitude	5 (0.2)	5 (0.2)	5 (0.2)	5 (0.2)	5 (0.2)	5 (0.2)	5 (0.2)	5 (0.2)	5 (0.2)	4.5 (0.2)	4 (0.2)	3 (0.2)	2 (0.2)	5 (0.5)
Crest Sinousity_2 Wavelength	30 (0.6)	30 (0.6)	30 (0.6)	30 (0.6)	30 (0.6)	30 (0.6)	30 (0.6)	30 (0.6)	30 (0.6)	32.5 (0.6)	35 (0.6)	37.5 (0.6)	40 (0.6)	30 (1)
Crest Sinousity_2 Amplitude	3 (0.3)	3 (0.1))	3 (0.1)	3 (0.1)	3 (0.1)	3 (0.1)	3 (0.1)	3 (0.1)	3 (0.1)	2.75 (0.1)	2.5 (0.1)	2 (0.1)	1.5 (0.1)	3 (0.05)
Depositional Rate: Sand	0.3 (0.01)	0.3 (0.01)	0.25 (0.01)	0.235 (0.01)	0.225 (0.01)	0.21 (0.01)	0.2 (0.01)	0.175 (0.01)	0.15 (0.01)	0.125 (0.01)	0.1 (0.01)	0.08 (0.01)	0.07 (0.01)	0.3
Depositional Length: Sand	4 (0.1)	3.5 (0.1)	3 (0.1)	2.85 (0.1)	2.75 (0.1)	2.6 (0.1)	2.5 (0.1)	2.25 (0.1)	2 (0.1)	1.75 (0.1)	1.5 (0.1)	1.25 (0.075)	1 (0.05)	70 (0.1)
Depositional Rate: Mud	0 (0)	0.1 (0.01)	0.14 (0.01)	0.155 (0.01)	0.16 (0.01)	0.17 (0.01)	0.18 (0.01)	0.2 (0.01)	0.22 (0.01)	0.24 (0.01)	0.25 (0.01)	0.26 (0.01)	0.27 (0.01)	0.1
Depositional Length: Mud	0 (0)	3.5 (0.1)	4 (0.1)	4.15 (0.1)	4.25 (0.1)	4.4 (0.1)	4.5 (0.1)	4.75 (0.1)	5 (0.1)	5.25 (0.1)	5.5 (0.1)	5.75 (0.1)	6 (0.1)	7.5 (1)
Average (StDev) sand fraction	*1 (0)*	*0.922 (0.003)*	*0.804 (0.008)*	*0.744 (0.008)*	*0.715 (0.008)*	*0.658 (0.01)*	*0.612 (0.01)*	*0.5 (0.09)*	*0.391 (0.009)*	*0.273 (0.011)*	*0.198 (0.014)*	*0.125 (0.09)*	*0.081 (0.09)*	0.985 (0.12)

Figure 1

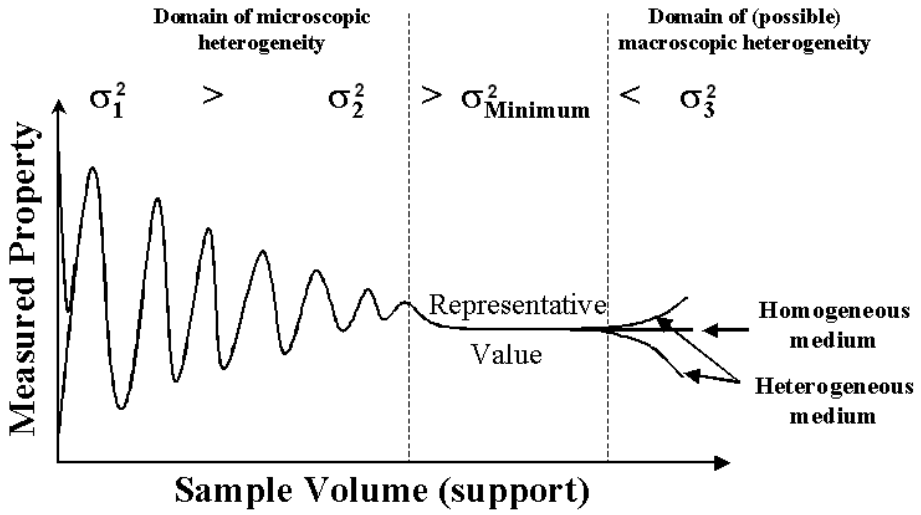

Figure 2

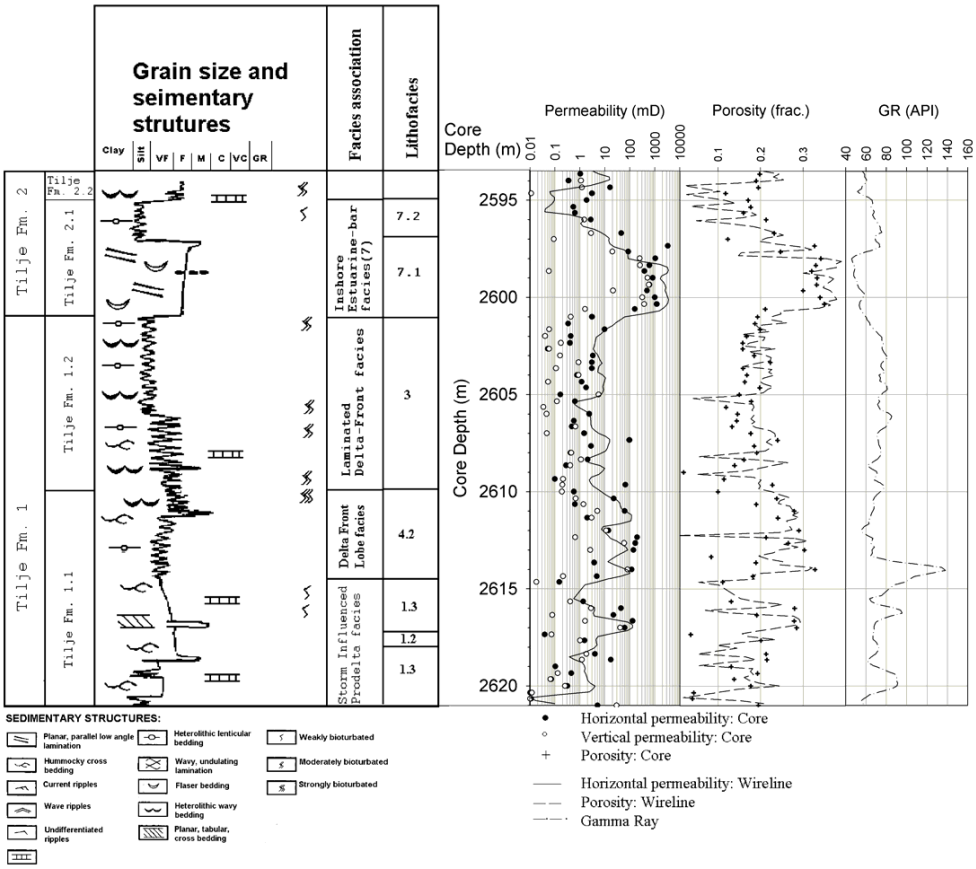

Figure 3

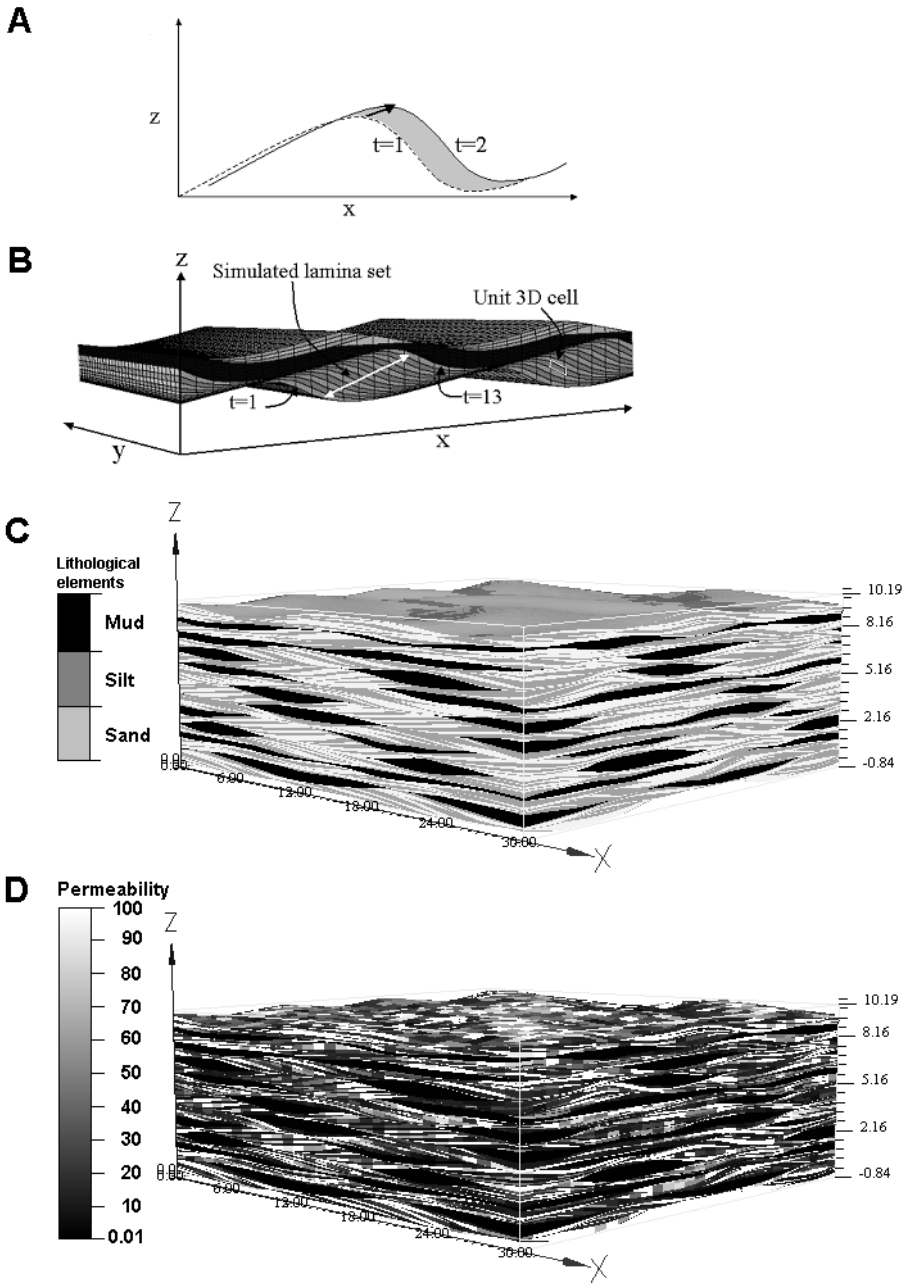
A
z
t=1
t=2
x
B
z
Simulated lamina set
Unit 3D cell
t=1
t=13
y
x
C
Z
Lithological elements
Mud
Silt
Sand
10.19
8.16
5.16
2.16
-0.84
0.00
6.00
12.00
18.00
24.00
30.00
X
D
Permeability
100
90
80
70
60
50
40
30
20
10
0.01
Z
10.19
8.16
5.16
2.16
-0.84
0.00
6.00
12.00
18.00
24.00
30.00
X

Figure 4

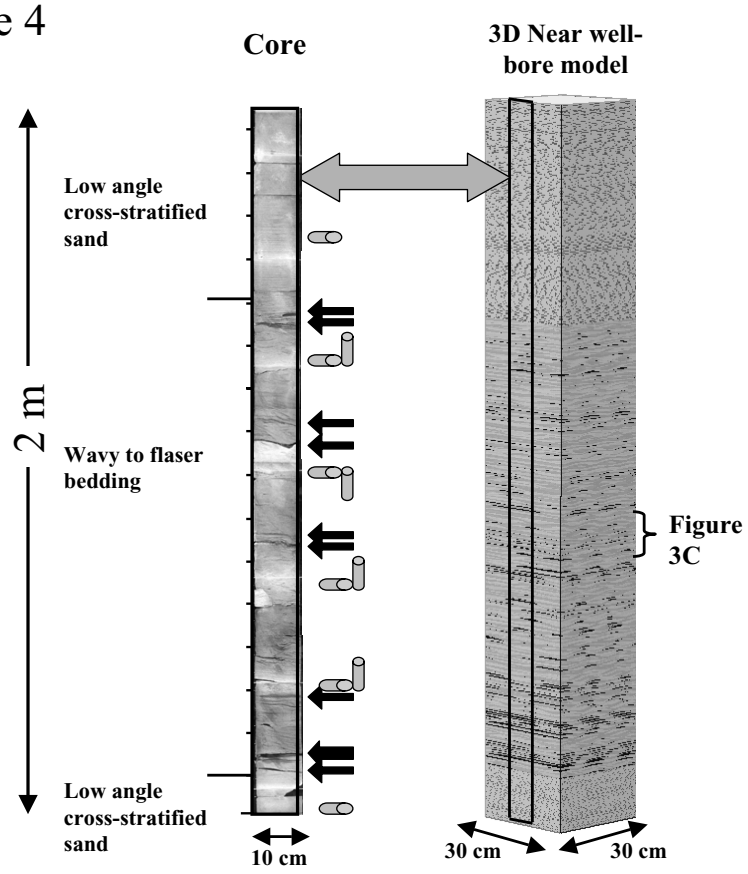

Figure 5a

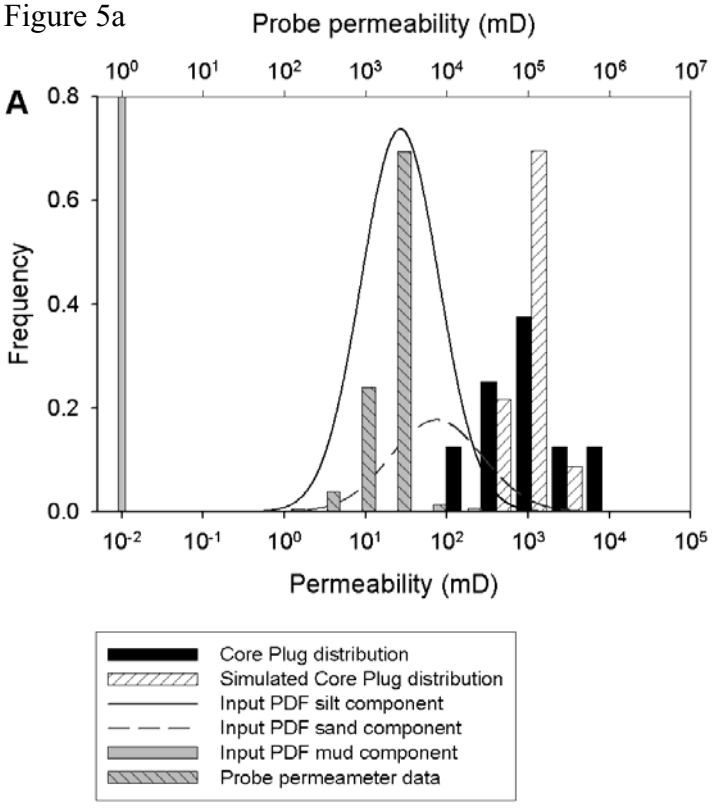

Figure 5b

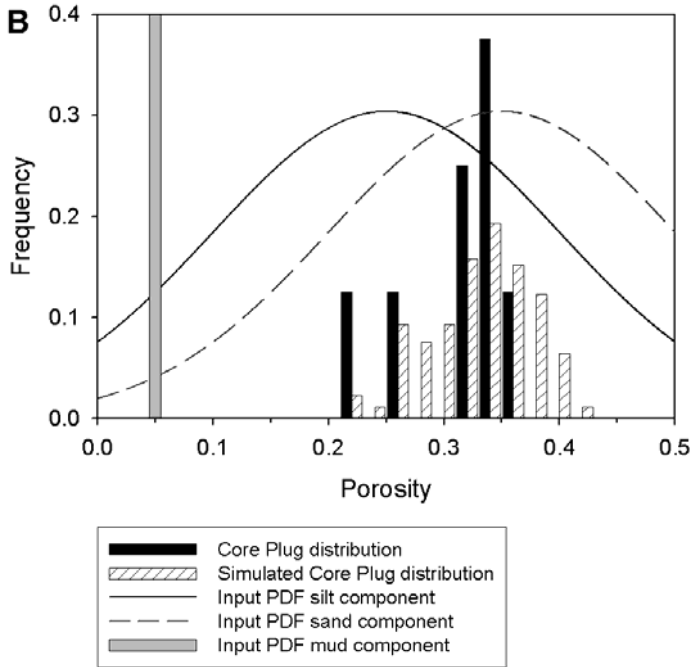

Figure 6

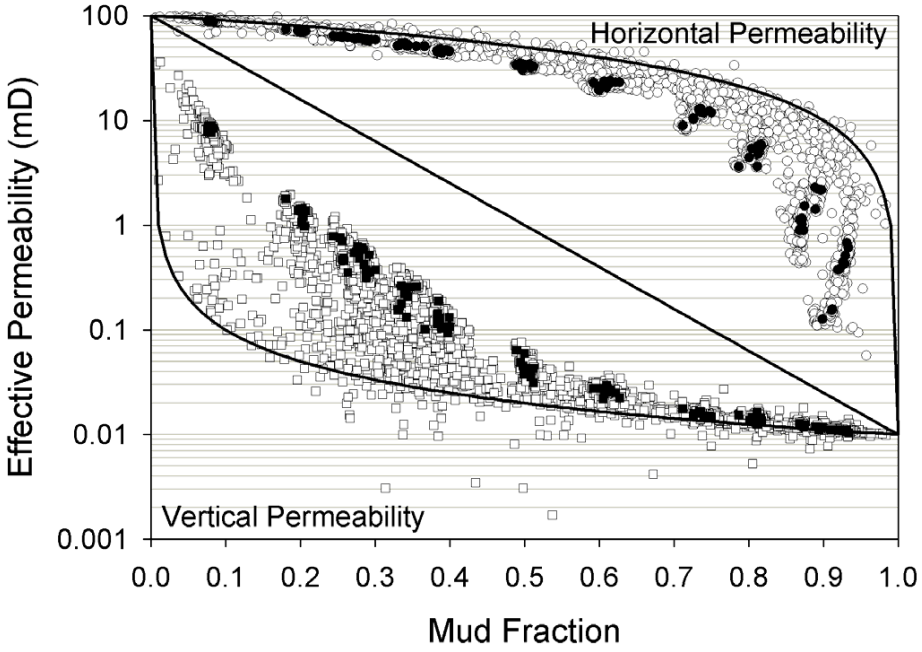

Figure 7

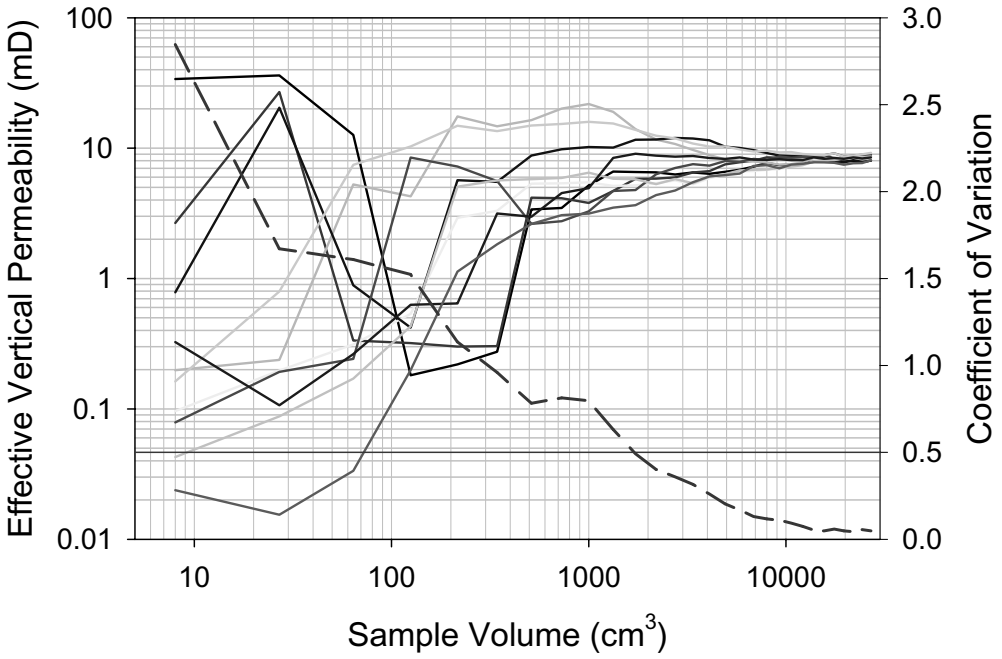

Figure 8

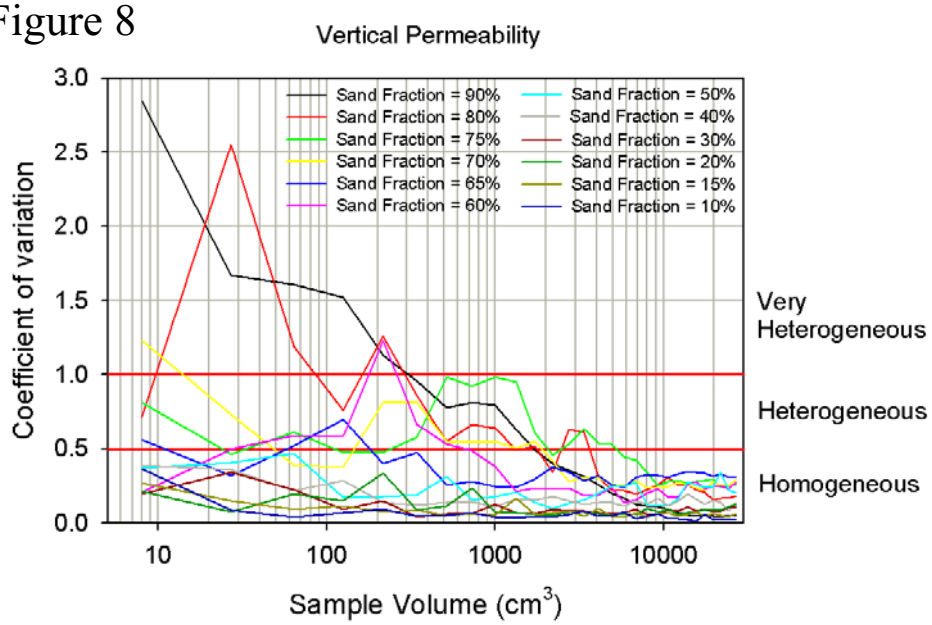

Figure 9

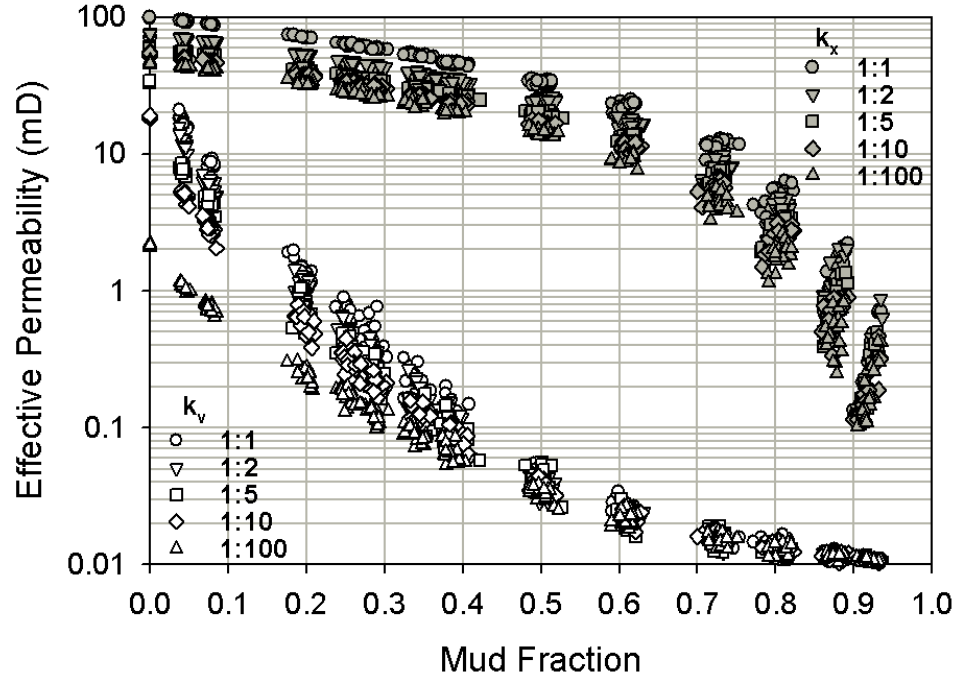

Figure 10A

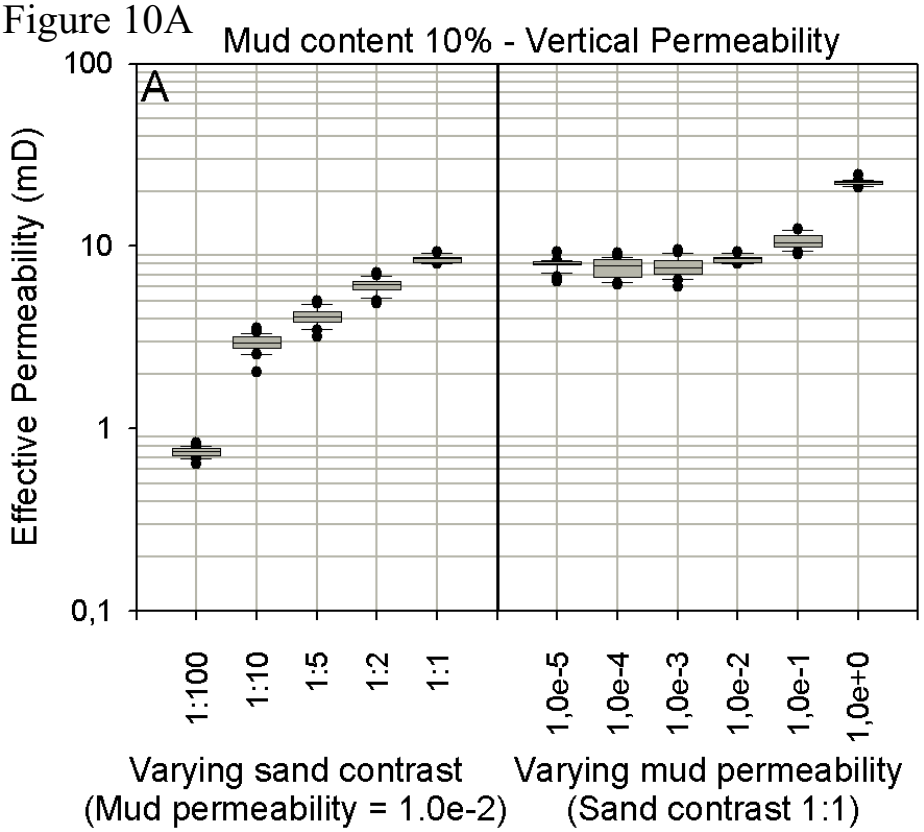

Figure 10B

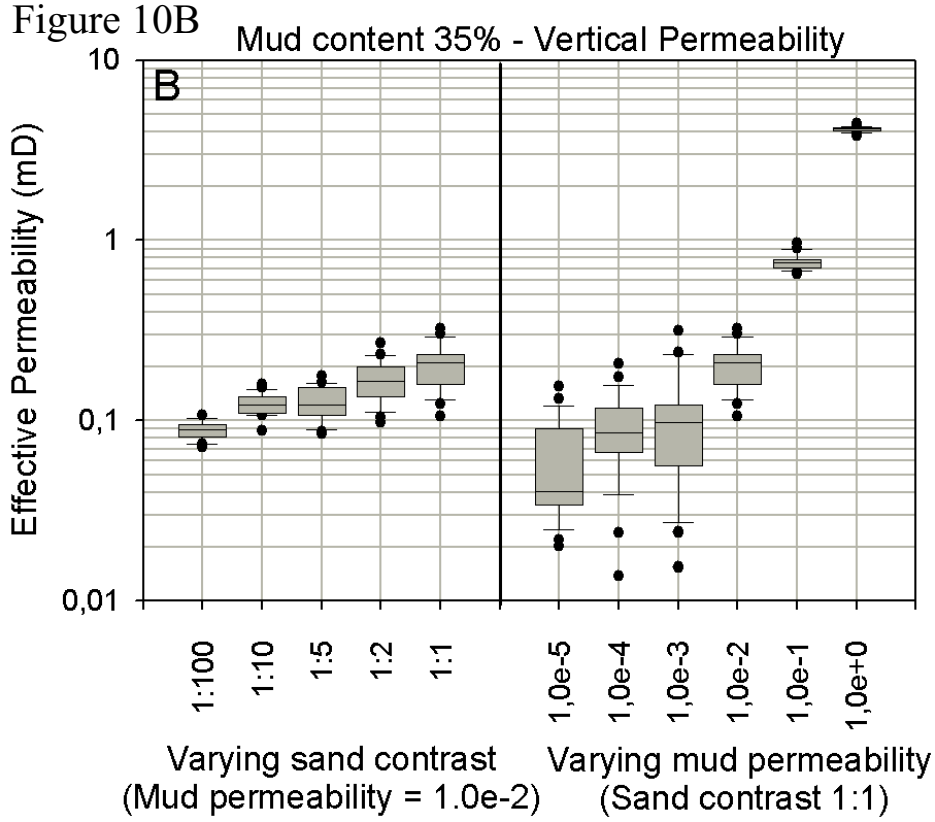

Figure 10C

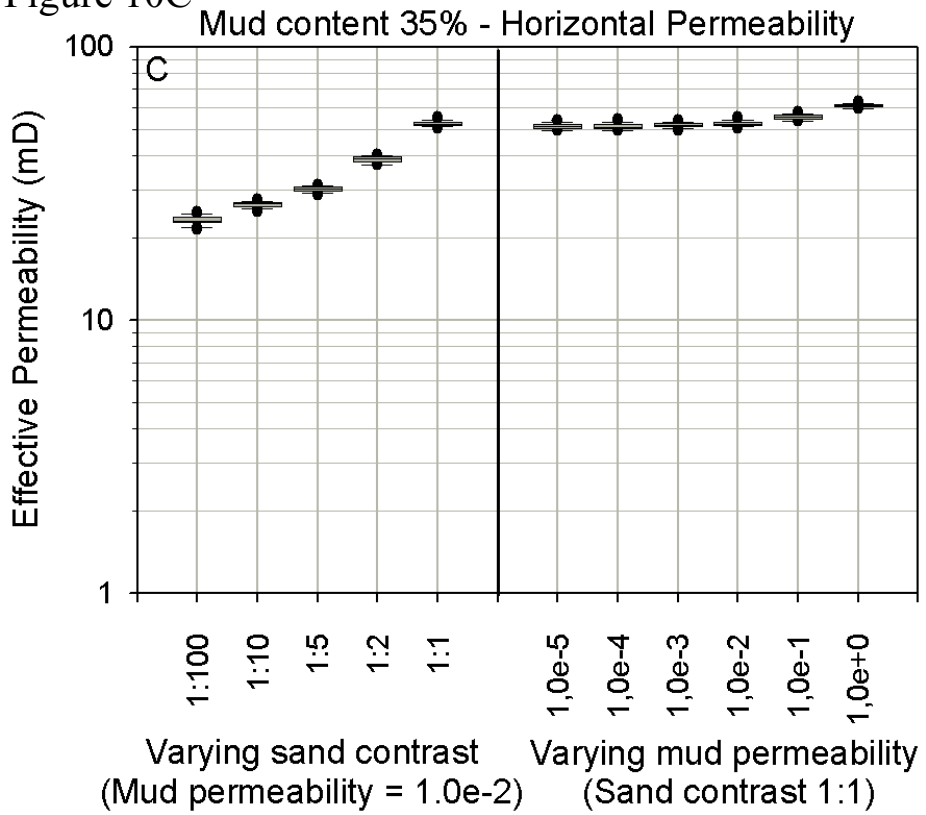

Figure 10D

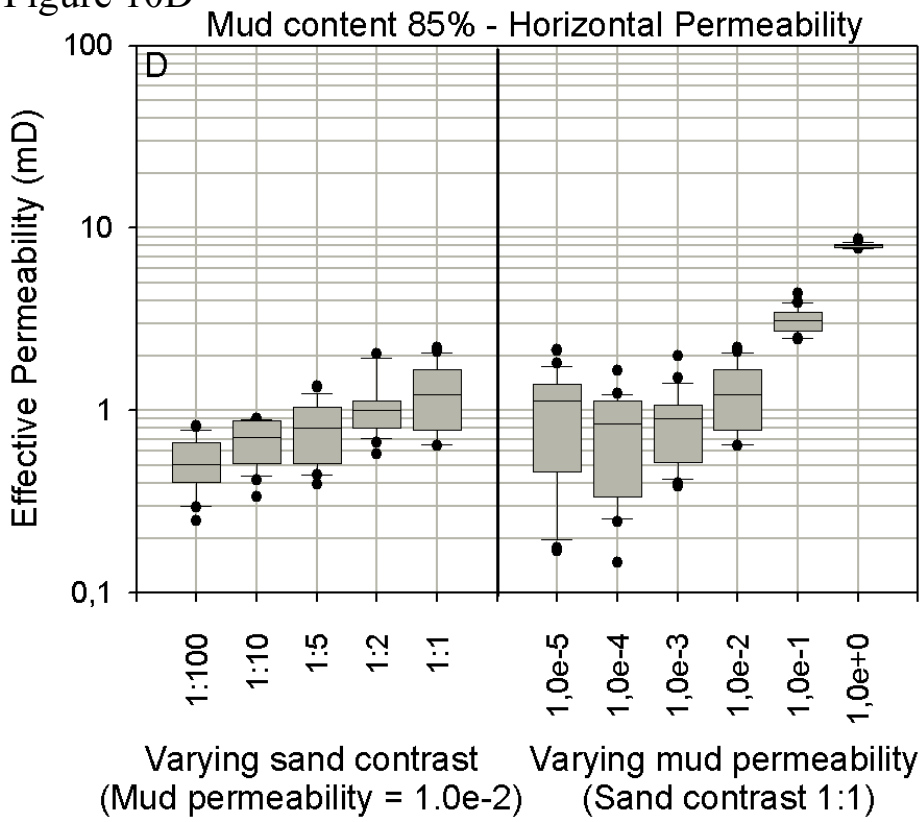

Figure 11A

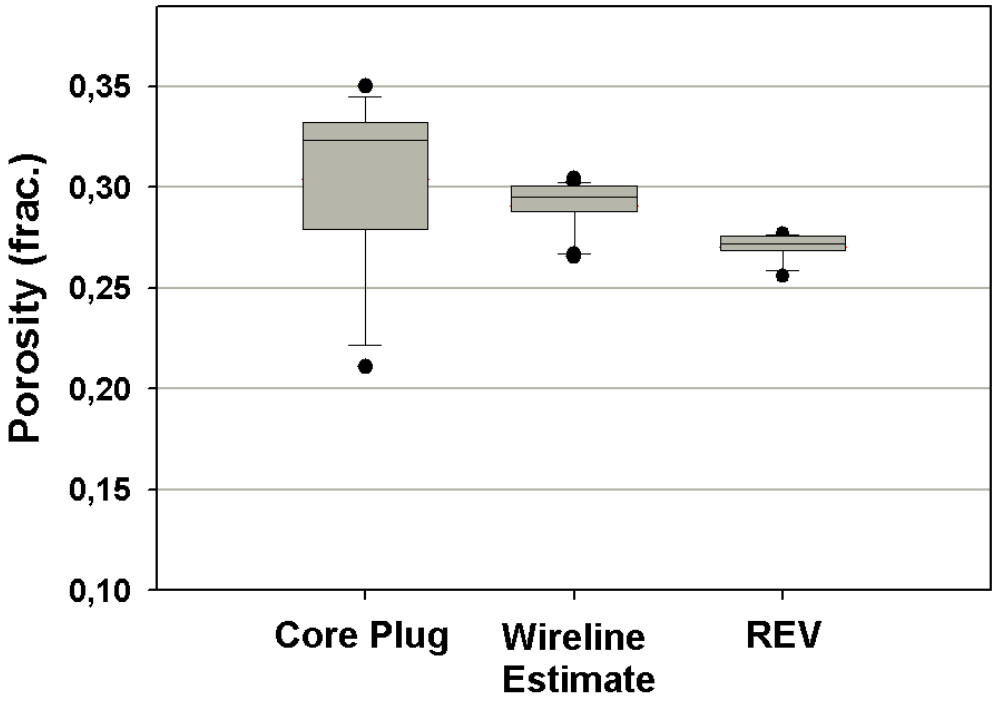

Figure 11B

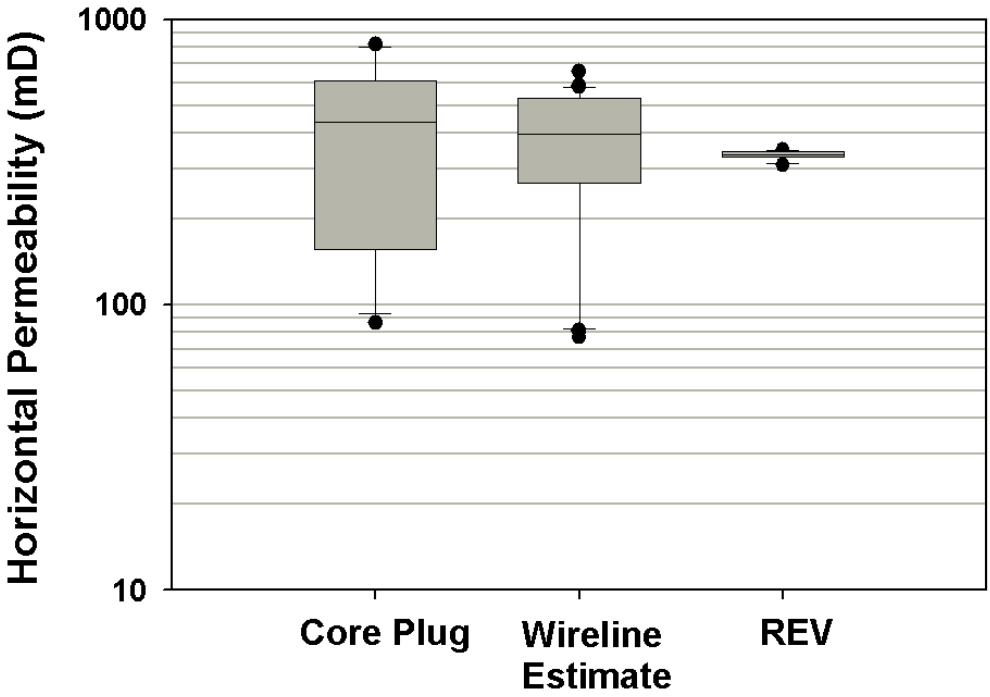

Figure 11C

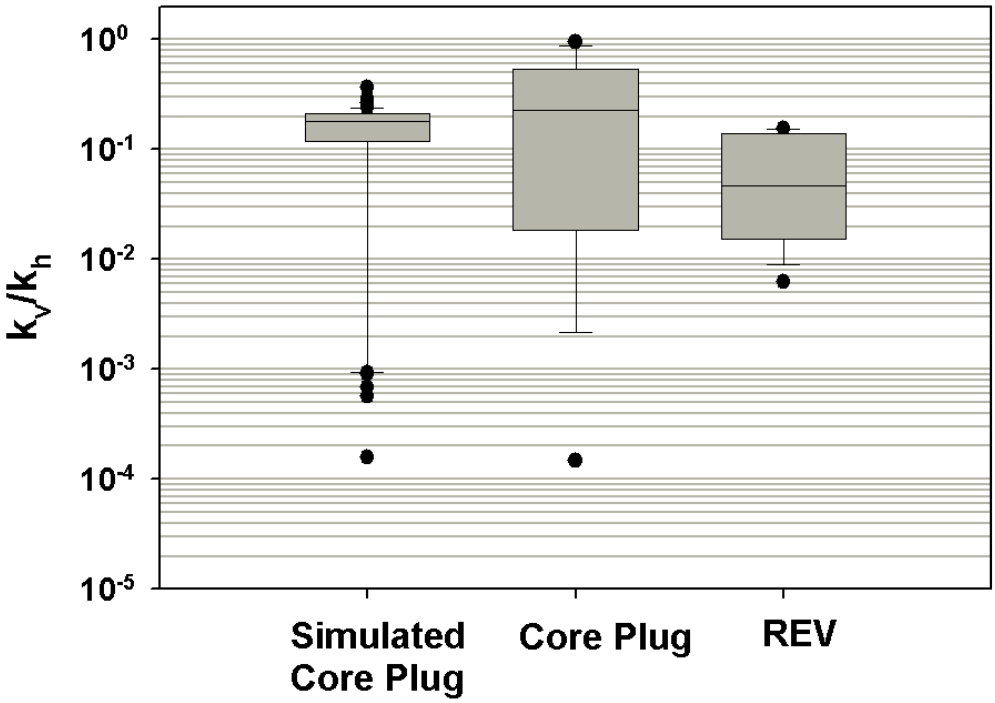

Appendix D Paper 3

Accepted for publication in Petroleum Geoscience as of 19. Spetember 2004.

Nordahl, K., Ringrose, P. S. and Wen, R.
Accepted for publication in Petroleum Geoscience as of 19 September 2004

Petrophysical characterisation of a heterolithic tidal reservoir interval using a process-based modelling tool

Kjetil Nordahl[1], Philip S. Ringrose[2], and Renjun Wen[3]
[1]Norwegian University of Science and Technology, Department of Mineral Resources and Engineering, Trondheim N-7491, Norway. Present address: Statoil Research Centre, Rotvoll, Trondheim N-7005, Norway.
[2]Statoil ASA, Exploration and Production, N-7501 Stjørdal, Norway.
[3]Geomodeling Technology Corp., Suite 230, 633 6th Avenue S.W. Calgary, Alberta, T2P 2Y5, Canada.

Abstract

Heterolithic lithofacies in the Jurassic Tilje Formation, offshore mid-Norway, consist of three components: sand, silt and mud intercalated at the cm scale, and are generally difficult to characterise petrophysically with core and wireline data. A near well-bore model of the lower part of the Tilje Formation in the Heidrun field is constructed to illustrate the application of these results to formation evaluation studies. The sedimentological model is developed by detailed parameterisation of a cored well interval and the petrophysical properties are based on core plug data, taking into account sampling bias and length scale. The variation in petrophysical properties as a function of sample volume is examined by calculating the representative elementary volume. The sensitivity of the representative permeability values to the contrast between the three components is studied and gives a better understanding of the flow behaviour of this system. These results are used to rescale the core plug data to a representative value and thereby quantify the uncertainty associated with the wireline-based estimates of porosity and horizontal permeability and to given an improved estimate of the k_v/k_h ratio.

Key words: *petrophysics, permeability, porosity, heterolithic sandstone.*

Introduction

Sedimentary architecture causes heterogeneity at many scales, which can affect reservoir performance (e.g. Haldorsen, 1986). At the bedding (sub-metre) scale, primary sedimentary structures can significantly influence the flow properties, as has been shown for a range of sedimentary systems (Weber, 1982; Corbett and Jensen, 1993; Hartkamp-Bakker and Donselaar, 1993; Hurst and Rosvoll, 1991). These studies show that porosity and permeability are strongly controlled by depositional processes through their influence on grain size, sorting, and fabric. Because of computational limits on the number of grid-cells in reservoir simulation, small-scale sedimentary structures cannot be included explicitly, but have to be represented by effective or representative values.

The problem of integrating data with different sample support in heterogeneous reservoirs has also been widely appreciated (Haldorsen, 1986; Enderlin et al., 1991; Worthington, 1994; Corbett et al.,

1998). In particular, the integration between core data (usually represented by discrete core plugs) with continuous wireline data is challenging since heterogeneities are often on the same scale as the measurement resolution. To integrate the two data sets, the normal approach is to upscale the measurements with the smallest sample support to the scale of the larger.

Methods for generating numerical models of the subsurface domain are reviewed by Koltermann and Gorelick (1996). Population of these models with petrophysical properties and calculating the effective flow properties at a larger scale can be done in a variety of ways (Renard and Marsily, 1997). For simple geometries (e.g. a stratified medium) exact analytical solutions can be found. In more complex cases, numerical methods can be used to estimate effective properties. Usually, only two component systems (sand and mud) are evaluated (Begg and King, 1985; Desbarats, 1987; Deutsch, 1989; Durlofsky and Chung, 1990).

Regardless of the upscaling technique, the question remains as to what scale the measurements should be rescaled to. Bear (1972) introduced the concept of Representative Elementary Volume (REV). This is based on effective medium theory, which assumes that the correlation lengths are shorter than the model domain. If the sample support is small compared to the length scale of the heterogeneity, the measured value will vary with a change in the support since varying degree of heterogeneity is included in the sample volume. At some scale (the REV), the fluctuations are minimized and a representative amount of heterogeneity can be measured (Figure 1).

The tidal deltaic Tilje formation (Martinius et al., this volume), is particularly heterogeneous and exhibits variability at many scales. Brandsæter et al. (2001) showed that the ratio between vertical and horizontal permeability (k_v/k_h ratio) was one of the most important parameters influencing oil recovery in this formation. At the bedding scale, thin intercalations of mudstone and sandstone layers have a strong influence on the flow properties (these two lithological components are hereafter referred to as sand and mud). These facies are dominated by heterolithic current ripple bedforms which have been described as flaser, wavy or lenticular bedding (Reineck and Wunderlich, 1968). Flaser and lenticular

bedding represent end-members of a range of tidal bedding types, with discontinuous mud lamina and discontinuous sand ripples, respectively. Wavy bedding describes more regular interbedding with approximately equal amounts of sand and mud. These mm to cm scale heterogeneities are not well characterised by the core plug or the wireline log measurements. Core plug measurements are at a volume scale below the characteristic length scale of the heterogeneity and the wireline logs tend to average out the responses from the different lithological components present. Integration between these two data sets is thus problematic. Figure 2 shows the studied interval of well H1 from the lower part of the Tilje formation in the Heidrun Field. This figure shows that the petrophysical variability is high, both within and between the different facies associations, such that there is in general a mis-match between the core and the wireline values.

This paper considers these problems using a process-based stochastic modelling tool (SBED™) (Wen et al., 1998). With this method, a realistic near wellbore model is created. The near wellbore model is defined here as a numerical representation of the sedimentological components and petrophysical properties in a rectangular shaped volume along the wellbore with a lateral dimension on the scale of the conventional wireline tool resolution. This also approximately corresponds to the lateral correlation lengths of the sedimentological and petrophysical elements in tidal facies. To be able to evaluate the tidal bedding system in general, a range of bedding models with different mud contents were created. Permeability is shown to vary with the sample volume and the REV can be calculated on these models. Furthermore, the sensitivity of flow behaviour to the permeability contrast between the different lithological components is explored. Finally, the near wellbore model is used to quantify the uncertainty associated with traditional averaging of core and wireline data to give improved estimates of the petrophysical properties in the studied interval.

The near wellbore model

Modelling of small-scale (cm-dm) sedimentological bedforms has been widely studied, and pioneering work on synthetic bedform modelling was published by Rubin (1988). The SBED™ method was

developed by Wen et al. (1998) and makes a significant step towards a petrophysically useful method by extending the approach of Rubin (1988) to include stochastic elements and 3D property modelling. The method used in SBED is based on manipulation of the following surface function:

$$z(x,y)^t = A\sin\left(\frac{x}{L_x} + \Theta_x\right) + B\sin\left(\frac{y}{L_y} + \Theta_y\right) + g(x,y) \qquad (1)$$

where x and y are spatial coordinates, t is a nominal time increment, A and B are amplitudes of the bedform in the current (x) and crest (y) directions, L_x and L_y are wavelengths of the bedform in the current and crest directions, Θ_x and Θ_y are initial phase angels (radians) and g(x,y) is a 2D gaussian random function. The input parameters to the program describe the bedform morphology in cross-section and plan-view (by a sine-function) and also how the surfaces move in space and time by vectors to mimic bedform migration (Figure 3A). The displacement creates a 3D volume separated by the surfaces giving a simulated lamina (Figure 3B). After a sequence of surfaces representing a lamina set, $z(x,y)^{t=n}$, a hiatus is simulated and erosion by a new time series is initiated (i.e. a new lamina set). The migration of bedforms, that in nature is a result of periodic avalanching and suspension fallout on the bedform lee- and stoss-side, is here simulated by displacement of successive sine curves. This is a simpler approach than process-based methods in which grain deposition is simulated. The input parameter set comprises a set of values to give a particular type of sedimentary bedform. The stochastic elements of the code reflect the natural variability in the deposits and ensure that a number of equiprobable realizations of the bedform model can be generated. Figure 3C shows an example of a realization of a geometry model. Statistical parameterisation of the sedimentological observations from core gives us the opportunity to determine the mean value of the deterministic part of the code while allowing the natural variability to be included in the stochastic elements. Table 1 gives some of the sedimentological parameters considered for this interval. The key parameters are the geometry, thickness variation and frequency of the mud layers, since these will have a strong influence on the vertical and horizontal permeability. Also listed in Table 1 are the main input parameter groups that are used to mimic the depositional process.

Within this geometrical bedding framework, petrophysical properties (porosity and permeability) are simulated using correlated 2D gaussian random fields. On the resulting permeability grid (Figure 3D), directional flow is simulated numerically by imposing a constant head gradient between opposite sides of the model and no-flow boundaries on the perpendicular sides. The single-phase steady state flow equation is then solved by a finite-difference method (described by Warren and Price 1961, White and Horne 1987, and Renard and Marsily 1997). By rotating the boundary condition setup, and repeating the flow simulation, the diagonal elements of the permeability tensor are found (denoted here as k_x, k_y and k_z,). Since porosity is an additive property (Narasimhan, 1983), the bulk porosity of the bedding model is simply found by taking the arithmetic average of the individual grid-cell values.

In this study only single-phase flow has been considered. However, where sedimentary structures have a significant effect on single-phase permeability, the multiphase effect on permeability is likely to be even greater. Multiphase flow aspects also need to be considered in reservoir studies and Pickup et al. (2000) performed two-phase upscaling on similar synthetic tidal bedding models as used here.

Bedding geometry model

The geometrical model represents the sedimentological features observed in the core such as the lamina and lamina set characteristics (Table 1). After dividing the core into lithofacies, a detailed log of mud content and lamina set thickness distribution within the cored interval was made, and these statistics were then used to develop the bedding models. To illustrate the modelling method, lithofacies 7.1 from the upper part of Figure 2 was selected. Ringrose et al. (this volume) consider the entire interval in Figure 2 for estimation of vertical permeability. The selected lithofacies is interpreted as an accretionary channel bank deposit (Martinius et al. 2001) and is dominated by flaser bedded deposits separated by thicker mud layers. The number and thickness of the mud and sand lamina sets (Table 2) were considered to have an important control on effective permeability. In order to ensure

that the near wellbore model of this lithofacies is realistic, the same parameters were measured on the numerical model. A realistic model is obtained when the two data sets are statistically similar (Table 2). Figure 4 shows part of this interval with one realization of the near wellbore model. Table 4 gives the geometrical input parameters while Table 3 gives the petrophysical parameters for this specific facies.

The petrophysical model

Each grid-cell in the model has a constant lateral dimension (1 by 1 cm) and a vertical dimension related to the lamina thickness (usually on the mm-scale, see Figure 3), and is by definition an isotropic and homogeneous petrophysical element. The model dimensions are 0.3 m by 0.3 m by 0.3 m and consist of c. one million cells. The grid cell scale is approximately the scale of the probe-permeameter device, c. 2-5mm (Halvorsen and Hurst, 1990, Ringrose et al., this volume). One detailed probe-permeability grid was available in the selected lithofacies. The main direct measurement of porosity and permeability are however the core plugs. In order to constrain the petrophysical model to data, we simulated the process of taking core plugs with 30cm spacing from the SBED™ model. The input petrophysical properties were then adjusted until a match was obtained between the real core plug data set and the simulated core plug data set. The simulated core plugs have the same dimension and orientation as the real core plugs and consist of approximately 600-800 grid-cells depending on the lamina thickness. There are limitations to this approach. Firstly, there should be a sufficient number of real core plugs from each facies to produce a stable histogram. Secondly, the real core plugs are often taken from the more sand rich zones avoiding the mud layers (see Figure 4), but the simulated core plugs are unbiased. Thirdly, several solutions are possible by changing the mean or variance of the input distribution (i.e. the solution is not unique). This is especially the case for porosity. The input permeability has to match both the upscaled vertical and horizontal core plug distributions giving a better constraint to the options available. Figure 5A and 5B show the results of this method for horizontal permeability and porosity, respectively, for the selected facies in the interval. There is a good match between the simulated and the real core plug data set, both validating

the petrophysical model and giving the three-component distribution of porosity and (isotropic) permeability. Figure 5A also show the available probe permeameter data and the distribution is similar to the distribution to the sand and silt components. Table 3 gives the petrophysical parameters for these curves and Figure 4 shows a realization of the final bedding model for the selected facies.

Even though there is an acceptable match between the core plug values and the model results, the latter tend to have slightly lower variability than the former. This is mainly because it is not possible to include all natural variability in geometry and petrophysics. For example, diagenetic features and fractures are not included in the synthetic bedding models. Although the Tilje Formation in the Heidrun Field is not severely affected by diagenesis, in other cases diagenesis could be equally important as the influence of the primary sedimentary structures. However, it is considered that the near wellbore model created here captures the most important features affecting the bedding-scale petrophysical properties.

There are few reported measurements on the mud component from these intercalated bedding types, but Ringrose et al. (this volume) discuss plausible values for mud permeability. A constant value of 0.01 mD is chosen here and then the sensitivity to this parameter on effective vertical and horizontal permeability is evaluated. Although 0.01 mD may be a rather high permeability for mud, for single-phase simulation, it is the contrast between the lithological elements that is most important.

Petrophysical variability with sample support

Several theories have been developed to estimate effective properties of heterogeneous media. In simple geometrical cases exact solutions exist, and for infinite, continuous parallel layers the horizontal and vertical effective permeability is given by the arithmetic and harmonic averages, respectively. In the case of a random, uncorrelated, isotropic lognormal permeability distribution, the geometric average has been shown to give a good estimate (Warren and Price, 1961). Although these estimates are useful, they do not generally apply to real sedimentary deposits, which often show more

complex geometry and variability. Effective media theories assume that the heterogeneity can be modelled as an inclusion embedded in a homogeneous matrix. If the inclusion has a simple form, analytical expressions for permeability can be calculated (e.g. Dagan, 1979). In percolation theory, assuming two components where one is non-permeable and the components are distributed randomly in space, the threshold for flow can be evaluated as a function of the conducting component (e.g. Begg and King, 1985). Randomly dispersed shales in a sandstone medium were evaluated numerically by Desbarats (1987), who showed that the effective permeability depends on the shale volume fraction, the spatial correlation structure and the dimensionality of the flow system. Deterministic modelling of sedimentary structures has also been performed (e.g. Corbett et al., 1992; Pickup et al., 1995; Ringrose et al., 1999), where the main focus was on fluvial and aeolian deposits. In these previous studies, only two components (sand and shale or two types of sand) were considered. The assumption of a two-component system is a simplification of tidal deposits since the sand lamina set consists of both sand and silt sized particles organized as cross-stratification in addition to the mud component. In addition, both the sand and the mud components are highly spatial correlated in these tidal deposits.

When the correlation lengths of the different components are smaller than the model domain, a property measured on a sub domain will depend on the size, position and orientation of this sub domain. Bear (1972) showed that at some sample support (the REV), the variability is minimized and a representative property could be measured (Figure 1). Norris and Lewis (1991) calculated in 2D the representative elementary area (REA) for a range of tidal facies based on binary images of an outcrop sample and found that for horizontal permeability the same REA applied regardless of the mud content. Jackson et al. (2003), dividing heterolithic rock cubes into smaller samples, showed that the effective property in 3D could be estimated with simple averaging schemes and that the choice of estimator depended on bedding type.

In order to evaluate the fundamental properties of the heterolithic bedding system, a set of models with different mud fraction was developed ranging from sand-dominated flaser bedding to mud-dominated lenticular bedding. Baas (1994) studied the development of ripple morphology in unidirectional flow

using flume tank experiments and found that ripples approached an equilibrium size and shape with either increasing current velocity or depositional time. Oost and Baas (1994) also evaluated the effect of unsteady flow (common with tidal currents) in the bedform morphology development. These experimental results have been used to constrain the input parameters for our numerical model thereby obtaining realistic geometries. The geometrical input parameters for these general tidal bedforms are found in Table 4.

Firstly, to evaluate how the petrophysical properties vary with sample support, and to isolate the effect of geometry and mud fraction, a two-component system (sand and mud) was used where the petrophysical contrast between the components was constant and equal to 10^4 (sand permeability of 100 mD and mud permeability of 0.01 mD). Smaller sub-models were then extracted from the larger scale model in a systematic manner, where the sub-grid size (i.e. sample volume) is increased in a cubic series (in 30 steps) from the smallest sample in the centre of the realization to the full size (0.3^3 m^3). There was no observed dependency on the location of the centre point of the sub grids. The effective permeability for each sub grid was then calculated for the vertical direction (k_z) and in the horizontal direction along the migration direction for the ripples (k_x). A total of 12 different bedding models (with 10 realizations of each) with varying mud content were used and Figure 6 shows all the results from the simulation where each square represents a specific mud content and sample volume. Note that there is a larger spread in upscaled permeability (more than 2 orders of magnitude) for certain ranges, namely below 40% mud fraction for vertical permeability and above 70% mud fraction for horizontal permeability. This indicates that the effective permeability is dependent on the sample size in these mud fraction ranges. Figure 7 shows the effective vertical permeability vs. sample volume for one of these models; a flaser bedded model with 10% mud fraction where the mud occurs as isolated lenses between the sand lamina sets. Each solid line represents one realization. This example clearly shows that the largest variability occurs at small sample volumes and that the fluctuations are minimized at large scales, consistent with the REV concept outlined above. For each sub-gird size, the coefficient of variation (C_v) was calculated between the realizations (see Jensen et al., 1997, for fuller discussion of use of C_v for petrophysical analysis). As proposed by Corbett and

Jensen (1992), a C_v below 0.5 indicates a statistically homogenous medium, while above 1 the samples can be considered very heterogeneous. It is observed (Figure 7) that the C_v decreases as the sample size (sub-grid size) increases, indicating that the effective property approaches the REV. Note that this REV is related only to geometrical heterogeneity and that spatial correlation in permeability will be likely to increase the absolute size of the representative volume. Similar curves as in Figure 7 were obtained for all the other 11 tidal bedding models and the results for vertical permeability are shown in Figure 8, where it can be seen that the sample volume (for $C_v < 0.5$) varies with mud content (this is in contrast to conclusion of Norris and Lewis, 1991). For vertical permeability (figure 8) there is a steady increase of this inflection point with increasing mud content, but above 40% mud, all the C_v curves lies in the homogeneous region. This behaviour is related to percolation theory, which predicts the point at which one component will start to connect across the model domain. The change in variability expressed with the C_v curve is related to the change in correlation lengths of sand and mud lenses with respect to the model domain. Further analysis of porosity and horizontal permeability is given in Nordahl (2004) where the issues of stationarity, correlation lengths, percolating thresholds and how to define REV on these bedding models are discussed. The permeability values measured at the REV are indicated in Figure 6 by black squares. It is clear that the representative effective permeability trends deviate significantly from the commonly used arithmetic and harmonic averages, which only are correct in the case of a perfectly stratified medium. The effective permeability of the more realistic and complex models used here can thus not be properly estimated with these estimates. Ringrose et al. (2003; this volume) discuss different methods that can be used to describe this trend.

Effect of petrophysical contrast in a three-component system

The previous results were for a two-component system (sand and mud), and the variability observed as a function of sample support was a result only of the geometry of the two components. As mentioned above, most of the sand lamina sets in the Tilje Formation consists of (at least) two different grain size classes. Petrophysically, these facies can then be treated as a three-component system. In this section,

the effect of changing the petrophysical contrast between the two sand components (contrasting lamina) is evaluated and then, keeping this contrast constant, the effect of different permeability of the mud layers is assessed.

Effect of contrast between sand components

The effect of varying the petrophysical contrast within each sand lamina set (Table 3) is evaluated by keeping the permeability of one of the sand components constant and equal to 100 mD and decreasing the permeability of the other component (the silty component). In this case the largest sample volume for each realization was used, such that in all cases the REV has been reached ($C_v < 0.5$). In Figure 9, the effective vertical and horizontal permeability is plotted against the mud fraction for the different contrast cases. In the low mud range, effective permeability is closely related to mud fraction and follows clear separate trends for each contrast case. For vertical permeability there is a change at around 40-50% mud content where the different cases merge towards one curve. The data for horizontal permeability have similar characteristics; however, the convergence of the five contrast cases occurs at around 80% mud fraction. This is again related to the percolation threshold and will be discussed below. Desbarats (1987) found similar threshold values using a markedly different two-component model.

Effect of contrast between sand and mud

The petrophysical properties of the mud layers, and especially the permeability, are difficult to measure and represent a large uncertainty. To evaluate this uncertainty we kept the contrast between the sand and silt component constant (and equal to 1) and varied the mud permeability from 10^{-5} to 10^{0} in six steps (Table 3). The models with mud content of 10%, 35% and 85% are used to evaluate the effects in different flow regimes. The results are plotted in Figure 10 A-D, along with a summary of the study of varying the contrast within sand lamina set (from Figure 9). In the case with only 10% mud, the vertical permeability is dominated by the magnitude of the contrast between the sand components and almost unaffected by varying the mud permeability (Figure 10A) meaning that the

mud lenses only act as weak baffles to the vertical flow. The same was found for horizontal permeability (not shown). Near the percolation threshold for vertical flow (35% mud), vertical permeability shows a strong dependency on the mud permeability (Figure 10B), while horizontal permeability is only weakly affected by the contrast between the sand components (Figure 10C). However, at higher mud contents (85%, Figure 10D), the sand ripples start to disconnect in the horizontal plane meaning that the percolation threshold for horizontal flow is reached. This gives a higher sensitivity to mud properties and less to the variation in permeability contrast within sand lamina set. The results above clearly show how effective permeability in complex, heterolithic deposits can be understood with respect to connectivity of sand and mud laminasets. That is, concepts from both effective medium theory and percolation theory must be used to properly assess this system. These results also indicate that the data collection should be linked with the bedding type. For example, close to and below the percolation thresholds, which are very different for vertical and horizontal flow, mud properties have most influence on effective permeability while the contrast between the cross-stratified components are more important above the percolating threshold.

Error associated with wireline estimates

An important application of these results is that the uncertainty associated with the wireline estimates of porosity and horizontal permeability can be evaluated. Porosity is usually estimated by using a neutron or density wireline log with a calibration to the core porosity. Although porosity is not an extensive property, it is volume-normalised and consequently additive (Narasimhan, 1983). Since the wireline tool physically measures quantities closely related to the total porosity (e.g. Hook, 2003), the integration between core porosity and the wireline tools often is quite reliable. However, in heterolithic deposits, the core plugs tend to be a biased sample (see Figure 4) since the mud layers are only occasionally sampled and this may adversely influence the integration. A traditional method to estimate horizontal permeability is to establish a regression equation between core porosity and core permeability and use this to estimate wireline permeability from the wireline estimate of porosity or by the use of some semi-empirical equations (e.g. Kozeny-Carman). Permeability being an intensive,

non-additive property will, in general, not be predictable with respect to porosity. This is especially the case when the sample support is very different, as in the case of core plugs and wireline tools, and when the scale of heterogeneity is between these two volume scales. With the SBED™ tool, porosity and permeability input distributions are taken directly from core plugs, probe permeameter measurements or thin sections, and assigned for each lamina and then rescaled to the scale of interest with a realistic bedding model. We thus have a method to address the uncertainty in the wireline estimate.

To illustrate this, models of lithofacies 7.1 have been used. This facies is from the upper part of the studied interval, which is a dominantly flaser-bedded facies with some thicker mud layers separating the different sets (see also Figure 2 and 4 and Table 2). The near wellbore model of this facies was evaluated at a scale large enough for representative properties to be obtained (in this case 10^6 cm^3). Figure 4 shows the core photo with the positions of the core plugs and the thicker mud layers characteristic of this facies indicated. Note that the core plugs in general miss the mud layers giving a biased dataset.

Although porosity is an easier parameter to estimate, the bias in the core plug data set towards sand properties will influence on the calibration process with the wireline tool. Figure 11A shows the distribution of the core plugs, the wireline estimate and a data set measured on a representative scale from the near wellbore model. In accordance with the REV concept, a reduction in the variance is observed when going from the measures representing the smallest volume to the largest. However, due to under-sampling of the mud layers, the correct and representative porosity value is somewhat lower. In this case, the error is not large compared to the wireline estimate, but it illustrates well the problem with biased sampling.

Figure 11B shows the result for horizontal permeability. In such a low-mud content facies, the dependency of the mud properties on horizontal permeability is small (see also figure 10C). However,

by using the estimate made at a representative scale we see that the variance in the data set is reduced, thereby giving a less uncertain estimate of this property.

The ratio between vertical and horizontal permeability (k_v/k_h) is both a difficult property to measure and an important property in reservoir simulation (Brandsæter et al., 2001). This parameter is particular sensitive to the geometry and the petrophysical properties of the mud layers. There is no wireline estimate for this property, and estimates from production data are often uncertain. However, by using the near wellbore model, a representative value for k_v/k_h for this facies can be found. Figure 11C shows that this estimate is lower than the estimate from core plug data, which is expected because of the bias in this data set. The minimum value of the simulated k_v/k_h ratio is higher than the minimum value from core plugs. This is because the few mud layers sampled (by the core plugs) are continuous in the sample but are discontinuous at the scale of the model. This difference in mud layer continuity from core plugs to a larger-scale 3D model has also been noted by Jackson et al. (2003). The k_v/k_h ratio will be very dependent on the chosen mud permeability, but even with the rather high value used here (0.01 mD), the difference to the core plug estimate is significant.

There are still issues that have to be addressed in the future to further reduce uncertainty. The true properties of the different components and especially the mud properties will be critical, and the probe permeameter data can play an important role to assess the sand lamina set variability. To be able to directly simulate the wireline tool responses on the near wellbore model would greatly advance the basis for an improved integration. Since some of the sedimentological elements models have correlation lengths that approach the model size, it would be useful to use more advanced upscaling techniques (e.g. periodic boundary conditions; Durlofsky, 1991) to calculate the effective properties. In addition, the effect of multiphase flow in this heterogeneous system is not considered here and should be investigated. As a result, much more work is still required to properly characterise these heterolithic deposits. However, the introduction of the near wellbore model, common to the

sedimentologist, the petrophysicist and the reservoir engineer, is an important step towards a better and fully integrated characterisation of these reservoirs.

Conclusion

Estimation of petrophysical properties in reservoirs where there are large petrophysical variations at the scale of core plugs and wireline logs is challenging. A key element of this paper is that in these heterogeneous reservoir intervals, the core plug values cannot be used directly in calibration and integration with wireline data since they represent measurements from a different sample support and a biased sample.

A process-based numerical modelling tool has been used to evaluate the near wellbore region of a tide influenced and heterogeneous reservoir interval in the Heidrun field in the Haltenbanken area, offshore mid-Norway. A method for parameterisation of the core data useful for this modelling tool has been proposed and successfully used to create realistic facies models from the interval. Also a method to establish the underlying distributions of a three-component sedimentary system from simulation of core plugs is outlined. The near wellbore model is used to rescale the core plug data to the scale of interest giving a better basis for comparing with other well data.

The variation of effective properties as a function of sample support has been evaluated. It is found that the variability is reduced at some sample volume and that the size of this volume was dependent on the mud content. The trends observed between representative permeability values and mud fraction are related to the percolation thresholds. By changing the contrast between the sand components and between the sand and the mud, different sensitivity to these contrasts were identified and this should guide the data collection in the well.

The results were also used to evaluate the uncertainty associated with the wireline estimates. The k_v/k_h ratio is often the most difficult parameter to estimate from available well data, and we have shown

how a better and less uncertain estimate can be made. Ringrose et al. (this volume) discuss the estimation of vertical permeability both in the Heidrun field and in the deeper buried and more complex Smørbukk field.

Acknowledgement

The first author will thank the Formation Evaluation Project at Norwegian University of Science and Technology for financial support. Comments from Inge Brandsæter, Arve Næss, Allard Martinius and Sverre Ola Johnsen during the work are appreciated. The comments from two anonymous reviewers are gratefully acknowledged. Simulations were performed using the SBED™ software package (Geomodeling Technology Corp.).We thank Statoil ASA for permission to publish the data.

References

Baas, J. H. 1994. A flume study on the development and equilibrium morphology of current ripples in very fine sand. *Sedimentology*, **41**, 185-209.

Bear, J. 1972. Dynamics of fluids in porous media. American Elsevier, New York.

Begg, S. H. and King, P. R. 1985. Modelling the effects of shales on reservoir performance: Calculation of effective vertical permeability. Paper SPE 13529 presented at the 1985 SPE Symposium on Reservoir Simulation, Dallas, TX, Feb. 10-13.

Brandsæter, I. Wist, H. T., Næss, A. et al. 2001. Ranking of stochastic realizations of complex tidal reservoirs using streamline simulation criteria. *Petroleum Geoscience*, **7**, S53-S63.

Corbett, P. W. M., Ringrose, P. S., Jensen, J. L. and Sorbie, K. S. 1992. Laminated clastic reservoirs: the interplay of capillary pressure and sedimentary architecture. Paper SPE 24699 presented at the 67th SPE Annual Technical Conference and Exhibition.

Corbett. P. W. K. and Jensen, J. L. 1992. Estimating the mean permeability: how many measurements do you need? *First Break*, **10**, 89-94.

Corbett, P. W. M. and Jensen, J. L. 1993. Application of probe permeametry to the prediction of two-phase flow performance in laminated sandstones (lower Brent Group, North Sea). *Marine and Petroleum Geology*, **10**, 335-346.

Corbett, P. W. M., Jensen, J. L. and Sorbie, K. S. 1998. A review of upscaling and cross-scaling issues in core and log data interpretation and prediction. *In*: Harvey, P. K. and Lovell, M. A. (eds.) *Core-Log Integration*, Geological Society, London, Special Publications, **136**, 9-16.

Dagan, G. 1979. Models of groundwater flow in statistically homogeneous porous formations. *Water Resources Research*, **15**, No. 1, 47-63.

Desbarats, A. J. 1987. Numerical estimation of effective permeability in sand-shale formations. *Water Resources Research*, **23**, No. 2, 273-286.

Deutsch, C. 1989. Calculating effective absolute permeability in sandstone/shale sequences. *SPE Formation Evaluation*, **4**, No. 3, 343-348.

Durlofsky, L. J. and Chung, E. Y. 1990. Effective Permeability of heterogeneous reservoir regions. *In*: Guérillot, D. and Guillon, O. (eds.) *2nd European Conference on the Mathematics of Oil Recovery*, Paris, 57-64.

Durlofsky, L. J. 1991. Numerical calculation of equivalent grid block permeability tensors for heterogeneous porous media. *Water Resources Research*, **27**, 699-708.

Enderlin, M. B., Hansen, D. K. T. and Hoyt, B. R. 1991. Rock volumes: Considerations for relating well log and core data. *In*: Lake, L. W., Carroll, H. B. and Wesson, T. C. (eds.) *Reservoir Characterization II*, Academic Press, San Diego, 277-288.

Haldorsen, H. H. 1986. Simulator parameter assignment and the problem of scale in reservoir engineering. *In*: Lake, L. W. and Carroll, H. B. (eds.) *Reservoir Characterization*, Academic Press, Orlando, 293-340.

Halvorsen, C. and Hurst, A. 1990. Principles, practice and applications of laboratory mini-permeametry. *In*: Worthington, P. F. (ed.) *Advances in Core Evaluation: Accuracy and Precision in Reserves Estimation*, *Reviewed proceedings of the First Society of Core Analysts European Core Analysis Symposium,* London. Gordon and Breach Science Publishers, 521-549.

Hartkamp-Bakker, C. A. and Donselaar, M. E. 1993. Permeability patterns in point bar deposits: Tertiary Loranca Basin, central Spain. *In*: Flint, S. S. and Bryant, I. D. (eds.) *The Geological modelling of hydrocarbon reservoirs and outcrop analogues,* Special Publication of the International Association of Sedimentologist, **15**, 157-168.

Hook, J. R. 2003. An introduction to porosity. *Petrophysics*, **44**, No. 3, 205-212.

Hurst, A. and Rosvoll, K. 1991. Permeability variations in sandstone and their relationship to sedimentary structures. *In*: Lake, L. W., Carroll, H. B. and Wesson, T. C. (eds.) *Reservoir Characterization II*, Academic Press, San Diego, 166-196.

Jackson, M. D., Muggeridge, A. H., Yoshida, S. and Johnson, D. 2003. Upscaling permeability measurements within complex heterolithic tidal sandstones. *Mathematical Geology*, **35**, No. 5, 499-519.

Jensen, J. L., Lake, L. W., Corbett, P. W. M. and Goggin, D. J. 1997. *Statistics for Petroleum Engineers and Geoscientists*. Prentice Hall PTR, New Jersey.

Koltermann, C. E. and Gorelick, S. M. 1996. Heterogeneity in sedimentary deposits: A review of structure imitating, process-imitating and descriptive approaches. *Water Resources Research*, **32**, No. 9, 2617-2658.

Martinius, A. W., Kaas, I., Næss, A., Helgensen, G., Kjærefjord, J. M. and Leith, D. A. 2001. Sedimentology of the heterolithic and tide-dominated Tilje Formation (Early Jurassic, Halten Terrace, offshore mid-Norway). *In*: Martinsen, O. M. and Dreyer, T. (eds.) *Sedimentary Environments Offshore Norway – Palaeozoic to Recent*. NPF Special Publication **10**, 103-144, Elsevier Science B. V, Amsterdam.

Martinius, A. W., Ringrose, P. S., Brostrøm, C., Elfenbein, C., Næss, A. and Ringås, J. E. (this volume). Reservoir challenges of heterolithic tidal hydrocarbon fields (Halten Terrace, Mid Norway).

Narasimhan, T. N. A note on volume-averaging. 1983. *In*: Pinder, G. F. (ed.) *Flow through porous media*. A Computational Mechanics Publication, CML Publications, 46-50.

Nordahl, K. 2004. *A petrophysical evaluation of tidal heterolithic deposits: application of a near wellbore model for reconciliation of scale dependent well data*. PhD thesis, Norwegian University of Science and Technology, Trondheim, Norway.

Norris, R. J. and Lewis, J. J. M. 1991. The geological modelling of effective permeability in complex heterolithic facies. Paper SPE 22692 presented at the 66th Annual Technical Conference and Exhibition, Dallas October 6-9, 359-374.

Oost, A. P. and Baas, J. H. 1994. The development of small scale bedforms in tidal environments: an empirical model for unsteady flow and its applications. *Sedimentology*, **41**, 883-903.

Pickup, G. E., Ringrose, P. S., Corbett, P. W. M., Jensen, J. L. and Sorbie, K. A. 1995. Geology, geometry and effective flow. *Petroleum geoscience*, **1**, 37-42.

Pickup, G., Ringrose, P. S. and Sharif, A. 2000. Steady-state upscaling: from lamina-scale to full-field model. *SPE Journal*, **5**, No. 2, 208-217.

Nordahl, K., Ringrose, P. S. and Wen, R.
Accepted for publication in Petroleum Geoscience as of 19 September 2004

Reineck, H-E. and Wunderlich, F. 1968. Classification and origin of flaser, and lenticular bedding. *Sedimentology*, **11**, 99-104.

Renard, Ph. and de Marsily, G. 1997. Calculating equivalent permeability: a review. *Advances in Water Resources*, **20**, No. 5-6, 253-278.

Ringrose, P. S., Pickup, G. E., Jensen, J. L. and Forrester, M. 1999. The Ardoss reservoir gridblock analogue: Sedimentology, statistical representivity and flow upscaling. *In*: Schatzinger, R. and Jordan, J. (eds.), *Reservoir Characterization – Recent Advances*, AAPG Memoir **71**, 265-276.

Ringrose, P. S., Skjetne, E. and Elfenbein, C. 2003. Permeability estimation functions based on forward modeling of sedimentary heterogeneity. Paper SPE 84275 presented at the SPE Annual Technical Conference and Exhibition, Denver, Colorado, 5-8 October 2003.

Ringrose , P., Nordahl, K. and Wen, R. (this volume). Vertical permeability estimation in tidal deltaic reservoir systems. Rubin, D. M. 1987. Cross-bedding, Bedforms, and Paleocurrents. *Concepts in Sedimentology and Paleontology*, *Volume 1*, Society of Economic Paleotologists and Mineralogists Special Publication.

Rubin, D. M. 1988. Cross-bedding, bedforms, and palaeocurrents. *Concepts in Sedimentology and Paleontology, Volume 1*, Society of Economic Palaeontologists and Mineralogists Special Publication.

Warren, J. E. and Price, H. S. 1961. Flow in heterogeneous porous media. *Society of Petroleum Engineer Journal*, **1**, 153-169.

Weber, K. J. 1982. Influence of common sedimentary structures on fluid flow in reservoir models. *Journal of Petroleum Technology*, **34**, 665-672.

Wen, R., Martinius, A. W., Næss, A. and Ringrose, P. 1998. Three-dimensional simulation of small-scale heterogeneity in tidal deposits – a process-based stochastic simulation method. *In*: Buccianti, A, Nardi, G. and Potenza, R. (eds.) *Proceedings of the 4th Annual Conference of the International Association of Mathematical Geology (IAMG)*, Ischia, 129-134.

White, C. D. and Horne, R. N. 1987. Computing absolute transmissibility in the presence of fine-scale heterogeneity. SPE Paper 16011, Presented at the 9th SPE Symposium on Reservoir Simulation, San Antonio, TX, February 1-4, 209-220.

Worthington, P. F. 1994. Effective integration of core and wireline data. *Marine and Petroleum Geology*, **11**, No. 4, 457-466.

Figure 1: Concept of Representative Elementary Volume (REV). In this paper, the microscopic domain refers to the scale from lamina to bed set, while the macroscopic domain to a scale larger than the lithofacies. Modified after Bear (1972).

Figure 2: Core data and wireline estimate from the studied interval in the Tilje Formation. The facies associations are from Martinius et al. (2001).

Figure 3: A: Schematic sketch of the generation of lamina surfaces in SBED between the t=1 and t=2 in the time series of equation 1. The grey area is the preserved lamina and the arrow indicates the vector that displaces the surface to mimic bedform migration. Note that the y-direction is not shown and that the preserved lamina is a 3D volume. B: Simulated 3D sand and mud laminaset in SBED. C: A realization of a sedimentological model. The three different lithological components present in the geometrical model can be clearly seen; sand (grey), silt (dark grey) and mud (black). D: A realization of a permeability model. The model size in C and D is 30 by 30 by 10 cm.

Figure 4: Core photo and 3D near wellbore model of the selected lithofacies 7.1 (see Figure 2 and Table 4). The cylinders indicate the positions of the vertical and horizontal core plugs and the arrows indicate the thick mud layers. Note that the core plugs do not generally sample the mud layers (biased samples).

Figure 5: Comparison between the core plug data (black bars) and the simulated core plugs (crosshatched bars) for horizontal permeability (A) and porosity (B). The solid (silt) and dashed (sand) curves show the input distributions that were used to obtain the simulated core plug distribution. The input porosity distribution was truncated at 50% porosity. The mud component was given a low and constant value (grey bar). Inserted in Figure 5A is also the probe-permeameter distribution, which has approximately the same variability as the input sand and silt curves.

Figure 6: Simulated horizontal (k_x, white circles) and vertical (k_z, white squares) permeability representing different sample volumes and mud contents (total of 3600 data points). The values measured at the REV are marked by black squares (k_z) and circles (k_x). The solid lines represent the harmonic, geometric and arithmetic averages.

Figure 7: Example of variation in vertical permeability with sample volume in a low mud content (10%) flaser bedded model. Each solid line represents one realization and the dashed line is the C_V curve calculated between the ten realizations at each volume step. At volumes larger than about 2000 cm^3, the C_V value becomes lower than 0.5.

Figure 8: The C_V curve for vertical permeability for 12 different tidal bedding models with varying mud fraction. Each C_V - line is based on similar calculations as Figure 7.

Figure 9: Effective vertical (white) and horizontal (grey) permeability with varying contrast between the sand and silt component (constant mud permeability). The plot is based on 240 realizations all at a REV scale. See table 3 for petrophysical input parameters.

Figure 10: Effect of changing the mud permeability. Inserted are also the relevant results from Figure 9.Three mud fraction models are used: A) low mud content case (10%), B) and C) near the percolating threshold for vertical flow (35%), and D) a high mud content (85%) lenticular bedded model near the percolation threshold for horizontal flow. See table 3 for petrophysical input parameters.

Figure 11: Comparison of porosity (A), horizontal permeability (B) and kv/kh-ratio (C) estimated or measured from different sources and sample volumes. The lower and upper limits of the box indicate the 25^{th} and the 75^{th} percentile while the whiskers represent the 10^{th} and the 90^{th} percentile. The solid line is the median and the black dots are the outliers. The values at the REV are measured on the bedding model at a representative scale and the distribution is based on ten realizations. There exist no wireline estimate for the kv/kh-ratio.

Table 1: Recorded sedimentological core data (left) and main input parameter groups in SBED™ (right).

Core Parameters	Geometrical input parameters
Lamina thickness (mean and standard deviation)	Bedform morphology (plan form and cross-section)
Sand/Mud laminaset thickness (mean and standard deviation)	Migration speed and direction
Periodic components (wavelength and amplitude)	Depositional rate and length for sand and mud
Bedding type (i.e. geometry of mud layers)	

Table 2: Core statistics for of sand and mud lamina set thickness in the selected lithofacies 7.1.

Component	Parameter	Core	Simulation
Sand lamina set	n	11	117
	Arithmetic average	20.14	21.1
	Standard deviation	18.64	1.98
	Median	15.9	21
	Mode	N/A	21
	Minimum	2	20.5
	Maximum	59.2	42.2
	Total cm	221.5	2468.4
Mud lamina set	n	11	117
	Arithmetic average	0.68	0.421
	Standard deviation	0.35	0.18
	Median	0.8	0.4
	Mode	0.8	0.5
	Minimum	0.1	0.1
	Maximum	1.2	0.9
	Total cm	7.5	49.2
Sand fraction		0.967	0.98
Number of mud layers per meter		4.8	4.65

Table 3: Petrophysical input parameters used; mean (standard deviation). The upper part relates to Figure 6-10.

	Sand Component	Silt Component	Mud Component
Sand-Silt Contrast 1:1	100 mD	100 mD	0.01 mD
Sand-Silt Contrast 1:2	100 mD	50 mD	0.01 mD
Sand-Silt Contrast 1:5	100 mD	20 mD	0.01 mD
Sand-Silt Contrast 1:10	100 mD	10 mD	0.01 mD
Sand-Silt Contrast 1:100	100 mD	1 mD	0.01 mD
Sand-Mud Contrast 10^{0}	100 mD	100 mD	1 mD
Sand-Mud Contrast 10^{-1}	100 mD	100 mD	0.1 mD
Sand-Mud Contrast 10^{-2}	100 mD	100 mD	0.01 mD
Sand-Mud Contrast 10^{-3}	100 mD	100 mD	0.001 mD
Sand-Mud Contrast 10^{-4}	100 mD	100 mD	0.0001 mD
Sand-Mud Contrast 10^{-5}	100 mD	100 mD	0.00001 mD
Lithofacies 7.1 (fig. 4, 5 and 11)	Mean ln 6 (0.2) StDev ln 1.2 (0)	Mean ln 4.5 (0.2) StDev ln 1 (0)	0.01 mD (0)

Table 4: Input geometrical parameters for the tidal bedding models; mean (standard deviation). The bedform morphology parameters have dimensions in centimetre, while the depositional parameters are relative length and rate. The variability were modelled with a spherical variogram with range = 3 cm for all the parameters. MF = Mud Fraction.

Control parameter	MF_0	MF_0.1	MF_0.2	MF_0.25	MF_0.3	MF_0.35	MF_0.4	MF_0.5	MF_0.6	MF_0.7	MF_0.8	MF_0.85	MF_0.9	Example facies (fig. 4 and 11)
Bedform_1 Wavelength	20 (1)	20 (1)	20 (1)	20 (1)	20 (1)	20 (1)	20 (1)	20 (1)	20 (1)	19 (0.9)	18 (0.8)	12 (0.7)	9 (0.1)	20 (1)
Bedform_1 Amplitude	0.2 (0.05)	0.2 (0.05)	0.2 (0.05)	0.2 (0.05)	0.2 (0.05)	0.2 (0.05)	0.2 (0.05)	0.2 (0.05)	0.2 (0.05)	0.19 (0.045)	0.18 (0.04)	0.12 (0.035)	0.1 (0.01)	0.2 (0.05)
Bedform_2 Wavelength	18 (0.5)	18 (0.5)	18 (0.5)	18 (0.5)	18 (0.5)	18 (0.5)	18 (0.5)	18 (0.5)	18 (0.5)	17 (0.45)	15 (0.4)	10 (0.035)	8 (0.03)	18 (0.5)
Bedform_2 Amplitude	0.18 (0.05)	0.18 (0.05)	0.18 (0.05)	0.18 (0.05)	0.18 (0.05)	0.18 (0.05)	0.18 (0.05)	0.18 (0.05)	0.18 (0.05)	0.17 (0.045)	0.15 (0.04)	0.1 (0.035)	0.09 (0.001)	0.18 (0.05)
Crest Sinousity_1 Wavelength	20 (0.5)	20 (0.5)	20 (0.5)	20 (0.5)	20 (0.5)	20 (0.5)	20 (0.5)	20 (0.5)	20 (0.5)	22.5 (0.5)	25 (0.5)	30 (0.5)	35 (0.5)	20 (0.2)
Crest Sinousity_1 Amplitude	5 (0.2)	5 (0.2)	5 (0.2)	5 (0.2)	5 (0.2)	5 (0.2)	5 (0.2)	5 (0.2)	5 (0.2)	4.5 (0.2)	4 (0.2)	3 (0.2)	2 (0.2)	5 (0.5)
Crest Sinousity_2 Wavelength	30 (0.6)	30 (0.6)	30 (0.6)	30 (0.6)	30 (0.6)	30 (0.6)	30 (0.6)	30 (0.6)	30 (0.6)	32.5 (0.6)	35 (0.6)	37.5 (0.6)	40 (0.6)	30 (1)
Crest Sinousity_2 Amplitude	3 (0.3)	3 (0.1))	3 (0.1)	3 (0.1)	3 (0.1)	3 (0.1)	3 (0.1)	3 (0.1)	3 (0.1)	2.75 (0.1)	2.5 (0.1)	2 (0.1)	1.5 (0.1)	3 (0.05)
Depositional Rate: Sand	0.3 (0.01)	0.3 (0.01)	0.25 (0.01)	0.235 (0.01)	0.225 (0.01)	0.21 (0.01)	0.2 (0.01)	0.175 (0.01)	0.15 (0.01)	0.125 (0.01)	0.1 (0.01)	0.08 (0.01)	0.07 (0.01)	0.3
Depositional Length: Sand	4 (0.1)	3.5 (0.1)	3 (0.1)	2.85 (0.1)	2.75 (0.1)	2.6 (0.1)	2.5 (0.1)	2.25 (0.1)	2 (0.1)	1.75 (0.1)	1.5 (0.1)	1.25 (0.075)	1 (0.05)	70 (0.1)
Depositional Rate: Mud	0 (0)	0.1 (0.01)	0.14 (0.01)	0.155 (0.01)	0.16 (0.01)	0.17 (0.01)	0.18 (0.01)	0.2 (0.01)	0.22 (0.01)	0.24 (0.01)	0.25 (0.01)	0.26 (0.01)	0.27 (0.01)	0.1
Depositional Length: Mud	0 (0)	3.5 (0.1)	4 (0.1)	4.15 (0.1)	4.25 (0.1)	4.4 (0.1)	4.5 (0.1)	4.75 (0.1)	5 (0.1)	5.25 (0.1)	5.5 (0.1)	5.75 (0.1)	6 (0.1)	7.5 (1)
Average (StDev) sand fraction	*1 (0)*	*0.922 (0.003)*	*0.804 (0.008)*	*0.744 (0.008)*	*0.715 (0.008)*	*0.658 (0.01)*	*0.612 (0.01)*	*0.5 (0.09)*	*0.391 (0.009)*	*0.273 (0.011)*	*0.198 (0.014)*	*0.125 (0.09)*	*0.081 (0.09)*	0.985 (0.12)

Figure 1

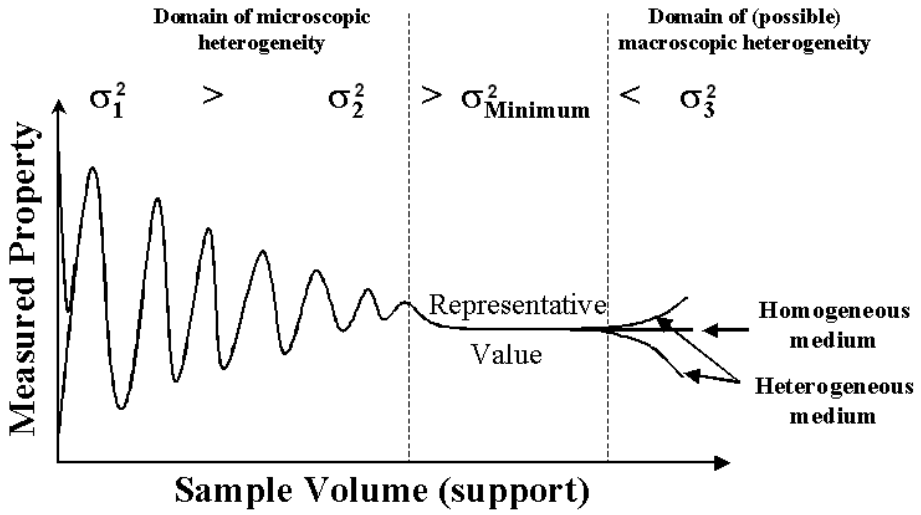

Figure 2

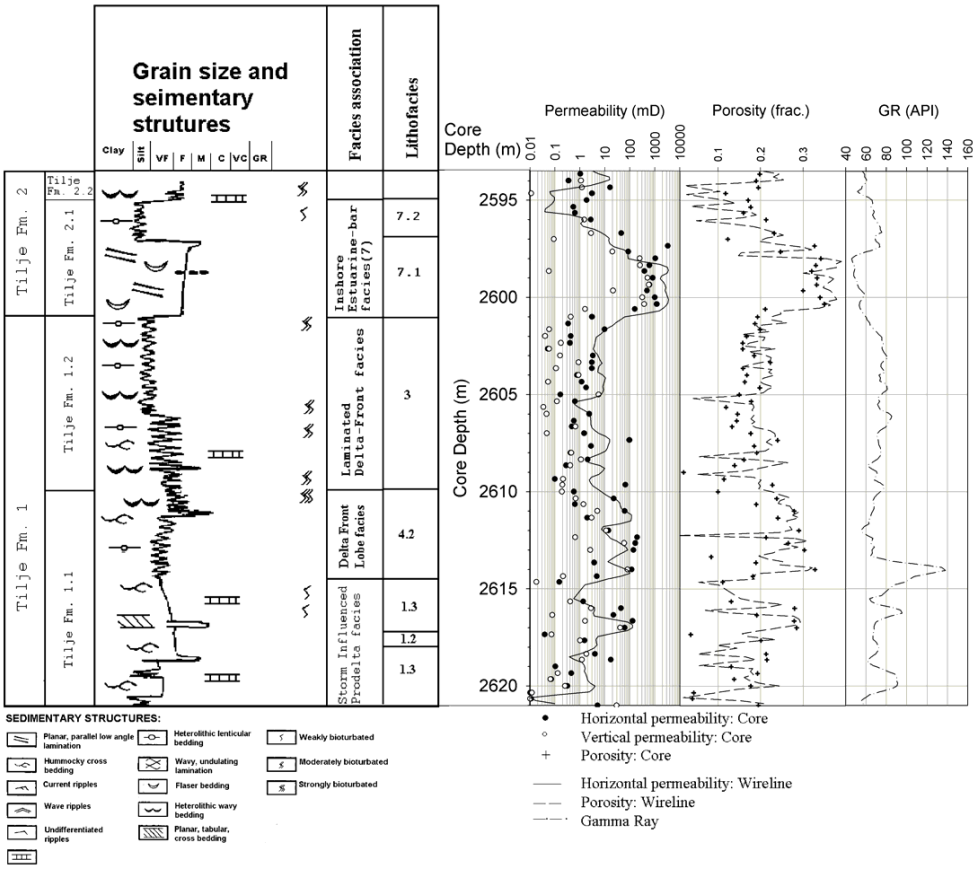

Figure 3

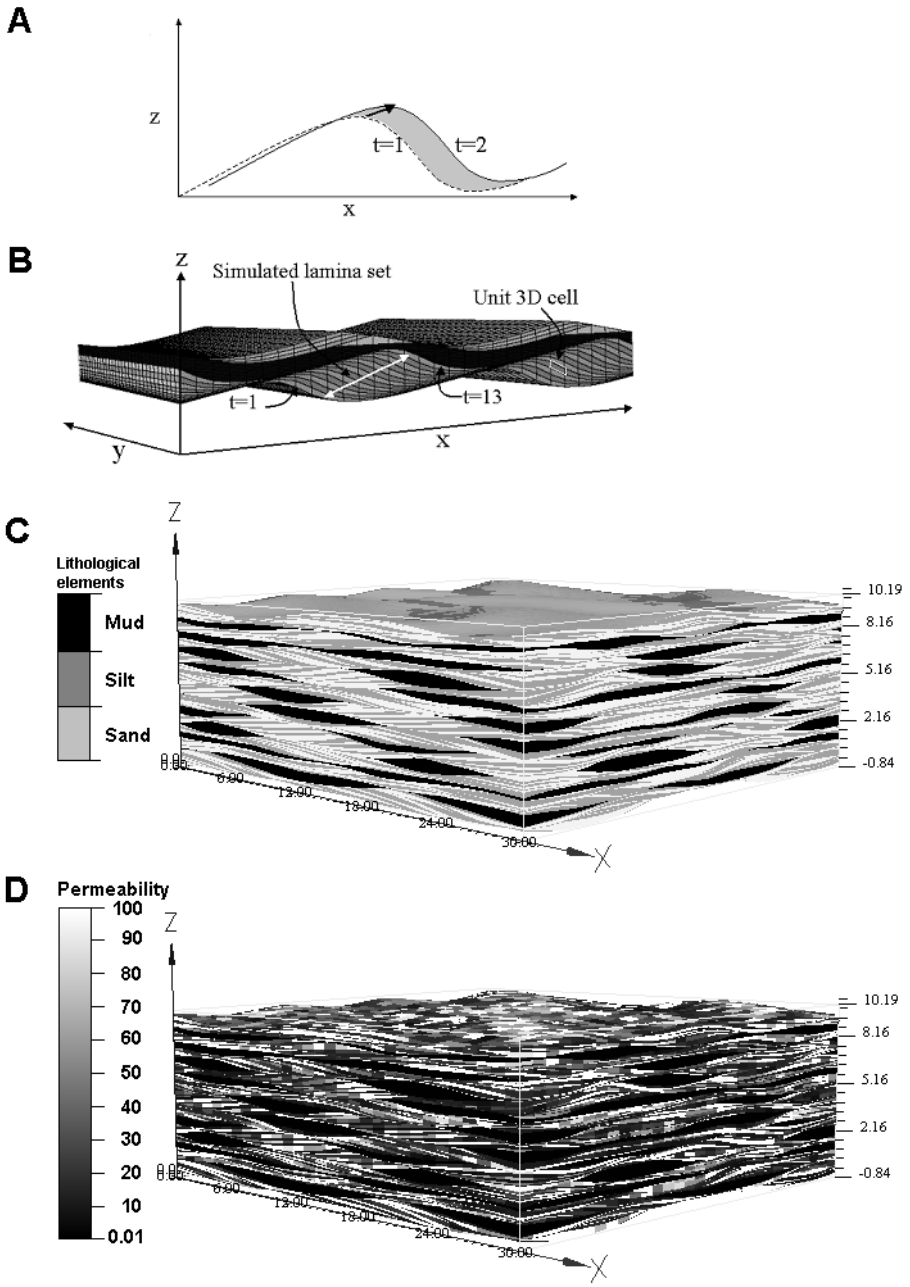
A
z
t=1
t=2
x
B
z
Simulated lamina set
Unit 3D cell
t=1
t=13
y
x
C
Z
Lithological elements
Mud
Silt
Sand
10.19
8.16
5.16
2.16
-0.84
0.00
6.00
12.00
18.00
24.00
30.00
X
D
Permeability
100
90
80
70
60
50
40
30
20
10
0.01
Z
10.19
8.16
5.16
2.16
-0.84
0.00
6.00
12.00
18.00
24.00
30.00
X

Figure 4

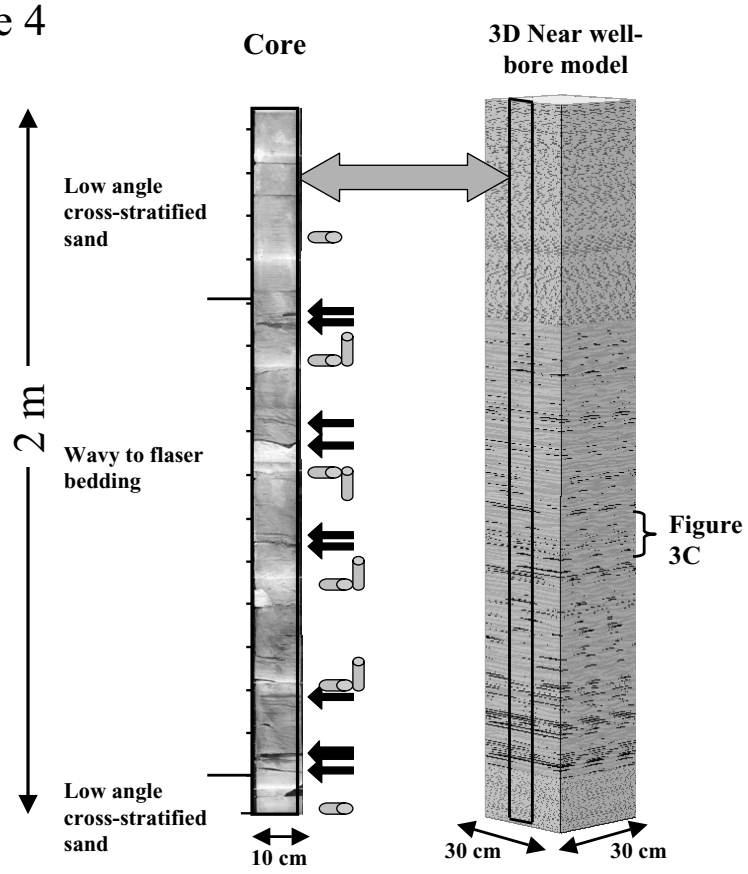

Figure 5a

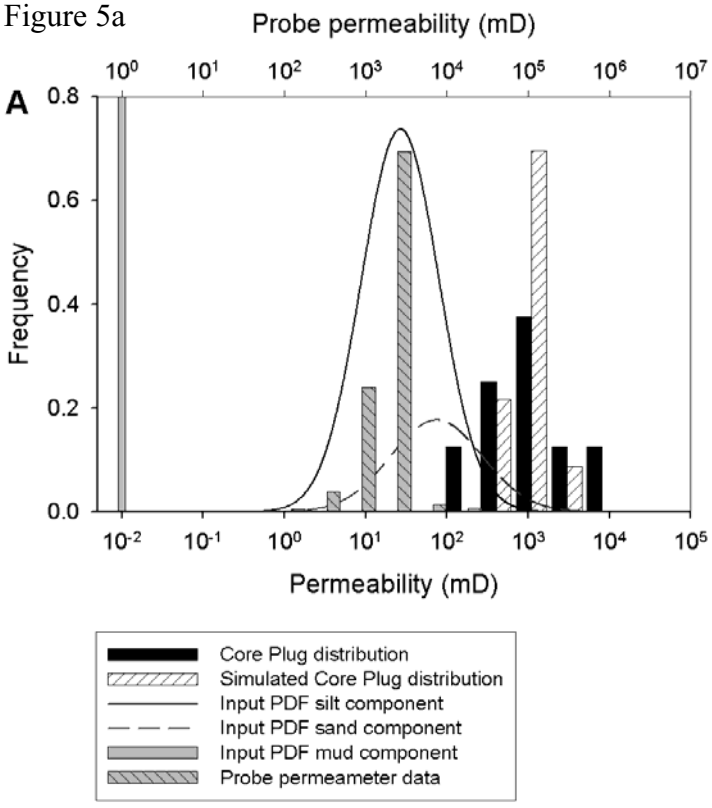

Figure 5b

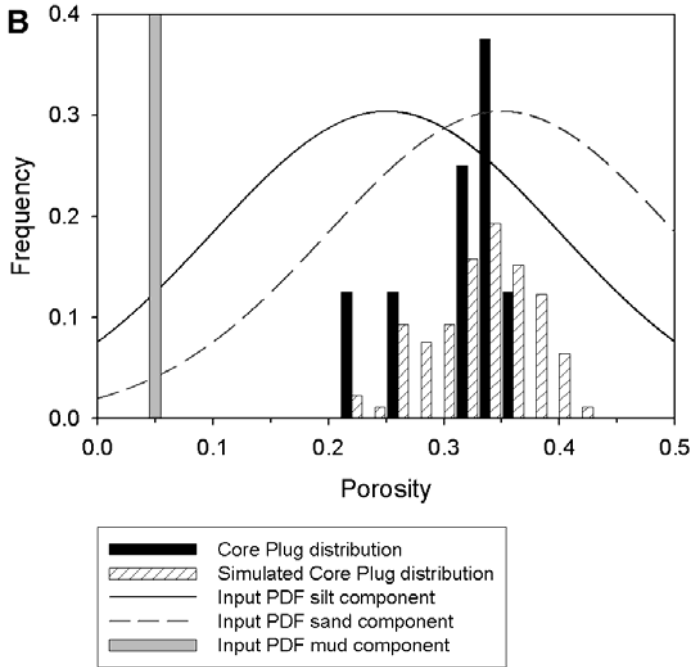

Figure 6

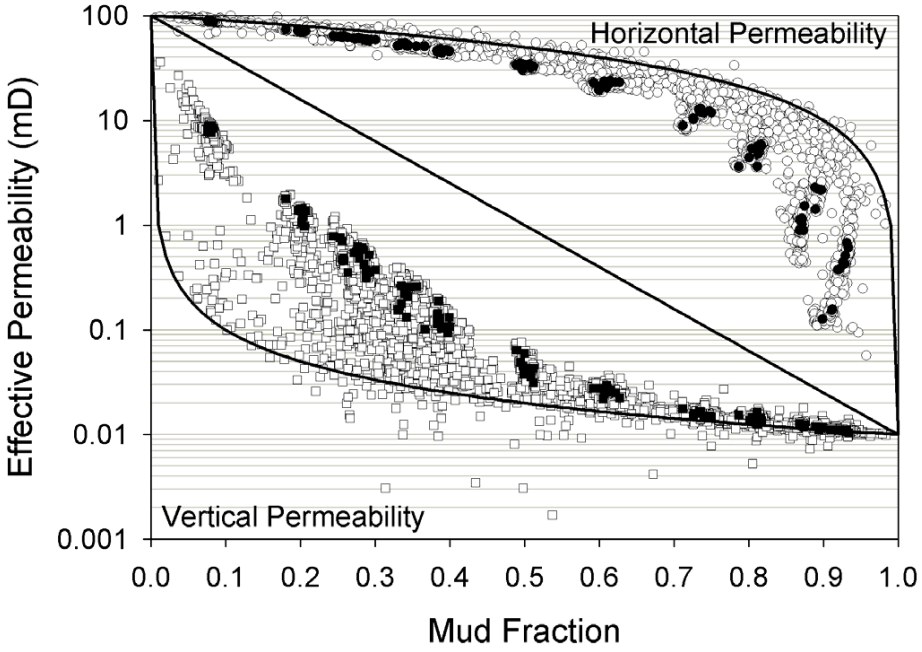

Figure 7

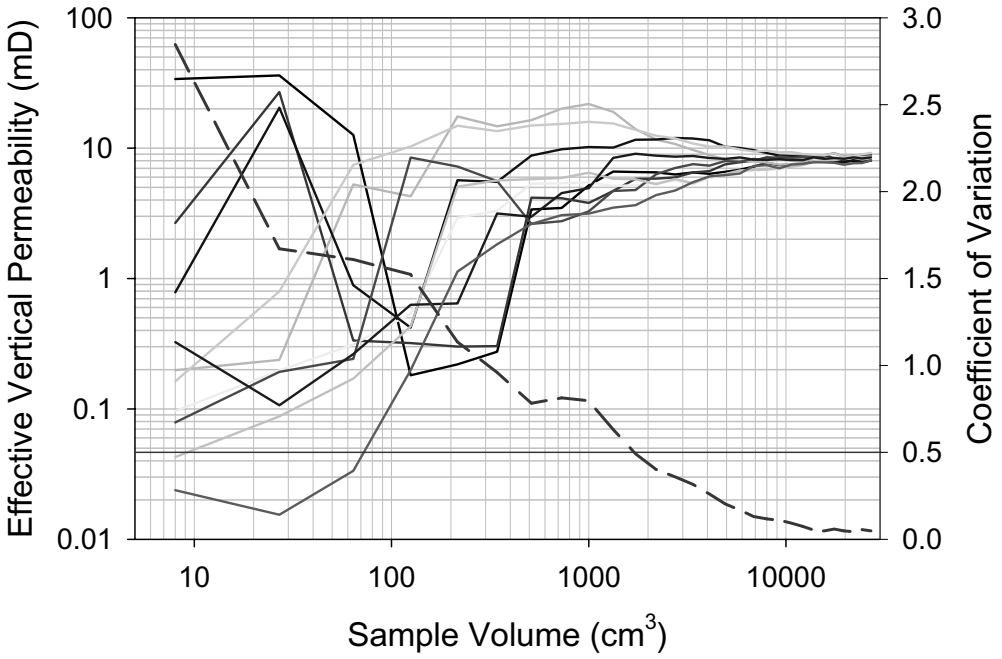

Figure 8

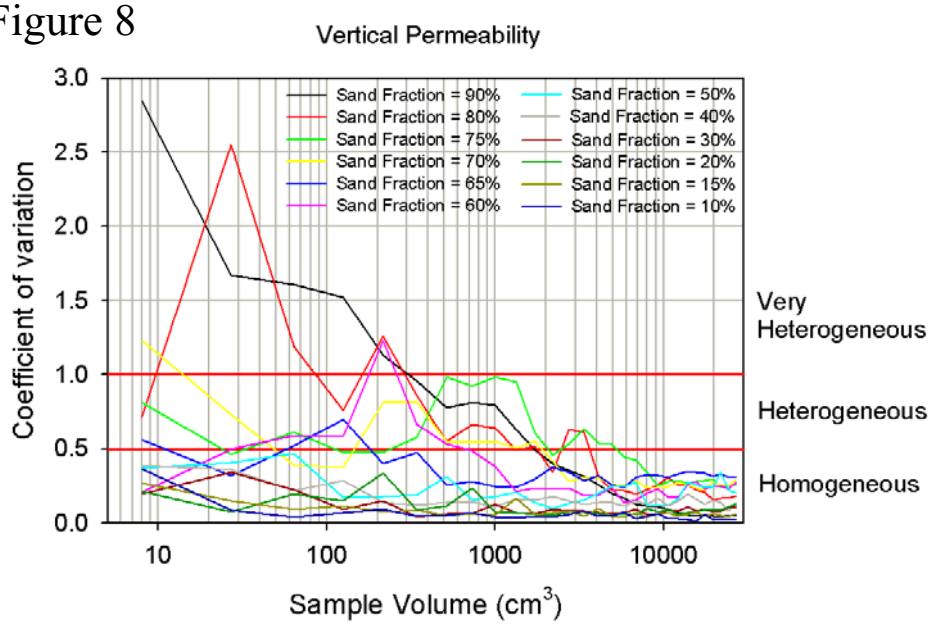

Figure 9

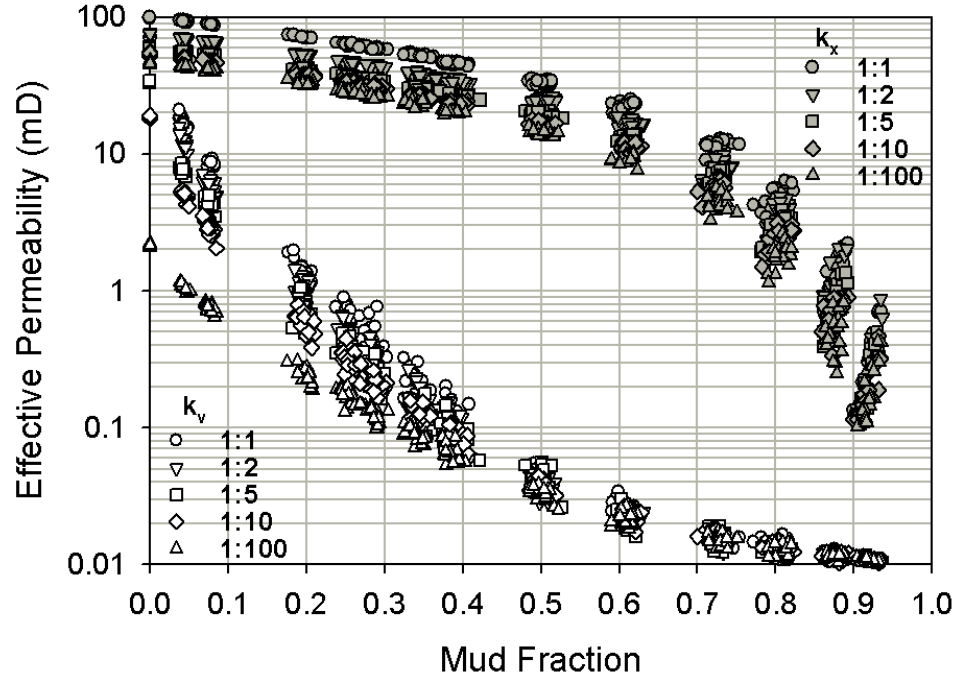

Figure 10A

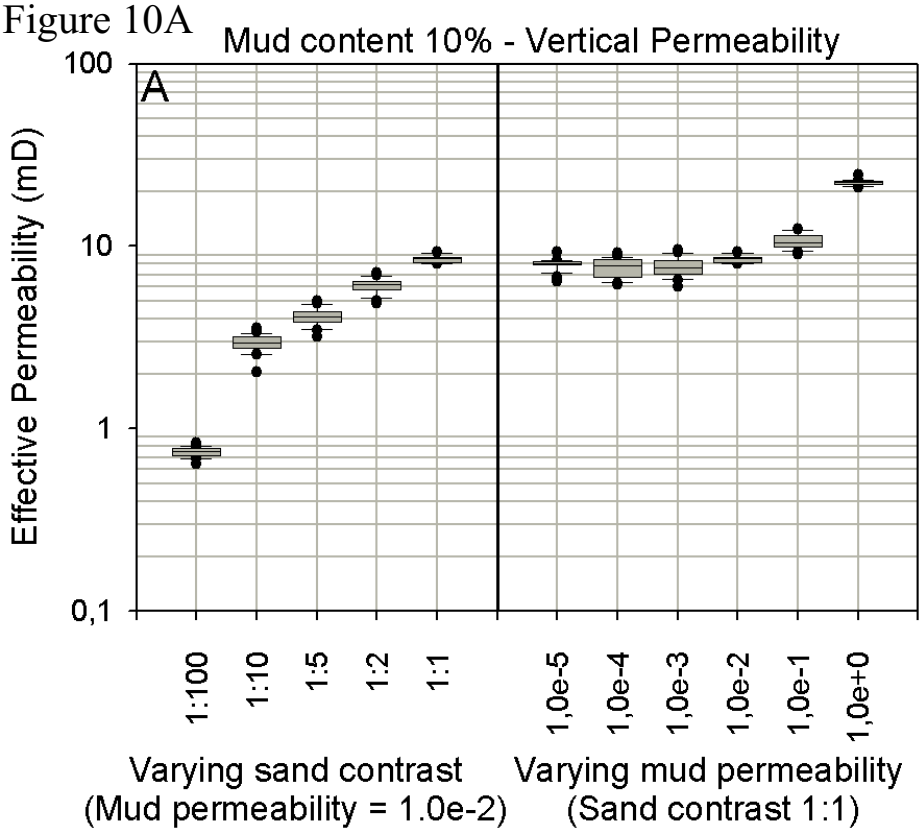

Figure 10B

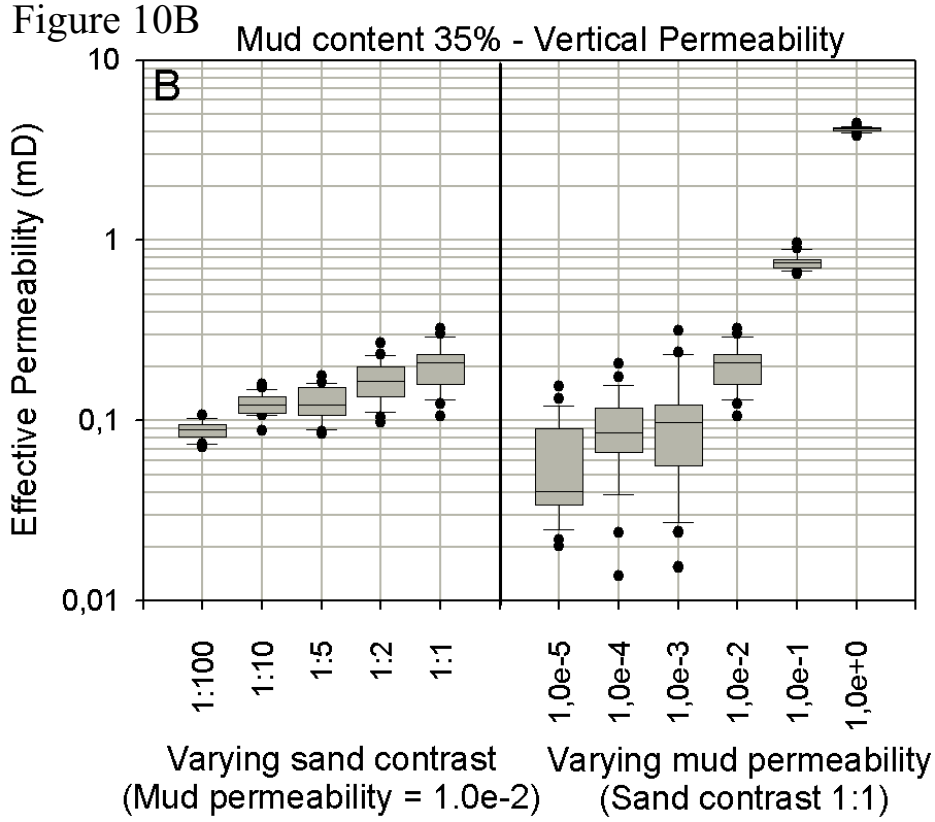

Figure 10C

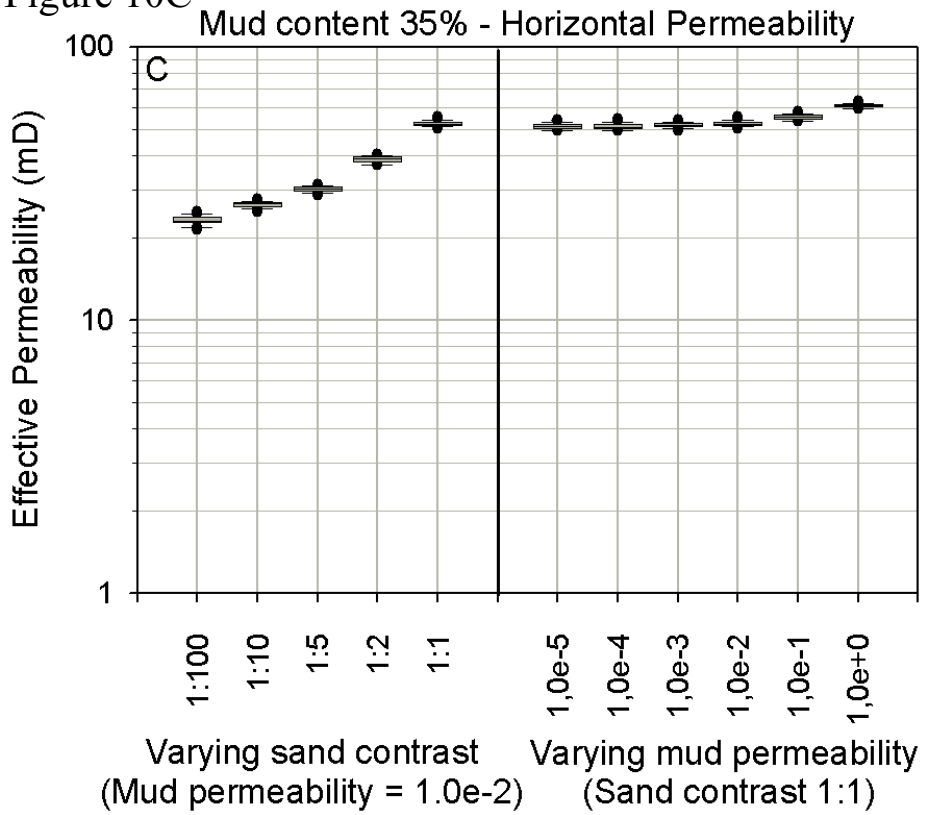

Figure 10D

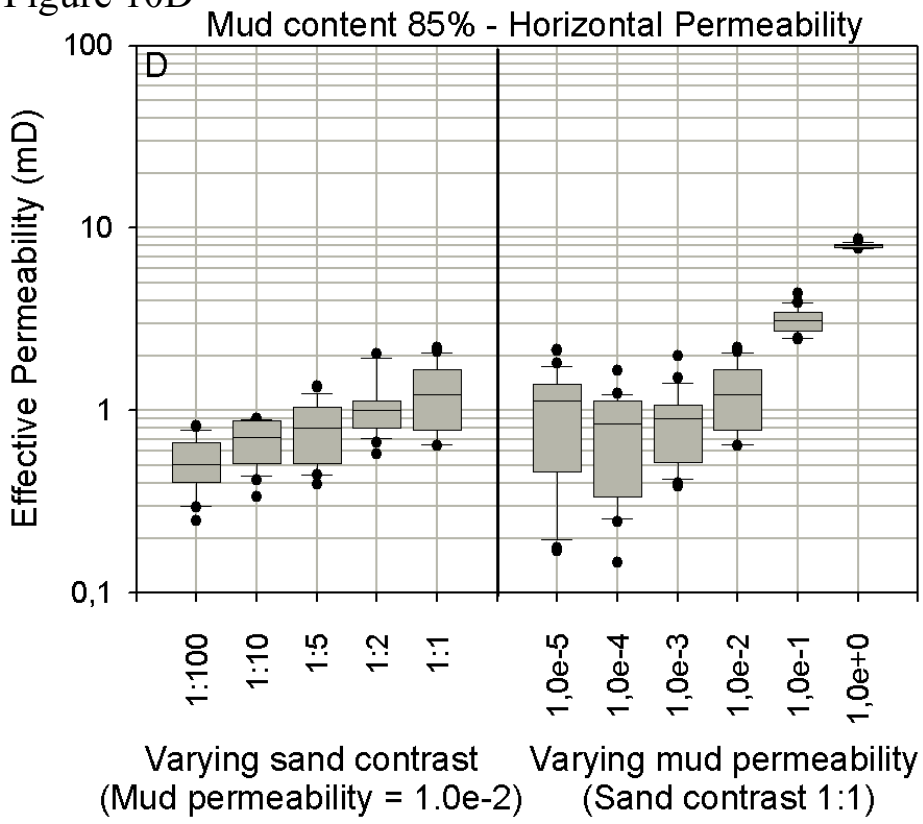

Figure 11A

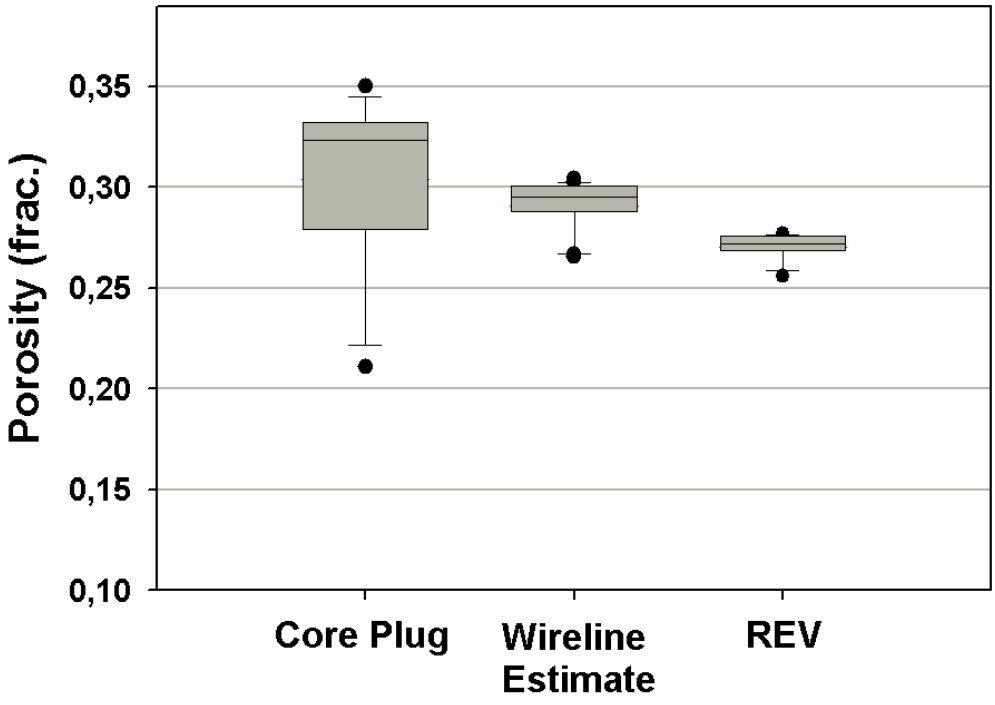

Figure 11B

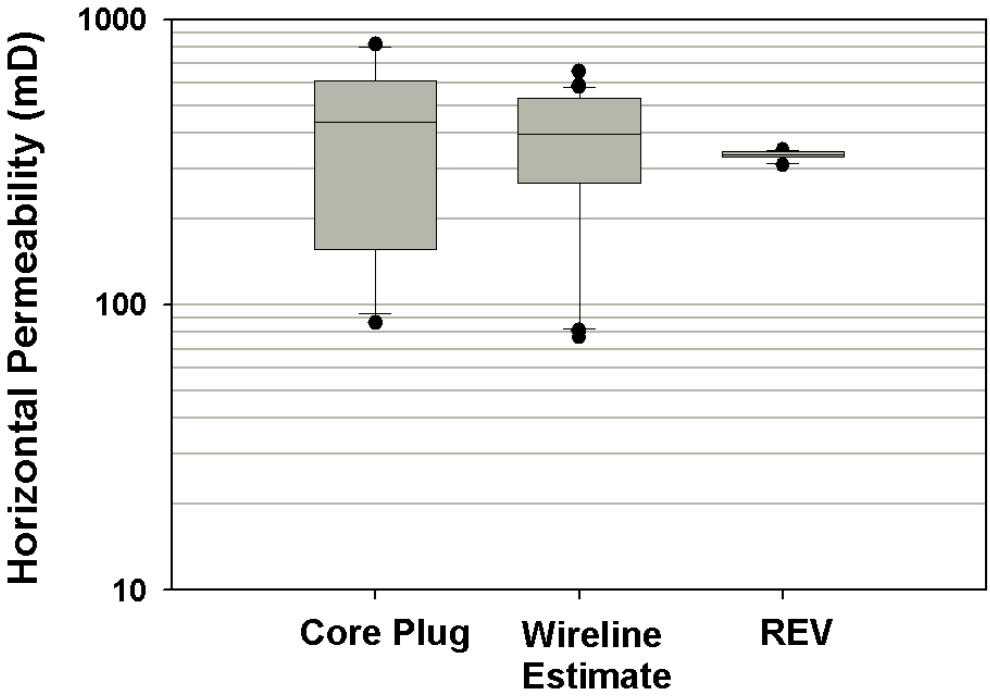

Figure 11C